

SUSTAINABLE OXIDATION CATALYSIS VIA HYPERVALENT IODINE
INTERMEDIATES

A Dissertation

by

ASIM MAITY

Submitted to the Graduate and Professional School of
Texas A&M University
in partial fulfillment of the requirements for the degree of

DOCTOR OF PHILOSOPHY

Chair of Committee,	David C. Powers
Committee Members,	François P. Gabbaï
	Daniel A. Singleton
	Jodie L. Lutkenhaus
Head of Department,	Simon W. North

May 2022

Major Subject: Chemistry

Copyright 2022 Asim Maity

ABSTRACT

Design of sustainable synthetic methods for oxidation reactions is one of the fundamental challenges in chemistry, and both aerobic conditions and electrochemistry provide attractive means to carry out sustainable oxidation reactions. Biological C–H oxidation catalysis routinely proceeds via highly reactive oxidized metal sites generated from O₂; similar oxidation reactions are usually carried out in contemporary synthesis using O₂ surrogates such as hypervalent iodine reagents. These reagents are often used in stoichiometric quantities leading to poor atom economy. In 2018, we reported the development of aerobic hypervalent iodine catalysis predicated on diverting aldehyde autoxidation intermediates towards the oxidation of aryl iodides for sustainable synthesis of both I(III) and I(V) reagents. Many of the transformations for which hypervalent iodine intermediates have been developed, including α -functionalization of carbonyls and metal-free C–H/N–H cross-coupling reactions, were successfully carried out aerobically. We discovered that aryl iodides with weakly-coordinating 2-substituted groups (such as *tert*-butylsulfonyl) yielded the corresponding I(V) reagents due to disproportionation of initially formed I(III) derivatives under the autoxidation reaction conditions and leveraged that for aerobic alcohol oxidation chemistry. Under autoxidation conditions, 1,2-diols afforded alcohol oxidation accompanied with C–C bond cleavage — characteristic of Dess-Martin Periodinane (DMP). Thus, this discovery serves as the first example of aerobic oxidation catalysis involving DMP analogue.

Detailed mechanistic studies of the aerobic oxidation chemistry led to identification of facile one-electron oxidation and the development of electrocatalytic hypervalent iodine chemistry. We demonstrated the viability of hypervalent iodine electrocatalysis in the context of both intra- and intermolecular C–H amination reactions, forming carbazole and aromatic hydrazine

derivatives, respectively via iodanyl radical catalysis. To expand the scope of amination reactions, we have developed new class of *N*-aminopyridinium reagents through benzyl C–H aminopyridylation, and utilized in the synthesis of tetrahydroisoquinolines and α -aminated carbonyl compounds.

Finally, a new family of aminating reagents, based on *N*-aminopyridinium scaffolds, were developed in response to the oxidative lability of many amine precursors under the strongly oxidizing conditions required for iodine-centered oxidation.

Given the breadth of chemistry available for hypervalent iodine compounds, demonstration of strategies to facilitate the aerobic and electrochemical generation of hypervalent iodine species promises to significantly impact the sustainable use of hypervalent iodine intermediates in synthesis.

DEDICATION

Dedicated to my loving family and all my teachers

ACKNOWLEDGEMENTS

This dissertation would not have been possible without the help, support, and guidance of many people. First and foremost, I would like to express my sincere gratitude to my advisor Prof. David C. Powers, for his invaluable advice, continuous support, and patience during my Ph.D. studies. I always wanted to be a part of a new lab for my Ph.D., and I joined TAMU only to work with him. Even though his initial projects were based on inorganic chemistry, he accommodated my desire to work on organic synthesis and encouraged me to design new projects. He always supported me when I wanted to learn or try new things. Being one of his initial crop of students, I learned a lot of chemistry lab techniques directly from him. Though his feedback for document edits seemed frustrating in those times, looking back it was all worth it as my science communication skills had improved the most during Ph.D. Apart from being an outstanding advisor, he has been a great friend and source of inspiration.

I would also like to thank my committee members Prof. Daniel Singleton, Prof. François P. Gabbaï, and Prof. Jodie L. Lutkenhaus, for their valuable suggestions during our meeting.

I would like to sincerely thank all my past and present group members for fostering a fun and collaborative work environment that made working in the lab enjoyable. Special thanks go to Dr. Anuvab Das, Dr. Sung-Min Hyun, Dr. Wen-Yang Gao, Gerard ‘Trip’ Van Trieste, Andrew ‘Andy’ Ezazi, and Brandon L. Frey for being good friends and making the lab exciting through many jokes and pranks. I also had the pleasure to mentor very talented undergrads and would like to thank all of them— Alan K. Wortman, Kimberlie Chudej, Mellissa Roverse, Haleigh Stafford, Nathanael D. Hoskinson, and Roberto G. Herrera—for helping me improve my mentoring and teaching skills.

I am grateful to the Chemistry Department at Texas A&M University for giving me the opportunity to pursue Ph.D. at such a collaborative and resourceful place. I am incredibly thankful to Sandy Horton for helping me wade through the rules and regulations of graduate school. On the technical side, I would like to thank Drs. Gregory P. Wylie, Vladimir Bakmutov, and Doug Elliott for training me on NMR and EPR instruments and helping me with NMR kinetics and *in situ* EPR experiments. I am especially grateful to Yohannes H. Rezenom for all the mass spectrometry experiments during spin-trapped EPR studies.

I would like to thank Anushree Mondal for being my best friend and the pillar of support throughout my graduate studies. I have been fortunate enough to have a wonderful circle of friends in College Station who made life fun outside the lab and joined me in many trips to the national parks. I'd like to specifically thank Dr. Anuvab Das, Dr. Sayan Banerjee, and Dr. Rajat Maji for all their know-how and for helping to settle in a new place.

Finally, I am forever grateful to my family for their continuous and unparalleled love, help, and support. I am indebted to my parents for all their hard work and sacrifices to make me who I am. I am grateful to my sister for always being there for me as a friend and believing in me. This journey wouldn't have been possible if not for them.

CONTRIBUTORS AND FUNDING SOURCES

Contributors

This work was supervised by a dissertation committee consisting of my advisor Professor David C. Powers, Professors François P. Gabbaï and Daniel A. Singleton of the Department of Chemistry, and Professor Jodie L. Lutkenhaus of the Department of Chemical Engineering.

Several portions of this thesis were developed in collaboration with co-workers. Brandon L. Frey contributed to the literature survey presented in Chapter I. Dr. Sung-Min Hyun contributed to the kinetics data presented in Chapter II and III and performed the diacetoxylation of 4-fluorostyrene and aerobic C–H/N–H coupling reactions in Chapter II. Alan K. Wortman, a Texas A&M undergraduate, helped with the preparation of substituted 1-phenylethyl alcohols described in Chapter III. Dr. Ashley D. Cardenal contributed to the measurement of disproportionation kinetics of compound **III.2a** in Chapter III. Prof. David C. Powers carried out the computational calculations on the disproportionation of **III.2a** and **III.2e** in Chapter III. Brandon L. Frey contributed to the synthesis of the biphenylacetmides and cyclic voltametric studies described in Chapter IV. Nathanael D. Hoskinson, a Texas A&M undergraduate, helped with the aerobic oxidation part of the robustness analysis in Chapter IV. Dr. Sung-Min Hyun helped with acquisition and analysis of single-crystal X-ray diffraction described in Chapter V. Pritam Rowchowdhury carried out the synthesis of benzyl-*N*-aminopyridiniums and its tosylated products described in Chapter V. Drs. Gregory P. Wylie and Doug Elliott helped with EPR measurements in Chapter V.

Funding Sources

This work was made possible in part by financial support from Texas A&M University, the Texas A&M College of Science Strategic Transformative Research Program (STRP), the Welch Foundation (A-1907), the National Science Foundation (CAREER-1848135), and the National Institute of Health (R35GM138114).

TABLE OF CONTENTS

	Page
ABSTRACT.....	ii
DEDICATION.....	iv
ACKNOWLEDGEMENTS.....	v
CONTRIBUTORS AND FUNDING SOURCES.....	vii
TABLE OF CONTENTS.....	ix
LIST OF FIGURES.....	xi
LIST OF TABLES.....	xxi
CHAPTER I INTRODUCTION: SUSTAINABLE OXIDATION CATALYSIS VIA HYPERVALENT IODINE INTERMEDIATES.....	1
I.1 Introduction.....	1
I.2 Sustainable Oxidants Based on Active Oxygen Content.....	2
I.3 Background on Hypervalent Iodine Compounds.....	4
I.4 Synthesis of Hypervalent Iodine(III) Reagents with Sustainable Oxidant.....	9
I.5 Synthesis of Hypervalent Iodine(V) Reagents with Sustainable Oxidants.....	15
I.6 Conclusions.....	16
CHAPTER II OXIDASE CATALYSIS VIS AEROBICALLY GENERATED HYPERVALENT IODINE INTERMEDIATES.....	17
II.1 Introduction.....	17
II.2 Results and Discussion.....	20
II.2.1 Intercepting Aldehyde Autoxidation for Aerobic Oxidation of Aryl Iodides.....	21
II.2.2 Application of Aerobic Oxidation of Aryl Iodides to Oxidase Chemistry.....	24
II.2.3 Application of Aerobic Oxidation of Aryl Iodides to Oxidase Catalysis.....	25
II.2.4 Aerobic Oxidation Mechanism.....	27
II.3 Conclusions.....	29
II.4 Experimental Details.....	30
II.4.1 General Considerations.....	30
II.4.2 Synthesis and Characterization Details.....	31
CHAPTER III OXIDATION CATALYSIS BY AN AEROBICALLY GENERATED DESS- MARTIN PERIODINANE ANALOGUE.....	69

LIST OF FIGURES

	Page
Figure I-1. The low ionization potential of iodine is manifest in families of oxidized iodine compounds.	5
Figure I-2. Orbital picture for the 3c-4e bonding in hypervalent iodine compounds.	6
Figure I-3. The chemistry of hypervalent iodine compounds is often described using terminology common to organometallic catalysis.	8
Figure I-4. Hydrogen peroxide reacts with (ditrifluoroacetoxy)iodobenzene to form singlet oxygen ($^1\text{O}_2$) and iodobenzene.	9
Figure I-5. The combination of hydrogen peroxide and acetic anhydride generate peracetic acid <i>in situ</i> , which is responsible for oxidation of iodobenzene (I.1a) to (diacetoxyiodo)benzene (I.2a).	10
Figure I-6. <i>In situ</i> generation of trifluoroperacetic acid from UHP and trifluoroacetic anhydride provides access to [bis(trifluoroacetoxy)iodo]arenes from the corresponding iodoarenes.	11
Figure I-7. H_2O_2 was combined with concentrated HCl to form hypochlorous acid (HOCl) <i>in situ</i> , the active chlorinating reagent for the synthesis of (dichloroiodo)arenes from iodoarenes.	11
Figure I-8. Diaryliodonium triflates were synthesized using urea-hydrogen peroxide adduct (UHP) in a sustainable method leading to symmetric and unsymmetric iodonium salts.	12
Figure I-9. Examples of anodically generated hypervalent iodine compounds.	13
Figure I-10. Recyclable iodoarene mediators for <i>ex cell</i> electrochemistry.	14
Figure I-11. Anodic oxidation of aryl iodides under flow conditions.	14
Figure I-12. RuCl_3 -mediated disproportionation of initially formed hypervalent iodine(III) intermediates provided access to the corresponding iodylarenes.	15
Figure II-1 Oxygenase versus oxidase aerobic oxidation chemistry.	17
Figure II-2. Utilization of O_2 as terminal oxidant in synthetic chemistry.	19
Figure II-3. Radical-chain mechanism for aldehyde autoxidation.	20
Figure II-4. Application of aerobic oxidation chemistry to the synthesis of a family of hypervalent iodine reagents.	23

Figure II-5. Aerobic oxidation of PhI provides a broad platform to directly utilize O ₂ as the terminal oxidant in substrate oxidation reactions.....	25
Figure II-6. Oxidase catalysis via aerobically generated hypervalent iodine intermediates.....	26
Figure II-7. Aerobic oxidation of iodobenzene is suppressed in the presence of radical inhibitors.....	27
Figure II-8. Aerobic oxidation of aryl iodides is accomplished by intercepting the oxidizing intermediates of aldehyde autoxidation chemistry.....	28
Figure II-9. Measurement of aerobic oxidation kinetics of iodobenzene in CDCl ₃ with no added initiator.....	54
Figure II-10. Measurement of aerobic oxidation kinetics of iodobenzene in CDCl ₃ with initiator.	55
Figure II-11. Kinetics experiments for aerobic oxidation of 4-iodotoluene with no added initiator.	56
Figure II-12. Measurement of aerobic oxidation kinetics of 4-iodotoluene in CDCl ₃ with initiator.	57
Figure II-13. Kinetics experiments for aerobic oxidation of iodobenzene with no added initiator.	58
Figure II-14. Measurement of aerobic oxidation kinetics of PhI in AcOH- <i>d</i> ₄ with initiator.	59
Figure II-15. NMR spectrum collected during aerobic oxidation of PhI with the peaks attributable to peroxo E highlighted in red.....	60
Figure II-16. Mass spectrometry analysis of (a) the reaction mixture of CH ₃ CHO, PhI, CoCl ₂ ·6H ₂ O, and O ₂ and (b) the reaction mixture of CH ₃ CHO, CoCl ₂ ·6H ₂ O, and O ₂	61
Figure II-17. ¹ H NMR plots of magnetization transfer experiment that demonstrates that acetaldehyde and intermediate E are in rapid equilibrium on the NMR time scale.....	62
Figure II-18. ¹ H NMR spectrum of compound II.3b recorded in CD ₃ OD at 23 °C.....	63
Figure II-19. ¹ H NMR spectrum of compound II.3c recorded in CD ₃ OD at 23 °C.....	64
Figure II-20. ¹ H NMR spectrum of compound II.3d recorded in CD ₃ OD at 23 °C.....	65
Figure II-21. ¹ H NMR spectrum of compound II.3e recorded in CD ₃ OD at 23 °C.....	66
Figure II-22. ¹ H NMR spectrum of compound II.3f recorded in CD ₃ OD at 23 °C.	67

Figure II-23. ¹ H NMR spectrum of compound II.3g recorded in CD ₃ OD at 23 °C.....	68
Figure III-1. Rapid disproportionation of aerobically generated iodosylbenzenes can enable aerobic oxidation via iodylbenzene intermediates.	70
Figure III-2. Role of Co(II) salt in aerobic oxidation of aryl iodides.	71
Figure III-3. Aldehyde-promoted aerobic oxidation can provide access to a variety of iodylbenzene derivatives.	72
Figure III-4. Oxidation chemistry scope of aerobically generated iodylbenzene reagent III.3a	75
Figure III-5. Aerobic oxidation secondary alcohols catalyzed by III.1a provides access to a wide variety of ketones.	77
Figure III-6. Application of III.1a in aerobic alcohol oxidation catalysis.	78
Figure III-7. Aerobic oxidation kinetics of 2-(<i>tert</i> -butylsulfonyl)iodobenzene in CDCl ₃	79
Figure III-8. ¹ H NMR experiment for addition of AcOH to III.2a	80
Figure III-9. Analysis of impurity in independently synthesized III.2a via EPR studies.	81
Figure III-10. Mass spectrometry analysis of III.2a prepared by Method A.	82
Figure III-11. Measurement of aerobic oxidation kinetics of 4-iodotoluene (III.1e) in CDCl ₃ . ..	83
Figure III-12. Measurement of aerobic oxidation kinetics of III.2a in AcOH- <i>d</i> ₄	84
Figure III-13. Proposed catalytic cycle for I(V) mediated aerobic oxidation catalysis.	85
Figure III-14. Reaction Profile for Cyclohexanol Oxidation by III.3a with and without Co(II).	112
Figure III-15. Measurement of aerobic oxidation kinetics of 2-(<i>tert</i> -butylsulfonyl)iodobenzene in CDCl ₃	113
Figure III-16. Measurement of aerobic oxidation of 4-iodotoluene in CDCl ₃	114
Figure III-17. Structure-dependent disproportionation thermodynamics.	117
Figure III-18. ¹ H NMR of compound III.3b measured in DMSO- <i>d</i> ₆ at 23 °C.	126
Figure III-19. ¹³ C NMR of compound III.3b measured in DMSO- <i>d</i> ₆ at 23 °C.	127
Figure III-20. ¹ H NMR of compound III.3c measured in D ₂ O at 23 °C.	128
Figure III-21. ¹³ C NMR of compound III.3c measured in D ₂ O at 23 °C.	129

Figure III-22. ^1H NMR of compound III.3i measured in $\text{DMSO-}d_6$ at 23 °C.	130
Figure III-23. ^{13}C NMR of compound III.3i measured in $\text{DMSO-}d_6$ at 23 °C.	131
Figure IV-1. Strategies for electrosynthetic chemistry.	133
Figure IV-2. Proposed mechanism of aldehyde-promoted aerobic autoxidation of aryl iodides.	134
Figure IV-3. Gas chromatogram of the headspace of 4-iodotoluene oxidation in HFIP indicating the evolution of H_2 at the cathode.	136
Figure IV-4. Intramolecular C–H / N–H coupling via hypervalent iodine electrocatalysis.	138
Figure IV-5. Cyclic voltammograms of various amines for intermolecular chemistry.	140
Figure IV-6. (a) Intermolecular C–H / N–H coupling via hypervalent iodine electrocatalysis.	141
Figure IV-7. Potential mechanisms for the observed acetate-dependent hypervalent iodine electrocatalysis.	142
Figure IV-8. Cyclic voltammograms studies of 4-iodoanisole.	143
Figure IV-9. Electrolysis and headspace analysis of [TBA]OAc in acetonitrile.	144
Figure IV-10. Electrolysis and headspace analysis of [TBA]OAc in HFIP.	144
Figure IV-11. ^1H NMR spectra of HFIP titration with [TBA]OAc in CD_3CN	146
Figure IV-12. Job plot constructed from the ^1H NMR data shown in Figure IV-11.	147
Figure IV-13. Summary of the results of robustness analysis.	148
Figure IV-14. Increasing reversibility of 4-iodotoluene oxidation in HFIP is observed in cyclic voltammograms collected with increasing scan rate.	192
Figure IV-15. Plot of (a) scan rate vs. peak anodic current (I_{pa}) of 4-iodotoluene [$R^2 = 0.89$] and (b) square root of scan rate vs. peak anodic current (I_{pa}) [$R^2 = 0.98$].	192
Figure IV-16. ^1H NMR spectra of HFIP titration with [TBA]OAc in CD_3CN	194
Figure IV-17. Job plot constructed from the ^1H NMR data shown in Figure IV-16.	195
Figure IV-18. Linear fitting of K_{eq} vs. $\Delta\delta\text{CA}$ for solutions 8 (—), 9 (—), 10 (—), and 11 (—).	196
Figure IV-19. Plot of scan rate vs. peak anodic current (I_{pa}) of 4-iodoanisole [$R^2 = 0.91$].	200

Figure IV-20. Comparison of current response in the cyclic voltammogram of 4-iodoanisole (IV.3a) with the addition of either (a) acetate, or (b) substrate (IV.1a).	200
Figure IV-21. Comparison of Faradaic efficiency with selected publications in recent years on electrocatalytic substrate functionalization.	202
Figure IV-22. ¹ H NMR spectrum of compound IV.S1h in CDCl ₃ (400 MHz) at 23 °C.....	203
Figure IV-23. ¹³ C NMR spectrum of compound IV.S1h in CDCl ₃ (100 MHz) at 23 °C.	204
Figure IV-24. ¹ H NMR spectrum of compound IV.1u in CDCl ₃ (400 MHz) at 23 °C.....	205
Figure IV-25. ¹³ C NMR spectrum of compound IV.1u in CDCl ₃ (100 MHz) at 23 °C.....	206
Figure IV-26. ¹ H NMR spectrum of compound IV.1v in CDCl ₃ (400 MHz) at 23 °C.....	207
Figure IV-27. ¹³ C NMR spectrum of compound IV.1v in CDCl ₃ (100 MHz) at 23 °C.....	208
Figure IV-28. ¹ H NMR spectrum of compound IV.2e in CDCl ₃ (400 MHz) at 23 °C.	209
Figure IV-29. ¹³ C NMR spectrum of compound IV.2e in CDCl ₃ (100 MHz) at 23 °C.	210
Figure IV-30. ¹ H NMR spectrum of compound IV.2q in CDCl ₃ (400 MHz) at 23 °C.....	211
Figure IV-31. ¹³ C NMR spectrum of compound IV.2q in CDCl ₃ (125 MHz) at 23 °C.....	212
Figure IV-32. ¹ H NMR spectrum of compound IV.2t in CDCl ₃ (400 MHz) at 23 °C.....	213
Figure IV-33. ¹³ C NMR spectrum of compound IV.2t in CDCl ₃ (100 MHz) at 23 °C.....	214
Figure IV-34. ¹ H NMR spectrum of compound IV.2u in CDCl ₃ (400 MHz) at 23 °C.....	215
Figure IV-35. ¹³ C NMR spectrum of compound IV.2u in CDCl ₃ (100 MHz) at 23 °C.....	216
Figure IV-36. ¹ H NMR spectrum of compound IV.2v in CDCl ₃ (400 MHz) at 23 °C.....	217
Figure IV-37. ¹³ C NMR spectrum of compound IV.2v in CDCl ₃ (100 MHz) at 23 °C.....	218
Figure IV-38. ¹ H NMR spectrum of compound IV.5f in CDCl ₃ (400 MHz) at 23 °C.....	219
Figure IV-39. ¹³ C NMR spectrum of compound IV.5f in CDCl ₃ (100 MHz) at 23 °C.....	220
Figure IV-40. ¹ H NMR spectrum of compound IV.5g in CDCl ₃ (500 MHz) at 23 °C.....	221
Figure IV-41. ¹³ C NMR spectrum of compound IV.5g in CDCl ₃ (125 MHz) at 23 °C.....	222
Figure IV-42. ¹ H NMR spectrum of compound IV.5h in CDCl ₃ (400 MHz) at 23 °C.....	223

Figure IV-43. ^{13}C NMR spectrum of compound IV.5h in CDCl_3 (100 MHz) at 23 °C.....	224
Figure IV-44. ^1H NMR spectrum of compound IV.5i in CDCl_3 (400 MHz) at 23 °C.....	225
Figure IV-45. ^{13}C NMR spectrum of compound IV.5i in CDCl_3 (100 MHz) at 23 °C.....	226
Figure V-1. Representative C–H amination methods.....	229
Figure V-2. Photocatalytic derivatization of benzyl <i>N</i> -aminopyridiniums.....	230
Figure V-3. Photocatalytic carboamination promoted by deaminative functionalization of V.2 in presence of olefins provides access to a family of 1,4-substituted tetrahydroisoquinolines V.5	231
Figure V-4. Functionalization of <i>N</i> -benzylpyridinium V.2 with (a) nucleophilic heterocycle V.6 and (b) silyl enol ethers V.8	233
Figure V-5. Proposed mechanism for carboamination reaction.	234
Figure V-6. Displacement ellipsoid plot for <i>cis</i> - V.5e plotted at 50% probability.....	274
Figure V-7. Displacement ellipsoid plot of V.5s plotted at 50% probability.	274
Figure V-8. EPR spectra for photochemical deaminative functionalization of V.2a in presence of PBN was obtained in acetonitrile.....	278
Figure V-9. ^1H NMR spectrum of compound V.2a in CDCl_3 (400 MHz) at 23 °C.	279
Figure V-10. ^{13}C NMR spectrum of compound V.2a in CDCl_3 (100 MHz) at 23 °C.	280
Figure V-11. ^1H NMR spectrum of compound V.2b in CDCl_3 (400 MHz) at 23 °C.	281
Figure V-12. ^{13}C NMR spectrum of compound V.2b in CDCl_3 (100 MHz) at 23 °C.....	282
Figure V-13. ^1H NMR spectrum of compound V.2c in CD_3CN (400 MHz) at 23 °C.....	283
Figure V-14. ^{13}C NMR spectrum of compound V.2c in CD_3CN (100 MHz) at 23 °C.....	284
Figure V-15. ^1H NMR spectrum of compound V.2d in CDCl_3 (400 MHz) at 23 °C.....	285
Figure V-16. ^{13}C NMR spectrum of compound V.2d in CDCl_3 (100 MHz) at 23 °C.....	286
Figure V-17. ^1H NMR spectrum of <i>cis</i> - V.5a in CDCl_3 (400 MHz) at 23 °C.	287
Figure V-18. ^{13}C NMR spectrum of <i>cis</i> - V.5a in CDCl_3 (100 MHz) at 23 °C.	288
Figure V-19. ^1H NMR spectrum of <i>trans</i> - V.5a in CDCl_3 (400 MHz) at 23 °C.....	289

Figure V-20. ^{13}C NMR spectrum of <i>trans</i> - V.5a in CDCl_3 (100 MHz) at 23 °C.	290
Figure V-21. ^1H NMR spectrum of <i>cis</i> - V.5b in CDCl_3 (400 MHz) at 23 °C.	291
Figure V-22. ^{13}C NMR spectrum of <i>cis</i> - V.5b in CDCl_3 (100 MHz) at 23 °C.	292
Figure V-23. ^1H NMR spectrum of <i>trans</i> - V.5b in CDCl_3 (400 MHz) at 23 °C.	293
Figure V-24. ^{13}C NMR spectrum of <i>trans</i> - V.5b in CDCl_3 (100 MHz) at 23 °C.	294
Figure V-25. ^1H NMR spectrum of <i>cis</i> - V.5c in CDCl_3 (400 MHz) at 23 °C.	295
Figure V-26. ^{13}C NMR spectrum of <i>cis</i> - V.5c in CDCl_3 (100 MHz) at 23 °C.	296
Figure V-27. ^1H NMR spectrum of <i>trans</i> - V.5c in CDCl_3 (400 MHz) at 23 °C.	297
Figure V-28. ^{13}C NMR spectrum of <i>trans</i> - V.5c in CDCl_3 (100 MHz) at 23 °C.	298
Figure V-29. ^1H NMR spectrum of <i>cis</i> - V.5d in CDCl_3 (400 MHz) at 23 °C.	299
Figure V-30. ^{13}C NMR spectrum of <i>cis</i> - V.5d in CDCl_3 (100 MHz) at 23 °C.	300
Figure V-31. ^1H NMR spectrum of <i>cis</i> - V.5e in CDCl_3 (400 MHz) at 23 °C.	301
Figure V-32. ^{13}C NMR spectrum of <i>cis</i> - V.5e in CDCl_3 (100 MHz) at 23 °C.	302
Figure V-33. ^1H NMR spectrum of <i>trans</i> - V.5e in CDCl_3 (400 MHz) at 23 °C.	303
Figure V-34. ^{13}C NMR spectrum of <i>trans</i> - V.5e in CDCl_3 (100 MHz) at 23 °C.	304
Figure V-35. ^1H NMR spectrum of <i>cis</i> - V.5f in CDCl_3 (400 MHz) at 23 °C.	305
Figure V-36. ^{13}C NMR spectrum of <i>cis</i> - V.5f in CDCl_3 (100 MHz) at 23 °C.	306
Figure V-37. ^1H NMR spectrum of <i>trans</i> - V.5f in CDCl_3 (400 MHz) at 23 °C.	307
Figure V-38. ^{13}C NMR spectrum of <i>trans</i> - V.5f in CDCl_3 (100 MHz) at 23 °C.	308
Figure V-39. ^1H NMR spectrum of <i>cis</i> - V.5g in CDCl_3 (400 MHz) at 23 °C.	309
Figure V-40. ^{13}C NMR spectrum of <i>cis</i> - V.5g in CDCl_3 (100 MHz) at 23 °C.	310
Figure V-41. ^1H NMR spectrum of <i>trans</i> - V.5g in CDCl_3 (400 MHz) at 23 °C.	311
Figure V-42. ^{13}C NMR spectrum of <i>trans</i> - V.5g in CDCl_3 (100 MHz) at 23 °C.	312
Figure V-43. ^1H NMR spectrum of <i>cis</i> - V.5h in CDCl_3 (400 MHz) at 23 °C.	313

Figure V-44. ^1H NMR spectrum of <i>trans</i> - V.5h in CDCl_3 (400 MHz) at 23 °C.	314
Figure V-45. ^{13}C NMR spectrum of <i>trans</i> - V.5h in CDCl_3 (100 MHz) at 23 °C.	315
Figure V-46. ^1H NMR spectrum of <i>cis</i> - V.5i in CDCl_3 (400 MHz) at 23 °C.	316
Figure V-47. ^{13}C NMR spectrum of <i>cis</i> - V.5i in CDCl_3 (100 MHz) at 23 °C.	317
Figure V-48. ^1H NMR spectrum of <i>trans</i> - V.5i in CDCl_3 (400 MHz) at 23 °C.	318
Figure V-49. ^{13}C NMR spectrum of <i>trans</i> - V.5i in CDCl_3 (100 MHz) at 23 °C.	319
Figure V-50. ^1H NMR spectrum of <i>trans</i> - V.5j in CDCl_3 (400 MHz) at 23 °C.	320
Figure V-51. ^{13}C NMR spectrum of <i>trans</i> - V.5j in CDCl_3 (100 MHz) at 23 °C.	321
Figure V-52. ^1H NMR spectrum of <i>cis</i> - V.5k in CDCl_3 (400 MHz) at 23 °C.	322
Figure V-53. ^{13}C NMR spectrum of <i>cis</i> - V.5k in CDCl_3 (100 MHz) at 23 °C.	323
Figure V-54. ^1H NMR spectrum of <i>cis</i> - V.5l in CDCl_3 (400 MHz) at 23 °C.	324
Figure V-55. ^{13}C NMR spectrum of <i>cis</i> - V.5l in CDCl_3 (100 MHz) at 23 °C.	325
Figure V-56. ^1H NMR spectrum of <i>trans</i> - V.5l in CDCl_3 (400 MHz) at 23 °C.	326
Figure V-57. ^{13}C NMR spectrum of <i>trans</i> - V.5l in CDCl_3 (100 MHz) at 23 °C.	327
Figure V-58. ^1H NMR spectrum of <i>cis</i> - V.5m in CDCl_3 (400 MHz) at 23 °C.	328
Figure V-59. ^{13}C NMR spectrum of <i>cis</i> - V.5m in CDCl_3 (100 MHz) at 23 °C.	329
Figure V-60. ^1H NMR spectrum of <i>cis</i> - V.5n in CDCl_3 (400 MHz) at 23 °C.	330
Figure V-61. ^{13}C NMR spectrum of <i>cis</i> - V.5n in CDCl_3 (100 MHz) at 23 °C.	331
Figure V-62. ^1H NMR spectrum of <i>trans</i> - V.5n in CDCl_3 (400 MHz) at 23 °C.	332
Figure V-63. ^{13}C NMR spectrum of <i>trans</i> - V.5n in CDCl_3 (100 MHz) at 23 °C.	333
Figure V-64. ^1H NMR spectrum of <i>cis</i> - V.5o in CDCl_3 (400 MHz) at 23 °C.	334
Figure V-65. ^{13}C NMR spectrum of <i>cis</i> - V.5o in CDCl_3 (100 MHz) at 23 °C.	335
Figure V-66. ^1H NMR spectrum of <i>trans</i> - V.5o in CDCl_3 (400 MHz) at 23 °C.	336
Figure V-67. ^{13}C NMR spectrum of <i>trans</i> - V.5o in CDCl_3 (100 MHz) at 23 °C.	337

Figure V-68. ^1H NMR spectrum of <i>cis</i> - V.5p in CDCl_3 (400 MHz) at 23 °C.	338
Figure V-69. ^{13}C NMR spectrum of <i>cis</i> - V.5p in CDCl_3 (100 MHz) at 23 °C.	339
Figure V-70. ^1H NMR spectrum of <i>trans</i> - V.5p in CDCl_3 (400 MHz) at 23 °C.	340
Figure V-71. ^{13}C NMR spectrum of <i>trans</i> - V.5p in CDCl_3 (100 MHz) at 23 °C.	341
Figure V-72. ^1H NMR spectrum of <i>cis</i> - V.5q in CDCl_3 (400 MHz) at 23 °C.	342
Figure V-73. ^{13}C NMR spectrum of <i>cis</i> - V.5q in CDCl_3 (100 MHz) at 23 °C.	343
Figure V-74. ^1H NMR spectrum of <i>trans</i> - V.5q in CDCl_3 (400 MHz) at 23 °C.	344
Figure V-75. ^{13}C NMR spectrum of <i>trans</i> - V.5q in CDCl_3 (100 MHz) at 23 °C.	345
Figure V-76. ^1H NMR spectrum of <i>cis</i> - V.5r in CDCl_3 (400 MHz) at 23 °C.	346
Figure V-77. ^{13}C NMR spectrum of <i>cis</i> - V.5r in CDCl_3 (100 MHz) at 23 °C.	347
Figure V-78. ^1H NMR spectrum of <i>trans</i> - V.5r in CDCl_3 (400 MHz) at 23 °C.	348
Figure V-79. ^{13}C NMR spectrum of <i>trans</i> - V.5r in CDCl_3 (100 MHz) at 23 °C.	349
Figure V-80. ^1H NMR spectrum of compound V.5s in CDCl_3 (400 MHz) at 23 °C.	350
Figure V-81. ^{13}C NMR spectrum of compound V.5s in CDCl_3 (100 MHz) at 23 °C.	351
Figure V-82. ^1H NMR spectrum of rotamer 1 of compound V.7 in CDCl_3 (400 MHz) at 23 °C.	352
Figure V-83. ^{13}C NMR spectrum of rotamer 1 of compound V.7 in CDCl_3 (100 MHz) at 23 °C.	353
Figure V-84. ^1H NMR spectrum of rotamer 2 of compound V.7 in CDCl_3 (400 MHz) at 23 °C.	354
Figure V-85. ^{13}C NMR spectrum of rotamer 2 of compound V.7 in CDCl_3 (100 MHz) at 23 °C.	355
Figure V-86. ^1H NMR spectra for thermal interconversion of rotamers (V.7) at 23 °C in CDCl_3 solvent.	356
Figure V-87. ^1H NMR spectrum of compound V.9a in CDCl_3 (400 MHz) at 23 °C.	357
Figure V-88. ^{13}C NMR spectrum of compound V.9a in CDCl_3 (100 MHz) at 23 °C.	358
Figure V-89. ^1H NMR spectrum of compound V.9b in CDCl_3 (400 MHz) at 23 °C.	359

Figure V-90. ¹³ C NMR spectrum of compound V.9b in CDCl ₃ (100 MHz) at 23 °C.	360
Figure V-91. ¹ H NMR spectrum of compound V.9c in CDCl ₃ (400 MHz) at 23 °C.	361
Figure V-92. ¹³ C NMR spectrum of compound V.9c in CDCl ₃ (100 MHz) at 23 °C.	362
Figure V-93. ¹ H NMR spectrum of compound V.9d in CDCl ₃ (400 MHz) at 23 °C.	363
Figure V-94. ¹³ C NMR spectrum of compound V.9d in CDCl ₃ (100 MHz) at 23 °C.	364
Figure V-95. ¹ H NMR spectrum of compound V.9e in CDCl ₃ (400 MHz) at 23 °C.	365
Figure V-96. ¹³ C NMR spectrum of compound V.9e in CDCl ₃ (100 MHz) at 23 °C.	366
Figure V-97. ¹ H NMR spectrum of compound V.9f in CDCl ₃ (400 MHz) at 23 °C.	367
Figure V-98. ¹³ C NMR spectrum of compound V.9f in CDCl ₃ (100 MHz) at 23 °C.	368
Figure V-99. ¹ H NMR spectrum of compound V.9g in CDCl ₃ (400 MHz) at 23 °C.	369
Figure V-100. ¹³ C NMR spectrum of compound V.9g in CDCl ₃ (100 MHz) at 23 °C.	370
Figure VI-1. Hypervalent iodine catalyzed aerobic spirocyclization reaction under photochemical conditions.	373
Figure VI-2. Green chemistry comparison between aryl iodide and Pd catalyzed C–N cross coupling reactions.	374

LIST OF TABLES

	Page
Table I-1. List of general oxidants in order of their respective active oxygen content. ¹⁰	2
Table II-1. Optimization of aerobic oxidation of iodobenzene.....	22
Table III-1. Optimization table for I(V) mediated cyclohexanol oxidation.....	74
Table III-2. Co-catalyzed background reactions.....	105
Table III-3. Comparison of experimental metrical parameters for I(III) compound III.2a with optimized structures using various basis sets and functionals.	116
Table III-4. Comparison of experimental metrical parameters for I(V) compound III.3a with optimized structures using various basis sets and functionals.	117
Table III-5. Coordinates for optimized geometry of PhI using SMD solvation model (CH ₂ Cl ₂).	117
Table III-6. Coordinates for optimized geometry of PhIO using SMD solvation model (CH ₂ Cl ₂).	118
Table III-7. Coordinates for optimized geometry of PhIO ₂ using SMD solvation model (CH ₂ Cl ₂).	119
Table III-8. Coordinates for optimized geometry of III.1a using SMD solvation model (CH ₂ Cl ₂).	120
Table III-9. Coordinates for optimized geometry of III.2a using SMD solvation model (CH ₂ Cl ₂).	121
Table III-10. Coordinates for optimized geometry of III.3a using SMD solvation model (CH ₂ Cl ₂).	122
Table III-11. Coordinates for optimized geometry of <i>p</i> -sulfone I(I) using SMD solvation model (CH ₂ Cl ₂).	123
Table III-12. Coordinates for optimized geometry of <i>p</i> -sulfone I(III) using SMD solvation model (CH ₂ Cl ₂).	124
Table III-13. Coordinates for optimized geometry of <i>p</i> -sulfone I(V) using SMD solvation model (CH ₂ Cl ₂).	125
Table IV-1. Optimization of intramolecular C–H amination, varying solvent and temperature.	135

Table IV-2. Optimization of intermolecular C–H amination.....	139
Table IV-3. Data for the Job plot performed by ¹ H NMR titration in CD ₃ CN.....	146
Table IV-4. Onset potentials for oxidation of various substituted aryl iodides.....	185
Table IV-5. Effect of electrode materials on intramolecular C–H amination.....	185
Table IV-6. Full optimization table for intramolecular C–H amination.....	186
Table IV-7. Comparison of the electrolyte concentration used in this manuscript with those in other recent electrocatalytic methods.....	187
Table IV-8. Onset and peak potentials of biarylacetamide substrates.....	188
Table IV-9. Yield of selected substrate background reaction in the absence of aryl iodide.....	189
Table IV-10. Data for the Job plot performed by ¹ H NMR titration in CD ₃ CN.....	195
Table IV-11. Optimization of the electrochemical oxidation of 4-iodotoluene under constant current electrolysis.....	197
Table IV-12. Optimization of catalyst screening and effect of additives under constant current electrolysis.....	198
Table V-1. Examination of the impact of solvent on tetrahydroisoquinoline synthesis.....	270
Table V-2. Examination of the impact of photocatalyst on tetrahydroisoquinoline synthesis.....	270
Table V-3. Examination of the impact of reagent stoichiometry on tetrahydroisoquinoline synthesis.....	272
Table V-4. Examination of the impact of temperature on tetrahydroisoquinoline synthesis.....	273
Table V-5. X-ray experimental details of <i>cis</i> - V.5e (CCDC 2084507).....	275
Table V-6. X-ray experimental details of V.5s (CCDC 2084508).....	276

CHAPTER I

INTRODUCTION: SUSTAINABLE OXIDATION CATALYSIS VIA HYPERVALENT IODINE INTERMEDIATES*

I.1 Introduction

Oxidation reactions, in which electron equivalents are removed from a substrate, are often critical steps in the synthesis of functional organic molecules. By definition, oxidation reactions require the use of an electron acceptor (*i.e.*, terminal oxidant). Because the reduced byproducts generated from the terminal oxidant are often lost as chemical waste, the chemical structure of the terminal oxidant dictates the sustainability of the oxidation reaction. Biological oxidation chemistry often utilizes dioxygen (O₂) as the terminal oxidant and generates water as the ultimate byproduct.^{1, 2} As such, these enzymatic oxidation reactions are nearly ideal from the perspective of sustainability. Analogous utilization of O₂ as a terminal oxidant in synthetic chemistry remains a significant challenge because 1) the triplet ground state of O₂ imposes kinetic barriers to O₂ utilization,³ 2) O₂ often engages in poorly selective radical chain reactions,⁴ 3) the electron inventories of O₂ reduction (four-electron) and substrate oxidation (two electrons) are mismatched;^{5, 6} and, 4) O₂ utilization can present safety concerns depending on the specific reaction conditions employed.⁷ The challenges associated with direct O₂ utilization as a terminal oxidant in selective synthesis have stimulated the development of alternative chemical oxidants

* Data, figures, and text in this chapter were adapted with permission from reference Frey; B. L.; Maity, A.; Tan, H.; Roychowdhury, P.; Powers, D. C. *Iodine Catalysis in Organic Synthesis*; Muniz, K., Ishihara, K. (Eds.); Wiley-VCH, **2022**, 335–386. Copyright © 2022 the John Wiley and Sons, Inc. and Maity, A.; Cardenal, A. D.; Gao, W.-Y.; Ashirov, R.; Hyun, S.-M.; Powers, D. C. *Inorg. Chem.* **2019**, *58*, 10543–10553, Copyright © 2019, American Chemical Society.

for application in specific synthetic contexts. Implicit in the use of designer chemical oxidants is an increase in the waste associated with oxidation chemistry and in turn reduced sustainability.

I.2 Sustainable Oxidants Based on Active Oxygen Content

The principles of green chemistry articulated by Anastas *et al.*^{8,9} codify the concept of atom economy and the impact of the nature of waste on the efficiency of a chemical process. Active oxygen content, which is defined as the percent weight ratio of the oxygen transferred to product divided by the formula weight of the reagent, can be used as a guiding parameter for evaluating the sustainability of oxidants.¹⁰ Table I-1 lists the active oxygen content and associated waste products generated from a variety of commonly encountered terminal oxidants.

Table I-1. List of general oxidants in order of their respective active oxygen content.¹⁰

Substrate + Oxidant \longrightarrow Product + Reduced Oxidant (Stoichiometric waste)		
Oxidant	Active Oxygen Content (wt %)	Waste Generated
O ₂ or O ₂ / reductant ^a	100 (50)	None (H ₂ O)
H ₂ O ₂	47	H ₂ O
KMnO ₄	30.4	Mn(II) salt
NaOCl	21.6	NaCl
O ₂ / CH ₃ CHO	21.1	CH ₃ CO ₂ H
CH ₃ CO ₃ H	21.1	CH ₃ CO ₂ H
<i>t</i> BuOOH	17.8	<i>t</i> BuOH
H ₂ O ₂ -Urea	17.0	H ₂ O-Urea
KHSO ₅	10.5	KHSO ₄
<i>m</i> -CPBA	9.3	<i>m</i> -CBA
NaIO ₄	7.5	NaIO ₃
PhIO	7.3	PhI
NaBO ₃ ·4H ₂ O	7.2	NaBO ₂
Oxone ^b	2.6	K ₂ S ₂ O ₈ ·KHSO ₄ ·K ₂ SO ₄

^aThis analysis assumes the reduced byproduct is H₂O. If chemical reductants are employed (*i.e.*, H₂, NADH, CH₃CHO, etc.) the active oxygen content will be lower depending on the mass of the generated byproducts. ^bOxone (2KHSO₅·KHSO₄·K₂SO₄). *m*-CPBA = *meta*-chloroperbenzoic acid, *m*-CBA = *meta*-chlorobenzoic acid.

While O₂ is an attractive oxidant based on its active oxygen content, chemical strategies that utilize both oxygen atoms for substrate functionalization (*i.e.*, dioxygenase reactivity) are rare.¹¹ More typically, O₂ utilization is accomplished in the presence of an appropriate reductant, which addresses the incongruous electron inventory of O₂ reduction and substrate functionalization. Consequently only 50% of active oxygen content of O₂ is utilized and the other 50% is lost as waste (ideally H₂O). Hydrogen peroxide (H₂O₂) is also considered a green oxidant and has 47% active oxygen content when utilized in direct substrate oxidation chemistry with attendant generation of H₂O as the byproduct. Utilization of H₂O₂ as an oxidant in hypervalent iodine chemistry often requires acetic anhydride, to generate peracetic acid *in situ*, or the use of urea-hydrogen peroxide (UHP) adduct, both of which reduce the active oxygen content of the reagent. Other commonly encountered chemical oxidants, such as NaOCl, CH₃CO₃H, *m*-CPBA, NaIO₄, NaBO₃·4H₂O, and Oxone display significantly lower active oxygen contents. The recent renaissance of organic electrosynthesis offers an alternative strategy to sustainable oxidation chemistry: Anodic substrate oxidation provides the opportunity to avoid stoichiometric redox reagents and the associated waste streams.¹² The frequent requirement for high concentrations of supporting electrolyte can reduce the chemical efficiency of electrosynthetic approaches.

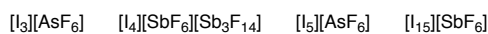
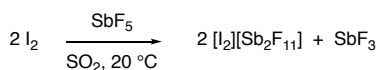
Hypervalent iodine compounds are a class of metal-free oxidants that are often used as terminal oxidants in both organic and inorganic synthesis. Although hypervalent iodine compounds are attractive oxidants due to the abundance of iodoarene starting materials and lower toxicity compared to transition metal catalysts, when employed as terminal oxidants hypervalent iodine reagents display poor atom economy. For example, when reduced, iodosylbenzene (PhIO) generates a stoichiometric quantity of iodobenzene and only features 7.3% active oxygen content.

In addition, hypervalent iodine species are typically prepared with stoichiometric metal-based oxidants (KMnO₄, Oxone, NaIO₄, etc.) or organic peracids (*m*-CPBA, CH₃CO₃H) which amplifies the overall chemical inefficiency of using these reagents in synthesis.

I.3 Background on Hypervalent Iodine Compounds

Iodine was discovered in 1811 by Bernard Courtois and was named by Joseph Louis Gay-Lussac in 1813 (the name “iodine” derives from the Greek word *ιώδης*, which means “violet colored”).¹³ The chemistry of iodine, which is the largest, least electronegative, and most ionizable of the non-radioactive halogens,¹⁴ is dominated by the (0) and (−1) oxidation states (*i.e.* I₂ and I[−]). Facile interconversion of I(0) and I(−1) by oxidation-reduction chemistry underpins the I[−] / I₃[−] redox couple that is critical to the chemistry of dye-sensitized solar cells.¹⁵ The ionizability of iodine is manifest in a rich body of iodine-centered redox chemistry and the availability of families of compounds featuring iodine in oxidation states greater than zero (Figure I-1). For example, exposure of I₂ to SbF₅ results in the formation of the [I₂⁺]-containing salt [I₂][Sb₂F₁₁] (Figure I-1a).^{16, 17} Dimerization of I₂⁺ to afford I₄²⁺ has been observed,^{18, 19} and higher-order iodine cations, such as I₃⁺, I₅⁺, I₇⁺, and I₁₅⁺ have been characterized.¹⁸ Higher oxidation state iodine species are also commonly encountered in iodine oxyacids of I(I), I(III), I(V), and I(VII) (*i.e.*, HIO, HIO₂, HIO₃, and HIO₄), iodine oxides, and iodine fluoride (*i.e.*, IF₇) (Figure I-1b). Higher oxidation states of iodine are also encountered in organoiodine chemistry (Figure I-1c).

(a) polyiodine cations



(b) oxyacids and fluorides



(c) higher valent organic iodine species

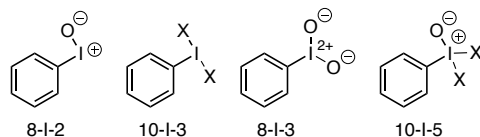


Figure I-1. The low ionization potential of iodine is manifest in families of oxidized iodine compounds. Examples include (a) polyiodine cations, (b) iodine oxyacids and fluorides, and (c) λ^3 - and λ^5 -iodanes.

In 1886, Willgerodt reported the preparation of PhICl_2 , which features an I(III) center, upon passage of Cl_2 through a solution containing PhI .²⁰ Since this original discovery, an enormous array of I(III) derivatives have been prepared. PhICl_2 is a T-shaped molecule and formally features a dactet electronic configuration at iodine. As such, these compounds are termed hypervalent, which Musher defined as: “atomic centers which exceed the number of valences allowed by the traditional theory, and thus utilize more electron-bonding pairs than provide stability in the Lewis Langmuir theory.”²¹ Various nomenclature schemes have been utilized to describe hypervalent I(III) compounds. According to IUPAC convention for compounds with non-standard coordination numbers, organic compounds containing I(III) centers are referred to as λ^3 -iodanes.²² Martin-Arduengo N–X–L nomenclature, in which N is the number of valence electrons formally assigned to iodine, X is the identity of the hypervalent element, and L is the number of ligands attached to the hypervalent atom, is also frequently used to describe higher valent organoiodides.²³ ²⁴ In addition, a large array of I(V)-containing compounds (*i.e.*, Dess-Martin periodinane (DMP))

and 2-Iodoxybenzoic acid (IBX); λ^5 -iodanes), which feature a dodecet electronic configuration at iodine, have been prepared.²⁵⁻³⁰ There are no examples of organic I(VII)-containing compounds.

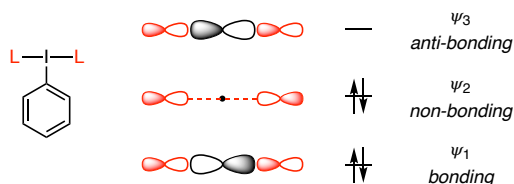


Figure I-2. Orbital picture for the 3c-4e bonding in hypervalent iodine compounds. Population of ψ_2 , which is ligand centered, allows accommodation of the formal octet violations at iodine without utilizing d-orbital hybridization. In neutral I(III) derivatives, L represents an anionic donor ligand.

Historically, bonding models based on either 1) participation of vacant iodine-centered d-orbitals in hybridization, or 2) bonds with greater than 50% ionic character, which would result in localization of electron density on ligand-borne orbitals, have been advanced to rationalize the apparent valence expansion at iodine in λ^3 - and λ^5 -iodanes.³¹ In 1951, Rundle and Pimentel advanced the now-accepted model for hypervalent iodine bonding based on overlap of the 5p orbital at iodine with ligand-centered orbitals to give rise to the electron-rich 3c-4e bonding picture illustrated in Figure I-2.^{32, 33} Population of bond ψ_1 and non-bonding ψ_2 gives rise to the observed linear L–I–L triads. Violation of the octet at iodine is avoided by localization of two electrons in ligand-borne ψ_2 . In addition to avoiding violation of the octet rule, this picture rationalizes the observation of highly ionic bonding in hypervalent iodine compounds and the preference for electronegative substituents to occupy the hypervalent bond. Further experimental support for the ionic bonding in hypervalent iodine molecules is the observation that the iodine center can serve as an acceptor in halogen bonding interactions.^{34, 35} Due to population of both bonding and non-bonding orbitals, the I–L bond lengths in hypervalent iodine species are typically intermediate between the sum of the covalent and ionic radii of the relevant atoms.³⁶ The bonding picture of

I(V) derivatives mirrors that of I(III) compounds except that there are two (orthogonal) hypervalent 3c-4e bonds.

Iodosylbenzene derivatives (*i.e.* 8-I-2 species) also feature I(III) centers. While these species are often drawn with I–L multiple bonds (*i.e.* PhI=O), the large radius of iodine results in insignificant π -bonding.³⁷ Poor π overlap results in highly polarized bonding, (*i.e.* PhI⁺–O⁻). The extensive polarization of the I–O bond often results in solid-state –I–O–I–O– polymerization driven by charge pairing,³⁸⁻⁴⁰ which results in poorly soluble materials. Iodosylbenzenes are metastable with respect to disproportionation to I(I) and I(V) species, although sufficiently large kinetic barriers to disproportionation often allow for straightforward handling of I(III) species. For example, the disproportionation of (PhIO)_n to generate iodobenzene and iodylbenzene is spontaneous,⁴¹ but requires either catalysts (*i.e.*, RuCl₃)⁴² or elevated temperatures⁴³ to proceed at appreciable rates. The mechanism of disproportionation has not been extensively investigated but has been suggested to proceed via oxygen-atom transfer chemistry in an *O*-bridged diiodine intermediate.⁴⁴ As a result of the aforementioned disproportionation thermodynamics, iodylbenzenes are weaker oxidants than iodosylbenzenes.

The reaction chemistry of hypervalent iodine compounds resembles that of the more toxic main-group analogues based on Hg(II), Tl(III), and Pb(IV)²⁶ and is frequently described using terminology common to organometallic mechanisms.⁴⁵ The oxidation of PhI to PhICl₂ described above represents an oxidative addition reaction at the iodine center (Figure I-3a).²⁰ Ligand exchange chemistry is often facile at iodine; for example, the alkoxide ligand exchange at iodine pictured in Figure I-3b is rapid at room temperature.⁴⁶ Both associative and dissociative exchange

mechanisms have been proposed.⁴⁷ Reductive elimination, in which ligand coupling from the hypervalent iodine center is accomplished with concurrent formation of an aryl iodide are ubiquitous (Figure I-3c). Both inner-sphere ligand coupling and outer-sphere, nucleophilic aromatic substitution pathways have been suggested for the observed elimination reactions.^{48, 49} Reductive elimination processes are driven by the hypernucleofugacity of PhI. Finally, group-transfer chemistry of iodosylbenzenes, for example in the synthesis of metal oxo complexes^{48, 50, 51} as well as in hydroxylation catalysis, is very frequently encountered (Figure I-3d).^{52, 53} The importance of hypervalent iodine compounds has resulted in an extensive review literature of the chemistry and reactivity of these compounds.^{26-30, 54, 55} Similar to the oxidation-reduction cycling that underpins hypervalent iodine catalysis, oxidation-reduction cycling with other main-group elements, such as phosphorous, has recently emerged as an opportunity in metal-free catalysis.⁵⁶⁻

59

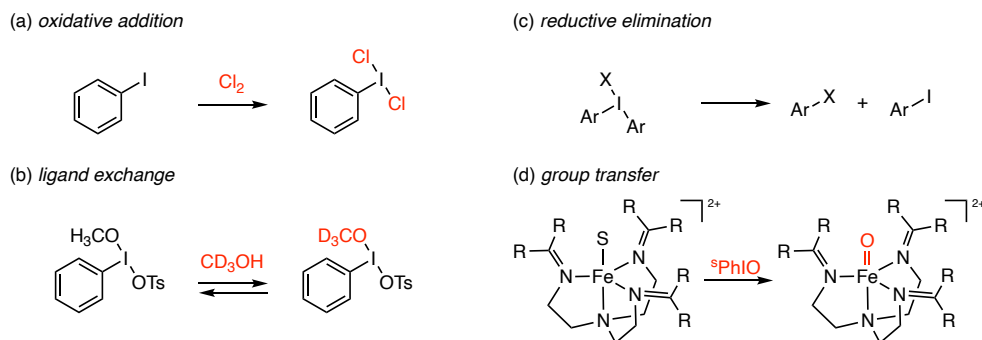


Figure I-3. The chemistry of hypervalent iodine compounds is often described using terminology common to organometallic catalysis. Hypervalent iodine compounds participate in (a) two-electron iodine-centered oxidation, (b) ligand exchange chemistry, (c) reductive elimination reactions, and (d) group-transfer processes. R = N(CH₃)₃; S = CH₃CN; ^sPhIO = 2-(*tert*-butylsulfonyl)iodosylbenzene.

I.4 Synthesis of Hypervalent Iodine(III) Reagents with Sustainable Oxidant

Since Willgerodt's reported preparation of PhICl_2 in 1886, several I(III) derivatives have been prepared and majority of these preparations involve using peroxide or peracids such as H_2O_2 and peracetic acid, respectively. H_2O_2 is considered to be an environmentally benign oxidant due to its 47% active oxygen content and the potential generation of water as the byproduct. H_2O_2 is produced via the Riedl–Pfleiderer process where 2-alkylanthraquinone is first reduced to 2-alkylhydroanthraquinone by hydrogenation and again oxidized aerobically to regenerate 2-alkylanthraquinone and H_2O_2 .⁶⁰ Decomposition of H_2O_2 to H_2O and O_2 is exothermic (-94.6 kJ/mol),⁶¹ and the use of concentrated solutions presents significant safety hazards. Hence, H_2O_2 is typically employed as $\leq 30\%$ aqueous solution. An alternative way to safely deliver H_2O_2 into the reaction is by using urea adduct of hydrogen peroxide (UHP), which is an odorless, water-soluble, crystalline solid that has an active oxygen content of 17%.⁶²

There are no examples of direct oxidation of iodoarenes with H_2O_2 alone, which may be due to the spontaneous decomposition of H_2O_2 by I(III) compounds to form singlet oxygen ($^1\text{O}_2$) and reduced I(I) (Figure I-4).⁶³ H_2O_2 is often employed as an oxidant in combination with acid anhydrides and hydrohalic acids, which promote the *in situ* generation of peracids and hypohalous acids, respectively. Here, we organize presentation of H_2O_2 -based methods by the type of hypervalent iodine compounds generated.

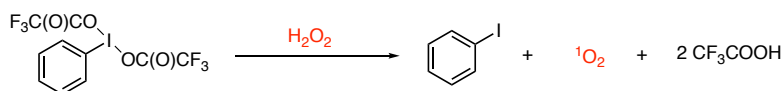


Figure I-4. Hydrogen peroxide reacts with (ditrifluoroacetoxy)iodobenzene to form singlet oxygen ($^1\text{O}_2$) and iodobenzene.

Peracid-based oxidation of iodoarenes was first reported by Boeseken and Schneider in 1931 who synthesized (diacetoxyiodo)benzene by treatment of iodobenzene in chloroform with

55% peracetic acid.⁶⁴ In 1953, Pausacker reported a modified synthesis in which 30% H₂O₂ and acetic anhydride were stirred together at 40 °C to generate peracetic acid followed by addition of iodobenzene (**I.1a**) to the resulting solution (Figure I-5).⁶⁵ This method avoids the use of highly concentrated peracetic acid solution and was the earliest example with H₂O₂ as the terminal oxidant for the synthesis of I(III) compounds. To date, this method is among the most widely used for the synthesis of PhI(OAc)₂ (**I.2a**).

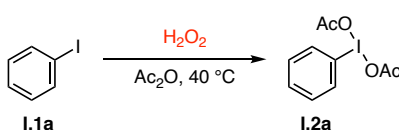


Figure I-5. The combination of hydrogen peroxide and acetic anhydride generate peracetic acid *in situ*, which is responsible for oxidation of iodobenzene (I.1a**) to (diacetoxyiodo)benzene (**I.2a**).**

[Bis(trifluoroacetoxy)iodo]arenes (**I.3**) are stronger oxidants than PhI(OAc)₂ due to the more electron-withdrawing trifluoroacetoxy groups on the iodine center.⁶⁶ Zhdankin *et al.* reported a direct synthetic route to **I.3** using trifluoroperacetic acid, generated *in situ* by combination of 80% H₂O₂ with trifluoroacetic anhydride.⁶⁷ Although the described procedure was more efficient than previous synthetic methods based on ligand exchange reactions of hypervalent iodine(III) compounds with trifluoroacetic acid,^{68, 69} silver trifluoroacetate,⁷⁰ or trimethylsilyl trifluoroacetate,⁷¹ the use of such high concentration of H₂O₂ poses serious safety hazards. In 2006, Wirth *et al.* described a modification of the procedure using UHP (urea hydrogen peroxide adduct) as the terminal oxidant, which enabled *in situ* formation of trifluoroperacetic acid, leading to efficient formation of [bis(trifluoroacetoxy)iodo]arenes (**I.3**) (Figure I-6).⁷²

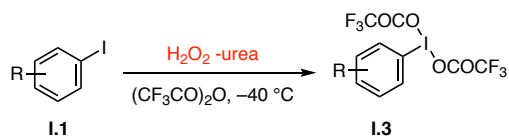


Figure I-6. *In situ* generation of trifluorooperacetic acid from UHP and trifluoroacetic anhydride provides access to [bis(trifluoroacetoxy)iodo]arenes from the corresponding iodoarenes.

(Dichloroiodo)arenes (**I.4**), are widely used reagents for the chlorination of unsaturated hydrocarbons and also as terminal oxidants for transition metal catalysis.⁷³ Historically, (dichloroiodo)benzene has been synthesized by bubbling chlorine gas into a solution of iodobenzene at a low temperature. Use of toxic and corrosive chlorine gas can be avoided using hydrochloric acid in combination with oxidants like KClO_3 ,⁷⁴ KMnO_4 ,⁷⁵ concentrated HNO_3 ,⁷⁵ $\text{Na}_2\text{S}_2\text{O}_8$,⁷⁶ CrO_3 ,⁷⁷ NaClO_2 , or NaClO .⁷⁸ These methods suffer from (super)stoichiometric use of terminal oxidants and poor substrate scope with respect to electron-withdrawing substituents on the iodoarenes. Jarnej and co-workers reported an alternative route for the synthesis of (dichloroiodo)arenes from a mixture of $\text{HCl}/\text{H}_2\text{O}_2$ (30% aqueous solution) in 1,1,1-trifluoroethanol (TFE) which acts both as a solvent and activator for H_2O_2 (Figure 12.8).⁷⁹ In this protocol, hypochlorous acid (HOCl) is generated *in situ* and acts as the active oxidant and chlorinating agent. This method tolerates alkyl substituents as well as electron-withdrawing groups such as carboxyl-, nitro-, and chloro substituents. But, in the presence of electron-donating groups like dimethyl, trimethyl or methoxy substituents, the corresponding (dichloroiodo)arenes decompose to the chlorinated arene products.

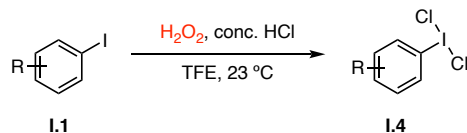


Figure I-7. H_2O_2 was combined with concentrated HCl to form hypochlorous acid (HOCl) *in situ*, the active chlorinating reagent for the synthesis of (dichloroiodo)arenes from iodoarenes.

Diaryliodonium salts are typically synthesized via a two-step process involving iodoarene oxidation followed by arylation of the I(III) with a suitable arene; thus, catalysis is often limited, and sustainable synthesis of these reagents is important to decrease the environmental impact. Building on the demonstration of UHP in the synthesis of iodine(III) reagents, Olofsson *et al.* developed a UHP-based synthesis of diaryliodonium triflates. The authors utilized the *in situ* formation of triflic peroxide using UHP and triflic anhydride (Tf₂O) to oxidize the iodoarenes in presence of suitable arenes to furnish diaryliodonium triflates (**I.5**) in a single step. The developed methodology was effective in synthesizing both symmetric and unsymmetric iodonium salts in good yield but, use of oxidatively labile substrate like anisole or pyridine led to undesired side-products or pyridine *N*-oxides, respectively without any desired product formation (Figure I-8).

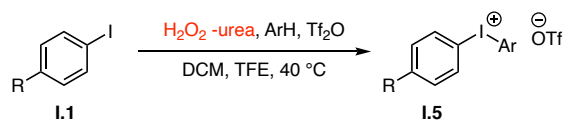


Figure I-8. Diaryliodonium triflates were synthesized using urea-hydrogen peroxide adduct (UHP) in a sustainable method leading to symmetric and unsymmetric iodonium salts.

Electrochemistry provides an alternative sustainable method for oxidation of aryl iodides as electric current is used in place of stoichiometric oxidants. The first example of electrochemical synthesis of hypervalent iodine(III) reagents was reported in 1960 by Schmidt and Meinert, who described the anodic oxidation of iodobenzene in the presence of silver fluoride (AgF), which acts as both the fluorine source and supporting electrolyte, to generate (difluoriodo)benzene (PhIF₂).⁸⁰ With difficulty in reproducing this synthesis,⁸¹ Fuchigami and co-workers developed direct electrolysis of 4-iodonitrobenzene (**I.1b**) in presence of Et₃N·3HF in 1994 to afford fluorinated I(III) product (**I.5b**, Figure I-9a).⁸² But, electrolysis of iodobenzene and 4-iodotoluene led to benzylic fluorination and diaryliodonium products, respectively. Later Hara *et al.* were successful

in synthesizing 4-(difluoriodo)toluene from 4-iodotoluene using $\text{Et}_3\text{N}\cdot 5\text{HF}$ as the supporting electrolyte and fluorine source under constant potential electrolysis at 1.5 V vs. Ag^+/Ag (**I.5c**, Figure I-9b).⁸³ Most of the recent electrochemical synthesis of hypervalent iodine are developed *in situ* where unstable, or dangerous reagents are generated without the need for isolation and later used in *ex cell* reactions under non-electrochemical conditions. This approach often leads to improved yields and safer reaction conditions but unstable towards isolation.^{84, 85} Nishiyama and co-workers developed anodic oxidation of iodoarenes in fluorinated solvents, such as trifluoroethanol (TFE) to afford [bis(trifluoroethoxy)iodo]benzene (**I.6a**, Figure I-9c).⁸⁶⁻⁸⁸ Fluorinated alcohol solvents are known to help stabilize radical cation intermediates and consequently improve single electron oxidation events of iodoarenes at anode surfaces.^{66, 89-91}

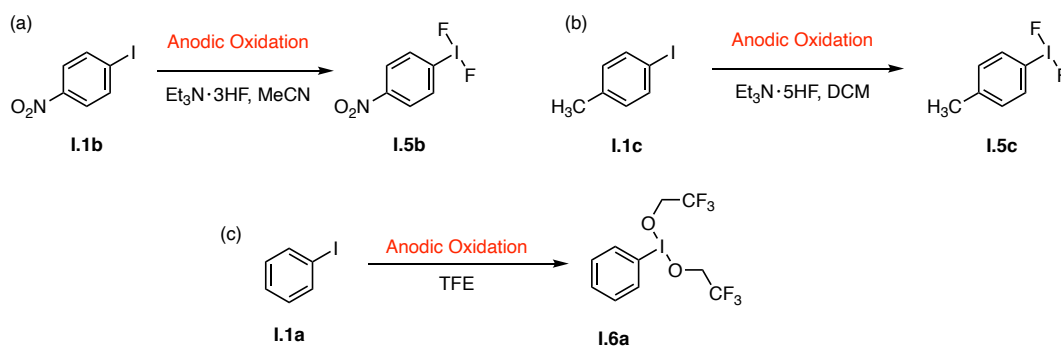


Figure I-9. Examples of anodically generated hypervalent iodine compounds.

One of the drawbacks of an electrochemical reaction is that challenge imposed by the need to separate the desired products from catalyst, reagent, and supporting electrolyte. To overcome this challenge, Francke and coworkers developed low-molecular-weight, charged iodoarenes as potential *ex cell* mediators in which the supporting electrolyte and the iodoarene mediator were combined (Figure I-10).⁹²⁻⁹⁴ The first examples developed were quaternary ammonium substituted 4-iodoarenes. Anodic oxidation of iodoarene **I.1d** in fluorinated solvents provided access to the corresponding hypervalent iodine compound **I.7d**, which was subsequently utilized in *ex cell C-*

N bond forming reactions.^{92, 93} Francke and co-workers later advanced iodoarylsulfonates (**I.1e**, **I.1f**) and iodoobenzoates (**I.1g-I.1i**) as redox-active supporting electrolytes.⁹⁴

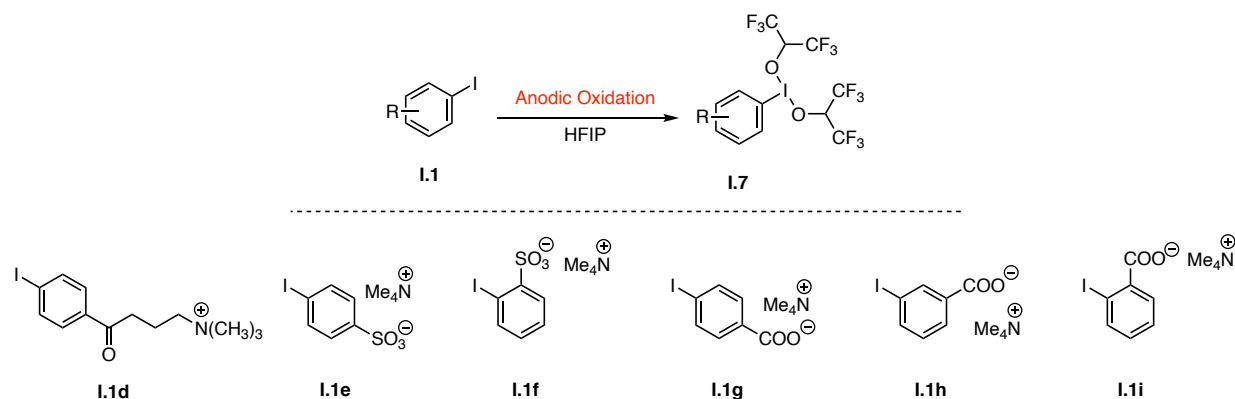


Figure I-10. Recyclable iodoarene mediators for *ex cell* electrochemistry.

Electrochemical oxidation of iodoarenes via flow chemistry has also been developed by Wirth and co-workers where the amount of supporting electrolyte can be drastically reduced to attenuate the waste stream (Figure I-11).⁹⁵⁻⁹⁸ Flow conditions offer advantages compared to mechanical stirring, such as better mixing, more efficient heat transfer, easy scale-up,⁹⁹ and can be especially useful in industrial settings for energy conservation¹⁰⁰, multistep synthesis¹⁰¹ or end-to-end production.¹⁰²

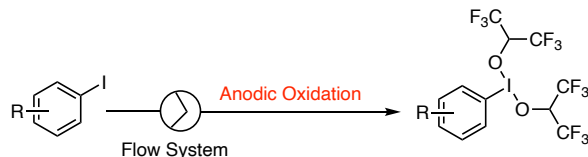


Figure I-11. Anodic oxidation of aryl iodides under flow conditions.

I.5 Synthesis of Hypervalent Iodine(V) Reagents with Sustainable Oxidants

Iodylarenes are typically prepared using harsh oxidation conditions such as potassium peroxysulfate in concentrated sulfuric acid,¹⁰³ sodium periodate,^{104, 105} Oxone,¹⁰⁶ peracetic acid at elevated temperatures.¹⁰⁷ Iodylarenes can also be prepared from the disproportionation of corresponding iodosylbenzenes at high temperatures.¹⁰⁸ Zhdankin and co-workers reported a two-step, one-pot strategy to access iodylarenes using H₂O₂ as the terminal oxidant by coupling *in situ* generation of peracid with subsequent disproportionation chemistry catalyzed by RuCl₃ (0.8 mol%).⁴² This method was effective in furnishing iodylarenes bearing both electron-donating and electron-withdrawing groups, but formation of 2-iodoxybenzoic acid (IBX) from 2-iodobenzoic acid was unsuccessful (Figure I-12). When independently synthesized PhI(OAc)₂ (**I.2a**) was treated with RuCl₃ (0.4 mol%) in an aqueous acetonitrile solution at room temperature, immediate formation of equimolar amount of iodylbenzene (**I.8a**) and iodobenzene (**I.1a**) were observed, which is consistent with disproportionation being operative in the synthesis of I(V) species.¹⁰⁹

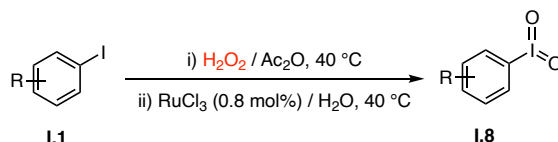


Figure I-12. RuCl₃-mediated disproportionation of initially formed hypervalent iodine(III) intermediates provided access to the corresponding iodylarenes.

Hypervalent iodine(V) reagents can be electrochemically synthesized, but require harsh reaction conditions. Oxidation of 2-iodobenzoic acid in 0.2 M H₂SO₄ aqueous with a boron doped diamond electrode at potentials greater than 1.8 V vs. SCE produced 2-iodoxybenzoic acid.^{110, 111} Interestingly, applied potentials between 1.6–1.8 V vs. SCE produces the I(III) 2-iodosylbenzoic acid and increasing potentials above 1.8 V vs. SCE yields the I(V) product. The usefulness of boron doped diamond electrode can be attributed to its stability and high over potential for O₂ evolution.

I.6 Conclusions

Our interest in hypervalent iodine chemistry has, in large part, been motivated by the utility of these reagents as non-toxic, selective oxidants in synthetic chemistry. Iodosylbenzene derivatives have been applied to α -oxidation of carbonyls,¹¹² oxidative 1,2-difunctionalization of olefins,¹¹³ oxidative dearomatization chemistry,¹¹⁴⁻¹¹⁷ cross-coupling reactions,^{118, 119} and have found important application as group-transfer reagents in organometallic catalysis.^{29, 120} The facility of ligand exchange at hypervalent iodine centers underpins the breadth of substrate functionalization chemistry that can be achieved with hypervalent iodine compound: In addition to oxygen transfer, halogen, nitrogen, and hydrocarbyl transfer reactions are all common. I(V) reagents display complementary substrate functionalization chemistry, most notably towards alcohol and amine dehydrogenation reactions.²⁵⁻³⁰

The development of either 1) methods to synthesize hypervalent iodine compounds using sustainable sources such as O₂ and electrical current (generated from renewable sources like solar photovoltaics), or 2) methods to employ hypervalent iodine species as catalysts in tandem with green oxidants could provide a platform for sustainable oxidation methods for wide variety of reactions. Here, we summarize progress towards sustainable synthesis and use of hypervalent iodine compounds.

CHAPTER II

OXIDASE CATALYSIS VIS AEROBICALLY GENERATED HYPERVALENT IODINE INTERMEDIATES*

II.1 Introduction

O₂ is a readily available, environmentally benign, thermodynamically strong oxidant. The development of chemical strategies to couple O₂ reduction directly to substrate oxidation would enable sustainable synthetic methods.^{11, 121, 122} However, selective and efficient utilization of O₂ is challenging due to the triplet ground state of O₂, which imposes substantial kinetic barriers to O₂ reduction and gives rise to poorly selective radical chemistry,^{3, 4} and due to the disparity between the electron inventories of four-electron O₂ reduction and two-electron substrate oxidation.⁵ Broadly, there are two approaches to O₂ utilization: (1) oxygenase chemistry, in which O₂ serves as both an oxidant and the source of oxygen content in organic reaction products; and (2) oxidase chemistry, in which O₂ serves as a proton and electron acceptor but is not incorporated into the organic reaction products (Figure II-1).¹²³

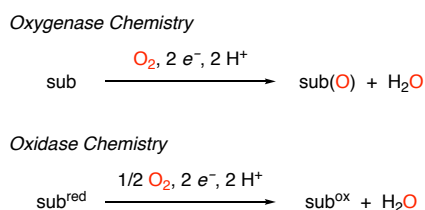


Figure II-1 Oxygenase versus oxidase aerobic oxidation chemistry. In oxygenase chemistry, O₂ functions both as the electron acceptor as well as the source of oxygen content during substrate functionalization. In oxidase chemistry, O₂ functions only as a proton and electron acceptor and is not incorporated in the oxidized substrate. Oxidase strategies are conceptually more broadly applicable to synthetic chemistry, as they allow a variety of substrate functionalization modes to be coupled to O₂ as the terminal oxidant.

*Data, figures, and text in this chapter were adapted with permission from Maity, A.; Hyun, S.-M.; Powers, D. C. *Nat. Chem.* **2018**, *10*, 200–204, Copyright © 2017 Nature Publishing Group.

Oxidase chemistry is synthetically attractive because many desirable oxidation reactions do not require substrate oxygenation. Pd-catalyzed aerobic oxidation has emerged as a particularly powerful platform to couple O₂ reduction to substrate oxidation chemistry, and this chemistry is predicated on leveraging the wide array of catalytic reactions that involve Pd(II) intermediates to access broadly applicable synthetic chemistry with O₂ (Figure II-2a).¹²⁴ To efficiently manage the oxidation of Pd(0) by Pd(II), electron transfer mediators (ETMs), such as hydroquinone, are often employed.^{125, 126} Hydroquinone spontaneously reacts with O₂ to generate quinone and quinone readily oxidizes Pd(0) to Pd(II). Use of hydroquinone as an ETM has enabled O₂ reduction to be coupled with aerobic alkene functionalization, C–C and C–O coupling reactions, and alcohol oxidation chemistry.^{123, 127, 128} Other ETMs, such as nitroxyl radicals,¹²⁹⁻¹³¹ polyoxometallates,¹³²⁻¹³⁶ flavins¹³⁷ have been developed, and similar redox relay strategies have been utilized to facilitate Cu-^{129, 138-147} and Ru-catalyzed¹⁴⁸⁻¹⁵² aerobic oxidation catalysis. The ETMs that are commonly used in aerobic oxidation reactions are generally weak oxidants and thus O₂-coupled catalysis is limited to reactions mediated by low-valent catalyst intermediates.

Enzymatic oxidation catalysis, such as the C–H hydroxylation chemistry accomplished by cytochrome P450s and methane monooxygenase (MMO), utilizes O₂ (in combination with a sacrificial reductant such as NADH) to generate strongly oxidizing high-valent intermediates.¹⁵³⁻¹⁵⁷ In the absence of broadly applicable strategies for O₂ utilization, synthetic chemists have developed myriad reagents that participate in selective two-electron oxidation chemistry. For example, hypervalent iodine reagents are a broadly useful class of selective two electron chemical oxidants based on 3-centered, 4-electron (3c–4e) iodine–ligand bonds.^{27, 29, 158} These reagents find

application in diverse chemical settings, including C–H hydroxylation and amination, olefin functionalization, oxidative dearomatization, and as group-transfer reagents in catalysis. The broad utility of hypervalent iodine reagents derives from the facile ligand exchange chemistry available at iodine. Ligand exchange reactions allow hypervalent iodine reagents to be utilized in oxidative oxygen-, nitrogen-, halogen- and hydrocarbyl-transfer chemistry.^{106, 120, 159} The current liabilities of hypervalent iodine reagents include the frequent need for stoichiometric quantities of these compounds and the synthesis of these reagents from wasteful metal-based oxidants such as KMnO_4 , NaIO_4 , and Oxone, or organic peracids such as *m*-chloroperbenzoic acid.¹⁶⁰ At the time of this work, there were no methods available for the direct synthesis of hypervalent iodine compounds from O_2 .^{161, 162} Liu and co-workers have suggested O_2 -coupled generation of I(V) intermediates during aerobic alcohol oxidation,¹⁶¹ but the active oxidant in this chemistry has subsequently been reassigned as Br_2 .¹⁶² We were attracted to aerobic oxidation of aryl iodides based on the hypothesis that the resulting hypervalent iodine reagents, in conjunction with ligand exchange at iodine, could provide a new platform for oxidase chemistry. Here, we intercept aldehyde autoxidation intermediates to prepare a family of hypervalent iodine reagents using O_2 as the terminal oxidant, and demonstrate the utility of aerobic oxidation of aryl iodides in oxidase catalysis to functionalize a variety of substrate classes (Figure II-2b).¹⁶³

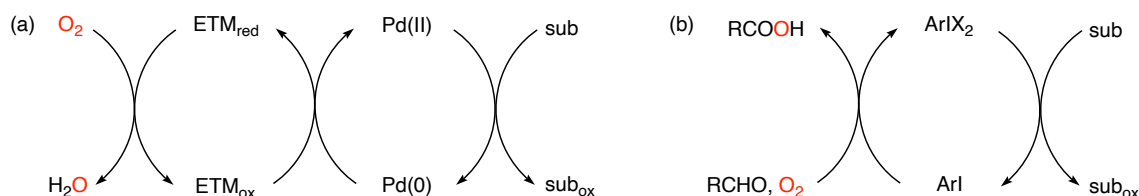


Figure II-2. Utilization of O_2 as terminal oxidant in synthetic chemistry. (a) Electron-transfer mediators (ETMs) have been used to enable Pd-catalyzed aerobic oxidation. (b) Aldehyde-promoted aerobic synthesis of hypervalent iodine intermediates enables complementary substrate oxidation chemistry; sub = substrate.

II.2 Results and Discussion

Aldehyde autoxidation chemistry, which converts aldehydes to carboxylic acids under the action of O_2 , is among the earliest reactions of O_2 with organic molecules to be characterized.¹⁶⁴ In 1832, Wöhler and Liebig reported the autoxidation of benzaldehyde to benzoic acid.¹⁶⁵ Bäckström advanced the now accepted radical chain mechanism for aldehyde autoxidation in 1927 (Figure II-3), which involves hydrogen-atom abstraction (HAA) from aldehyde **A** to generate acyl radical **B**, reaction of **B** with O_2 to generate acyl peroxy radical **C**, and HAA to generate an equivalent of peracid **D** and the acyl radical chain carrier **B**.¹⁶⁶ Subsequent Baeyer-Villiger reaction via intermediate **E** generates two equivalents of acid **F**.¹⁶⁷ The synthetic utility of autoxidation intermediates in reaction development has been realized.¹⁶⁸⁻¹⁷² For example, aerobically generated acyl radical intermediates have been intercepted for olefin addition chemistry and aerobically generated peracids have been utilized for oxygen-atom transfer chemistry (OAT).¹⁷³⁻¹⁷⁷

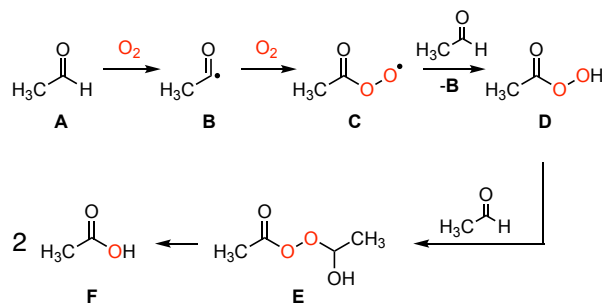


Figure II-3. Radical-chain mechanism for aldehyde autoxidation. Autoxidation of aldehydes to carboxylic acids proceeds via initial hydrogen-atom abstraction (HAA) from an aldehyde (**A**) to generate an acyl radical (**B**). Subsequent reaction between **B** and O_2 generates acyl superoxo **C**. HAA from a second equivalent of **A** generates peracid **D** and chain carrier **B**. Conversion of peracid **D** to carboxylic acids is accomplished by a Baeyer-Villiger reaction via intermediate **E**. Here, we intercept reactive oxidants generated during autoxidation (*i.e.*, **D** and **E**) to access hypervalent iodine reagents. Coupling O_2 reduction to the synthesis of hypervalent iodine compounds provides a platform for oxidase chemistry.

II.2.1 Intercepting Aldehyde Autoxidation for Aerobic Oxidation of Aryl Iodides

We initiated our investigation of aerobic oxidation of aryl iodides by examining the viability of the oxidation of PhI (**II.1a**) with O₂ in the presence of a variety of simple aldehydes in 1,2-dichloroethane (DCE) at 23 °C (Table II-1). We found that, although benzaldehyde was ineffective in promoting the oxidation of iodobenzene (Table II-1, entry 1), isobutyraldehyde and butyraldehyde led to the observation of 2% and 6% yield of I(III) bis-esters, respectively (entries 2 and 3). Use of acetaldehyde afforded PhI(OAc)₂ (**II.2a**) in 42–91% yield (yields obtained from five identical reactions, entry 4). We speculated that the variability of oxidation efficiency was due to inconsistent initiation of radical autoxidation chemistry. Addition of a sub-stoichiometric amount of various metal salts (1 mol%) that have been demonstrated to initiate autoxidation (entries 5–7)^{178, 179} led to identification of CoCl₂·6H₂O as a highly effective autoxidation initiator, leading to PhI(OAc)₂ in 99% yield. AcOH is the only by-product of aldehyde-promoted PhI oxidation, and PhI(OAc)₂ can be isolated as a pure compound following a simple aqueous extraction to remove Co salts. Using CoCl₂·6H₂O as radical chain initiator, PhI oxidation can be accomplished with air as the O₂ source (63% yield). Aerobic oxidation of PhI to generate PhI(OAc)₂ could be carried out on gram scale (97% yield, 1.59 g isolated product). The developed aerobic oxidation is compatible with a broad range of organic solvents. In addition to DCE, high yields are obtained in coordinating solvents, such as CH₃CN (entry 8), and protic solvents, such as AcOH (entry 9). In contrast, PhI oxidation does not proceed in THF, which we hypothesize is due to inhibition of autoxidation by the presence of relatively weak C–H bonds (*vide infra*).

Table II-1. Optimization of aerobic oxidation of iodobenzene. Aerobic oxidation was optimized by examining the impact of experimental variables on the oxidation of iodobenzene to iodobenzene diacetate. Consistent with oxidation of PhI by autoxidation intermediates, the addition of autoxidation initiators is required to achieve consistent high yields of PhI oxidation. ^aFor optimization experiments, yields were determined by ¹H NMR spectroscopy from crude reaction mixture using mesitylene as internal standard.

c1ccc(I)cc1 (II.1a) $\xrightarrow[\text{conditions, 23 } ^\circ\text{C}]{\text{O}_2, \text{CH}_3\text{CHO}}$ c1ccc(I(OC(=O)R)OC(=O)R)cc1 (II.2a)

Entry	RCHO	Solvent	Initiator (1.0 mol%)	Yield ^a
1	PhCHO	DCE	None	0
2	i-PrCHO	DCE	None	2%
3	n-PrCHO	DCE	None	6%
4	CH ₃ CHO	DCE	None	42-91%
5	CH ₃ CHO	DCE	Cu(OAc) ₂ ·H ₂ O	48%
6	CH ₃ CHO	DCE	Mn(OAc) ₂ ·4H ₂ O	75%
7	CH ₃ CHO	DCE	CoCl ₂ ·6H ₂ O	99%
8	CH ₃ CHO	AcOH	CoCl ₂ ·6H ₂ O	98%
9	CH ₃ CHO	CH ₃ CN	CoCl ₂ ·6H ₂ O	73%
10	CH ₃ CHO	THF	CoCl ₂ ·6H ₂ O	0

With conditions in hand for the aerobic oxidation of PhI, we examined the O₂-coupled synthesis of a family of hypervalent iodine reagents that have been applied in synthetic chemistry (Figure II-4). Aerobic oxidation tolerates a range of electron-donating and -withdrawing substituents on the aryl iodide (compounds **II.1**), and hydrolysis of the initially formed I(III) diacetates (**II.2a-g**) provides ready access to iodosylbenzene derivatives (**II.3a-g**) in uniformly high yield. Substitution of the aromatic ring has been demonstrated to provide a synthetic handle to tune both the activity and the aggregation state of aryl I(III) reagents.^{180, 181} Addition of TsOH to the oxidation of PhI affords Koser's reagent (**II.2h**), an acid-activated iodosylbenzene

derivative, in 84% yield.¹⁸² Similarly, addition of carboxylic acids to the reaction mixture directly affords the corresponding I(III) esters: oxidation in the presence of trifluoroacetic acid (TFA) and benzoic acid results in $\text{PhI}(\text{CF}_3\text{COO})_2$ (**II.2i**) and $\text{PhI}(\text{OBz})_2$ (**II.2j**) in 52 and 48% yields, respectively. Aldehyde promoted oxidation of 2-iodobenzoic acid (**II.1k**), 2-(2-iodophenyl)propan-2-ol (**II.1l**) and 1,1,1,3,3,3-hexafluoro-2-(2-iodophenyl)propan-2-ol (**II.1m**) affords I(III) compounds **II.2k**, **II.2l**, and **II.2m**, respectively.

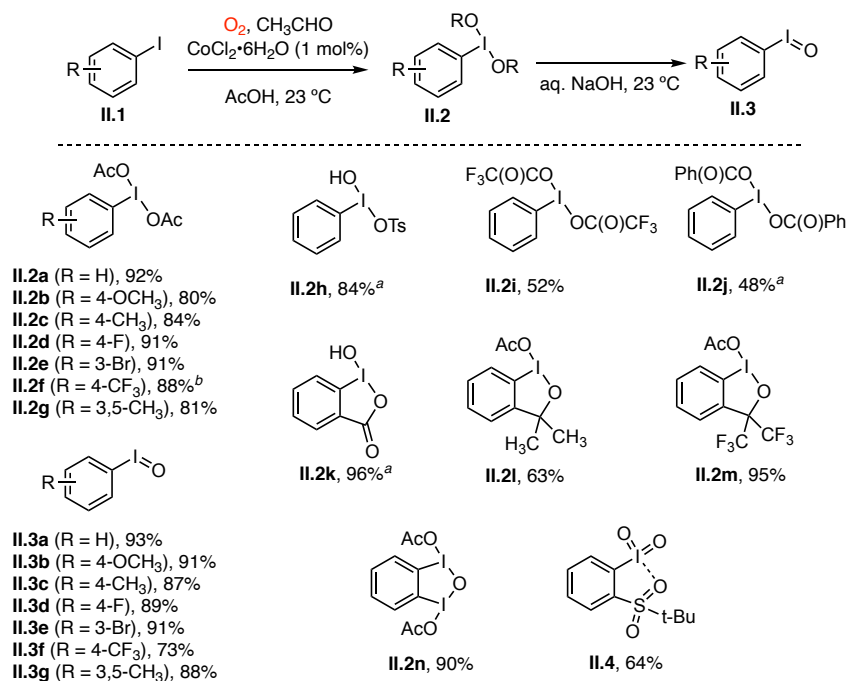


Figure II-4. Application of aerobic oxidation chemistry to the synthesis of a family of hypervalent iodine reagents. ^aReaction solvent in these oxidation reactions was 1,2-dichloroethane (DCE). ^bFor this substrate, dimerization product $(4\text{-CF}_3\text{C}_6\text{H}_4\text{I}(\text{OAc}))_2\text{O}$ was obtained.

Benziodoxole-based hypervalent iodine reagents, in which the *ortho*-substituent chelates to the oxidized iodine center (*i.e.*, **II.2k-m**), are widely utilized in atom and group-transfer chemistry. The developed conditions also provide access to bis-I(III) compound **II.2n**, by four-electron oxidation of 1,2-diiodobenzene (**II.1n**), in 90% yield. Finally, we examined oxidation of 2-*tert*-butylsulfonyliodobenzene (**II.1o**) to access 2-*tert*-butylsulfonyliodosylbenzene (**II.4**), a

hypervalent iodine derivative that has found application in hydroxylation catalysis due to its substantially increased solubility versus unsubstituted iodosylbenzene.¹⁸³ Unlike the aforementioned oxidation reactions, which generate I(III) derivatives in high yield, oxidation of 2-tert-butylsulfonyliodobenzene affords I(V) derivative **II.4**. The unanticipated overoxidation in this case is probably due to disproportionation of an initially formed I(III) derivative.

II.2.2 Application of Aerobic Oxidation of Aryl Iodides to Oxidase Chemistry

Access to chemical platforms for oxidase chemistry, in which O₂ is utilized as the terminal oxidant without participating in substrate oxygenation, would provide an approach to coupling diverse modes of substrate oxidation directly to O₂ reduction. Here, we demonstrate that aerobic oxidation of aryl iodides can be used to couple O₂ reduction to 1,2-difunctionalization of olefins, carbonyl α -functionalization, oxidative dearomatization chemistry, and direct C–H amination chemistry (Figure II-5). For each of the transformations illustrated in Figure II-5, control reactions in the absence of aryl iodides resulted in no conversion to the illustrated oxidation products. Aerobic oxidation of aryl iodides can be utilized in substrate oxygenation. Aerobic 1,2-*bis*-acetoxylation of styrene derivatives,¹⁸⁴ illustrated by the conversion of 4-fluorostyrene (**II.5**) to *bis*-acetate **II.6** in 88% yield, can be accomplished via a one-pot procedure (Figure II-5a). In the specific case of styrene functionalization, a one-pot, two-step protocol, in which PhI(OAc)₂ is prepared prior to styrene addition, was necessary. The incompatibility of radical chain autoxidation of PhI with the presence of styrene is consistent with the facility of radical addition to styrenes. One-step aerobic carbonyl α -oxidation reactions proceed readily. Acetophenone (**II.7**) undergoes α -tosylation¹⁸⁵ to afford oxygenated compound **II.8** in 74% yield by the action of standard autoxidation conditions with the addition of *p*-toluene sulfonic acid (*p*-TSA) (Figure II-5b).

Similarly, β -ketoester **II.9** is readily tosylated to afford α -oxygenate **II.10** in 61% yield (Fig. II-5c). Use of 20 mol% PhI in the α -tosylation of acetophenone led to the observation of 33% yield of compound **II.8**, which provided a proof-of-principle that PhI could be used as a catalyst for aerobic oxidation chemistry. We hypothesize that the poor catalyst turnover observed in these reactions may be due to relatively slow α -oxygenation of carbonyl substrates by aerobically generated I(III); if substrate functionalization is slow relative to aldehyde autoxidation, insufficient I(I) will be generated to intercept reactive autoxidation intermediates.

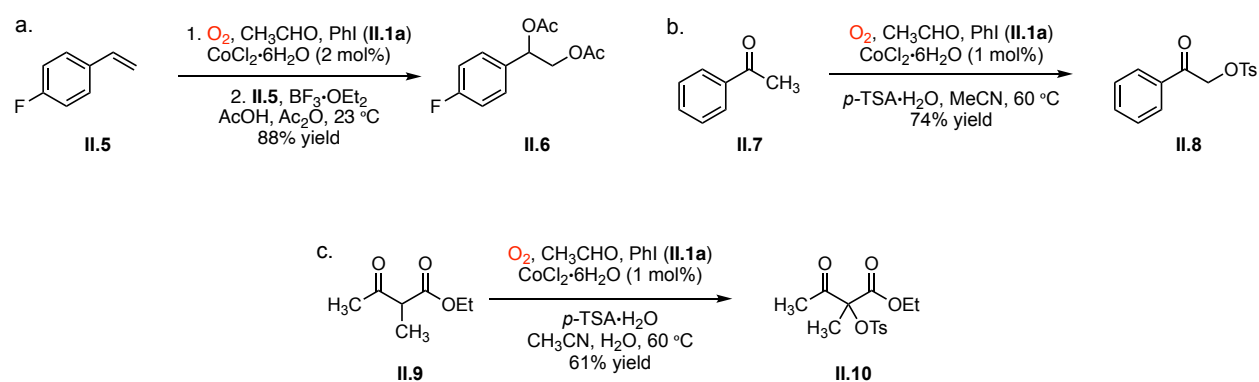


Figure II-5. Aerobic oxidation of PhI provides a broad platform to directly utilize O₂ as the terminal oxidant in substrate oxidation reactions. Utilization of PhI oxidation to oxygenate substrates is highlighted by (a) 1,2-difunctionalization of olefins, (b) α -oxygenation of acetophenone, and (c) α -oxygenation of β -keto esters. *p*-TSA: *para*-toluenesulfonic acid.

II.2.3 Application of Aerobic Oxidation of Aryl Iodides to Oxidase Catalysis

The ability to accomplish ligand exchange chemistry in hypervalent iodine compounds allows the developed aerobic oxidation of aryl iodides to be applied to substrate oxidation chemistry that does not involve incorporation of oxygen in the reaction products. For example, in the α -oxidation of β -ketoester **II.9**, replacing *p*-TSA with tetrabutylammonium bromide ([TBA]Br) results in aerobic bromination to afford compound **II.11** (57% yield), not the α -oxygenation product **II.10** as demonstrated above (Figure II-5b). Unlike the oxygenation reactions pictured in Figure II-5, which require stoichiometric aryl iodide to access synthetically useful

oxidation yields, bromination could be achieved with a catalytic amount of aryl iodide. With 20 mol% 1,2-diiodobenzene (**II.1n**), bromination proceeds in 72% yield (Figure II-6a). PhI is also a competent catalyst for bromination, but superior yields are obtained with 1,2-diiodobenzene as catalyst. We have extended aryl-iodide-catalysed aerobic oxidation to oxidative dearomatization chemistry and C–H amination chemistry. Using 20 mol% 1,2-diiodobenzene, Weinreb¹⁸⁶ amide **II.12** undergoes aerobic dearomatization to afford lactam **II.13** in 77% yield (Figure II-6b). Dehydrogenative N–H/C–H coupling to arylate amines with unfunctionalized aromatics can also be accomplished by the action of aryl iodide catalysis. With 10 mol% 1,2-diiodobenzene, amine **II.14** undergoes arylation with benzene to afford phenylsulfonamide **II.15** in 78% yield (Figure II-6c).¹⁸⁷ In each of the reactions pictured in Figure II-6, aerobic oxidation is accomplished with AcOH as the only stoichiometric by-product.

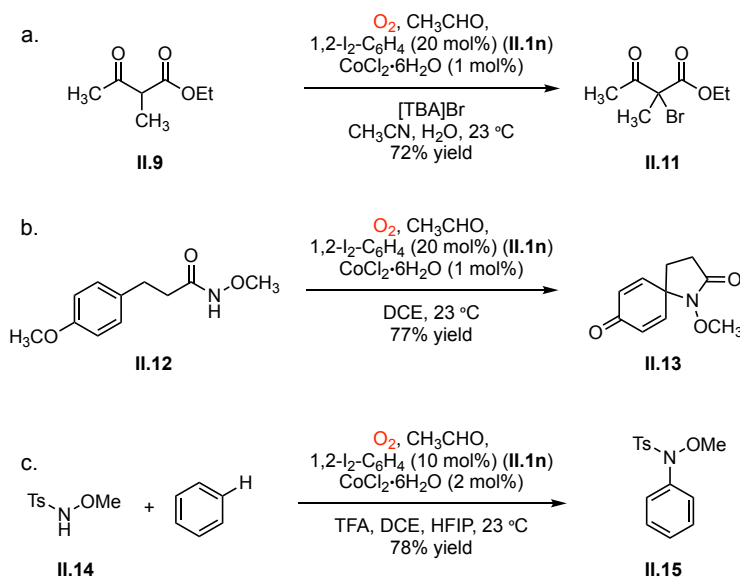


Figure II-6. Oxidase catalysis via aerobically generated hypervalent iodine intermediates. Ligand exchange chemistry at hypervalent iodine reagents, and *in situ* aerobic oxidation, supports oxidase catalysis of heterofunctionalization reactions, such as: (a) aerobic bromination of β -keto esters, (b) oxidative dearomatization chemistry; and (c) direct aerobic C–H amination chemistry. [TBA]Br: tetrabutylammonium bromide, DCE: 1,2-dichloroethane, TFA: trifluoroacetic acid, HFIP: 1,1,1,3,3,3-hexafluoroisopropanol.

II.2.4 Aerobic Oxidation Mechanism

Aldehyde-promoted aerobic oxidation of aryl iodides was developed based on the hypothesis that strongly oxidizing intermediates in aldehyde autoxidation chemistry could be coopted for the oxidation of aryl iodides. Consistent with this hypothesis, the use of reaction solvents with relatively weak C–H bonds (that is, THF) or the addition of 2,6-di-*tert*-butyl-4-methylphenol (BHT), a common radical inhibitor, suppressed the formation of hypervalent iodine products (Figure II-7).

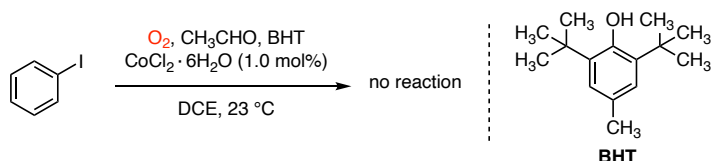


Figure II-7. Aerobic oxidation of iodobenzene is suppressed in the presence of radical inhibitors.

To further probe the mechanism of PhI oxidation, we followed the kinetics of PhI consumption and $\text{PhI}(\text{OAc})_2$ evolution by ^1H NMR spectroscopy in CDCl_3 (Figure II-8). In the absence of $\text{CoCl}_2 \cdot 6\text{H}_2\text{O}$, an induction period is observed and evolution of $\text{PhI}(\text{OAc})_2$ displays sigmoidal growth consistent with a radical chain process (See Figure II-9 for full kinetics data). In the presence of $\text{CoCl}_2 \cdot 6\text{H}_2\text{O}$, $\text{PhI}(\text{OAc})_2$ evolution still displays sigmoidal growth, but the induction period for PhI oxidation to $\text{PhI}(\text{OAc})_2$ is substantially shortened, which is consistent with more rapid initiation of a radical chain process (See Experimental Details section for full kinetics data).

Similar kinetic profiles were measured for the oxidation of 4-iodotoluene and for the oxidation of PhI in *d*₄-AcOH. During these ^1H NMR experiments, we did not observe ^1H NMR resonances of peracetic acid, but we did note the initial evolution and subsequent disappearance

of a quartet at 5.41 ppm, a singlet at 2.01 ppm and a doublet at 1.35 ppm, which integrate in a 1:3:3 ratio. We attributed these signals to Baeyer–Villiger intermediate **E**.¹⁸⁸ Consistent with this assignment, high-resolution mass spectrometry of the oxidation reaction reveals the presence of a signal at $m/z = 143.0318$ ($M+Na^+$ for **E**). Intermediate **E** is also observed when PhI oxidation is carried out in $AcOH-d_4$. Observation of **E**, which is the adduct of a molecule of aerobically generated AcOOH and a molecule of CH_3CHO , confirms that aldehyde autoxidation is operative during aerobic oxidation of aryl iodides. Magnetization transfer experiments demonstrate that compound **E** is in equilibrium with acetaldehyde and peracetic acid on the timescale of PhI oxidation. At that time, we couldn't differentiate between aerobically generated AcOOH or compound **E**, the adduct of AcOOH with CH_3CHO , as the active oxidant in PhI oxidation.

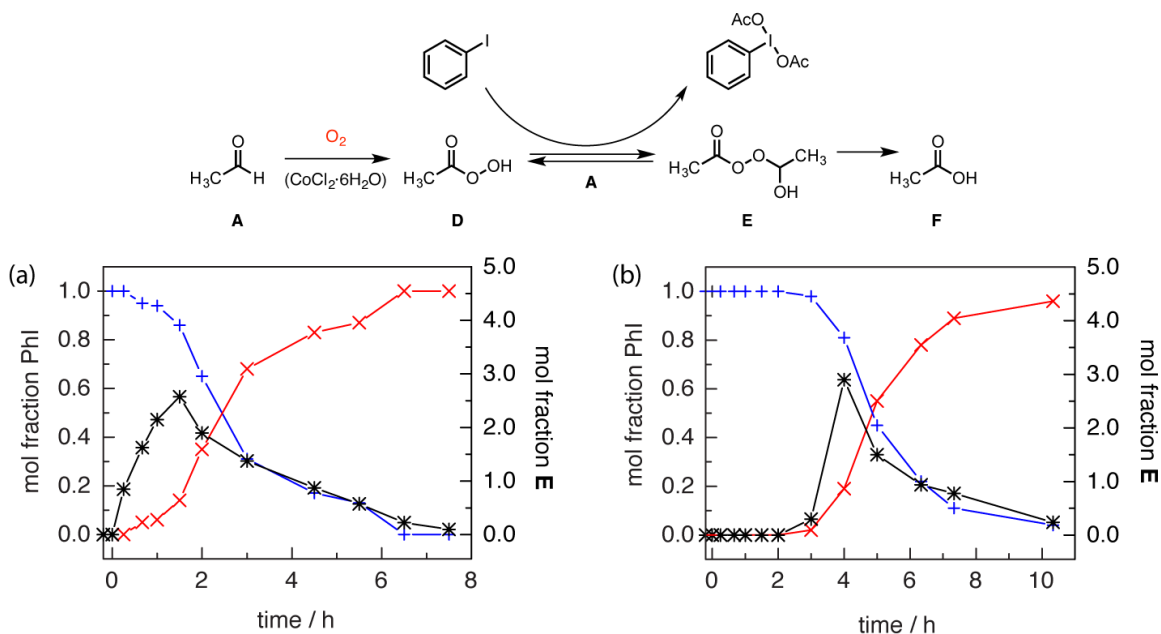


Figure II-8. Aerobic oxidation of aryl iodides is accomplished by intercepting the oxidizing intermediates of aldehyde autoxidation chemistry. Monitoring the kinetics of consumption of PhI (+) and evolution of $PhI(OAc)_2$ (x) by 1H NMR in the presence (a) or absence (b) of $CoCl_2 \cdot 6H_2O$, added as a radical initiator, indicates that Co(II) catalyzes the oxidation of PhI by initiating autoxidation. At intermediate times during PhI oxidation, peroxy intermediate **E** (*) is observed (by both 1H NMR and mass spectrometry) which confirms that autoxidation is operative during aryl iodide oxidation.

II.3 Conclusions

Development of a broadly applicable platform for oxidase catalysis, which utilizes O₂ as the terminal oxidant without necessitating the incorporation of oxygen during substrate functionalization, would provide new opportunities to utilize O₂ as a sustainable oxidant in chemical synthesis. Aldehyde autoxidation chemistry, in which an aldehyde is converted to a carboxylic acid under the action of O₂, is among the earliest examples of aerobic oxidation in organic chemistry and proceeds via reactive peroxy radicals and peracids. Here, we redirect the reactive two-electron oxidants that are generated during aldehyde autoxidation to provide access to a family of hypervalent iodine reagents. The synthesis strategy leverages the intrinsic proclivity of O₂ to participate in radical chain chemistry (*i.e.*, autoxidation) to prepare selective two-electron oxidants for use in synthesis. The importance of generating hypervalent iodine-based oxidants, and not utilizing aldehyde autoxidation intermediates directly for substrate oxidation, is highlighted by the diversity of oxidative substrate functionalization chemistry that can be coupled to O₂ reduction using aryl iodides. We have demonstrated that aryl-iodide-supported oxidase chemistry and catalysis can be leveraged for aerobic olefin functionalization, carbonyl α -oxidation to introduce both oxygen and halogen functionality, oxidative dearomatization reactions and aerobic C–H amination chemistry. We anticipate that aryl-iodide-catalyzed aerobic oxidation chemistry will provide new opportunities and strategies to directly utilize O₂ in sustainable chemical synthesis.

II.4 Experimental Details

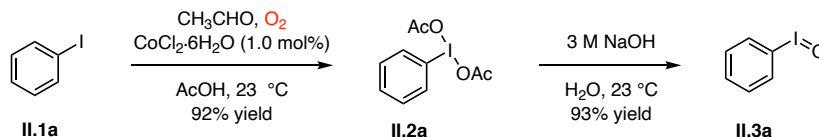
II.4.1 General Considerations

Materials All chemicals and solvents were obtained as ACS reagent grade and used as received. Iodobenzene and styrene were obtained from Beantown Chemical. Acetaldehyde, 2-iodonitrobenzene, 3-(4-methoxyphenyl)propionic acid, and *p*-toluenesulfonic acid monohydrate were obtained from Alfa Aesar. Sodium hydroxide and ethyl acetate were obtained from EMD Millipore. 2-iodobenzoic acid, 4-iodoanisole, 4-iodotoluene, benzoic acid, 3-bromoiodobenzene, 2,5-dimethyliodobenzene, 1,1,1,3,3,3-hexafluoro-2-phenyl-2-propanol, butylated hydroxytoluene, acetophenone, 2-methylethyl acetoacetate, 1,2-dichloroethane, 4-fluorostyrene, borontrifluoride diethyletherate, diethyl ether, methanol, THF, hexanes, acetic acid, and acetic anhydride were obtained from Sigma Aldrich. Tetrabutylammonium bromide was purchased from Chem-Impex Int'l Inc. 1,2-Diiodobenzene and silica gel (0.060 – 0.200 mm, 60 Å for column chromatography) were obtained from Acros Organics. CH₂Cl₂ and acetonitrile were obtained from Fisher Scientific. *O*-methylhydroxylamine hydrochloride, butyraldehyde, isobutyraldehyde, and trifluoroacetic acid was obtained from TCI. NMR solvents were purchased from Cambridge Isotope Laboratories and were used as received. O₂ (99.6%) was obtained from Conroe Welding Supply. All reactions were carried out under ambient atmosphere unless otherwise noted. *N*-Methoxy-4-methylbenzenesulfonamide (18),¹⁸⁷ 2-(2-iodophenyl)propan-2-ol,¹⁸⁹ and 2-*tert*-butyliodosylbenzene¹⁹⁰ was prepared according to literature procedures

Characterization Details NMR spectra were recorded on a Mercury-300, an Inova-500, or an Avance III 400 FT NMR spectrometer. ¹H acquisitions were referenced against residual proton resonances in deuterated solvents: CDCl₃ (7.26 ppm, ¹H; 77.16 ppm, ¹³C), DMSO-d₆ (2.50 ppm,

^1H ; 39.52 ppm, ^{13}C) and CD_3OD (3.31 ppm, ^1H). ^1H NMR data are reported as follows: chemical shift (δ , ppm), (multiplicity: s (singlet), d (doublet), t (triplet), m (multiplet), br (broad), integration).¹⁹¹

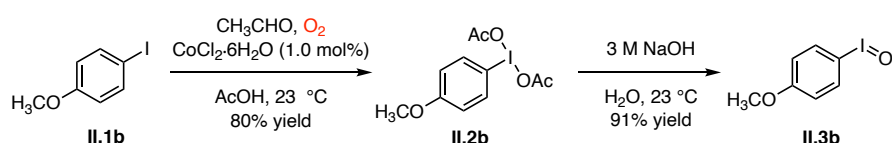
II.4.2 Synthesis and Characterization Details



Synthesis of iodobenzene diacetate (II.2a). A 20-mL scintillation vial was charged with glacial AcOH (2.0 mL), iodobenzene (**II.1a**, 82.2 mg, 0.401 mmol, 1.00 equiv), and $\text{CoCl}_2 \cdot 6\text{H}_2\text{O}$ (0.9 mg, 0.004 mmol, 1 mol%) and was fitted with a rubber septum. The reaction vessel was purged with O_2 for 5 min before acetaldehyde (224 μL , 4.07 mmol, 10.2 equiv) was added in one portion. The reaction mixture was stirred under 1 atm O_2 , delivered by inflated balloon, at 23 °C for 5 h. The solvent was removed *in vacuo* and residue was dissolved in CH_2Cl_2 . The organic layer was washed with distilled water and extracted with CH_2Cl_2 (3×7 mL). The organic layer was dried over MgSO_4 and solvent was removed *in vacuo* to afford 119 mg of iodobenzene diacetate (**II.2a**) as a white solid (92% yield). Characterization of **II.2a**: ^1H NMR (δ , 23 °C, CDCl_3): 8.09 (d, $J = 7.3$ Hz, 2H), 7.63–7.47 (m, 3H), 2.01 (s, 6H). ^{13}C NMR (δ , 23 °C, CDCl_3): 176.5, 135.0, 131.8, 131.0, 121.7, 20.5. The obtained spectral data are in good agreement with those reported in literature.¹⁹²

Synthesis of iodosylbenzene (II.3a). A 20-mL scintillation vial was charged with iodobenzene diacetate (**II.2a**, 97.1 mg, 0.301 mmol, 1.00 equiv) and 3 M NaOH (5 mL). The reaction mixture was stirred for 3 h at 23 °C. The resulting suspension was then filtered to afford

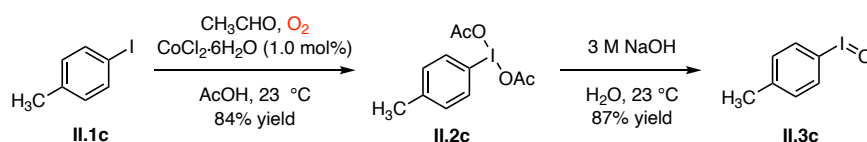
62 mg of iodosylbenzene (**II.3a**) as a yellow solid (93% yield). Characterization of **II.3a**: ^1H NMR (δ , 23 °C, CD_3OD): 8.04 (dd, $J = 7.5, 2.1$ Hz, 2H), 7.60–7.56 (m, 3H). These ^1H NMR data correspond to the *bis*-methoxy adduct of **2a**; in the absence of a coordinating solvent **II.3a** is an insoluble polymeric material. ^{13}C NMR data have not been collected due to poor solubility of **II.3a**. HRMS (ESI $^+$): Calcd. for $\text{C}_6\text{H}_6\text{IO}$ $[\text{M}+\text{H}]^+$ m/z 220.9463. Found: 220.9453. The obtained spectral data are in good agreement with those reported in literature.¹⁹³



Synthesis of 4-methoxy-iodobenzene diacetate (II.2b). A 20-mL scintillation vial was charged with glacial AcOH (2.0 mL), 4-methoxy-iodobenzene (**II.1b**, 94.3 mg, 0.402 mmol, 1.00 equiv), and $\text{CoCl}_2\cdot 6\text{H}_2\text{O}$ (0.9 mg, 0.004 mmol, 1 mol%) and was fitted with a rubber septum. The reaction vessel was purged with O_2 for 5 min before acetaldehyde (224 μL , 4.07 mmol, 10.1 equiv) was added in one portion. The reaction mixture was stirred under 1 atm O_2 , delivered by inflated balloon, at 23 °C for 10 h. The solvent was removed *in vacuo* and residue was dissolved in CH_2Cl_2 . The organic layer was washed with distilled water and extracted with CH_2Cl_2 (3×7 mL). The organic layer was dried over MgSO_4 and solvent was removed *in vacuo* to afford 113 mg of 4-methoxy-iodobenzene diacetate (**II.2b**) as a white solid (80% yield). Characterization of **II.2b**: ^1H NMR (δ , 23 °C, CDCl_3): 8.01 (d, $J = 9.0$ Hz, 2H), 6.96 (d, $J = 9.1$ Hz, 2H), 3.86 (s, 3H), 1.99 (s, 6H). ^{13}C NMR (δ , 23 °C, CDCl_3): 176.4, 162.1, 137.1, 116.6, 111.6, 55.6, 20.4. The obtained spectral data are in good agreement with those reported in literature.¹⁹⁴

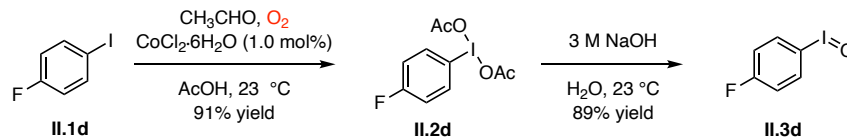
Synthesis of 4-methoxy iodosylbenzene (II.3b). A 20-mL scintillation vial was charged with 4-methoxy-iodobenzene diacetate (**II.2b**, 104 mg, 0.295 mmol, 1.00 equiv) and 3 M NaOH

(5 mL). The reaction mixture was stirred for 3 h at 23 °C. The resulting suspension was then filtered to afford 67 mg of 4-methoxy iodosylbenzene (**II.3b**) as a yellow solid (91% yield). Characterization of **II.3b**: ^1H NMR (δ , 23 °C, CD_3OD): 7.95 (d, $J = 9.1$ Hz, 2H), 7.18 (d, $J = 9.1$ Hz, 2H), 3.89 (s, 3H). These ^1H NMR data correspond to the *bis*-methoxy adduct of **II.3b**, which is generated upon dissolution of **II.3b** in CD_3OD . ^{13}C NMR data have not been collected due to poor solubility of **II.3b**. HRMS (ESI $^+$): Calcd. for $\text{C}_7\text{H}_7\text{INaO}_2$ $[\text{M}+\text{Na}]^+$ m/z 272.9388. Found: 272.9373. Compound **II.3b** has been previously described, but ^1H NMR data have not been published.¹⁹⁵



Synthesis of 4-methyl-iodobenzene diacetate (II.2c). A 20-mL scintillation vial was charged with glacial AcOH (2.0 mL), 4-methyl-iodobenzene (**II.1c**, 87.2 mg, 0.399 mmol, 1.00 equiv), and $\text{CoCl}_2\cdot 6\text{H}_2\text{O}$ (0.9 mg, 0.004 mmol, 1 mol%) and was fitted with a rubber septum. The reaction vessel was purged with O_2 for 5 min before acetaldehyde (224 μL , 4.07 mmol, 10.2 equiv) was added in one portion. The reaction mixture was stirred under 1 atm O_2 , delivered by inflated balloon, at 23 °C for 5 h. Solvent was removed *in vacuo* and the residue was dissolved in CH_2Cl_2 . The organic layer was washed with distilled water and extracted with CH_2Cl_2 (3×7 mL). The organic layer was dried over MgSO_4 and solvent was removed *in vacuo* to afford 113 mg of 4-methyl-iodobenzene diacetate (**II.2c**) as a white solid (84% yield). Characterization of **II.2c**: ^1H NMR (δ , 23 °C, CDCl_3): 7.97(d, $J = 8.2$ Hz, 2H), 7.29 (d, $J = 8.0$ Hz, 2H), 2.44 (s, 3H), 2.00 (s, 6H). ^{13}C NMR (δ , 23 °C, CDCl_3): 176.2, 142.5, 134.8, 131.6, 118.2, 21.4, 20.2. The obtained spectral data are in good agreement with those reported in literature.¹⁹⁴

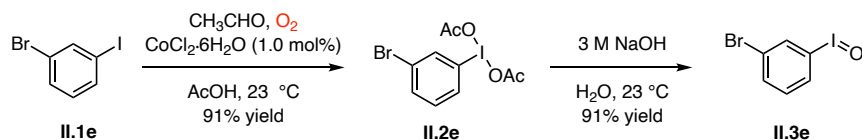
Synthesis of 4-methyl iodosylbenzene (II.3c). A 20-mL scintillation vial was charged with 4-methyl-iodobenzene diacetate (**II.2c**, 100 mg, 0.298 mmol, 1.00 equiv) and 3 M NaOH (5 mL). The reaction mixture was stirred for 3 h at 23 °C. The resulting suspension was then filtered to afford 61 mg of 4-methyl iodosylbenzene (**II.3c**) as a yellow solid (87% yield). Characterization of **II.3c**: ¹H NMR (δ, 23 °C, CD₃OD): 7.90 (d, *J* = 8.4 Hz, 2H), 7.38 (d, *J* = 8.2 Hz, 2H), 2.44 (s, 3H). These ¹H NMR data correspond to the *bis*-methoxy adduct of **II.3c**, which is generated upon dissolution of **II.3c** in CD₃OD. ¹³C NMR data have not been collected due to poor solubility of **II.3c**. HRMS (ESI⁺): Calcd. for C₇H₈IO [M+H]⁺ *m/z* 234.9620. Found: 234.9608. Compound **II.3c** has been previously described, but ¹H NMR data have not been published.¹⁹⁶



Synthesis of 4-fluoro-iodobenzene diacetate (II.2d). A 20-mL scintillation vial was charged with glacial AcOH (2.0 mL), 4-fluoro-iodobenzene (**II.1d**, 89.1 mg, 0.401 mmol, 1.00 equiv), and CoCl₂·6H₂O (0.9 mg, 0.004 mmol, 1 mol%) and was fitted with a rubber septum. The reaction vessel was purged with O₂ for 5 min before acetaldehyde (224 μL, 4.07 mmol, 10.1 equiv) was added in one portion. The reaction mixture was stirred under 1 atm O₂, delivered by inflated balloon, at 23 °C for 5 h. Solvent was removed *in vacuo* and the residue was dissolved in CH₂Cl₂. The organic layer was washed with distilled water and extracted with CH₂Cl₂ (3 × 7 mL). The organic layer was dried over MgSO₄ and solvent was removed *in vacuo* to afford 124 mg of 4-fluoro-iodobenzene diacetate (**II.2d**) as a white solid (91% yield). Characterization of **II.2d**: ¹H NMR (δ, 23 °C, CDCl₃): 8.08 (dd, *J* = 9.1, 4.9 Hz, 2H), 7.18 (t, *J* = 8.6 Hz, 2H), 2.01 (s, 6H). ¹³C

NMR (δ , 23 °C, CDCl₃): 176.3, 164.2 (d, $J=253.1$ Hz), 137.4 (d, $J=8.7$ Hz), 118.4 (d, $J=22.6$ Hz), 115.4, 20.2. The obtained spectral data are in good agreement with those reported in literature.¹⁹⁷

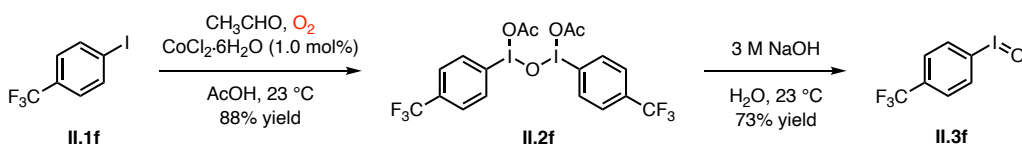
Synthesis of 4-fluoro iodosylbenzene (II.3d). A 20-mL scintillation vial was charged with 4-fluoro-iodobenzene diacetate (**II.2d**, 101 mg, 0.298 mmol, 1.00 equiv) and 3 M NaOH (5 mL). The reaction mixture was stirred for 3 h at 23 °C. The resulting suspension was then filtered to afford 63 mg of 4-fluoro-iodosylbenzene (**II.3d**) as a yellow solid (89% yield). Characterization of **II.3d**: ¹H NMR (δ , 23 °C, CD₃OD): 8.06 (dd, $J = 7.8, 5.4$ Hz, 2H), 7.33 (t, $J = 8.7$ Hz, 2H). These ¹H NMR data correspond to the *bis*-methoxy adduct of **II.3d**, which is generated upon dissolution of **II.3d** in CD₃OD. ¹³C NMR data have not been collected due to poor solubility of **II.3d**. HRMS (ESI⁺): Calcd. for C₆H₅FIO [M+H]⁺ m/z 238.9369. Found: 238.9357. Compound **II.3d** has been previously described, but ¹H NMR data have not been published.



Synthesis of 3-bromo-iodobenzene diacetate (II.2e). A 20-mL scintillation vial was charged with glacial AcOH (2.0 mL), 3-bromo-iodobenzene (**II.1e**, 113 mg, 0.399 mmol, 1.00 equiv), and CoCl₂·6H₂O (0.9 mg, 0.004 mmol, 1 mol%) and was fitted with a rubber septum. The reaction vessel was purged with O₂ for 5 min before acetaldehyde (224 μ L, 4.07 mmol, 10.2 equiv) was added in one portion. The reaction mixture was stirred under 1 atm O₂, delivered by inflated balloon, at 23 °C for 5 h. Solvent was removed *in vacuo* and the residue was dissolved in CH₂Cl₂. The organic layer was washed with distilled water and extracted with CH₂Cl₂ (3 \times 7 mL). The organic layer was dried over MgSO₄ and solvent was removed *in vacuo* to afford 146 mg of 3-bromo-iodobenzene diacetate (**II.2e**) as a white solid (91% yield). Characterization of **II.2e**: ¹H

NMR (δ , 23 °C, CDCl₃): 8.22 (s, 1H), 8.02 (d, J = 8.1 Hz, 1H), 7.71 (d, J = 8.1 Hz, 1H), 7.37 (d, J = 8.0 Hz, 1H), 2.02 (s, 6H). ¹³C NMR (δ , 23 °C, CDCl₃): 176.8, 137.5, 135.1, 133.6, 132.3, 124.1, 121.5, 20.6. The obtained spectral data are in good agreement with those reported in literature.¹⁹⁸

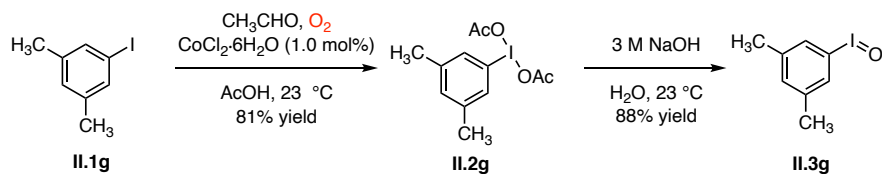
Synthesis of 3-bromo iodosylbenzene (II.3e). A 20-mL scintillation vial was charged with 3-bromo-iodobenzene diacetate (II.2e, 121 mg, 0.302 mmol, 1.00 equiv) and 3 M NaOH (5 mL). The reaction mixture was stirred for 3 h at 23 °C. The resulting suspension was then filtered to afford 82 mg of 3-bromo-iodosylbenzene (II.3e) as a yellow solid (91% yield). Characterization of II.3e: ¹H NMR (δ , 23 °C, CD₃OD): 8.18 (s, 1H), 8.00 (d, J = 8.0 Hz, 1H), 7.75 (d, J = 8.0 Hz, 1H), 7.53–7.47 (m, 1H). These ¹H NMR data correspond to the *bis*-methoxy adduct of II.3e, which is generated upon dissolution of II.3e in CD₃OD. ¹³C NMR data have not been collected due to poor solubility of II.3e. HRMS (ESI⁺): Calcd. for C₆H₅BrIO [M+H]⁺ m/z 298.8568. Found: 298.8556. Compound II.3e has been previously described, but ¹H NMR data have not been published.



Synthesis of μ -oxo-bis[(acetoxyiodo)-4-trifluoromethylbenzene] (II.2f). A 20-mL scintillation vial was charged with glacial AcOH (2.0 mL), 4-trifluoromethyl-iodobenzene (II.1f, 109 mg, 0.402 mmol, 1.00 equiv), and CoCl₂·6H₂O (0.9 mg, 0.004 mmol, 1 mol%) and was fitted with a rubber septum. The reaction vessel was purged with O₂ for 5 min before acetaldehyde (224 μ L, 4.07 mmol, 10.1 equiv) was added in one portion. The reaction mixture was stirred under 1 atm O₂, delivered by inflated balloon, at 23 °C for 5 h. The solvent was removed *in vacuo* and residue was dissolved in CH₂Cl₂. The organic layer was washed with distilled water and extracted

with CH₂Cl₂ (3 × 7 mL). The organic layer was dried over MgSO₄ and solvent was removed *in vacuo* to afford 119 mg of the title compound **II.2f** as a white solid (88% yield). Characterization of **II.2f**: ¹H NMR (δ, 23 °C, CDCl₃): 7.92 (d, *J* = 8.3 Hz, 2H), 7.53 (d, *J* = 8.3 Hz, 2H), 1.94 (s, 3H). ¹³C NMR of the sample was not recorded as the compound was unstable over the course of the NMR acquisition. The obtained spectral data are in good agreement with those reported in literature.¹⁹⁴

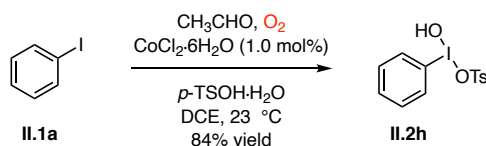
Synthesis of 4-trifluoromethyl iodobenzene (II.3f). A 20-mL scintillation vial was charged with μ-oxo-bis[(acetoxiyodo)-4-trifluoromethyl-benzene] (**II.2f**, 78.3 mg, 0.115 mmol, 1.00 equiv) and 3 M NaOH (5 mL). The reaction mixture was stirred for 3 h at 23 °C. The resulting suspension was then filtered to afford 48 mg of 4-trifluoromethyl iodobenzene (**II.3f**) as a yellow solid (73% yield). Characterization of **II.3f**: ¹H NMR (δ, 23 °C, CD₃OD): 8.23 (d, *J* = 8.3 Hz, 2H), 7.90 (d, *J* = 8.3 Hz, 2H). These ¹H NMR data correspond to the *bis*-methoxy adduct of **II.3f**, which is generated upon dissolution of **II.3f** in CD₃OD. ¹³C NMR data have not been collected due to poor solubility of **II.3f**. HRMS (ESI⁺): Calcd. for C₇H₅F₃IO [M+H]⁺ *m/z* 288.9337. Found: 288.9324. Compound **II.3f** has been previously described, but ¹H NMR data have not been published.¹⁹⁹



Synthesis of 3,5-dimethyl-iodobenzene diacetate (II.2g). A 20-mL scintillation vial was charged with glacial AcOH (2.0 mL), 3,5-dimethyl-iodobenzene (**II.1g**, 93.1 mg, 0.401 mmol, 1.00 equiv), and CoCl₂·6H₂O (0.9 mg, 0.004 mmol, 1 mol%) and was fitted with a rubber septum.

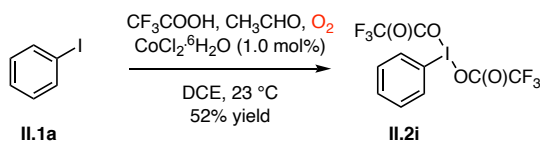
The reaction vessel was purged with O₂ for 5 min before acetaldehyde (224 μL, 4.07 mmol, 10.1 equiv) was added in one portion. The reaction mixture was stirred under 1 atm O₂, delivered by inflated balloon, at 23 °C for 10 h. Solvent was removed *in vacuo* and the residue was dissolved in CH₂Cl₂. The organic layer was washed with distilled water and extracted with CH₂Cl₂ (3 × 7 mL). The organic layer was dried over MgSO₄ and solvent was removed *in vacuo* to afford 114 mg of 3,5-dimethyl-iodobenzene diacetate (**II.2g**) as a white solid (81% yield). Characterization of **II.2g**: ¹H NMR (δ, 23 °C, CDCl₃): 7.72 (s, 2H), 7.20 (s, 1H), 2.38 (s, 6H), 2.00 (s, 6H). ¹³C NMR (δ, 23 °C, CDCl₃): 176.4, 141.1, 133.7, 132.5, 121.3, 21.3, 20.4. The obtained spectral data are in good agreement with those reported in literature.¹⁹⁴

Synthesis of 3,5-dimethyl iodosylbenzene (II.3g). A 20-mL scintillation vial was charged with 3,5-dimethyl-iodobenzene diacetate (**II.2g**, 106 mg, 0.303 mmol) and 3 M NaOH (5 mL). The reaction mixture was stirred for 3 h at 23 °C. The resulting suspension was then filtered to afford 66 mg of 3,5-dimethyl-iodosylbenzene (**II.3g**) as a yellow solid (88% yield). Characterization of **II.3g**: ¹H NMR (δ, 23 °C, CD₃OD): 7.66 (s, 2H), 7.24 (s, 1H), 2.39 (s, 6H). These ¹H NMR data correspond to the *bis*-methoxy adduct of **II.3g**, which is generated upon dissolution of **II.3g** in CD₃OD. ¹³C NMR data have not been collected due to poor solubility of **II.3g**. HRMS (ESI⁺): Calcd. for C₈H₁₀IO [M+H]⁺ m/z 248.9776. Found: 248.9763. Compound **II.3g** has been previously described, but ¹H NMR data have not been published.²⁰⁰



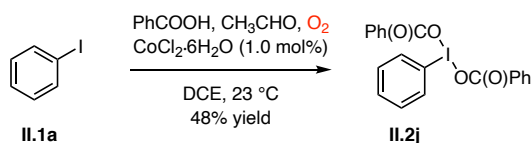
Synthesis of hydroxy(phenyl)-λ³-iodaneyl 4-methylbenzenesulfonate (II.2h). A 20-mL scintillation vial was charged with DCE (2.0 mL), iodobenzene (**II.1a**, 88.1 mg, 0.431 mmol, 1.00

equiv), and $\text{CoCl}_2 \cdot 6\text{H}_2\text{O}$ (0.9 mg, 0.004 mmol, 1 mol%) and was fitted with a rubber septum. The reaction vessel was purged with O_2 for 5 min before acetaldehyde (224 μL , 4.06 mmol, 10.2 equiv) was added in one portion. The reaction mixture was stirred under 1 atm O_2 , delivered by inflated balloon, at 23 $^\circ\text{C}$ for 16 h. At this time, p -T $\text{SOH} \cdot \text{H}_2\text{O}$ (90 mg, 0.475 mmol, 1.10 equiv) dissolved in minimum amount of acetonitrile was added to the reaction mixture via syringe. The reaction mixture was stirred for 5h at 23 $^\circ\text{C}$, at which time a white precipitate was isolated by filtration, washed with hexanes, and dried *in vacuo* to afford 141 mg of the title compound (**II.2h**) as a white solid (84% yield). ^1H NMR (δ , 23 $^\circ\text{C}$, CD_3OD): 8.36 (d, J = 8.2 Hz, 2H), 7.87–7.82 (m, 1H), 7.73–7.66 (m, 4H), 7.23 (d, J = 8.1 Hz, 2H), 2.37 (s, 3H). ^{13}C NMR (δ , 23 $^\circ\text{C}$, CD_3OD): 143.0, 141.9, 137.0, 134.9, 132.8, 129.8, 126.9, 122.1, 21.3. The obtained spectral data are in good agreement with those reported in literature.²⁰¹

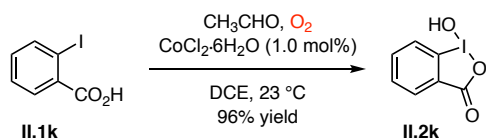


Synthesis of phenyl- λ^3 -iodanediyl bis(2,2,2-trifluoroacetate) (II.2i). A 20-mL scintillation vial was charged with glacial AcOH (2.0 mL), iodobenzene (82.2 mg, 0.401 mmol, 1.00 equiv), trifluoroacetic acid (91.1 mg, .799 mmol, 1.99 equiv), and $\text{CoCl}_2 \cdot 6\text{H}_2\text{O}$ (0.9 mg, 0.004 mmol, 1 mol%) and was fitted with a rubber septum. The reaction vessel was purged with O_2 for 5 min before acetaldehyde (224 μL , 4.07 mmol, 10.2 equiv) was added in one portion. The reaction mixture was stirred under 1 atm O_2 , delivered by inflated balloon, at 23 $^\circ\text{C}$ for 12 h. The solvent was removed *in vacuo* and residue was dissolved in CH_2Cl_2 . The organic layer was washed with distilled water, 5% NaHCO_3 solution, and extracted with CH_2Cl_2 (3×7 mL). The organic layer was dried over MgSO_4 and solvent was removed *in vacuo* to afford 76mg of iodobenzene

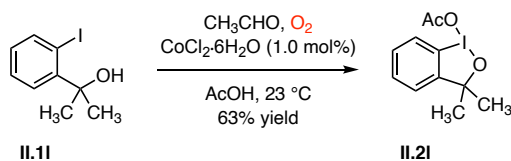
ditrifluoroacetate (**II.2i**) as a microcrystalline white solid (44% yield). $^1\text{H NMR}$ (δ , 23 °C, CDCl_3 with one drop CF_3COOH) δ 8.21 (d, $J = 8.2$ Hz, 2H), 7.76 (t, $J = 7.5$ Hz, 1H), 7.64 (d, $J = 8.0$ Hz, 2H). The obtained spectral data are in good agreement with those reported in literature.



Synthesis of phenyl- λ^3 -iodanediyl dibenzoate (II.2j). A 20-mL scintillation vial was charged with DCE (2.0 mL), iodobenzene (**II.1a**, 82.2 mg, 0.401 mmol, 1.00 equiv), benzoic acid (PhCOOH , 486 mg, 3.98 mmol, 9.92 equiv), and $\text{CoCl}_2\cdot 6\text{H}_2\text{O}$ (0.9 mg, 0.004 mmol, 1 mol%) and was fitted with a rubber septum. The reaction vessel was purged with O_2 for 5 min before acetaldehyde (224 μL , 4.07 mmol, 10.2 equiv) was added in one portion. The reaction mixture was stirred under 1 atm O_2 , delivered by inflated balloon, at 23 °C for 12 h. The solvent was removed *in vacuo* and residue was dissolved in CH_2Cl_2 . The organic layer was washed with distilled water and extracted with CH_2Cl_2 (3×7 mL). The organic layer was dried over MgSO_4 and solvent was removed *in vacuo* to afford 85mg of iodobenzene dibenzoate (**II.2j**) as a white solid (48% yield). $^1\text{H NMR}$ (δ , 23 °C, CDCl_3) δ 8.24 (d, $J = 7.9$ Hz, 2H), 7.93 (d, $J = 7.2$ Hz, 4H), 7.64-7.46 (m, 5H), 7.36 (t, $J = 7.6$ Hz, 4H). $^{13}\text{C NMR}$ (δ , 23 °C, CDCl_3) δ 171.5, 135.0, 132.6, 131.8, 131.1, 130.3, 130.2, 128.3, 122.5. The obtained spectral data are in good agreement with those reported in literature.²⁰²

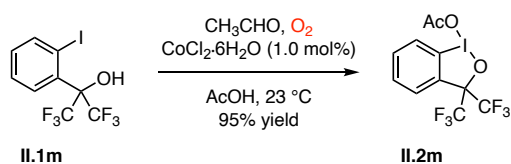


Synthesis of 1-Hydroxy-1,2-benziodoxol-3(1H)-one (II.2k). A 20-mL scintillation vial was charged with DCE (2.0 mL), 2-iodobenzoic acid (**II.1k**, 50.2 mg, 0.202 mmol, 1.00 equiv), and $\text{CoCl}_2\cdot 6\text{H}_2\text{O}$ (0.5 mg, 0.002 mmol, 1 mol%) and was fitted with a rubber septum. The reaction vessel was purged with O_2 for 5 min before acetaldehyde (112 μL , 2.03 mmol, 10.1 equiv) was added in one portion. The reaction mixture was stirred under 1 atm O_2 , delivered by inflated balloon, at 23 $^\circ\text{C}$ for 16 h. The reaction mixture was diluted with hexanes. The precipitate was isolated by filtration and was washed with 2 mL water. The solid was dried *in vacuo* to afford 51 mg of the title compound (**II.2k**) as an off-white solid (96% yield). ^1H NMR (δ , 23 $^\circ\text{C}$, $\text{DMSO-}d_6$): 8.03 (s, 1H, OH proton exchangeable with D_2O), 8.01–7.98 (m, 1H), 7.95–7.92 (m, 1H), 7.84 (s, 1H), 7.69 (td, $J = 7.3, 1.0$ Hz, 1H). ^{13}C NMR (δ , 23 $^\circ\text{C}$, $\text{DMSO-}d_6$): 167.8, 134.5, 131.6, 131.2, 130.4, 126.4, 120.5. The obtained spectral data are in good agreement with those reported in literature.²⁰³

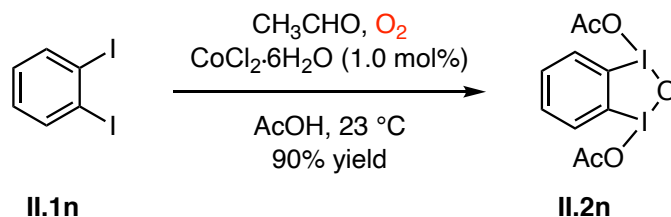


Synthesis of 1,3-Dihydro-1-hydroxy-3,3-dimethyl-1,2-benziodoxole (II.2l). A 20-mL scintillation vial was charged with glacial AcOH (2.0 mL), 2-(2-iodophenyl)propan-2-ol (**II.1l**, 75.9 mg, 0.290 mmol, 1.00 equiv), and $\text{CoCl}_2\cdot 6\text{H}_2\text{O}$ (0.7 mg, 0.003 mmol, 1 mol%) and was fitted with a rubber septum. The reaction vessel was purged with O_2 for 5 min before acetaldehyde (168 μL , 2.99 mmol, 10.3 equiv) was added in one portion. The reaction mixture was stirred under 1 atm O_2 , delivered by inflated balloon, at 23 $^\circ\text{C}$ for 10 h. The solvent was removed *in vacuo* and residue was dissolved in CH_2Cl_2 . The organic layer was washed with distilled water and extracted

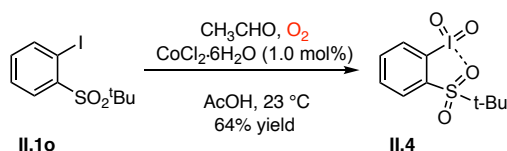
with CH₂Cl₂ (3 × 7 mL). The organic layer was dried over MgSO₄ and solvent was removed *in vacuo*. The obtained residue was washed with hexanes to afford 59 mg of the title compound (**II.2I**) as white solid (63% yield). ¹H NMR (δ, 23 °C, CDCl₃): 7.79 (d, *J* = 7.5 Hz, 1H), 7.50–7.45 (m, 2H), 7.18 (d, *J* = 9.1 Hz, 1H), 2.11 (s, 3H), 1.52 (s, 6H). ¹³C NMR (δ, 23 °C, CDCl₃): 177.4, 149.4, 130.4, 129.95, 129.87, 126.2, 115.7, 84.6, 29.2, 21.5. The obtained spectral data are in good agreement with those reported in literature.²⁰⁴



Synthesis of 3,3-bis(trifluoromethyl)-1λ³-benzo[*d*][1,2]iodaoxol-1(3*H*)-yl acetate (II.2m**).** A 20-mL scintillation vial was charged with glacial AcOH (2.0 mL), 1,1,1,3,3,3-hexafluoro-2-(2-iodophenyl)propan-2-ol (**II.1m**, 149 mg, 0.403 mmol, 1.00 equiv), and CoCl₂·6H₂O (0.9 mg, 0.004 mmol, 1 mol%) and was fitted with a rubber septum. The reaction vessel was purged with O₂ for 5 min before acetaldehyde (224 μL, 4.07 mmol, 10.1 equiv) was added in one portion. The reaction mixture was stirred under 1 atm O₂, delivered by inflated balloon, at 23 °C for 5 h and then another portion of acetaldehyde (112 μL, 2.03 mmol, 4.98 equiv) was added and the reaction mixture was stirred for 5 h at 23 °C. The solvent was removed *in vacuo* and residue was dissolved in CH₂Cl₂. The organic layer was washed with distilled water and extracted with CH₂Cl₂ (3 × 7 mL). The organic layer was dried over MgSO₄ and solvent was removed *in vacuo* to afford 164 mg of the title compound (**II.2m**) as a white solid (95% yield). ¹H NMR (δ, 23 °C, CDCl₃): 7.93 (d, *J* = 8.2 Hz, 1H), 7.61–7.79 (m, 3H), 2.18 (s, 3H). ¹³C NMR (δ, 23 °C, CDCl₃): 176.6, 133.4, 131.5, 131.0, 130.2, 129.6 (quintet (qu), *J* = 2.0 Hz), 123.4 (q, *J* = 287.7 Hz), 115.7, 85.6, 20.4. The obtained spectral data are in good agreement with those reported in literature.²⁰⁵



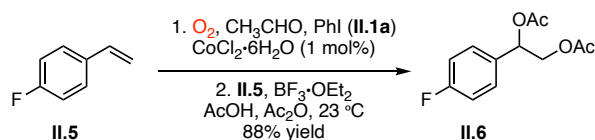
Synthesis of 1,3-Diacetoxy-1,3-dihydro-1,3,2-benziodooxole (II.2n). A 20-mL scintillation vial was charged with glacial AcOH (2.0 mL), 1,2-diiodobenzene (**II.1n**, 132 mg, 0.400 mmol, 1.00 equiv), and $\text{CoCl}_2 \cdot 6\text{H}_2\text{O}$ (0.9 mg, 0.004 mmol, 1 mol%) and was fitted with a rubber septum. The reaction vessel was purged with O_2 for 5 min before acetaldehyde (224 μL , 4.07 mmol, 10.0 equiv) was added in one portion. The reaction mixture was stirred under 1 atm O_2 , delivered by inflated balloon, at 23 $^\circ\text{C}$ for 10 h. Solvent was reduced *in vacuo* and hexanes were added. The observed white precipitate was isolated by filtration, washed with hexanes, and dried *in vacuo* to afford 167 mg of the title compound (**II.2n**, 90% yield). ^1H NMR (δ , 23 $^\circ\text{C}$, CDCl_3): 8.03 (dd, $J = 6.1, 3.4$ Hz, 2H), 7.63 (dd, $J = 6.1, 3.4$ Hz, 2H), 2.09 (s, 6H). ^{13}C NMR (δ , 23 $^\circ\text{C}$, CDCl_3): 178.1, 135.3, 131.9, 21.6. The obtained spectral data are in good agreement with those reported in literature.¹⁸⁷



Synthesis of 1-(tert-butylsulfonyl)-2-iodobenzene (II.4). A 20-mL scintillation vial was charged with glacial AcOH (2.0 mL), 1-(tert-butylsulfonyl)-2-iodobenzene (**II.1o**, 130 mg, 0.401 mmol, 1.00 equiv), and $\text{CoCl}_2 \cdot 6\text{H}_2\text{O}$ (0.9 mg, 0.004 mmol, 1 mol%) and was fitted with a rubber septum. The reaction vessel was purged with O_2 for 5 min before acetaldehyde (224 μL , 4.07 mmol, 10.1 equiv) was added in one portion. The reaction mixture was stirred under 1 atm O_2 , delivered by inflated balloon, at 23 $^\circ\text{C}$ for 10 h. The solvent was removed *in vacuo* and residue

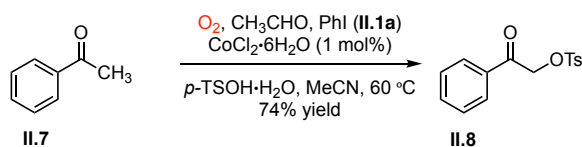
was treated with 2:1 hexanes:CH₂Cl₂ to induce precipitation of white solid. The precipitate was isolated by filtration, washed with hexanes, and dried *in vacuo* to afford 91 mg of the title compound (**II.4**) as a white solid (64% yield). Characterization of **II.4**: ¹H NMR (δ, 23 °C, DMSO-*d*₆): 8.46 (d, *J* = 7.6 Hz, 1H), 8.13 (t, *J* = 7.1 Hz, 1H), 7.97–7.84 (m, 2H), 1.32 (s, 9H). ¹³C NMR (δ, 23 °C, DMSO-*d*₆): 148.0, 135.1, 132.0, 131.2, 124.0, 61.2, 23.2. The spectral data are in good agreement with those reported in literature.¹⁹⁰

Application of Aerobic Oxidation to Substrate Functionalization



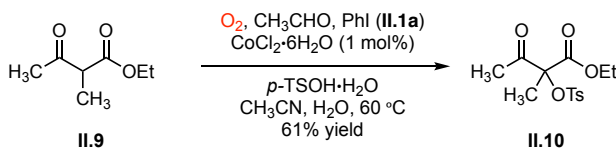
Synthesis of 1-(4-fluorophenyl)ethane-1,2-diyl diacetate (10). A 20-mL vial was charged with AcOH (0.9 mL), Ac₂O (0.1 mL), iodobenzene (**II.1a**, 61.0 mg, 0.299 mmol, 1.50 equiv), and CoCl₂·6H₂O (0.5 mg, 4 μmol, 2 mol%) and fitted with a rubber septum. The reaction vial was purged with O₂ for 5 min and then acetaldehyde (168 μL, 3.00 mmol, 15.0 equiv) was added to the reaction mixture. The reaction mixture was stirred for 6 h at 23 °C under 1 atm O₂ (supplied via a balloon). 4-Fluorostyrene (**II.5**, 24.0 μL, 0.201 mmol, 1.00 equiv) and 0.202 M BF₃·OEt₂ solution in AcOH (100 μL, 20.2 μmol, 10 mol%) were added and stirred at 23 °C for 6 h. Saturated aqueous NaHCO₃ and CH₂Cl₂ were added to the reaction mixture and the aqueous layer was extracted with CH₂Cl₂ (2 × 3 mL). Solvent was removed *in vacuo* and the residue was purified column chromatography on SiO₂ (9:1 hexane:ethyl acetate) to afford 42.4 mg of the title compound (**II.6**, 88% yield). ¹H NMR (δ, 23 °C, CDCl₃): 7.37–7.32 (m, 2H), 7.05–7.02 (t, 2H), 4.30–4.27 (m, 2H), 2.11 (s, 3H), 2.05 (s, 3H). ¹³C NMR (δ, 23 °C, CDCl₃): 170.5, 169.9, 162.7 (d, *J* = 274.2

Hz), 132.4 (d, $J = 3.3$ Hz), 128.6 (d, $J = 8.3$ Hz), 115.6 (d, $J = 21.5$ Hz), 72.6, 65.9, 21.1, 20.7. ^{19}F NMR (δ , 23 °C, CDCl_3): -112.9 ppm ($\text{C}_6\text{H}_5\text{F}$ was used as a standard, -113.1 ppm). The obtained spectral data are in good agreement with those reported in literature.²⁰⁶

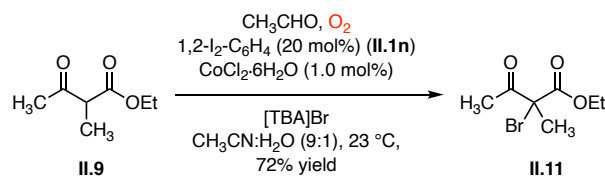


Synthesis of 2-tosyl-1-phenylethan-1-one (II.8). A 50-mL three-neck flask was fitted with a reflux condenser and a rubber septum and was charged with acetonitrile (8 mL), acetophenone (II.7, 62 μL , 0.532 mmol, 1.00 equiv), iodobenzene (II.1a, 67 μL , 0.600 mmol, 1.13 equiv),* and $\text{CoCl}_2 \cdot 6\text{H}_2\text{O}$ (1.2 mg, 0.0050 mmol, 1.0 mol%). O_2 was bubbled through the reaction before acetaldehyde (168 μL , 3.0 mmol, 15.0 equiv) was added in one portion. The reaction mixture was stirred at 23 °C for 10 min before $p\text{-TSOH} \cdot \text{H}_2\text{O}$ (114 mg, 0.599 mmol, 1.12 equiv), dissolved in acetonitrile (2.0 mL), was delivered to the reaction mixture via syringe. The reaction mixture was stirred under constant O_2 bubbling at 60 °C for 16 h. The reaction mixture was diluted with CH_2Cl_2 , washed with water, 10% NaHCO_3 , and dried over MgSO_4 . Solvent was removed *in vacuo* and the residue was purified by column chromatography (3:1 hexanes:ethyl acetate) to afford 112 mg of the title compound (II.8, 74% yield). ^1H NMR (δ , 23 °C, CDCl_3): 7.87–7.82 (m, 4H), 7.61 (t, $J = 7.4$ Hz, 1H), 7.47 (t, $J = 7.5$ Hz, 2H), 7.35 (d, $J = 7.9$ Hz, 2H), 5.27 (s, 2H), 2.45 (s, 3H). ^{13}C NMR (δ , 23 °C, CDCl_3): 190.4, 145.4, 134.3, 133.9, 132.8, 130.1, 129.1, 128.31, 128.15, 70.1, 21.9. The obtained spectral data are in good agreement with those reported in literature.²⁰⁷

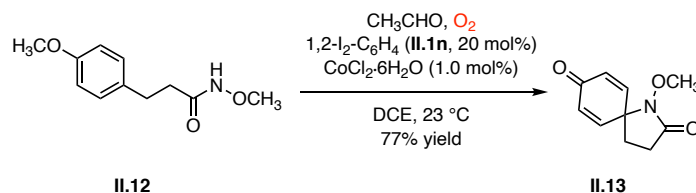
* When 20 mol% PhI was used, compound II.8 was isolated in 33% yield.



Synthesis of ethyl 2-methyl-3-oxo-2-(tosyloxy)butanoate (II.10). A 50-mL three-neck flask was fitted with reflux condenser and a rubber septum and was charged with acetonitrile (8 mL), 2-methyl ethylacetoacetate (**II.9**) (86 mg, 0.60 mmol, 1.0 equiv), iodobenzene (67 μL , 0.60 mmol, 1.0 equiv), and $\text{CoCl}_2\cdot 6\text{H}_2\text{O}$ (1.4 mg, 0.0058 mmol, 1.0 mol%). O_2 was bubbled through the reaction before acetaldehyde (340 μL , 6.05 mmol, 10.0 equiv) was added in one portion. The reaction mixture was stirred at 23 $^\circ\text{C}$ for 10 min before p -TSOH $\cdot\text{H}_2\text{O}$ (126 mg, 0.662 mmol, 1.11 equiv), dissolved in acetonitrile (3 ml), was delivered to the reaction mixture via syringe. The reaction mixture was stirred under constant O_2 bubbling, at 60 $^\circ\text{C}$ for 16 h. The reaction mixture was diluted with CH_2Cl_2 , washed with water, 10% NaHCO_3 , dried over MgSO_4 . Solvent was removed *in vacuo* and the residue was purified by column chromatography (3:1 hexanes:ethyl acetate) to afford 114 mg of the title compound (**II.10**, 61% yield). ^1H NMR (δ , 23 $^\circ\text{C}$, CDCl_3): 7.84 (d, $J = 8.3$ Hz, 2H), 7.34 (d, $J = 8.0$ Hz, 2H), 4.26 (q, $J = 7.1$ Hz, 2H), 2.44 (s, 3H), 2.29 (s, 3H), 1.85 (s, 3H), 1.29 (t, $J = 7.2$ Hz, 3H). ^{13}C NMR (δ , 23 $^\circ\text{C}$, CDCl_3): 200.7, 166.6, 145.2, 135.1, 129.9, 127.7, 90.6, 63.0, 25.4, 21.8, 20.2, 13.9. The obtained spectral data are in good agreement with those reported in literature.²⁰⁸



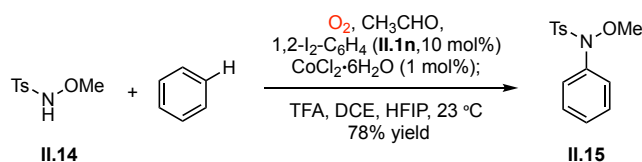
Synthesis of ethyl 2-bromo-2-methyl-3-oxobutanoate (II.9). A 20-mL scintillation vial was charged with MeCN:H₂O (9:1, 5 mL), 2-methyl ethylacetoacetate (**13**) (44.9 mg, 0.311 mmol, 1.00 equiv), 1,2-diiodobenzene (**II.1n**, 21 mg, 0.064 mmol, 20 mol%),* and CoCl₂·6H₂O (0.7 mg, 0.003 mmol, 1.0 mol%) and was fitted with a rubber septum. The reaction vessel was purged with O₂ for 5 min before acetaldehyde (174 μL, 3.10 mmol, 9.97 equiv) was added in one portion. [TBA]Br (110 mg, 0.341 mmol, 1.10 equiv) was dissolved in 2 mL MeCN:H₂O (9:1) and added to the reaction mixture via syringe. The reaction mixture was stirred under 1 atm O₂, delivered by inflated balloon, at 23 °C for 16 h. Solvent was removed *in vacuo* and the residue was purified by column chromatography (9:1 hexanes:diethyl ether) to afford 50 mg of the title compound (**II.11**) as a pale yellow oil (72% yield). ¹H NMR (δ, 23 °C, CDCl₃): 4.28 (q, *J* = 7.1 Hz, 2H), 2.44 (s, 3H), 1.98 (s, 3H), 1.31 (t, *J* = 7.1 Hz, 3H). ¹³C NMR (δ, 23 °C, CDCl₃): 198.4, 168.4, 63.3, 62.8, 29.8, 25.9, 25.4, 14.0. The obtained spectral data are in good agreement with those reported in literature.²⁰⁹



Synthesis of 1-methoxy-1-azaspiro[4.5]deca-6,9-dien-8-one (II.13). A 20-mL scintillation vial was charged with DCE (2.0 mL), *N*-methoxy-3-(4-methoxyphenyl)propanamide

* When 1.0 equivalents of PhI were used, compound **II.11** was isolated in 57% yield.

(**II.12**, 42.1 mg, 0.201 mmol, 1.00 equiv), 1,2-diodobenzene (**II.1n**, 14 mg, 0.042 mmol, 20 mol%),* and $\text{CoCl}_2 \cdot 6\text{H}_2\text{O}$ (0.5 mg, 0.002 mmol, 1 mol%) and was fitted with a rubber septum. The reaction vessel was purged with O_2 for 5 min before acetaldehyde (112 μL , 2.01 mmol, 10.0 equiv) was added in one portion. The reaction mixture was stirred under 1 atm O_2 , delivered by inflated balloon, at 23 $^\circ\text{C}$ for 16 h. The reaction mixture was diluted with CH_2Cl_2 , washed with water, 10% NaHCO_3 , and dried over MgSO_4 . Solvent was removed *in vacuo* and the residue was purified by column chromatography (1:1 hexanes:ethyl acetate) to afford 30 mg of the title compound (**II.13**, 77% yield). ^1H NMR (δ , 23 $^\circ\text{C}$, CDCl_3): 6.83 (d, $J = 8.4$ Hz, 2H), 6.37 (d, $J = 8.4$ Hz, 2H), 3.79 (s, 3H), 2.54 (t, $J = 7.9$ Hz, 2H), 2.17 (t, $J = 7.9$ Hz, 2H). ^{13}C NMR (δ , 23 $^\circ\text{C}$, CDCl_3) 184.5, 171.9, 147.4, 131.3, 65.4, 62.1, 29.8, 27.7, 26.1. The obtained spectral data are in good agreement with those reported in literature.^{186, 187}



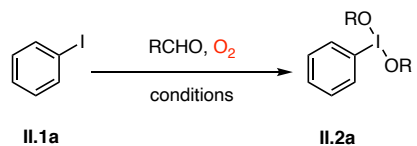
Synthesis of *N*-methoxy-4-methyl-*N*-phenylbenzenesulfonamide (II.15**).** A 20-mL vial was charged with DCE (0.25 mL), 1,1,1,3,3,3-hexafluoro-2-propanol (HFIP, 0.25 mL), 1,2-diodobenzene (**II.1n**, 5.0 mg, 0.015 mmol, 10 mol%),[†] $\text{CoCl}_2 \cdot 6\text{H}_2\text{O}$ (0.4 mg, 3 μmol , 2 mol%), tosyl-*N*-methoxy amine (**II.14**, 30.2 mg, 0.150 mmol, 1.00 equiv), benzene (160 μL , 1.79 mmol,

* When 1.0 equivalents of PhI were used, compound **II.13** was isolated in 76% yield.

[†] When 1.0 equivalents of 1,2-diodobenzene were used, compound **II.15** was isolated in 78% yield.

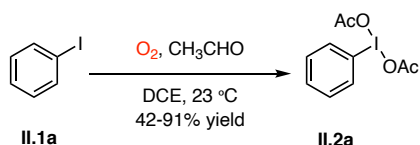
12.0 equiv), and trifluoroacetic acid (57.4 μL , 0.750 mmol, 5 equiv) and was fitted with a rubber septum. The reaction vial was purged with O_2 for 5 min and then acetaldehyde (11 μL , 0.20 mmol, 1.3 equiv) was added to the reaction mixture. The reaction mixture was stirred for 3 h at 23 $^\circ\text{C}$ under 1 atm O_2 (supplied via a balloon). An additional portion of acetaldehyde (11 μL , 0.20 mmol, 1.3 equiv) was added and the reaction mixture was stirred for 12 h at 23 $^\circ\text{C}$ under 1 atm O_2 . Solvent was removed *in vacuo*. The residue was dissolved in CH_2Cl_2 (5 mL), excess solid NaHCO_3 was added, the mixture was filtered, and solvent was removed *in vacuo*. The residue was purified by column chromatography on SiO_2 using a 96:4 hexanes:ethyl acetate eluent to afford 32.4 mg of the title compound (**II.15**, 78% yield). ^1H NMR (δ , 23 $^\circ\text{C}$, CDCl_3): 7.43–7.41 (m, 2H), 7.27–7.26 (m, 3H), 7.22–7.21 (m, 2H), 7.13–7.11 (m, 2H), 3.89 (s, 3H), 2.42 (s, 3H) ppm. ^{13}C NMR (δ , 23 $^\circ\text{C}$, CDCl_3): 144.7, 140.9, 130.0, 129.6, 129.0, 128.3, 127.5, 123.5, 64.2, 21.7 ppm. The recorded spectral data are in good agreement with those reported in literature.

Optimization of Aerobic Oxidation of Iodobenzene



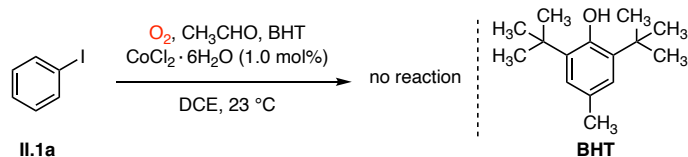
Representative Procedure. A 20-mL scintillation vial was charged with DCE (2.0 mL), iodobenzene (**II.1a**, 83.8 mg, 0.411 mmol, 1.00 equiv), and $\text{CoCl}_2 \cdot 6\text{H}_2\text{O}$ (0.9 mg, 0.004 mmol, 1 mol%) and was fitted with a rubber septum. The reaction vessel was purged with O_2 for 5 min before acetaldehyde (224 μL , 4.07 mmol, 9.90 equiv) was added in one portion. The reaction mixture was stirred under 1 atm O_2 , delivered by inflated balloon, at 23 $^\circ\text{C}$ for 16 h. Solvent was removed *in vacuo* and the crude residue was analyzed by ^1H NMR.

Evaluation of Aerobic Oxidation of Iodobenzene in the Absence of A Radical Initiator



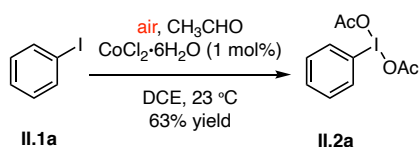
A 20-mL scintillation vial was charged with DCE (2.0 mL) and iodobenzene (83.8 mg, 0.411 mmol, 1.00 equiv) and was fitted with a rubber septum. The reaction vessel was purged with O_2 for 5 min before acetaldehyde (224 μL , 4.07 mmol, 9.90 equiv) was added in one portion. The reaction mixture was stirred under 1 atm O_2 , delivered by inflated balloon, at 23 $^\circ\text{C}$ for 16 h. Removal of the solvent *in vacuo* afforded the title compound (41-91% yield). ^1H NMR (δ , 23 $^\circ\text{C}$, CDCl_3): 8.09 (d, $J = 7.3$ Hz, 2H), 7.63-7.47 (m, 3H), 2.01 (s, 6H).

Evaluation of Aerobic Oxidation of Iodobenzene in the Presence of BHT



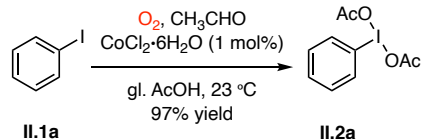
A 20-mL scintillation vial was charged with DCE (2.0 mL), iodobenzene (**II.1a**, 83.8 mg, 0.411 mmol, 1.00 equiv), BHT (89 mg, 4.039 mmol, 10.00 equiv), and $\text{CoCl}_2 \cdot 6\text{H}_2\text{O}$ (0.9 mg, 0.004 mmol, 1 mol%) and was fitted with a rubber septum. The reaction vessel was purged with O_2 for 5 min before acetaldehyde (224 μL , 4.07 mmol, 9.90 equiv) was added in one portion. The reaction mixture was stirred under 1 atm O_2 , delivered by inflated balloon, at 23 $^\circ\text{C}$ for 16 h. Removal of the solvent *in vacuo* and ^1H NMR analysis indicated that iodobenzene, not iodobenzene diacetate, was present.

Aerobic Oxidation of Iodobenzene with Air as O_2 Source



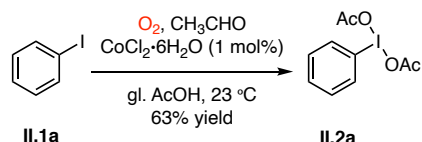
A 20-mL scintillation vial was charged with DCE (2.0 mL), iodobenzene (**II.1a**, 83.8 mg, 0.411 mmol, 1.00 equiv), and $\text{CoCl}_2 \cdot 6\text{H}_2\text{O}$ (0.9 mg, 0.004 mmol, 1 mol%) and was fitted with a rubber septum. Then acetaldehyde (224 μL , 4.07 mmol, 9.90 equiv) was added in one portion. The reaction mixture was stirred under air, delivered by inflated balloon, at 23 $^\circ\text{C}$ for 16 h. Solvent was removed *in vacuo* and the crude residue was analyzed by ^1H NMR (**II.2a**, 63% yield).

Gram-Scale Synthesis of Iodobenzene Diacetate (II.2a)



A 20-mL scintillation vial was charged with glacial AcOH (6 mL), iodobenzene (**II.1a**, 1.04 g, 5.10 mmol, 1.00 equiv), and CoCl₂·6H₂O (6.7 mg, 0.028 mmol, 0.50 mol%) and was fitted with a rubber septum. The reaction vessel was purged with O₂ for 5 min before acetaldehyde (1.00 mL, 17.8 mmol, 3.54 equiv) was added in one portion. The reaction mixture was stirred under 1 atm O₂, delivered by inflated balloon, at 23 °C for 6 h. Then another portion of acetaldehyde (1.00 mL, 17.8 mmol, 3.54 equiv) and CoCl₂·6H₂O (6.7 mg, 0.028 mmol, 0.50 mol%) were dissolved in 1 mL glacial AcOH and delivered to the reaction mixture via a syringe. It was then stirred under 1 atm O₂, delivered by inflated balloon, at 23 °C for 12 h. The reaction mixture was diluted with CH₂Cl₂, washed with 5% sodium bicarbonate solution, water and brine. The organic layer was dried over MgSO₄ and solvent was removed *in vacuo* to afford 1.59 g of iodobenzene diacetate (**II.2a**) as a white solid (97% yield). Product was identified with ¹H NMR.

10 Gram Scale Synthesis of Iodobenzene Diacetate (II.2a)



A 20-mL scintillation vial was charged with glacial AcOH (30 mL), iodobenzene (**II.1a**, 10.0 g, 49.0 mmol, 1.00 equiv), and CoCl₂·6H₂O (29.1 mg, 0.122 mmol, 0.25 mol%) and was fitted with a rubber septum. The reaction vessel was purged with O₂ for 5 min before acetaldehyde (10.0 mL, 178 mmol, 3.64 equiv) was added in one portion. The reaction mixture was stirred under

1 atm O₂, delivered by inflated balloon, at 23 °C for 6 h. Then three portions of acetaldehyde (10.0 mL, 178 mmol, 3.64 equiv) and CoCl₂·6H₂O (29.1 mg, 0.122 mmol, 0.25 mol%) were dissolved in 5 mL glacial AcOH each time and delivered to the reaction mixture via a syringe in an interval of 8h and stirred under 1 atm O₂, delivered by inflated balloon, at 23 °C. It was then stirred for 6h more after all addition under 1 atm O₂, delivered by inflated balloon, at 23 °C. The reaction mixture was diluted with CH₂Cl₂, washed with 5% sodium bicarbonate solution, water and brine. The organic layer was dried over MgSO₄ and solvent was removed *in vacuo* to afford 9.92 g of iodobenzene diacetate (**II.2a**) as a white solid (63% yield). Product was identified with ¹H NMR.

Kinetics of Iodobenzene Oxidation in CDCl₃

Measurement of aerobic oxidation kinetics of iodobenzene in CDCl₃ with no added initiator. A 20-mL scintillation vial was charged with CDCl₃ (4.0 mL) and iodobenzene (**II.1a**, 163.2 mg, 0.800 mmol, 1.00 equiv) and was fitted with a rubber septum. The reaction vessel was purged with O₂ for 5 min. An aliquot (0.200 mL) was removed and the ¹H NMR spectrum was recorded. Acetaldehyde (450 μL, 8.04 mmol, 10.1 equiv) was added to the reaction vessel and the reaction mixture was stirred at 23 °C under 1 atm O₂, delivered by inflated balloon. Aliquots (0.200 mL) were removed periodically for ¹H NMR analysis. Monitoring was continued until the reaction had reached completion, as evidenced by the disappearance of ¹H NMR resonances attributable to iodobenzene. Data and spectra are collected in Figure II-9.

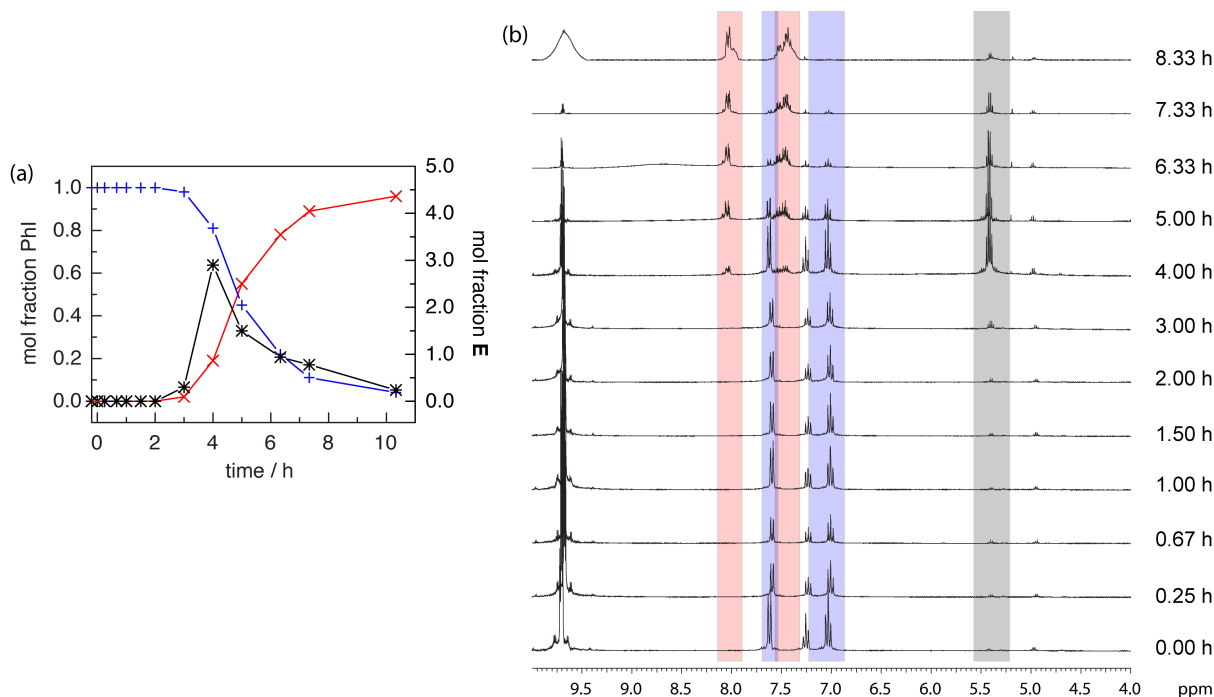


Figure II-9. Measurement of aerobic oxidation kinetics of iodobenzene in CDCl_3 with no added initiator. (a) Mol fraction of PhI (+), $\text{PhI}(\text{OAc})_2$ (x), and peroxy E (*) as a function of time for oxidation of PhI in CDCl_3 at 23 °C without $\text{CoCl}_2 \cdot 6\text{H}_2\text{O}$. (b) Stacked ^1H NMR spectra obtained periodically during the oxidation of PhI with signals attributable to PhI (—), $\text{PhI}(\text{OAc})_2$ (—), and peroxy E (—) highlighted.

Measurement of aerobic oxidation kinetics of iodobenzene in CDCl_3 with initiator. A 20-mL scintillation vial was charged with CDCl_3 (4.0 mL), iodobenzene (**II.1a**, 163.2 mg, 0.800 mmol, 1.00 equiv), and $\text{CoCl}_2 \cdot 6\text{H}_2\text{O}$ (1.0 mg, 7.70 μmol , 1 mol%) and fitted with a rubber septum. The reaction vessel was purged with O_2 for 5 min. An aliquot (0.200 mL) was removed and the ^1H NMR spectrum was recorded. Acetaldehyde (450 μL , 8.04 mmol, 10.1 equiv) was added to the reaction vessel and the reaction mixture was stirred at 23 °C under 1 atm O_2 , delivered by inflated balloon. Aliquots (0.200 mL) were removed periodically for ^1H NMR analysis. Monitoring was continued until the reaction had reached completion, as evidenced by the disappearance of ^1H NMR resonances attributable to iodobenzene. Data and spectra are collected in Figure II-10.

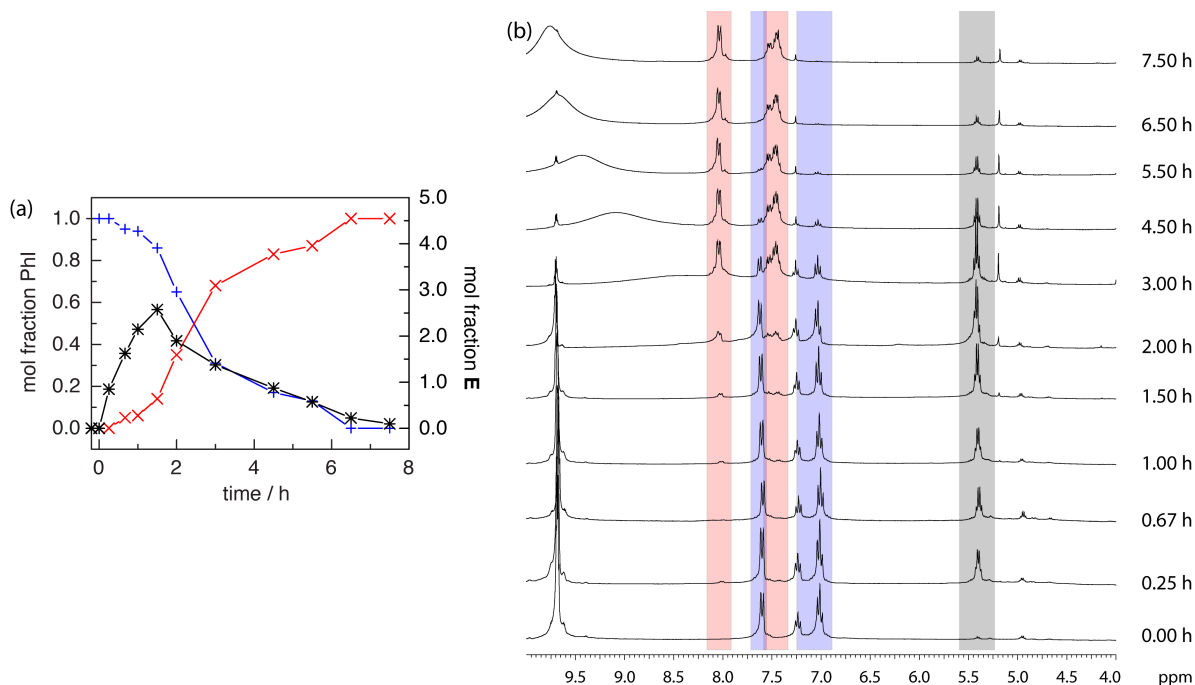


Figure II-10. Measurement of aerobic oxidation kinetics of iodobenzene in CDCl₃ with initiator. (a) Mol fraction of PhI (+), PhI(OAc)₂ (x), and peroxy E (*) as a function of time for oxidation of PhI in CDCl₃ at 23 °C in the presence of CoCl₂·6H₂O (1 mol%). (b) Stacked ¹H NMR spectra obtained periodically during the oxidation of PhI with signals attributable to PhI (—), PhI(OAc)₂ (—), and peroxy E (—) highlighted.

Kinetics of 4-Iodotoluene Oxidation in CDCl₃

Measurement of aerobic oxidation kinetics of 4-iodotoluene in CDCl₃ with no added initiator. A 20-mL scintillation vial was charged with CDCl₃ (4.0 mL) and 4-iodotoluene (**II.1c**, 174.4 mg, 0.800 mmol, 1.00 equiv) and was fitted with a rubber septum. 1,4-Dibromobenzene (94.4 mg, 0.400 mmol) was added to the reaction mixture as internal standard. The reaction vessel was purged with O₂ for 5 min. An aliquot (0.200 mL) was removed and the ¹H NMR spectrum was recorded. Acetaldehyde (450 μL, 8.04 mmol, 10.1 equiv) was added to the reaction vessel and the reaction mixture was stirred at 23 °C under 1 atm O₂, delivered by inflated balloon. Aliquots (0.200 mL) were removed periodically for ¹H NMR analysis. Monitoring was continued until the

reaction had reached completion, as evidenced by the disappearance of ^1H NMR resonances attributable to 4-iodotoluene. Data and spectra are collected in Figure II-11.

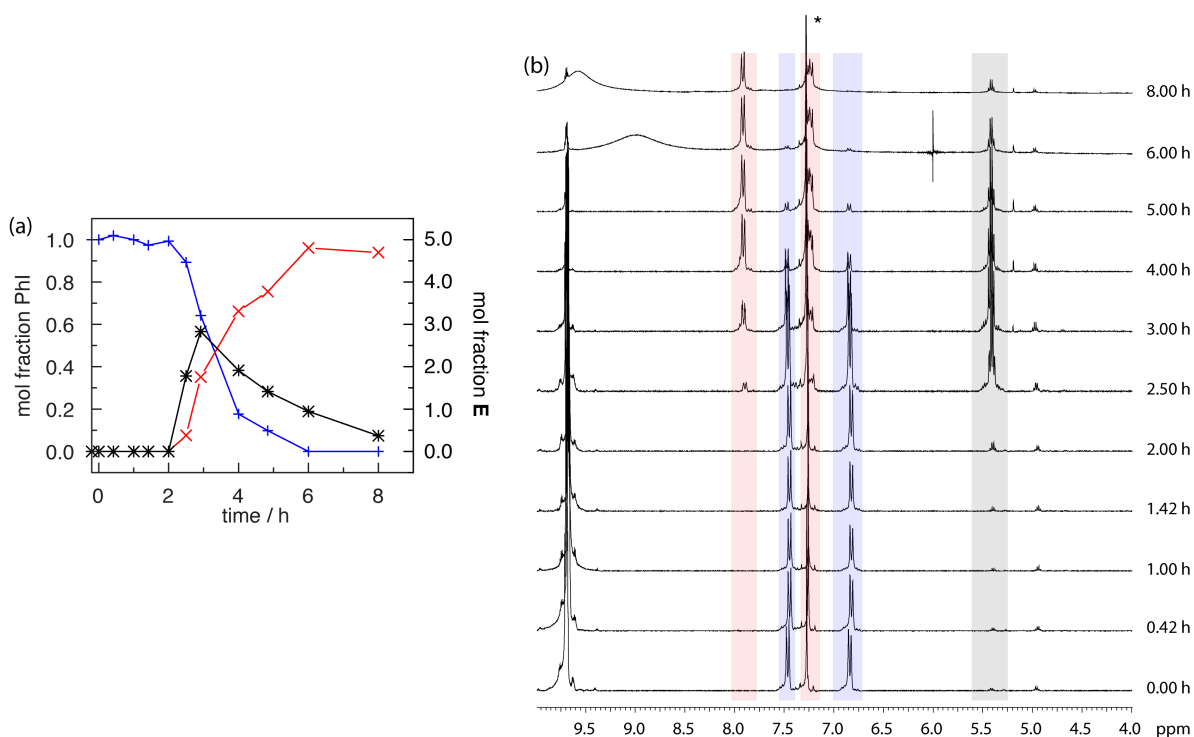


Figure II-11. Kinetics experiments for aerobic oxidation of 4-iodotoluene with no added initiator. (a) Mol fraction of 4-iodotoluene (+), II.2c (x), and peroxy E (*) as a function of time for oxidation of 4-iodotoluene in CDCl_3 at 23°C in the presence of $\text{CoCl}_2\cdot 6\text{H}_2\text{O}$ (1 mol%). (b) Stacked ^1H NMR spectra obtained periodically during the oxidation of 4-iodotoluene with signals attributable to 4-iodotoluene (—), $\text{PhI}(\text{OAc})_2$ (—), and peroxy E (—) highlighted; * = 1,4-dibromobenzene added as internal standard.

Measurement of aerobic oxidation kinetics of 4-iodotoluene in CDCl_3 with initiator.

A 20-mL scintillation vial was charged with CDCl_3 (4.0 mL), 4-iodotoluene (II.1c, 174.4 mg, 0.800 mmol, 1.00 equiv), and $\text{CoCl}_2\cdot 6\text{H}_2\text{O}$ (1.0 mg, 7.70 μmol , 1 mol%) and was fitted with a rubber septum. 1,4-Dibromobenzene (94.4 mg, 0.400 mmol) was added to the reaction mixture as internal standard. The reaction vessel was purged with O_2 for 5 min. An aliquot (0.200 mL) was removed and the ^1H NMR spectrum was recorded. Acetaldehyde (450 μL , 8.04 mmol, 10.1 equiv) was added to the reaction vessel and the reaction mixture was stirred at 23°C under 1 atm

O₂, delivered by inflated balloon. Aliquots (0.200 mL) were removed periodically for ¹H NMR analysis. Monitoring was continued until the reaction had reached completion, as evidenced by the disappearance of ¹H NMR resonances attributable to 4-iodotoluene. Data and spectra are collected in Figure II-12.

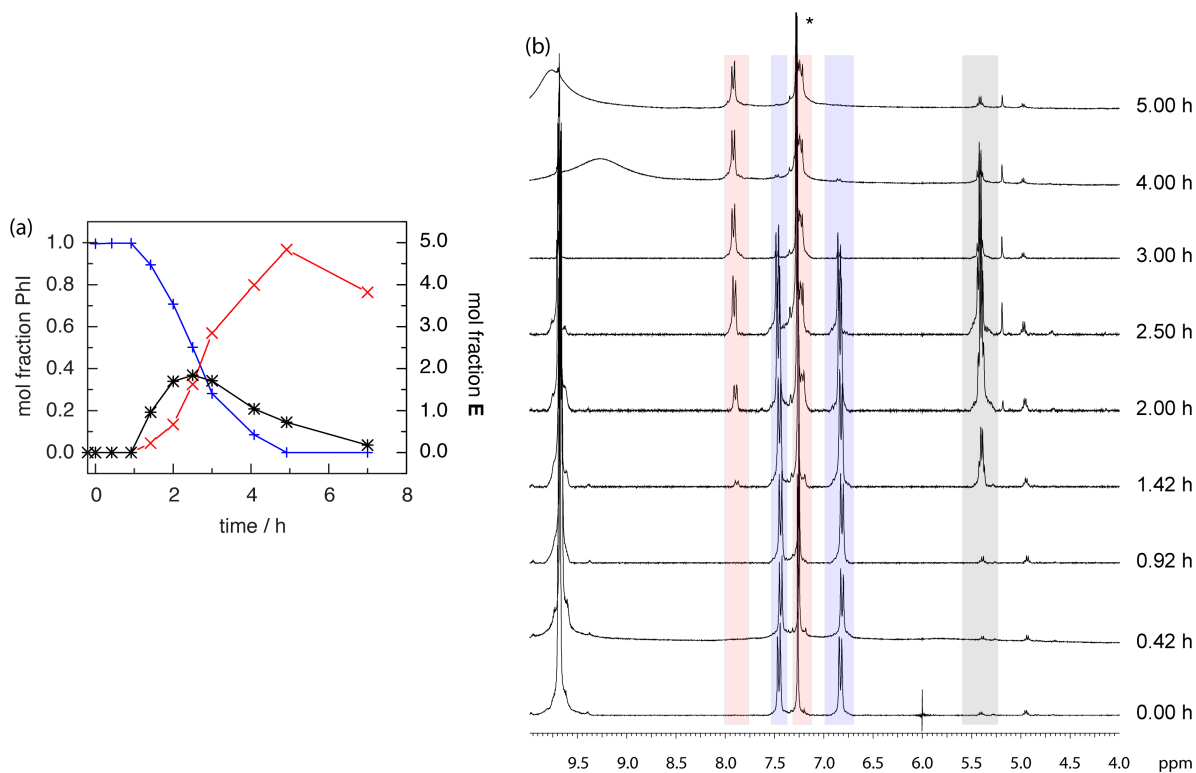


Figure II-12. Measurement of aerobic oxidation kinetics of 4-iodotoluene in CDCl₃ with initiator. (a) Mol fraction of 4-iodotoluene (+), II.1c (x), and peroxy E (*) as a function of time for oxidation of 4-iodotoluene in CDCl₃ at 23 °C in the presence of CoCl₂·6H₂O (1 mol%). (b) Stacked ¹H NMR spectra obtained periodically during the oxidation of 4-iodotoluene with signals attributable to 4-iodotoluene (—), PhI(OAc)₂ (—), and peroxy E (—) highlighted; * = 1,4-dibromobenzene added as internal standard.

Kinetics of Iodobenzene Oxidation in AcOH- d_4

Measurement of aerobic oxidation kinetics of iodobenzene in AcOH- d_4 with no added initiator. A 20-mL scintillation vial was charged with AcOH- d_4 (4.0 mL) and iodobenzene (**II.1a**, 163.2 mg, 0.800 mmol, 1.00 equiv) and was fitted with a rubber septum. Mesitylene (50 μ L, 0.359 mmol) was added to the reaction mixture as internal standard. The reaction vessel was purged with O₂ for 5 min, and an aliquot (0.200 mL) was removed and ¹H NMR spectroscopy was recorded. Acetaldehyde (450 μ L, 8.04 mmol, 10.1 equiv) was added to the reaction vessel and the reaction mixture was stirred at 23 °C under 1 atm O₂, delivered by inflated balloon. Monitoring was continued up to 10 h. Data are collected in Figure II-13.

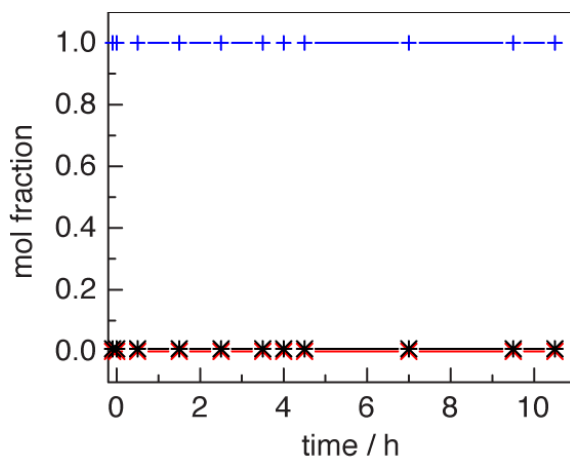


Figure II-13. Kinetics experiments for aerobic oxidation of iodobenzene with no added initiator. (a) Mol fraction of PhI (+), PhI(OAc)₂ (x), and peroxy E (*) as a function of time for oxidation of PhI in AcOH- d_4 at 23 °C without CoCl₂·6H₂O (1 mol%). Under these conditions, oxidation of PhI is not observed.

Measurement of aerobic oxidation kinetics of iodobenzene in AcOH- d_4 with initiator. A 20-mL scintillation vial was charged with AcOH- d_4 (4.0 mL), iodobenzene (**II.1a**, 163.2 mg, 0.800 mmol, 1.00 equiv), and CoCl₂·6H₂O (1.0 mg, 7.70 μ mol, 1 mol%) and was fitted with a rubber septum. Mesitylene (50 μ L, 0.359 mmol) was added to the reaction mixture as internal standard.

The reaction vessel was purged with O₂ for 5 min, and an aliquot (0.200 mL) was removed and ¹H NMR spectroscopy was recorded. Acetaldehyde (450 μL, 8.04 mmol, 10.1 equiv) was added to the reaction vessel and the reaction mixture was stirred at 23 °C under 1 atm O₂, delivered by inflated balloon. Monitoring was continued until the reaction had reached completion, as evidenced by the disappearance of ¹H NMR resonances attributable to iodobenzene. Data and spectra are collected in Figure II-14.

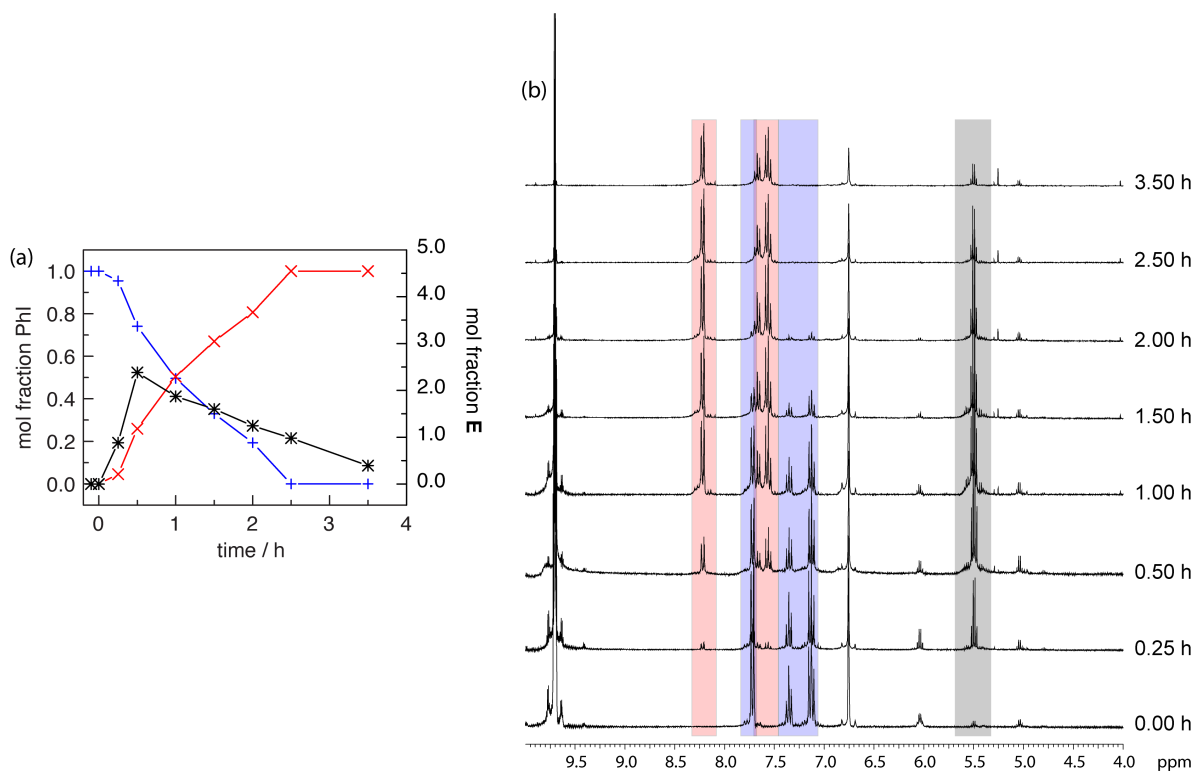


Figure II-14. Measurement of aerobic oxidation kinetics of PhI in AcOH-*d*₄ with initiator. (a) Mol fraction of PhI (+), PhI(OAc)₂ (x), and peroxy E (*) as a function of time for oxidation of PhI in AcOH-*d*₄ at 23 °C in the presence of CoCl₂·6H₂O (1 mol%). (b) Stacked ¹H NMR spectra obtained periodically during the oxidation of PhI with signals attributable to PhI (—), PhI(OAc)₂ (—), and peroxy E (—) highlighted.

Characterization of Peroxo Intermediate E

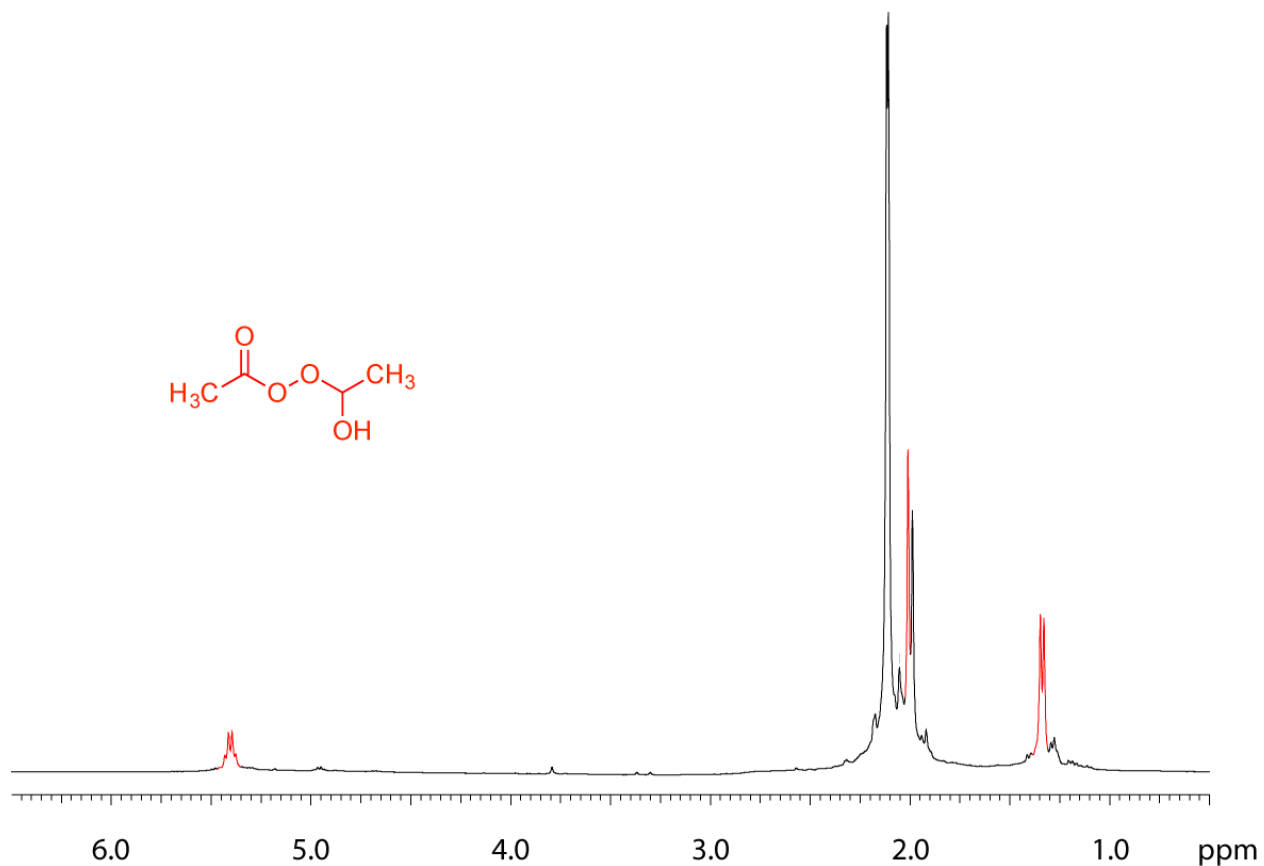


Figure II-15. NMR spectrum collected during aerobic oxidation of PhI with the peaks attributable to peroxo E highlighted in red. The highlighted peaks are coincident with a spectrum obtained by combining AcOOH with CH₃CHO.

Analysis by Mass Spectrometry

***In situ* characterization during iodobenzene Oxidation.** A 20-mL scintillation vial was charged with CHCl_3 (1.50 mL), iodobenzene (41.0 mg, 0.201 mmol, 1.00 equiv), and $\text{CoCl}_2 \cdot 6\text{H}_2\text{O}$ (0.3 mg, 2.31 μmol , 1 mol%) and was fitted with a rubber septum. The reaction vessel was purged with O_2 for 5 min. Acetaldehyde (115 μL , 2.06 mmol, 10.2 equiv) was added to the reaction vessel and the reaction mixture was stirred at 23 $^\circ\text{C}$ under 1 atm O_2 , delivered by inflated balloon, for 1.5 h which the peroxy **E** was in the maximum concentration determined by kinetics measurement. At this time, the crude reaction mixture was injected for HRMS analysis. HRMS (ESI⁺): calcd. for $\text{C}_4\text{H}_8\text{NaO}_4$ [M+Na]⁺ m/z 143.0320. Found: 143.0318. Data is summarized in Figure II-16a.

Characterization of **E from autoxidation with iodobenzene present.** A 20-mL scintillation vial was charged with CHCl_3 (1.50 mL) and $\text{CoCl}_2 \cdot 6\text{H}_2\text{O}$ (0.3 mg, 2.31 μmol , 1 mol%) and was fitted with a rubber septum. The reaction vessel was purged with O_2 for 5 min. Acetaldehyde (115 μL , 2.06 mmol, 10.2 equiv) was added to the reaction vessel and the reaction mixture was stirred at 23 $^\circ\text{C}$ under 1 atm O_2 , delivered by inflated balloon, for 1.5 h which the peroxy **E** was in the maximum concentration determined by kinetics measurement. At this time, the crude reaction mixture was injected for HRMS analysis. HRMS (ESI⁺): calcd. for $\text{C}_4\text{H}_8\text{NaO}_4$ [M+Na]⁺ m/z 143.0320. Found: 143.0318. Data is summarized in Figure II-16b.

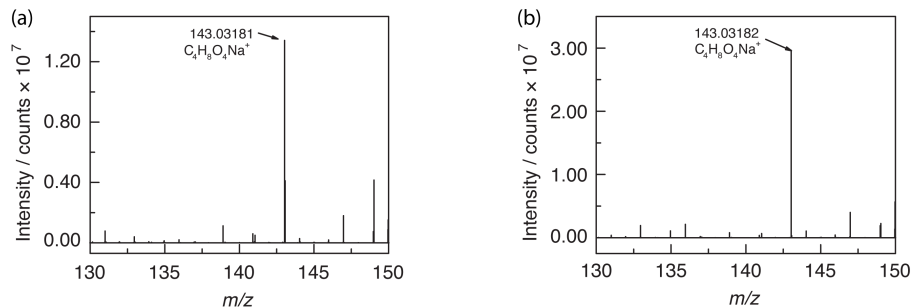


Figure II-16. Mass spectrometry analysis of (a) the reaction mixture of CH_3CHO , PhI , $\text{CoCl}_2 \cdot 6\text{H}_2\text{O}$, and O_2 and (b) the reaction mixture of CH_3CHO , $\text{CoCl}_2 \cdot 6\text{H}_2\text{O}$, and O_2 . The presence of Baeyer-Villiger intermediate **E** is evident in both analyses.

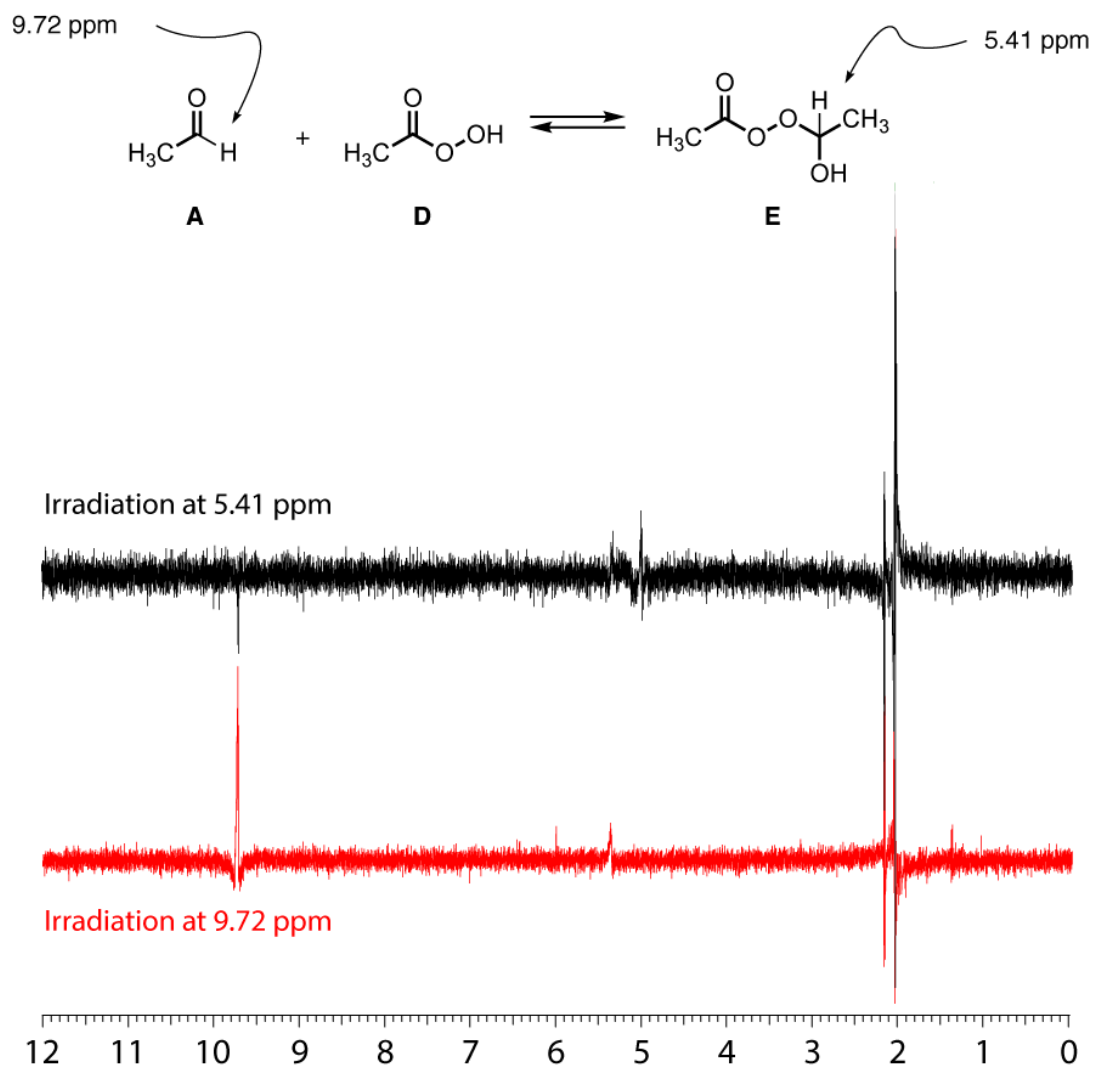


Figure II-17. ¹H NMR plots of magnetization transfer experiment that demonstrates that acetaldehyde and intermediate E are in rapid equilibrium on the NMR time scale. Top: Irradiation of the methine signal of compound E (resonance at 5.41 ppm) results in selective enhancement of the aldehydic proton signal of acetaldehyde (9.72 ppm). Bottom: Irradiation of the aldehydic signal of acetaldehyde (resonance at 9.72 ppm) results in selective enhancement of the methine proton signal of compound E (5.41 ppm).

Spectra of New Compounds

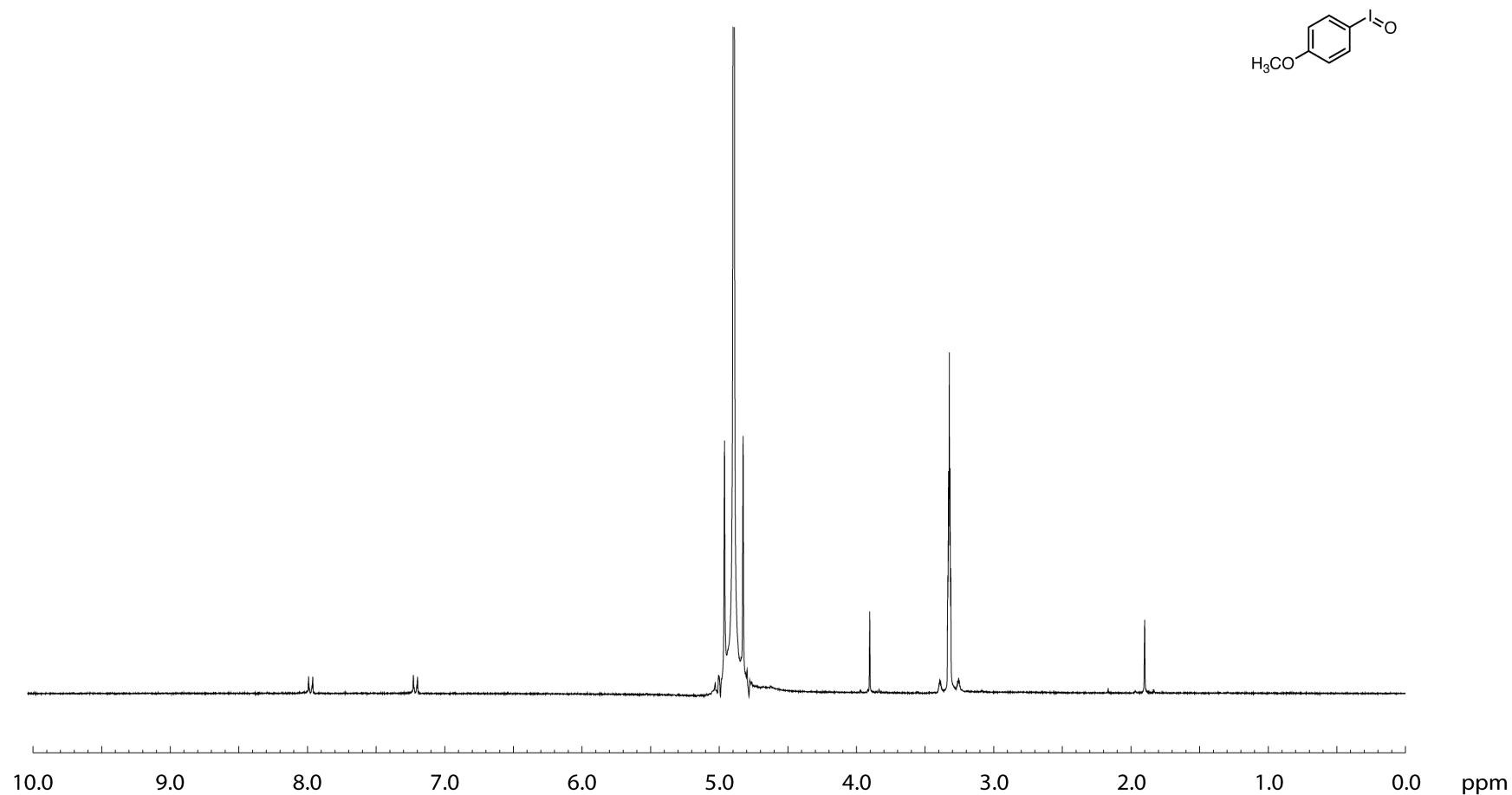


Figure II-18. ^1H NMR spectrum of compound **II.3b** recorded in CD_3OD at $23\text{ }^\circ\text{C}$. The solvent signal has been truncated to zoom in on peaks of interest. In CD_3OD , compound **II.3b** is likely converted to a *bis*-methoxy iodine; most iodosylbenzene derivatives are insufficiently soluble for ^1H NMR spectroscopy in the absence of coordinating solvents.

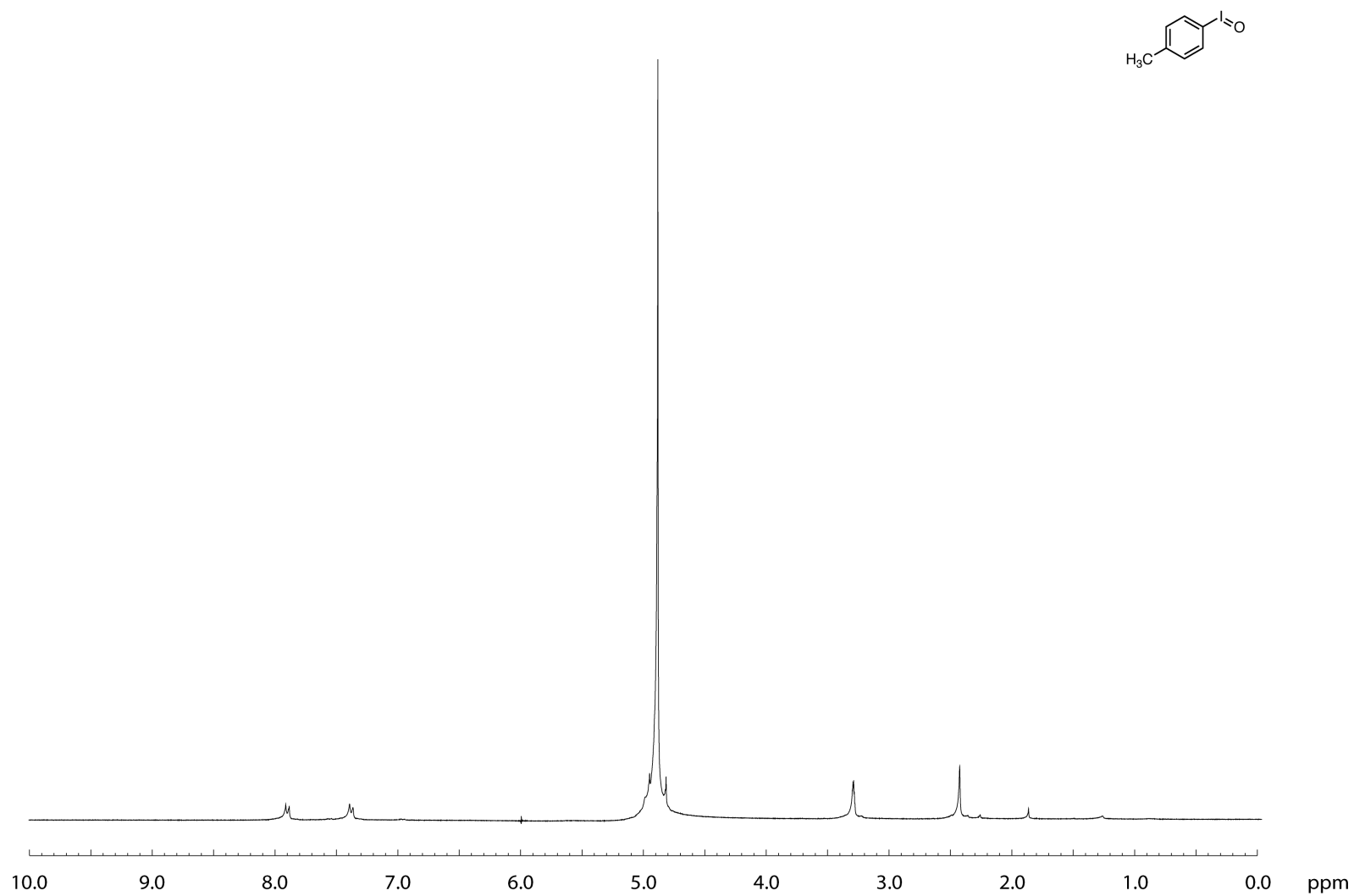


Figure II-19. ^1H NMR spectrum of compound **II.3c** recorded in CD_3OD at $23\text{ }^\circ\text{C}$. The solvent signal has been truncated to zoom in on peaks of interest. In CD_3OD , compound **II.3c** is likely converted to a *bis*-methoxy iodine; most iodosylbenzene derivatives are insufficiently soluble for ^1H NMR spectroscopy in the absence of coordinating solvents.

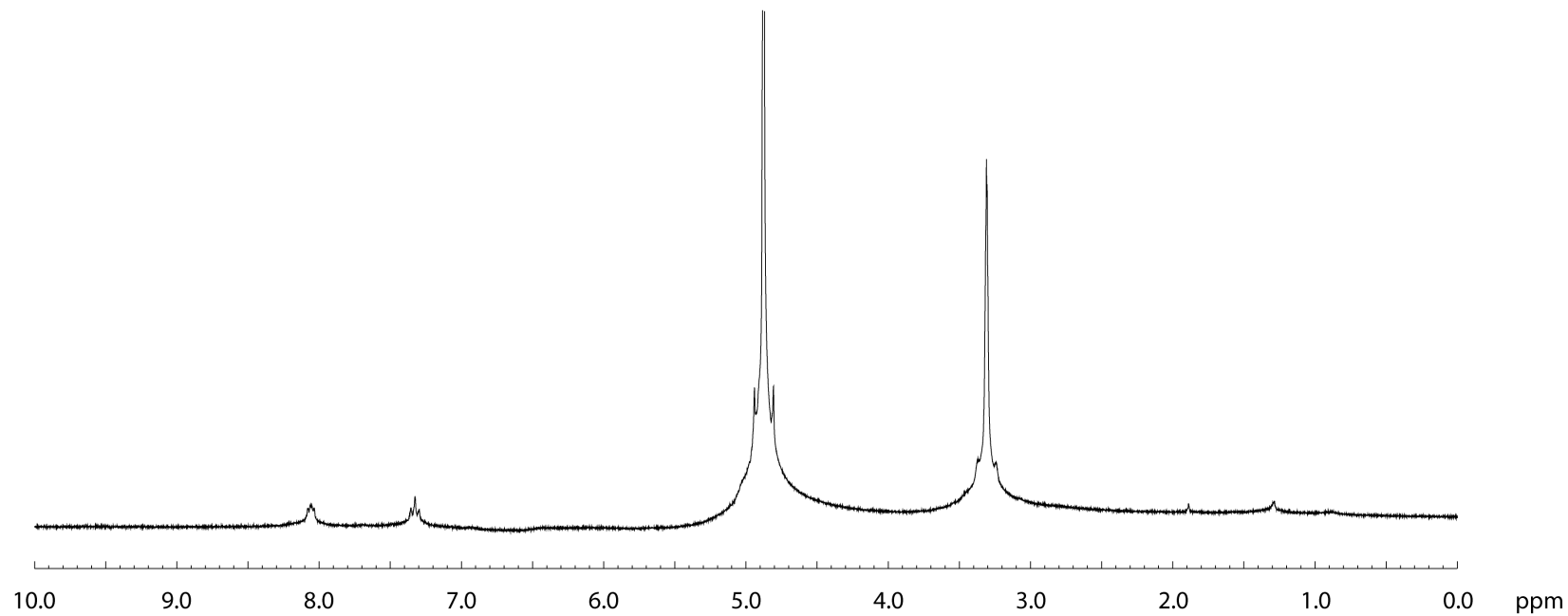
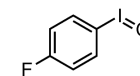


Figure II-20. ^1H NMR spectrum of compound **II.3d** recorded in CD_3OD at $23\text{ }^\circ\text{C}$. The solvent signal has been truncated to zoom in on peaks of interest. In CD_3OD , compound **II.3d** is likely converted to a *bis*-methoxy iodine; most iodosylbenzene derivatives are insufficiently soluble for ^1H NMR spectroscopy in the absence of coordinating solvents.

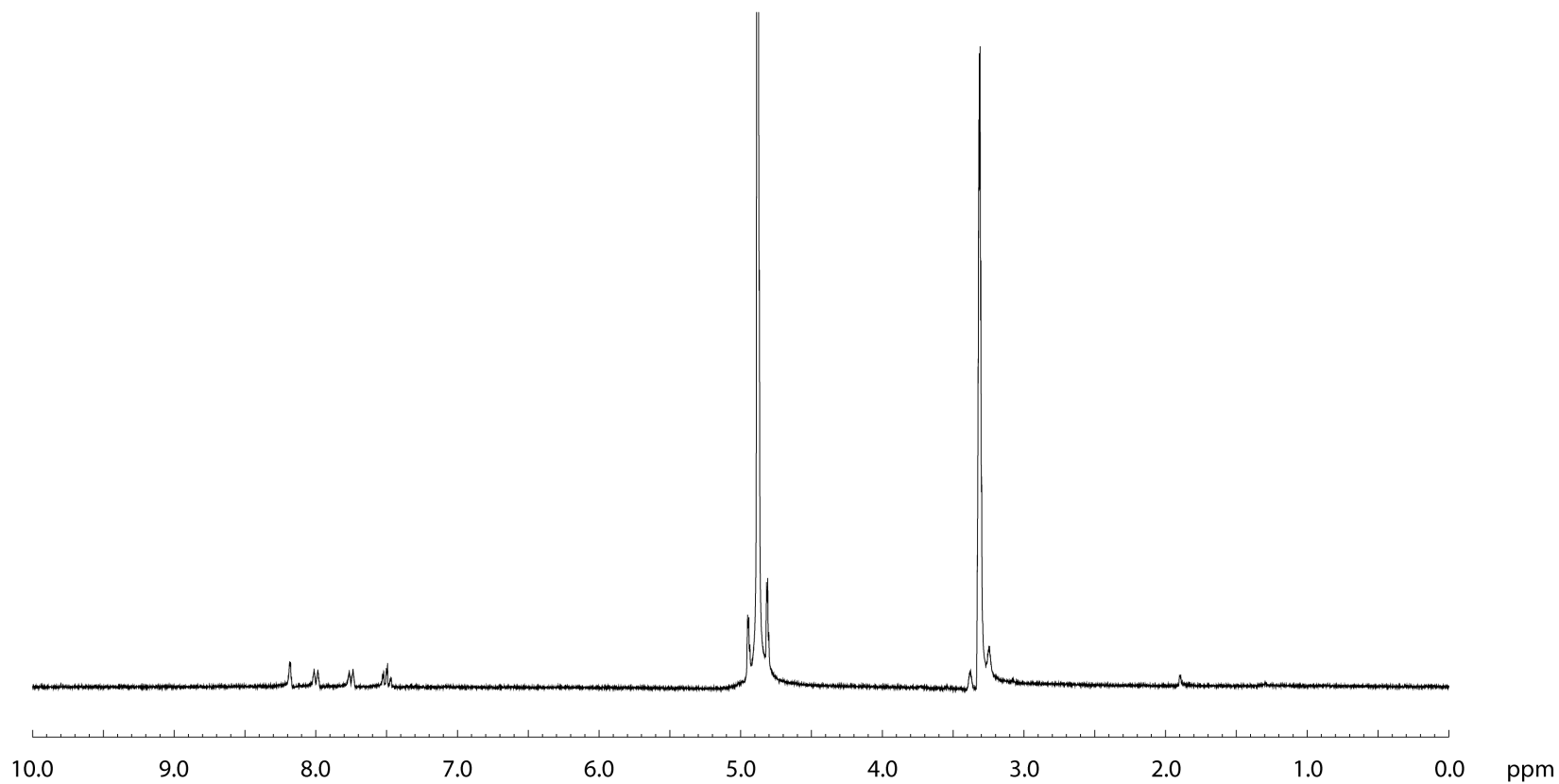
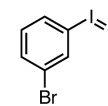


Figure II-21. ^1H NMR spectrum of compound **II.3e** recorded in CD_3OD at $23\text{ }^\circ\text{C}$. The solvent signal has been truncated to zoom in on peaks of interest. In CD_3OD , compound **II.3e** is likely converted to a *bis*-methoxy iodine; most iodosylbenzene derivatives are insufficiently soluble for ^1H NMR spectroscopy in the absence of coordinating solvents.

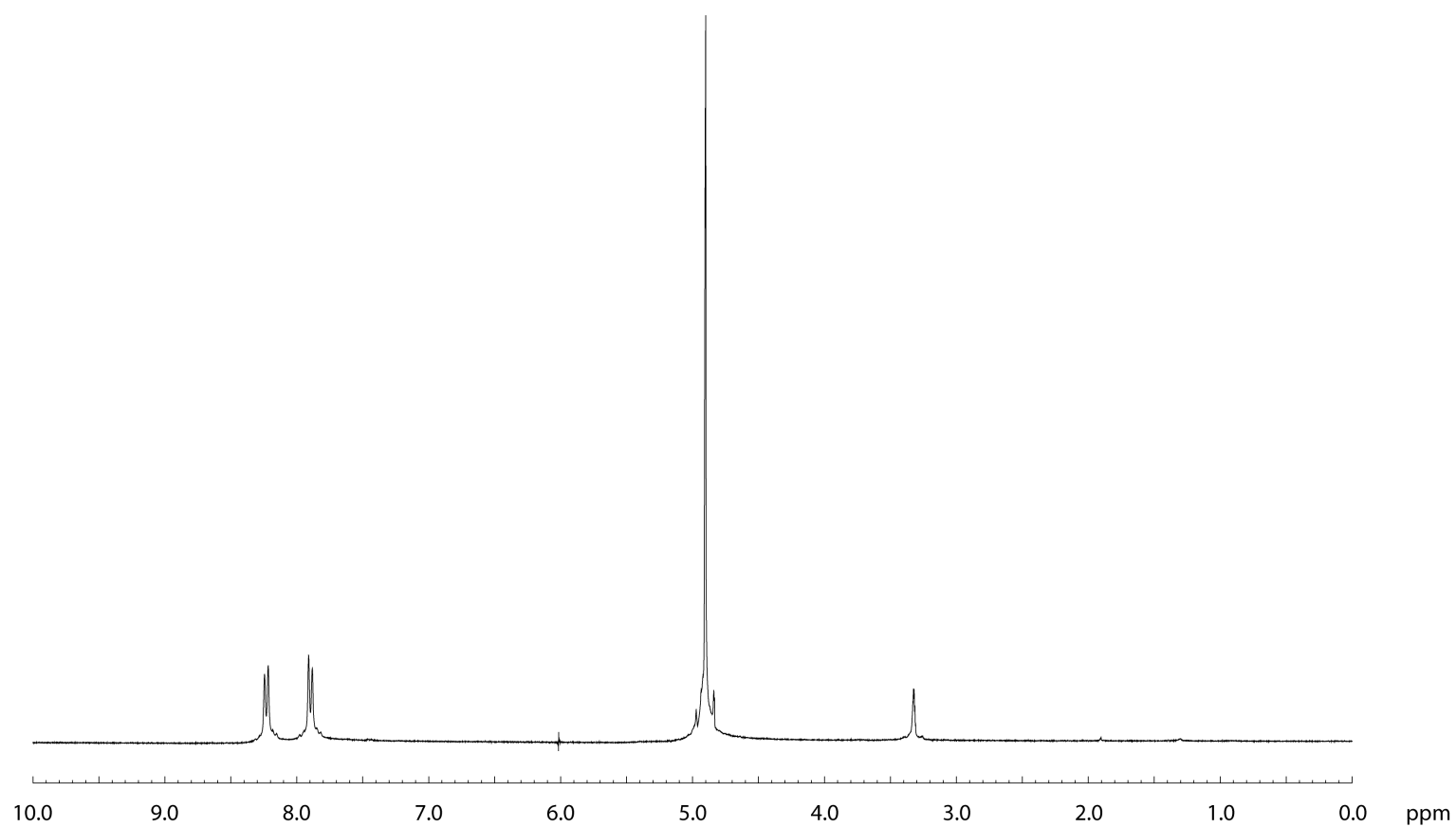
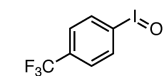


Figure II-22. ^1H NMR spectrum of compound **II.3f** recorded in CD_3OD at $23\text{ }^\circ\text{C}$. The solvent signal has been truncated to zoom in on peaks of interest. In CD_3OD , compound **II.3f** is likely converted to a *bis*-methoxy iodine; most iodosylbenzene derivatives are insufficiently soluble for ^1H NMR spectroscopy in the absence of coordinating solvents.

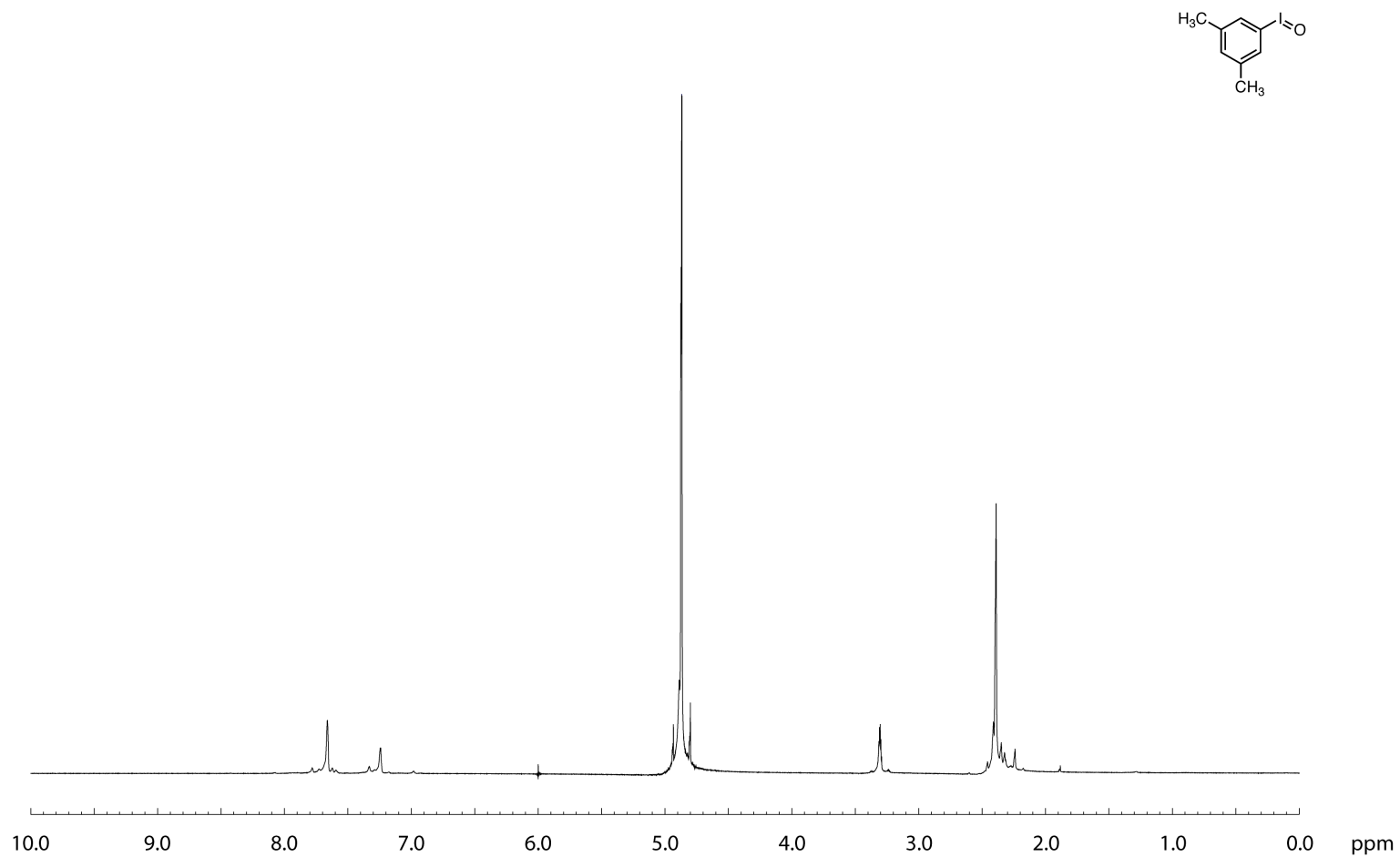


Figure II-23. ^1H NMR spectrum of compound **II.3g** recorded in CD_3OD at $23\text{ }^\circ\text{C}$. The solvent signal has been truncated to zoom in on peaks of interest. In CD_3OD , compound **II.3g** is likely converted to a *bis*-methoxy iodine; most iodosylbenzene derivatives are insufficiently soluble for ^1H NMR spectroscopy in the absence of coordinating solvents.

CHAPTER III

OXIDATION CATALYSIS BY AN AEROBICALLY GENERATED DESS-MARTIN PERIODINANE ANALOGUE*

III.1 Introduction

O₂ is a conceptually ideal oxidant for synthesis,^{11, 121, 122} but challenges such as 1) the proclivity of O₂ to participate in unselective single-electron transfer chemistry, 2) the kinetic barriers associated with reaction of the triplet ground state of O₂ with singlet organic molecules,^{3, 4} and 3) the difficulty in choreographing four-electron O₂ reduction with two-electron substrate oxidation, often prevent application of O₂ as a selective reagent in organic synthesis.^{5, 6} In some cases, redox mediators—small molecules that participate in predictable oxidation chemistry with O₂—have enabled O₂ reduction to be coupled to substrate oxidation chemistry. For example, the hydroquinone–quinone redox couple has been exploited to couple O₂ reduction with a variety of Pd-catalyzed processes.^{126, 210} In the absence of general strategies to utilize O₂ directly, an array of synthetic two-electron oxidants, such as hypervalent iodine reagents, have been developed. Generally, these reagents are not directly derived from O₂ and use of these reagents results in the formation of stoichiometric quantities of chemical waste. The need for more sustainable methods for oxidation chemistry demands the development of new strategies and methods for O₂ utilization.

* Data, figures, and text in this chapter were adapted with permission from reference Maity, A.; Hyun, S.-M.; A. K. Wortman; Powers, D. C. *Angew. Chem. Int. Ed.* **2018**, *57*, 7205–7209, Copyright © 2018 the John Wiley and Sons, Inc. Maity, A.; Cardenal, A. D.; Gao, W.-Y.; Ashirov, R.; Hyun, S.-M.; Powers, D. C. *Inorg. Chem.* **2019**, *58*, 10543–10553, Copyright © 2019, American Chemical Society.

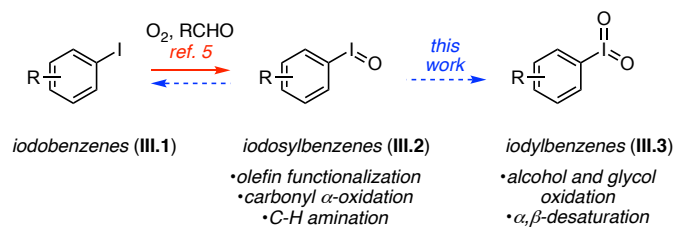


Figure III-1. Rapid disproportionation of aerobically generated iodosylbenzenes can enable aerobic oxidation via iodylbenzene intermediates.

We recently reported the aerobic oxidation of aryl iodides (III.1) to iodosylbenzenes (III.2) using strong oxidants generated during aldehyde autoxidation and applied the aerobically generated I(III) reagents to olefin functionalization, carbonyl α -oxidation, and N–H arylation.¹⁶³ Contemporaneously, Miyamoto and Uchiyama *et al.* reported iodoarene-catalyzed aerobic glycol cleavage reactions and Hofmann rearrangements under similar aldehyde-promoted aerobic oxidation conditions.²¹¹ We reasoned that the scope of aerobic oxidation chemistry that can be achieved via hypervalent iodine intermediates would be substantially expanded if the aerobic oxidation of iodobenzenes could be extended to the synthesis of I(V) reagents (iodylbenzenes, III.3). I(V) reagents,^{158, 212-217} such as Dess–Martin periodinane (DMP)^{218, 219} and 2-iodoxybenzoic acid (IBX),²²⁰ display complementary substrate oxidation chemistry as compared to iodosylbenzenes (III.2), and have been applied to the oxidation of primary and secondary alcohols,^{221, 222} 1,2-^{220, 223} and 1,4-diols,^{224, 225} and amines,^{226, 227} as well as the dehydrogenation of carbonyl compounds to generate α, β -unsaturated carbonyls,²²⁸⁻²³⁰ and benzylic C–H bond oxidation.²³¹ Currently, iodylbenzenes are prepared by the action of strong chemical oxidants, such as periodate, hypochlorite, dimethyldioxirane, or Oxone, in strongly acidic conditions,¹⁰⁶ or by the metal-catalyzed⁴² or high-temperature⁴³ disproportionation of iodosylbenzenes. The harsh reaction conditions and strong oxidants typically employed in the synthesis of I(V) reagents limit the utility of I(V) intermediates in catalysis.²³²⁻²³⁸ Herein, we demonstrate that aerobic oxidation of I(I) to

generate I(III) compounds can be coupled with facile disproportionation of I(III) to enable oxidation catalysis via iodylbenzene intermediates.²³⁹

III.2 Results and Discussions

III.2.1 Aerobic Synthesis of I(V) Reagents

During our initial investigation of the aerobic oxidation of iodobenzenes (**III.1**) to iodosylbenzenes (**III.2**), we noted that oxidation of 2-(*tert*-butylsulfonyl)iodobenzene (**III.1a**) afforded iodylbenzene **III.3a**, rather than the corresponding I(III) derivative **III.2a**.^{163, 183} Chelating substituents in the 2-position are frequently employed in hypervalent iodine chemistry to enhance solubility by breaking up I–O–I–O polymers that are common for iodosylbenzenes.²⁴⁰ To achieve reproducible aerobic oxidation chemistry, these investigations were carried out in the presence of CoCl₂ (1 mol%), which serves as an initiator of aldehyde autoxidation (Figure III-2).^{163, 241}

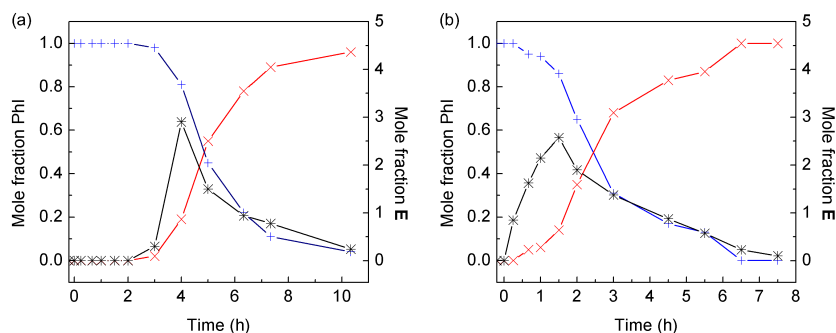


Figure III-2. Role of Co(II) salt in aerobic oxidation of aryl iodides. Mole fraction of PhI (—), PhI(OAc)₂ (—), and 1-hydroxyethyl ethaneperoxoate (**E**, —) as a function of time for oxidation of PhI in CDCl₃ with acetaldehyde at 23 °C (a) without CoCl₂·6H₂O (b) with CoCl₂·6H₂O. Without any initiator, irreproducible induction period for oxidation of aryl iodides is observed.

With interest in developing an aerobic synthesis of soluble I(V) reagents, we have investigated the aerobic oxidation of a family of iodobenzenes bearing potentially chelating

aerobically generated iodylbenzenes such as **III.3b** and **III.3e** were found to be less efficient reagents for cyclohexanol oxidation (entries 6 and 7, 0% and 66% yield of cyclohexanone, respectively).

To characterize the reactivity profile of **III.3a** as an oxidant for organic substrate functionalization, we canvassed the reactivity **III.3a** in a variety of reactions that are typical of IBX and DMP. While **III.3a** efficiently oxidizes secondary alcohols (Figure III-4a), it does not effect the dehydrogenation of the resulting carbonyl compounds to generate α,β -unsaturated carbonyls: Addition of excess **III.3a** to the oxidation of cyclohexanol, or treatment of cyclohexanone with **III.3a**, did not result in dehydrogenation to afford 2-cyclohexenone, even in the presence of additives such as dimethyl sulfoxide (DMSO) or *N*-oxides, which have previously been used to promote I(V)-mediated desaturation chemistry.²²⁸ Treatment of primary alcohols, such as benzyl alcohol (**III.6a**) and geraniol (**III.6b**), resulted in the corresponding aldehydes **III.7a** and **III.7b** in 99% and 81% yield, respectively (Figure III-4b). Compound **III.3a** effects oxidative cleavage of 1,2-diols—oxidation of hydroxybenzoin (**III.8**) with **III.3a** results in oxidative C–C cleavage to generate benzaldehyde (**III.9**) in 86% yield (Figure III-4c)—which is characteristic of the chemistry of DMP.²²³ In contrast, IBX typically provides access to dicarbonyls.²⁴² **III.3a** effects the oxidation of 1,4-diol **III.10** to lactone **III.11** in 60% yield, based on recovered starting materials. Compound **III.3a** does not promote benzylic C–H oxidation (for example, oxidation of ethylbenzene), which has been observed for some I(V) derivatives, but **III.3a** can be applied to the oxidative dehydrogenation of amines to generate imines (**III.13a** and **III.13b**), oximes (**III.13c**), and *N*-heterocycles (**III.13d**); see Figure III-4d.

Table III-1. Optimization table for I(V) mediated cyclohexanol oxidation. Iodylbenzene derivative **III.3a** was found to efficiently oxidize cyclohexanol in stoichiometric reactions, and iodobenzene **III.1a** is a competent oxidation catalyst.

Entry	Conditions	Solvent	T (°C)	ArI (equiv)	Initiator (1.0 mol%)	Yield
1	A	DMSO	23	III.3a (1.0)	-	0%
2	A	DMSO	50	III.3a (1.0)	-	5%
3	A	DMSO	70	III.3a (1.0)	-	25%
4	A	MeCN	70	III.3a (1.0)	-	0%
5	A	MeNO ₂	70	III.3a (1.0)	-	95%
6	A	MeNO ₂	70	III.3b (1.0)	-	0%
7	A	MeNO ₂	70	III.3e (1.0)	-	66%
8	B	MeNO ₂	70	III.1a (15 mol%)	CoCl ₂ ·6H ₂ O	86%
9	B	MeNO ₂	70	III.1a (15 mol%)	-	22%
10	B	MeNO ₂	70	III.1a (15 mol%)	Cu(OAc) ₂ · H ₂ O	30%
11	B	MeNO ₂	70	III.1a (15 mol%)	Mn(OAc) ₂ · 4H ₂ O	35%
12	B	MeNO ₂	70	III.1a (15 mol%)	CoCl ₂ ·6H ₂ O	77%
13	B	MeNO ₂	70	III.1a (15 mol%)	CoCl ₂ ·6H ₂ O	57%
14	B	MeNO ₂	70	-	CoCl ₂ ·6H ₂ O	15%
15	B	MeNO ₂	70	III.1e (15 mol%)	CoCl ₂ ·6H ₂ O	24%

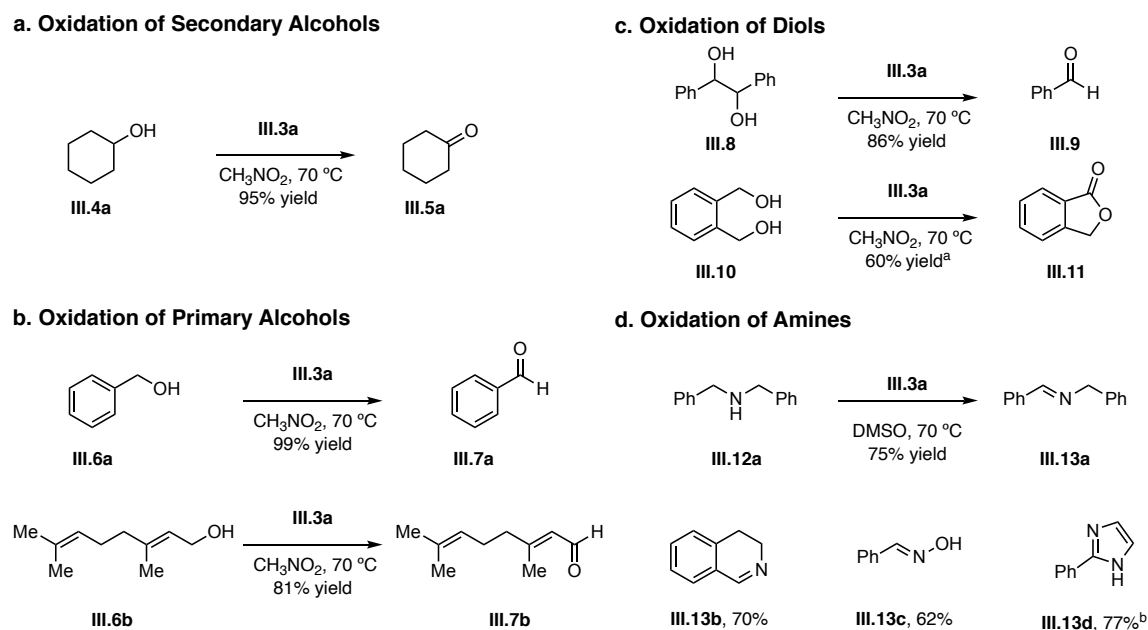


Figure III-4. Oxidation chemistry scope of aerobically generated iodylbenzene reagent **III.3a.** Compound **III.3a** oxidizes (a) secondary alcohols to ketones, (b) primary alcohols to aldehydes, (c) mediates glycol cleavage to aldehydes, oxidizes 1,4-diols to lactols, and (d) accomplishes dehydrogenative amine oxidation. ^ayield based on recovered starting material. ^bfrom 2-phenyl-4,5-dihydro-1*H*-imidazole.

Iodylbenzene-mediated oxidation reactions typically rely on stoichiometric amounts of I(V) reagents and we hypothesized that the strong oxidants (such as Oxone) typically needed to generate I(V) derivatives limit application of I(V) derivatives in catalysis. Further, we hypothesized that facile generation of I(V) derivatives (**III.3**) under our aerobic oxidation chemistry could be extended to I(V) oxidation catalysis and we turned our attention to the application of iodylbenzene **III.3a** as an intermediate in aerobic oxidation catalysis (Figure III-5 and III-6). To accomplish in situ aerobic oxidation at the elevated temperatures required for substrate oxidation (70 °C), acetaldehyde (bp = 20.2 °C) was replaced with *n*-butyraldehyde (bp = 74.8 °C). Examination of the impact of **III.1a** loading on the efficiency of cyclohexanol oxidation led us to pursue the following experiments with 15 mol% of **III.1a** as catalyst (Table III-1, Entry 8). With 15 mol% **III.1a**, cyclohexanol (**III.4a**) oxidation proceeds in 86% yield (for optimization

experiments see Table III-1). Alcohol oxidation catalysis can be achieved using air in place of pure O₂; using air, cyclohexanol oxidation is accomplished in 66% yield. In the absence of **III.1a**, 15% yield of cyclohexanone (**III.5a**) was obtained, which arises from background Co(II)-catalyzed alcohol oxidation (for background reactions for all substrates reported see Experimental Details section).^{243, 244} Using **III.1a** as catalyst, we have investigated the oxidation chemistry of a series of secondary alcohols (Figure III-5). Substituted aryl and heteroaryl ethanols participate in alcohol oxidation to afford the corresponding acetophenone derivatives (**III.5b–l**). Notably, electron-deficient (**III.5e** and **III.5g**) and electron-rich (**III.5d**, **III.5j**, and **III.5l**) derivatives are tolerated, as well as heteroaryl substituents (**III.5i**). Oxidation of methoxy-substituted alcohol **III.4f** affords acetophenone derivative **III.5f** in low yield, which may be because of the background reaction of weak C–H bonds with reactive oxidants during aldehyde autoxidation. Oxidation of aliphatic alcohols also generates ketones; cyclopentanone (**III.5m**), cyclohexanone (**III.5a**), cycloheptanone (**III.5n**), and 2-hexanone (**III.5o**) are all accessed by oxidation of the corresponding alcohol. α,α -Disubstituted acetophenone **III.5k** was accessed in 64% yield, but the presence of larger α -substituents results in diminished oxidation efficiency (α,α -diphenyl ketone **III.5p** is generated in 33% yield). Oxidation of benzoin (**III.4q**), an α -hydroxycarbonyl, affords dicarbonyl **III.5q** in 60% yield. Olefinic substrates are tolerated in the aerobic oxidation catalysis. As examples, 2-cyclohexenone (**III.5r**) is generated from the oxidation of 2-cyclohexenol (**III.4r**) and cholesterol (**III.4s**) participates in aerobic oxidation to afford **III.5s** in 57% yield.

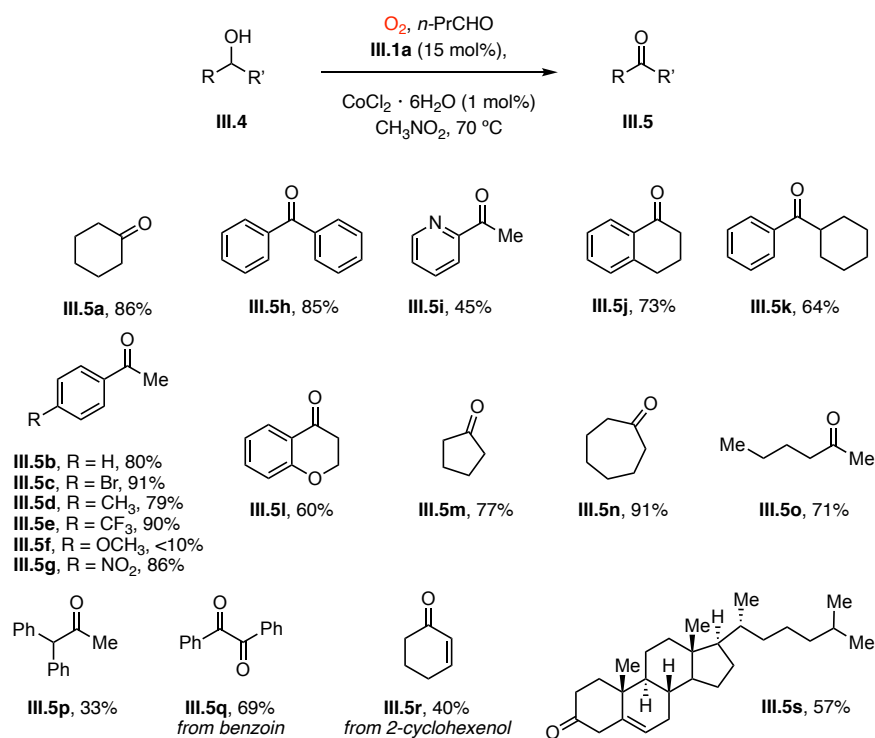


Figure III-5. Aerobic oxidation secondary alcohols catalyzed by III.1a provides access to a wide variety of ketones. *n*-PrCHO = *n*-butryaldehyde.

Application of the optimized reaction conditions to iodoarene-catalyzed oxidation of primary alcohols results in the formation of carboxylic acids (Figure III-6a). Benzyl alcohols **III.6a** and **III.6c**, heteroaromatic benzyl alcohol **III.6d**, as well as long-chain aliphatic alcohols **III.6e** and **III.6f**, participate in aerobic oxidation to afford the corresponding carboxylic acids in good yield. The observation of carboxylic acids in catalytic reactions, but aldehydes in stoichiometric reactions, is likely the result of initial oxidation of primary alcohol to the corresponding aldehyde, followed by subsequent autoxidation to the corresponding carboxylic acid under the reaction conditions used to generate iodylbenzenes. The reactive intermediates of autoxidation also likely interfere with application of the developed aerobic oxidation catalysis to geraniol (**III.6b**); exposure of **III.6b** to the developed catalytic conditions results in a mixture of products. Aryl-iodide-catalyzed aerobic oxidation of 1,2-diol **III.8** affords benzoic acid **III.9** in 79% yield (Figure III-6b) and oxidation of 1,4-diol **III.10** generates lactone **II.11** in 73% yield (Figure III-6c).

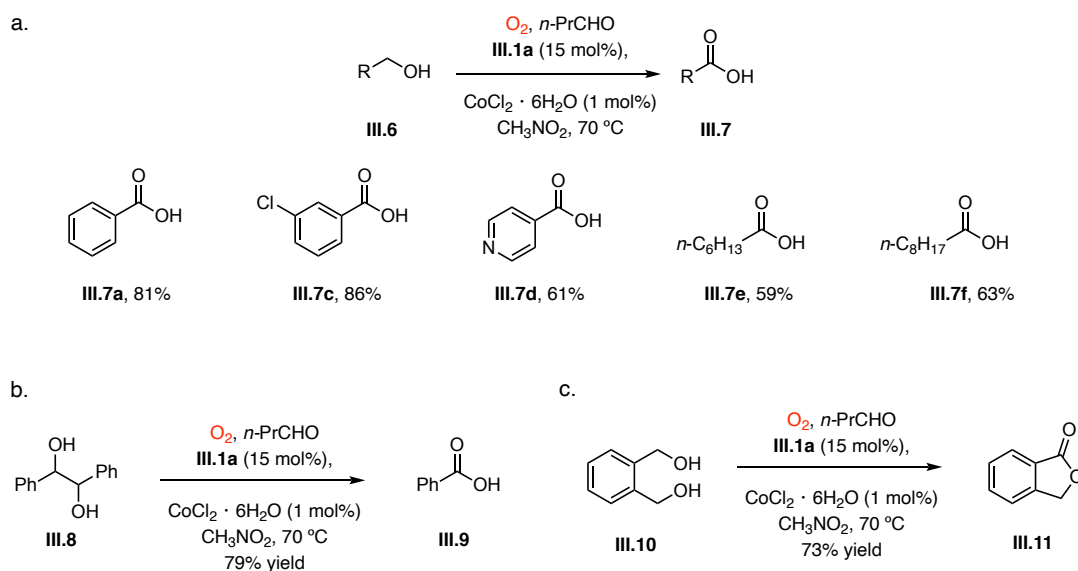


Figure III-6. Application of III.1a in aerobic alcohol oxidation catalysis. (a) Oxidation of primary alcohols and (b) 1,2-diols results in the formation of carboxylic acids and oxidation of (c) 1,4-diols affords lactones under aerobic I(V) catalysis. The overoxidation in the catalytic reaction arises from autoxidation of the initially formed products under the aerobic conditions. *n*-PrCHO = *n*-butryaldehyde.

III.2.3 Proposed Mechanism of Aerobic Oxidation Catalysis via I(V) Reagents

Initially, we proposed that the observation of I(V) reagent **III.3a** under aerobic oxidation conditions was due to AcOH-promoted disproportionation of an initially formed iodosylbenzene intermediate (**III.2a**) based on the following observations: 1) *In situ* monitoring of the oxidation of iodoarene **III.1a** revealed that **III.1a** and I(V) compound **III.3a** were the only observable iodine-containing species and that I(III) compound **III.2a** (or *bis*-acetate adduct **III.2a'**) was not present in the reaction mixture (Figure III-7); and 2) disproportionation of independently synthesized iodosylarene **III.2a** to generate equimolar amount of I(I) and I(V) was observed upon addition of AcOH (Figure III-8). The proposed acid-promoted disproportionation was consistent with literature detailing *O*-bridged intermediates in disproportionation reactions in acidic media.^{44, 245, 246} During subsequent investigations of the reaction chemistry of **III.2a** with AcOH, we have observed that in contrast to the observed disproportionation, diacetate **III.2a'** formed in the

presence of AcOH and this species appears to be resistant to disproportionation. To clarify the divergent results regarding the disproportionation of **III.2a**, we have pursued the following series of experiments.²⁴⁷

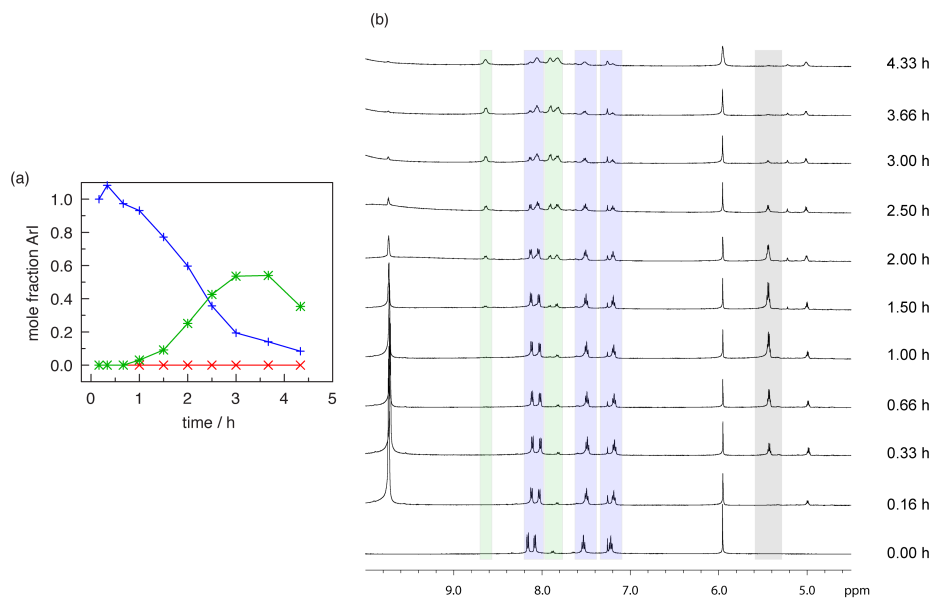


Figure III-7. Aerobic oxidation kinetics of 2-(*tert*-butylsulfonyl)iodobenzene in CDCl₃. Mol fraction of **III.1a (+), **III.2a** (x), and **III.3a** (*) as a function of time for oxidation of **III.1a** in CDCl₃ at 23 °C in the presence of CoCl₂·6H₂O (1 mol%).**

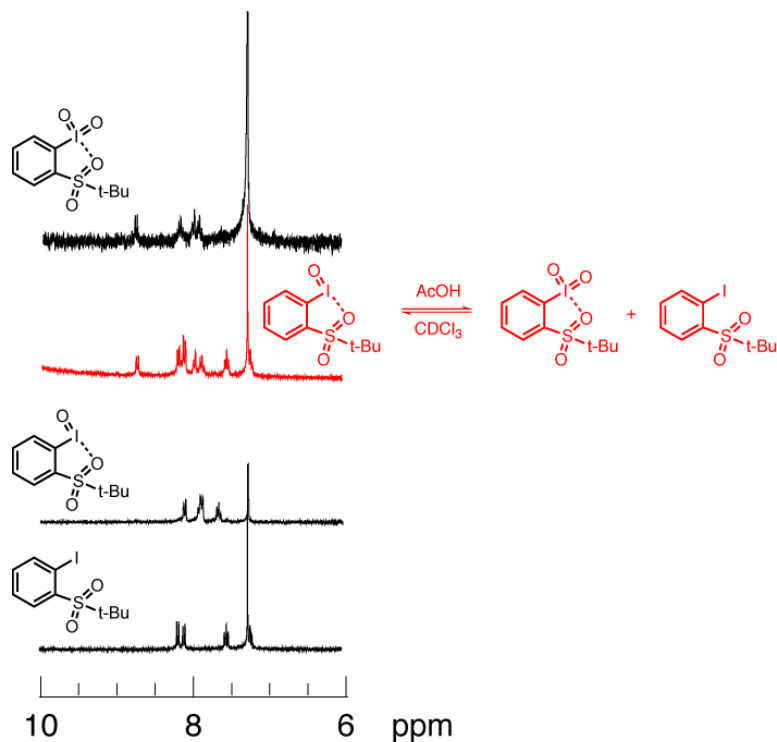


Figure III-8. ^1H NMR experiment for addition of AcOH to **III.2a**. Addition of 1.0 equivalents of AcOH to a sample of **III.2a** in CDCl_3 led to the immediate disproportionation to equimolar amounts of **III.1a** and **III.3a**.

For the NMR experiment illustrated in Figure III-8, compound **III.2a** was prepared according to the literature procedure based on treatment of **III.1a** with KClO_3 and HCl , followed by hydrolysis with NaOH to provide analytically pure sample (Figure III-9a, Method A).¹⁸³ We speculated that the unpredictable disproportionation rates displayed by independently synthesized **III.2a** may be due to the presence of a trace impurity from the preparation that is not detected by combustion analysis. Samples of **III.1a** prepared by Method A exhibited substantial variation with respect to disproportionation rate: In a series of ^1H NMR experiments using mesitylene as an internal standard, half-lives ranging from less than a minute to six hours have been observed. To evaluate the potential presence of impurities in the samples of **III.1a**, we have pursued EPR and mass spectrometry-based experiments. Exposure of a sample of **III.1a** prepared by KClO_3/HCl method to *N-tert-butyl- α -phenylnitron*e (PBN), which is a commonly used EPR spin trap,²⁴⁸ in

CDCl_3 results in the EPR spectrum shown in Figure III-9b, which can be fit as the admixture of the spectrum of oxidized PBN as well as the spectrum of the PBN adduct of hydroxy radical (Figure III-9c).

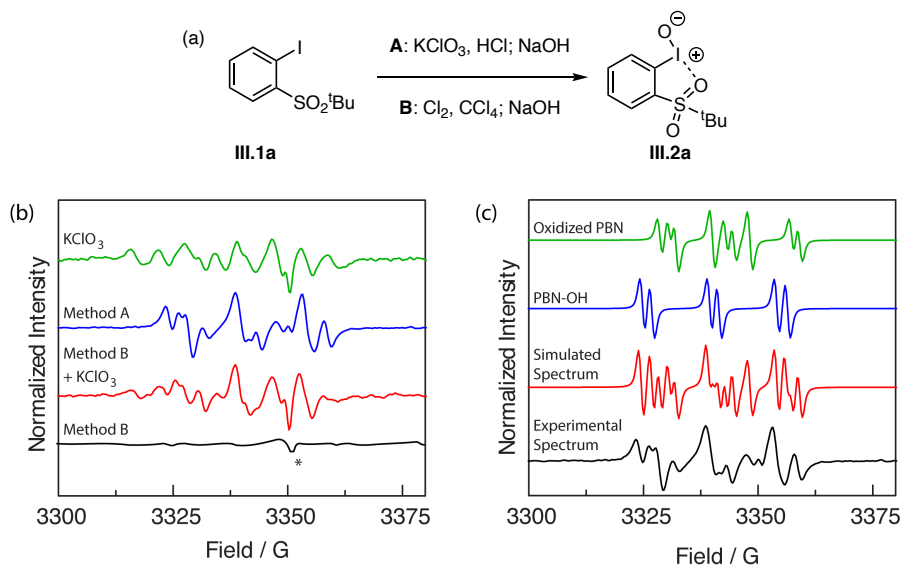


Figure III-9. Analysis of impurity in independently synthesized III.2a via EPR studies. (a) III.2a was synthesized following literature method (A) and a modified method (B). (b) EPR spectra obtained following PBN addition to III.2a prepared by Method B (—), and with added KClO₃ (—), III.2a prepared by Method A (—), and KClO₃ (—); * this signal is from the resonator background. (c) Simulated EPR components: Experimentally obtained spectrum following PBN addition to III.2a prepared by Method B with added KClO₃ (—), spectral simulation as admixture of oxidized PBN and hydroxy radical adduct (—), simulated PBN-adduct of hydroxyl radical (—), and simulated spectrum for oxidized PBN (—).

The intensity of the spectral features increases upon exposure of the sample to ambient light and an identical EPR spectrum can be obtained from KClO₃ in CDCl_3 (See Experimental Details section for additional data). These observations are consistent with the presence of a trace quantity of chlorate that was not removed despite extensive washing; UV irradiation of chlorate has been reported to promote a variety of radical-generating processes.²⁴⁹ Dissolution of the sample of III.2a prepared by Method A in HNO_3 and analysis by ICP-MS indicated the presence of K^+ . Chlorate is not detectable by IR analysis, however, negative-mode ESI-MS of III.2a prepared by Method A indicates the presence of ClO_3^- ($m/z = 82.953$ (expt); 82.954 (calc)) (Figure

III-10).

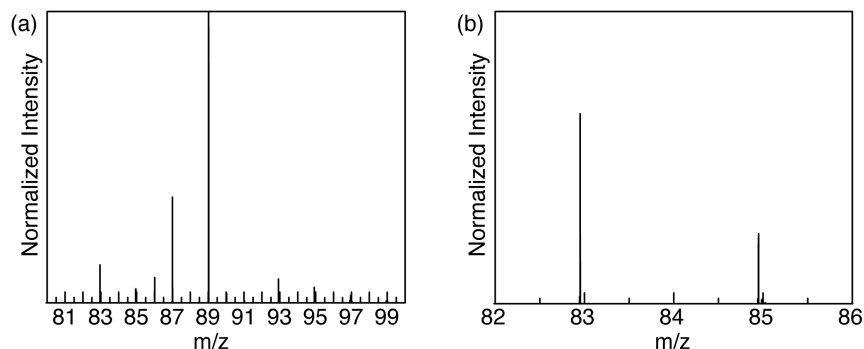


Figure III-10. Mass spectrometry analysis of III.2a prepared by Method A. (a) Negative-mode ESI-MS of III.2a synthesized by Method B demonstrating the presence of ClO_3^- ($m/z = 82.953$ (expt); 82.954 (calc)). (b) Expansion of the chlorate region of the mass spectrum.

We suspected that the source of the observed potassium is the KClO_3 used to prepare III.2a. Based on the hypothesis that trace impurities associated with KClO_3 were leading to the irreproducible disproportionation behavior of III.2a, we modified the synthetic protocol as follows: Cl_2 was bubbled through a solution of III.1a in CCl_4 , the resulting solid was isolated, and was then treated with 5M NaOH solution (Figure III-9a, Method B). The resulting samples of III.2a display reproducible disproportionation chemistry. Exposure of material prepared by Method B to PBN did not give rise to an observable EPR signal (Figure III-9b). Addition of KClO_3 to the sample of III.2a prepared from Method B led to the evolution of an EPR spectrum that overlays the spectrum obtained from Method A (Figure III-9b) and the intensity of the signal increased upon exposure to light (see Experimental Details section for additional data). In addition, ICP-MS analysis of III.2a prepared by Method B did not show the presence of any trace metal ions.

Regarding the formation of iodylarene III.3a by aldehyde-promoted aerobic oxidation, the

above experimental data suggest that our original proposal of acid-promoted disproportionation of **III.2a** was based on the irreproducible disproportionation kinetics of material prepared by Method A. Following experiments were carried out to better understand the aerobic synthesis of I(V) reagents:

(1) While the oxidation of 4-iodotoluene (**III.1e**) to the corresponding iodylbenzene (**III.3e**) under the action of O₂, CH₃CHO, and Co(II) proceeds via the initial formation of 4-iodotoluene diacetate (**III.2e'**) followed by subsequent oxidation of I(III) to I(V) as illustrated in Figure III-11, oxidation of iodoarene **III.1a** affords iodylarene **III.3a** without the observation of iodosylarene **III.2a** or *bis*-acetate **III.2e'** (Figure III-7).²³⁹

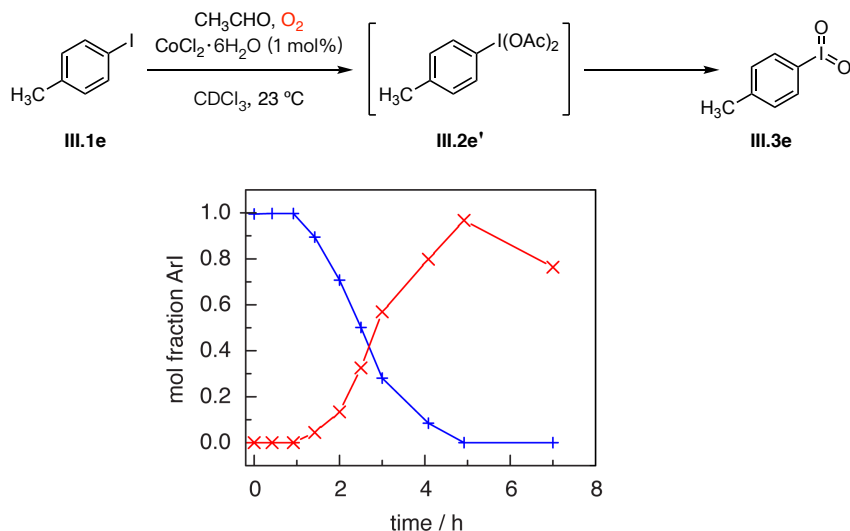


Figure III-11. Measurement of aerobic oxidation kinetics of 4-iodotoluene (III.1e**) in CDCl₃.** Mol fraction of **III.1e** (+) and **III.2e'** (x) as a function of time for oxidation of 4-iodotoluene (**III.1e**) in CDCl₃ at 23 °C in the presence of CoCl₂·6H₂O (1 mol%). Poor solubility of **III.3e** prevents determination of the concentration of this species.

(2) Addition of the isolable reaction components of aldehyde-promoted aerobic oxidation, including acetaldehyde, acetic acid, CoCl₂, and Co(OAc)₃ (see Experimental Details section for additional data), does not induce disproportionation of *bis*-acetate **III.2a'**.

(3) Exposure of an independently prepared sample of I(III) compound **III.2a** to aldehyde-promoted aerobic oxidation (O_2 , CH_3CHO , and Co(II) in $\text{AcOH-}d_4$) resulted in the observation of both iodylarene **III.3a** and iodoarene **III.1a** by $^1\text{H NMR}$ (Figure III-12). The presence of iodoarene **III.1a** during the aerobic oxidation of **III.2a** suggests that a disproportionation mechanism may be operative, although the mechanism of disproportionation is still unclear.

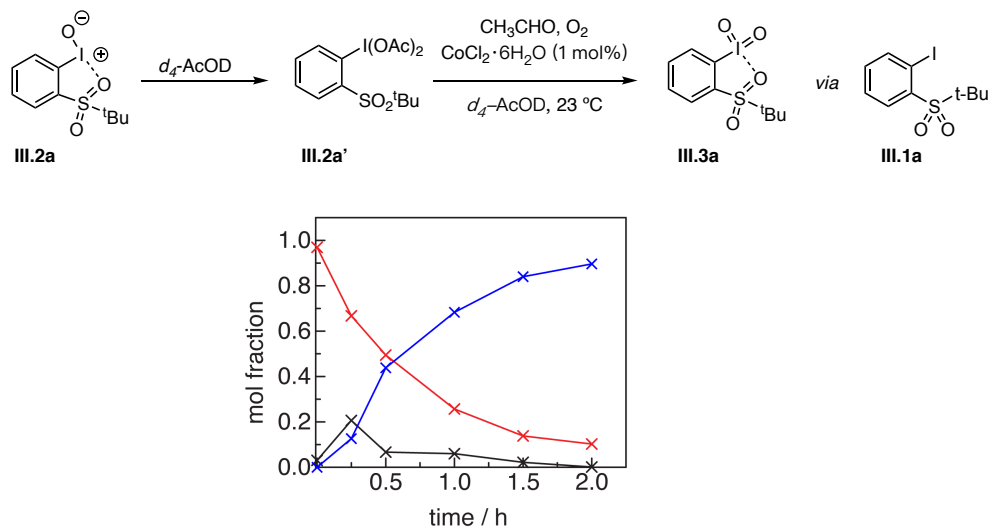


Figure III-12. Measurement of aerobic oxidation kinetics of **III.2a in $\text{AcOH-}d_4$.** Mol fraction of **III.1a** (\times), **III.2a** (\times) and **III.3a** (\times) as a function of time for oxidation of **III.2a** in $\text{AcOH-}d_4$ at 23°C in presence of acetaldehyde and $\text{CoCl}_2 \cdot 6\text{H}_2\text{O}$ (1 mol%).

Taking into consideration all the observations outlined above, we propose that substrate oxidation proceeds via the catalytic cycles pictured in Figure III-13. Initial oxidation of aryl iodide **III.1a** generates iodosylbenzene **III.2a**. Facile disproportionation of **III.2a** under autoxidation conditions generates equimolar quantities of **III.1a** and **III.3a**. Substrate oxidation by **III.3a** generates **III.2a**, which, following disproportionation, affords **III.1a** that is poised to participate in subsequent aldehyde-promoted aerobic oxidation. The critical role of I(V) intermediates in substrate oxidation chemistry is revealed by comparison of the chemistry of iodosylbenzenes that participate in facile disproportionation with those that do not rapidly disproportionate. Hence,

iodobenzene **III.1a** could be utilized for aerobic I(V) catalysis as it participates in facile disproportionation.

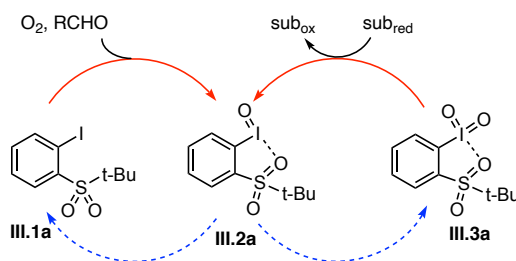


Figure III-13. Proposed catalytic cycle for I(V) mediated aerobic oxidation catalysis.

Density functional theory (DFT) calculations—carried out with the M06-2X²⁵⁰ functional (basis sets: LANL2DZ²⁵¹⁻²⁵³ for I and 6-31G(d,p)^{254, 255} for other atoms) and the solvation model based on density (SMD)²⁵⁶—indicate that disproportionation of **III.2a** to generate **III.1a** and **III.3a** is thermodynamically favored ($\Delta G = -8.8 \text{ kcal/mol}^{-1}$; see computational details part in Experimental Details section). In contrast to **III.2a**, iodobenzene **III.1e** does not participate in facile disproportionation; *in situ* monitoring of the oxidation of **III.1e** by 1H NMR spectroscopy indicates that initial oxidation affords the I(III) derivative **III.2e'**, which subsequently converts slowly to the I(V) derivative **III.3e** (Figure III-11). Independently prepared **III.3e** effects oxidation of cyclohexanol in 66% yield, whereas **III.1e** (which generates the iodobenzene derivative **III.2e'** that does not rapidly disproportionate) is an ineffective oxidation catalyst (24% yield of cyclohexanone from cyclohexanol; for comparison, the Co-catalyzed background provides a 15% yield). These data indicate that the efficiency of aerobic oxidation catalysis is significantly compromised when facile disproportionation of I(III) is not available.

III.3 Conclusions

In conclusion, we have reported the first aerobically generated I(V) reagents that participate in substrate oxidation chemistry. By coupling aerobic oxidation of I(I) to I(III) with facile disproportionation of the initially formed I(III) reagents, efficient access to I(V) is accomplished. The I(V) reagent generated in this protocol is functionally analogous to DMP and provides a platform to couple O₂ reduction with oxidation of alcohols, diols, and amines. *In situ* generation of iodylbenzene intermediates supports aerobic oxidation catalysis and we have demonstrated that efficient catalysis requires access to the I(V) oxidation state. These studies add to the growing field of aerobically generated oxidants that underpin development of sustainable oxidation chemistry. We anticipate that development of new strategies to couple O₂ reduction to iodobenzene oxidation, without the intermediacy of reactive aldehyde autoxidation intermediates, will engender broadly applicable hypervalent-iodine-catalyzed aerobic oxidation chemistry.

III.4 Experimental Details

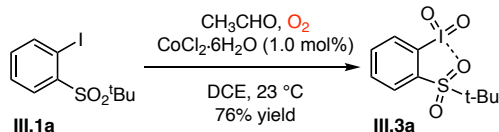
III.4.1 General Considerations

Materials All chemicals and solvents were obtained as ACS reagent grade and used as received. Iodobenzene and cyclohexanol were obtained from Beantown Chemical. Acetaldehyde, geraniol, and 2-iodonitrobenzene were obtained from Alfa Aesar. Sodium hydroxide and ethyl acetate were obtained from EMD Millipore. $\text{CoCl}_2 \cdot 6\text{H}_2\text{O}$, 2-iodobenzoic acid, 4-iodoanisole, 4-iodotoluene, 3-bromoiodobenzene, 2,5-dimethyliodobenzene, 2-adamantanol, benzoin, cyclopentanol, cyclopentanone, cycloheptanone, 4'-nitroacetophenone, 4'-(trifluoromethyl)acetophenone, 2,2-dimethyl-1-propanol, 4'-bromoacetophenone, 4'-methylacetophenone, 2-cyclohexen-1-ol, 1-heptanol, 1-nonanol, 4-chromanol, 1-phenylethanol, cholesterol, dibenzylamine, N-hydroxybenzylamine hydrochloride, benzophenone, 1,2,3,4-tetrahydroisoquinoline, 2-phenyl-2-imidazoline, cyclohexanone, 2-hexanol, sodium borohydride, 1,2-diiodobenzene, 1,2-dichloroethane (DCE), diethyl ether, methanol, tetrahydrofuran (THF), hexanes, and acetic acid were obtained from Sigma Aldrich. Silica gel (0.060 – 0.200 mm, 60 Å for column chromatography) was obtained from Acros Organics. CH_2Cl_2 and acetonitrile were obtained from Fisher Scientific. Butyraldehyde was obtained from TCI. NMR solvents were purchased from Cambridge Isotope Laboratories and were used as received. O_2 (99.6%) was obtained from Conroe Welding Supply. Substituted phenyl ethyl alcohols (**III.4**) were prepared from the corresponding ketones (**III.5**) by NaBH_4 reduction according to literature methods.²⁵⁷ All reactions were carried out under ambient atmosphere unless otherwise noted.

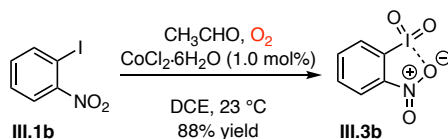
Characterization Details NMR spectra were recorded on Mercury 300 FT NMR for ^1H acquisitions and were referenced against solvent signals: CDCl_3 (7.26 ppm, ^1H ; 77.16 ppm, ^{13}C),

D₂O (4.79 ppm, ¹H) and DMSO-d₆ (2.50 ppm, ¹H).¹⁹¹ ¹H NMR data are reported as follows: chemical shift (δ, ppm), (multiplicity: s (singlet), d (doublet), t (triplet), m (multiplet), br (broad), integration). ¹³C NMR data are reported as follows: chemical shift (δ, ppm). Mass spectrum was recorded on Q Exactive™ Focus Hybrid Quadrupole-Orbitrap™ Mass Spectrometer from ThermoFisher Scientific. GC experiments were conducted on ThermoFisher Scientific Trace 1310 Gas Chromatograph. Melting points (mp) were measured using MelTemp II from Laboratory Devices Inc. For reports of melting points (mp), decomp stands for decomposition and expl stands for explosion.

III.4.2 Synthesis and Characterization Details

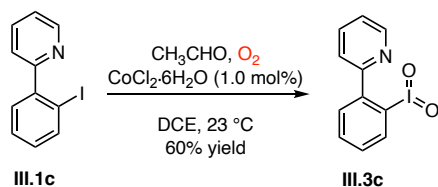


Synthesis of 1-(*tert*-butylsulfonyl)-2-iodobenzene (III.3a). A 20-mL scintillation vial was charged with glacial AcOH (2.0 mL), 1-(*tert*-butylsulfonyl)-2-iodobenzene (**III.1a**, 130 mg, 0.401 mmol, 1.00 equiv), and $\text{CoCl}_2 \cdot 6\text{H}_2\text{O}$ (0.9 mg, 0.004 mmol, 1 mol%) and was fitted with a rubber septum. The reaction vessel was purged with O_2 for 5 min before acetaldehyde (224 μL , 4.07 mmol, 10.1 equiv) was added in one portion. The reaction mixture was stirred under 1 atm O_2 , delivered by inflated balloon, at 23 $^\circ\text{C}$ for 10 h. The solvent was concentrated to 1 mL under reduced pressure and residue was treated with 2:1 hexanes: CH_2Cl_2 to induce precipitation of white solid. The precipitate was isolated by filtration, washed with hexanes, and dried *in vacuo* to afford 108 mg of the title compound **III.3a** as a white solid (76% yield). Characterization of **III.3a**: ^1H NMR (δ , 23 $^\circ\text{C}$, $\text{DMSO}-d_6$): 8.46 (d, $J = 7.6$ Hz, 1H), 8.13 (t, $J = 7.1$ Hz, 1H), 7.97–7.84 (m, 2H), 1.32 (s, 9H). ^{13}C NMR (δ , 23 $^\circ\text{C}$, $\text{DMSO}-d_6$): 148.0, 135.1, 132.0, 131.2, 124.0, 61.2, 23.2. mp 169–170 $^\circ\text{C}$ (expl). The spectral data are in good agreement with those reported in literature.¹⁶³



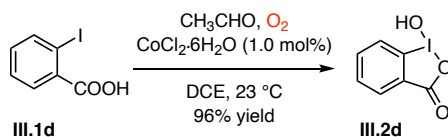
Synthesis of 2-nitroiodobenzene (III.3b). A 20-mL scintillation vial was charged with DCE (2.0 mL), 2-nitroiodobenzene (**III.2b**, 51.2 mg, 0.205 mmol, 1.00 equiv), and $\text{CoCl}_2 \cdot 6\text{H}_2\text{O}$ (0.5 mg, 0.002 mmol, 1 mol%) and was fitted with a rubber septum. The reaction vessel was purged with O_2 for 5 min before acetaldehyde (112 μL , 2.03 mmol, 10.0 equiv) was added in one portion. The reaction mixture was stirred under 1 atm O_2 , delivered by inflated balloon, at 23 $^\circ\text{C}$, for 16 h.

The solvent was concentrated to 1 mL under reduced pressure and the resulting solution was diluted with 5 mL hexane to induce precipitation. The precipitate was filtered off to afford 50 mg of the title compound **III.3b** as a pale-yellow solid (88% yield). Characterization of **III.3b**: ^1H NMR (δ , 23 °C, DMSO- d_6): 8.37 (dd, J = 8.1, 1.1 Hz, 1H), 8.30 (dd, J = 7.7, 1.3 Hz, 1H), 8.19 (td, J = 7.5, 1.0 Hz, 1H), 7.89 (td, J = 7.7, 1.1 Hz, 1H). ^{13}C NMR (δ , 23 °C, DMSO- d_6): δ 144.5, 144.2, 137.1, 133.4, 125.5, 125.3. mp 196-199 °C. HRMS (ESI $^+$): Calcd. for $\text{C}_6\text{H}_4\text{NINaO}_4$ [$\text{M}+\text{Na}$] $^+$ m/z 303.9083. Found: 303.9078.

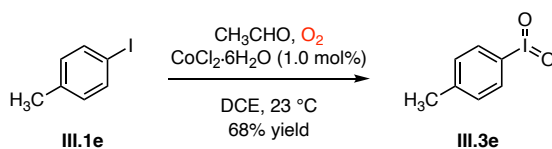


Synthesis of 2-(2-iodophenyl)pyridine (III.3c). A 20-mL scintillation vial was charged with acetic acid (2.0 mL), 2-(2-iodophenyl)pyridine (**III.2c**, 79.5 mg, 0.283 mmol, 1.00 equiv), and $\text{CoCl}_2\cdot 6\text{H}_2\text{O}$ (0.7 mg, 0.003 mmol, 1 mol%) and was fitted with a rubber septum. The reaction vessel was purged with O_2 for 5 min before acetaldehyde (149 μL , 2.71 mmol, 10.0 equiv) was added in one portion. The reaction mixture was stirred under 1 atm O_2 , delivered by inflated balloon, at 23 °C, for 16 h. The solvent was concentrated to 1 mL under reduced pressure and residue was treated with 2:1 hexanes: CHCl_3 to induce precipitation. The precipitate was then filtered off and washed with hexane to afford 53 mg of the title compound **III.3c** as an off-white solid (60% yield). Characterization of **III.3c**: ^1H NMR (δ , 23 °C, D_2O): 8.69 (dd, J = 5.1, 0.8 Hz, 1H), 8.37-8.30 (m, 2H), 8.24 (d, J = 8.2 Hz, 1H), 8.13 (td, J = 7.8, 1.4 Hz, 1H), 7.87 (td, J = 7.6, 1.7 Hz, 2H), 7.59 (ddd, J = 7.5, 5.2, 1.1 Hz, 1H). ^{13}C NMR (δ , 23 °C, D_2O): 149.3, 144.8, 142.3,

140.9, 134.1, 132.6, 132.0, 127.3, 125.4, 124.0, 120.5. mp 170-172 °C (decomp). HRMS (ESI⁺): Calcd for C₁₁H₈INNaO₂ [M+Na]⁺ m/z 335.9497. Found: 335.9487.

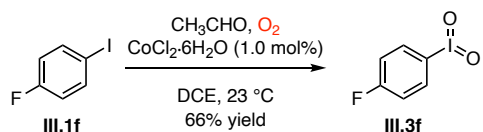


Synthesis of 1-Hydroxy-2-iodobenzodioxol-3(1H)-one (III.2d). Compound **III.3d** was prepared according to literature reported method.¹⁶³ A 20-mL scintillation vial was charged with DCE (2.0 mL), 2-iodobenzoic acid (**III.1d**, 50.2 mg, 0.202 mmol, 1.00 equiv), and CoCl₂·6H₂O (0.5 mg, 0.002 mmol, 1 mol%) and was fitted with a rubber septum. The reaction vessel was purged with O₂ for 5 min before acetaldehyde (112 μL, 2.03 mmol, 10.1 equiv) was added in one portion. The reaction mixture was stirred under 1 atm O₂, delivered by inflated balloon, at 23 °C, for 16 h. The reaction mixture was diluted with hexane and the solid residue was filtered off, washed with 2 mL water. The solid left was dried *in vacuo* to afford 51 mg of the title compound **III.2d** as an off-white solid (96% yield). Characterization of **III.2d**: ¹H NMR (δ, 23 °C, DMSO-*d*₆): 8.03 (s, 1H, OH proton exchangeable with D₂O), 8.01-7.98 (m, 1H), 7.95-7.92 (m, 1H), 7.84 (s, 1H), 7.69 (td, *J* = 7.3, 1.0 Hz, 1H). ¹³C NMR (δ, 23 °C, DMSO-*d*₆): 167.8, 134.5, 131.6, 131.2, 130.4, 126.4, 120.5. mp 247-250 °C (lit. 250-252 °C).

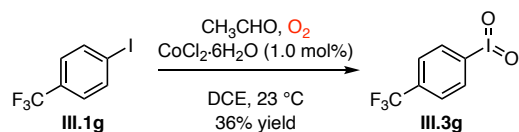


Synthesis of *p*-methyliodolylbenzene (III.3e). A 20-mL scintillation vial was charged with DCE (2.0 mL), 4-iodotoluene (**III.1e**, 87.1 mg, 0.399 mmol, 1.00 equiv), and CoCl₂·6H₂O (0.9 mg, 0.004 mmol, 1 mol%) and was fitted with a rubber septum. The reaction vessel was purged with O₂ for 5 min before acetaldehyde (224 μL, 4.07 mmol, 10.0 equiv) was added in one portion.

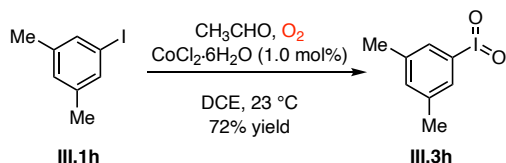
The reaction mixture was stirred under 1 atm O₂, delivered by inflated balloon, at 23 °C, for 16 h. The solvent was concentrated to 1 mL under reduced pressure and the resulting solution was diluted with 5 mL hexane. The precipitate was filtered off to afford 67 mg of the title compound as **III.3e** a yellow-white powder (68% yield). Characterization of **III.3e**: ¹H NMR (δ, 23 °C, DMSO-*d*₆): 7.83 (d, *J* = 8.2 Hz, 2H), 7.39 (d, *J* = 7.9 Hz, 2H), 2.38 (s, 3H). ¹³C NMR (δ, 23 °C, DMSO-*d*₆): 141.4, 136.9, 131.5, 129.4, 126.5, 20.9. HRMS (ESI⁺): Calcd for C₇H₇INaO₂ [M+Na]⁺ *m/z* 272.9388. Found: 272.9387. mp 190-192 °C (decomp) lit. 213 °C (decomp). The spectral data are in good agreement with those reported in literature.⁴²



Synthesis of *p*-fluoroiodobenzene (III.3f**).** A 20-mL scintillation vial was charged with DCE (2.0 mL), 4-fluoroiodobenzene (**III.1f**, 89.3 mg, 0.401 mmol, 1.00 equiv), and CoCl₂·6H₂O (0.9 mg, 0.004 mmol, 1 mol%) and was fitted with a rubber septum. The reaction vessel was purged with O₂ for 5 min before acetaldehyde (224 μL, 4.07 mmol, 10.0 equiv) was added in one portion. The reaction mixture was stirred under 1 atm O₂, delivered by inflated balloon, at 23 °C, for 16 h. The solvent was removed *in vacuo* and the residue was washed with hexanes twice. The residue was dried *in vacuo* to afford 66 mg of the title compound **III.3f** as a yellow-white powder (66% yield). Characterization of **III.3f**: ¹H NMR (δ, 23 °C, DMSO-*d*₆): δ 8.05-8.00 (m, 2H), 7.46-7.40 (m, 2H). ¹³C NMR (δ, 23 °C, DMSO-*d*₆): δ 165.8, 162.5, 129.7 (d, *J* = 36 Hz), 116.2 (d, *J* = 90 Hz). mp 210-212 °C (expl) lit. 234 °C (decomp). HRMS (ESI⁺): Calcd for C₆H₄FINaO₂ [M+Na]⁺ *m/z* 276.9138. Found: 276.9133. The spectral data are in good agreement with those reported in literature.⁴²

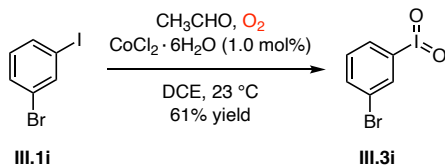


Synthesis of *p*-trifluoromethyliodolylbenzene (III.3g). A 20-mL scintillation vial was charged with DCE (2.0 mL), 4-trifluoromethyliodobenzene (III.1g, 109 mg, 0.401 mmol, 1.00 equiv), and $\text{CoCl}_2\cdot 6\text{H}_2\text{O}$ (0.9 mg, 0.004 mmol, 1 mol%) and was fitted with a rubber septum. The reaction vessel was purged with O_2 for 5 min before acetaldehyde (224 μL , 4.07 mmol, 10.0 equiv) was added in one portion. The reaction mixture was stirred under 1 atm O_2 , delivered by inflated balloon, at 23 $^\circ\text{C}$, for 16 h. The solvent was removed *in vacuo* and the residue was washed with hexanes twice. The residue was dried *in vacuo* to afford 43 mg of the title compound III.3g as a yellow-white powder (36% yield). Characterization of III.3g: $^1\text{H NMR}$ (δ , 23 $^\circ\text{C}$, $\text{DMSO-}d_6$): 8.17 (d, $J = 7.6$ Hz, 2H), 7.95 (d, $J = 8.0$ Hz, 2H). HRMS (ESI $^+$): Calcd for $\text{C}_7\text{H}_4\text{F}_3\text{INaO}_2$ $[\text{M}+\text{Na}]^+$ m/z 326.9106. Found: 326.9102. mp 232-234 $^\circ\text{C}$ (decomp) lit. 213-216 $^\circ\text{C}$ (decomp). The spectral data are in good agreement with those reported in literature.⁴²



Synthesis of 3,5-dimethyliodolylbenzene (III.3h). A 20-mL scintillation vial was charged with DCE (2.0 mL), 3,5-dimethyliodobenzene (III.1h, 93.2 mg, 0.401 mmol, 1.00 equiv), and $\text{CoCl}_2\cdot 6\text{H}_2\text{O}$ (0.9 mg, 0.004 mmol, 1 mol%) and was fitted with a rubber septum. The reaction vessel was purged with O_2 for 5 min before acetaldehyde (224 μL , 4.07 mmol, 10.1 equiv) was added in one portion. The reaction mixture was stirred under 1 atm O_2 , delivered by inflated balloon, at 23 $^\circ\text{C}$, for 16 h. The solvent was removed *in vacuo* and the residue was washed with

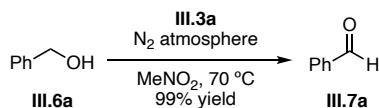
hexane twice. The residue was dried *in vacuo* to afford 76 mg of the title compound **III.3h** as an off-white solid (72% yield). Characterization of **III.3h**: ^1H NMR (δ , 23 °C, DMSO- d_6): 7.55 (s, 2H), 7.19 (s, 1H), 2.35 (s, 6H). mp 196-198 °C (decomp) lit. 217 °C (expl). The spectral data are in good agreement with those reported in literature.¹⁰⁶



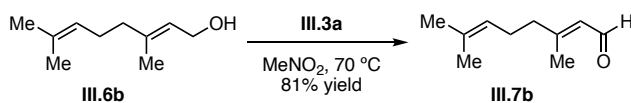
Synthesis of 3-bromoiodobenzene (III.3i). A 20-mL scintillation vial was charged with DCE (2.0 mL), 3-bromoiodobenzene (**III.1i**, 113 mg, 0.399 mmol, 1.00 equiv), and $\text{CoCl}_2 \cdot 6\text{H}_2\text{O}$ (0.9 mg, 0.004 mmol, 1 mol%) and was fitted with a rubber septum. The reaction vessel was purged with O_2 for 5 min before acetaldehyde (224 μL , 4.07 mmol, 10.2 equiv) was added in one portion. The reaction mixture was stirred under 1 atm O_2 , delivered by inflated balloon, at 23 °C, for 16 h. The solvent was removed *in vacuo* and the residue was washed with hexane twice. The residue was dried *in vacuo* to afford 77 mg of the title compound **III.3i** as an off-white powder (61% yield). Characterization of **III.3i**: ^1H NMR (δ , 23 °C, DMSO- d_6): 8.08 (s, 1H), 7.95 (d, $J = 7.9$ Hz, 1H), 7.74 (dt, $J = 7.9, 0.9$ Hz, 1H), 7.54 (t, $J = 7.8$ Hz, 1H). ^{13}C NMR (δ , 23 °C, DMSO- d_6): 153.2, 133.9, 131.1, 128.9, 125.5, 121.7. mp 204-206 °C (decomp). HRMS (ESI $^+$): Calcd for $\text{C}_6\text{H}_4\text{IBrNaO}_2$ [$\text{M} + \text{Na}$] $^+$ m/z 336.8337. Found: 336.8332.

Application of Aerobic Oxidation to Organic Oxidation Chemistry

Stoichiometric Oxidation Chemistry

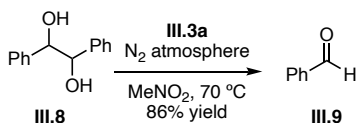


Oxidation of Benzyl Alcohol (III.6a). A 10-mL round-bottom flask was charged with MeNO₂ (2.0 mL), 1-(*tert*-butylsulfonyl)-2-iodylbenzene (**III.3a**, 85 mg, 0.238 mmol, 1.16 equiv), and benzyl alcohol (**III.6a**, 22.2 mg, 0.205 mmol, 1.00 equiv) and capped with a rubber septum. The reaction mixture was bubbled with nitrogen for 10 min and stirred under nitrogen atmosphere at 70 °C for 24 h. Then the reaction mixture was concentrated under reduced pressure and analyzed by ¹H NMR with mesitylene as internal standard to afford benzaldehyde in 99% yield. The reaction when carried out under ambient atmosphere, benzoic acid was formed due to facile autoxidation of benzaldehyde.

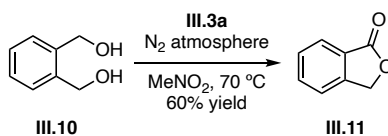


Oxidation of Geraniol (III.6b). A 20-mL scintillation vial was charged with MeNO₂ (2.0 mL), 1-(*tert*-butylsulfonyl)-2-iodylbenzene (**III.3a**, 85 mg, 0.238 mmol, 1.16 equiv), and geraniol (**6b**, 31.3 mg, 0.204 mmol, 1.00 equiv) and was tightly capped. The reaction mixture was stirred at 70 °C for 24 h. Then it was diluted with 5 mL ethyl acetate and sequentially washed with 10% NaHCO₃ and sat. aq. NaCl. The organic layer was dried anhydrous MgSO₄, concentrated and purified by silica-gel column chromatography (5% ethyl acetate in hexanes) to afford 25 mg (81%) of the titled compound **III.7b** as a pale-yellow oil. ¹H NMR (δ, 23 °C, CDCl₃): 9.99 (d, *J* = 8.1

Hz, 1H), 5.90-5.86 (m, 1H), 5.09-5.04 (m, 1H), 2.27-2.20 (m, 4H), 2.16 (s, 3H), 1.68 (s, 3H), 1.61 (s, 3H). The spectral data are in good agreement with those reported in literature.²⁵⁸

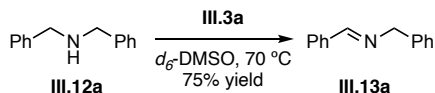


Oxidation of hydroxybenzoin (III.8). A 10-mL round-bottom flask was charged with MeNO₂ (2.0 mL), 1-(*tert*-butylsulfonyl)-2-iodylbenzene (**III.3a**, 51 mg, 0.143 mmol, 1.37 equiv), and hydroxybenzoin (**III.8**, 22.3 mg, 0.104 mmol, 1.00 equiv) and capped with a rubber septum. The reaction mixture was bubbled with nitrogen for 10 min and stirred at 70 °C for 24 h. Then the reaction mixture was concentrated under reduced pressure and analyzed by ¹H NMR with mesitylene as internal standard to afford benzaldehyde (**III.9**) in 86% yield. The reaction when carried out under ambient atmosphere, benzoic acid was formed due to facile autoxidation of benzaldehyde.

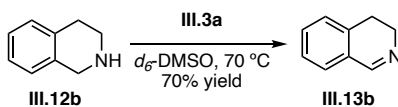


Oxidation of benzene-1,2-dimethanol (III.10). A 10-mL round bottomed flask was charged with MeNO₂ (2.0 mL), 1-(*tert*-butylsulfonyl)-2-iodylbenzene (**III.3a**, 105 mg, 0.294 mmol, 1.46 equiv), and benzene-1,2-dimethanol (**III.10**, 28.1 mg, 0.202 mmol, 1.00 equiv) and capped with a rubber septum. The reaction mixture was bubbled with nitrogen for 10 min and stirred under nitrogen atmosphere at 70 °C for 24 h. Then the reaction mixture was concentrated under reduced pressure and analyzed by ¹H NMR with mesitylene as internal standard to afford the title compound **III.11** in 30% yield (60% based on recovered starting material), with 20% of

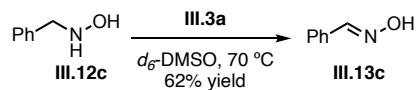
the corresponding lactol, and 50% starting material. When 2 equiv of oxidant was used, *o*-phthalaldehyde was formed in 39% yield.



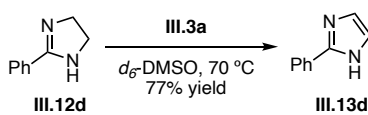
Oxidation of dibenzylamine (III.12a). A 20-mL scintillation vial was charged with DMSO-*d*₆ (1.0 mL), 1-(*tert*-butylsulfonyl)-2-iodylbenzene (**III.3a**, 142 mg, 0.398 mmol, 1.96 equiv), and dibenzylamine (**III.12a**, 40.1 mg, 0.203 mmol, 1.00 equiv) and was tightly capped. The reaction mixture was stirred at 70 °C for 24 h. Then it was analyzed by ¹H NMR with mesitylene as internal standard. Yield 75%.



Oxidation of 1,2,3,4-tetrahydroisoquinoline (III.12b). A 20-mL scintillation vial was charged with DMSO (2.0 mL), 1-(*tert*-butylsulfonyl)-2-iodylbenzene (**III.3a**, 141 mg, 0.396 mmol, 2.02 equiv), and 1,2,3,4-tetrahydroisoquinoline (**III.12b**, 26.1 mg, 0.196 mmol, 1.00 equiv) and was tightly capped. The reaction mixture was stirred at 70 °C for 24 h. Then it was diluted with 5 mL ethyl acetate and washed with 10% NaHCO₃ and Brine solution. The organic layer was dried anhydrous MgSO₄, concentrated and purified by silica gel chromatography (50% ethyl acetate / hexanes) to afford 19 mg (70%) of the titled compound **III.13b** as a yellow oil. ¹H NMR (δ, 23 °C, CDCl₃): 8.33 (bs, 1H), 7.39-7.28 (m, 3H), 7.16 (d, *J* = 7.1 Hz, 1H), 3.80-3.74 (m, 2H), 2.75 (t, *J* = 7.7 Hz, 2H). The spectral data are in good agreement with those reported in literature.²⁵⁹

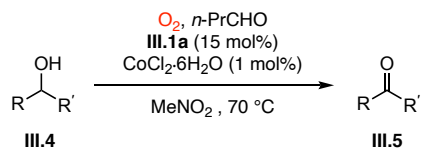


Oxidation of *N*-benzylhydroxylamine (III.12c). A 20-mL scintillation vial was charged with DMSO-*d*₆ (1.0 mL), 1-(*tert*-butylsulfonyl)-2-iodylbenzene (**III.3a**, 145 mg, 0.407 mmol, 2.06 equiv) and *N*-hydroxybenzylamine (**III.12c**, 24.3 mg, 0.197 mmol, 1.00 equiv) and was tightly capped. The reaction mixture was stirred at 70 °C for 24 h. Then it was analyzed by ¹H NMR with mesitylene as internal standard. Yield 62%.

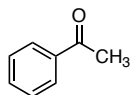


Oxidation of 2-phenyl-4,5-dihydro-1*H*-imidazole (III.12d). A 20-mL scintillation vial was charged with DMSO (2.0 mL), 1-(*tert*-butylsulfonyl)-2-iodylbenzene (**III.3a**, 149 mg, 0.418 mmol, 2.11 equiv), and 2-phenyl-2-imidazoline (**III.12d**, 29.2 mg, 0.198 mmol, 1.00 equiv) and was tightly capped. The reaction mixture was stirred at 70 °C for 24 h. Then it was diluted with 5 mL ethyl acetate and washed sequentially with 10% NaHCO₃ sat. aq. NaCl. The organic layer was dried anhydrous MgSO₄, concentrated, and purified by silica gel column chromatography (50% ethyl acetate / hexanes) to afford 22 mg (77%) of the titled compound **III.13d** as a white solid. ¹H NMR (δ, 23 °C, CDCl₃): 7.86 (dd, *J* = 8.2, 1.4 Hz, 2H), 7.43-7.34 (m, 3H), 7.16 (s, 2H). mp 141-144 °C (lit. 142-148 °C). The spectral data are in good agreement with those reported in literature.²⁶⁰

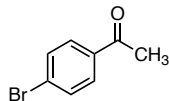
ArI-Catalyzed Aerobic Oxidation of Secondary Alcohols



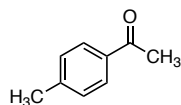
Method A. A 25-mL three-neck flask fitted with condenser (5 °C) was charged with nitromethane (5 mL), 1-(*tert*-butylsulfonyl)-2-iodobenzene (**III.1a**, 32.4 mg, 0.100 mmol, 15.0 mol%), and CoCl₂·6H₂O (1.70 mg, 0.007 mmol, 1.04 mol%). O₂ was bubbled through the reaction before butyraldehyde (90 μL, 1.0 mmol, 1.5 equiv) was added in one portion and stirred at 23 °C for 20 min. Then subsequent alcohol (**III.4**, 0.667 mmol, 1.0 equiv) was dissolved in 1.0 ml nitromethane (CH₂Cl₂ was used where the alcohol was insoluble in nitromethane) and delivered via syringe to the reaction mixture. The reaction mixture was stirred under constant O₂ bubbling (at the approximate flow rate of 30-35 mL/min), at 70 °C. Three more portions of butyraldehyde (90.0 μL, 1.00 mmol, 1.49 equiv) was added at an interval of 2h and the reaction was stirred for 14h in total. Then the solvent was concentrated under reduced pressure and reaction mixture was diluted with dichloromethane, washed with water followed by satd. NaHCO₃ solution and dried over anhyd. MgSO₄. The solvent was concentrated under reduced pressure, purified by column chromatography to afford corresponding ketone (**III.5**).



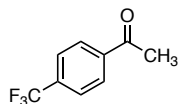
Acetophenone (**III.5b**). Purified by silica-gel column chromatography (10% ethyl acetate in hexanes). Yield: 64 mg (80%). ¹H NMR (δ, 23 °C, CDCl₃): 7.96 (dd, *J* = 8.4, 1.3 Hz, 2H), 7.59-7.53 (m, 1H), 7.44-7.49 (m, 2H), 2.61 (s, 3H). The spectral data are in good agreement with those reported in literature.²⁶¹



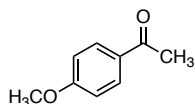
4-Bromoacetophenone (III.5c). Purified by silica-gel column chromatography (10% ethyl acetate in hexanes). Yield: 121 mg (91%). $^1\text{H NMR}$ (δ , 23 °C, CDCl_3): 7.82 (d, $J = 7.4$ Hz, 2H), 7.60 (d, $J = 7.2$ Hz, 2H), 2.58 (s, 3H). mp 50-53 °C (lit. 49-51 °C). The spectral data are in good agreement with those reported in literature.²⁶²



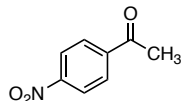
4-Methylacetophenone (III.5d). Purified by silica-gel column chromatography (10% ethyl acetate in hexanes). Yield: 71 mg (79%). $^1\text{H NMR}$ (δ , 23 °C, CDCl_3): 7.86 (d, $J = 8.1$ Hz, 2H), 7.26 (d, $J = 6.7$ Hz, 2H), 2.58 (s, 3H), 2.42 (s, 3H). The spectral data are in good agreement with those reported in literature.²⁶³



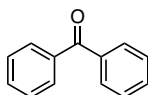
4-Trifluoromethylacetophenone (III.5e). Purified by silica-gel column chromatography (10% ethyl acetate in hexanes). Yield: 113 mg (90%). $^1\text{H NMR}$ (δ , 23 °C, CDCl_3): 8.07 (d, $J = 8.0$ Hz, 2H), 7.74 (d, $J = 8.0$ Hz, 2H), 2.65 (s, 3H). mp 33-35 °C (lit. 30-33 °C). The spectral data are in good agreement with those reported in literature.²⁶⁴



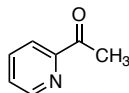
4-Methoxyacetophenone (III.5f). Purified by silica-gel column chromatography (20% ethyl acetate in hexanes). Yield: 10 mg (9%). $^1\text{H NMR}$ (δ , 23 °C, CDCl_3): 7.94 (d, $J = 8.9$ Hz, 2H), 6.93 (d, $J = 9.0$ Hz, 2H), 3.87 (s, 3H), 2.56 (s, 3H). mp 50-53 °C (lit. 49-51 °C). The spectral data are in good agreement with those reported in literature.²⁶²



4-Nitroacetophenone (III.5g). Purified by silica-gel column chromatography (10% ethyl acetate in hexanes). Yield: 95 mg (86%). $^1\text{H NMR}$ (δ , 23 °C, CDCl_3): 8.29 (d, $J = 6.6$ Hz, 2H), 8.10 (d, $J = 6.6$ Hz, 2H), 2.66 (s, 3H). mp 77-80 °C (lit. 75-78 °C). The spectral data are in good agreement with those reported in literature.²⁶⁵



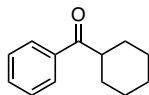
Benzophenone (III.5h). Purified by silica-gel column chromatography (10% ethyl acetate in hexanes). Yield: 103 mg (85%). $^1\text{H NMR}$ (δ , 23 °C, CDCl_3): 7.86 (d, $J = 7.1$ Hz, 4H), 7.67-7.51 (m, 6H). mp 46-48 °C (lit. 47-51 °C). The spectral data are in good agreement with those reported in literature.²⁶³



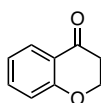
2-Acetylpyridine (III.5i). Purified by silica-gel column chromatography (25% ethyl acetate in hexanes). Yield: 37 mg (45%). $^1\text{H NMR}$ (δ , 23 °C, CDCl_3): 8.68-8.67 m (1H), 8.04-8.02 m (1H), 7.84-7.80 m (1H), 7.48-7.45 m (1H), 2.72 s (3H). The spectral data are in good agreement with those reported in literature.²⁶⁶



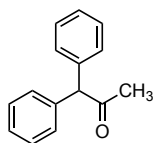
α -Tetralone (III.5j). Purified by silica-gel column chromatography (10% ethyl acetate in hexanes). Yield: 69 mg (73%). $^1\text{H NMR}$ (δ , 23 °C, CDCl_3): 8.03 (d, $J = 7.8$ Hz, 1H), 7.46 (td, $J = 7.5, 1.4$ Hz, 1H), 7.32-7.22 (m, 2H), 2.96 (t, $J = 6.1$ Hz, 2H), 2.65 (t, $J = 6.5$ Hz, 2H), 2.14 (t, $J = 6.4$ Hz, 2H). The spectral data are in good agreement with those reported in literature.²⁶⁷



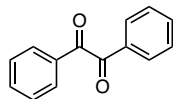
Phenylcyclohexyl ketone (III.5k). Purified by silica-gel column chromatography (10% ethyl acetate in hexanes). Yield: 79 mg (64%). $^1\text{H NMR}$ (δ , 23 °C, CDCl_3): 7.97 (d, $J = 8.1$ Hz, 2H), 7.56 (t, $J = 7.2$ Hz, 1H), 7.48 (t, $J = 7.6$ Hz, 2H), 3.33-3.24 (m, 1H), 1.94-1.86 (m, 4H), 1.79-1.74 (m, 1H), 1.59-1.27 (m, 5H). mp 56-58 °C (lit. 55-57 °C). The spectral data are in good agreement with those reported in literature.²⁶⁸



4-Chromanone (III.5l). Purified by silica-gel column chromatography (10% ethyl acetate in hexanes). Yield: 59 mg (60%). $^1\text{H NMR}$ (δ , 23 °C, CDCl_3): 7.89 (dd, $J = 8.1, 1.5$ Hz, 1H), 7.50-7.42 (m, 1H), 7.04-6.94 (m, 2H), 4.53 (t, $J = 6.6$ Hz, 2H), 2.80 (t, $J = 6.6$ Hz, 2H). mp 37-40 °C (lit. 35-38 °C). The spectral data are in good agreement with those reported in literature.²⁶⁷

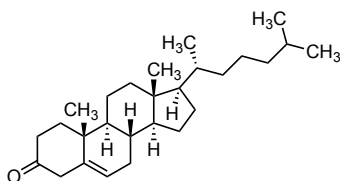


Diphenylacetone (III.5p). Purified by silica-gel column chromatography (10% ethyl acetate in hexanes). Yield: 46 mg (33%). $^1\text{H NMR}$ (δ , 23 °C, CDCl_3): 7.33-7.18 (m, 10H), 5.08 (s, 1H), 2.21 (s, 3H). mp 60-62 °C (lit. 59-63 °C). The spectral data are in good agreement with those reported in literature.²⁶⁹



Benzil (III.5q). Purified by silica-gel column chromatography (10% ethyl acetate in hexanes). Yield: 97 mg (69%). $^1\text{H NMR}$ (δ , 23 °C, CDCl_3): 7.98 (d, $J = 7.0$ Hz, 4H), 7.66 (t, $J =$

7.4 Hz, 2H), 7.52 (t, J = 7.8 Hz, 4H). mp 91-93 °C (lit. 94-95 °C). The spectral data are in good agreement with those reported in literature.²⁷⁰



Cholest-5-ene-3-one (III.5s). Purified by silica-gel column chromatography (10% ethyl acetate in hexanes). Yield: 146 mg (57%). mp 126-128 °C (lit. 129 °C). The spectral data are in good agreement with those reported in literature.²⁷¹

Method B. A 25-mL Schlenk tube was charged with nitromethane (1.0 mL), 1-(*tert*-butylsulfonyl)-2-iodobenzene (**III.1a**, 32.4 mg, 0.100 mmol, 15.0 mol%), and CoCl₂·6H₂O (1.70 mg, 0.007 mmol, 1.04 mol%). O₂ was bubbled through the reaction before butyraldehyde (250 μL, 2.78 mmol, 4.14 equiv) was added in one portion and stirred at room temperature for 20 min. Then subsequent alcohol (**III.4**, 0.670 mmol, 1.00 equiv) was dissolved in 1.0 ml nitromethane and delivered via syringe to the reaction mixture. The reaction mixture was stirred under O₂ atmosphere at 70 °C for 12h. Then the crude reaction mixture was analyzed by GC.



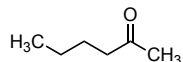
Cyclohexanone (III.5a). Yield: 86% (bp = 155 °C), crude reaction mixture was measured from GC with mesitylene as internal standard.



Cyclopentanone (III.5m). Yield: 77% (bp = 130.6 °C), crude reaction mixture was measured in GC with mesitylene (bp = 164.7 °C) as internal standard.



Cycloheptanone (III.5n). Yield: 91% (bp = 181.0 °C), crude reaction mixture was measured in GC with mesitylene (bp = 164.7 °C) as internal standard.

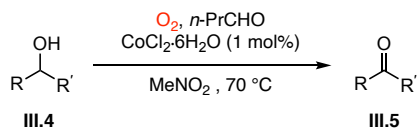


2-Hexanone (III.5o). Yield: 71% (bp = 127 °C), crude reaction mixture was measured in GC with mesitylene (bp = 164.7 °C) as internal standard.



Cyclohex-2-ene-1-one (III.5r). Yield: 40% (bp = 173.0 °C), crude reaction mixture was measured in GC with mesitylene (bp = 164.7 °C) as internal standard.

Analysis of Co-Catalyzed Background Reaction



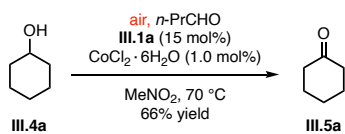
A 25-mL Schlenk tube was charged with nitromethane (2.0 mL) and $\text{CoCl}_2 \cdot 6\text{H}_2\text{O}$ (1.70 mg, 0.007 mmol, 1.04 mol%). O_2 was bubbled through the reaction before butyraldehyde (250 μL , 2.78 mmol, 4.14 equiv) was added in one portion and stirred at 23 °C for 20 min. Then, alcohol (0.67 mmol, 1.00 equiv) was dissolved in 1.0 ml nitromethane and delivered via syringe to the reaction mixture. The reaction mixture was stirred under O_2 (at the approximate flow rate of 30-35 mL/min) atmosphere at 70 °C for 12 h. Then the crude reaction mixture was analyzed by GC. All the results are tabulated in Table III-2.

Table III-2. Co-catalyzed background reactions.

Product	Yield	Yield w/o ArI	Yield w/o ArI & CoCl ₂
Cyclohexanone	86	15%	Trace
Acetophenone	80	22	15
4-Methylacetophenone	79	44	2
4-bromoacetophenone	91	62	5
2-acetyl pyridine	45	22	9
cyclopentanone	77	46	n.d.
Tetralone	72	34	n.d.
Cyclohex-2-ene-1-one	40	6	4
4-trifluoromethylacetophenone	90	40	n.d.
4-nitroacetophenone	86	34	n.d.
2-hexanone	71	15	n.d.
Cycloheptanone	91	44	n.d.
Benzil (from benzoin)	69	Benzoic acid (44%)- trace amt. of benzil	No reaction
Phenyl cyclohexyl ketone	64	31	n.d.
Benzoic acid (from benzyl alcohol)	81	51	14 (benzaldehyde)
<i>m</i> -CBA (from 3-cholorbenzyl alcohol)	86	22	n.d.
Nonanoic acid	63	Trace	No reaction
Heptanoic acid	59	Trace	No reaction
Lactol (from benzene-1,2-dimethanol)	79	No reaction	No reaction
Benzoic acid (from hydroxybenzoin)	73	38	n.d.
Chromanone	60	20	n.d.
Cholest-5-ene-3-one	57	No reaction	n.d.
Benzophenone	85	23	n.d.

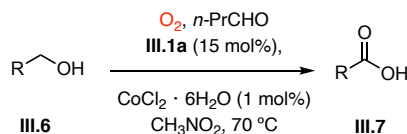
n.d. – not determined

Catalytic Oxidation of Cyclohexanol in Presence of Air

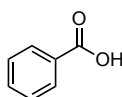


A 25-mL Schlenk tube was charged with nitromethane (1.0 mL), 1-(*tert*-butylsulfonyl)-2-iodobenzene (**III.1a**, 32.4 mg, 0.100 mmol, 15.0 mol%), and CoCl₂·6H₂O (1.70 mg, 0.007 mmol, 1.04 mol%). Air was bubbled through the reaction before butyraldehyde (250 μ L, 2.78 mmol, 4.14 equiv) was added in one portion and stirred at room temperature for 20 min. Then cyclohexanol (67.1 mg, 0.671 mmol, 1.00 equiv) was dissolved in 1.0 ml nitromethane and delivered via syringe to the reaction mixture. The reaction mixture was stirred under air (with flow rate of 30-35 mL/min) at 70 °C for 12h. Then the crude reaction mixture was analyzed by GC with the yield determined to be 66%.

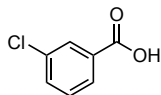
ArI-Catalyzed Aerobic Oxidation of Primary Alcohols



Method A. A 25-mL three-neck flask fitted with condenser (5 °C) was charged with nitromethane (5 mL), 1-(*tert*-butylsulfonyl)-2-iodobenzene (**III.1a**, 32.4 mg, 0.100 mmol, 15.0 mol%), and CoCl₂·6H₂O (1.70 mg, 0.007 mmol, 1.04 mol%). O₂ was bubbled through the reaction before butyraldehyde (90 μL, 1.0 mmol, 1.5 equiv) was added in one portion and stirred at room temperature for 20 min. Then, alcohol (**III.6**, 0.667 mmol, 1.00 equiv) was dissolved in 1.0 ml nitromethane (CH₂Cl₂ was used where the alcohol was insoluble in nitromethane) and delivered via syringe to the reaction mixture. The reaction mixture was stirred under constant O₂ bubbling (at the approximate flow rate of 30-35 mL/min), at 70 °C. Three more portions of butyraldehyde (90.0 μL, 1.00 mmol, 1.49 equiv) was added at an interval of 2 h and the reaction was stirred for 14 h in total. Then the solvent was reduced and crude reaction mixture was analyzed.

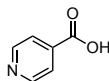


Benzoic acid (**III.7a**). Purified by silica-gel column chromatography (10% ethyl acetate in hexanes). Yield: 66 mg (81%). ¹H NMR (δ, 23 °C, CDCl₃): 8.12 (d, *J* = 7.0 Hz, 2H), 7.65-7.60 (m, 1H), 7.48 (t, *J* = 7.5 Hz, 2H). mp 124-126 °C (lit. 121-125 °C). The spectral data are in good agreement with those reported in literature.²⁷²



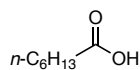
3-Chlorobenzoic acid (**III.7c**). Purified by silica-gel column chromatography (10% ethyl acetate in hexanes). Yield: 90 mg (86%). ¹H NMR (δ, 23 °C, CDCl₃): 8.10 (t, *J* = 1.8 Hz, 1H),

8.02 (t, $J = 1.3$ Hz, 1H), 7.60 (ddd, $J = 8.0, 2.1, 1.1$ Hz, 1H), 7.43 (t, $J = 7.9$ Hz, 1H). mp 150-153 °C (lit. 153-157 °C). The spectral data are in good agreement with those reported in literature.²⁶⁵

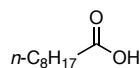


4-Picolinic acid or Isonicotinic acid (III.7d). The general procedure for Method B was modified for this substrate in that the reaction was carried out on a 0.34 mmol scale. Purified by silica-gel column chromatography (5% MeOH in CH₂Cl₂). Yield: 26 mg (61%). ¹H NMR (δ , 23 °C, DMSO-*d*₆): 8.78 (d, $J = 6.0$ Hz, 2H), 7.82 (d, $J = 6.0$ Hz, 2H). mp >300 °C (lit. >300 °C). The spectral data are in good agreement with those reported in literature.²⁷³

Method B. A 25-mL Schlenk tube was charged with nitromethane (1.0 mL), 1-(*tert*-butylsulfonyl)-2-iodobenzene (**III.1a**, 32.4 mg, 0.100 mmol, 15.0 mol%) and CoCl₂·6H₂O (1.70 mg, 0.007 mmol, 1.04 mol%). O₂ was bubbled through the reaction before butyraldehyde (250 μ L, 2.78 mmol, 4.14 equiv) was added in one portion and stirred at room temperature for 20 min. Then subsequent alcohol (**6**, 0.667 mmol, 1.00 equiv) was dissolved in 1.0 ml nitromethane and delivered via syringe to the reaction mixture. The reaction mixture was stirred under O₂ atmosphere at 70 °C for 12h. Then the crude reaction mixture was analyzed by GC.

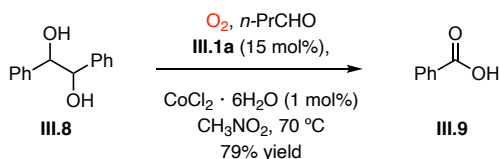


Heptanoic acid (III.7e). Yield: 59% (bp = 223.0 °C), crude reaction mixture was measured in GC with mesitylene (bp = 164.7 °C) as internal standard.

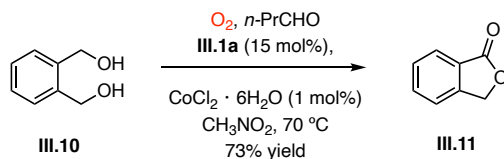


Nonanoic acid (7f). Yield: 63% (bp = 269.0 °C), crude reaction mixture was measured in GC with mesitylene (bp = 164.7 °C) as internal standard.

ArI-Catalyzed Aerobic Oxidation of Diols



Oxidation of hydroxybenzoin (III.8). A 25-mL three-neck flask fitted with condenser (5 °C) was charged with nitromethane (5 mL), hydroxybenzoin (III.8, 143 mg, 0.67 mmol, 1.0 equiv), 1-(*tert*-butylsulfonyl)-2-iodobenzene (III.1a, 32 mg, 0.10 mmol, 15 mol%), and CoCl₂·6H₂O (1.70 mg, 0.007 mmol, 1.04 mol%). O₂ was bubbled through the reaction before butyraldehyde (90 μL, 1.0 mmol, 1.5 equiv) was added in one portion and stirred at room temperature for 20 min. The reaction mixture was then heated at 70 °C and stirred under constant O₂ bubbling (at the approximate flow rate of 30-35 mL/min). Three more portions of butyraldehyde (90 μL, 1.0 mmol, 1.5 equiv) was added at an interval of 2 h and the reaction was stirred for 14 h in total. Then crude reaction mixture was concentrated under reduced pressure and purified by silica-gel column chromatography (20% ethyl acetate in hexanes) to afford 130 mg (79%) of the title compound III.9 as a white solid. ¹H NMR (δ, 23 °C, CDCl₃): 8.12 (d, *J* = 7.0 Hz, 2H), 7.65-7.60 (m, 1H), 7.48 (t, *J* = 7.5 Hz, 2H). mp 126-129 °C (lit. 121-125 °C). The spectral data are in good agreement with those reported in literature.²⁰¹



Oxidation of benzene-1,2-dimethanol (III.10). A 25-mL three-neck flask fitted with condenser (5 °C) was charged with nitromethane (5 mL), 1,2-benzenedimethanol (**III.10**, 92.5 mg, 0.67 mmol, 1.0 equiv), 1-(*tert*-butylsulfonyl)-2-iodobenzene (**III.1a**, 32 mg, 0.10 mmol, 15 mol%), and CoCl₂·6H₂O (1.7 mg, 0.007 mmol, 1.04 mol%). O₂ was bubbled through the reaction before butyraldehyde (90 μL, 1.0 mmol, 1.5 equiv) was added in one portion and stirred at 23 °C for 20 min. The reaction mixture was then heated at 70 °C and stirred under constant O₂ bubbling (at the approximate flow rate of 30-35 mL/min). Three more portions of butyraldehyde (90 μL, 1.0 mmol, 1.5 equiv) was added at an interval of 2 h and the reaction was stirred for 14 h in total. The crude reaction mixture was concentrated under reduced pressure and purified by silica gel column chromatography (10% ethyl acetate in hexanes) to afford 66 mg (73%) of the title compound **III.11** as white solid. ¹H NMR (δ, 23 °C, CDCl₃): 7.93 (d, *J* = 7.4 Hz, 1H), 7.69 (t, *J* = 7.5 Hz, 1H), 7.56-7.49 (m, 2H), 5.33 (s, 2H). mp 73-75 °C (lit. 75-76 °C). The spectral data are in good agreement with those reported in literature.²⁷⁴

Measurement of Oxygen Flow for Catalysis Reaction

A 1000-mL measuring cylinder was filled with deionized water to the brim and submerged upside down in a water bucket. Then a needle with constant oxygen flow rate was inserted into measuring cylinder and water displacement by oxygen was recorded. The experiment was repeated four times with flow rate determined to be 30-35 mL/min.

Role of $\text{CoCl}_2 \cdot 6\text{H}_2\text{O}$ in Catalysis Reaction

Aldehyde autoxidation occurs via radical chain propagation mechanism which requires initiation step.¹⁷⁷ Previously, we have evaluated various metal salts as initiators, and $\text{CoCl}_2 \cdot 6\text{H}_2\text{O}$ was found to be the best for oxidation of iodobenzene to diacetoxyiodobenzene. The initiation of autoxidation is evidence by the data summarized in Figure III-2. The Co-mediated initiation likely proceeds via reaction of Co(II) with O_2 to generate a superoxide intermediate²⁷⁵ that serves to initiate the autoxidation radical chain.

For the reported catalytic condition in this manuscript, autoxidation of *n*-butyraldehyde requires $\text{CoCl}_2 \cdot 6\text{H}_2\text{O}$ to act as radical chain initiator. From control reaction, modest Co-catalyzed background reactions were observed for some substrates (Table III-2). To further clarify the role of $\text{CoCl}_2 \cdot 6\text{H}_2\text{O}$ in the catalytic reaction condition, background reactions for all the substrates were carried out and yields for background reactions were found to be lower than the catalytic condition.

NaBr additives have been reported to be needed to increase the rate of Co(II) induced alcohol oxidation in presence of peracetic acid and Co-catalyzed oxidation of primary aliphatic alcohols have been reported to not proceed.²⁷⁶ In the present investigation, both 1-heptanol and 1-nonanol were oxidized to corresponding carboxylic acids in catalytic reaction condition with 59% and 63% yield respectively.

Reaction Profile for Cyclohexanol Oxidation by III.3a with and without Co(II)

A 20-mL scintillation vial was charged with nitromethane (3 mL), 1-(*tert*-butylsulfonyl)-2-iodylbenzene (**III.3a**, 77.4 mg, 0.217 mmol, 1.01 equiv), and cyclohexanol (**III.4a**, 21.7 mg, 0.217 mmol, 1.00 equiv) and was tightly capped (Sample 1). Another 20-mL scintillation vial was charged with nitromethane (3 mL), 1-(*tert*-butylsulfonyl)-2-iodylbenzene (**III.3a**, 87.1 mg, 0.244 mmol, 1.00 equiv), cyclohexanol (**III.4a**, 24.4 mg, 0.244 mmol, 1.00 equiv), and $\text{CoCl}_2 \cdot 6\text{H}_2\text{O}$ (**3a**, 0.500 mg, 0.002 mmol, 1.00 mol%) and was tightly capped (Sample 2). Both the reaction mixtures were stirred at 70 °C and aliquot of 100 μL reaction mixture were taken out from both for GC analysis against an internal standard at regular time intervals. The kinetics data (Figure III-14) for both with and without $\text{CoCl}_2 \cdot 6\text{H}_2\text{O}$ is plotted below and demonstrates that addition of $\text{CoCl}_2 \cdot 6\text{H}_2\text{O}$ to the reaction mixture does not accelerate alcohol oxidation.

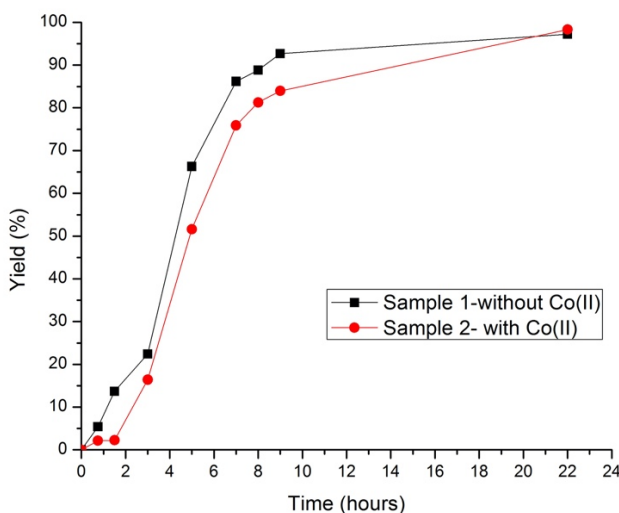


Figure III-14. Reaction Profile for Cyclohexanol Oxidation by III.3a with and without Co(II). % Yield of sample 1 (—) and sample 2 (—) as a function of time for the oxidation of cyclohexanol by compound III.3a in stoichiometric condition. Sample 1 was without $\text{CoCl}_2 \cdot 6\text{H}_2\text{O}$ and Sample 2 was charged with $\text{CoCl}_2 \cdot 6\text{H}_2\text{O}$ (1 mol%).

Kinetics Data

Measurement of aerobic oxidation kinetics of 2-(*tert*-butylsulfonyl)iodobenzene in CDCl₃. A 20-mL scintillation vial was charged with CDCl₃ (4.0 mL), 2-(*tert*-butylsulfonyl)iodobenzene (**1a**, 0.130 g, 0.401 mmol, 1.00 equiv), and CoCl₂·6H₂O (1.0 mg, 4.20 μmol, 1 mol%), and fitted with a rubber septum. 1,1,2,2-tetrachloroethane (20 μL, 0.189 mmol) was added to the reaction mixture as internal standard. The reaction vessel was purged with O₂ for 5 min. An aliquot (0.200 mL) was removed and the ¹H NMR spectrum was recorded. Acetaldehyde (245 μL, 4.03 mmol, 10.0 equiv) was added to the reaction vessel and the reaction mixture was stirred at 23 °C under 1 atm O₂, delivered by inflated balloon. Aliquots (0.200 mL) were removed periodically for ¹H NMR analysis. Monitoring was continued until the reaction had reached completion, as evidenced by the disappearance of ¹H NMR resonances attributable to iodobenzene. Data and spectra are collected in Figure III-15.

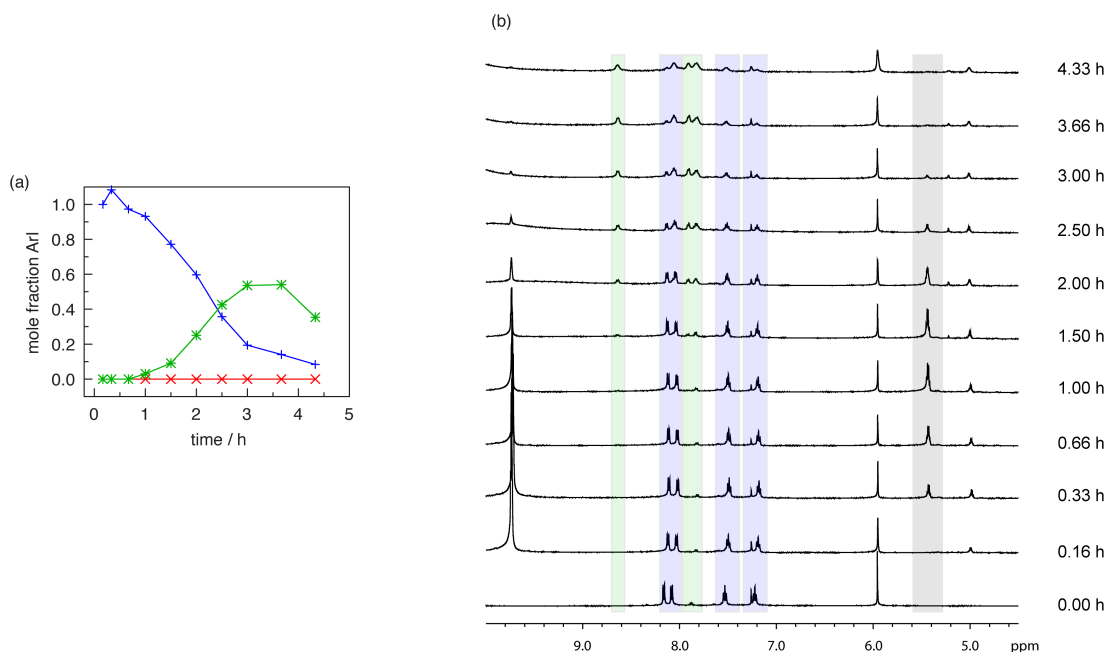


Figure III-15. Measurement of aerobic oxidation kinetics of 2-(*tert*-butylsulfonyl)iodobenzene in CDCl₃. Mol fraction of III.1a (+), III.2a (x), and III.3a (*) as a function of time for oxidation of III.1a in CDCl₃ at 23 °C in the presence of CoCl₂·6H₂O (1 mol%). (b) Stacked ¹H NMR spectra obtained periodically during the oxidation of III.1a with signals attributable to 1a (—), 2a (—), and 3a (—) highlighted. Poor solubility of III.3a accounts for the apparent decreasing concentration at longer reaction times.

Measurement of aerobic oxidation kinetics of 4-iodotoluene in CDCl₃. A 20-mL scintillation vial was charged with CDCl₃ (4.0 mL), 4-iodotoluene (**1e**, 174.4 mg, 0.800 mmol, 1.00 equiv), and CoCl₂·6H₂O (1.0 mg, 7.70 μmol, 1 mol%) and was fitted with a rubber septum. 1,4-Dibromobenzene (94.4 mg, 0.400 mmol) was added to the reaction mixture as internal standard. The reaction vessel was purged with O₂ for 5 min. An aliquot (0.200 mL) was removed and the ¹H NMR spectrum was recorded. Acetaldehyde (450 μL, 8.04 mmol, 10.1 equiv) was added to the reaction vessel and the reaction mixture was stirred at 23 °C under 1 atm O₂, delivered by inflated balloon. Aliquots (0.200 mL) were removed periodically for ¹H NMR analysis. Monitoring was continued until the reaction had reached completion, as evidenced by the disappearance of ¹H NMR resonances attributable to **III.1e**. Data and spectra are collected in Figure III-16.

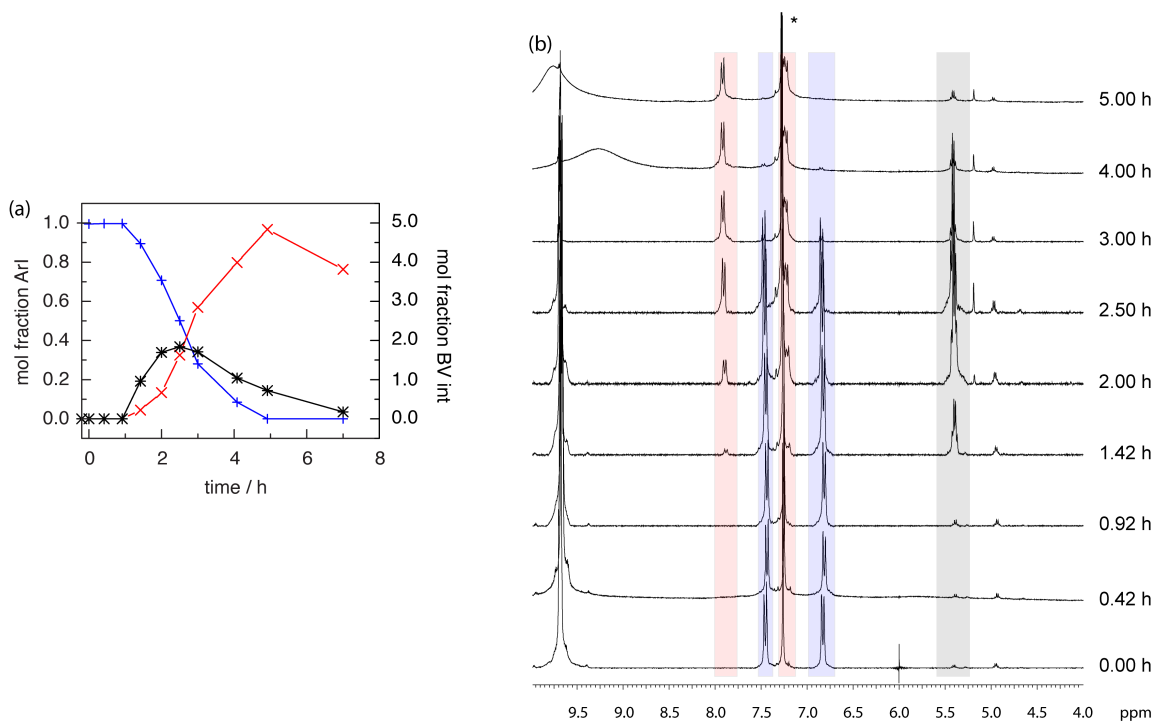


Figure III-16. Measurement of aerobic oxidation of 4-iodotoluene in CDCl₃. Mol fraction of **III.1e** (+), **III.2e** (x), and Baeyer-Villiger intermediate 1-hydroxyethyl ethaneperoxoate (*) as a function of time for oxidation of 4-iodotoluene (**III.1e**) in CDCl₃ at 23 °C in the presence of CoCl₂·6H₂O (1 mol%). (b) Stacked ¹H NMR spectra obtained periodically during the oxidation of

1e with signals attributable to **III.1e** (—), **III.2e** (—), and the Baeyer-Villiger intermediate (—) highlighted; * = 1,4-dibromobenzene added as internal standard. Poor solubility of **III.3e** prevents determination of the concentration of this species.

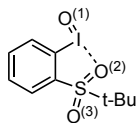
Computational Details

Calculations were performed using the Gaussian 09, Revision D.01 suite of software.²⁷⁷ Various basis sets and functionals were evaluated for geometry optimization and results were compared against crystallographically determined structures of **III.2a** and **III.3a**.²⁴⁰ In each case, stationary points were characterized with frequency calculations using the same basis set and functional used for the geometry optimization. M062X geometries (LANL2DZ basis set for I, 6-31+G** for other atoms) reproduced experimental metrical parameters. Optimizations and frequency calculations were carried out using an SMD solvation model. Both dichloromethane and nitromethane solvation were evaluated and the identity of the solvent was found to have negligible impact on the resulting geometries and disproportionation thermodynamics.

Gas-phase geometry optimizations and TD-DFT calculations were carried out using an SDD basis set for Rh and 6-31G* for all other atoms.^{254,278} Single-point solvent corrections (THF) were carried out using a Polarizable Continuum Model using the integral equation formalism variant. B3LYP geometries well reproduced experimental metrical parameters, obtained by X-ray crystallography (tabulated in Tables III-3 and III-4) and provided similar structural parameters as optimizations carried out with either M06^{250, 279} or M06-L²⁸⁰ functionals.

Geometry comparison

Table III-3. Comparison of experimental metrical parameters for I(III) compound III.2a with optimized structures using various basis sets and functionals. The best agreement between experiment and theory was obtained using the M062X functional, LANL2DZ basis set



for I, and 6-31+G** for all other atoms.

Bonds	Expt.	Conditions A*	Conditions B†	Conditions C‡	Conditions D§
I–O(1)	1.848(6)	1.9363	1.90703	1.87669	1.85825
I–O(2)	2.707(5)	2.8089	2.80428	2.81286	2.80589
I–C	2.128(7)	2.1913	2.17896	2.14103	2.11909
S–O(2)	1.441(5)	1.4935	1.49378	1.47950	1.45396
S–O(3)	1.425(5)	1.4801	1.48018	1.46691	1.44234
C–I–O(1)	94.8(3)	95.6986	95.90032	95.16019	97.31658
O(2)–I–O(1)	167.3(2)	167.7664	168.04528	167.28958	169.58619

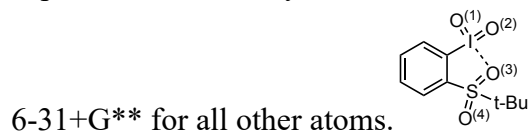
* Conditions A: B3LYP with sdd for I and 6-31+G** for other atoms. Similar computations have previously been utilized to compute hypervalent iodine geometries and energies: Ling, L.; Liu, K.; Li, X.; Li, Y. *ACS Catal.* **2015**, *5*, 2458–2468.

† Conditions B: B3LYP with LANL2DZ for I and 6-31+G** for other atoms.

‡ Conditions C: M062X with LANL2DZ for I and 6-31+G** for other atoms.

§ Conditions D: M062X with (aug-)cc-pVTZ for I, (aug-)cc-pV(X+d)Z for S, and (aug)cc-pVTZ for other atoms. Similar computations have previously be utilized to compute hypervalent iodine geometries and energies: Jiang, H.; Sun, T.-Y.; Wang, X.; Xie, Y.; Zhang, X.; Wu, Y.-D.; Schaefer, H. F. III. *Org. Lett.* **2017**, *19*, 6502–6505.

Table III-4. Comparison of experimental metrical parameters for I(V) compound III.3a with optimized structures using various basis sets and functionals. The best agreement between experiment and theory was obtained using the M062X functional, LANL2DZ basis set for I, and



Bonds	Expt.	Conditions A	Conditions B	Conditions C	Conditions D
I–O(1)	1.796(2)	1.8482	1.82929	1.79914	1.79913
I–O(2)	1.822(2)	1.8439	1.82738	1.79715	1.79649
I–O(3)	2.693(2)	2.8024	2.78872	2.73815	2.76880
I–C	2.140(4)	2.2359	2.21555	2.15551	2.13711
S–O(3)	1.455(3)	1.4862	1.49441	1.48109	1.45548
S–O(4)	1.439(3)	1.4706	1.47830	1.46494	1.44081
C–I–O(1)	95.1	93.0508	94.06264	93.85952	95.70322
O(2)–I–O(1)	166.1	155.4518	163.45711	166.0360	163.99788

Computed Structure-Dependent Disproportionation Thermodynamics

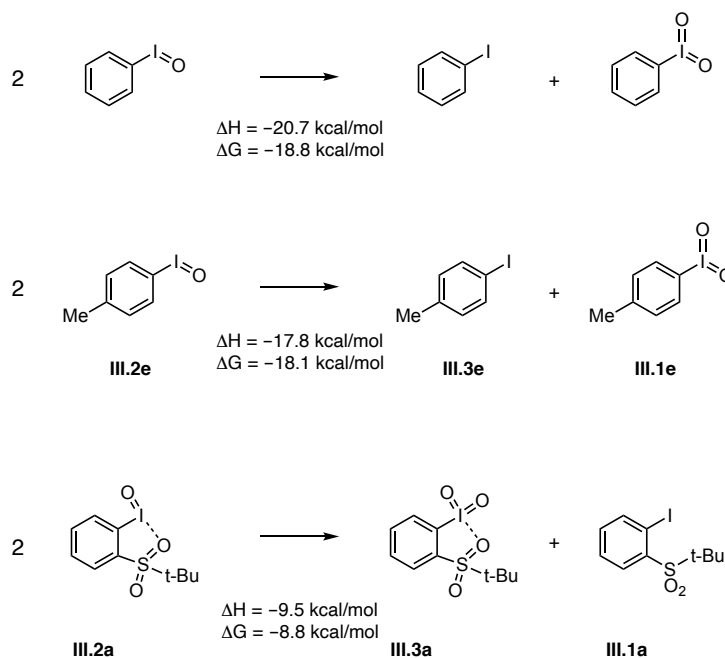


Figure III-17. Structure-dependent disproportionation thermodynamics. The thermodynamic parameters reported below are derived from DFT calculations carried out with Conditions C (M062X with LANL2DZ for I and 6-31+G** for other atoms).

Table III-5. Coordinates for optimized geometry of PhI using SMD solvation model (CH₂Cl₂).

Atom	X	Y	Z
C	-3.344652	0.000000	-0.000002
C	-2.645423	-1.206382	-0.000002
C	-1.249524	-1.214042	-0.000001
C	-0.566395	0.000002	0.000000
C	-1.249525	1.214042	0.000000
C	-2.645427	1.206380	-0.000002
H	-4.430301	-0.000003	-0.000003
H	-3.182607	-2.150206	-0.000003
H	-0.706760	-2.153797	-0.000001
H	-0.706766	2.153801	0.000000
H	-3.182609	2.150205	-0.000002
I	1.554995	0.000000	0.000001

Table III-6. Coordinates for optimized geometry of PhIO using SMD solvation model (CH₂Cl₂).

Atom	X	Y	Z
C	3.483889	0.022108	0.134418
C	2.782692	1.220705	0.002784
C	1.393408	1.209752	-0.122477
C	0.728843	-0.014493	-0.116653
C	1.412839	-1.220209	0.019773
C	2.802633	-1.194811	0.140783
H	4.565065	0.036788	0.232548
H	3.313205	2.167881	-0.000370
H	0.843037	2.139808	-0.224947
H	0.876240	-2.163716	0.029878
H	3.347561	-2.127862	0.246134
I	-1.384242	-0.034968	-0.247850
O	-1.900761	0.207766	1.562631

Table III-7. Coordinates for optimized geometry of PhIO₂ using SMD solvation model (CH₂Cl₂).

Atom	X	Y	Z
C	3.573311	0.032900	0.111449
C	2.851764	1.226515	0.132362
C	1.461380	1.205867	0.010822
C	0.839046	-0.025399	-0.128379
C	1.529456	-1.230348	-0.155215
C	2.918074	-1.191312	-0.031610
H	4.654148	0.055474	0.211367
H	3.365600	2.175230	0.251111
H	0.875294	2.120274	0.045597
H	1.007027	-2.177735	-0.255531
H	3.483850	-2.117522	-0.040312
I	-1.277465	-0.046000	-0.230201
O	-1.521322	1.582480	0.508263
O	-1.568488	-1.298362	1.035720

Table III-8.Coordinates for optimized geometry of III.1a using SMD solvation model (CH₂Cl₂).

Atom	X	Y	Z
C	0.726764	2.412046	-0.304257
C	0.242902	1.097638	-0.321072
C	-1.087228	0.836802	0.030703
C	-1.902969	1.904466	0.416929
C	-1.411445	3.206614	0.444436
C	-0.094069	3.465954	0.076918
H	1.753998	2.596456	-0.600812
H	-2.935815	1.713764	0.688149
H	-2.068680	4.016463	0.745635
H	0.294550	4.478750	0.082735
I	-2.055217	-1.051291	-0.003107
S	1.473066	-0.129050	-0.817082
O	2.466127	0.597831	-1.623741
O	0.801403	-1.281112	-1.429769
C	2.317727	-0.684268	0.718356
C	3.394979	-1.659747	0.236214
H	3.921288	-2.036803	1.118645
H	2.958222	-2.510785	-0.293518
H	4.121109	-1.164831	-0.414107
C	1.308801	-1.379495	1.625245
H	0.853445	-2.244325	1.135837
H	1.843763	-1.726463	2.515469
H	0.518479	-0.697140	1.954340
C	2.942584	0.528526	1.403318
H	3.602153	1.078384	0.726328
H	3.541414	0.165208	2.244713
H	2.184986	1.209569	1.801901

Table III-9. Coordinates for optimized geometry of III.2a using SMD solvation model (CH₂Cl₂).

Atom	X	Y	Z
C	-1.008420	2.430924	-0.319947
C	-0.482769	1.137608	-0.330532
C	0.856727	0.922554	-0.020216
C	1.672528	1.984609	0.342600
C	1.139630	3.273978	0.375558
C	-0.193064	3.500956	0.036407
H	-2.047086	2.589467	-0.595306
H	2.715098	1.788465	0.586232
H	1.778014	4.106022	0.655760
H	-0.598247	4.507208	0.044782
I	1.864058	-0.964941	-0.101790
S	-1.582266	-0.197263	-0.777477
O	-0.706803	-1.317252	-1.187478
O	-2.556972	0.321337	-1.743300
C	-2.482466	-0.708070	0.737721
C	-3.434413	-1.813549	0.272901
H	-3.968126	-2.183151	1.153848
H	-4.168690	-1.434612	-0.442568
H	-2.891833	-2.650573	-0.175364
C	-3.253289	0.492708	1.280857
H	-3.896944	0.938916	0.517356
H	-3.890520	0.137791	2.097061
H	-2.585501	1.257629	1.687381
C	-1.467976	-1.232937	1.748789
H	-0.939487	-2.110929	1.368123
H	-2.016360	-1.526154	2.649685
H	-0.740420	-0.466143	2.036174
O	3.475321	-0.327650	0.619092

Table III-10. Coordinates for optimized geometry of III.3a using SMD solvation model (CH₂Cl₂).

Atom	X	Y	Z
C	-1.239045	2.401194	-0.436195
C	-0.640275	1.146903	-0.345548
C	0.680849	1.027907	0.074338
C	1.415412	2.149765	0.420937
C	0.814111	3.408165	0.341140
C	-0.503514	3.534260	-0.091216
H	-2.265014	2.485861	-0.782250
H	2.446249	2.034879	0.749074
H	1.386640	4.290242	0.609178
H	-0.963242	4.514120	-0.166328
I	1.800091	-0.813989	0.104857
S	-1.617721	-0.286919	-0.768901
O	-0.631448	-1.360761	-1.029206
O	-2.553109	0.091115	-1.831064
C	-2.570911	-0.769462	0.722086
C	-3.392818	-1.983515	0.278814
H	-3.948390	-2.343125	1.150243
H	-4.109395	-1.715341	-0.501833
H	-2.753853	-2.794803	-0.080820
C	-3.473020	0.391945	1.128723
H	-4.102756	0.720635	0.297236
H	-4.127307	0.040809	1.932758
H	-2.899659	1.241703	1.510341
C	-1.578871	-1.134439	1.822094
H	-0.948780	-1.979335	1.529500
H	-2.152113	-1.429002	2.706580
H	-0.947620	-0.285207	2.106779
O	3.191316	-0.095637	0.991068
O	2.342295	-0.895422	-1.606610

Table III-11. Coordinates for optimized geometry of *p*-sulfone I(I) using SMD solvation model (CH₂Cl₂).

Atom	X	Y	Z
C	0.321344	1.216110	-0.442563
C	-1.058081	1.216170	-0.247405
C	-1.732778	-0.000018	-0.147606
C	-1.058087	-1.216221	-0.247273
C	0.321329	-1.216202	-0.442437
C	0.994487	-0.000057	-0.529975
H	0.863175	2.152454	-0.537027
H	-1.595437	-2.156356	-0.180917
H	0.863126	-2.152578	-0.536761
I	-3.823263	0.000015	0.162520
S	2.761859	-0.000043	-0.784767
O	3.108362	-1.266895	-1.448927
O	3.108359	1.266702	-1.449159
C	3.544451	0.000056	0.875622
C	3.119411	1.263131	1.619804
H	3.652828	1.285806	2.575549
H	3.380847	2.165389	1.060217
H	2.046646	1.267985	1.835318
C	5.050736	0.000007	0.601718
H	5.356791	0.891159	0.047076
H	5.566814	-0.000087	1.566800
H	5.356652	-0.891098	0.046953
C	3.119378	-1.262862	1.620024
H	2.046616	-1.267603	1.835572
H	3.652882	-1.285407	2.575721
H	3.380736	-2.165242	1.060581
H	-1.595414	2.156311	-0.181147

Table III-12. Coordinates for optimized geometry of *p*-sulfone I(III) using SMD solvation model (CH₂Cl₂).

Atom	X	Y	Z
C	-0.571155	-1.387275	-0.191980
C	0.806878	-1.415464	0.008657
C	1.515516	-0.226076	-0.114043
C	0.918110	0.985097	-0.427904
C	-0.461031	1.008135	-0.631339
C	-1.184467	-0.175288	-0.504450
H	-1.160018	-2.296591	-0.119417
H	1.523989	1.884230	-0.517752
H	-0.963601	1.933455	-0.897788
I	3.620468	-0.179088	0.167369
S	-2.951852	-0.146457	-0.770137
O	-3.236259	0.956726	-1.700929
O	-3.357047	-1.511432	-1.147164
C	-3.728707	0.248608	0.848159
C	-3.320320	-0.823719	1.853508
H	-3.861777	-0.637978	2.786844
H	-3.581343	-1.825338	1.500344
H	-2.249317	-0.786567	2.074492
C	-5.235427	0.211934	0.579567
H	-5.557908	-0.778524	0.247747
H	-5.749617	0.446646	1.516536
H	-5.527136	0.953981	-0.169145
C	-3.274614	1.637780	1.287344
H	-2.203600	1.665965	1.509296
H	-3.809849	1.893067	2.207509
H	-3.506513	2.393285	0.531947
O	3.830250	1.674222	-0.115633
H	1.307294	-2.349195	0.245734

Table III-13. Coordinates for optimized geometry of *p*-sulfone I(V) using SMD solvation model (CH₂Cl₂).

Atom	X	Y	Z
C	0.676903	1.203052	-0.427500
C	-0.696628	1.194927	-0.189857
C	-1.326067	-0.030742	-0.030428
C	-0.665361	-1.249068	-0.105784
C	0.707107	-1.237760	-0.348447
C	1.354471	-0.012005	-0.491639
H	1.208193	2.138152	-0.575037
H	-1.196835	-2.190441	-0.001349
H	1.260536	-2.167667	-0.437280
I	-3.417121	-0.013718	0.335879
S	3.119584	0.003836	-0.802752
O	3.451028	-1.257931	-1.481474
O	3.428354	1.276592	-1.471346
C	3.943060	0.005021	0.837337
C	3.504919	1.247993	1.607452
H	4.060826	1.271243	2.550252
H	3.730871	2.163647	1.054198
H	2.437829	1.224184	1.849062
C	5.441411	0.047257	0.523976
H	5.711739	0.955316	-0.021400
H	5.980860	0.042503	1.476091
H	5.755330	-0.826427	-0.053759
C	3.570215	-1.277860	1.575651
H	2.506232	-1.308350	1.829502
H	4.137354	-1.302654	2.511582
H	3.830141	2.166098	0.993681
O	-3.875016	-1.384357	-0.740982
O	-3.757914	1.536288	-0.516831
H	-1.260785	2.122633	-0.152618

NMR Spectra:

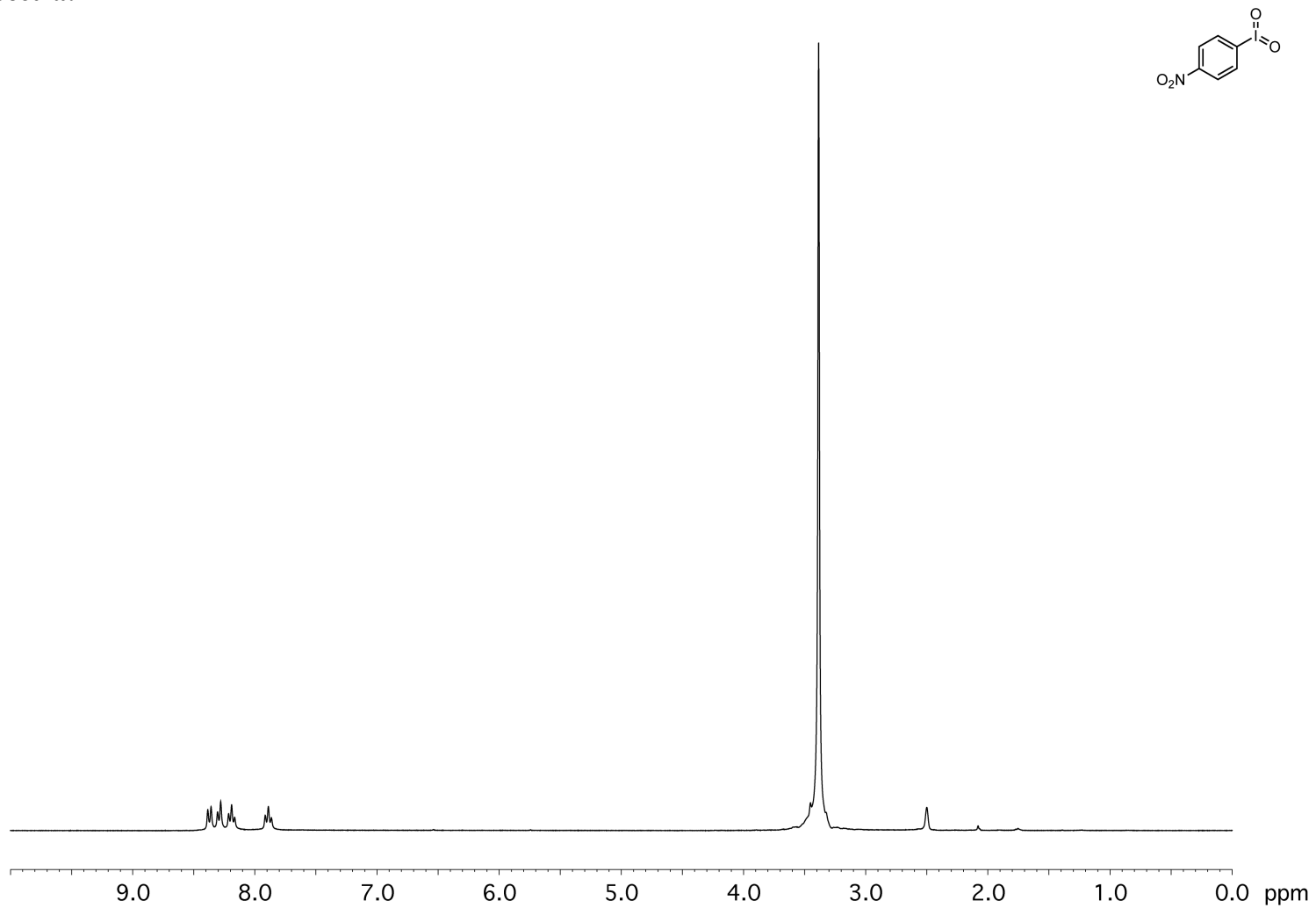


Figure III-18. ¹H NMR of compound III.3b measured in DMSO-*d*₆ at 23 °C.

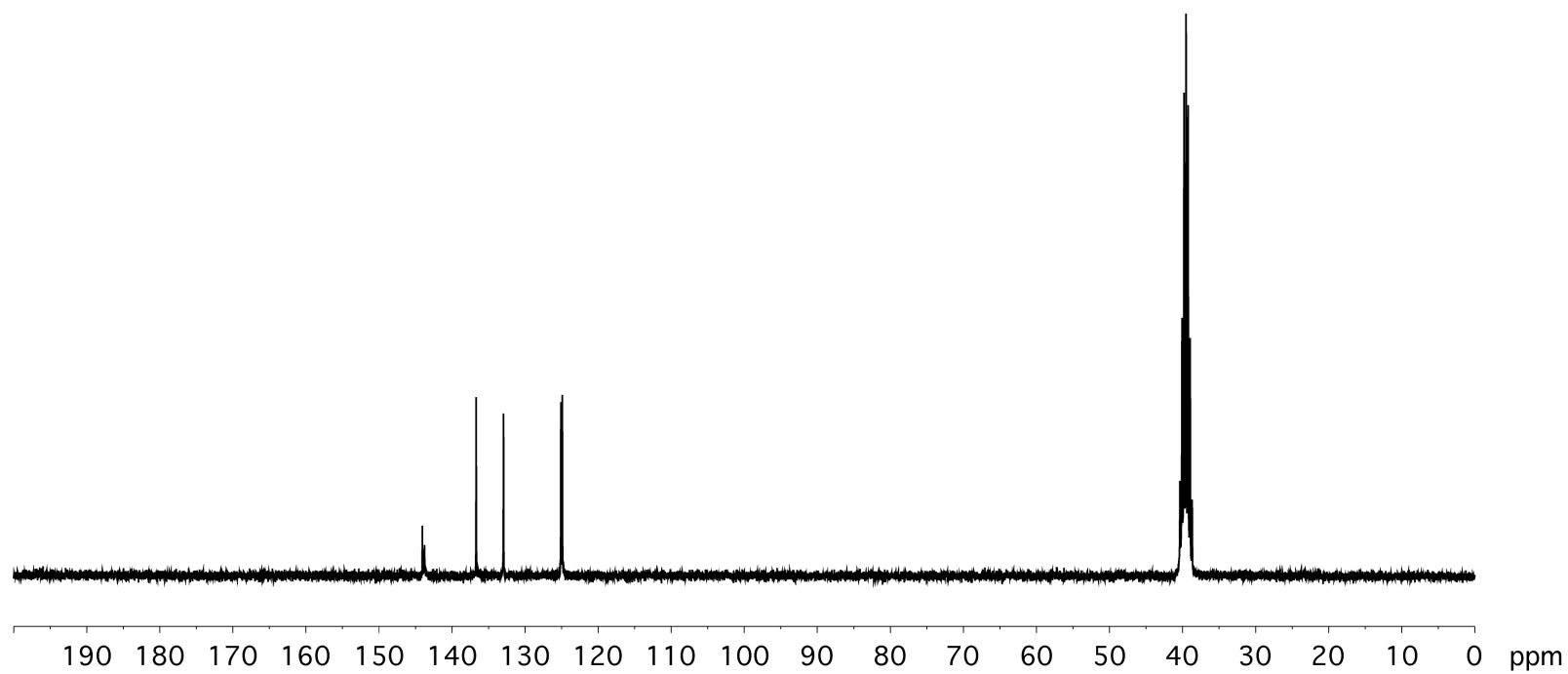
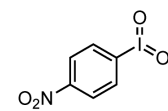


Figure III-19. ^{13}C NMR of compound III.3b measured in DMSO- d_6 at 23 °C.

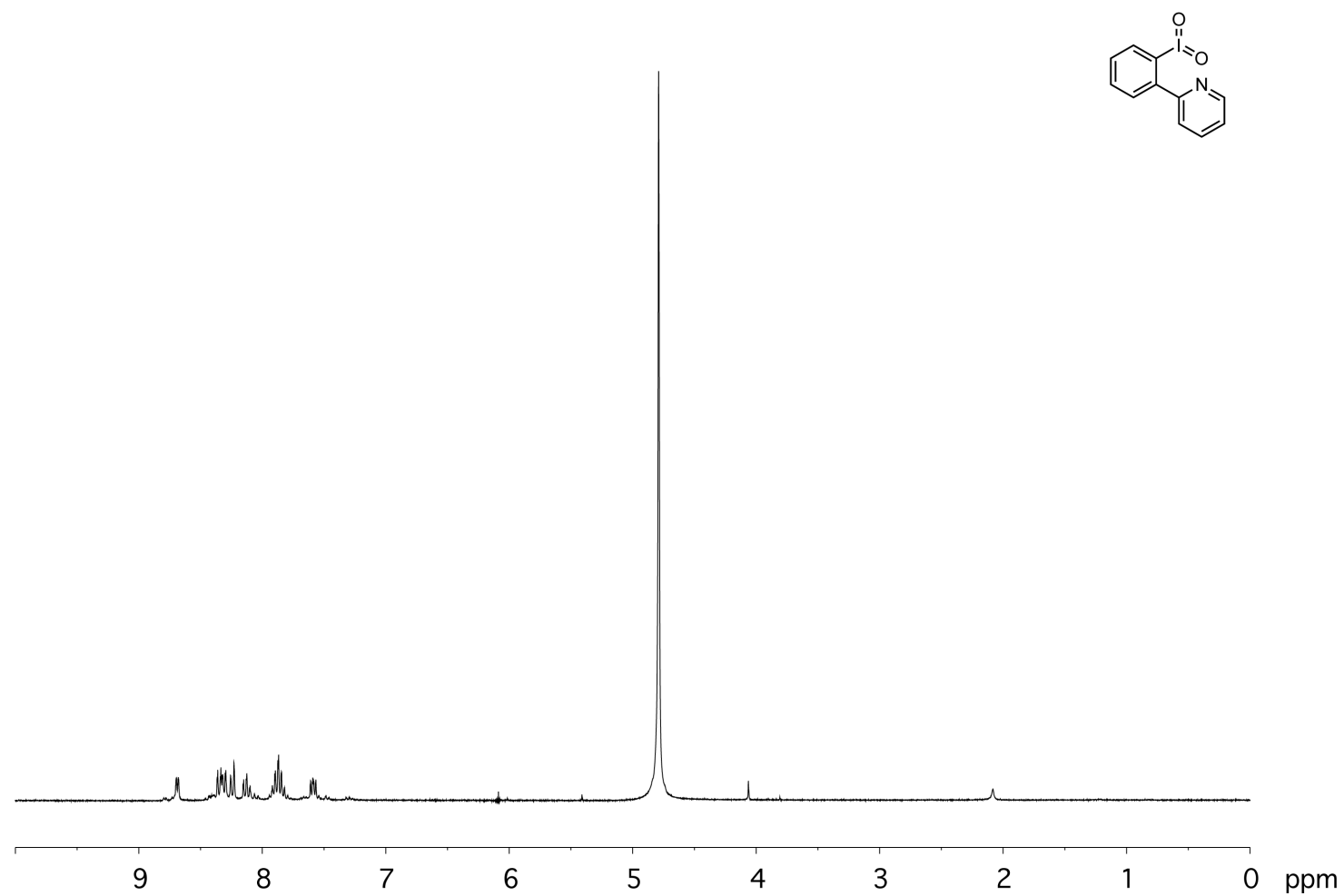


Figure III-20. ¹H NMR of compound III.3c measured in D₂O at 23 °C.

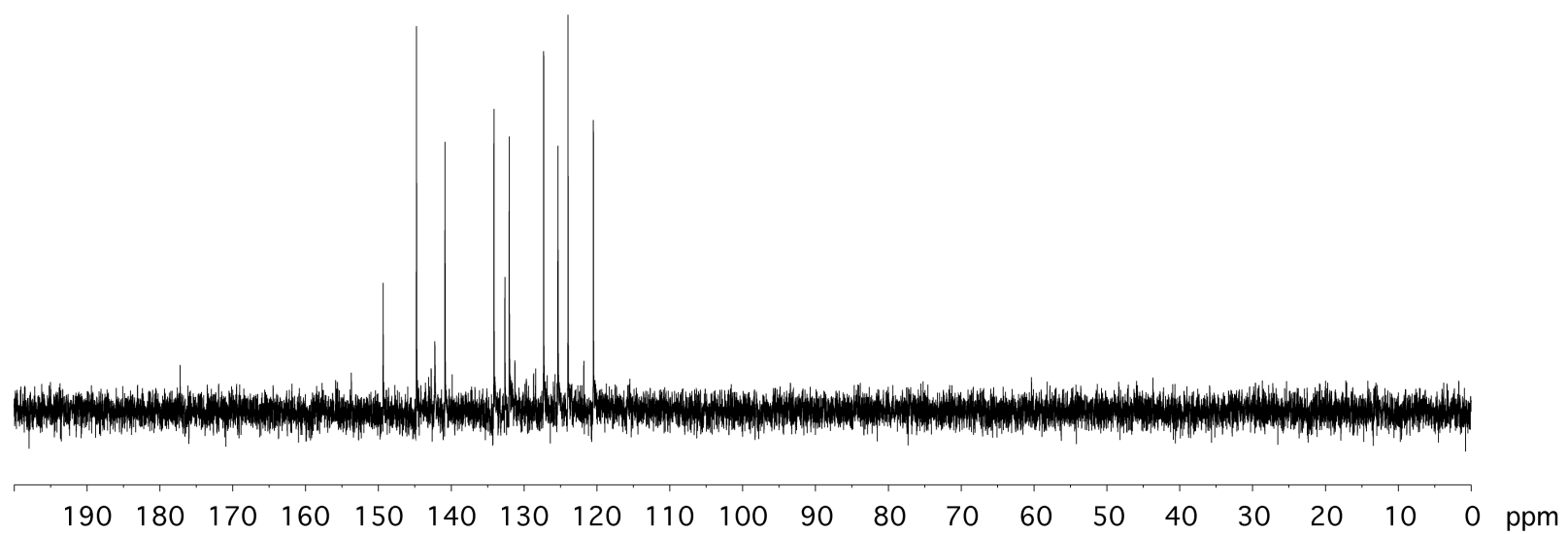
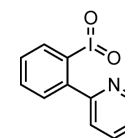


Figure III-21. ^{13}C NMR of compound III.3c measured in D_2O at 23 °C.

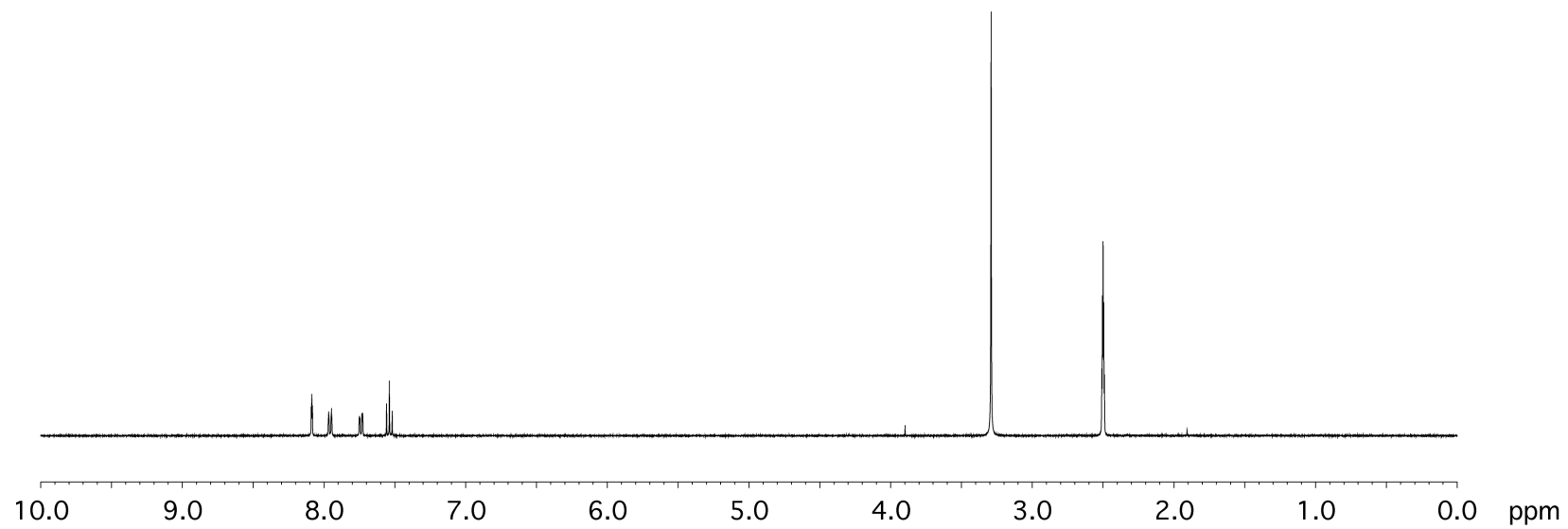
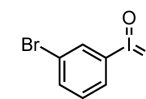


Figure III-22. ^1H NMR of compound III.3i measured in $\text{DMSO-}d_6$ at $23\text{ }^\circ\text{C}$.

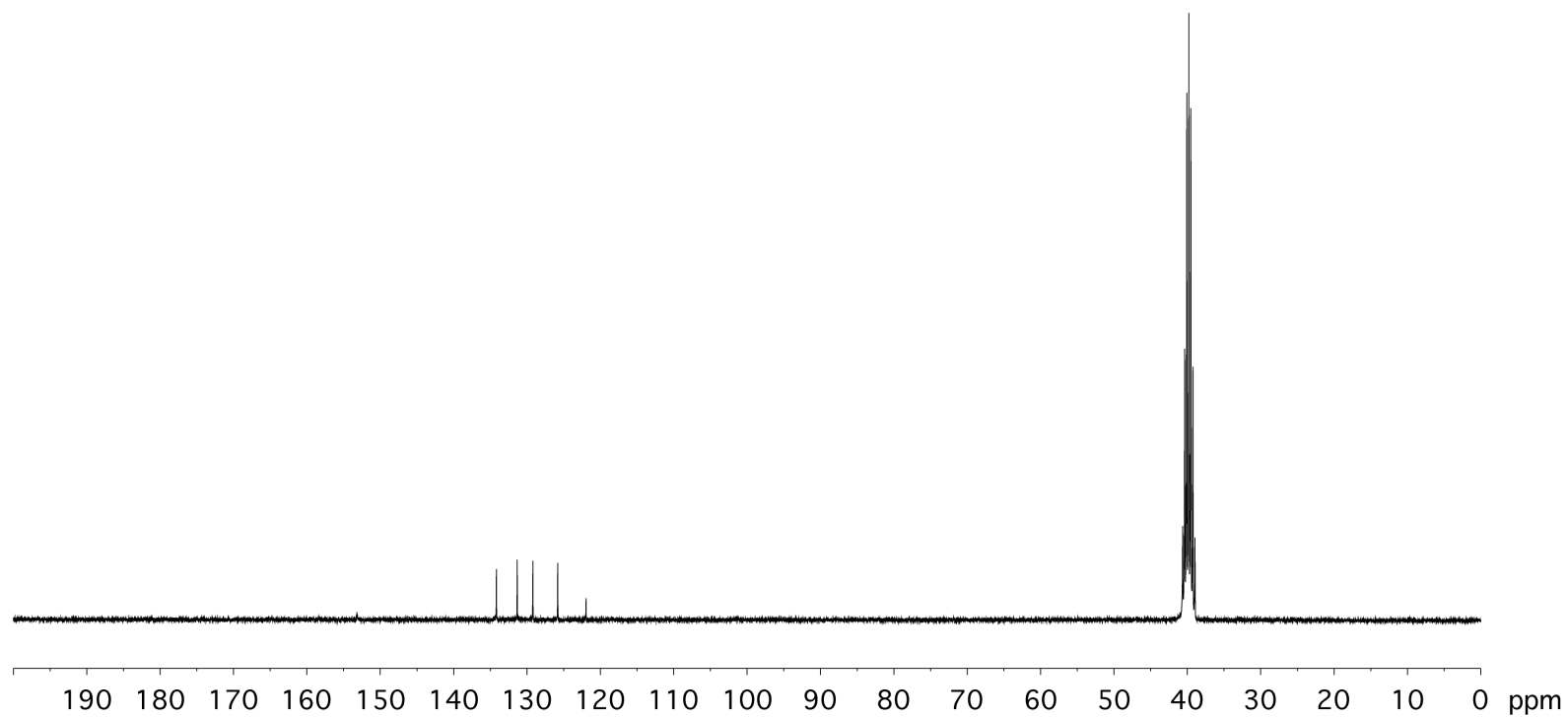
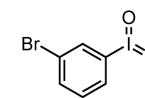


Figure III-23. ^{13}C NMR of compound III.3i measured in $\text{DMSO-}d_6$ at $23\text{ }^\circ\text{C}$.

CHAPTER IV

ELECTROCATALYTIC C–H AMINATION VIA ANODICALLY GENERATED HYPERVALENT IODINE INTERMEDIATES*

IV.1 Introduction

Electrochemistry is an attractive approach to sustainable synthesis that obviates the need for stoichiometric redox reagents and, thus, generation of the attendant waste streams.²⁸¹⁻²⁸⁸ Because of its inherent tunability and scalability, electrosynthesis could impact the enormous variety of organic transformations in which electrons are added to, or removed from, substrates. In practice, challenges such as (1) the sluggish interfacial electron transfer rates for many organic molecules, which necessitate application of substantial overpotential to achieve practical current densities,²⁸⁹ and (2) the need to couple the single-electron events that are typical of electrochemistry with the multielectron events required for bond-breaking and -making in organic reactions, can limit direct electrosynthesis (Figure IV-1).²⁹⁰ Indirect electrocatalysis, in which small molecule redox catalysts (i.e., electrocatalysts) convey applied potential from the working electrode to the bulk reaction medium, has emerged as an important strategy in selective organic electrocatalysis.²⁹¹⁻²⁹⁴ Soluble electrocatalysts facilitate interfacial electron transfer, circumvent unselective side reactions, and can couple a diverse array of substrate functionalization mechanisms to the electrochemical stimulus. Important methods based on quinone-,^{295, 296} amine-,²⁹⁷⁻²⁹⁹ nitroxyl radical-,³⁰⁰⁻³⁰⁶ and transition metal-redox catalysts³⁰⁷⁻³¹⁴ have been disclosed.

* Data, figures, and text in this chapter were adapted with permission from reference Maity, A.; Frey, B. L.; Hoskinson, N. D.; Powers, D. C. Electrocatalytic C–N Coupling via Anodically Generated Hypervalent Iodine Intermediates. *J. Am. Chem. Soc.* **2020**, *142*, 4990–4995, Copyright © 2019, American Chemical Society and Hyun, S.-M.; Yuan, M.; Maity, A.; Gutierrez, O.; Powers, D. C. *Chem* **2019**, *5*, 2388–2404, Copyright © 2019 Elsevier Inc.

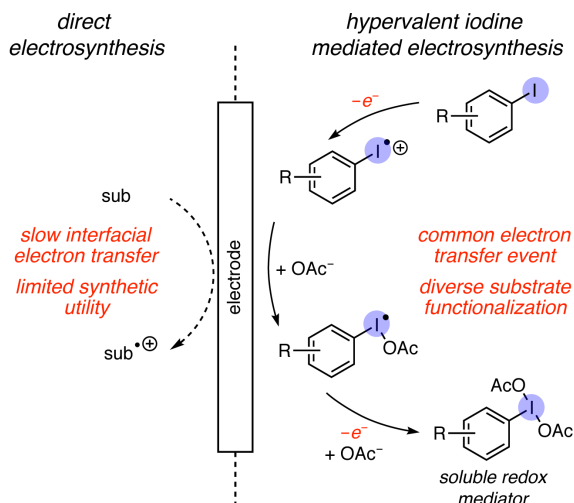


Figure IV-1. Strategies for electrosynthetic chemistry. The generation of soluble redox mediators, such as hypervalent iodine intermediates, provides the opportunities to couple a diverse set of substrate functionalization mechanisms to a common interfacial electron transfer event.

Hypervalent iodine reagents are a class of organic oxidants that have been deployed in a wide variety of substrate functionalization reactions.^{29, 55, 120, 159, 213, 315} Electrochemical oxidation of aryl iodides typically requires substantial overpotential;³¹⁶ thus, hypervalent iodine electrochemistry has largely been limited to *ex cell* applications,^{86, 88, 92-94, 317} in which aryl iodides are electrolyzed in the absence of substrate and subsequently used as stoichiometric reagents, or implemented in the context of flow systems.^{82, 97, 98, 318-321} *Ex cell* methods require stoichiometric generation of hypervalent iodine species, which obviate many of the potential advantages of electrochemistry vis-a-vis sustainability, and fail to address the central challenge of hypervalent iodine electrocatalysis, which is achieving selective oxidation of aryl iodides in the presence of substrates.

During the development of aerobic hypervalent iodine catalysis,^{163, 239} we proposed that the aerobic generation of hypervalent iodine compounds proceeded through the intermediacy of acetate-stabilized iodanyl radicals (*i.e.*, I(II) species; Figure IV-2).³²² We hypothesized that anodic oxidation of aryl iodides in acetate-rich media could provide access to the same acetate-stabilized

iodanyl radicals and thus enable the development of hypervalent iodine electrocatalysis. Here, we report that acetate-dependent anodic oxidation of aryl iodides enables hypervalent iodine electrocatalysis of both intra- and intermolecular C–H/N–H coupling reactions. Further, we report a series of mechanistic studies that demonstrate the importance of transient iodanyl radical intermediates in electrocatalysis.³²³

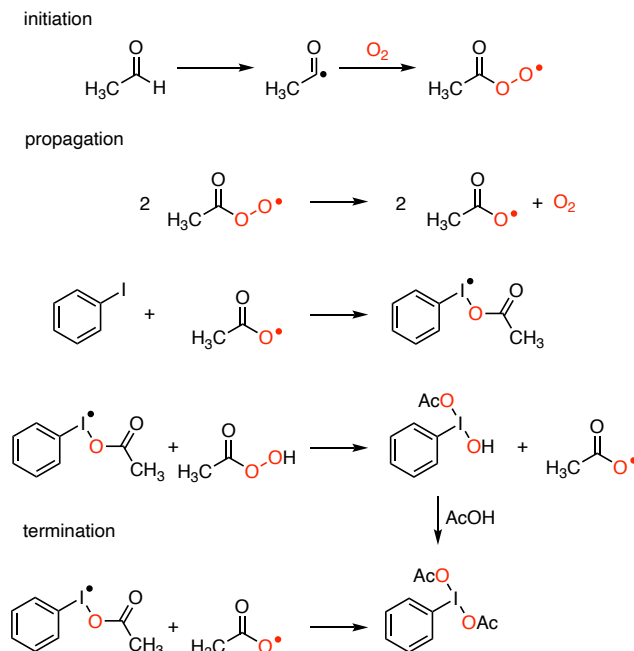


Figure IV-2. Proposed mechanism of aldehyde-promoted aerobic autoxidation of aryl iodides.

IV.2 Results and Discussion

We chose the intramolecular C–H/N–H coupling of *N*-([1,1'-biphenyl]-2-yl)acetamide (**IV.1a**) to afford *N*-acetylcarbazole (**IV.2a**) as an initial reaction target to evaluate hypervalent iodine electrochemistry because this transformation has important precedent both with stoichiometric hypervalent iodine promoters and hypervalent iodine catalysis in the presence of peracid terminal oxidants.³²⁴⁻³²⁶ We initiated our investigations of hypervalent iodine electrocatalysis by examining the onset potential for variously substituted iodoarenes by cyclic

voltammetry (CV, see Experimental Details Section) and identified 4-iodoanisole (**IV.3a**) as an attractive initial catalyst target (onset potential ~ 1.40 V vs. Ag⁺/Ag).

Table IV-1. Optimization of intramolecular C–H amination, varying solvent and temperature. Reaction conditions: 0.20 mmol of substrate, 0.05 mmol of catalyst, 0.40 mmol [TBA]OAc, 0.2 M [TBA]PF₆, 5.0 mL of solvent, glassy carbon anode, Pt cathode, and AgNO₃/Ag reference electrode.

Entry	ArI	Additive (2 equiv)	T (°C)	Solvent	Yield (%)
1	4-iodoanisole (1 equiv)	-	23	HFIP	0
2	4-iodoanisole (2 equiv)	[TBA]OAc	23	HFIP	61
3	–	[TBA]OAc	23	HFIP	0
4	4-iodoanisole (25 mol%)	[TBA]OAc	23	HFIP	76
5	4-iodoanisole (20 mol%)	[TBA]OAc	23	HFIP	56
6	4-iodoanisole (15 mol%)	[TBA]OAc	23	HFIP	40
6	4-iodotoluene	[TBA]OAc	23	HFIP	0
7	iodobenzene	[TBA]OAc	23	HFIP	0

Constant potential electrolysis (CPE) of a 1:1 mixture of **IV.1a** and **IV.3a** in 1,1,1,3,3,3-hexafluoroisopropanol (HFIP) with 0.2 M [TBA]PF₆ as supporting electrolyte resulted in no C–N

bond-forming chemistry (Table IV-1, entry 1) and partial decomposition of the starting material (87% of **IV.1a** was recovered following electrolysis; TBA = tetrabutylammonium).³²⁷ Based on the hypothesis that acetate ligands can stabilize initially generated iodanyl radicals,³²² we examined the electrolysis of a mixture of **IV.1a** and **IV.3a** with added [TBA]OAc and found that 2.0 equiv of [TBA]OAc, with respect to substrate, promotes electrochemical C–N coupling in 61% yield (Table IV-1, entry 2). No C–N coupled product was obtained in absence of aryl iodide (Table IV-1, entry 3). The loading of **IV.3a** can be lowered; we find that 25 mol% affords 76% yield. Following intramolecular C–N bond-forming chemistry, analysis of the crude reaction mixture by ¹H NMR indicates <5% catalyst decomposition. Examination of other solvents, reaction temperatures, N-protecting groups, and electrode materials did not result in substantively better reaction efficiency (See Experimental Details section for additional data). Redox balance in the observed chemistry is achieved by proton reduction (presumably of HFIP) to generate H₂, which was observed by GC analysis of the reaction headspace (Figure IV-3).

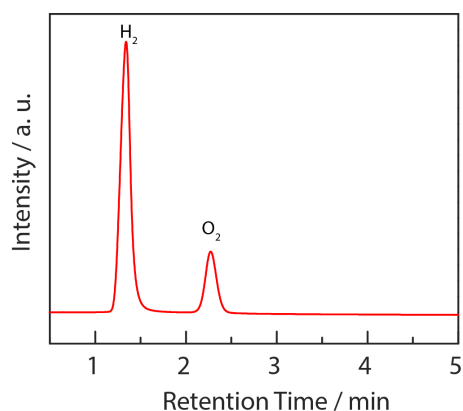


Figure IV-3. Gas chromatogram of the headspace of 4-iodotoluene oxidation in HFIP indicating the evolution of H₂ at the cathode. The oxygen (O₂) peak is from air; the reaction was set up under ambient conditions. A 10-mL glass vial was charged with 4-iodotoluene (43.1 mg, 0.197 mmol, 1.00 equiv), tetrabutylammonium acetate (121 mg, 0.401 mmol, 2.03 equiv), tetrabutylammonium hexafluorophosphate (390 mg, 1.01 mmol, 5.02 equiv), and HFIP (5.0 mL). The reaction vessel was fitted with glassy carbon anode, platinum cathode, and a Ag⁺/Ag reference electrode. A constant potential of 1.8 V vs. Ag⁺/Ag was applied to the reaction mixture and stirred at 23 °C until ~80 C charge (~4.15 F/mol) is passed. The headspace of the reaction mixture was analyzed by gas chromatography to determine the products of the cathodic half of the reaction.

IV.2.1 Electrocatalytic Intramolecular C–H Amination

With the optimized conditions in hand (Table IV-1, entry 4), we evaluated the scope of intramolecular C–N bond-forming chemistry (Figure IV-4). Reactions were run until 80 C of charge was passed (4.15 F/mol), which typically resulted in reaction times of 6–12 h. Using 4-iodoanisole (**IV.3a**) as catalyst, we found that both 5- and 4'-halogenation are well tolerated (**IV.2b–g**), as is the introduction of weakly electron withdrawing groups like 5-formyl (**IV.2h**) or 4'-phenyl (**IV.2i**). Under these conditions, substrates with more electron-withdrawing substituents, such as 5-nitro (**IV.2j**) and 5-methylcarboxylate (**IV.2k**), did not afford the expected carbazole. Based on the hypothesis that these more electron-deficient substrates may require a more oxidizing hypervalent iodine catalyst, we employed 2,2'-diiodo-4,4',6,6'-tetramethyl-1,1'-biphenyl (**IV.3b**)³²⁸ as catalyst (onset potential for oxidation is 1.68 V vs. Ag⁺/Ag for **IV.3b** compared to the onset potential of **IV.3a** which is 1.40 V vs. Ag⁺/Ag). The more oxidizing conditions allowed both **IV.2j** and **IV.2k** to be accessed (43% and 71% yields, respectively). Electron donating groups were tolerated in the 4'-position (i.e., **IV.2l** and **IV.2m**). In contrast, introduction of methyl and methoxy groups at the 5-position (i.e., **IV.1n** and **IV.1o**) led to starting material decomposition and trace amount of carbazole. We speculate that the presence of electron donating substituents at the 5- position decreases the onset potential of the substrate below that of the aryl iodide catalyst and thus leads to direct and unselective substrate activation. Consistent with this hypothesis, CPE of 5-*tert*-butyl acetamide (**IV.1p**) in the absence of aryl iodide catalyst afforded **IV.2p** in 65% yield (background reactions of the other substrates in Figure IV-4 indicate that only **IV.1p** and **IV.1v** participate in appreciable C–N coupling chemistry in the absence of **3**, see Experimental Details section for additional data). The broader tolerance for substitution in the 4'-position than the 5-position is consistent with the smaller impact of substituents in this position on the onset

potential for direct substrate oxidation. Intramolecular cyclization is also tolerant to substitution at the 2'- (**IV.2q**) and 3-positions (**IV.2r** and **IV.2s**) and can be accomplished in multifunctional substrates, as highlighted by the synthesis of **IV.2v**, a precursor to anti-HIV natural product clauszoline-K.^{329, 330}

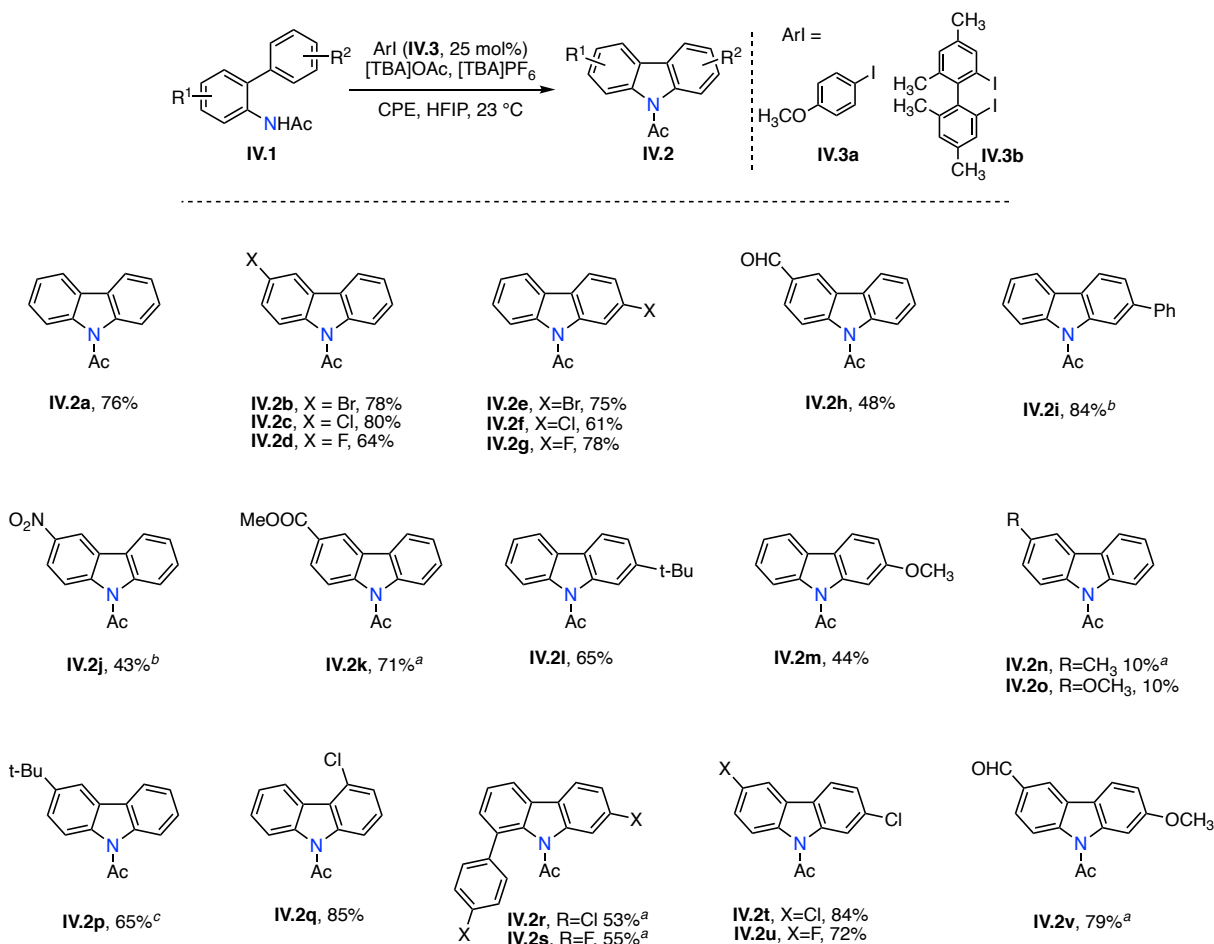
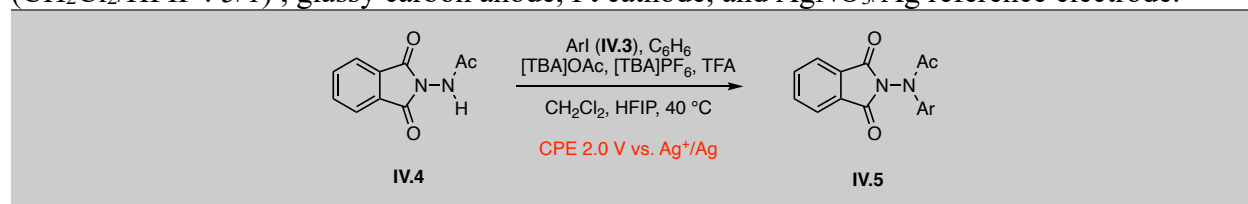


Figure IV-4. Intramolecular C–H / N–H coupling via hypervalent iodine electrocatalysis. Standard conditions: catalyst **III.3a**, CPE at 1.5 V vs. Ag⁺/Ag for 80 C, undivided cell, glassy carbon anode, platinum-plated cathode, and Ag⁺/Ag reference electrode. ^aCatalyst **III.3b**, CPE at 1.9 V vs. Ag⁺/Ag for 80 C. ^bCatalyst **III.3a**, constant current electrolysis (CCE) at 5 mA for 5 F/mol. ^cCPE in the absence of catalyst. HFIP=1,1,1,3,3,3-hexafluoroisopropanol.

IV.2.2 Electrocatalytic Intermolecular C–H Amination

Hypervalent iodine electrocatalysis can also be applied to intermolecular C–N bond-forming chemistry. Catalyst **IV.3b** was used as the aryl iodide mediator due to its previously reported success in furnishing intermolecular C–H amination reactions.³³¹ CPE of a CH₂Cl₂/HFIP solution of hydrazine derivative **IV.4** and 10 equiv of benzene in the presence of 1 equiv of **IV.3b** affords 81% yield of *N*-phenylated compound **IV.5a** (Table IV-2). The catalyst loading can be decreased to 25 mol% without significantly compromising the yield (71% of isolated product). Similar to the above-described intramolecular C–N bond-forming chemistry, no C–N coupling products are observed in the absence of either aryl iodide or [TBA]OAc.

Table IV-2. Optimization of intermolecular C–H amination. Reaction conditions: 0.20 mmol of substrate, 0.05 mmol of catalyst, 0.40 mmol [TBA]OAc, 0.2 M [TBA]PF₆, 5.0 mL of solvent (CH₂Cl₂/HFIP : 5/1), glassy carbon anode, Pt cathode, and AgNO₃/Ag reference electrode.



Entry	ArI	ArI Loading	Yield (%)
1	4-iodoanisole	1 equiv	0
2	Iodobenzene	1 equiv	0
3	4-iodotoluene	1 equiv	0
4	1,2-diiodobenzene	1 equiv	65
5	2,2'-diiodo-4,4',6,6'-tetramethyl-1,1'-biphenyl	1 equiv	81
6	2,2'-diiodo-4,4',6,6'-tetramethyl-1,1'-biphenyl	25 mol%	71
7	2,2'-diiodo-4,4',6,6'-tetramethyl-1,1'-biphenyl	20 mol%	59
8	-	-	0

Amine derivatives that feature onset potentials for direct oxidation below that of **IV.3b** (i.e., 2.0 V vs. Ag⁺/Ag), such as TsNHOMe, TrocNHOMe, and acetanilide did not engage in intermolecular C–N coupling (Figure IV-5).

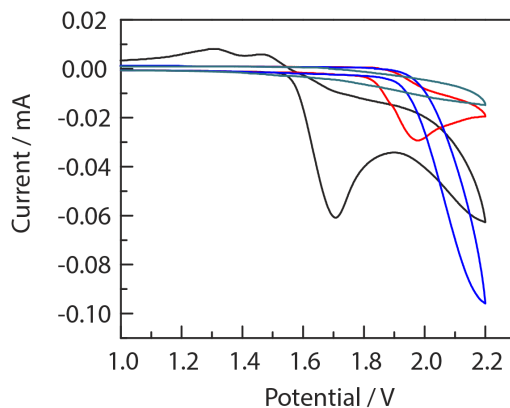


Figure IV-5. Cyclic voltammograms of various amines for intermolecular chemistry. acetanilide (—), TrocNHOMe (—), TsNHOMe (—) and *N*-(1,3-dioxoisindolin-2-yl)acetamide (**IV.4**, —). CV conditions: 0.2 M [TBA]PF₆ solution of HFIP, glassy carbon working electrode, and Pt counter electrode. Troc= 2,2,2-trichloroethoxycarbonyl.

With the optimized condition in hand, scope of intermolecular C–H amination reaction was examined (Figure IV-6a). The intermolecular C–H amination reactions with halogenated aryl group were accomplished in 35–82% yields (**IV.5b–f**). Positional selectivity for difunctionalized arenes (i.e., **IV.5f–i**) is consistent with electrophilic aromatic substitution preferences. Electron-rich hydrocarbons like toluene, xylene, and naphthalene were not viable substrates in the intermolecular N–H arylation. Hydrogenolysis of the N–N bond in compounds **IV.5** leads to *N*-acyl aniline derivatives (**IV.6**), which can be challenging to synthesize by transition-metal-catalyzed cross-coupling reactions due to the stability of ammonia adducts of many transition metals (Figure IV-6b).³³² Alternately, compounds **IV.5** can be elaborated to the corresponding arylhydrazines (**IV.7**), which are useful precursors to various heterocyclic compounds, by treatment with hydrazine (Figure IV-6b).³³³

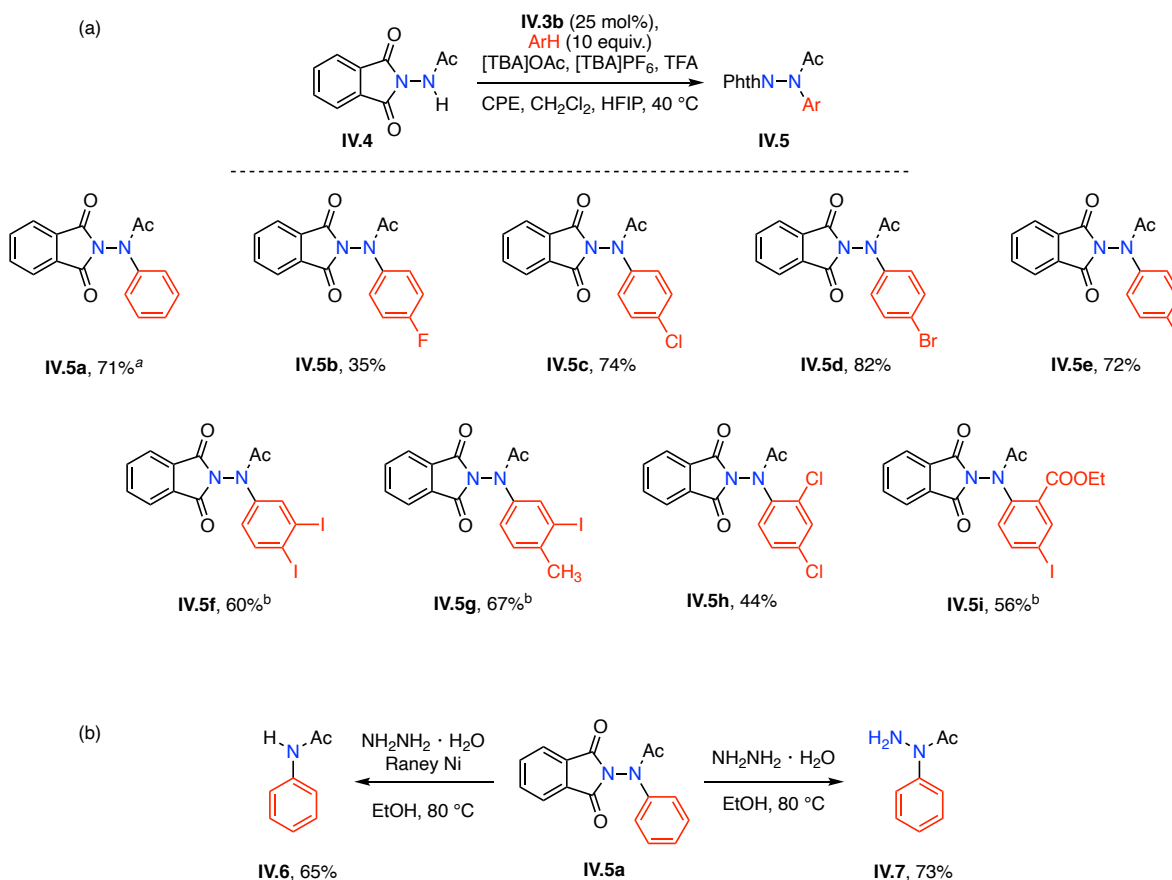


Figure IV-6. (a) Intermolecular C–H / N–H coupling via hypervalent iodine electrocatalysis. Standard conditions: catalyst **IV.3b**, CPE for 80 C, 2.0 V vs. Ag⁺/Ag, undivided cell, glassy carbon anode, platinum-plated cathode, and Ag⁺/Ag reference. ^aCPE at 1.8 V. ^b5 equiv of ArH. HFIP=1,1,1,3,3,3-hexafluoroisopropanol. (b) Products of intermolecular C–H amination could be derivatized to afford acetanilides (**IV.6**) and phenyl acetyl hydrazines (**IV.7**)

IV.2.3 Electrocatalytic C–H Amination Mechanism

With interest in gaining deeper understanding of the observed acetate-dependent hypervalent iodine electrocatalysis, we considered two potential anodic oxidation mechanisms (Figure IV-7). The initial interfacial electron transfer could be between the working electrode and the aryl iodide to generate an I(II) intermediate (**IV.8**), which would then be trapped by exogenous acetate ion to generate acetoxy iodanyl radical **IV.9** (Figure IV-7, path a). Subsequent oxidation chemistry would ultimately lead to I(III) compound **IV.10**. Alternatively, the observed acetate-dependent chemistry might arise from an interrupted Kolbe electrolysis³³⁴ in which initially

formed acetoxy radicals add to aryl iodides to generate iodanyl radical intermediates (9), which would subsequently undergo further oxidation to I(III) compound **IV.10** (Figure IV-7, path b). Available evidence, summarized below, is most consistent with the former mechanistic scenario.

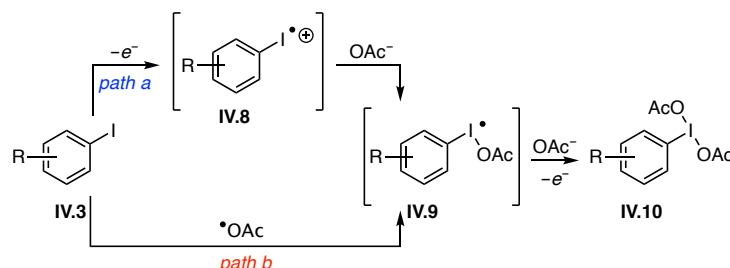


Figure IV-7. Potential mechanisms for the observed acetate-dependent hypervalent iodine electrocatalysis. a) Interfacial electron transfer with aryl iodide would initially generate a I(II) cation. b) Interfacial electron transfer with acetate would initially generate acetoxy radicals.

Examination of the CV of **IV.3a** as a function of scan rate in HFIP indicates that while the oxidation is irreversible at low scan rates (i.e., < 100 mV/s), electrochemical reversibility emerges at higher scan rates (>250 mV/s, Figure IV-8a). Addition of [TBA]OAc to a CV experiment of **IV.3a** in HFIP results in both the loss of reversibility and the substantial increase in the anodic current (I_{pa}), indicating that the electrochemically generated species is trapped by added acetate (Figure IV-8b). The measured peak potential is linearly correlated with the square root of scan rate, which indicates electron transfer from a solution-borne, not surface adsorbed, species (Figure IV-8c).^{335, 336} Trapping of electrochemically generated iodanyl radicals is not limited to acetate. A variety of common hypervalent iodine ligands including pyridine, cyanide, trifluoroacetate, and fluoride all give rise to the same enhanced current and suppressed reversibility that is diagnostic of trapping the electrochemically generated species.

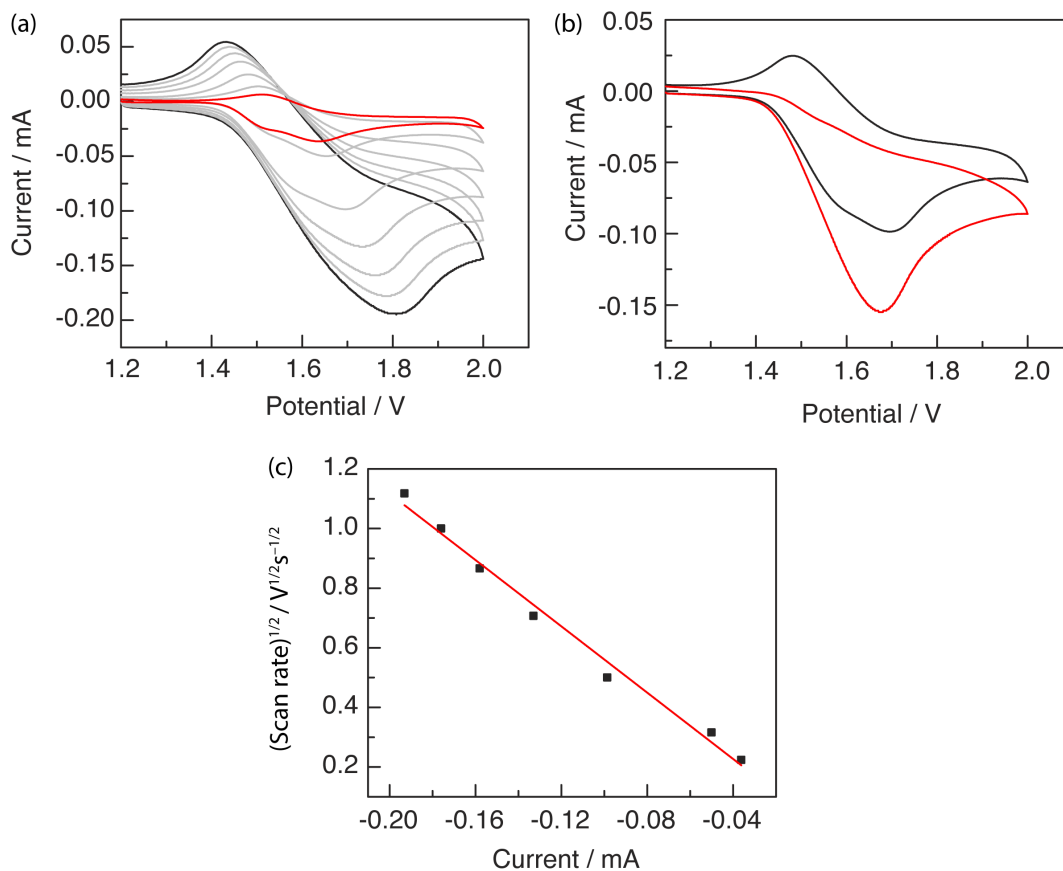


Figure IV-8. Cyclic voltammograms studies of 4-iodoanisole. (a) Increasing reversibility of **IV.3a** oxidation in HFIP is observed in CVs collected with increasing scan rate: 0.05 (—), 0.1, 0.25, 0.50, 0.75, 1.0, and 1.2 V/s (—). (b) CVs of **IV.3a** in a 0.2 M [TBA]PF₆ solution of HFIP (—) and in presence of 2.0 equivalents of [TBA]OAc (—). (c) Plot of peak anodic current (I_{pa}) of **IV.3a** vs. square root of scan rate [$R^2 = 0.99$].

Regarding the potential that the reported hypervalent iodine chemistry arises from an interrupted Kolbe electrolysis, we observed that electrolysis of CH₃CN solutions containing [TBA]OAc and [TBA]PF₆ results in the products expected of Kolbe electrolysis: ethane, methane, and CO₂ (observed by GC analysis of reaction headspace, Figure IV-9). In contrast, acetate oxidation is suppressed in HFIP, the solvent in which the chemistry is (uniquely) effective (no volatiles are observed in headspace analysis as well as no oxidation peak in the CV, Figure IV-10).

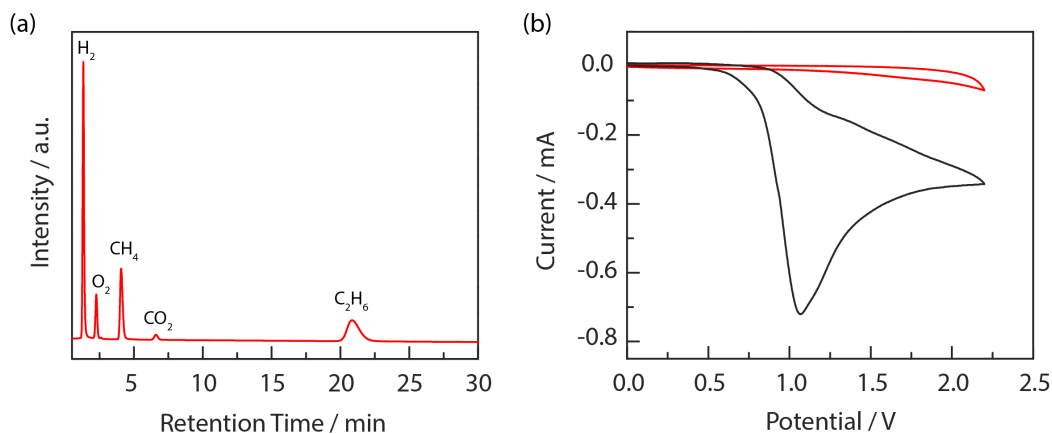


Figure IV-9. Electrolysis and headspace analysis of [TBA]OAc in acetonitrile. (a) Gas chromatogram of headspace of [TBA]OAc electrolysis in acetonitrile. Anodic oxidation of acetate leads to decarboxylation of initially formed acetoxy radical and produces methane (CH_4), carbon dioxide (CO_2) and ethane (C_2H_6). Hydrogen gas is observed as the product of cathodic half-cell reaction. The oxygen (O_2) peak is due to the ambient conditions used for reaction set-up. (b) Comparison of cyclic voltammograms of 0.2 M [TBA] PF_6 solution in acetonitrile: before (—) and after addition of [TBA]OAc (—). CV conditions: 10 mM [TBA]OAc, glassy carbon working electrode, Pt counter electrode, scan rate 0.1 V/s. A 10-mL glass vial was charged with tetrabutylammonium acetate (120 mg, 0.401 mmol, 1.00 equiv), tetrabutylammonium hexafluorophosphate (390 mg, 1.01 mmol, 2.52 equiv), and acetonitrile (5.0 mL) and was fitted with glassy carbon anode, platinum cathode, and Ag^+/Ag reference electrode. A constant potential of 1.8 V vs. Ag^+/Ag was applied to the reaction mixture and stirred at 23 °C until ~80 C charge (~2.07 F/mol) was passed. The headspace of the reaction mixture was then analyzed by gas chromatography.

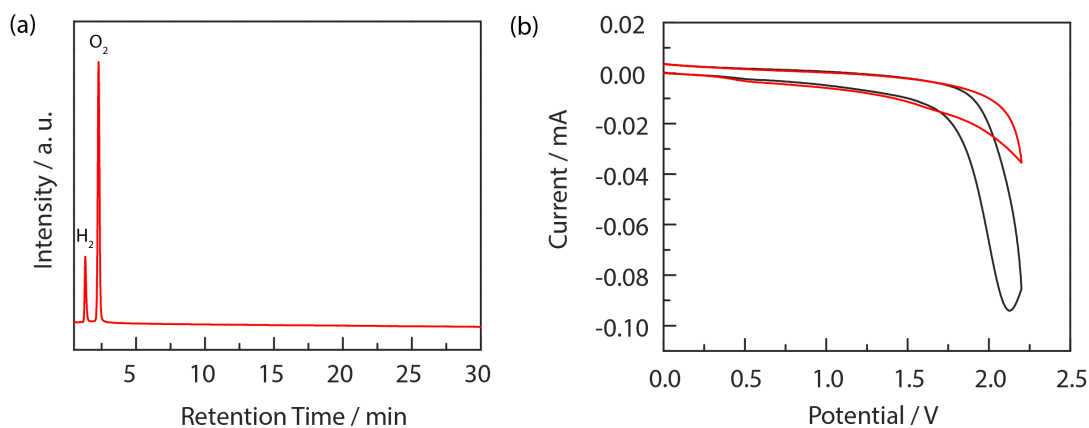


Figure IV-10. Electrolysis and headspace analysis of [TBA]OAc in HFIP. (a) Gas chromatogram of headspace of [TBA]OAc electrolysis in HFIP. In HFIP, anodic oxidation of acetate is suppressed and no products derived from decarboxylation are observed. The oxygen (O_2) peak is due to the ambient conditions used for reaction set-up. (b) Comparison of cyclic voltammograms of 0.2 M [TBA] PF_6 solution in HFIP: before (—) and after addition of

[TBA]OAc (—). CV conditions: 10 mM [TBA]OAc, glassy carbon working electrode, Pt counter electrode, scan rate 0.1 V/s. A 10-mL glass vial was charged with tetrabutylammonium acetate (120 mg, 0.401 mmol, 1.00 equiv), tetrabutylammonium hexafluorophosphate (390 mg, 1.01 mmol, 2.52 equiv), and HFIP (5.0 mL) and was fitted with glassy carbon anode, platinum cathode, and a Ag^+/Ag reference electrode. A constant potential of 1.8 V vs. Ag^+/Ag was applied to the reaction mixture and the reaction was stirred at 23 °C for 12 h. No significant current was observed during this period and only ~2 C of charge was passed. The headspace of the reaction mixture was analyzed by gas chromatography.

The suppression of Kolbe electrolysis is consistent with strong hydrogen bonding of acetate to the acidic O–H of HFIP ($\text{pK}_a = 9.3$).³³⁷ Consistent with this hypothesis, NMR analysis of solutions containing both HFIP and [TBA]OAc reveals a significant downfield shift in the methine resonance (Figure IV-11). As shown in Figure IV-11, the resonance of the methine proton (adjacent to OH group) was shifted upfield as the mole fraction of [TBA]OAc was increased. The Job plot, shown in Figure IV-12, was obtained plotting $\chi_{\text{HFIP}} \times \Delta\delta_{\text{ppm}}$ with χ_{HFIP} , indicating a 1:1 complex stoichiometry. NMR analysis provides an equilibrium constant for association of 0.767 (see Experimental Details section for additional data).

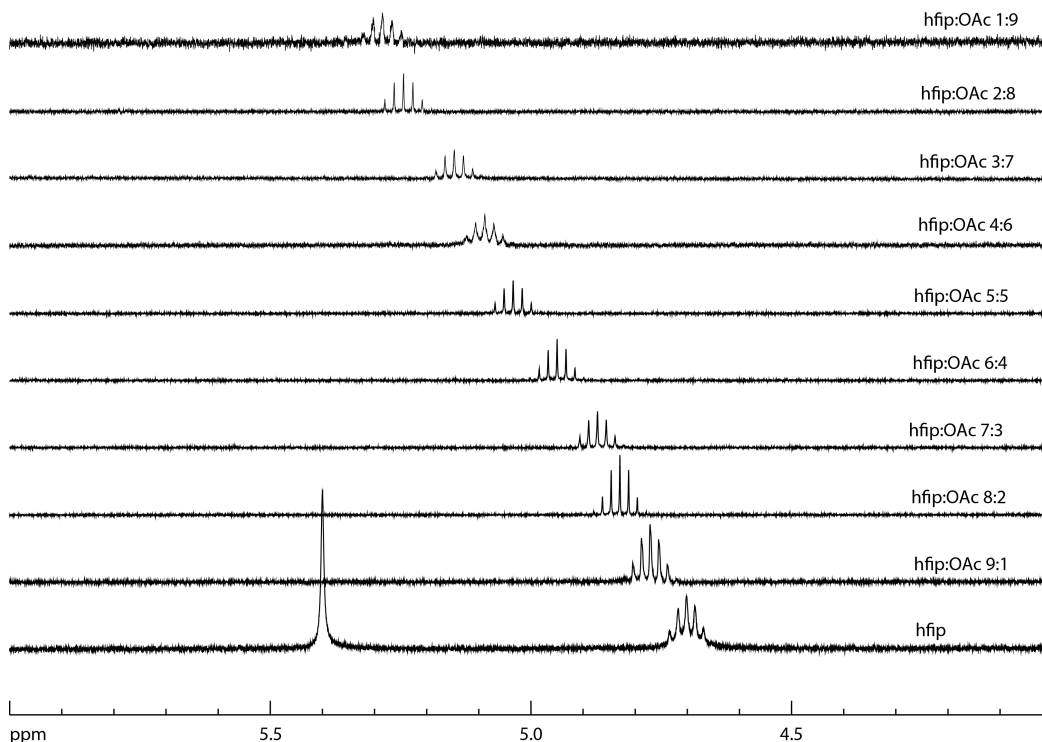


Figure IV-11. ^1H NMR spectra of HFIP titration with [TBA]OAc in CD_3CN . In this plot, change of chemical shift of 3° proton adjacent to OH group is measured as a function of [TBA]OAc concentration. Stock solutions (10 mM) of HFIP and [TBA]OAc were prepared separately in CD_3CN . Ten NMR samples were prepared with different proportions of the HFIP and [TBA]OAc solution so that the total concentration of ($[\text{HFIP}] + [[\text{TBA}]\text{OAc}]$) for each sample was 10 mM (Table IV-3). Each NMR sample was run at 23°C and the sample was allowed to equilibrate in the magnet for 5 min before the ^1H NMR spectrum was recorded.

Table IV-3. Data for the Job plot performed by ^1H NMR titration in CD_3CN .

Entry	HFIP (μL)	[TBA]OAc (μL)	HFIP (mM)	[TBA]OAc (mM)	χ_{HFIP}	δ (ppm)	$\Delta\delta$ (ppm)	$\chi_{\text{HFIP}} \times \Delta\delta_{\text{ppm}}$
1	1000	0	10	0	1	4.70	0	–
2	900	100	9	1	0.9	4.77	0.07	0.063
3	800	200	8	2	0.8	4.83	0.13	0.102
4	700	300	7	3	0.7	4.87	0.17	0.119
5	600	400	6	4	0.6	4.95	0.25	0.150
6	500	500	5	5	0.5	5.03	0.33	0.165
7	400	600	4	6	0.4	5.09	0.39	0.156
8	300	700	3	7	0.3	5.15	0.45	0.135
9	200	800	2	8	0.2	5.24	0.54	0.108
10	100	900	1	9	0.1	5.29	0.58	0.058

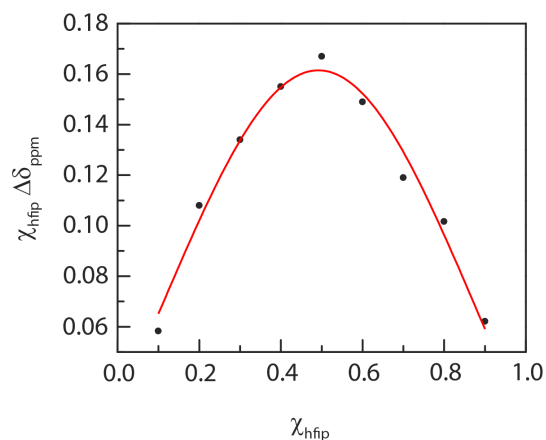


Figure IV-12. Job plot constructed from the ^1H NMR data shown in Figure IV-11. The maximum at ~ 0.5 indicates a 1:1 interaction between HFIP and [TBA]OAc.

IV.2.4 Robustness Analysis

Robustness analysis is utilized to scope out functional group tolerance of a particular reaction where external additive are introduced in the reaction mixture to measure its effect on reaction yield and how much additive is recovered after the reaction.³³⁸ Hypervalent iodine catalyzed C–N bond forming chemistry is most often accomplished with peracid terminal oxidants.^{328,325, 331} While recently developed aerobic hypervalent iodine chemistry proceeds through a distinct one-electron mechanism, the autoxidation chemistry used to couple O_2 reduction to aryl iodide oxidation, produces a significant steady state concentration of peracid. For this reason, the developed aerobic oxidation conditions display substrate scope limitations similar to those displayed by peracid conditions when assayed by robustness analysis.^{322, 338} We were interested in evaluating the robustness of the developed hypervalent iodine electrocatalysis to evaluate if a broader functional group tolerance may be achieved by avoiding the use or evolution of peracids. Figure IV-13 displays both the impact of a variety of small-molecule additives on the yield of intramolecular C–H/N–H coupling as well as the amount of recovered additive following the electrochemical reaction. The efficiency of electrocatalytic C–N coupling is superior to aerobic conditions for all additives and similar to that of peracetic acid. The electrochemical conditions

display higher additive recovery, in particular when challenged against oxidatively labile functional groups, such as alkynes and olefins (96% and 92%, respectively).

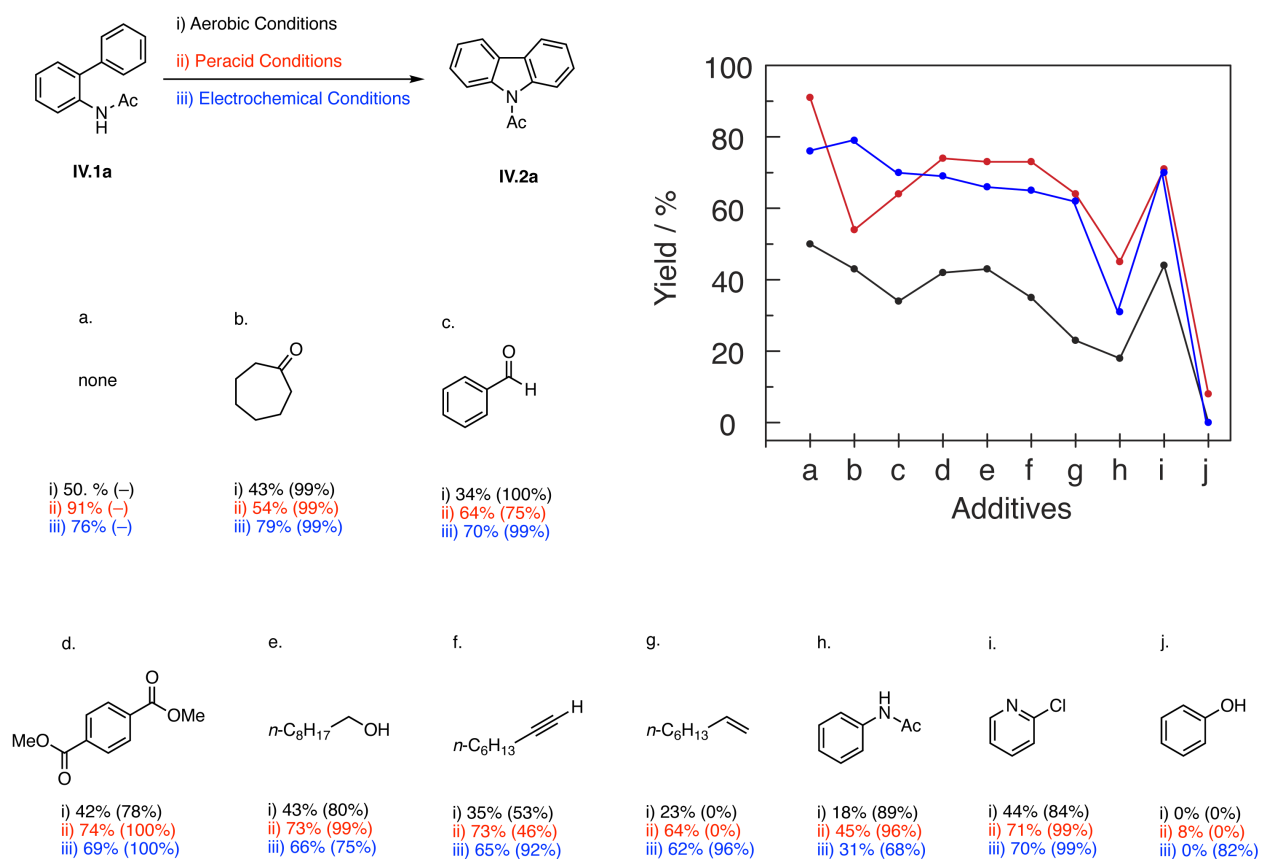


Figure IV-13. Summary of the results of robustness analysis. Reaction yield for aerobic conditions (—), *m*-CPBA conditions (—), and electrochemical conditions (—) are illustrated in the graph. The functional group tolerance for electrochemical conditions is superior than aerobic conditions and comparable with peracid conditions.

IV.3 Conclusions

In summary, we report the first example of hypervalent iodine electrocatalysis for C–H amination chemistry. The developed chemistry is applicable to both intra- and intermolecular C–N bond-forming reactions. Mechanistic experiments indicate the critical role of acetate to stabilize initially generated iodanyl radical intermediates. Given the breadth of the synthetic chemistry available to hypervalent iodine intermediates and the number of reports of hypervalent iodine electrocatalysis, demonstration of strategies to facilitate facile electrochemical generation of hypervalent iodine species promises to significantly impact the sustainable use of hypervalent iodine intermediates in synthesis.

IV.4 Experimental Details

IV.4.1 General Considerations

Materials All chemicals and solvents were obtained as ACS reagent grade and used as received. 2-Bromoaniline, 4-*tert*-butylphenylboronic acid, 2,4-dimethylphenylboronic acid, 3-bromo-5-methylanisole, tetrabutylammonium hexafluorophosphate ([TBA]PF₆), tetrabutylammonium acetate ([TBA]OAc), pyridine, and benzoyl chloride (BzCl) were obtained from Tokyo Chemical Industry (TCI). 2-Bromo-4-fluoroaniline, 2-bromo-*p*-anisidine, 2-bromo-4-nitroaniline, 4-fluorophenylboronic acid, 4-chlorophenylboronic acid, 4-trifluoromethylphenylboronic acid, 2-chlorophenylboronic acid, trifluoroacetic acid, 4-trifluoromethyliodobenzene, and 1,1,1,3,3,3-hexafluoro-2-phenyl-2-propanol were obtained from Matrix Scientific. 1,1,1,3,3,3-Hexafluoro-2-isopropanol (HFIP) was acquired from Oakwood Chemicals. Palladium acetate (Pd(OAc)₂) was acquired from Strem Chemicals. 2-Bromo-*p*-toluidine, methyl-4-amino-3-bromobenzoate, 4-biphenylboronic acid, 1,2-diiodobenzene, and trimethyl borate were obtained from Alfa Aesar. 2-Bromo-4-chloroaniline, 1,2-diiodobenzene, boron trifluoride diethyl etherate, [1,1'-biphenyl]-2-amine (**IV.S1a**), and silica gel (0.060 – 0.200 mm, 60Å for column chromatography) were obtained from Acros Organics. Tetrabutylammonium bromide ([TBA]Br), 4-methoxyphenylboronic acid, methanesulfonyl chloride (MsCl), and 2,3-dichloro-5,6-dicyano-1,4-benzoquinone (DDQ) were obtained from Chem-Impex Int'l Inc. Iodobenzene, 4-iodoanisole, 4-iodotoluene, 4-fluoriodobenzene, 2,6-dimethoxyiodobenzene, ethyl 3-iodobenzoate, 4-bromophenylboronic acid, 2,6-dibromoaniline, 2-iodobenzoic acid, Pd(PPh₃)₂Cl₂, Raney Ni, hydrazine monohydrate, tosyl chloride (TsCl), tetrahydrofuran (THF), hexanes, ethyl acetate, dichloromethane, N,N-dimethylformamide (DMF), acetic acid, acetic anhydride, and trifluoroacetic anhydride were obtained from Sigma Aldrich. Hydrochloric acid

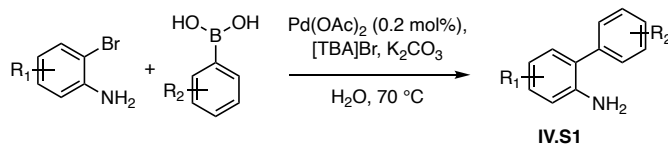
(36.5%), *N*-bromosuccinimide (NBS), anhydrous magnesium sulfate, anhydrous sodium carbonate, and anhydrous potassium carbonate were obtained from VWR. Sodium hydroxide was obtained from EMD Millipore. Acetonitrile and ethanol (200 proof) were obtained from Fischer Scientific. NMR solvents were purchased from Cambridge Isotope Laboratories and were used as received. All reactions were carried out under ambient atmosphere unless otherwise noted. 2-(2-Iodophenyl)propan-2-ol,³³⁹ 2,2'-diiodo-4,4',6,6'-tetramethyl-1,1'-biphenyl,³²⁸ 1,1,1,3,3,3-hexafluoro-2-(2-iodophenyl)propan-2-ol,³⁴⁰ *N*-(1,3-dioxoisindolin-2-yl)-*N*-phenylacetamide,³⁴¹ 4-amino-3-bromobenzaldehyde,³⁴² 2,4-dimethoxyiodobenzene,³⁴³ and Pd(PPh₃)₄³⁴⁴ were prepared according to literature procedures.

Characterization Details ¹H and ¹³C NMR spectral acquisitions were recorded on an Inova 500 FT NMR (Varian), a VNMRs 500 FT NMR (Varian), or an Acsend™ 400 NMR (Bruker) and were referenced against residual proteo solvent signals: CDCl₃ (7.26 ppm, ¹H; 77.16 ppm, ¹³C) and acetonitrile-d₃ (1.94 ppm, ¹H).¹⁹¹ ¹H NMR data are reported as follows: chemical shift (δ, ppm), (multiplicity: s (singlet), d (doublet), t (triplet), m (multiplet), br (broad), integration). ¹³C NMR data are reported as follows: chemical shift (δ, ppm). Mass spectrometry data was recorded on either Orbitrap Fusion™ Tribrid™ Mass Spectrometer or Q Exactive™ Focus Hybrid Quadrupole-Orbitrap™ Mass Spectrometer from ThermoFisher Scientific. An Agilent Trace 1300 GC with attached thermal conductivity detector and a custom-made 120 cm stainless steel column packed with Carbosieve-II was used for analysis of headspace gases. The column was kept at 200 °C and Ar was used as carrier gas. The detector was set to a temperature of 250 °C. Headspace gas (~300 μL) was transferred to the GC with a 0.50 mL Valco Precision Sampling Syringe (Series A-2) equipped with a Valco Precision sampling needle with a 5-point

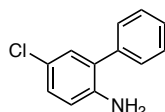
side port. Cyclic voltammetry (CV) experiments were carried out using CH Instruments Electrochemical Analyzer (Model CHI620A) in a three-electrode cell. For CV experiments, a glassy carbon working electrode, Pt counter electrode, and Ag-reference electrode were used (obtained from CH Instruments). For both constant potential and constant current electrolysis, glassy carbon, Pt, boron-doped carbon, and graphite working electrodes were purchased from IKA. An IKA Electrasyn 2.0 was used for constant current electrolysis and CH Instruments Electrochemical Analyzer (Model CHI620A) potentiostat was used for constant potential electrolysis. All electrochemical experiments were carried out in 10-mL Electrasyn glass vial. Reference electrodes were prepared using 0.1 M solution of [TBA]PF₆ in acetonitrile with 1.0 mM AgNO₃.

IV.4.2 Synthesis and Characterization Details

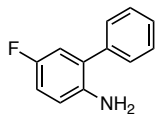
General Procedure for the Synthesis of Biarylanilines (IV.S1)



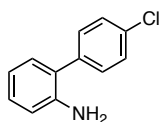
A 20-mL scintillation vial was charged with the appropriate substituted 2-bromoaniline (2.80 mmol, 1.00 equiv), the appropriate substituted phenylboronic acid (4.20 mmol, 1.50 equiv), Pd(OAc)₂ (1.3 mg, 6.0 μmol, 0.20 mol%), [TBA]Br (903 mg, 2.90 mmol, 1.00 equiv), K₂CO₃ (977 mg, 7.07 mmol, 2.52 equiv), and distilled water (4.0 mL). The reaction vessel was fitted with a rubber septum, purged with N₂ for 10 min, and the reaction mixture was heated at 70 °C for 16 h. The reaction mixture was cooled to 23 °C and was extracted with ethyl acetate (3 × 10 mL). The combined organic fractions were dried over MgSO₄ and solvent was removed under reduced pressure. The obtained residue was purified by SiO₂ gel chromatography (eluent 95:5 hexanes:ethyl acetate) to afford the biarylamines listed below.



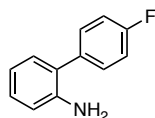
5-Chloro-[1,1'-biphenyl]-2-amine (IV.S1c). Prepared from 2-bromo-4-chloroaniline and phenylboronic acid, **IV.S1c** was obtained as a colorless oil (75% yield). ¹H NMR (δ, 23 °C, 400 MHz, CDCl₃): 7.51–7.43 (m, 4H), 7.42–7.38 (m, 1H), 7.16–7.09 (m, 2H), 6.73–6.69 (m, 1H), 3.76 (br, 2H). The obtained spectral data are in good agreement with those reported in literature.³⁴⁵



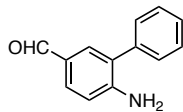
5-Fluoro-[1,1'-biphenyl]-2-amine (IV.S1d). Prepared from 2-bromo-4-fluoroaniline and phenylboronic acid, **IV.S1d** was obtained as a colorless oil (69% yield). $^1\text{H NMR}$ (δ , 23 $^\circ\text{C}$, 400 MHz, CDCl_3): 7.51–7.46 (m, 4H), 7.42–7.38 (m, 1H), 6.92–6.88 (m, 2H), 6.73–6.69 (m, 1H), 3.64 (br, 2H). The obtained spectral data are in good agreement with those reported in literature.³⁴⁶



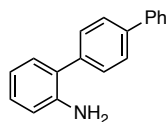
4'-Chloro-[1,1'-biphenyl]-2-amine (IV.S1f). Prepared from 2-bromoaniline and 4-chlorophenylboronic acid, **IV.S1f** was obtained as a colorless oil (41% yield). $^1\text{H NMR}$ (δ , 23 $^\circ\text{C}$, 400 MHz, CDCl_3): 7.44–7.39 (m, 4H), 7.20–7.15 (m, 1H), 7.10 (dd, $J = 7.6, 1.3$ Hz, 1H), 6.83 (td, $J = 7.5, 1.1$ Hz, 1H), 6.77 (dd, $J = 8.0, 0.9$ Hz, 1H), 3.72 (br, 2H). The obtained spectral data are in good agreement with those reported in literature.³⁴²



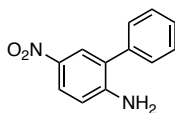
4'-Fluoro-[1,1'-biphenyl]-2-amine (IV.S1g). Prepared from 2-bromoaniline and 4-fluorophenylboronic acid, **IV.S1g** was obtained as a colorless oil (94% yield). $^1\text{H NMR}$ (δ , 23 $^\circ\text{C}$, 400 MHz, CDCl_3): 7.44 (dd, $J = 8.8, 5.5$ Hz, 2H), 7.18–7.10 (m, 4H), 6.84 (td, $J = 7.5, 1.2$ Hz, 1H), 6.78 (dd, $J = 8.0, 1.1$ Hz, 1H), 3.72 (br, 2H). The obtained spectral data are in good agreement with those reported in literature.³⁴²



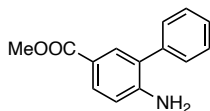
6-Amino-[1,1'-biphenyl]-3-carbaldehyde (IV.S1h). Prepared from 4-amino-3-bromobenzaldehyde and phenylboronic acid, **IV.S1h** was obtained as a colorless oil (71% yield). $^1\text{H NMR}$ (δ , 23 °C, 400 MHz, CDCl_3): 9.80 (s, 1H), 7.71 (dd, $J = 8.3, 1.9$ Hz, 1H), 7.66 (d, $J = 1.8$ Hz, 1H), 7.51–7.41 (m, 5H), 6.81 (d, $J = 8.3$ Hz, 1H), 4.44 (br, 2H). $^{13}\text{C NMR}$ (δ , 23 °C, 100 MHz, CDCl_3): 190.5, 149.6, 137.9, 133.25, 133.24, 130.9, 129.2, 128.9, 127.91, 127.77, 126.8, 114.7. HRMS-ESI: calculated for $[\text{M}+\text{H}] = 196.0910$, observed $[\text{M}+\text{H}] = 196.0913$.



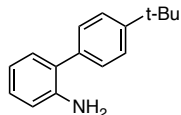
[1,1':4',1''-Terphenyl]-2-amine (IV.S1i). Prepared from 2-bromoaniline and 4-biphenylboronic acid, **IV.S1i** was obtained as a colorless oil (64% yield). $^1\text{H NMR}$ (δ , 23 °C, 400 MHz, CDCl_3): 7.71–7.66 (m, 4H), 7.58–7.55 (m, 2H), 7.49 (t, $J = 7.6$ Hz, 2H), 7.41–7.37 (m, 1H), 7.22–7.18 (m, 2H), 6.89–6.86 (m, 1H), 6.83–6.81 (m, 1H), 3.83 (br, 1H). The obtained spectral data are in good agreement with those reported in literature.³⁴⁵



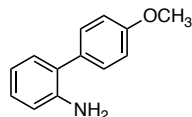
5-Nitro-[1,1'-biphenyl]-2-amine (IV.S1j). Prepared from 2-bromo-4-nitroaniline and phenylboronic acid, **IV.S1j** was obtained as a yellow oil (71% yield). $^1\text{H NMR}$ (δ , 23 °C, 400 MHz, CDCl_3): 8.09–8.06 (m, 2H), 7.52–7.48 (m, 2H), 7.44–7.40 (m, 3H), 6.73–6.71 (m, 1H), 4.48 (br, 2H). The obtained spectral data are in good agreement with those reported in literature.³⁴⁷



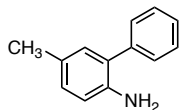
Methyl 6-amino-[1,1'-biphenyl]-3-carboxylate (IV.S1k). Prepared from methyl 4-amino-3-bromobenzoate and phenylboronic acid, **IV.S1k** was obtained as a colorless oil (61% yield). ¹H NMR (δ , 23 °C, 400 MHz, CDCl₃): 7.85–7.83 (m, 2H), 7.47–7.45 (m, 4H), 7.40–7.35 (m, 2H), 6.75 (d, J = 9.0 Hz, 1H), 4.26 (br, 2H), 3.86 (s, 3H). The obtained spectral data are in good agreement with those reported in literature.³⁴⁸



4-(Tert-butyl)-[1,1'-biphenyl]-2-amine (IV.S1l). Prepared from 2-bromoaniline and 4-tert-butylphenylboronic acid, **IV.S1l** was obtained as a colorless oil (59% yield). ¹H NMR (δ , 23 °C, 400 MHz, CDCl₃): 7.47 (d, J = 8.6 Hz, 2H), 7.40 (d, J = 8.6 Hz, 2H), 7.15 (td, J = 7.2, 1.6 Hz, 2H), 6.84–6.76 (m, 2H), 3.78 (br, 2H), 1.37 (s, 9H). The obtained spectral data are in good agreement with those reported in literature.³⁴⁵

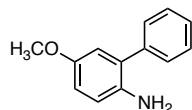


4-Methoxy-[1,1'-biphenyl]-2-amine (IV.S1m). Prepared from 2-bromoaniline and 4-methoxyphenylboronic acid, **IV.S1m** was obtained as a colorless oil (76% yield). ¹H NMR (δ , 23 °C, 400 MHz, CDCl₃): 7.43–7.41 (m, 2H), 7.19–7.14 (m, 2H), 7.03–7.01 (m, 2H), 6.85 (td, J = 7.4, 1.2 Hz, 1H), 6.79–6.77 (m, 1H), 3.88 (s, 3H), 3.77 (br, 2H). The obtained spectral data are in good agreement with those reported in literature.³⁴⁵

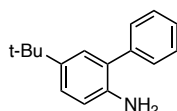


5-Methyl-[1,1'-biphenyl]-2-amine (IV.S1n). Prepared from 2-bromo-4-methylaniline and phenylboronic acid, **IV.S1n** was obtained as a light orange oil (53% yield). ¹H NMR (δ , 23 °C,

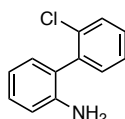
400 MHz, CDCl₃): 7.53–7.47 (m, 4H), 7.41–7.37 (m, 1H), 7.04–7.02 (m, 2H), 6.74 (d, J = 8.3 Hz, 1H), 3.58 (br, 2H), 2.34 (s, 3H). The obtained spectral data are in good agreement with those reported in literature.³⁴⁶



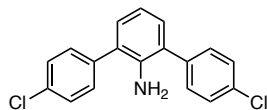
5-Methoxy-[1,1'-biphenyl]-2-amine (IV.S1o). Prepared from 2-bromo-4-methoxyaniline and phenylboronic acid, **IV.S1o** was obtained as a yellow oil (53% yield). ¹H NMR (δ, 23 °C, 400 MHz, CDCl₃): 7.50–7.45 (m, 4H), 7.40–7.36 (m, 1H), 6.82–6.73 (m, 3H), 3.79 (s, 3H), 3.53 (br, 2H). The obtained spectral data are in good agreement with those reported in literature.³⁴⁹



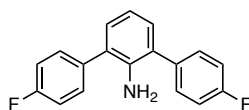
5-(Tert-butyl)-[1,1'-biphenyl]-2-amine (IV.S1p). Prepared from 2-bromo-4-(tert-butyl)aniline and phenylboronic acid, **IV.S1p** was obtained as a colorless solid (70% yield). ¹H NMR (δ, 23 °C, 400 MHz, CDCl₃): 7.53–7.46 (m, 4H), 7.38 (ddt, J = 7.7, 6.2, 1.6 Hz, 1H), 7.23 (dd, J = 8.3, 2.4 Hz, 1H), 7.19 (d, J = 2.3 Hz, 1H), 6.77 (d, J = 8.3 Hz, 1H), 3.69 (br, 2H), 1.34 (s, 9H). The obtained spectral data are in good agreement with those reported in literature.³⁴⁷



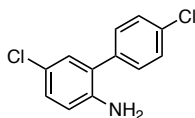
2'-Chloro-[1,1'-biphenyl]-2-amine (IV.S1q). Prepared from 2-bromoaniline and 2-chlorophenylboronic acid, **IV.S1q** was obtained as a colorless solid (36% yield). ¹H NMR (δ, 23 °C, 400 MHz, CDCl₃): 7.51 (dt, J = 6.9, 1.6 Hz, 1H), 7.36–7.30 (m, 3H), 7.22 (ddd, J = 8.0, 7.4, 1.6 Hz, 1H), 7.07–7.05 (m, 1H), 6.86–6.79 (m, 2H), 3.27 (s, 2H). The obtained spectral data are in good agreement with those reported in literature.³⁵⁰



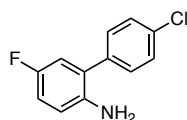
4,4''-Dichloro-[1,1':3',1''-terphenyl]-2'-amine (IV.S1r). Prepared from 2,6-dibromoaniline and 4-chlorophenylboronic acid, **IV.S1r** was obtained as a light yellow oil (51% yield). ¹H NMR (δ , 23 °C, 400 MHz, CDCl₃): 7.46 (dd, $J = 8.8, 5.4$ Hz, 4H), 7.15 (t, $J = 8.8$ Hz, 4H), 7.09 (d, $J = 7.5$ Hz, 2H), 6.87 (dd, $J = 7.8, 7.3$ Hz, 1H), 3.49 (s, 2H). The obtained spectral data are in good agreement with those reported in literature.³⁵¹



4,4''-Difluoro-[1,1':3',1''-terphenyl]-2'-amine (IV.S1s). Prepared from 2,6-dibromoaniline and 4-fluorophenylboronic acid, **IV.S1s** was obtained as a colorless solid (45% yield). ¹H NMR (δ , 23 °C, 400 MHz, CDCl₃): 7.43 (s, 8H), 7.09 (d, $J = 7.5$ Hz, 2H), 6.87 (t, $J = 7.5$ Hz, 1H), 3.76 (s, 2H). The obtained spectral data are in good agreement with those reported in literature.³⁵¹

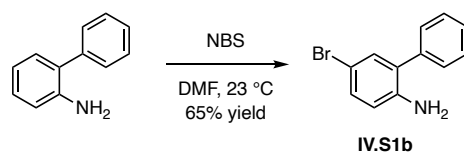


4',5-Dichloro-[1,1'-biphenyl]-2-amine (IV.S1t). Prepared from 2-bromo-4-chloroaniline and 4-chlorophenylboronic acid, **IV.S1t** was obtained as a colorless solid (40% yield). ¹H NMR (δ , 23 °C, 400 MHz, CDCl₃): 7.44–7.41 (m, 2H), 7.41–7.35 (m, 2H), 7.11 (dd, $J = 8.5, 2.5$ Hz, 1H), 7.10–7.06 (m, 1H), 6.68 (d, $J = 8.5$ Hz, 1H), 3.70 (br, 2H). The obtained spectral data are in good agreement with those reported in literature.³⁵²



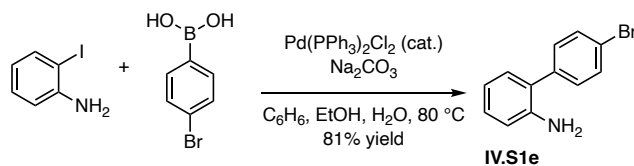
4'-Chloro-5-fluoro-[1,1'-biphenyl]-2-amine (IV.S1u). Prepared from 2-bromo-4-fluoroaniline and 4-chlorophenylboronic acid, **IV.S1u** was obtained as a colorless solid (63% yield). ¹H NMR (δ , 23 °C, 400 MHz, CDCl₃): 7.45–7.41 (m, 2H), 7.41–7.37 (m, 2H), 6.88 (td, J = 8.4, 3.0 Hz, 1H), 6.83 (dd, J = 9.2, 2.9 Hz, 1H), 6.69 (dd, J = 8.7, 4.8 Hz, 1H), 3.58 (br, 2H). The obtained spectral data are in good agreement with those reported in literature.³⁵²

Synthesis of 5-bromo-[1,1'-biphenyl]-2-amine (IV.S1b)



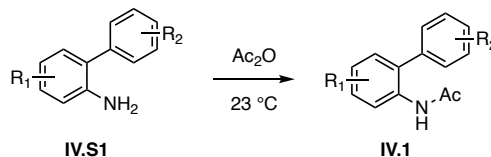
Compound **IV.S1b** was synthesized according to the following modification of a literature procedure.³⁵³ A 50-mL round-bottom flask was charged with [1,1'-biphenyl]-2-amine (850 mg, 5.00 mmol, 1.00 equiv) and DMF (20 mL). The resulting solution was cooled to 0 °C with an ice bath. A solution of NBS (1.05 g, 6.00 mmol, 1.20 equiv) dissolved in 10 mL of DMF was added to the reaction vessel dropwise at 0 °C. The reaction mixture was allowed to warm to 23 °C and was stirred for 2 h. The reaction mixture was diluted with distilled water (~50 mL) and extracted with CH₂Cl₂ (3 × 10 mL). The combined organic fractions were dried over MgSO₄ and solvent was removed under reduced pressure. The obtained residue was purified by SiO₂ gel chromatography (eluent 95:5 hexanes:ethyl acetate) to afford the desired product as yellow solid (810 mg, 65 % yield). ¹H NMR (δ , 23 °C, 400 MHz, CDCl₃): 7.47–7.34 (m, 6H), 7.26–7.23 (m, 1H), 6.67 (d, J = 9.1 Hz, 1H), 3.94 (br, 2H). The obtained spectral data are in good agreement with those reported in literature.³⁵⁴

Synthesis of 4'-bromo-[1,1'-biphenyl]-2-amine (IV.S1e)

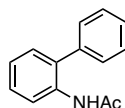


Compound **IV.S1e** was synthesized according to the following modification of a literature procedure.³⁵⁵ A 100-mL round-bottom flask was charged with 2-iodoaniline (619 mg, 2.83 mmol, 1.00 equiv), 4-bromophenylboronic acid (699 mg, 3.49 mmol, 1.23 equiv), Pd(PPh₃)₂Cl₂ (181 mg, 0.258 mmol, 9.14 mol%), Na₂CO₃ (1.01 g, 9.61 mmol, 3.4 equiv), benzene (25 mL), ethanol (1.5 mL), and distilled water (5 mL). The reaction vessel was fitted with a rubber septum, purged with N₂ for 10 min, and heated at 80 °C for 16 h. The reaction mixture was cooled to 23 °C and was then extracted with ethyl acetate (3 × 20 mL). The combined organic fractions were dried over MgSO₄ and solvent was removed under reduced pressure. The obtained residue was purified by SiO₂ gel chromatography (eluent 95:5 hexanes:ethyl acetate) to afford the title compound as white solid (570 mg, 81% yield). ¹H NMR (δ, 23 °C, 400 MHz, CDCl₃): 7.59 (d, J = 8.5 Hz, 2H), 7.37 (d, J = 8.5 Hz, 2H), 7.19 (td, J = 7.7, 1.4 Hz, 1H), 7.11 (dd, J = 7.6, 1.6 Hz, 1H), 6.86 (dd, J = 7.5, 1.2 Hz, 1H), 6.79 (dd, J = 8.0, 1.0 Hz, 1H), 3.74 (s, 2H). The obtained spectral data are in good agreement with those reported in literature.³⁵⁵

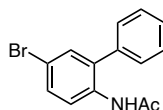
General Procedure for Acylation of Biarylanilines



A 20-mL scintillation vial was charged with the appropriate biarylamine (**IV.S1**, 2.0 mmol, 1.0 equiv) and acetic anhydride (Ac_2O , ~2 mL). The reaction mixture was stirred at 23 °C for 10 min. The reaction mixture was poured onto a pre-cooled saturated solution of K_2CO_3 (0 °C). The resulting precipitate was isolated by vacuum filtration, washed with distilled water (2×5 mL) and hexanes (2×5 mL), and dried under reduced pressure to provide the *N*-arylamides (**IV.1**) listed below.

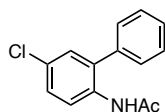


N-([1,1'-biphenyl]-2-yl)acetamide (**IV.1a**). Prepared from [1,1'-biphenyl]-2-amine (**IV.S1a**), **IV.1a** was obtained as a white solid (82% yield). ^1H NMR (δ , 23 °C, 400 MHz, CDCl_3): 8.27 (d, $J = 8.0$ Hz, 1H), 7.49 (t, $J = 7.3$ Hz, 2H), 7.44–7.37 (m, 4H), 7.24–7.18 (m, 2H), 7.11 (br, 1H), 2.02 (s, 3H). The obtained spectral data are in good agreement with those reported in literature.³⁵⁶

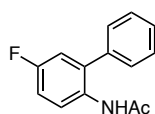


N-(5-bromo-[1,1'-biphenyl]-2-yl)acetamide (**IV.1b**). Prepared from 5-bromo-[1,1'-biphenyl]-2-amine (**IV.S1b**), **IV.1b** was obtained as a colorless solid (78% yield). ^1H NMR (δ , 23 °C, 400 MHz, CDCl_3): 8.22 (d, $J = 8.6$ Hz, 1H), 7.52–7.44 (m, 4H), 7.38–7.34 (m, 3H), 7.08 (br,

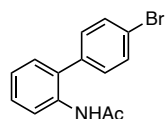
1H), 2.01 (s, 3H). The obtained spectral data are in good agreement with those reported in literature.³⁵⁶



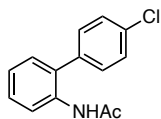
N-(5-chloro-[1,1'-biphenyl]-2-yl)acetamide (**IV.1c**). Prepared from 5-chloro-[1,1'-biphenyl]-2-amine (**IV.S1c**), **IV.1c** was obtained as a colorless solid (98% yield). ¹H NMR (δ, 23 °C, 400 MHz, CDCl₃): 8.26 (d, J = 8.8 Hz, 1H), 7.53–7.43 (m, 3H), 7.37–7.32 (m, 3H), 7.23 (d, J = 2.4 Hz, 1H), 7.08 (br, 1H), 2.02 (s, 3H). The obtained spectral data are in good agreement with those reported in literature.³⁵⁶



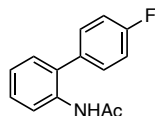
N-(5-fluoro-[1,1'-biphenyl]-2-yl)acetamide (**IV.1d**). Prepared from 5-fluoro-[1,1'-biphenyl]-2-amine (**IV.S1d**), **IV.1d** was obtained as a colorless solid (88% yield). ¹H NMR (δ, 23 °C, 400 MHz, CDCl₃): 8.07 (m, 1H), 7.47–7.29 (m, 5H), 7.11–7.00 (m, 2H), 6.94 (br, 1H), 2.05 (s, 3H). The obtained spectral data are in good agreement with those reported in literature.³⁵⁶



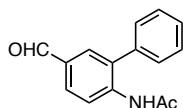
N-(4'-bromo-[1,1'-biphenyl]-2-yl)acetamide (**IV.1e**). Prepared from 4'-bromo-[1,1'-biphenyl]-2-amine (**IV.S1e**), **IV.1e** was obtained as a white solid (76 % yield). ¹H NMR (δ, 23 °C, 400 MHz, CDCl₃): 8.24–8.21 (m, 1H), 7.66–7.63 (m, 2H), 7.43–7.37 (m, 1H), 7.28–7.23 (m, 4H), 7.00 (br, 1H), 2.07 (s, 3H). The obtained spectral data are in good agreement with those reported in literature.³⁵⁶



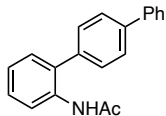
N-(4'-chloro-[1,1'-biphenyl]-2-yl)acetamide (**IV.1f**). Prepared from 4'-chloro-[1,1'-biphenyl]-2-amine (**IV.S1f**), **IV.1f** was obtained as a colorless solid (77% yield). $^1\text{H NMR}$ (δ , 23 $^\circ\text{C}$, 400 MHz, CDCl_3): 8.20 (d, $J = 7.9$ Hz, 1H), 7.46 (d, $J = 8.4$ Hz, 2H), 7.38 (ddd, $J = 8.4, 6.5, 2.1$ Hz, 1H), 7.31 (d, $J = 8.4$ Hz, 2H), 7.20 (d, $J = 7.0$ Hz, 2H), 6.98 (br, 1H), 2.04 (s, 3H). The obtained spectral data are in good agreement with those reported in literature.³⁵⁶



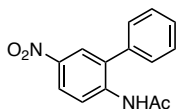
N-(4'-fluoro-[1,1'-biphenyl]-2-yl)acetamide (**IV.1g**). Prepared from 4'-fluoro-[1,1'-biphenyl]-2-amine (**IV.S1g**), **IV.1g** was obtained as a colorless solid (85% yield). $^1\text{H NMR}$ (δ , 23 $^\circ\text{C}$, 400 MHz, CDCl_3): 8.20 (d, $J = 8.0$ Hz, 1H), 7.38–7.32 (m, 3H), 7.20–7.15 (m, 4H), 7.01 (br, 1H), 2.03 (s, 3H). The obtained spectral data are in good agreement with those reported in literature.³⁵⁶



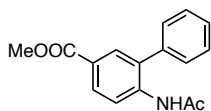
N-(5-formyl-[1,1'-biphenyl]-2-yl)acetamide (**IV.1h**). Prepared from 6-amino-[1,1'-biphenyl]-3-carbaldehyde (**IV.S1h**), **IV.1h** was obtained as an orange solid (61% yield). $^1\text{H NMR}$ (δ , 23 $^\circ\text{C}$, 400 MHz, CDCl_3): 9.94 (s, 1H), 8.61 (d, $J = 8.4$ Hz, 1H), 7.87 (dd, $J = 8.4, 2.0$ Hz, 1H), 7.76 (d, $J = 2.0$ Hz, 1H), 7.53 (dd, $J = 8.0, 6.5$ Hz, 2H), 7.49–7.47 (m, 1H), 7.42 (br, 1H), 7.39–7.37 (m, 3H), 2.05 (s, 3H). The obtained spectral data are in good agreement with those reported in literature.³⁵⁶



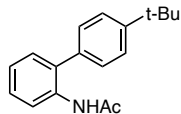
N-([1,1':4'1''-terphenyl]-2-yl)acetamide (**IV.1i**). Prepared from [1,1':4'1''-terphenyl]-2-amine (**IV.S1i**), **IV.1i** was obtained as a colorless solid (99% yield). $^1\text{H NMR}$ (δ , 23 °C, 400 MHz, CDCl_3): 8.28 (d, $J = 8.3$ Hz, 1H), 7.72 (d, $J = 8.2$ Hz, 2H), 7.66 (dd, $J = 8.2, 1.1$ Hz, 2H), 7.51–7.45 (m, 4H), 7.39 (tt, $J = 8.0, 1.7$ Hz, 2H), 7.29 (d, $J = 7.0$ Hz, 1H), 7.21 (d, $J = 7.3$ Hz, 1H), 7.18 (br, 1H), 2.06 (s, 3H). The obtained spectral data are in good agreement with those reported in literature.³⁴⁹



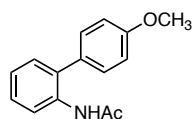
N-(5-nitro-[1,1'-biphenyl]-2-yl)acetamide (**IV.1j**). Prepared from 5-nitro-[1,1'-biphenyl]-2-amine (**IV.S1j**), **IV.1j** was obtained as a tan solid (84% yield). $^1\text{H NMR}$ (δ , 23 °C, 400 MHz, CDCl_3): 8.65 (d, $J = 9.1$ Hz, 1H), 8.25 (dd, $J = 9.2, 2.7$ Hz, 1H), 8.13 (d, $J = 2.7$ Hz, 1H), 7.59–7.52 (m, 3H), 7.42 (br, 1H), 7.41–7.38 (m, 2H), 2.07 (s, 3H). The obtained spectral data are in good agreement with those reported in literature.³⁵⁷



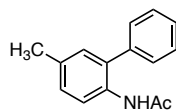
Methyl 6-acetamido-[1,1'-biphenyl]-3-carboxylate (**IV.1k**). Prepared from 6-amino-[1,1'-biphenyl]-3-carboxylate (**IV.S1k**), **IV.1k** was obtained as a colorless solid (85% yield). $^1\text{H NMR}$ (δ , 23 °C, 400 MHz, CDCl_3): 8.48 (d, $J = 8.2$ Hz, 1H), 8.03 (dd, $J = 8.7, 2.1$ Hz, 1H), 7.92 (d, $J = 2.1$ Hz, 1H), 7.52–7.45 (m, 3H), 7.38 (dd, $J = 8.2, 1.4$ Hz, 2H), 7.34 (br, 1H), 3.90 (s, 3H), 2.04 (s, 3H). The obtained spectral data are in good agreement with those reported in literature.³⁵⁷



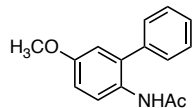
N-(4'-(*tert-butyl*)-[1,1'-biphenyl]-2-yl)acetamide (**IV.1I**). Prepared from 4'-(*tert-butyl*)-[1,1'-biphenyl]-2-amine (**IV.S1I**), **IV.1I** was obtained as a colorless solid (69% yield). $^1\text{H NMR}$ (δ , 23 °C, 400 MHz, CDCl_3): 8.24 (d, $J = 8.2$ Hz, 1H), 7.50 (d, $J = 8.2$ Hz, 2H), 7.36–7.30 (m, 3H), 7.26–7.23 (m, 2H), 7.16 (t, $J = 7.4$ Hz, 1H), 2.04 (s, 3H), 1.38 (s, 9H). The obtained spectral data are in good agreement with those reported in literature.³⁵⁶



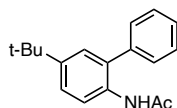
N-(4'-methoxy-[1,1'-biphenyl]-2-yl)acetamide (**IV.1m**). Prepared from 4'-methoxy-[1,1'-biphenyl]-2-amine (**IV.S1m**), **IV.1m** was obtained as a colorless solid (70% yield). $^1\text{H NMR}$ (δ , 23 °C, 400 MHz, CDCl_3): 8.28 (d, $J = 8.1$ Hz, 1H), 7.39–7.35 (m, 1H), 7.33–7.31 (m, 2H), 7.24 (d, $J = 7.3$ Hz, 1H), 7.18 (d, $J = 7.5$ Hz, 1H), 7.16 (br, 1H), 7.04 (d, $J = 8.7$ Hz, 2H), 3.90 (s, 3H), 2.06 (s, 3H). The obtained spectral data are in good agreement with those reported in literature.³⁵⁶



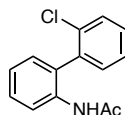
N-(5-methyl-[1,1'-biphenyl]-2-yl)acetamide (**IV.1n**). Prepared from 5-methyl-[1,1'-biphenyl]-2-amine (**IV.S1n**), **IV.1n** was obtained as a colorless solid (66% yield). $^1\text{H NMR}$ (δ , 23 °C, 400 MHz, CDCl_3): 8.11 (d, $J = 8.3$ Hz, 1H), 7.50 (t, $J = 7.3$ Hz, 2H), 7.44–7.43 (m, 1H), 7.41–7.38 (m, 2H), 7.20 (dd, $J = 8.3, 2.1$ Hz, 1H), 7.09 (s, 1H), 7.06 (br, 1H), 2.37 (s, 3H), 2.03 (s, 3H). The obtained spectral data are in good agreement with those reported in literature.³⁵⁶



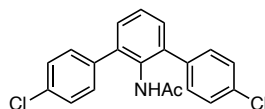
N-(5-methoxy-[1,1'-biphenyl]-2-yl)acetamide (**IV.1o**). Prepared from 5-methoxy-[1,1'-biphenyl]-2-amine (**IV.S1o**), **IV.1o** was obtained as a colorless solid (49% yield). $^1\text{H NMR}$ (δ , 23 $^\circ\text{C}$, 400 MHz, CDCl_3): 7.96 (d, $J = 8.9$ Hz, 1H), 7.47 (t, $J = 7.2$ Hz, 2H), 7.42–7.40 (m, 1H), 7.37–7.35 (m, 2H), 7.03 (br, 1H), 6.90 (dd, $J = 8.9, 2.8$ Hz, 1H), 6.81 (d, $J = 2.9$ Hz, 1H), 3.81 (s, 3H), 2.00 (s, 3H). The obtained spectral data are in good agreement with those reported in literature.³⁵⁶



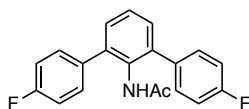
N-(5-(tert-butyl)-[1,1'-biphenyl]-2-yl)acetamide (**IV.1p**). Prepared from 5-(tert-butyl)-[1,1'-biphenyl]-2-amine (**IV.S1p**), **IV.1p** was obtained as a colorless solid (69% yield). $^1\text{H NMR}$ (δ , 23 $^\circ\text{C}$, 400 MHz, CDCl_3): 8.12 (d, $J = 8.5$ Hz, 1H), 7.49 (t, $J = 7.3$ Hz, 2H), 7.43–7.38 (m, 4H), 7.24 (d, $J = 2.3$ Hz, 1H), 7.04 (br, 1H), 2.01 (s, 3H), 1.33 (s, 9H). The obtained spectral data are in good agreement with those reported in literature.³⁵⁸



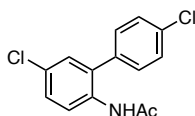
N-(2'-chloro-[1,1'-biphenyl]-2-yl)acetamide (**IV.1q**). Prepared from 2'-chloro-[1,1'-biphenyl]-2-amine (**IV.S1q**), **IV.1q** was obtained as an oil (35% yield). $^1\text{H NMR}$ (δ , 23 $^\circ\text{C}$, 400 MHz, CDCl_3): 8.20 (d, $J = 8.1$ Hz, 1H), 7.54–7.52 (m, 1H), 7.45–7.30 (m, 4H), 7.19 (d, $J = 6.2$ Hz, 2H), 6.80 (br, 1H), 1.99 (s, 3H). The obtained spectral data are in good agreement with those reported in literature.³⁵⁹



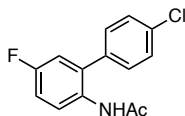
N-(4,4''-dichloro-[1,1':3',1''-terphenyl]-2'-yl)acetamide (**IV.1r**). Prepared from 4,4''-dichloro-[1,1':3',1''-terphenyl]-2'-amine (**IV.S1r**), **IV.1r** was obtained as a colorless solid (40% yield). ¹H NMR (δ, 23 °C, 400 MHz, CDCl₃): 7.44–7.28 (m, 11H), 6.52 (s, 1H), 1.74 (s, 3H). The obtained spectral data are in good agreement with those reported in literature.³²⁶



N-(4,4''-difluoro-[1,1':3',1''-terphenyl]-2'-yl)acetamide (**IV.1s**). Prepared from 4,4''-difluoro-[1,1':3',1''-terphenyl]-2'-amine (**IV.S1s**), **IV.1s** was obtained as a colorless solid (45% yield). ¹H NMR (δ, 23 °C, 400 MHz, CDCl₃): 7.42–7.32 (m, 7H), 7.09 (t, J = 8.7 Hz, 4H), 6.47 (s, 1H), 1.73 (s, 3H). The obtained spectral data are in good agreement with those reported in literature.³²⁶

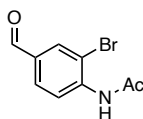


N-(4',5-dichloro-[1,1'-biphenyl]-2-yl)acetamide (**IV.1t**). Prepared from 4',5-dichloro-[1,1'-biphenyl]-2-amine (**IV.S1t**), **IV.1t** was obtained as a colorless solid (66% yield). ¹H NMR (δ, 23 °C, 400 MHz, CDCl₃): 8.19 (d, J = 8.9 Hz, 1H), 7.49–7.46 (m, 2H), 7.35–7.28 (m, 3H), 7.20 (d, J = 2.3 Hz, 1H), 6.94–6.94 (m, 1H), 2.03 (s, 3H). The obtained spectral data are in good agreement with those reported in literature.³⁶⁰



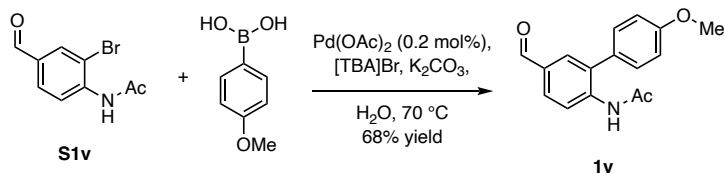
N-(4'-chloro-5-fluoro-[1,1'-biphenyl]-2-yl)acetamide (**IV.1u**). Prepared from 4'-chloro-5-fluoro-[1,1'-biphenyl]-2-amine (**IV.S1u**), **IV.1u** was obtained as a colorless solid (61% yield). ¹H NMR (δ, 23 °C, 400 MHz, CDCl₃): 8.11–8.07 (m, 1H), 7.47 (d, J = 8.4 Hz, 2H), 7.30 (d, J = 8.4

Hz, 2H), 7.08 (td, $J = 8.5, 2.9$ Hz, 1H), 6.94 (dd, $J = 8.9, 3.0$ Hz, 1H), 6.87 (s, 1H), 2.03 (s, 3H).
13C NMR (δ , 23 °C, 100 MHz, CDCl₃): 168.5, 135.8, 134.8, 130.7, 130.5, 129.6, 124.84, 124.76, 116.9, 116.6, 115.6, 115.4, 24.5. HRMS-ESI: calculated for [M+H]⁺ = 264.0586, observed [M+H]⁺ = 264.0584.



N-(2-bromo-4-formylphenyl)acetamide (**IV.S1v**). Prepared from 4-amino-3-bromobenzaldehyde, **IV.S1v** was obtained as a colorless solid (50% yield). ¹H NMR (δ , 23 °C, 400 MHz, CDCl₃): 9.88 (s, 1H), 8.64 (d, $J = 8.5$ Hz, 1H), 8.09 (d, $J = 1.8$ Hz, 1H), 7.86 (br, 1H), 7.82 (dd, $J = 8.5, 1.8$ Hz, 1H), 2.30 (s, 3H). The obtained spectral data are in good agreement with those reported in literature.³⁶⁰

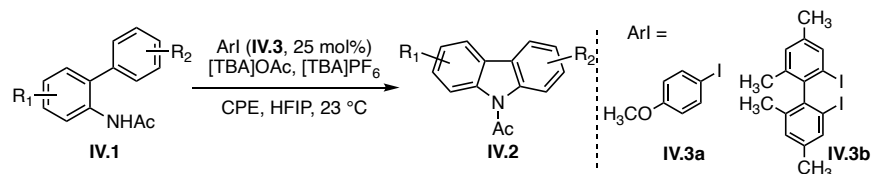
Synthesis of *N*-(5-formyl-4'-methoxy-[1,1'-biphenyl]-2-yl)acetamide (**IV.1v**)



A 20-mL scintillation vial was charged with *N*-(2-bromo-4-formylphenyl)acetamide (**IV.S1v**, 600 mg, 2.49 mmol, 1.00 equiv), 4-methoxyphenylboronic acid (568 mg, 3.74 mmol, 1.50 equiv), Pd(OAc)₂ (1.3 mg, 6.0 μmol, 0.20 mol%), [TBA]Br (903 mg, 2.90 mmol, 1.00 equiv), K₂CO₃ (977 mg, 7.07 mmol, 2.52 equiv), and distilled water (4.0 mL) and was fitted with a rubber septum. The reaction vessel was purged with N₂ for 10 min after which time the reaction mixture was heated at 70 °C for 16 h. The reaction mixture was cooled to 23 °C and was then extracted with ethyl acetate (3 × 10 mL). The combined organic fractions were dried over MgSO₄ and solvent was removed under reduced pressure. The obtained residue was purified by SiO₂ gel chromatography (eluent 95:5 hexanes:ethyl acetate) to afford 458 mg of the title compound (68% yield). ¹H NMR (δ, 23 °C, 400 MHz, CDCl₃): 9.94 (s, 1H), 8.60 (d, J = 8.4 Hz, 1H), 7.85 (dd, J = 8.5, 2.0 Hz, 1H), 7.74 (d, J = 2.0 Hz, 1H), 7.42 (br, 1H), 7.31 (d, J = 8.8 Hz, 2H), 7.05 (d, J = 8.8 Hz, 2H), 3.89 (s, 3H), 2.07 (s, 3H). ¹³C NMR (δ, 23 °C, 100 MHz, CDCl₃): 191.3, 168.5, 160.0, 140.7, 132.1, 131.4, 130.8, 130.5, 128.7, 120.3, 115.1, 55.6, 25.1. HRMS-ESI: calculated for [M+H]⁺ = 270.1125, observed [M+H]⁺ = 270.1116.

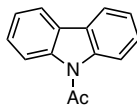
Electrocatalytic Intramolecular C–H Amination

General Procedure for Intramolecular Amination Reactions

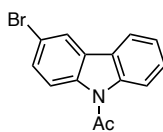


Constant Potential Conditions. A 10-mL glass vial was charged with *N*-arylacetamide (IV.1, 0.201 mmol, 1.00 equiv), 4-iodoanisole (IV.3a, 12.0 mg, 0.0512 mmol, 25.3 mol%), tetrabutylammonium acetate (121 mg, 0.401 mmol, 1.99 equiv), tetrabutylammonium hexafluorophosphate (390 mg, 1.01 mmol, 5.02 equiv), and HFIP (5.0 mL) and was fitted with glassy carbon anode, platinum cathode, and Ag⁺/Ag reference electrode. A constant potential of 1.5 V vs. Ag⁺/Ag was applied to the reaction mixture with stirring at 23 °C until ~80 C charge (~4.15 F/mol) is passed. The solvent was removed under reduced pressure. The obtained residue was purified by SiO₂ gel chromatography (eluent 95:5 hexanes:ethyl acetate) to afford the *N*-acyl carbazole product (IV.2) indicated below.

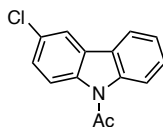
Constant Current Conditions. A 10-mL glass vial was charged with *N*-arylacetamide (IV.1, 0.201 mmol, 1.00 equiv), aryl iodide catalyst (IV.3, 0.0512 mmol, 25.3 mol%), tetrabutylammonium acetate (121 mg, 0.401 mmol, 1.99 equiv), and tetrabutylammonium hexafluorophosphate (390 mg, 1.01 mmol, 5.02 equiv), and HFIP (5.0 mL) and was fitted with glassy carbon anode and platinum cathode. A constant current of 5 mA was applied to the reaction mixture with stirring at 23 °C until 4.00 F/mol is passed. The solvent was removed under reduced pressure. The obtained residue was purified by SiO₂ gel chromatography (eluent 95:5 hexanes:ethyl acetate) to afford the *N*-acyl carbazole product (IV.2) indicated below.



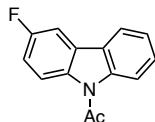
1-(9H-carbazol-9-yl)ethan-1-one (IV.2a). Prepared under constant potential conditions using **IV.3a** as catalyst. Yield: 32 mg (76% yield). $^1\text{H NMR}$ (δ , 23 °C, 400 MHz, CDCl_3): 8.15 (d, $J = 8.3$ Hz, 2H), 8.02 (d, $J = 6.7$ Hz, 2H), 7.51 (t, $J = 7.1$ Hz, 2H), 7.44 (t, $J = 7.5$ Hz, 2H), 2.90 (s, 3H). The obtained spectral data are in good agreement with those reported in literature.³⁶¹



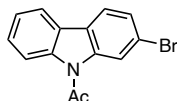
1-(3-bromo-9H-carbazol-9-yl)ethan-1-one (IV.2b). Prepared under constant potential conditions using **IV.3a** as catalyst. Yield: 45 mg (78% yield). $^1\text{H NMR}$ (δ , 23 °C, 400 MHz, CDCl_3): 8.20 (d, $J = 8.9$ Hz, 1H), 8.12–8.10 (m, 2H), 7.96 (d, $J = 7.7$ Hz, 1H), 7.57 (d, $J = 8.9$ Hz, 1H), 7.52 (d, $J = 8.5$ Hz, 1H), 7.41 (t, $J = 7.5$ Hz, 1H), 2.88 (s, 3H). The obtained spectral data are in good agreement with those reported in literature.³⁶¹



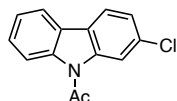
1-(3-chloro-9H-carbazol-9-yl)ethan-1-one (IV.2c). Prepared under constant potential conditions using **IV.3a** as catalyst. Yield: 39 mg (80% yield). $^1\text{H NMR}$ (δ , 23 °C, 400 MHz, CDCl_3): 8.26 (d, $J = 8.9$ Hz, 1H), 8.12 (d, $J = 8.4$ Hz, 1H), 7.98–7.95 (m, 2H), 7.54 (td, $J = 7.9$, 1.3 Hz, 1H), 7.46–7.40 (m, 2H), 2.89 (s, 3H). The obtained spectral data are in good agreement with those reported in literature.³⁶¹



1-(3-Fluoro-9H-carbazol-9-yl)ethan-1-one (IV.2d). Prepared under constant potential conditions using **IV.3a** as catalyst. Yield: 29 mg (64% yield). ^1H NMR (δ , 23 °C, 400 MHz, CDCl_3): 8.33-8.30 (m, 1H), 8.11 (d, $J = 8.4$ Hz, 1H), 7.97 (ddd, $J = 7.7, 1.4, 0.7$ Hz, 1H), 7.66–7.64 (m, 1H), 7.52 (ddd, $J = 8.5, 7.3, 1.3$ Hz, 1H), 7.41 (td, $J = 7.5, 0.9$ Hz, 1H), 7.20 (td, $J = 9.0, 2.7$ Hz, 1H), 2.90 (s, 3H). The obtained spectral data are in good agreement with those reported in literature.³²⁵

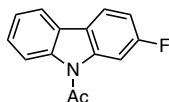


1-(2-Bromo-9H-carbazol-9-yl)ethan-1-one (IV.2e). Prepared under constant potential conditions using **IV.3a** as catalyst. Yield: 43 mg (75% yield). ^1H NMR (δ , 23 °C, 400 MHz, CDCl_3): 8.52 (d, $J = 1.5$ Hz, 1H), 8.08 (d, $J = 8.4$ Hz, 1H), 7.97 (d, $J = 7.7$ Hz, 1H), 7.83 (d, $J = 8.2$ Hz, 1H), 7.51 (d, $J = 8.4$ Hz, 2H), 7.40 (t, $J = 7.5$ Hz, 1H), 2.88 (s, 3H). ^{13}C NMR (δ , 23 °C, 100 MHz, CDCl_3): 170.0, 139.6, 138.6, 127.8, 127.1, 125.9, 125.3, 124.0, 121.1, 120.8, 120.2, 119.9, 116.0, 27.9. HRMS-ESI: calculated for $[\text{M}+\text{H}] = 288.0019$, observed $[\text{M}+\text{H}] = 288.0011$.

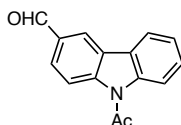


1-(2-Chloro-9H-carbazol-9-yl)ethan-1-one (IV.2f). Prepared under constant potential conditions using **IV.3a** as catalyst. Yield: 30 mg (61% yield). ^1H NMR (δ , 23 °C, 400 MHz, CDCl_3): 8.38 (s, 1H), 8.10 (d, $J = 8.4$ Hz, 1H), 7.98 (d, $J = 7.0$ Hz, 1H), 7.90 (d, $J = 8.3$ Hz, 1H),

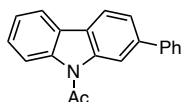
7.50 (t, $J = 7.2$ Hz, 1H), 7.43–7.37 (m, 2H), 2.89 (s, 3H). The obtained spectral data are in good agreement with those reported in literature.³⁶¹



1-(2-Fluoro-9H-carbazol-9-yl)ethan-1-one (IV.2g). Prepared under constant potential conditions using **IV.3a** as catalyst. Yield: 36 mg (78% yield). ¹H NMR (δ , 23 °C, 400 MHz, CDCl₃): 8.09 (td, $J = 6.6, 3.0$ Hz, 2H), 7.97–7.91 (m, 2H), 7.47 (ddd, $J = 8.5, 7.2, 1.3$ Hz, 1H), 7.40 (td, $J = 7.5, 1.0$ Hz, 1H), 7.14 (td, $J = 8.7, 2.3$ Hz, 1H), 2.89 (s, 3H). The obtained spectral data are in good agreement with those reported in literature.³⁶²



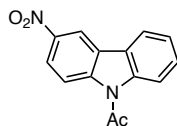
9-Acetyl-9H-carbazole-3-carbaldehyde (IV.2h). Prepared under constant potential conditions using **IV.3a** as catalyst. Yield: 20 mg (48% yield). ¹H NMR (δ , 23 °C, 400 MHz, CDCl₃): 10.15 (s, 1H), 8.44 (dd, $J = 1.7, 0.5$ Hz, 1H), 8.30 (d, $J = 8.6$ Hz, 1H), 7.98–7.94 (m, 2H), 7.82 (d, $J = 2.2$ Hz, 1H), 7.07 (dd, $J = 8.6, 2.2$ Hz, 1H), 3.97 (s, 3H), 2.93 (s, 3H). The obtained spectral data are in good agreement with those reported in literature.³⁶¹



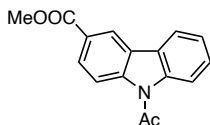
1-(2-Phenyl-9H-carbazol-9-yl)ethan-1-one (IV.2i). Prepared under constant current conditions using **IV.3a** as catalyst. Yield: 48 mg (84% yield). ¹H NMR (δ , 23 °C, 400 MHz, CDCl₃): 8.54 (d, $J = 0.7$ Hz, 1H), 8.22 (d, $J = 8.3$ Hz, 1H), 8.09–8.04 (m, 2H), 7.73 (dd, $J = 8.3,$

1.1 Hz, 2H), 7.67 (dd, $J = 8.0, 1.4$ Hz, 1H), 7.55–7.50 (m, 3H), 7.46–7.40 (m, 2H), 2.97 (s, 3H).

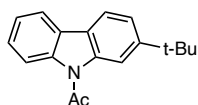
The obtained spectral data are in good agreement with those reported in literature.³⁶³



1-(3-Nitro-9H-carbazol-9-yl)ethan-1-one (IV.2j). Prepared under constant current conditions using **IV.3a** as catalyst. Yield: 22 mg (43% yield). ¹H NMR (δ , 23 °C, 400 MHz, CDCl₃): 8.90 (d, $J = 2.2$ Hz, 1H), 8.54 (d, $J = 9.2$ Hz, 1H), 8.41 (dd, $J = 9.2, 2.4$ Hz, 1H), 8.15–8.10 (m, 2H), 7.63 (td, $J = 7.9, 1.3$ Hz, 1H), 7.54–7.50 (m, 1H), 2.97 (s, 3H). The obtained spectral data are in good agreement with those reported in literature.³⁶⁴

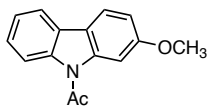


Methyl 9-acetyl-9H-carbazole-3-carboxylate (IV.2k). Prepared under constant potential conditions using **3b** as catalyst. CPE carried out 1.9 V vs. Ag⁺/Ag with HFIP/CH₂Cl₂ (5/1) solvent mixture. Yield: 38 mg (71% yield). ¹H NMR (δ , 23 °C, 400 MHz, CDCl₃): 8.73 (dd, $J = 1.8, 0.6$ Hz, 1H), 8.35 (dd, $J = 8.8, 0.5$ Hz, 1H), 8.22–8.19 (m, 2H), 8.11 (ddd, $J = 7.7, 1.4, 0.7$ Hz, 1H), 7.56 (ddd, $J = 8.5, 7.2, 1.3$ Hz, 1H), 7.47 (td, $J = 7.5, 0.9$ Hz, 1H), 4.02 (s, 3H), 2.95 (s, 3H). The obtained spectral data are in good agreement with those reported in literature.³²⁴

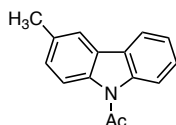


1-(2-Tert-butyl-9H-carbazol-9-yl)ethan-1-one (IV.2l). Prepared under constant potential conditions using **3a** as catalyst. Yield: 34 mg (65% yield). ¹H NMR (δ , 23 °C, 400 MHz, CDCl₃): 8.33 (s, 1H), 8.15 (d, $J = 8.3$ Hz, 1H), 7.97 (d, $J = 8.3$ Hz, 1H), 7.91 (d, $J = 7.6$ Hz, 1H), 7.45 (t, J

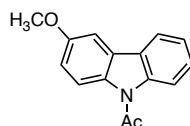
= 9.2 Hz, 2H), 7.37 (t, $J = 7.5$ Hz, 1H), 2.90 (s, 3H), 1.44 (s, 10H). The obtained spectral data are in good agreement with those reported in literature.³⁶³



1-(2-Methoxy-9H-carbazol-9-yl)ethan-1-one (IV.2m). Prepared under constant potential conditions using **IV.3a** as catalyst. Yield: 21 mg (44% yield). ¹H NMR (δ , 23 °C, 400 MHz, CDCl₃): 8.05 (d, $J = 7.8$ Hz, 1H), 7.93–7.89 (m, 2H), 7.87–7.85 (m, 1H), 7.42–7.34 (m, 2H), 6.99 (dd, $J = 8.5, 2.3$ Hz, 1H), 3.93 (s, 3H), 2.88 (s, 3H). The obtained spectral data are in good agreement with those reported in literature³⁶¹

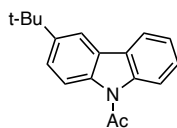


1-(3-Methyl-9H-carbazol-9-yl)ethan-1-one (IV.2n). Prepared under constant potential conditions using **IV.3b** as catalyst. CPE carried out 1.9 V vs. Ag⁺/Ag with HFIP/CH₂Cl₂ (5/1) solvent mixture. Yield: 4.4 mg (10% yield). ¹H NMR (δ , 23 °C, 400 MHz, CDCl₃): 8.23 (d, $J = 8.4$ Hz, 1H), 8.08 (d, $J = 8.5$ Hz, 1H), 7.97 (ddd, $J = 7.7, 1.4, 0.6$ Hz, 1H), 7.80 (t, $J = 0.9$ Hz, 1H), 7.49–7.45 (m, 1H), 7.38 (td, $J = 7.5, 1.0$ Hz, 1H), 7.30 (ddd, $J = 8.5, 1.8, 0.5$ Hz, 1H), 2.88 (s, 3H), 2.53 (s, 3H). The obtained spectral data are in good agreement with those reported in literature.³⁶⁵

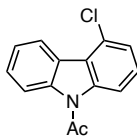


1-(3-Methoxy-9H-carbazol-9-yl)ethan-1-one (IV.2o). Prepared under constant potential conditions using **IV.3a** as catalyst. Yield: 4.8 mg (10% yield). ¹H NMR (δ , 23 °C, 400 MHz, CDCl₃): 7.91–7.89 (m, 2H), 7.52–7.48 (m, 2H), 7.39 (d, $J = 7.4$ Hz, 1H), 7.08 (d, $J = 2.4$ Hz, 1H),

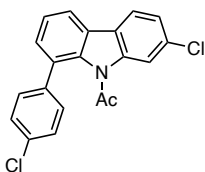
7.00 (d, $J = 2.4$ Hz, 1H), 3.90 (s, 3H), 2.63 (s, 3H). The obtained spectral data are in good agreement with those reported in literature.³⁶²



1-(3-Tert-butyl-9H-carbazol-9-yl)ethan-1-one (IV.2p). Prepared under constant potential conditions using **IV.3a** as catalyst. Yield: 36 mg (65% yield). ¹H NMR (δ , 23 °C, 400 MHz, CDCl₃): 8.27 (d, $J = 8.3$ Hz, 1H), 8.10 (d, $J = 8.8$ Hz, 1H), 8.04–8.01 (m, 2H), 7.55 (dd, $J = 8.8$, 2.1 Hz, 1H), 7.48 (ddd, $J = 8.4$, 7.2, 1.3 Hz, 1H), 7.40 (td, $J = 7.5$, 0.9 Hz, 1H), 2.89 (s, 3H), 1.46 (s, 9H). The obtained spectral data are in good agreement with those reported in literature.³²⁵

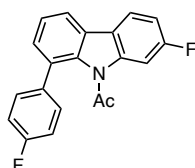


1-(4-Chloro-9H-carbazol-9-yl)ethan-1-one (IV.2q). Prepared under constant potential conditions using **IV.3a** as catalyst. Yield: 41 mg (85% yield). ¹H NMR (δ , 23 °C, 400 MHz, CDCl₃): 8.68 (dt, $J = 7.9$, 0.6 Hz, 1H), 8.25 (dd, $J = 7.0$, 2.1 Hz, 1H), 8.17 (d, $J = 8.5$ Hz, 1H), 7.54–7.52 (m, 1H), 7.46–7.36 (m, 3H), 2.90 (s, 3H). ¹³C NMR (δ , 23 °C, 125 MHz, CDCl₃): 170.2, 140.2, 138.8, 128.7, 127.9, 127.6, 125.4, 125.1, 123.9, 123.50, 123.41, 115.6, 114.8, 28.1. HRMS-ESI: calculated for [M+H] = 244.0524, observed [M+H] = 244.0521.

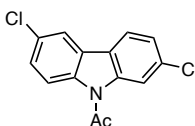


N-(4,4''-dichloro-[1,1':3',1''-terphenyl]-2'-yl)acetamide (IV.2r). Prepared under constant potential conditions using **IV.3b** as catalyst. CPE carried out 1.9 V vs. Ag⁺/Ag with HFIP/CH₂Cl₂

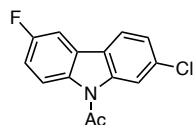
(5/1) solvent mixture. Yield: 38 mg (53% yield). $^1\text{H NMR}$ (δ , 23 °C, 400 MHz, CDCl_3): 8.24 (d, $J = 1.9$ Hz, 1H), 7.97 (dd, $J = 7.5, 1.3$ Hz, 1H), 7.91 (d, $J = 8.3$ Hz, 1H), 7.54–7.49 (m, 6H), 7.38 (dd, $J = 8.2, 1.8$ Hz, 1H), 1.82 (s, 4H). The obtained spectral data are in good agreement with those reported in literature.³²⁶



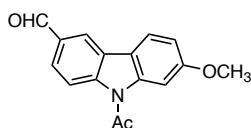
N-(4,4''-difluoro-[1,1':3',1''-terphenyl]-2'-yl)acetamide (**IV.2s**). Prepared under constant potential conditions using **IV.3b** as catalyst. CPE carried out 1.9 V vs. Ag^+/Ag with HFIP/ CH_2Cl_2 (5/1) solvent mixture. Yield: 35 mg (55% yield). $^1\text{H NMR}$ (δ , 23 °C, 400 MHz, CDCl_3): 7.96–7.93 (m, 3H), 7.57 (dd, $J = 8.8, 5.3$ Hz, 2H), 7.47 (d, $J = 7.6$ Hz, 1H), 7.42 (d, $J = 1.2$ Hz, 1H), 7.23–7.13 (m, 3H), 1.79 (s, 3H). The obtained spectral data are in good agreement with those reported in literature.³²⁶



1-(2,6-Dichloro-9H-carbazol-9-yl)ethan-1-one (**IV.2t**). Prepared under constant potential conditions using **IV.3a** as catalyst. Yield: 47 mg (84% yield). $^1\text{H NMR}$ (δ , 23 °C, 400 MHz, CDCl_3): 8.24 (d, $J = 1.7$ Hz, 1H), 8.11 (d, $J = 8.9$ Hz, 1H), 7.90–7.83 (m, 2H), 7.41 (ddd, $J = 21.6, 8.6, 2.0$ Hz, 2H), 2.86 (s, 3H). $^{13}\text{C NMR}$ (δ , 23 °C, 100 MHz, CDCl_3): 169.7, 139.6, 137.2, 134.0, 129.8, 127.7, 127.2, 124.6, 123.9, 120.9, 119.8, 117.4, 116.9, 27.8. HRMS-ESI: calculated for $[\text{M}+\text{H}] = 278.0134$, observed $[\text{M}+\text{H}] = 278.0132$.



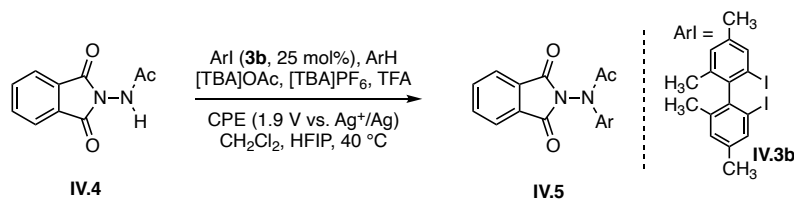
1-(2-Chloro-6-fluoro-9H-carbazol-9-yl)ethan-1-one (IV.2u). Prepared under constant potential conditions using **IV.3a** as catalyst. Yield: 37 mg (72% yield). ^1H NMR (δ , 23 °C, 400 MHz, CDCl_3): 8.24 (s, 1H), 8.17 (dd, $J = 9.2, 4.3$ Hz, 1H), 7.86 (d, $J = 8.3$ Hz, 1H), 7.62–7.60 (m, 1H), 7.39 (dd, $J = 8.3, 1.8$ Hz, 1H), 7.21 (td, $J = 9.0, 2.7$ Hz, 1H), 2.88 (s, 3H). ^{13}C NMR (δ , 23 °C, 100 MHz, CDCl_3): 169.5, 133.8, 124.3, 120.8, 117.5, 116.8, 115.0, 114.8, 27.6. HRMS-ESI: calculated for $[\text{M}+\text{H}] = 262.0429$, observed $[\text{M}+\text{H}] = 262.0430$.



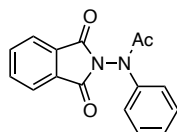
9-Acetyl-7-methoxy-9H-carbazole-3-carbaldehyde (IV.2v). Prepared under constant potential conditions using **IV.3b** as catalyst. CPE carried out 1.9 V vs. Ag^+/Ag with HFIP/ CH_2Cl_2 (5/1) solvent mixture. Yield: 41 mg (79% yield). ^1H NMR (δ , 23 °C, 400 MHz, CDCl_3): 10.12 (s, 1H), 8.42 (dd, $J = 1.7, 0.5$ Hz, 1H), 8.28 (d, $J = 8.6$ Hz, 1H), 7.96–7.91 (m, 2H), 7.80 (d, $J = 2.2$ Hz, 1H), 7.05 (dd, $J = 8.6, 2.2$ Hz, 1H), 3.94 (s, 3H), 2.91 (s, 3H). ^{13}C NMR (δ , 23 °C, 100 MHz, CDCl_3): 191.6, 170.2, 160.4, 142.3, 140.7, 132.3, 128.0, 127.2, 120.9, 120.5, 119.0, 116.2, 111.7, 102.0, 55.9, 27.8. HRMS-ESI: calculated for $[\text{M}+\text{H}] = 268.0968$, observed $[\text{M}+\text{H}] = 268.0962$.

Intermolecular C–H Amination Electrocatalysis

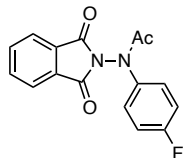
General Procedure for Intermolecular Amination Reactions



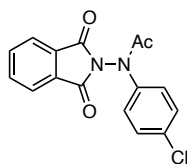
A 10-mL glass vial was charged with *N*-(1,3-dioxoisindolin-2-yl)acetamide (**IV.4**, 41.0 mg, 0.201 mmol, 1.00 equiv), 2,2'-diiodo-4,4',6,6'-tetramethyl-1,1'-biphenyl (**IV.3b**, 23.0 mg, 0.0495 mmol, 24.6 mol%), arene (2.01 mmol, 10.0 equiv), trifluoroacetic acid (TFA, 75.0 μ L, 5.00 equiv), tetrabutylammonium acetate (121 mg, 0.401 mmol, 1.99 equiv), tetrabutylammonium hexafluorophosphate (390 mg, 1.01 mmol, 5.02 equiv), HFIP (4.2 mL), and CH₂Cl₂ (0.8 mL) and was fitted with glassy carbon anode, platinum cathode and Ag⁺/Ag reference electrode. A constant potential of 2.0 V vs. Ag⁺/Ag was applied to the reaction mixture and stirred at 40 °C until ~80 C charge (~4.15 F/mol) is passed. The solvent was then concentrated under reduced pressure. The obtained residue was purified by SiO₂ gel chromatography (eluent 80:20 hexanes:ethyl acetate) to afford the products (**IV.5**) listed below.



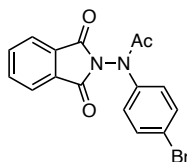
N-phenyl-*N*-(1,3-dioxoisindolin-2-yl)acetamide (**IV.5a**). Prepared from benzene at 1.8 V vs Ag⁺/Ag. With 5 equiv of PhH 32% yield was obtained. Yield: 40 mg (71% yield). ¹H NMR (δ , 23 °C, 400 MHz, CDCl₃): 7.89 (dd, *J* = 5.5, 3.1 Hz, 2H), 7.76 (dd, *J* = 5.5, 3.1 Hz, 2H), 7.70–7.68 (m, 2H), 7.45 (d, *J* = 7.5 Hz, 3H), 2.11 (s, 3H).¹⁸⁷



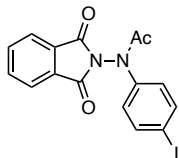
N-(4-fluorophenyl)-*N*-(1,3-dioxisoindolin-2-yl)acetamide (**IV.5b**). Prepared from fluorobenzene. Yield: 21 mg (35% yield). ^1H NMR (δ , 23 °C, 400 MHz, CDCl_3): 7.89 (dd, J = 5.5, 3.0 Hz, 2H), 7.77 (dd, J = 5.5, 3.1 Hz, 2H), 7.70 (dd, J = 9.0, 4.9 Hz, 2H), 7.14 (dd, J = 9.0, 8.2 Hz, 2H), 2.10 (s, 3H). The obtained spectral data are in good agreement with those reported in literature.³³¹



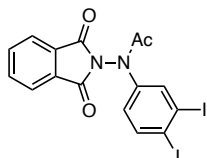
N-(4-chlorophenyl)-*N*-(1,3-dioxisoindolin-2-yl)acetamide (**IV.5c**). Prepared from chlorobenzene. Yield: 47 mg (74% yield). ^1H NMR (δ , 23 °C, 400 MHz, CDCl_3): 7.90 (dd, J = 5.5, 3.1 Hz, 2H), 7.78 (dd, J = 5.5, 3.1 Hz, 2H), 7.63 (d, J = 8.7 Hz, 2H), 7.43 (d, J = 8.7 Hz, 2H), 2.11 (s, 3H). The obtained spectral data are in good agreement with those reported in literature.¹⁸⁷



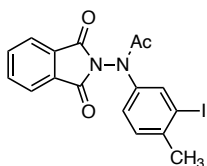
N-(4-bromophenyl)-*N*-(1,3-dioxisoindolin-2-yl)acetamide (**IV.5d**). Prepared from bromobenzene. Yield: 59 mg (82% yield). ^1H NMR (δ , 23 °C, 400 MHz, CDCl_3): 7.89 (dd, J = 5.4, 3.1 Hz, 2H), 7.78 (dd, J = 5.5, 3.1 Hz, 2H), 7.58 (d, J = 3.6 Hz, 4H), 2.11 (s, 3H). The obtained spectral data are in good agreement with those reported in literature.¹⁸⁷



N-(4-iodophenyl)-*N*-(1,3-dioxisoindolin-2-yl)acetamide (**IV.5e**). Prepared from iodobenzene. Yield: 58 mg (72% yield). ^1H NMR (δ , 23 °C, 400 MHz, CDCl_3): 7.89 (dd, $J = 5.5$, 3.1 Hz, 2H), 7.80–7.76 (m, 4H), 7.42 (d, $J = 8.5$ Hz, 2H), 2.11 (s, 3H). The obtained spectral data are in good agreement with those reported in literature.³³¹

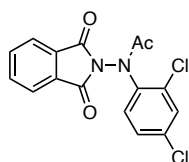


N-(3,4-diiodophenyl)-*N*-(1,3-dioxisoindolin-2-yl)acetamide (**IV.5f**). Prepared from 1,2-diiodobenzene (5 equiv). Yield: 64 mg (60% yield). ^1H NMR (δ , 23 °C, 400 MHz, CDCl_3): 8.16 (d, $J = 2.1$ Hz, 1H), 7.96–7.77 (m, 5H), 7.37 (dd, $J = 8.4$, 2.1 Hz, 1H), 2.12 (s, 3H). ^{13}C NMR (δ , 23 °C, 100 MHz, CDCl_3): 167.8, 164.9, 141.0, 140.5, 139.4, 135.0, 130.0, 129.7, 124.3, 109.9, 108.9, 21.8. HRMS-ESI: calculated for $[\text{M}+\text{H}] = 532.8854$, observed $[\text{M}+\text{H}] = 532.8844$.

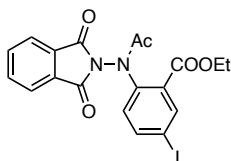


N-(1,3-dioxisoindolin-2-yl)-*N*-(3-iodo-4-methylphenyl)acetamide (**IV.5g**). Prepared from 2-iodotoluene (5 equiv). Yield: 62 mg (74% yield) with 1:10 mixture of *o*- (*N*-(1,3-dioxisoindolin-2-yl)-*N*-(3-iodo-2-methylphenyl)acetamide) and *p*-isomer (*N*-(1,3-dioxisoindolin-2-yl)-*N*-(3-iodo-4-methylphenyl)acetamide). ^1H NMR (δ , 23 °C, 500 MHz,

CDCl₃, *p*-isomer): 7.90–7.88 (m, 3H), 7.77 (dd, *J* = 5.5, 3.1 Hz, 2H), 7.54 (s, 1H), 7.21 (dd, *J* = 8.3, 2.4 Hz, 1H), 2.45 (s, 3H), 2.11 (s, 3H). ¹³C NMR (δ, 23 °C, 125 MHz, CDCl₃, *p*-isomer): 168.2, 165.0, 143.9, 140.8, 140.4, 134.9, 130.1, 129.8, 127.7, 124.5, 124.2, 102.5, 28.3, 21.8. HRMS-ESI: calculated for [M+H]= 421.0044, observed [M+H]= 421.0044.



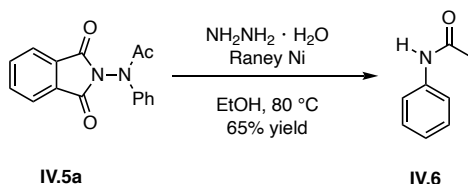
N-(2,4-dichlorophenyl)-*N*-(1,3-dioxisoindolin-2-yl)acetamide (**IV.5h**). Prepared from 1,3-dichlorobenzene. Yield: 31 mg (44% yield). ¹H NMR (δ, 23 °C, 400 MHz, CDCl₃): 7.90 (dd, *J* = 5.4, 3.2 Hz, 2H), 7.84 (d, *J* = 8.6 Hz, 1H), 7.79 (dd, *J* = 5.5, 3.1 Hz, 2H), 7.56 (d, *J* = 2.3 Hz, 1H), 7.34 (dd, *J* = 8.6, 2.4 Hz, 1H), 2.13 (s, 3H). ¹³C NMR (δ, 23 °C, 100 MHz, CDCl₃): 168.1, 136.8, 136.4, 134.8, 131.9, 131.0, 129.5, 128.8, 20.9. HRMS-ESI: calculated for [M+H]= 349.0141, observed [M+H]= 349.0134.



Ethyl 2-(*N*-(1,3-dioxisoindolin-2-yl)acetamido)-5-iodobenzoate (**IV.5i**). Prepared from ethyl 3-iodobenzoate (5 equiv). Yield: 53 mg (56% yield). ¹H NMR (δ, 23 °C, 400 MHz, CDCl₃): 8.20 (d, *J* = 2.1 Hz, 1H), 7.90 (dd, *J* = 8.4, 2.1 Hz, 1H), 7.85 (d, *J* = 8.5 Hz, 2H), 7.75 (dd, *J* = 5.5, 3.1 Hz, 2H), 7.55 (d, *J* = 8.4 Hz, 1H), 4.53 (q, *J* = 7.2 Hz, 2H), 2.16 (s, 3H), 1.41 (t, *J* = 7.2 Hz, 3H). ¹³C NMR (δ, 23 °C, 100 MHz, CDCl₃): 169.0, 164.97, 164.91, 142.3, 140.2, 138.6, 134.9, 134.4, 132.4, 130.0, 124.2, 95.7, 62.8, 21.9, 14.1. HRMS-ESI: calculated for [M+H]= 479.0098, observed [M+H]= 479.0101.

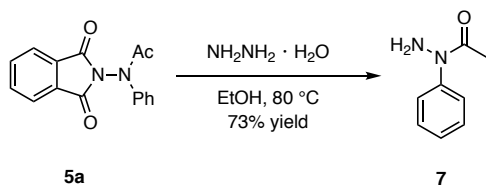
Derivatization of Intermolecular C–H Amination Products

Synthesis of Acetanilide (IV.6)



A 10-mL round-bottom flask was charged with *N*-phenyl-*N*-(1,3-dioxoisindolin-2-yl)acetamide (**IV.5a**, 50.1 mg, 0.178 mmol, 1.00 equiv), 80% $\text{N}_2\text{H}_4 \cdot \text{H}_2\text{O}$ (30.0 μL , 0.428 mmol, 2.88 equiv), Raney Ni (150 mg), and ethanol (5.0 mL) and was fitted with a reflux condenser. The reaction mixture was refluxed for 2 h and then cooled to 23 °C. Benzene (~5 mL) was added to the reaction mixture and the insoluble residue was removed by filtration. The filtrate was concentrated under reduced and the obtained residue was purified by SiO_2 gel chromatography (eluent 80:20 hexanes:ethyl acetate) to afford the title compound (**IV.6**) as a white solid (16 mg, 65% yield). ^1H NMR (δ , 23 °C, 400 MHz, CDCl_3): 7.50–7.48 (m, 2H), 7.35–7.32 (m, 3H), 7.13–7.09 (m, 1H), 2.18 (s, 3H). The obtained spectral data are in good agreement with those reported in literature.³⁶¹

Synthesis of *N*-phenylacetohydrazide (**IV.7**)

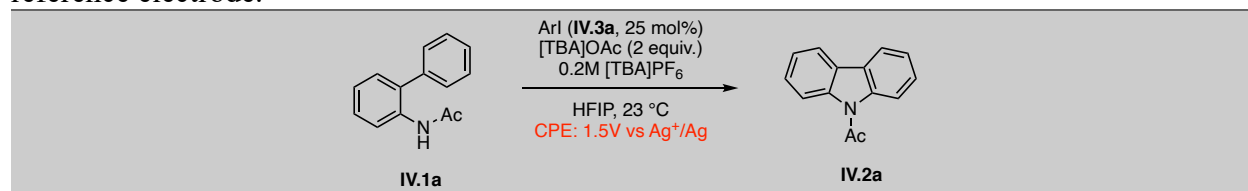


A 10-mL round-bottom flask was charged with *N*-phenyl-*N*-(1,3-dioxoisindolin-2-yl)acetamide (**IV.5a**, 48.0 mg, 0.171 mmol, 1.00 equiv), 80% $\text{N}_2\text{H}_4 \cdot \text{H}_2\text{O}$ (25.0 μL , 0.428 mmol, 2.50 equiv), and ethanol (5.0 mL) and was fitted with a reflux condenser. The reaction mixture was refluxed for 2 h and then cooled to $23\text{ }^\circ\text{C}$. Benzene ($\sim 5\text{ mL}$) was added to the reaction mixture and the insoluble residue was removed by filtration. The filtrate was then concentrated under reduced pressure. The obtained residue was purified by SiO_2 gel chromatography (eluent 80:20 hexanes:ethyl acetate) to afford the title compound (**IV.7**) as a white solid (18 mg, 73% yield). ^1H NMR (δ , $23\text{ }^\circ\text{C}$, 400 MHz, CDCl_3): 7.41 (t, $J = 7.5\text{ Hz}$, 2H), 7.33–7.28 (m, 3H), 4.83 (s, 2H), 2.00 (s, 3H). The obtained spectral data are in good agreement with those reported in literature.³⁶⁶

Table IV-4. Onset potentials for oxidation of various substituted aryl iodides. Conditions: Aryl Iodide (5.0 mM) in 0.2 M [TBA]PF₆ solution of HFIP with glassy carbon working electrode, Pt counter electrode and AgNO₃/Ag reference electrode. Scan rate = 0.10 V/s.

Entry	ArI	Onset potential / V vs. Ag ⁺ /Ag
1	4-iodoanisole	1.4
2	2,4-dimethoxyiodobenzene	1.41
3	2,6-dimethoxyiodobenzene	1.41
4	4-iodotoluene	1.65
5	2,2'-diiodo-4,4',6,6'-tetramethyl-1,1'-biphenyl	1.68, 1.83
6	iodobenzene	1.74
7	4-fluoroiodobenzene	1.79
8	2-iodobenzoic acid	1.90
9	4-trifluoromethyliodobenzene	2.00

Table IV-5. Effect of electrode materials on intramolecular C–H amination. Reaction conditions: 0.20 mmol of substrate, 0.05 mmol of catalyst, 5.0 mL of solvent, and AgNO₃/Ag reference electrode.



Entry	Anode	Cathode	Yield (%)
1	Glassy Carbon	0.05 M	76
2	Pt	0.10 M	0
3	Graphite	0.15 M	<10
4	Boron doped carbon (BDC)	0.20 M	35

Table IV-6. Full optimization table for intramolecular C–H amination. Effect of supporting electrolyte concentration, [TBA]OAc equivalence, protecting group, solvent, and temperature on electrocatalytic C–H amination reaction to form carbazoles. Reaction condition: 0.20 mmol of substrate (**IV.1a**), 0.05 mmol of catalyst (**IV.3a**), 5.0 mL of solvent, glassy carbon anode, Pt cathode and AgNO₃/Ag reference electrode.

IV.1a $\xrightarrow[\text{conditions}]{\text{4-Iodoanisole (IV.3a, 25 mol\%)}}$ IV.2a
CPE: 1.5V vs Ag⁺/Ag

Entry	[TBA]OAc	[TBA]PF ₆	R	T (°C)	Solvent	Yield (%)
1	2 equiv	0.05 M	Ac	23	HFIP	60
2	2 equiv	0.10 M	Ac	23	HFIP	70
3	2 equiv	0.15 M	Ac	23	HFIP	68
4	2 equiv	0.20 M	Ac	23	HFIP	76
5	1 equiv	0.20 M	Ac	23	HFIP	49
6	3 equiv	0.20 M	Ac	23	HFIP	75
7	5 equiv	0.20 M	Ac	23	HFIP	70
8	2 equiv	0.20 M	Ac	40	HFIP	37
9	2 equiv	0.20 M	Ac	23	MeCN	0
10	2 equiv	0.20 M	Ac	23	TFE	28
11	2 equiv	0.20 M	Ac	23	HFIP/MeCN (1/1)	0
12	2 equiv	0.20 M	Ac	23	HFIP/MeCN (2/1)	0
13	2 equiv	0.20 M	Ac	23	HFIP/MeCN (9/1)	45
14	2 equiv	0.20 M	Bz	23	HFIP	56
15	2 equiv	0.20 M	Ms	23	HFIP	64
16	2 equiv	0.20 M	Ts	23	HFIP	44
17	2 equiv	0.20 M	CF ₃ COO	23	HFIP	25

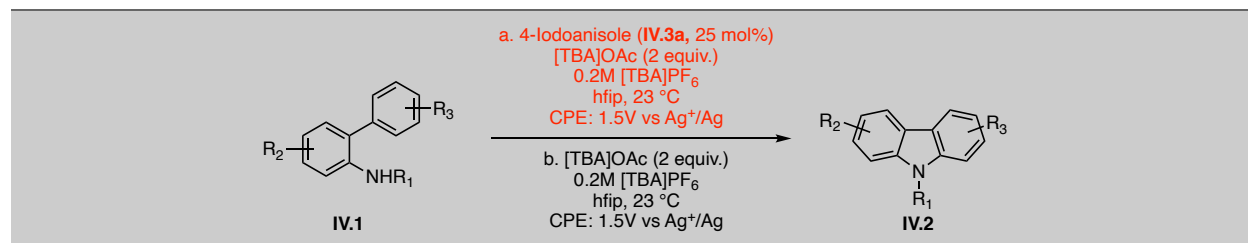
Table IV-7. Comparison of the electrolyte concentration used in this manuscript with those in other recent electrocatalytic methods.

Entry	Reference	Electrolyte Conc. (M)
1	<i>J. Am. Chem. Soc.</i> 2019 , <i>141</i> , 2825–2831	0.1
2	<i>ACS Catal.</i> 2019 , <i>9</i> , 746–754	0.1
3	<i>J. Am. Chem. Soc.</i> 2018 , <i>140</i> , 12511–12520	0.1
4	<i>J. Am. Chem. Soc.</i> 2018 , <i>140</i> , 2438–2441	0.1
5	<i>J. Am. Chem. Soc.</i> 2018 , <i>140</i> , 2076–2079	0.1
6	<i>J. Am. Chem. Soc.</i> 2017 , <i>139</i> , 15548–15553	0.1
7	<i>Science</i> 2017 , <i>357</i> , 575–579	0.1
8	<i>Chem. Eur. J.</i> 2018 , <i>24</i> , 12274–12279	0.2
9	<i>J. Am. Chem. Soc.</i> 2017 , <i>139</i> , 7448–7451	0.05
10	<i>Nature</i> 2019 , <i>573</i> , 398.	0.1
11	<i>J. Am. Chem. Soc.</i> 2019 , <i>141</i> , 6392–6402	0.2
12	<i>Angew. Chem. Int. Ed.</i> 2017 , <i>56</i> , 13088–13093	0.4
13	<i>ACS Cent. Sci.</i> 2019 , <i>5</i> , 1179–1186	0.5
14	<i>Acc. Chem. Res.</i> 2019 , <i>52</i> , 3432–3441	0.1
15	<i>J. Am. Chem. Soc.</i> 2019 , <i>141</i> , 14160–14167	0.1
16	<i>J. Am. Chem. Soc.</i> 2019 , <i>141</i> , 11115–11122	0.1
17	<i>Angew. Chem. Int. Ed.</i> 2018 , <i>57</i> , 10221–10225	0.1
18	<i>J. Am. Chem. Soc.</i> 2003 , <i>125</i> , 36–37.	0.4
19	<i>Angew. Chem. Int. Ed.</i> 2010 , <i>49</i> , 129–133.	0.1
20	<i>Angew. Chem. Int. Ed.</i> 2015 , <i>54</i> , 10555–10558.	0.1
21	<i>This work</i>	0.2

Table IV-8. Onset and peak potentials of biarylacetamide substrates. CV conditions: substrate 5 mM, 0.2 M [TBA]PF₆ solution of HFIP, glassy carbon working electrode, Pt counter electrode, Ag⁺/Ag reference electrode and scan rate = 0.10 V/s.

Entry	Substrate	Onset Potential (V vs. Ag ⁺ /Ag)	Peak Potential (V vs. Ag ⁺ /Ag)
1	IV.1a	1.50	1.69
2	IV.1b	1.50	1.73
3	IV.1c	1.50	1.73
4	IV.1d	1.55	1.72
5	IV.1e	1.50	1.74
6	IV.1f	1.50	1.71
7	IV.1g	1.54	1.70
8	IV.1h	1.76	1.96
9	IV.1i	1.44	1.58, 1.75
10	IV.1j	1.83	1.92
11	IV.1k	1.62	1.90
12	IV.1l	1.50	1.62
13	IV.1m	1.34	1.50
14	IV.1n	1.43	1.58
15	IV.1o	1.22	1.39
16	IV.1p	1.43	1.60
17	IV.1q	1.61	1.80
18	IV.1r	1.56	1.65, 1.82
19	IV.1s	1.50	1.68
20	IV.1t	1.61	1.83
21	IV.1u	1.57	1.76
22	IV.1v	1.48	1.63

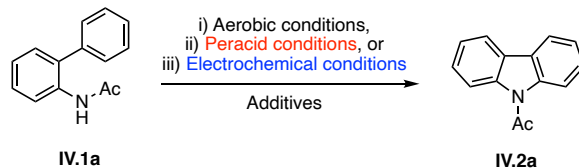
Table IV-9. Yield of selected substrate background reaction in the absence of aryl iodide. A 10-mL glass vial was charged with *N*-arylacetamide (1, 0.201 mmol, 1.00 equiv), tetrabutylammonium acetate (121 mg, 0.401 mmol, 1.99 equiv), tetrabutylammonium hexafluorophosphate (390 mg, 1.01 mmol, 5.02 equiv), and HFIP (5.0 mL) and was fitted with glassy carbon anode, platinum cathode, and Ag⁺/Ag reference electrode. A constant potential of 1.5 V vs. Ag⁺/Ag was applied to the reaction mixture with stirring at 23 °C until ~80 C charge (~4.15 F/mol) is passed if the current density was not too low. The solvent was removed under reduced pressure. Mesitylene was added directly to the crude reaction mixture as an internal standard and the yield was analyzed by ¹H NMR in CDCl₃.



Entry	Substrate	Yield ^a (%)	Yield ^b (%)	Onset Potential (V vs. Ag ⁺ /Ag)
1	IV.1a, R ₁ =R ₂ =H	76	0 ^c	1.50
2	IV.1b, R ₁ =Br, R ₂ =H	78	10 ^c	1.50
3	IV.1c, R ₁ =Cl, R ₂ =H	80	15 ^c	1.50
4	IV.1g, R ₁ =H, R ₂ =F	78	5 ^c	1.54
5	IV.1j, R ₁ =NO ₂ , R ₂ =H	43	0 ^c	1.83
6	IV.1k, R ₁ =COOMe, R ₂ =H	71	0 ^c	1.62
7	IV.1l, R ₁ =H, R ₂ = ^t Bu	65	0 ^c	1.50
8	IV.1m, R ₁ =H, R ₂ =OMe	44	0 ^d	1.34
9	IV.1o, R ₁ =OMe, R ₂ =H	10	0 ^d	1.22
11	IV.1p, R ₁ = ^t Bu, R ₂ =H	65	65	1.43
12	IV.1v, R ₁ =CHO, R ₂ =OMe	79	33	1.48

^c current density was too low. ^d decomposition of substrate was observed.

Procedure for Robustness Analysis



Aerobic conditions A 20-mL scintillation vial was charged with *N*-([1,1'-biphenyl]-2-yl)acetamide (**IV.1a**, 42.5 mg, 0.201 mmol, 1.00 equiv), 4-iodotoluene (11.0 mg, 0.0505 mmol, 25.0 mol%), $\text{CoCl}_2 \cdot 6\text{H}_2\text{O}$ (0.5 mg, 2.13 μmol , 1.06 mol%), 1,2-dichloroethane (DCE, 1.0 mL), and HFIP (0.50 mL) and the reaction mixture was fitted with a rubber septum. The reaction vessel was purged with O_2 for 2-3 min and acetaldehyde (120 μL , 2.13 mmol, 10.6 equiv) was added to the reaction vessel. Individual additives (0.201 mmol, 1.00 equiv) were dissolved in 2:1 DCE:HFIP (0.50 mL) and were added to the reaction vessel via syringe after 15 min. The reaction mixture was stirred at 23 $^\circ\text{C}$ under 1 atm O_2 , delivered by inflated balloon for 16 h. Mesitylene was added as an internal standard to the crude reaction mixture and then an aliquot (~ 0.1 mL) of the reaction mixture was taken into an NMR tube, diluted with CDCl_3 (~ 0.4 mL), and corresponding ^1H NMR was recorded. The yield and additive recovery were analyzed from the appropriate ^1H NMR. Data are collected in the Figure IV-13.

Peracid conditions A 20-mL scintillation vial was charged with *N*-([1,1'-biphenyl]-2-yl)acetamide (**IV.1a**, 32.1 mg, 0.152 mmol, 1.00 equiv), 2,2'-diiodo-4,4',6,6'-tetramethyl-1,1'-biphenyl (**IV.3b**, 7.07 mg, 0.0151 mmol, 10.0 mol%), dichloromethane (CH_2Cl_2 , 1.50 mL), HFIP (1.50 mL), and appropriate additives (0.151 mmol, 1.00 equiv). Peracetic acid (39% in acetic acid, 51.0 μL , 0.301 mmol, 1.99 equiv) was added to the reaction vessel, and the reaction mixture was stirred at 23 $^\circ\text{C}$ for 16 h. Mesitylene was added as an internal standard to the crude reaction mixture and then an aliquot (~ 0.1 mL) of the reaction mixture was taken into an NMR tube, diluted with

CDCl₃ (~0.4 ml), and corresponding ¹H NMR was recorded. The yield and additive recovery were analyzed from the appropriate ¹H NMR. Data are collected in the Figure IV-13.

Electrochemical conditions. A 10-mL glass vial was charged with *N*-([1,1'-biphenyl]-2-yl)acetamide (**IV.1a**, 0.201 mmol, 1.00 equiv), 4-iodoanisole (**IV.3a**, 12.0 mg, 0.0512 mmol, 25.3 mol%), appropriate additive (0.201 mmol, 1.00 equiv), tetrabutylammonium acetate (121 mg, 0.401 mmol, 1.99 equiv), tetrabutylammonium hexafluorophosphate (390 mg, 1.01 mmol, 5.02 equiv), and HFIP (5.0 mL). The reaction vessel was fitted with glassy carbon anode, platinum cathode, and Ag⁺/Ag reference electrode. A constant potential of 1.5V vs. Ag⁺/Ag was applied to the reaction mixture, which was stirred at 23 °C until ~80 C charge (~4.15 F/mol) was passed. Mesitylene was added as an internal standard to the crude reaction mixture and then an aliquot (~0.1 mL) of the reaction mixture was taken into an NMR tube, diluted with CDCl₃ (~0.4 ml), and corresponding ¹H NMR was recorded. The yield and additive recovery were analyzed from the appropriate ¹H NMR. Data are collected in the Figure IV-13.

Cyclic Voltammogram Studies of 4-Iodotoluene

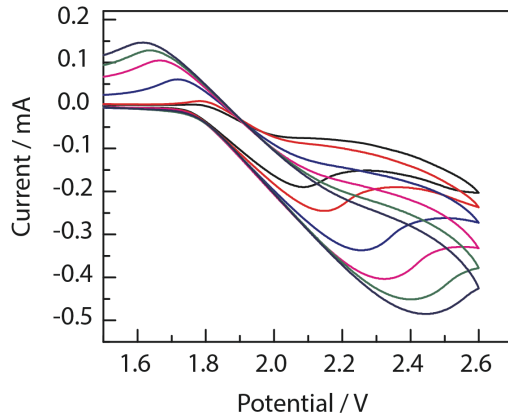


Figure IV-14. Increasing reversibility of 4-iodotoluene oxidation in HFIP is observed in cyclic voltammograms collected with increasing scan rate. 0.05 V/s (—), 0.1 V/s (—), 0.25 V/s (—), 0.50 V/s (—), 0.75 V/s (—), and 1.0 V/s (—). CV conditions: 10 mM 4-iodotoluene, 0.2 M [TBA]PF₆ solution of HFIP, glassy carbon working electrode, and Pt counter electrode.

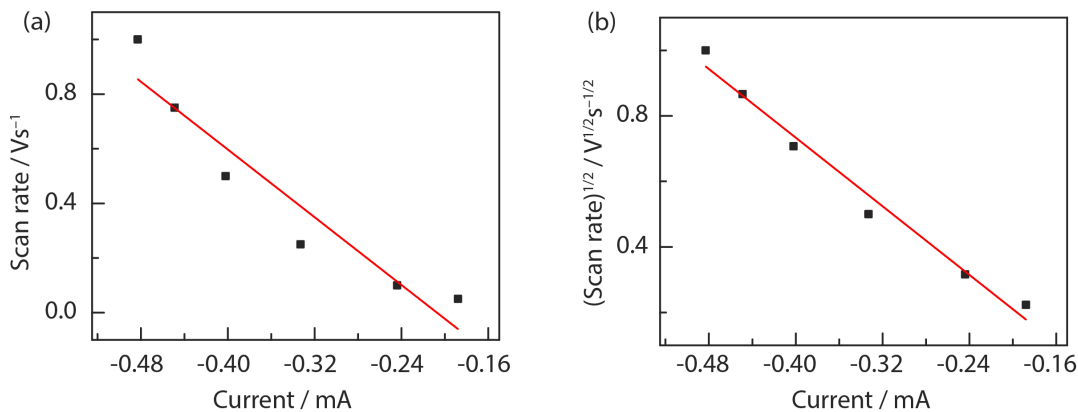


Figure IV-15. Plot of (a) scan rate vs. peak anodic current (I_{pa}) of 4-iodotoluene [$R^2 = 0.89$] and (b) square root of scan rate vs. peak anodic current (I_{pa}) [$R^2 = 0.98$]. The better fit for (b) suggests that no adsorption of aryl iodide was observed on the surface of the electrode.

Determination of the K_{eq} for HFIP binding to [TBA]OAc

In order to determine the equilibrium constant (K_{eq}) for acetate binding to HFIP, an NMR tube was charged with mesitylene (3.2 mg, 0.027 mmol), HFIP (5.0 μ L, 0.048 mmol), and CD_3CN (0.50 mL). The sample was allowed to equilibrate in the magnet for 5 min before the 1H NMR spectrum was recorded, and the spectrum was remeasured after 30 min to ensure that equilibrium had been reached. In a 20-mL scintillation vial a stock solution of [TBA]OAc (80 mg, 0.27 mmol) in CD_3CN (0.50 mL) was prepared. To the solution in NMR tube, 20 μ L of [TBA]OAc stock solution was added and the corresponding 1H NMR spectrum was recorded. Each NMR sample was run at 23 $^{\circ}C$ and the amount of HFIP and [TBA]OAc in a given sample was determined using mesitylene as the internal standard. As shown in Figure IV-16, the resonance of the 3 $^{\circ}$ proton (adjacent to OH group) was shifted downfield as the mole fraction of acetate anion was increased. The Job plot, shown in Figure IV-17, was obtained plotting $\chi_{HFIP} \times \Delta\delta_{ppm}$ with χ_{HFIP} , indicating a 1:1 complex stoichiometry.

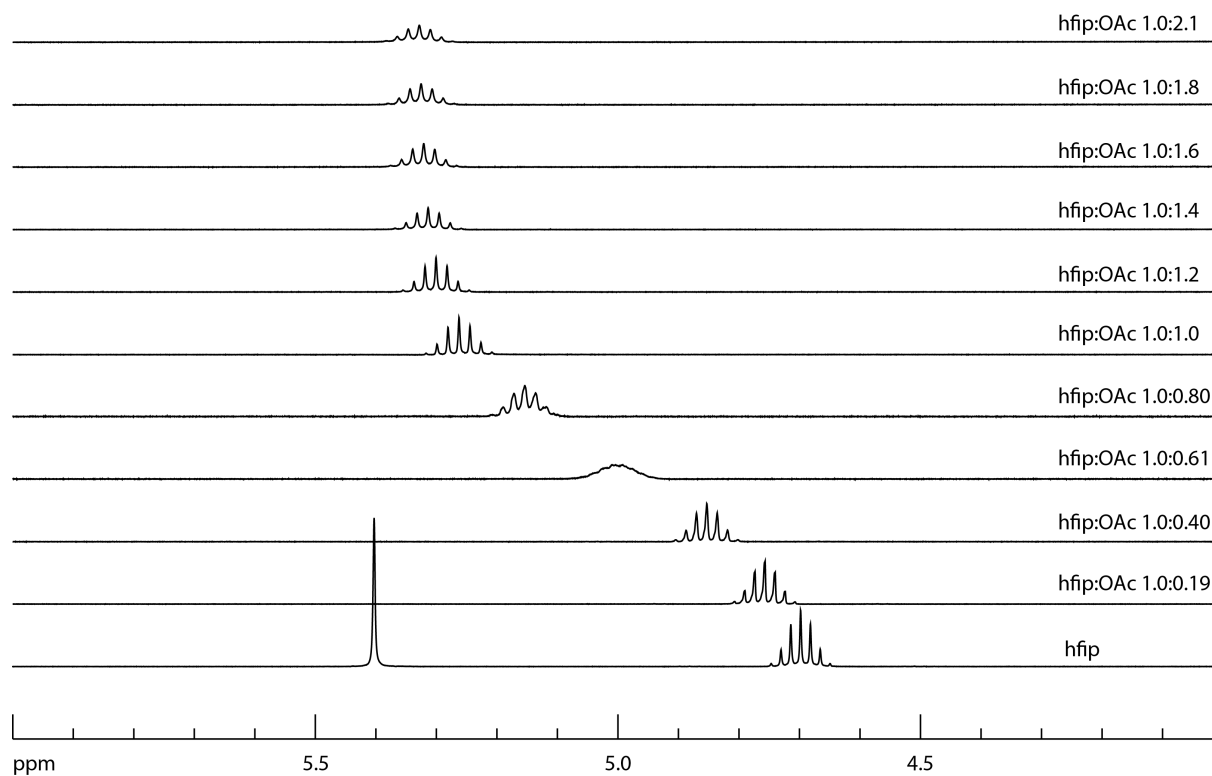


Figure IV-16. ^1H NMR spectra of HFIP titration with [TBA]OAc in CD_3CN . In this plot, change of chemical shift of 3° proton adjacent to OH group is measured as a function of [TBA]OAc concentration.

Table IV-10. Data for the Job plot performed by ^1H NMR titration in CD_3CN .

Entry	HFIP (mM)	[TBA]OAc (mM)	χ_{HFIP}	δ (ppm)	$\Delta\delta$ (ppm)	$\chi_{\text{HFIP}} \times \Delta\delta_{\text{ppm}}$
1	0.0489	–	1.00	4.70	0	–
2	0.0489	0.00932	0.840	4.78	0.08	0.0672
3	0.0489	0.0198	0.712	4.85	0.15	0.107
4	0.0489	0.0298	0.622	5.01	0.31	0.193
5	0.0489	0.0394	0.554	5.15	0.45	0.249
6	0.0489	0.0515	0.488	5.26	0.56	0.273
7	0.0489	0.0602	0.449	5.3	0.6	0.269
8	0.0489	0.0702	0.411	5.31	0.61	0.251
9	0.0489	0.0808	0.377	5.32	0.62	0.234
10	0.0489	0.0923	0.3467	5.33	0.63	0.218
11	0.0489	0.101	0.326	5.33	0.63	0.205

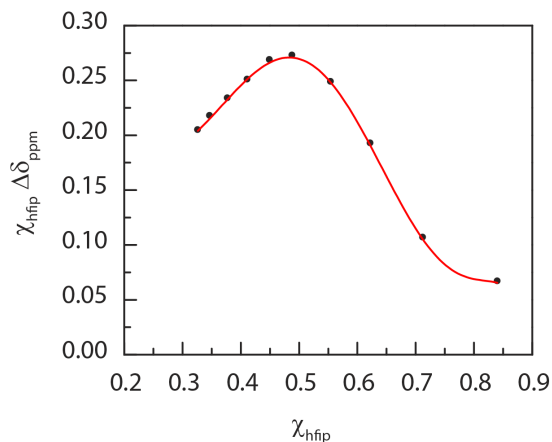


Figure IV-17. Job plot constructed from the ^1H NMR data shown in Figure IV-16. The maximum at ~ 0.5 indicates a 1:1 interaction between HFIP and [TBA]OAc.

The equilibrium constant for the formation of an adduct between HFIP and [TBA]OAc was calculated from Eq. IV-1³⁶⁷

$$K_{eq} = \frac{\Delta\delta_{obs}}{(\Delta\delta_{CA} - \Delta\delta_{obs})\left([HFIP] - \frac{[xx]\Delta\delta_{obs}}{\Delta\delta_{CA}}\right)} \quad \text{Equation IV-1}$$

Where,

$\Delta\delta_{obs}$ = difference between the chemical shifts of neat HFIP and that of in presence of [TBA]OAc

$\Delta\delta_{CA}$ = change in chemical shift between the completely complexed and uncomplexed molecule

For a range of possible $\Delta\delta_{CA}$ values, K_{eq} was determined following the equation IV-1 for entries 8-11 in Table IV-10 and the trial K_{eq} vs. $\Delta\delta_{CA}$ was plotted for each concentration shown in Figure IV-16.

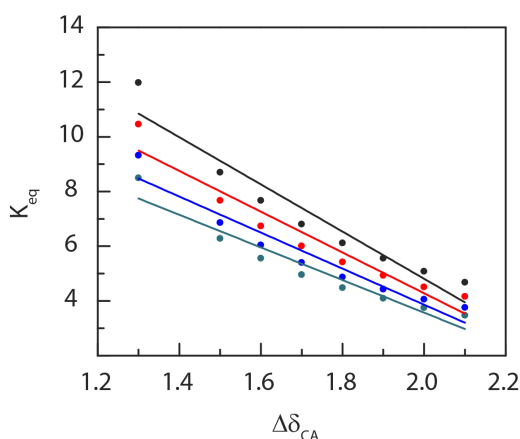


Figure IV-18. Linear fitting of K_{eq} vs. $\Delta\delta_{CA}$ for solutions 8 (—), 9 (—), 10 (—), and 11 (—). The equations for the best-fitted linear curve from the Figure IV-18 were given as: $y = 22.06 - 8.62x$ for solution 8 (—); $R^2 = 0.92$, Equation IV-2; $y = 19.19 - 7.46x$ for solution 9 (—); $R^2 = 0.91$, Equation IV-3; $y = 17.04 - 6.59x$ for solution 10 (—); $R^2 = 0.92$, Equation IV-4; $y = 15.49 - 5.96x$ for solution 11 (—); $R^2 = 0.93$, Equation IV-5.

Since the K_{eq} at a given temperature is constant for all the solutions, the value of $\Delta\delta_{CA}$ and K_{eq} was determined solving Eq. IV-2–5. The value of $\Delta\delta_{CA}$ was found to be 2.47 ppm. and the K_{eq} for HFIP hydrogen-bonding with [TBA]OAc was determined to be 0.767 ± 0.002 at 23 °C.

Initial Optimization Reactions Using Constant Current Electrolysis

Table IV-11. Optimization of the electrochemical oxidation of 4-iodotoluene under constant current electrolysis. Reaction conditions: 0.20 mmol of 4-iodotoluene, 0.2 M [TBA]PF₆, 5.0 mL of HFIP.

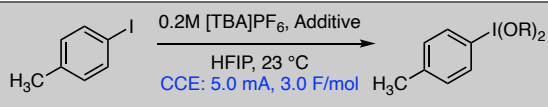
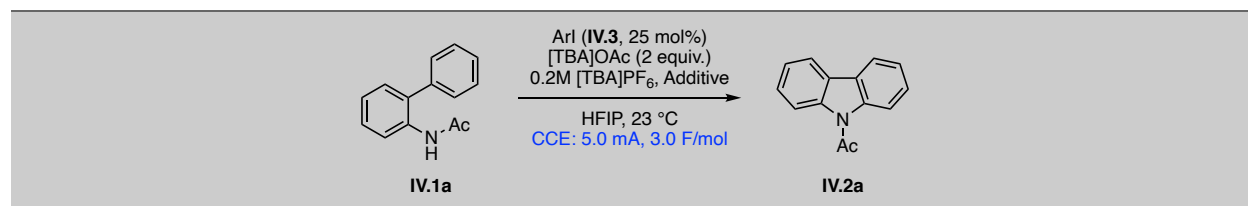
				
Entry	Anode	Cathode	Additive	Yield (%)
1	Glassy Carbon	Pt	[TBA]OAc (2 eq.)	60
2	Glassy Carbon	Pt	AcOH (5 eq.)	8
3	Glassy Carbon	Pt	-	40 (HFIP adduct)
4	Pt	Pt	[TBA]OAc (2 eq.)	28
5	Graphite	Pt	[TBA]OAc (2 eq.)	32
6	BDC	Pt	[TBA]OAc (2 eq.)	41

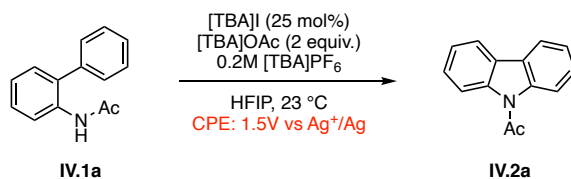
Table IV-12. Optimization of catalyst screening and effect of additives under constant current electrolysis. Reaction conditions: 0.20 mmol of substrate, 0.05 mmol of catalyst, additive 0.20 mmol, 0.40 mmol [TBA]OAc, 0.2 M [TBA]PF₆, 5.0 mL of HFIP, glassy carbon anode, and Pt cathode.



Entry	ArI	ArI Loading	Additive	Yield (%)
1	4-iodotoluene	25 mol%	-	40
2	4-iodoanisole	25 mol%	-	55
3	iodobenzene	25 mol%	-	22
4	2,6-dimethoxyiodobenzene	25 mol%	-	27
5	2,4-dimethoxyiodobenzene	25 mol%	-	37
6	1,2-diiodobenzene	25 mol%	-	34
7	2-iodobenzoic acid	25 mol%	-	27
8	2-(2-iodophenyl)propan-2-ol	25 mol%	-	37
9	1,1,1,3,3,3-hexafluoro-2-(2-iodophenyl)propan-2-ol	25 mol%	-	34
10	4-iodoanisole	1 equiv	-	62
11	4-iodoanisole	25 mol%	-	57
12	4-iodoanisole	10 mol%	-	46
13	4-iodoanisole	5 mol%	-	35
14	4-iodoanisole	25 mol%	CH ₂ Cl ₂	28
15	4-iodoanisole	25 mol%	MeCN	trace
16	4-iodoanisole	25 mol%	Cs ₂ O ₃	56
17	4-iodoanisole	25 mol%	BF ₃ ·OEt ₂	46
18	4-iodoanisole	25 mol%	CF ₃ COOH	trace

Control reaction for iodide mediated intramolecular C–N coupling

To exclude the possibility of catalyst decomposition mediated reaction chemistry (via iodide oxidation), background reaction with [TBA]I in place of 4-iodoanisole was attempted for the parent carbazole forming reaction using **IV.1a**.



A 10-mL glass vial was charged with *N*-([1,1'-biphenyl]-2-yl)acetamide (**IV.1a**, 0.201 mmol, 1.00 equiv), tetrabutylammonium iodide (18.5 mg, 0.05 mmol, 25.0 mol%), tetrabutylammonium acetate (121 mg, 0.401 mmol, 1.99 equiv), tetrabutylammonium hexafluorophosphate (390 mg, 1.01 mmol, 5.02 equiv), and HFIP (5.0 mL). The reaction vessel was fitted with glassy carbon anode, platinum cathode, and Ag⁺/Ag reference electrode. A constant potential of 1.5V vs. Ag⁺/Ag was applied to the reaction mixture, which was stirred at 23 °C. Due to low current densities the reaction was run until 45C charge (~2.33 F/mol) was passed, approximately 15 h. Mesitylene was added directly to the crude reaction mixture as an internal standard and the yield was analyzed by ¹H NMR in CDCl₃. The yield was found to be 35% with Faradaic efficiency of 30%.

The yield of 35% carbazole product (**IV.2a**) is significantly lower than the 76% yield of optimized reaction condition with aryl iodide catalyst (**IV.3a**). Though the Faradaic efficiency of 36% for [TBA]I is comparable with that of reaction with 4-iodoanisole (40%), the current density for [TBA]I reaction was significantly lower than aryl-iodide-catalyzed reaction (45C of charge

were passed for [TBA]I in 15h whereas 80C of charge is passed with 4-iodoanisole in 7-8h). In addition to this observation, high recovery of 4-iodoanisole (~95%) from parent reaction condition excludes the possibility of catalyst decomposition mediated chemistry.

Additional Cyclic Voltammogram Studies of 4-Iodoanisole

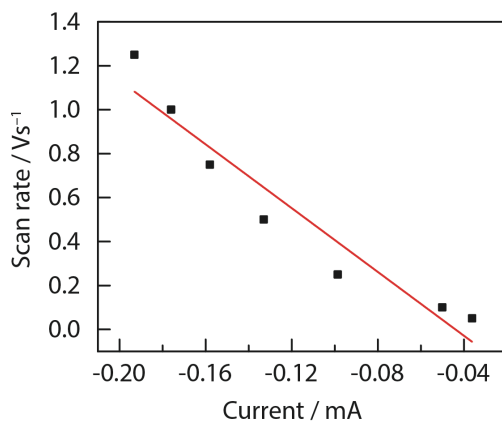


Figure IV-19. Plot of scan rate vs. peak anodic current (I_{pa}) of 4-iodoanisole [$R^2 = 0.91$]. The better fit for Figure IV-7c suggests that no adsorption of aryl iodide was observed on the surface of the electrode. Data collected from Figure IV-7a.

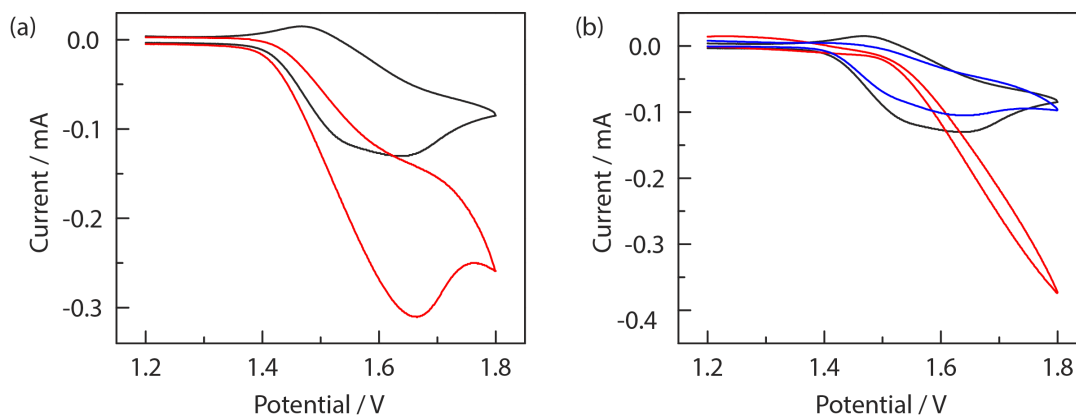


Figure IV-20. Comparison of current response in the cyclic voltammogram of 4-iodoanisole (IV.3a) with the addition of either (a) acetate, or (b) substrate (IV.1a). (a) Cyclic voltammogram of 4-iodoanisole (IV.3a) (—) and IV.3a with [TBA]OAc (—). (b) Cyclic voltammogram of 4-iodoanisole (IV.3a) (—), compound IV.1a (—), and IV.3a with IV.1a (—). The increased current with addition of [TBA]OAc is consistent with [TBA]OAc trapping an

electrochemically generated iodanyl radical. CV conditions: 0.2 M [TBA]PF₆ solution of HFIP, glassy carbon working electrode, Pt counter electrode, and scan rate = 0.25 V/s.

Calculation of Faradaic efficiency for various substrates

The Faradaic efficiency of the described reactions are calculated using the following formula:

$$\mathbf{Faradaic\ efficiency} = \frac{Q_{theoretical}}{Q_{experimental}} \times \frac{reaction\ yield}{100} \% \quad \mathbf{Equation\ IV-6}$$

Where, $Q_{theoretical}$ = amount of charge required for the reaction for 100% efficiency (2.0 F/mol)

$Q_{experimental}$ = amount of charge passed through the reaction (4.15 F/mol)

$reaction\ yield$ = respective yield of product in consideration

Figure IV-21. Comparison of Faradaic efficiency with selected publications in recent years on electrocatalytic substrate functionalization.

Entry	Reference	Faradaic Efficiency
1	<i>ACS Catal.</i> 2019 , <i>9</i> , 746–754	27-90%
2	<i>J. Am. Chem. Soc.</i> 2018 , <i>140</i> , 2438–2441	<20%
3	<i>J. Am. Chem. Soc.</i> 2017 , <i>139</i> , 7448-7451	<15%
4	<i>Nature</i> 2019 , <i>573</i> , 398	<30%
5	<i>J. Am. Chem. Soc.</i> 2019 , <i>141</i> , 6392–6402	<30%
6	<i>Angew. Chem. Int. Ed.</i> 2017 , <i>56</i> , 13088–13093	48%
7	<i>Angew. Chem. Int. Ed.</i> 2010 , <i>49</i> , 129–133	<21%
8	<i>J. Am. Chem. Soc.</i> 2017 , <i>139</i> , 2956–2959	17-55%
9	<i>J. Am. Chem. Soc.</i> 2007 , <i>129</i> , 6680–6681	26-60%
10	<i>J. Am. Chem. Soc.</i> 2018 , <i>140</i> , 11487–11494	<15 %
11	<i>J. Am. Chem. Soc.</i> 2015 , <i>137</i> , 9816–9819	35-51%
12	<i>J. Am. Chem. Soc.</i> 2007 , <i>129</i> , 2246–2247	42-60%
13	<i>J. Am. Chem. Soc.</i> 2009 , <i>131</i> , 11310–11311	<30%
14	<i>J. Org. Chem.</i> 1994 , <i>59</i> , 7190-7192	30-44%
15	<i>This paper</i>	21-40%

NMR Spectra of New Compounds

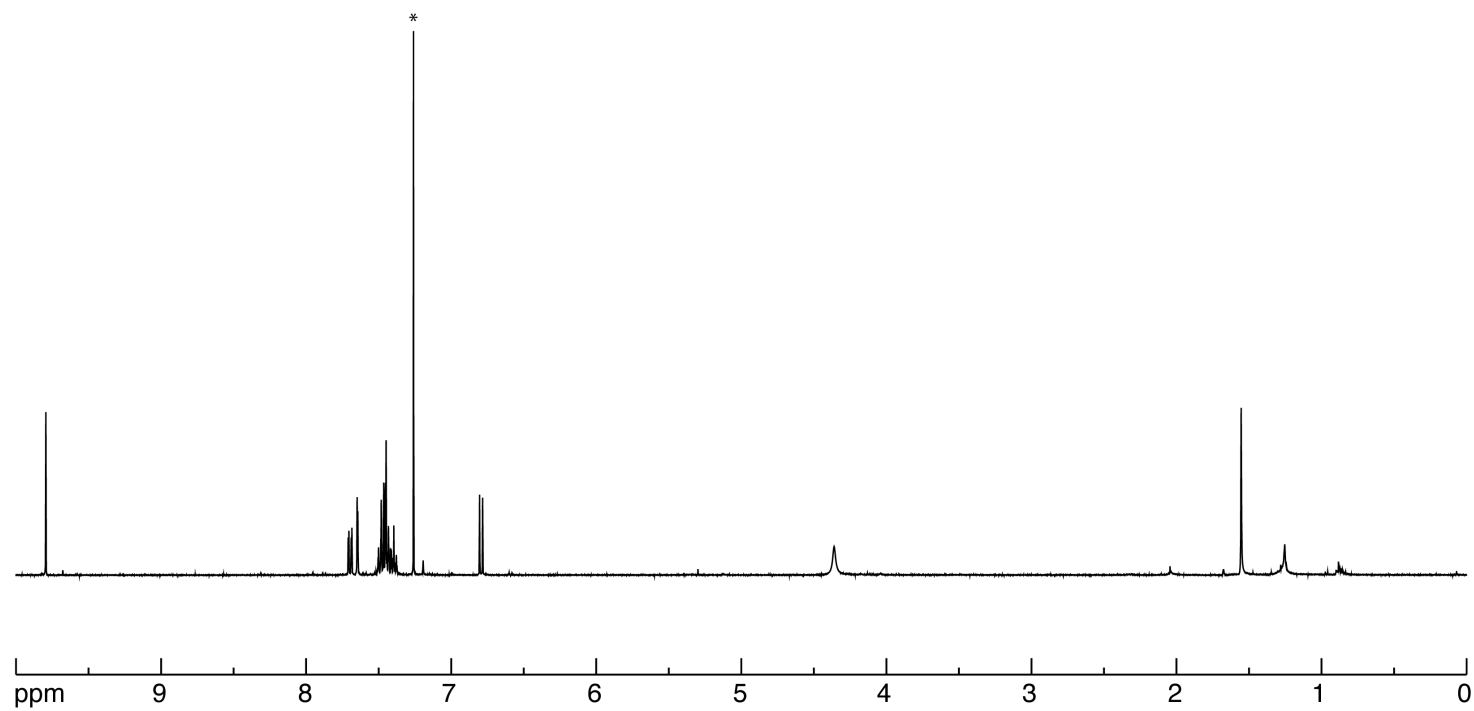
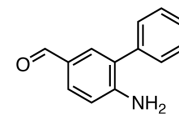


Figure IV-22. ^1H NMR spectrum of compound IV.S1h in CDCl_3 (400 MHz) at 23 °C. * CDCl_3 solvent peak.

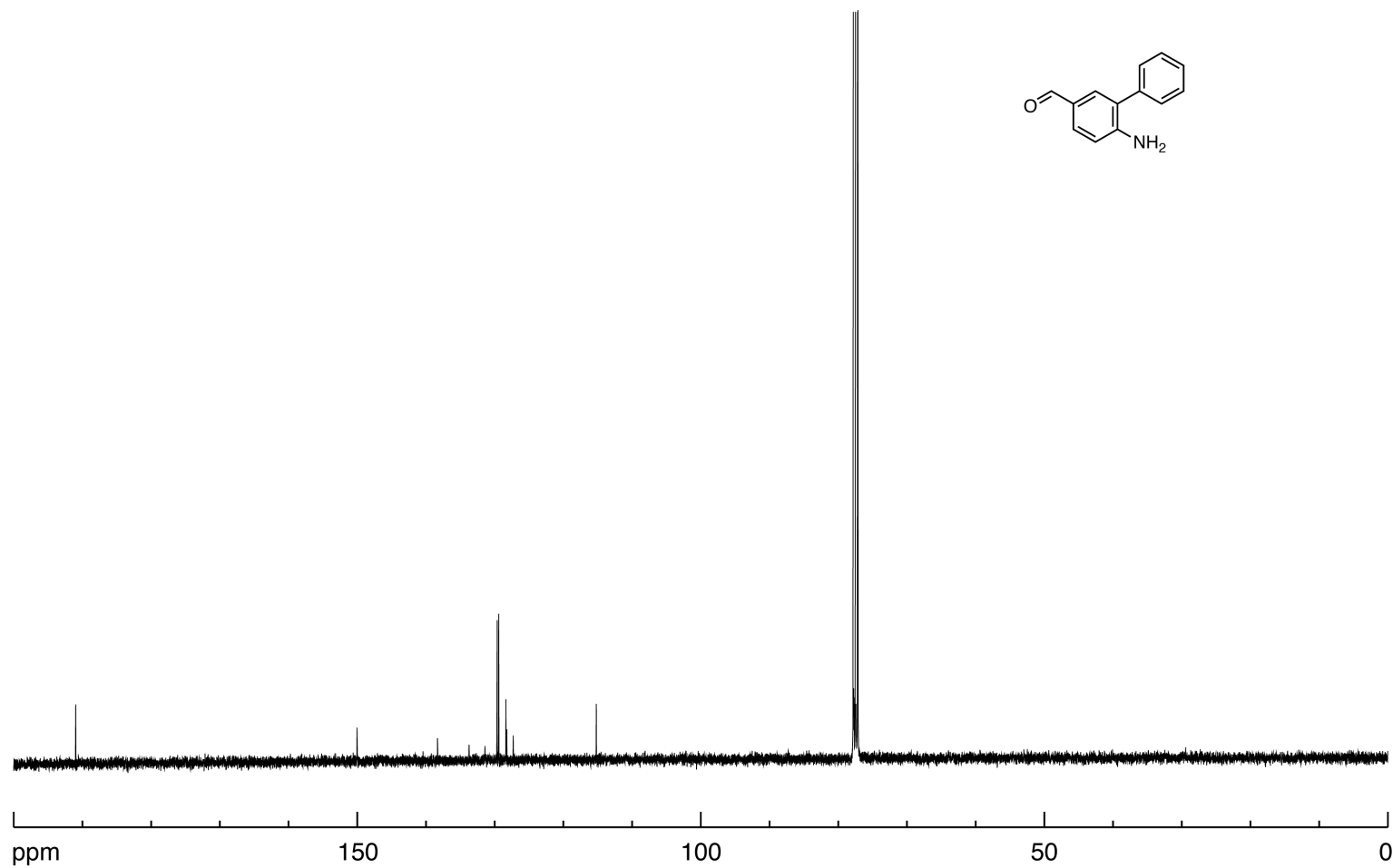


Figure IV-23. ¹³C NMR spectrum of compound IV.S1h in CDCl₃ (100 MHz) at 23 °C. *CDCl₃ solvent peak.

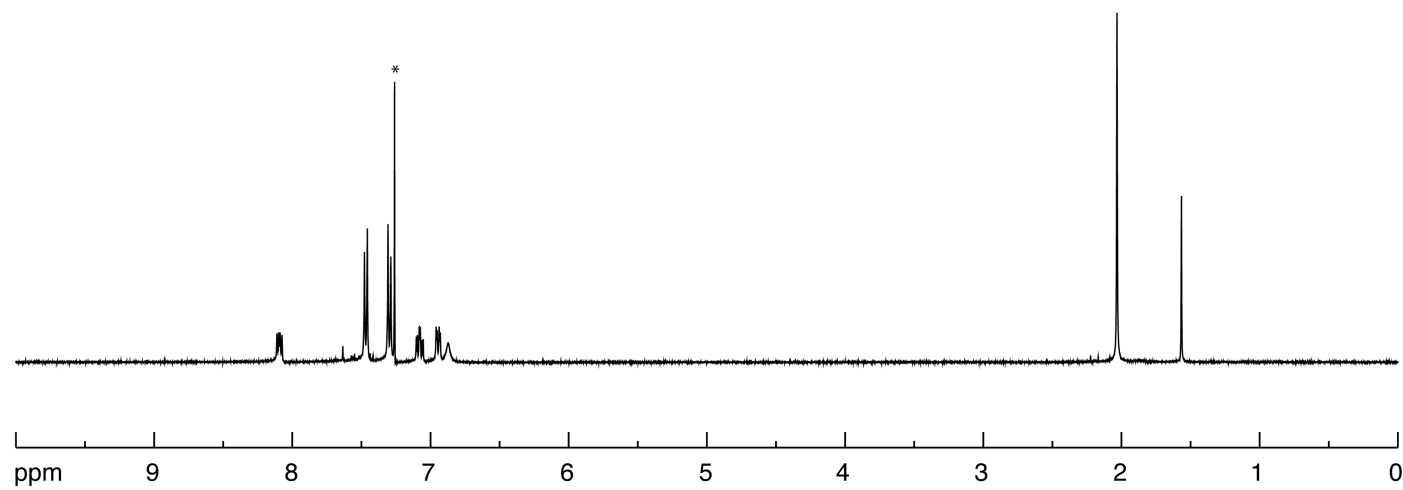
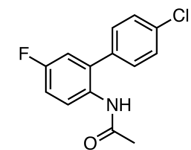


Figure IV-24. ¹H NMR spectrum of compound IV.1u in CDCl₃ (400 MHz) at 23 °C. *CDCl₃ solvent peak.

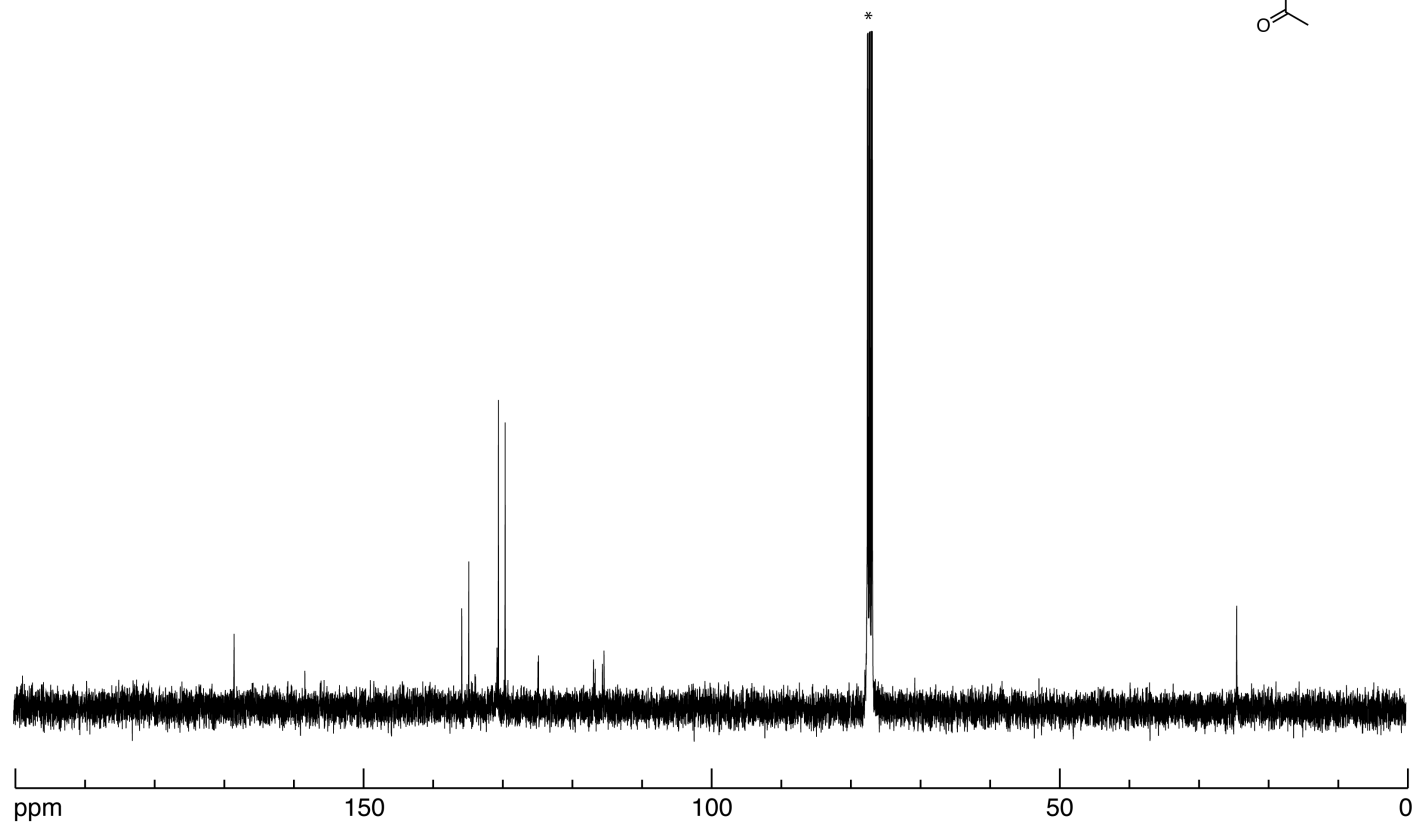
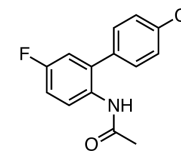


Figure IV-25. ¹³C NMR spectrum of compound IV.1u in CDCl₃ (100 MHz) at 23 °C. *CDCl₃ solvent peak.

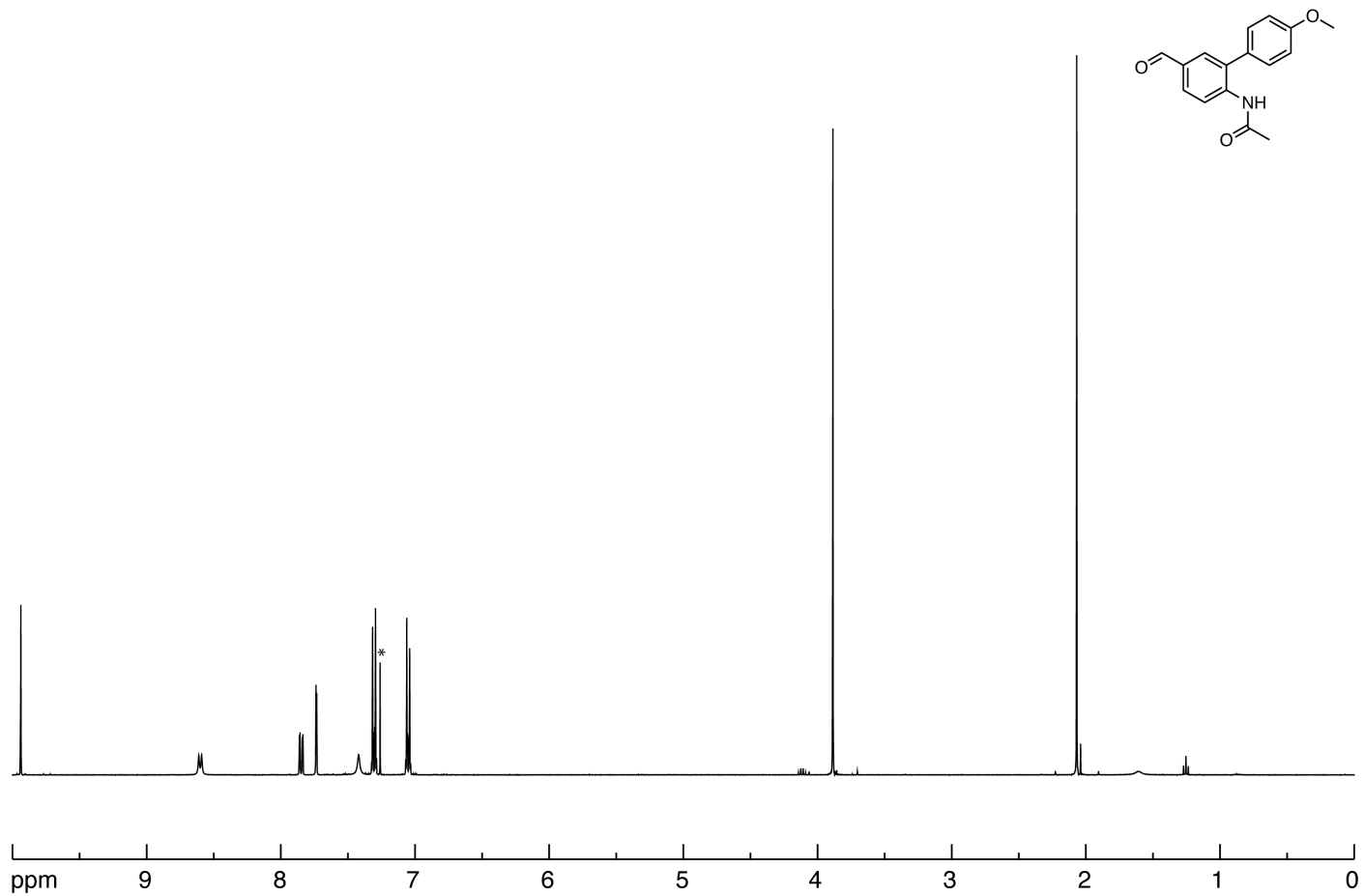


Figure IV-26. ¹H NMR spectrum of compound IV.1v in CDCl₃ (400 MHz) at 23 °C. *CDCl₃ solvent peak.

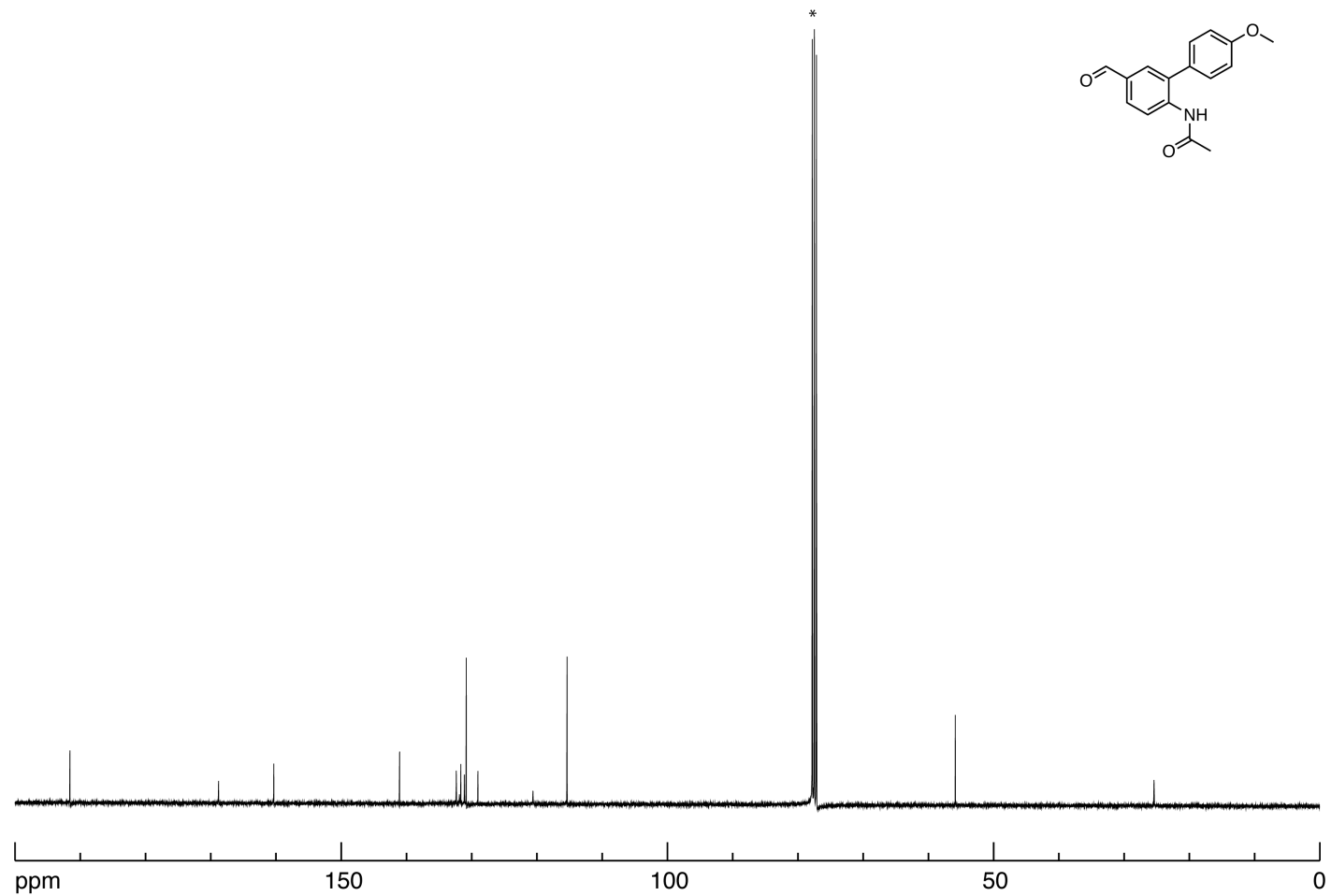


Figure IV-27. ¹³C NMR spectrum of compound IV.1v in CDCl₃ (100 MHz) at 23 °C. *CDCl₃ solvent peak.

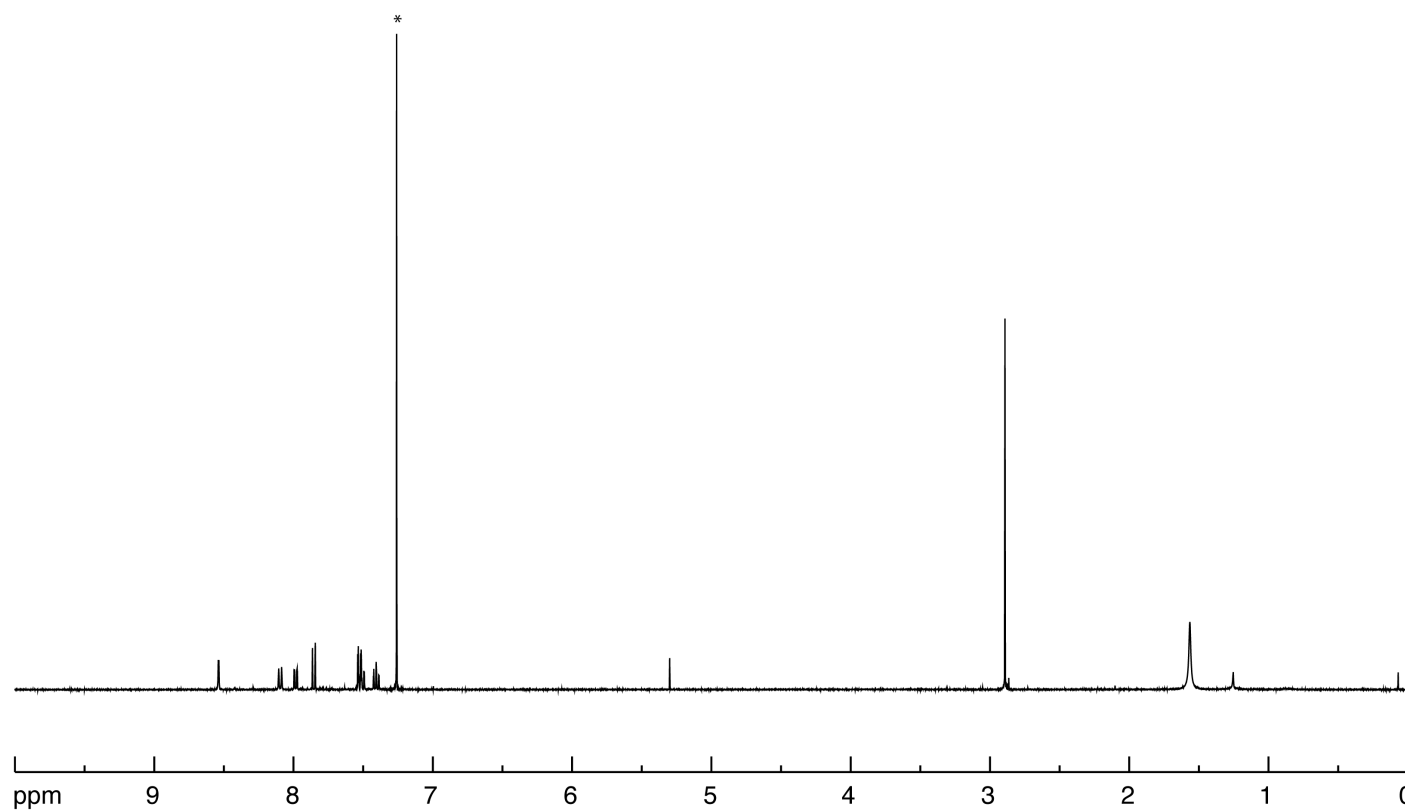
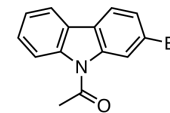


Figure IV-28. ^1H NMR spectrum of compound IV.2e in CDCl_3 (400 MHz) at 23 °C. * CDCl_3 solvent peak.

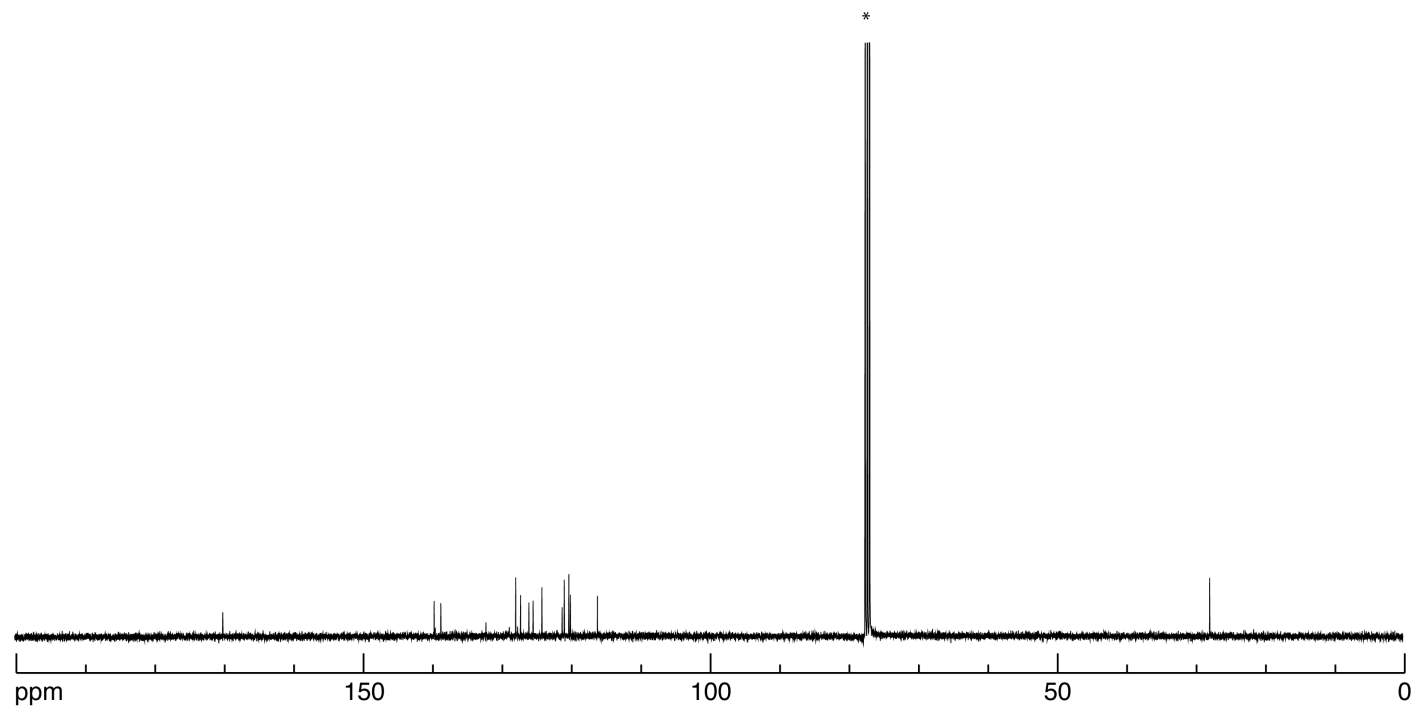
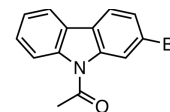


Figure IV-29. ¹³C NMR spectrum of compound IV.2e in CDCl₃ (100 MHz) at 23 °C. *CDCl₃ solvent peak.

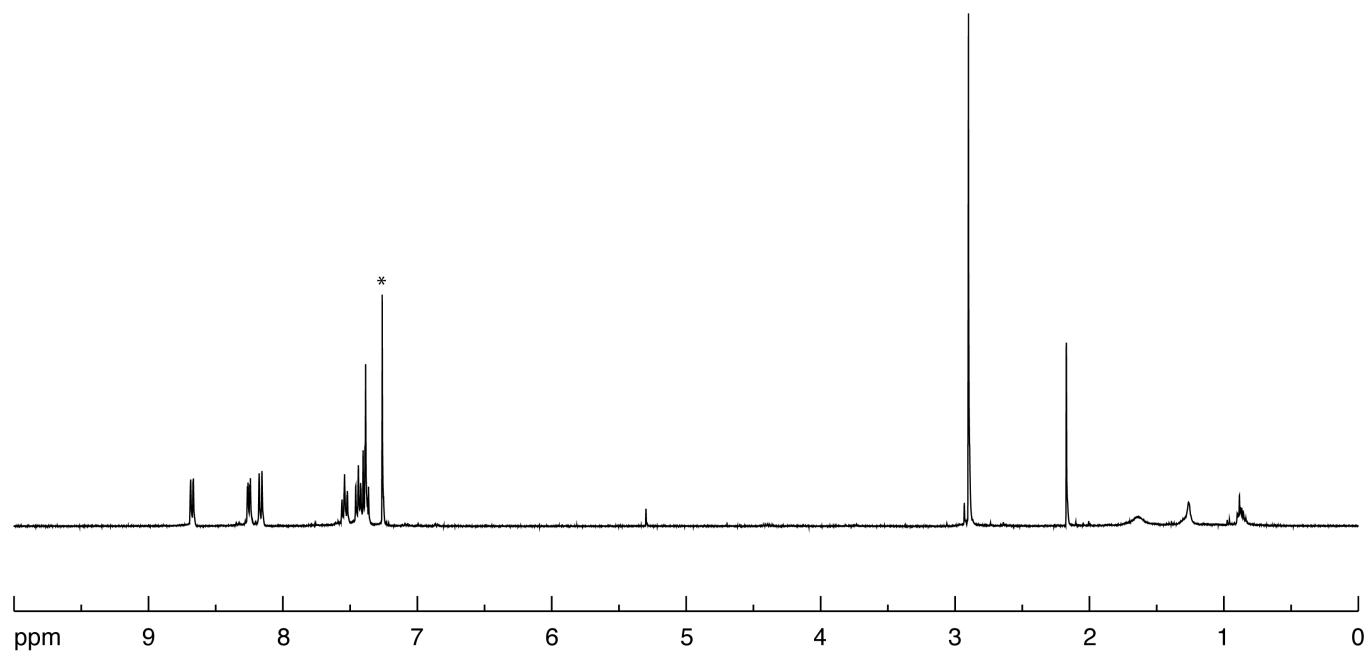
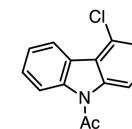


Figure IV-30. ^1H NMR spectrum of compound IV.2q in CDCl_3 (400 MHz) at 23 °C. * CDCl_3 solvent peak.

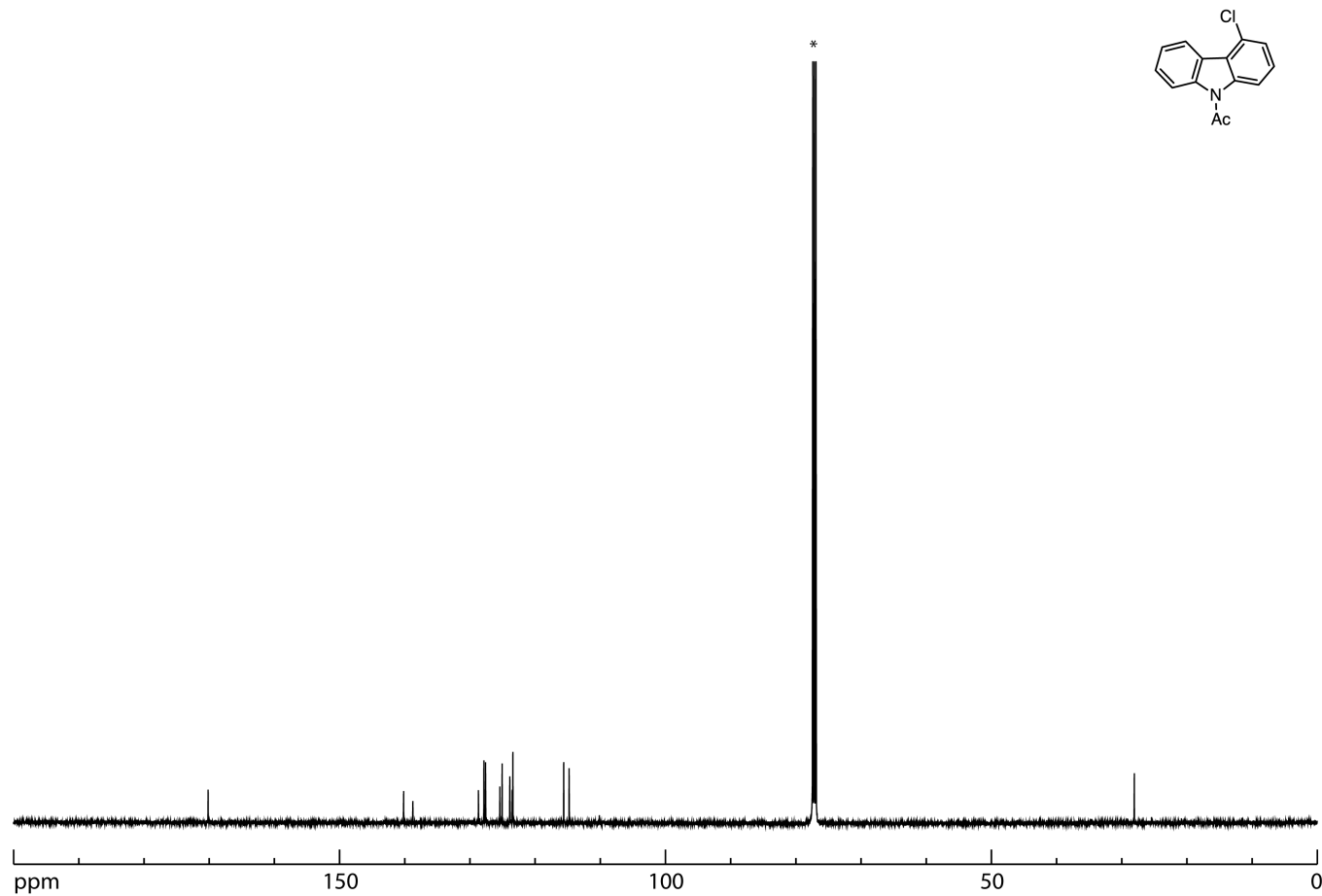


Figure IV-31. ¹³C NMR spectrum of compound IV.2q in CDCl₃ (125 MHz) at 23 °C. *CDCl₃ solvent peak.

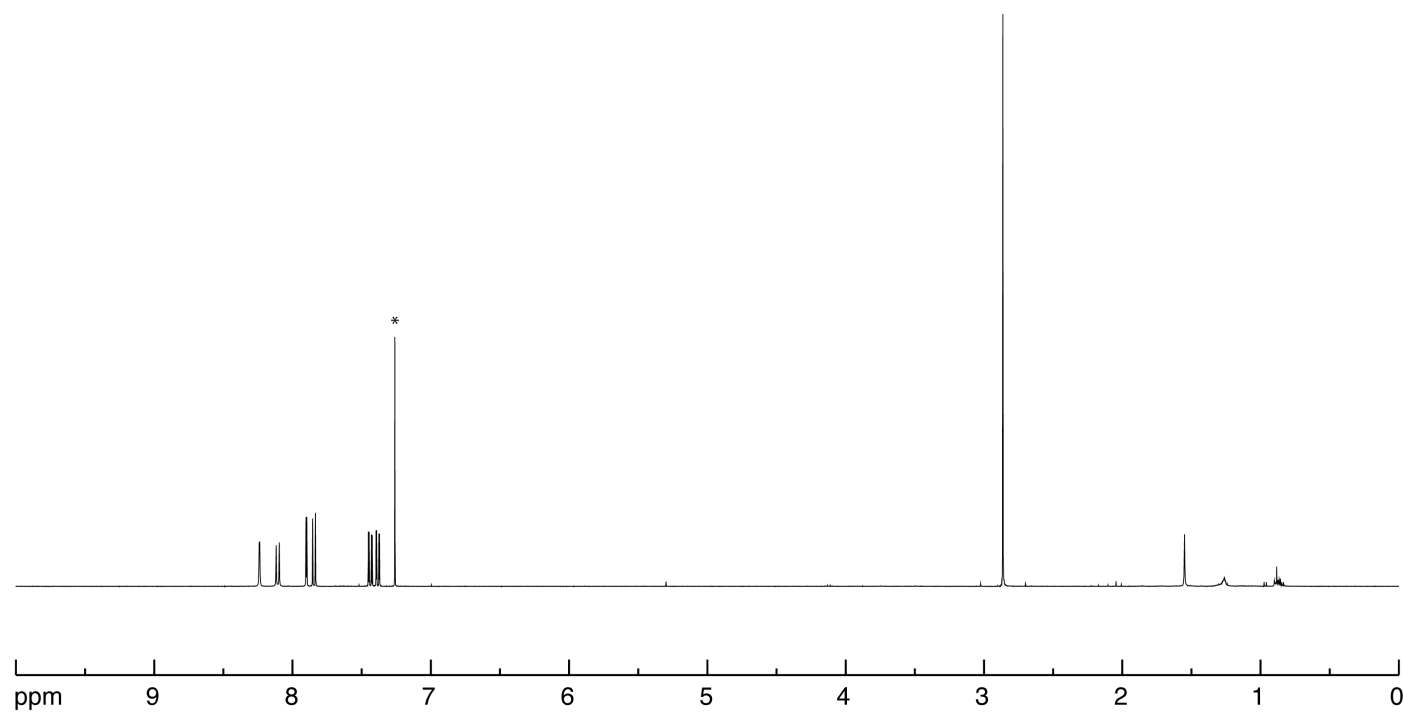
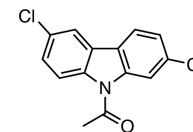


Figure IV-32. ^1H NMR spectrum of compound IV.2t in CDCl_3 (400 MHz) at 23 °C. * CDCl_3 solvent peak.

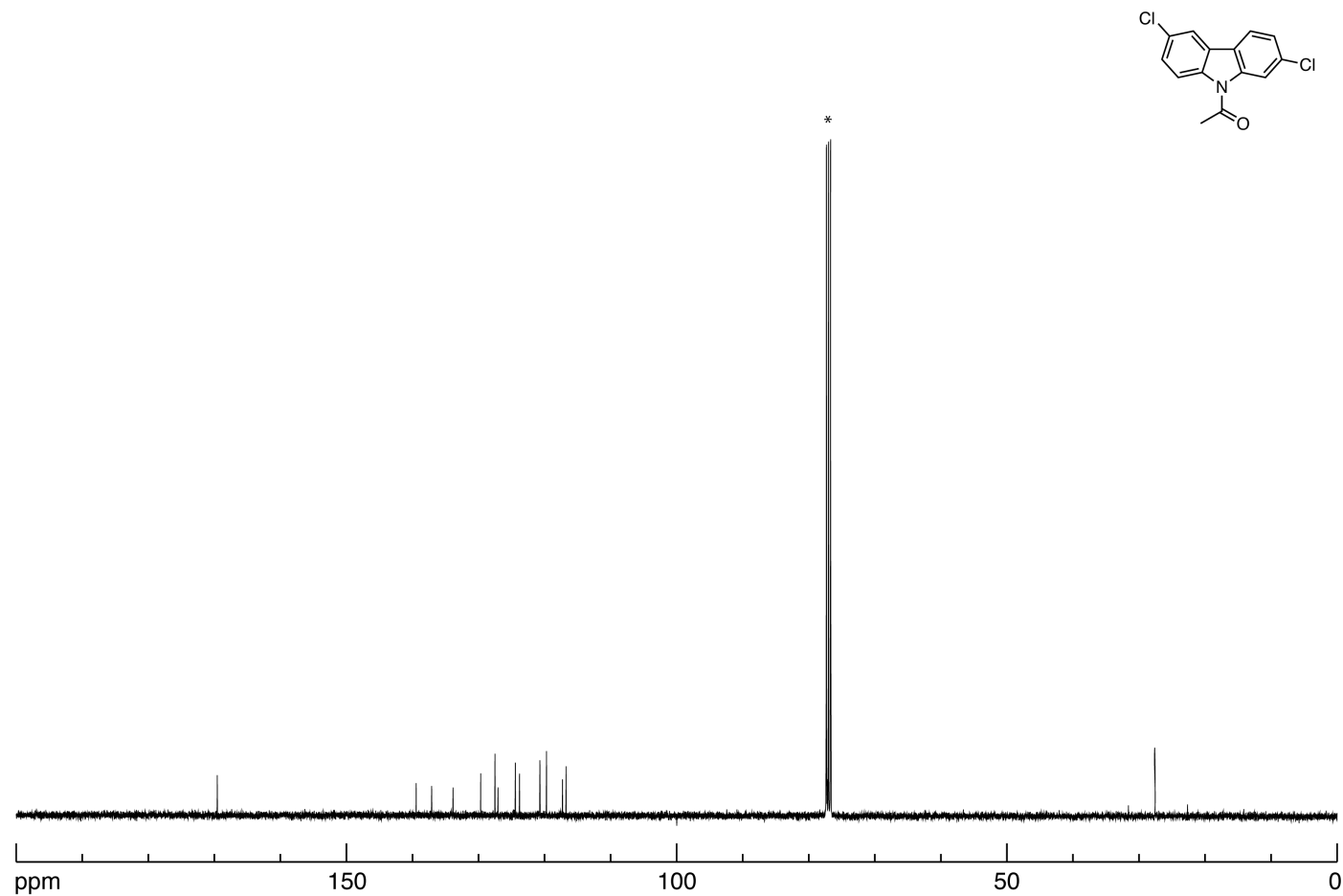


Figure IV-33. ^{13}C NMR spectrum of compound IV.2t in CDCl_3 (100 MHz) at 23 °C. * CDCl_3 solvent peak.

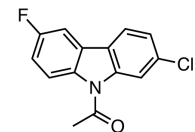
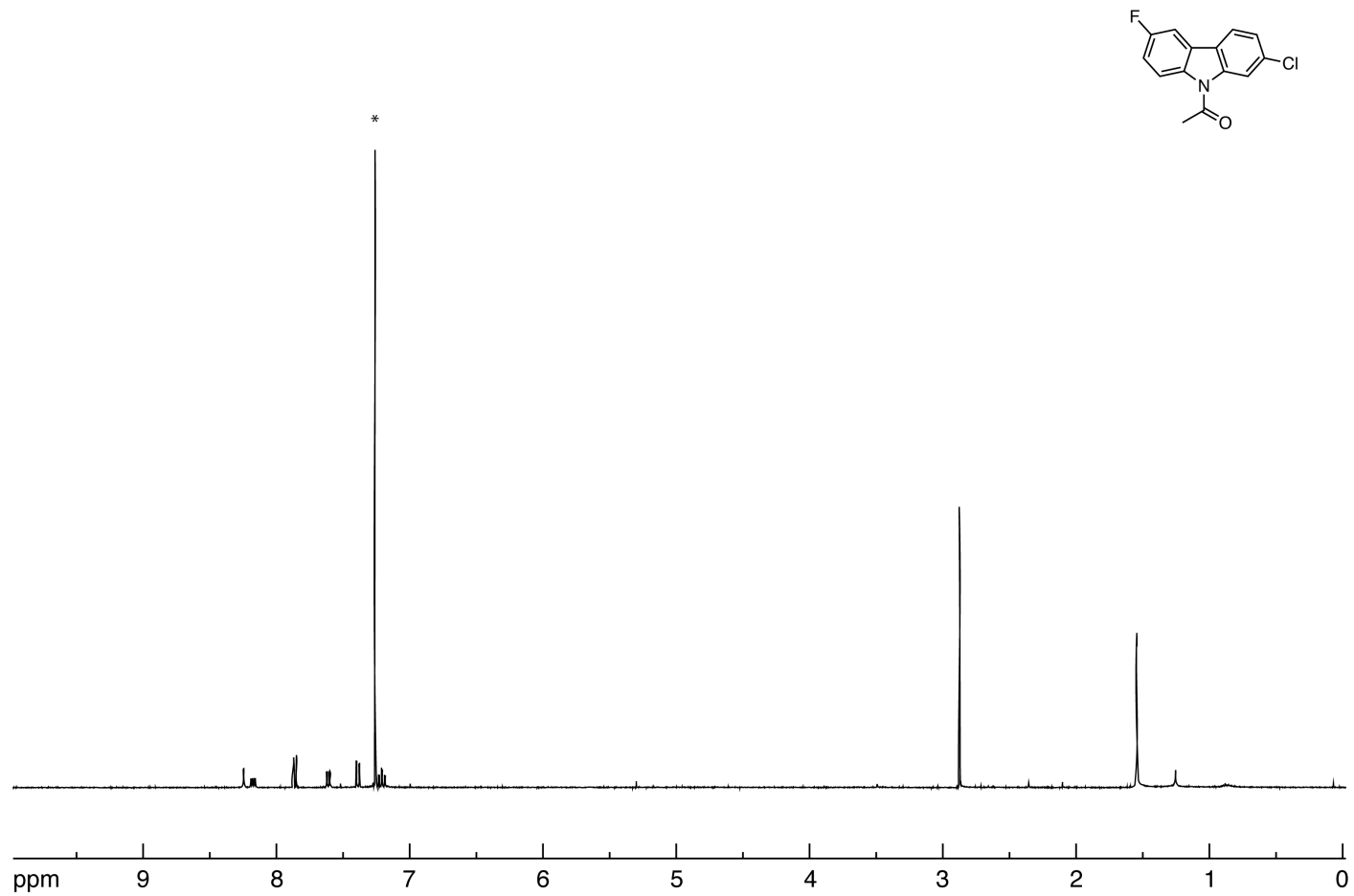


Figure IV-34. ¹H NMR spectrum of compound IV.2u in CDCl₃ (400 MHz) at 23 °C. *CDCl₃ solvent peak.

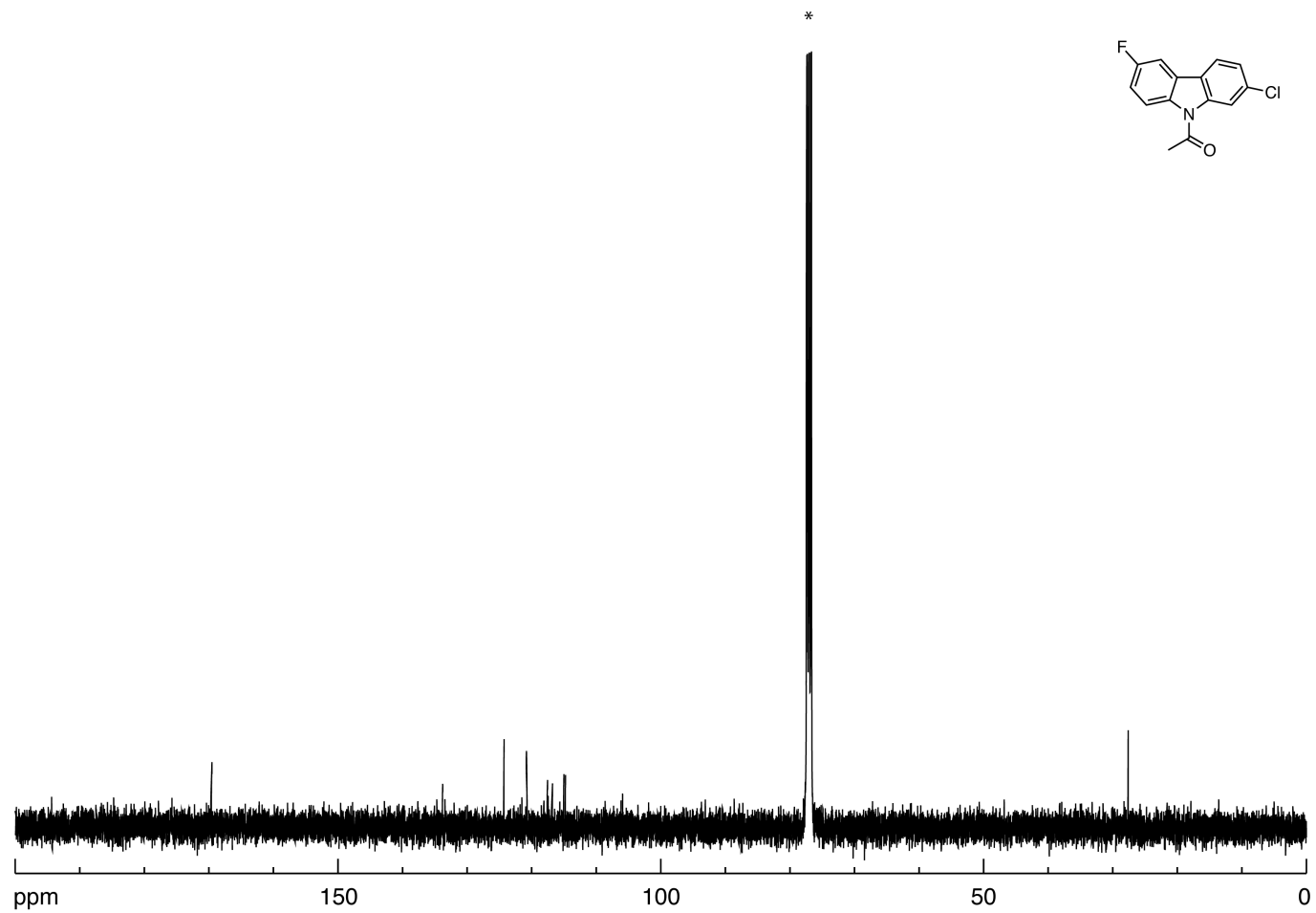


Figure IV-35. ¹³C NMR spectrum of compound IV.2u in CDCl₃ (100 MHz) at 23 °C. *CDCl₃ solvent peak.

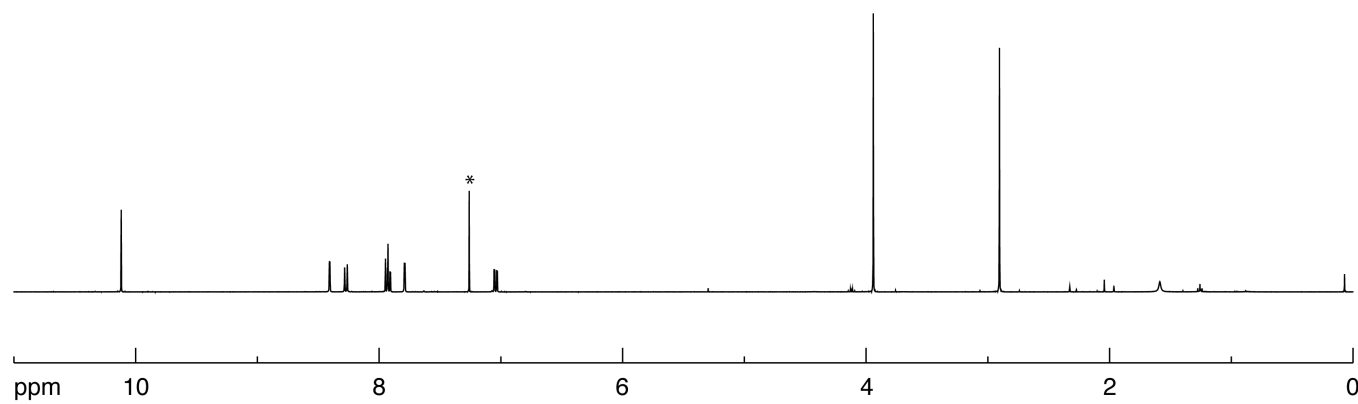
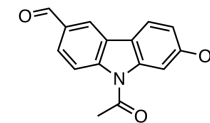


Figure IV-36. ^1H NMR spectrum of compound IV.2v in CDCl_3 (400 MHz) at 23 °C. * CDCl_3 solvent peak.

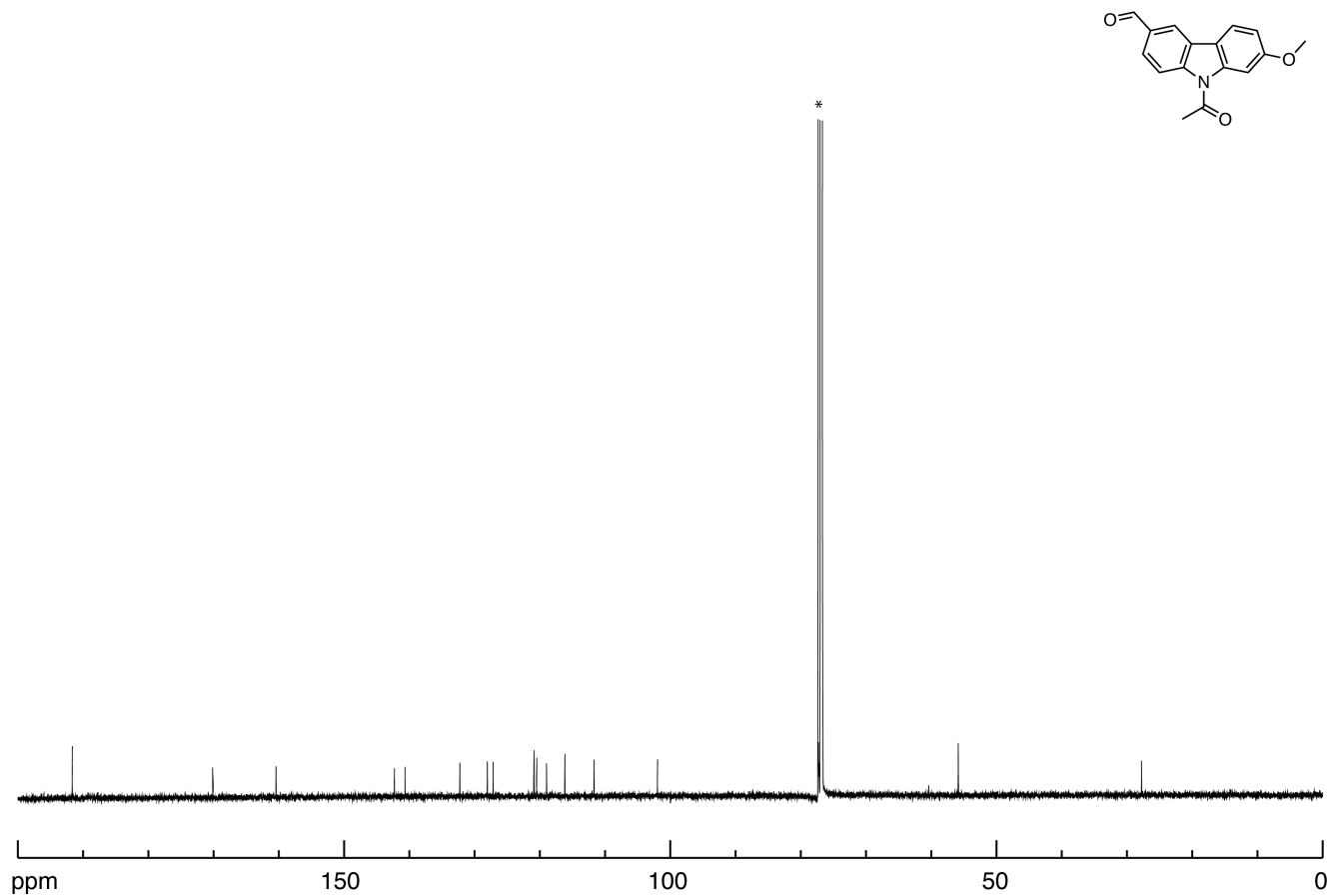


Figure IV-37. ¹³C NMR spectrum of compound IV.2v in CDCl₃ (100 MHz) at 23 °C. *CDCl₃ solvent peak.

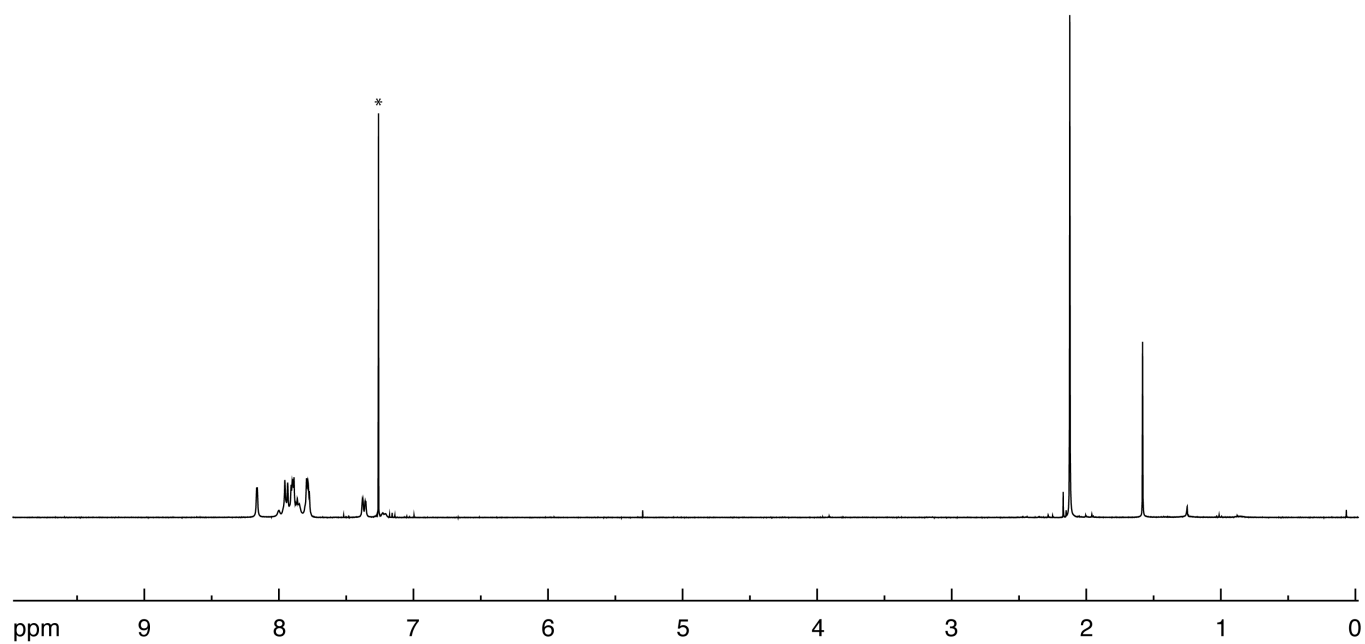
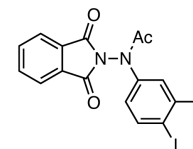


Figure IV-38. ^1H NMR spectrum of compound IV.5f in CDCl_3 (400 MHz) at 23 °C. * CDCl_3 solvent peak.

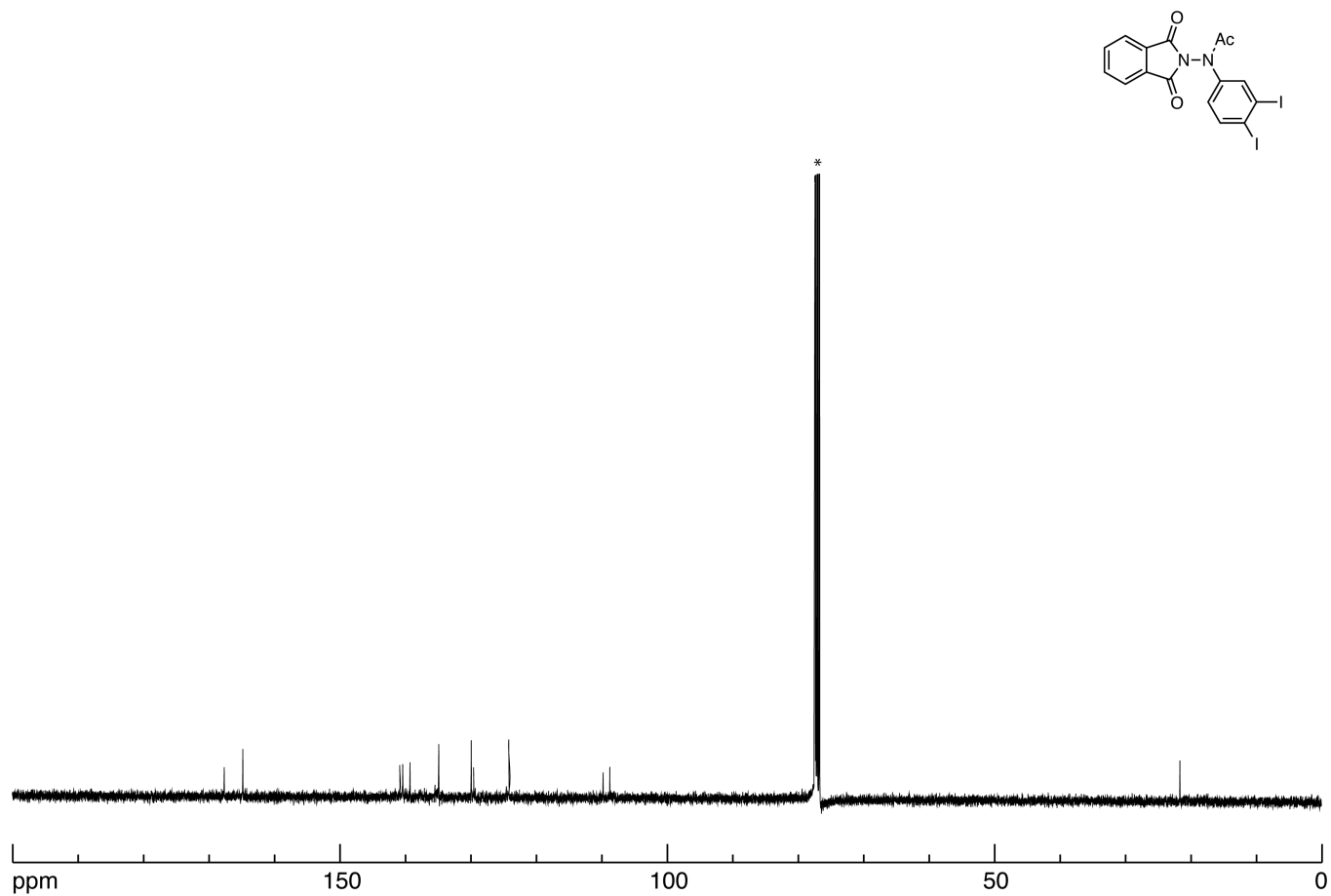


Figure IV-39. ¹³C NMR spectrum of compound IV.5f in CDCl₃ (100 MHz) at 23 °C. *CDCl₃ solvent peak.

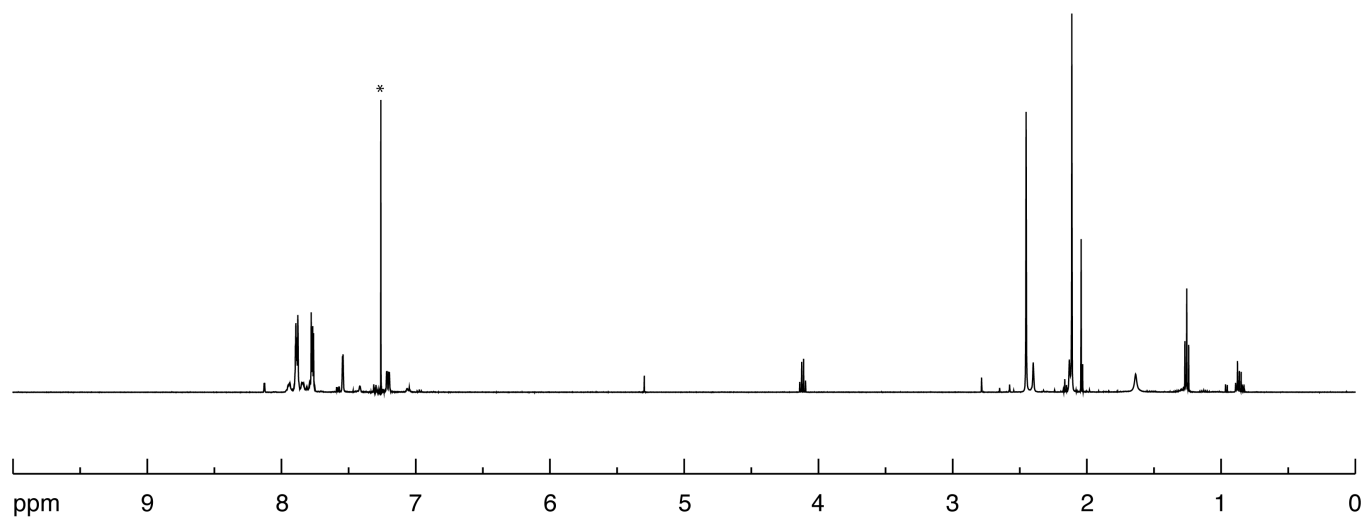
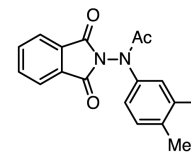


Figure IV-40. ^1H NMR spectrum of compound IV.5g in CDCl_3 (500 MHz) at 23 °C. * CDCl_3 solvent peak.

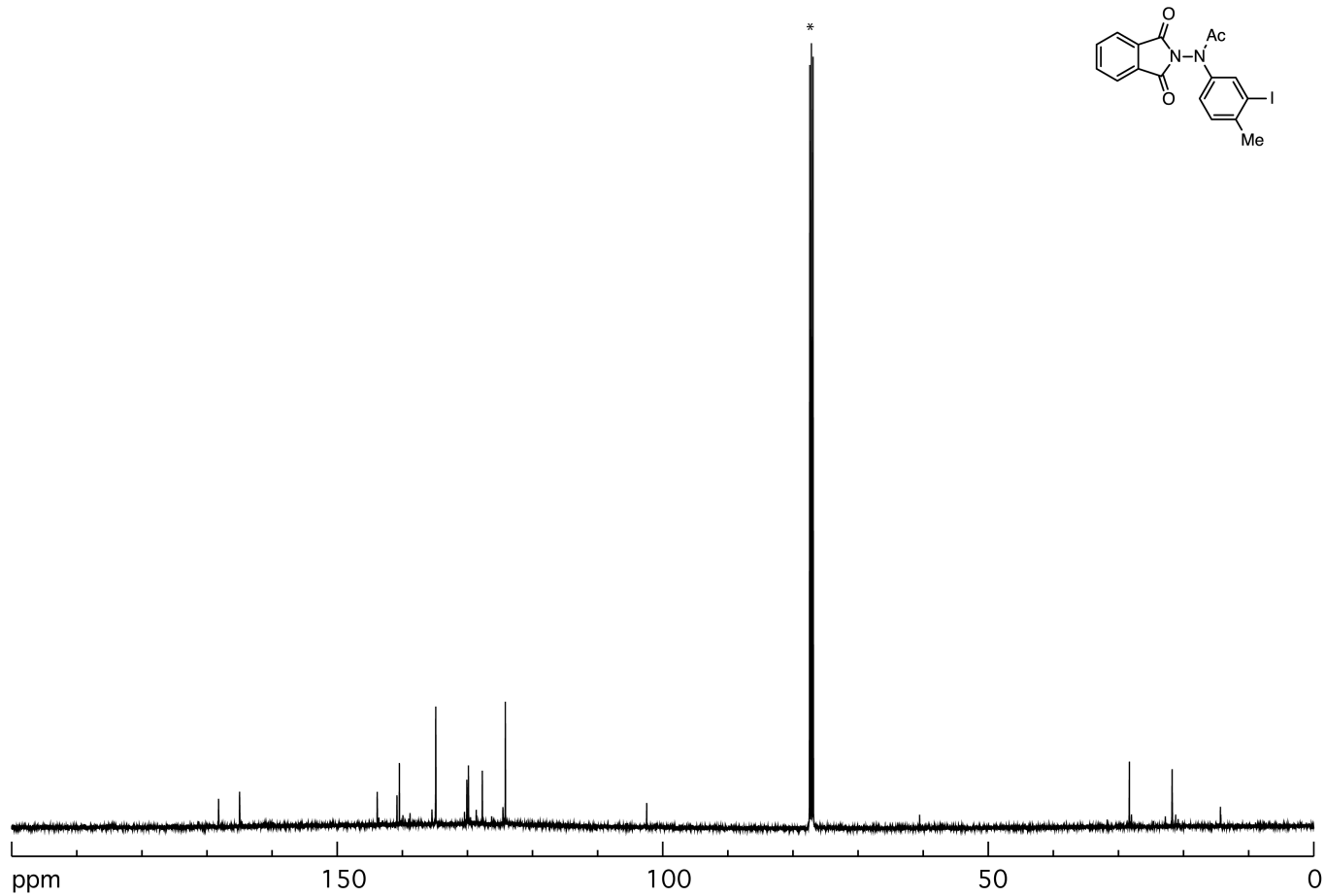


Figure IV-41. ¹³C NMR spectrum of compound IV.5g in CDCl₃ (125 MHz) at 23 °C. *CDCl₃ solvent peak.

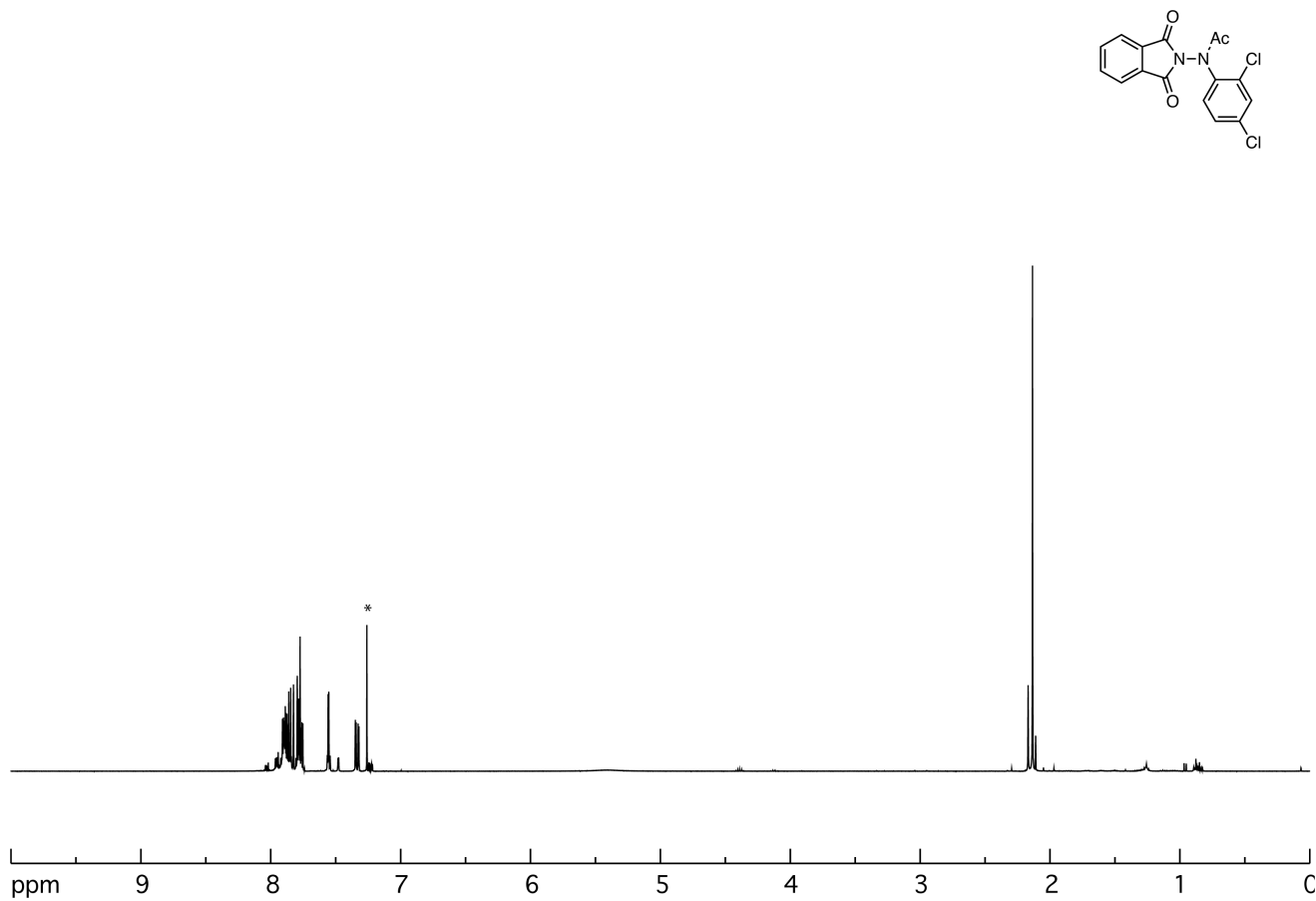


Figure IV-42. ¹H NMR spectrum of compound IV.5h in CDCl₃ (400 MHz) at 23 °C. *CDCl₃ solvent peak.

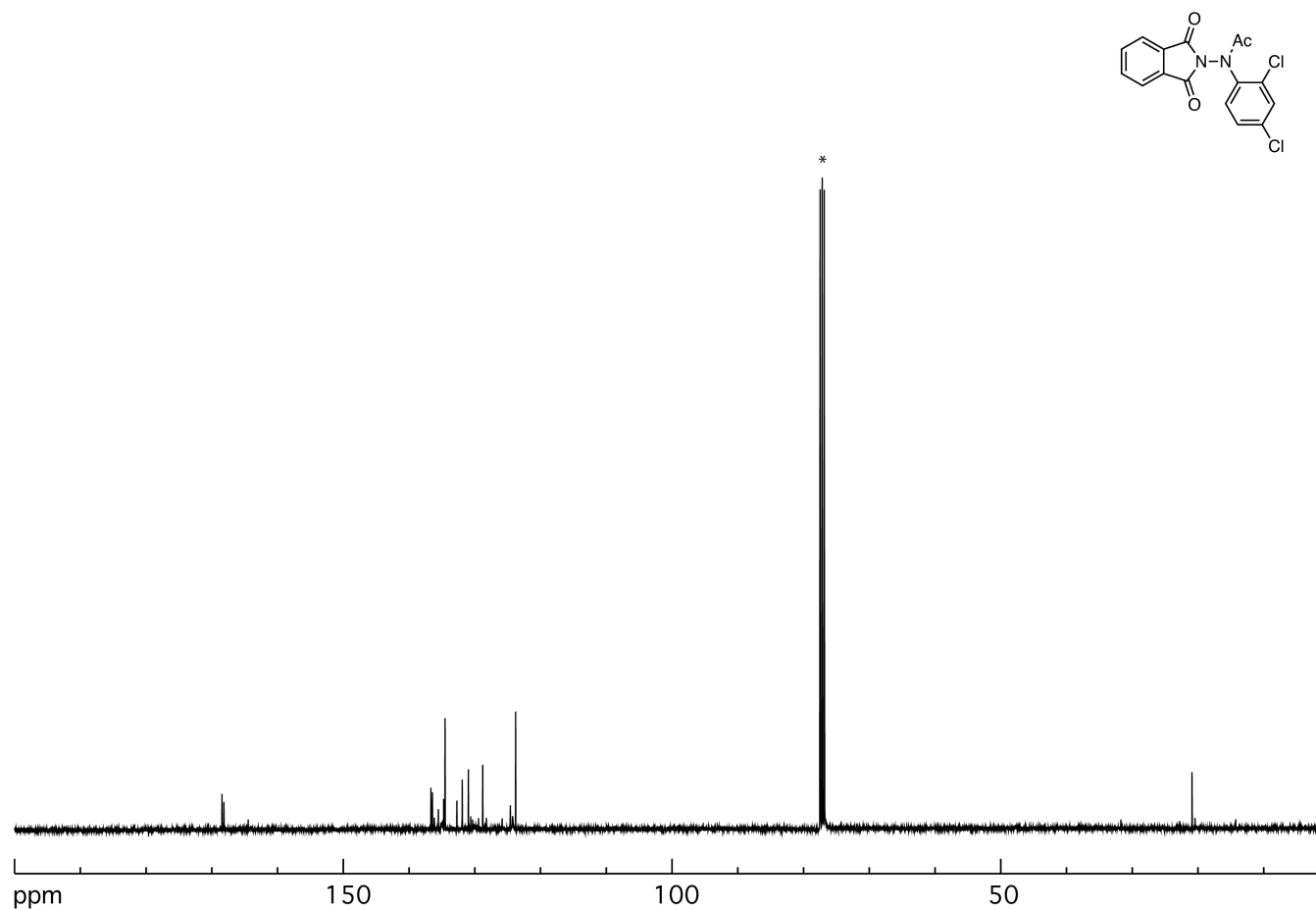


Figure IV-43. ¹³C NMR spectrum of compound IV.5h in CDCl₃ (100 MHz) at 23 °C. *CDCl₃ solvent peak.

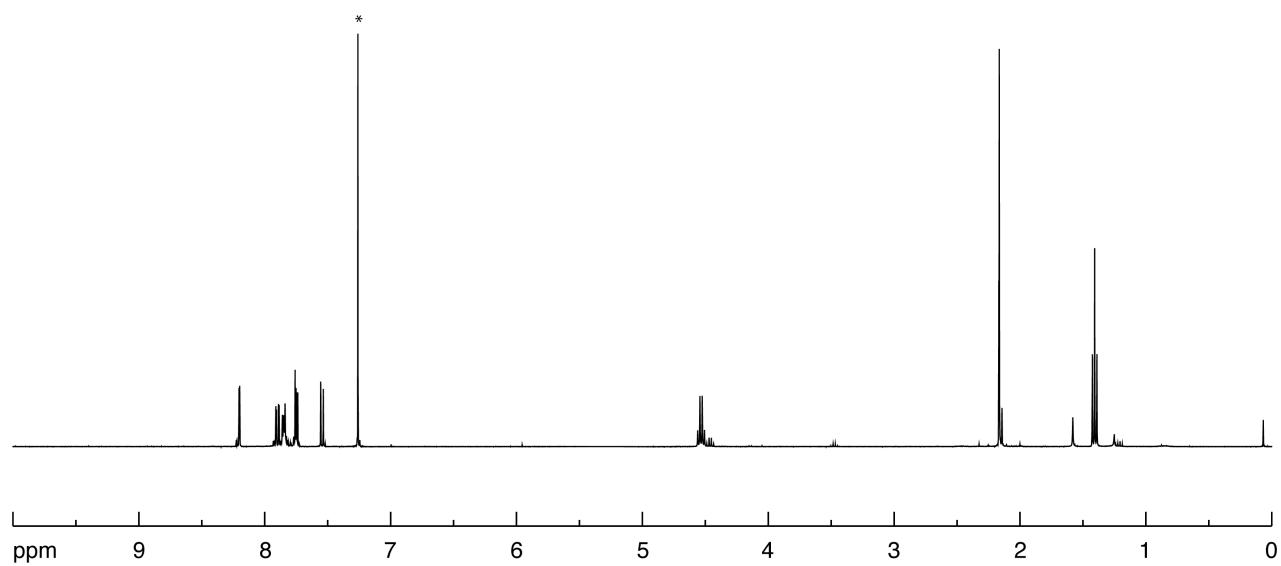
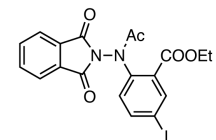


Figure IV-44. ^1H NMR spectrum of compound IV.5i in CDCl_3 (400 MHz) at 23 °C. * CDCl_3 solvent peak.

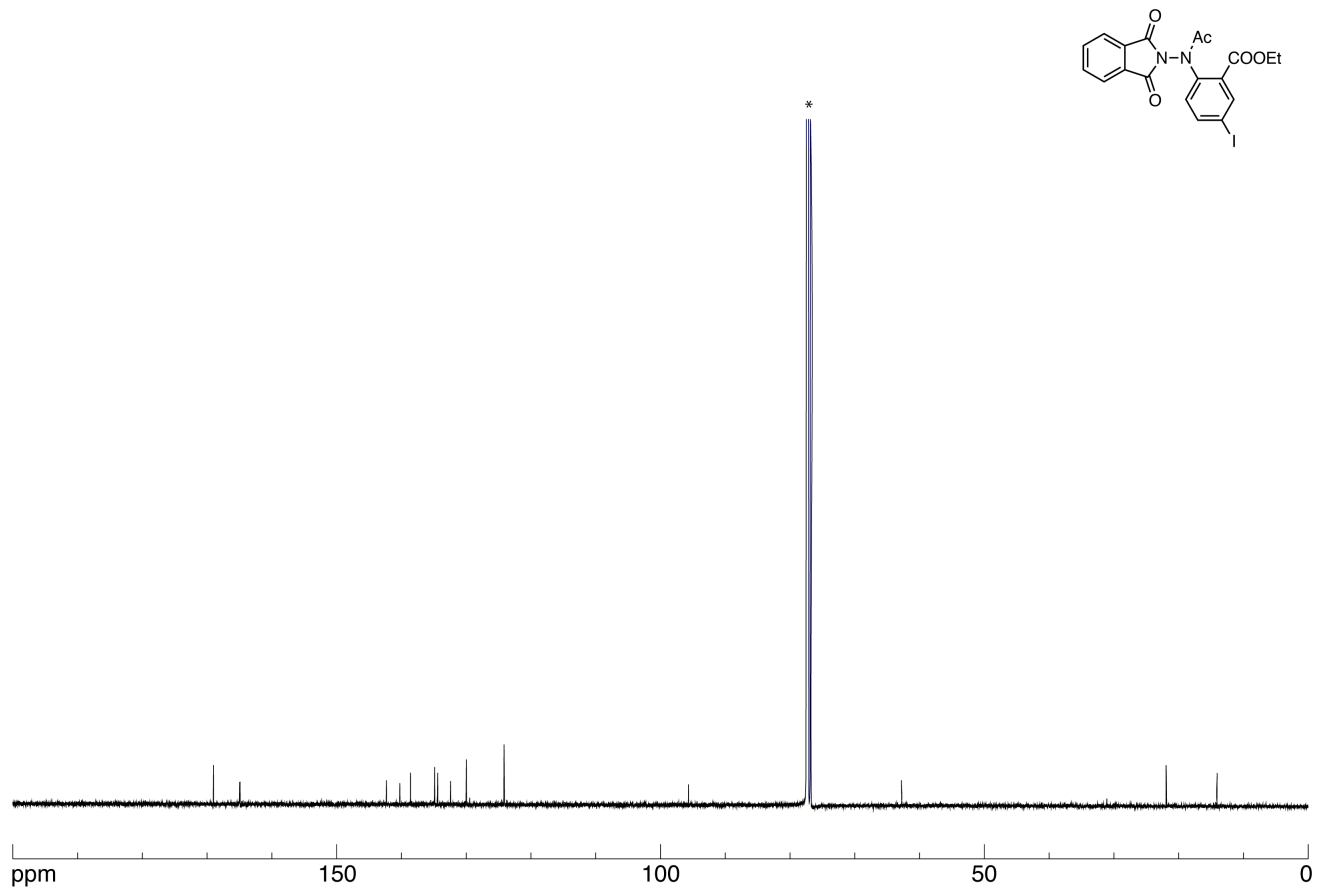


Figure IV-45. ¹³C NMR spectrum of compound IV.5i in CDCl₃ (100 MHz) at 23 °C. *CDCl₃ solvent peak.

CHAPTER V

DIVERSE AMINATION SEQUENCE ENABLED BY BIFUNCTIONAL *N*-AMINOPYRIDINIUM REAGENTS*

V.1 Introduction

The presence of amines and other nitrogen-based functional groups can profoundly impact the chemical and biological properties of organic small molecules and thus C–N bonds are ubiquitous in pharmacologically active organic scaffolds.³⁶⁸⁻³⁷¹ In both biology and synthetic chemistry, installation of C–N bonds typically requires substrate pre-oxidation, which inherently limits the efficiency and versatility of synthetic approaches to these important molecules.³⁷² A variety of C–H amination methods, based on either nitrene or nitrogen-centered radical intermediates, have been advanced to install *N*-containing functional groups without the need for substrate prefunctionalization (Figure V-1a).³⁷³⁻³⁸¹ In practice, electron-withdrawing groups, such as *N*-sulfonyl substituents, are typically required to activate aminating reagents for C–H functionalization and methods to elaborate the resulting sulfonamides to more complex nitrogen-containing molecules are limited.³⁸²⁻

389

* Data, figures, and text in this chapter were adapted with permission from reference Rowchudhury, P.; Maity, A.; Powers, D. C. Bifunctional *N*-Aminopyridinium Reagents Enable C–H Amination, Olefin Carboamination Cascades. *ChemRxiv* **2021**, 10.26434/chemrxiv.14677533.v1.

We recently introduced *N*-aminopyridinium salts as bifunctional reagents in C–H amination chemistry.³⁹⁰ The combination of a nucleophilic *N*-amino group and a reductively activatable N–N bond provided a platform to couple C–H amination with C–N cross coupling to achieve formal nitrene transfer to benzylic C–H bonds.³⁹¹ Here, we demonstrate that reductive activation of the same N–N bonds allows derivatization of the products of C–H amination via electrophilic *N*-centered radicals (Figure V-1b).³⁹²⁻⁴⁰² We highlight the amination/derivatization sequence in (1) the synthesis of tetrahydroisoquinolines, an important heterocycle in medicinal chemistry, which can be challenging to prepare by existing methods,⁴⁰³⁻⁴¹² and (2) the synthesis of α -aminoketones via formal aza-Rubottom chemistry.⁴¹³ These protocols enable conversion of benzylic C–H bonds to an array of nitrogen-containing products and significantly expand the utility of *N*-aminopyridiniums as lynchpins of molecular synthesis.

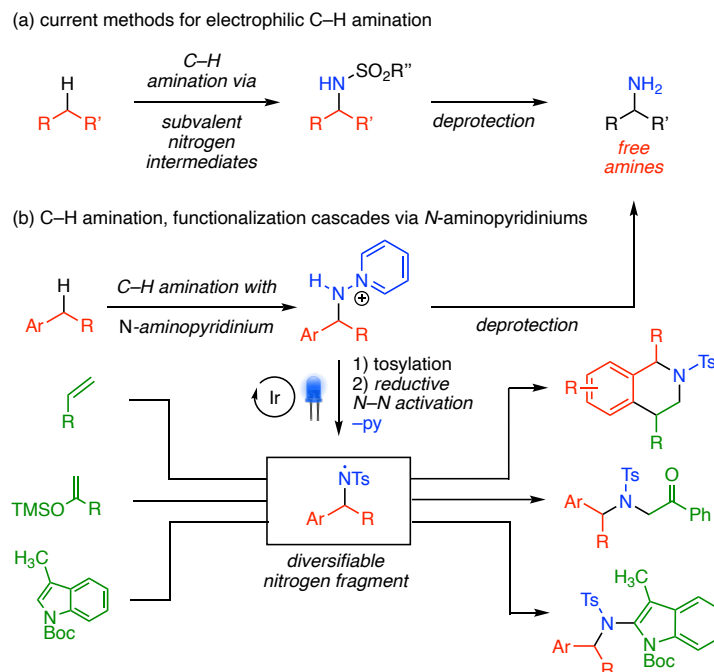


Figure V-1. Representative C–H amination methods. (a) Direct C–H amination via nitrene transfer or radical-mediated processes typically requires activation of the amine fragment with electron withdrawing substituents, which can be removed to ultimately generate free amines. (b) Here, we demonstrate C–H amination with *N*-aminopyridinium which provides the opportunity to diversify the products of C–H amination via amidyl radicals generated by reductive N–N cleavage.

V.2 Results and Discussion

During our initial studies of C–H aminopyridylation, we developed conditions that promoted selective benzylic C–H functionalization of a variety of ethyl and alkylbenzene derivatives. We envisioned that oxidative quenching of the excited state of an appropriate photoredox mediator would promote reductive cleavage of the N–N bond of these compounds to release pyridine and unveil an electrophilic aminyl radical. The generated aminyl radical could be engaged with exogenous substrate, such as an olefin, with the potential for additional C–C bond formation through cyclization in the presence of pendant

phenyl moiety (*vide infra*). Initial attempts to photolyze a solution of **V.1a** in the presence of aryl olefins and a variety of photoredox mediators were unsuccessful. We observed complete recovery of starting materials with no desired N–N cleavage (Figure V-2).

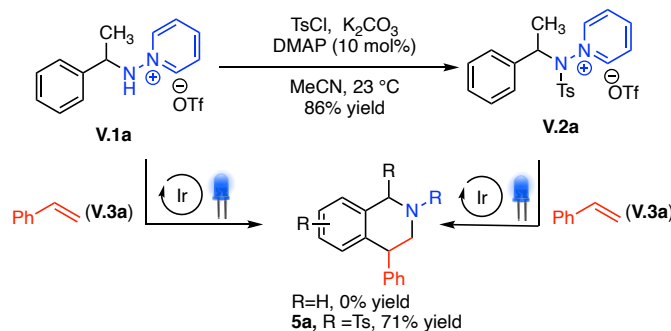


Figure V-2. Photocatalytic derivatization of benzyl *N*-aminopyridiniums. Functionalization of *N*-benzylpyridinium in presence of styrene afforded corresponding carboamination product in case of tosyl protected *N*-aminopyridinium derivative; presumably due to stabilization of incipient *N*-centered radical via tosyl group. Conditions: $[\text{Ir}(\text{ppy})_2(\text{dtbbpy})][\text{PF}_6]$ (**V.4**, 1 mol%), blue LED, CH_2Cl_2 , 0 °C

We reasoned that the inability to achieve N–N cleavage may arise from the instability of the aminyl radicals that would result from reductive extrusion of pyridine and hypothesized that the installation of a sulfonyl group would stabilize the incipient *N*-centered radical (Figure V-2). Tosylation of **V.1a** by treatment with TsCl , K_2CO_3 , and DMAP (10 mol%) afforded sulfonamide **V.2a**. Photolysis ($\lambda = 463 \text{ nm}$) of sulfonamide **V.2a** with $[\text{Ir}(\text{ppy})_2(\text{dtbbpy})][\text{PF}_6]$ (**V.4**, 1 mol%) in the presence of styrene (**V.3a**) resulted in the evolution of tetrahydroisoquinoline **V.5a** in 71% yield (1.4:1 ratio of *cis:trans* diastereomers). Tetrahydroisoquinoline **V.5a** represents the product of anti-Markovnikov carbonamination of styrene. Control reactions in the absence of light and/or photocatalyst did not yield any deaminative product. For details of the carboamination optimization,

including the impact of solvent, photocatalyst, reaction stoichiometry, and reaction temperature, see the Experimental Details section for additional data.

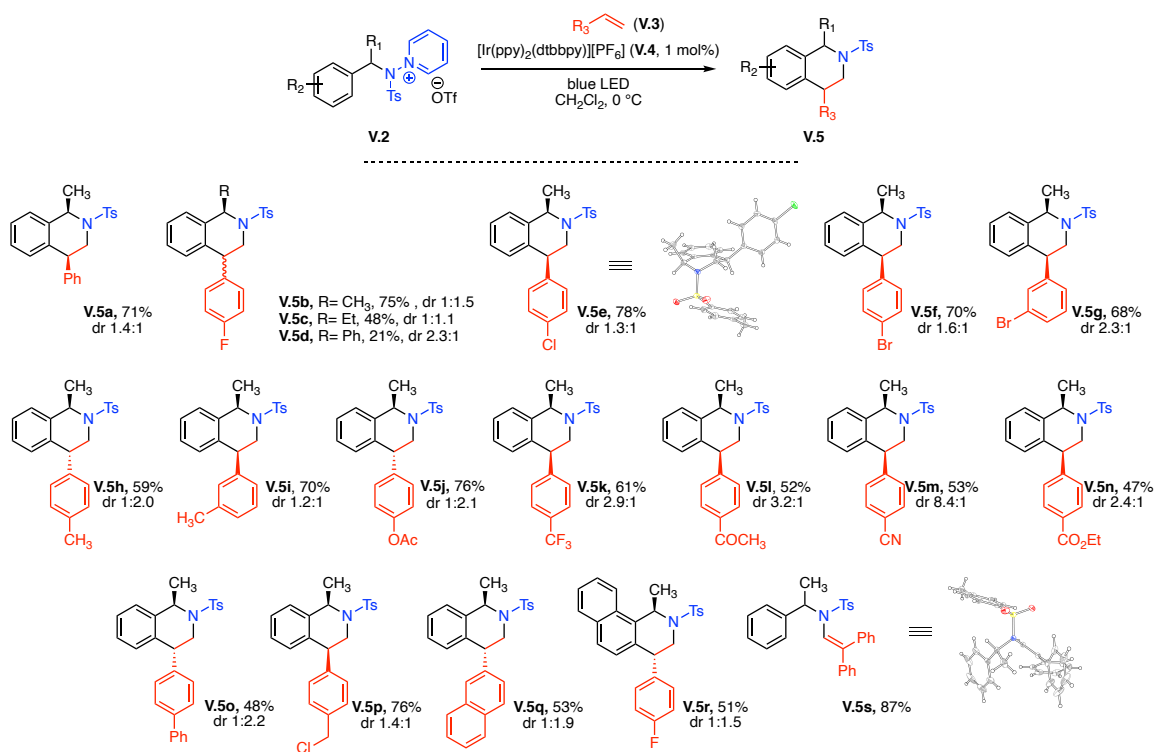


Figure V-3. Photocatalytic carboamination promoted by deaminative functionalization of V.2 in presence of olefins provides access to a family of 1,4-disubstituted tetrahydroisoquinolines V.5. Conditions: **V.2** (1.0 equiv), **V.3** (1.6 equiv), CH_2Cl_2 , 0 °C, 16 h.

The developed carboamination chemistry tolerates both substitutions of the aminopyridinium and styrene reaction partners. Reaction of 4-fluorostyrene with differently substituted aminopyridinium salts resulted in the formation of tetrahydroisoquinolines **V.5b-d**. Reaction of differently substituted halostyrenes with **V.2a** affords the corresponding tetrahydroisoquinolines (**V.5e-g**) as diastereomeric mixtures in 68-78% yield. The relative stereochemistry of the tetrahydroisoquinoline products was

assigned based on single-crystal X-ray diffraction analysis of chlorinated tetrahydroisoquinoline **V.5e** (for crystallographic details, see Experimental Details section for additional data). Electron-donating substituents such as 4- and 3-methylstyrenes afforded tetrahydroisoquinolines **V.5h** and **V.5i** with *trans*- and *cis*-diastereomers being major products, respectively. Deaminative carboamination of 4-acetoxystyrene provided tetrahydroisoquinoline **V.5j** in 76% yield with the *trans* diastereomer being major product. Tetrahydroisoquinolines **V.5k-n**, derived from electron-deficient styrenes, were accessed in 47-61% yield with *cis* diastereoselectivity. Reaction with weakly withdrawing 4-vinyl-1,1'-biphenyl afforded tetrahydroisoquinoline **V.5o** in 48% yield with a mixture of 1:2.2 *cis*: *trans* diastereoisomers. Deaminative carboamination of 4-(chloromethyl)styrene yielded **V.5p** in 76% yield with *cis* isomer as the major product. It should be noted that no significant side-reaction via hydrogen atom abstraction (HAA) at the benzylic position of 4-(chloromethyl)styrene was observed. Bulky olefinic substrate such as 2-vinylnaphthalene yielded **V.5q** in 53% yield with *trans* isomer as the major component. The reaction is also tolerant to substitution on the *N*-benzylaminopyridinium coupling partners. For example, coupling of **V.2d**, the *N*-benzylaminopyridinium derived from 1-ethylnaphthalene, with 4-fluorostyrene yielded the corresponding benzo-fused tetrahydroisoquinoline **V.5r** in 51% yield with a mixture of 1:1.5 *cis*: *trans* diastereomers.

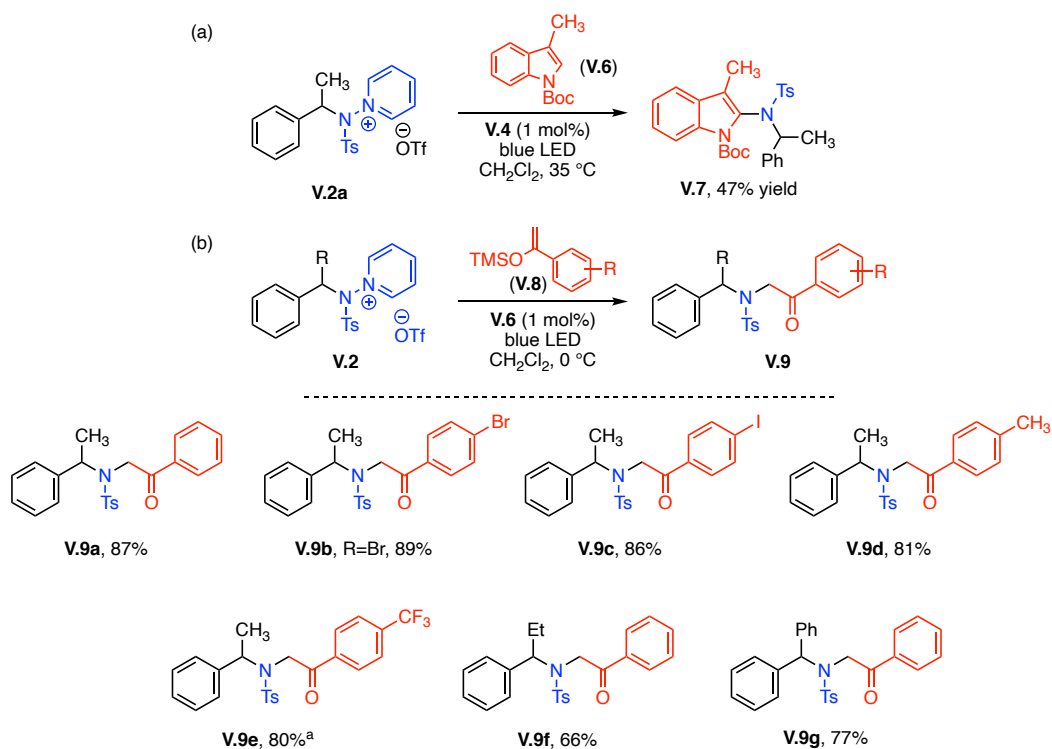


Figure V-4. Functionalization of *N*-benzylpyridinium **V.2 with (a) nucleophilic heterocycle **V.6** and (b) silyl enol ethers **V.8**. conditions for (a): **V.2a** (1.0 equiv), **V.6** (3.0 equiv), CH₂Cl₂, 35 °C, 16 h. conditions for (b): **V.2** (1.0 equiv), **V.8** (2.0 equiv), CH₂Cl₂, 0 °C, 16 h. ^a4 equivalents of **V.8e** were used; with 2 equivalents the yield of **V.9e** was 61%.**

In addition to olefinic substrates, the electrophilic radicals generated by reductive activation of the N–N bonds in *N*-benzylaminopyridiniums engage in amination reactions with nucleophilic heterocycles, such as *N*-Boc-indole **V.6** to afford 2-aminated indole **V.7** in 47% yield (Figure V-4a), and silyl enol ethers (**V.8**) to afford α -amino carbonyls **V.9** (Figure V-4b). The amination of silyl enol ethers via *N*-aminopyridiniums,⁴¹⁴ which represents a formal aza-Rubottom reaction, tolerates both substitution of the nucleophilic partner **V.8** (*i.e.*, preparation of **V.9a–e**) as well as variation of the benzylic substituents on the *N*-benzylpyridinium partner **V.2** (*i.e.*, preparation of **V.9f** and **V.9g**).

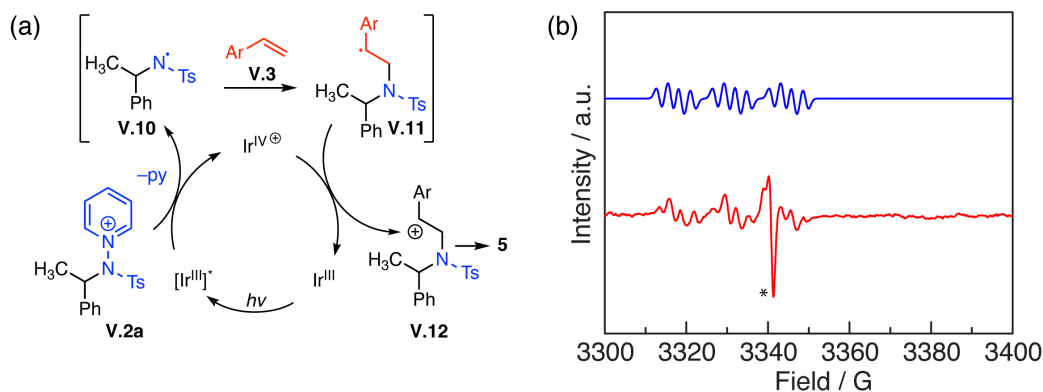


Figure V-5. Proposed mechanism for carboamination reaction.(a) Potential carboamination catalytic cycle. Electron transfer from the excited state of $[\text{Ir}(\text{ppy})_2(\text{dtbbpy})][\text{PF}_6]$ to **V.2a** results in reductive N–N cleavage to unveil amidyl radical **V.10** and Ir(IV). Addition to olefin **V.3** generates benzylic radical **V.11**. Oxidation by Ir(IV) generates a benzylic cation **V.12**, which alkylates the pendent arene to afford tetrahydroisolinolines **V.5**. (b) EPR spectra for photochemical deaminative functionalization of **V.2a** in presence of PBN was obtained in acetonitrile. The observed triplet of quartet in the photolyzed spectrum is attributed to PBN-trapped amidyl radical with $a_{\text{N}(\text{PBN})} = 13.85$ G, $a_{\text{H}} = 3.20$ G, and $a_{\text{N}(\text{amidyl})} = 2.52$ G; (—) without photolysis, (—) experimental spectrum with blue light irradiation, and (—) simulated spectrum.

Reductive functionalization of *N*-benzylaminopyridiniums (**V.2**) can be envisioned as arising from the mechanism illustrated in Figure V-5a (illustrated for olefin carboamination to generate tetrahydroisoquinolines).⁴¹⁵ Electron transfer from an excited state of the Ir photocatalyst to **V.2** results in N–N cleavage to an amidyl radical (**V.10**), pyridine, and an Ir(IV) intermediate. Reaction of the generated amidyl radical **V.10** with olefin **V.3** generates benzylic radical **V.11**. Oxidation of **V.11** by Ir(IV) would afford cationic intermediate **V.12** and regenerate the photocatalyst. Electrophilic addition to the arene to the cation in **V.12** furnishes tetrahydroisoquinoline **V.5**. In support of this scheme, addition of *N*-tert-butyl- α -phenylnitron (PBN) to the carboamination of **V.2a** resulted in observation of the PBN adduct of amidyl radical **V.10** by both X-band EPR spectroscopy and high-resolution APCI-MS (Figure V-5b).⁴¹⁶ In addition, deaminative functionalization

of **V.2a** in the presence of 1,1-diphenylethylene yielded the corresponding olefinic product **V.5s** in 87% yield as opposed to the expected tetrahydroisoquinoline (Figure V-3), which is presumably due to elimination from stabilized carbocation **V.12s** in preference to arene alkylation to generate the corresponding tetrahydroisoquinoline.

V.3 Conclusions

In summary, here we described utilization of benzyl C–H aminopyridylation products in olefin carboamination and formal aza-Rubottom oxidation of silyl enol ethers. The nucleophilicity of *N*-aminopyridinium allows these reagents to engage in C–H amination chemistry, and reductive N–N cleavage unveils electrophilic amidyl radical intermediates as diversifiable nitrogen synthons. The realization of C–H functionalization chemistry with *N*-aminopyridinium reagents both significantly expands the structural complexity that is available to this burgeoning class of bifunctional reagents and significantly expands the synthetic utility products accessible via C–H amination.

V.4 Experimental Details

V.4.1 General Considerations

Materials All chemicals and solvents were obtained as ACS reagent grade and used as received. Styrene was acquired from BeanTown Chemical (BTC). Diphenylmethane, 4-(dimethylamino)pyridine (DMAP), 4-chlorostyrene, and 4-bromostyrene were purchased from Alfa Aesar. *N*-Iodosuccinimide, 4-Fluorostyrene, 4-acetoxystyrene, and 2-bromostyrene were purchased from Matrix Scientific. Ethylbenzene, 4'-ethylacetophenone, 4-ethylphenyl acetate, propylbenzene, *p*-toluenesulfonyl chloride, and 1-(chloromethyl)-4-vinylbenzene were purchased from Tokyo Chemical Industry (TCI). 2,3-Dichloro-5,6-dicyano-1,4-benzoquinone (DDQ), 4-bromostyrene, and 4-trifluoromethylstyrene were acquired from Oakwood. 1-Ethyl-naphthalene, [Ir(ppy)₂(dtbbpy)]PF₆, [Ir(dF(CF₃)ppy)₂(dtbpy)][PF₆], [Ru(bpy)₃][PF₆]₂, Eosin Y, tetrahydrofuran (THF), hexanes, ethyl acetate, dichloromethane, and *N,N*-dimethylformamide (DMF) were obtained from Sigma Aldrich. Anhydrous magnesium sulfate and anhydrous potassium carbonate were obtained from VWR. Acetonitrile and methanol were obtained from Fischer Scientific. Dry dichloromethane (purchased from Fisher scientific, HPLC grade) was obtained from a drying column and stored over activated 4 Å molecular sieves.⁴¹⁷ NMR solvents were purchased from Cambridge Isotope Laboratories and were used as received. All reactions were carried out under ambient atmosphere unless otherwise noted. 1-(4-Vinylphenyl)ethan-1-one,⁴¹⁸ ethyl 4-vinylbenzoate,⁴¹⁹ 4-vinylbenzonitrile,⁴²⁰ 4-vinyl-1,1'-biphenyl,⁴²⁰ 2-vinylnaphthalene,⁴²¹ *tert*-butyl-3-methyl-1*H*-indole-1-carboxylate,⁴²² and 4-substituted silyl enol ethers⁴²³ were

prepared according to literature procedures. YUNBO blue LED strip lights (460-465 nm) were purchased from Amazon.

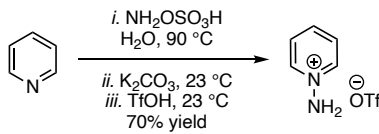
Characterization Details ^1H and ^{13}C NMR spectral acquisitions were recorded on an Inova 500 FT NMR (Varian), a VNMR5 500 FT NMR (Varian), or an AscendTM 400 NMR (Bruker) and were referenced against residual proteo solvent signals: CDCl_3 (5.26 ppm, ^1H ; 77.16 ppm, ^{13}C) and acetonitrile- d_3 (1.94 ppm, ^1H).¹⁹¹ ^1H NMR data are reported as follows: chemical shift (δ , ppm), (multiplicity: s (singlet), d (doublet), t (triplet), m (multiplet), br (broad), integration). ^{13}C NMR data are reported as follows: chemical shift (δ , ppm). Mass spectrometry data were recorded on either Orbitrap FusionTM TribridTM Mass Spectrometer or Q ExactiveTM Focus Hybrid Quadrupole-OrbitrapTM Mass Spectrometer from ThermoFisher Scientific. EPR spectra were recorded at X-band (9.35 GHz) on a Bruker ELEXSYS Spectrometer at 23 °C in 2 mm EPR tubes. EPR simulations were performed with EASYSPIN (version 5.2.17) using “garlic” function.⁴²⁴

X-Ray Diffraction Details Experimental details of crystallization are included in the synthetic procedures for the relevant compounds. A Bruker APEX 2 Duo X-ray (three-circle) diffractometer was used for crystal screening, unit cell determination, and data collection for the X-ray crystal structures of *cis*-**V.7c** and **V.7r**. Crystal suitable for X-ray diffraction were mounted on a MiTeGen dual-thickness micro-mount and placed under a cold N_2 stream (Oxford). The X-ray radiation employed was generated from a Mo sealed X-ray tube ($K_\alpha = 0.70173 \text{ \AA}$ with a potential of 40 kV and a current of 40 mA). Bruker

AXS APEX II software was used for data collection and reduction. Absorption corrections were applied using the program SADABS. A solution was obtained using XT/XS in APEX2 and refined in Olex2.⁴²⁵⁻⁴²⁷ Hydrogen atoms were placed in idealized positions and were set riding on the respective parent atoms. All non-hydrogen atoms were refined with anisotropic thermal parameters. The structure was refined (weighted least squares refinement on F2) to convergence.⁴²⁷

V.4.2 Synthesis and Characterization Details

B.1 Synthesis of *N*-Aminopyridinium Triflate

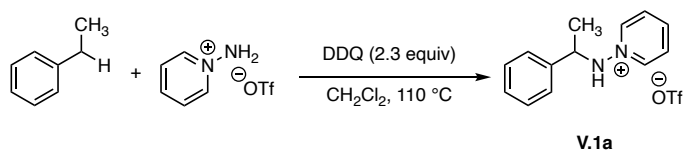


N-Aminopyridinium triflate was prepared by the following modification of literature methods.⁴²⁸ A 100-mL round-bottomed flask was charged with pyridine (21.4 mL, 265 mmol, 3.00 equiv) and a freshly prepared solution of hydroxylamine-*O*-sulfonic acid (10.0 g, 88.4 mmol, 1.00 equiv) in distilled water (25.0 mL) at $23\text{ }^\circ\text{C}$. The resulting solution was stirred at $90\text{ }^\circ\text{C}$ for 20 min, at which time the reaction mixture was cooled to $23\text{ }^\circ\text{C}$ and potassium carbonate (15.8 g, 115 mmol, 1.30 equiv) was added. Volatiles were removed under reduced pressure and the residue was taken up in ethanol (50.0 mL). Insoluble residues were removed by vacuum filtration and the filtrate was acidified with 60% trifluoromethanesulfonic acid to $\text{pH} = 5$. An off-white precipitate was obtained upon storing the resulting solution overnight at $-20\text{ }^\circ\text{C}$. Isolation of this precipitate by vacuum

filtration followed by thorough washing with diethyl ether afforded the title compound as an off-white solid (15.1 g, 70% yield). ¹H NMR (δ , 23 °C, 400 MHz, CD₃CN): 8.58 (dt, J = 4.6, 1.7 Hz, 2H), 8.28 (t, J = 7.8 Hz, 1H), 7.92 (t, 2H), 7.13 (bs, 2H). The obtained spectral data are in good agreement with those reported in literature.³⁹¹

B.2 Synthesis of *N*-benzylaminopyridiniums

Synthesis of 1-((1-Phenylethyl)amino)pyridin-1-ium triflate (V.1a)



Compound **1a** was prepared following literature procedure.³⁹¹ A 25-mL thick-walled glass tube was charged with *N*-aminopyridinium triflate (48.8 mg, 0.201 mmol, 1.00 equiv), ethylbenzene (32.0 μ L, 0.260 mmol, 1.31 equiv), 2,3-dichloro-5,6-dicyano-1,4-benzoquinone (DDQ, 104 mg, 0.460 mmol, 2.30 equiv), and CH₂Cl₂ (1.00 mL). The reaction vessel was sealed with a Teflon screw top and heated at 110 °C for 40 h. The reaction mixture was cooled to 23 °C. Solids were removed by vacuum filtration and washed with CH₂Cl₂. The filtrate was concentrated under reduced pressure. The residue was purified by SiO₂ gel chromatography (eluent 85:15 CH₂Cl₂:acetonitrile) to afford the title compound as a brown oil (50.0 mg, 72% yield). ¹H NMR (δ , 23 °C, 400 MHz, CDCl₃): 8.71 (dd, J = 6.9, 1.2 Hz, 2H), 8.31 (bs, 1H), 8.26-8.22 (m, 1H), 7.81-7.78 (m, 2H), 7.29-

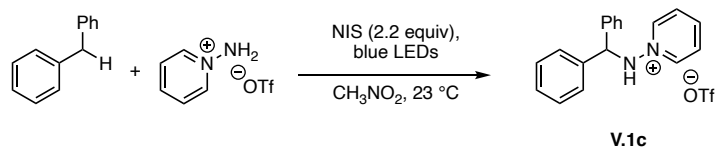
7.23 (m, 5H), 4.57 (q, $J = 3.3, 1.9$ Hz, 1H), 1.66 (d, $J = 6.6$ Hz, 3H). The obtained spectral data are in good agreement with those reported in literature.³⁹¹

Synthesis of 1-((1-Phenylpropyl)amino)pyridin-1-ium triflate (V.1b)



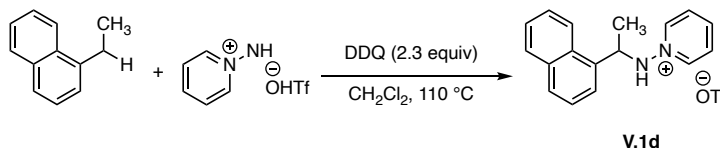
Compound **V.1b** was prepared following literature procedure.³⁹¹ A 25-ml Schlenk flask was charged with *N*-aminopyridinium triflate (48.8 mg, 0.200 mmol, 1.00 equiv), propylbenzene (139 μ L, 0.998 mmol, 4.99 equiv), *N*-iodosuccinimide (NIS, 100 mg, 0.440 mmol, 2.20 equiv), and CH₃NO₂ (0.20 mL) under an N₂ atmosphere. The resulting solution was degassed by three freeze-pump-thaw cycles and stirred for 30 h at 23 °C while being irradiated by blue LEDs. The reaction mixture was concentrated under reduced pressure. The obtained residue was purified by SiO₂ gel chromatography (eluent 85:15 CH₂Cl₂:acetonitrile) to afford the title compound as brown solid (42.6 mg, 59% yield). ¹H NMR (δ , 23 °C, 400 MHz, CDCl₃): δ 8.70 (d, $J = 5.7$ Hz, 2H), 8.36 (dd, $J = 5.1, 0.4$ Hz, 1H), 8.22-8.18 (m, 1H), 7.79-7.75 (m, 2H), 7.29-7.27 (m, 3H), 7.22 (dd, $J = 7.5, 2.0$ Hz, 2H), 4.29-4.27 (m, 1H), 2.20-2.14 (m, 1H), 1.98-1.90 (m, 1H), 0.90 (t, $J = 7.4$ Hz, 3H). The obtained spectral data are in good agreement with those reported in literature.³⁹¹

Synthesis of 1-(Benzhydrylamino)pyridin-1-ium triflate (V.1c)



Compound **V.1c** was prepared following literature procedure.³⁹¹ A 25-ml Schlenk flask was charged with *N*-aminopyridinium triflate (48.8 mg, 0.200 mmol, 1.00 equiv), diphenylmethane (43.7 mg, 0.259 mmol, 1.30 equiv), *N*-iodosuccinimide (NIS, 100 mg, 0.440 mmol, 2.20 equiv), and CH₂Cl₂ (0.20 mL) under an N₂ atmosphere. The resulting solution was degassed by three freeze-pump-thaw cycles and stirred for 30 h at 23 °C while being irradiated by blue LEDs. The reaction mixture was concentrated under reduced pressure. The obtained residue was purified by SiO₂ gel chromatography (eluent 85:15 CH₂Cl₂:acetonitrile) to afford the title compound as white solid (58.2 mg, 71% yield). ¹H NMR (δ, 23 °C, 400 MHz, CDCl₃): 8.80 (d, *J* = 6.3 Hz, 2H), 8.62 (bs, 1H), 8.17 (t, *J* = 7.7 Hz, 1H), 7.73 (t, *J* = 7.1 Hz, 2H), 7.40-7.27 (m, 10H), 5.67 (s, 1H). The obtained spectral data are in good agreement with those reported in literature.³⁹¹

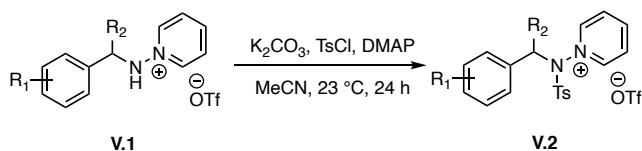
Synthesis of 1-((1-(Naphthalen-1-yl)ethyl)amino)pyridine-1-ium triflate (V.1d)



Compound **V.1d** was prepared following literature procedure.³⁹¹ A 25-mL thick-walled glass tube was charged with *N*-aminopyridinium triflate (48.8 mg, 0.201 mmol, 1.00 equiv), 1-ethylnaphthalene (40.0 μL, 0.258 mmol, 1.29 equiv), 2,3-dichloro-5,6-dicyano-

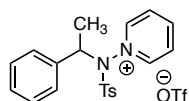
1,4-benzoquinone (DDQ, 104 mg, 0.460 mmol, 2.30 equiv), and CH₂Cl₂ (1.00 mL). The reaction vessel was sealed with a Teflon screw top and heated at 110 °C for 40 h. The reaction mixture was cooled to 23 °C. Solids were removed by vacuum filtration and washed with CH₂Cl₂. The filtrate was concentrated under reduced pressure. The residue was purified by SiO₂ gel chromatography (eluent 85:15 CH₂Cl₂:acetonitrile) to afford the title compound as a brown oil (62.8 mg, 79% yield). ¹H NMR (δ, 23 °C, 400 MHz, CDCl₃): 8.72 (d, *J* = 6.9 Hz, 3H), 8.19 (d, *J* = 7.8 Hz, 1H), 8.08 (t, *J* = 7.8 Hz, 1H), 7.83 (dd, *J* = 26.4, 8.0 Hz, 2H), 7.66 (t, *J* = 7.4 Hz, 3H), 7.52 (ddd, *J* = 9.6, 8.0, 1.5 Hz, 2H), 7.43 (t, *J* = 7.7 Hz, 1H), 5.45 (dd, *J* = 5.7, 4.3 Hz, 1H), 1.84 (d, *J* = 6.6 Hz, 3H). The obtained spectral data are in good agreement with those reported in literature.³⁹¹

Tosylation of *N*-benzylaminopyridiniums



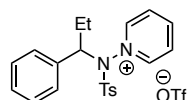
A 25-mL round-bottomed flask was charged with the appropriate *N*-benzylaminopyridinium (V.2, 1.00 mmol, 1.00 equiv) and acetonitrile (5.0 mL). K₂CO₃ (415 mg, 3.00 mmol, 3.00 equiv), TsCl (343 mg, 1.80 mmol, 1.80 equiv), and DMAP (12.2 mg, 0.100 mmol, 10.0 mol%) were added to the reaction vessel. The resulting mixture was degassed by sparging with N₂ for 10-15 min before being stirred at 23 °C for 24 h under nitrogen atmosphere. Solids were removed by vacuum filtration. The filtrate was

concentrated under reduced pressure and the residue was purified by silica gel column chromatography (eluent ethyl acetate followed by 85:15 CH₂Cl₂:acetonitrile). The obtained residue was further purified by recrystallization (1:2 CH₂Cl₂:Et₂O mixture) to afford the title compound.



1-((4-Methyl-N-(1-phenylethyl)phenyl)sulfonamido)pyridin-1-ium triflate (V.2a).

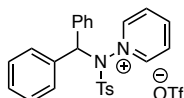
Prepared from *N*-benzylaminopyridinium **V.1a** and obtained as a pale-yellow solid (430 mg, 86% yield). ¹H NMR (δ, 23 °C, 400 MHz, CDCl₃): 8.82 (d, *J* = 5.0 Hz, 1H), 8.68 (t, *J* = 7.8 Hz, 1H), 8.30 (t, *J* = 4.2 Hz, 1H), 7.94 (dd, *J* = 21.8, 6.1 Hz, 2H), 7.66 (d, *J* = 8.3 Hz, 2H), 7.42 (d, *J* = 8.5 Hz, 2H), 7.30 (s, 3H), 7.22 (dd, *J* = 7.7, 1.7 Hz, 2H), 5.78 (d, *J* = 7.0 Hz, 1H), 2.49 (s, 3H), 1.71 (d, *J* = 6.9 Hz, 3H). ¹³C NMR (δ, 23 °C, 100 MHz, CDCl₃): 149.5, 147.9, 135.8, 131.7, 131.3, 130.1, 129.7, 128.5, 128.1, 121.9, 119.2, 63.5, 22.0, 18.9. ¹⁹F NMR (δ, 23 °C, 376 MHz, CDCl₃): -78.3. HRMS-APCI: calculated for [M⁺] = 353.1318, observed [M⁺] = 353.1315.



1-((4-Methyl-N-(1-phenylpropyl)phenyl)sulfonamido)pyridin-1-ium triflate

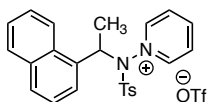
(V.2b). Prepared from *N*-benzylaminopyridinium **V.1b** and obtained as a brown solid (372 mg, 72% yield). ¹H NMR (δ, 23 °C, 500 MHz, CDCl₃): δ 8.72-8.69 (m, 2H), 8.36 (t, *J* = 7.1 Hz, 1H), 7.81 (s, 1H), 7.68 (s, 1H), 7.64-7.62 (m, 2H), 7.41 (d, *J* = 8.2 Hz, 2H), 7.36-7.30 (m, 3H), 7.15 (d, *J* = 7.1 Hz, 2H), 5.57 (dd, *J* = 9.1, 6.7 Hz, 1H), 2.48 (s, 3H), 2.14-

2.03 (m, 2H), 0.90 (t, $J = 7.3$ Hz, 3H). ^{13}C NMR (δ , 23 °C, 100 MHz, CDCl_3): δ 150.08, 150.07, 150.07, 150.06, 149.8, 148.93, 148.92, 148.92, 148.0, 134.1, 131.9, 131.35, 131.35, 130.8, 130.5, 129.9, 129.0, 128.55, 128.53, 128.53, 128.48, 128.47, 69.6, 25.2, 22.1, 11.3. ^{19}F NMR (δ , 23 °C, 376 MHz, CDCl_3): -78.3 . HRMS-APCI: calculated for $[\text{M}^+] = 367.1475$, observed $[\text{M}^+] = 367.1473$.



1-((N-benzhydryl-4-methylphenyl)sulfonamido)pyridin-1-ium triflate (V.2c).

Prepared from *N*-benzylaminopyridinium **V.1c** and obtained as a white solid (479 mg, 85% yield). ^1H NMR (δ , 23 °C, 500 MHz, CD_3CN): 8.83 (dd, $J = 7.0, 1.3$ Hz, 2H), 8.53 (tt, $J = 7.8, 1.3$ Hz, 1H), 7.95 (dd, $J = 7.8, 7.0$ Hz, 2H), 7.49 (d, $J = 8.5$ Hz, 2H), 7.45-7.43 (m, 4H), 7.36 (dd, $J = 8.6, 0.6$ Hz, 2H), 7.22-7.20 (m, 6H), 6.43 (s, 1H), 2.46 (s, 3H). ^{13}C NMR (δ , 23 °C, 100 MHz, CD_3CN): 150.5, 149.1, 148.8, 137.6, 132.2, 131.6, 130.11, 130.08, 129.96, 129.1, 118.3, 73.3, 21.9. ^{19}F NMR (δ , 23 °C, 376 MHz, CDCl_3): -78.3 . HRMS-APCI: calculated for $[\text{M}^+] = 415.1475$, observed $[\text{M}^+] = 415.1473$.

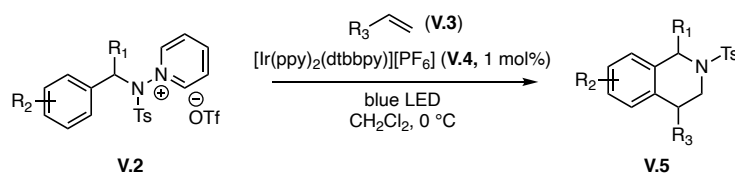


1-((4-Methyl-N-(1-(naphthalen-1-yl)ethyl)phenyl)sulfonamido)pyridin-1-ium

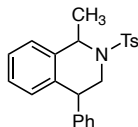
triflate (V.2d). Prepared from *N*-benzylaminopyridinium **V.1d** and obtained as a yellow solid (446 mg, 81% yield). ^1H NMR (δ , 23 °C, 400 MHz, CDCl_3): 8.92-8.90 (m, 1H), 8.60-8.58 (m, 1H), 8.45 (d, $J = 8.5$ Hz, 2H), 7.90 (d, $J = 8.1$ Hz, 1H), 7.80-7.74 (m, 2H), 7.64 (dt, $J = 6.6, 1.9$ Hz, 3H), 7.49-7.48 (m, 1H), 7.41-7.39 (m, 2H), 7.18 (t, $J = 11.8$ Hz, 3H),

6.77 (bs, 1H), 2.48 (s, 3H), 2.00 (d, $J = 7.0$ Hz, 3H). ^{13}C NMR (δ , 23 °C, 100 MHz, CDCl_3): 149.6, 149.5, 148.3, 148.1, 134.0, 131.4, 131.2, 130.4, 130.1, 129.8, 128.4, 128.30, 127.0, 126.5, 125.6, 122.5, 122.2, 119.3, 22.0. ^{19}F NMR (δ , 23 °C, 376 MHz, CDCl_3): -78.3. HRMS-APCI: calculated for $[\text{M}^+] = 403.1475$, observed $[\text{M}^+] = 403.1473$.

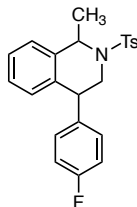
Deaminative Tetrahydroisoquinoline Syntheses



A 25-mL Schlenk tube was charged with appropriate *N*-benzylaminopyridinium (V.2, 0.100 mmol, 1.00 equiv), olefin (V.3, 0.160 mmol, 1.60 equiv), [Ir(ppy)₂(dtbbpy)][PF₆] (V.4, 1.0 mg, 1.10 μmol, 1.10 mol%), and CH₂Cl₂ (0.40 mL) under N₂ atmosphere. The resulting solution was degassed by three freeze-pump-thaw cycles and stirred for 16 h at 0 °C while being irradiated by blue LEDs. The reaction mixture was warmed to 23 °C and concentrated under reduced pressure. The obtained residue was purified by SiO₂ gel chromatography (eluent 90:10 hexanes:ethyl acetate) to afford the title compound. Diastereomers were separated via SiO₂ chromatography using an eluent gradient (*i.e.*, 100:0 – 90:10 hexanes:ethyl acetate). The diastereomeric ratio (dr) of the products are reported as a mixture of *cis* : *trans* isomers.



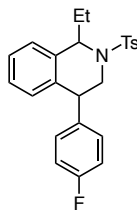
1-Methyl-4-phenyl-2-tosyl-1,2,3,4-tetrahydroisoquinoline (V.5a). Prepared from styrene (**V.3a**) and 1-((4-methyl-*N*-(1-phenylethyl)phenyl)sulfonamido)pyridin-1-ium triflate (**V.2a**) and obtained as a white solid (26.8 mg, 71% yield, 1.4:1 dr). *Cis isomer*: ^1H NMR (δ , 23 °C, 400 MHz, CDCl_3): 7.70 (d, $J = 8.3$ Hz, 2H), 7.32-7.14 (m, 7H), 7.10 (d, $J = 1.5$ Hz, 2H), 7.02 (s, 1H), 6.70 (d, $J = 7.8$ Hz, 1H), 5.26 (q, $J = 6.8$ Hz, 1H), 4.08-3.96 (m, 2H), 3.34 (dd, $J = 13.6, 11.1$ Hz, 1H), 2.38 (s, 3H), 1.52 (d, $J = 6.8$ Hz, 3H). ^{13}C NMR (δ , 23 °C, 100 MHz, CDCl_3): 143.4, 142.2, 138.32, 138.26, 136.5, 129.8, 129.7, 129.2, 128.9, 127.3, 127.1, 126.9, 126.6, 126.6, 52.3, 45.7, 44.5, 22.9, 21.6. *Trans isomer*: ^1H NMR (δ , 23 °C, 400 MHz, CDCl_3): 7.41 (d, $J = 8.4$ Hz, 2H), 7.23-7.03 (m, 8H), 6.91 (d, $J = 7.6$ Hz, 1H), 6.82 (dd, $J = 7.8, 1.6$ Hz, 2H), 5.18 (q, $J = 6.7$ Hz, 1H), 4.14 (t, $J = 3.6$ Hz, 1H), 3.75 (qd, $J = 14.1, 3.6$ Hz, 2H), 2.34 (s, 3H), 1.53 (d, $J = 6.7$ Hz, 3H). ^{13}C NMR (δ , 23 °C, 100 MHz, CDCl_3): 143.5, 142.9, 138.8, 136.9, 135.0, 130.2, 129.5, 128.7, 128.3, 127.3, 127.1, 127.0, 126.8, 126.5, 52.6, 45.9, 44.4, 22.8, 21.6. HRMS-ESI: calculated for $[\text{M}+\text{H}] = 378.1522$, observed $[\text{M}+\text{H}] = 378.1521$.



4-(4-Fluorophenyl)-1-methyl-2-tosyl-1,2,3,4-tetrahydroisoquinoline (V.5b).

Prepared from 4-fluorostyrene (V.3b) and 1-((4-methyl-*N*-(1-phenylethyl)phenyl)sulfonamido)pyridin-1-ium triflate (V.2a) and obtained as a white solid (29.6 mg, 75% yield, 1:1.5 dr). *Cis isomer*: ^1H NMR (δ , 23 °C, 400 MHz, CDCl_3): 7.70 (d, $J = 8.1$ Hz, 2H), 7.26-6.98 (m, 10H), 6.69-6.67 (m, 1H), 5.24 (q, $J = 6.7$ Hz, 1H), 4.05-3.96 (m, 2H), 3.31-3.26 (m, 1H), 2.38-2.35 (m, 3H), 1.50 (d, $J = 6.8$ Hz, 3H). ^{13}C NMR (δ , 23 °C, 100 MHz, CDCl_3): 162.1 (d, $^1J_{\text{C-F}} = 240$ Hz), 143.4, 138.3, 138.2, 137.9, 137.9, 136.3, 130.7, 130.6, 129.8, 129.8, 129.6, 127.1, 126.9, 126.8, 126.7, 115.8 (d, $^2J_{\text{C-F}} = 21$ Hz), , 52.3, 45.7, 43.8, 22.9, 21.6. ^{19}F NMR (δ , 23 °C, 376 MHz, CDCl_3): -115.4. *Trans isomer*: ^1H NMR (δ , 23 °C, 400 MHz, CDCl_3): 7.40 (d, $J = 8.3$ Hz, 2H), 7.40 (d, $J = 8.3$ Hz, 2H), 7.26-7.22 (m, 2H), 7.26-7.22 (m, 2H), 7.18-7.12 (m, 2H), 7.18-7.12 (m, 2H), 7.05 (d, $J = 8.0$ Hz, 2H), 7.05 (d, $J = 8.0$ Hz, 2H), 6.90 (d, $J = 7.6$ Hz, 1H), 6.90 (d, $J = 7.6$ Hz, 1H), 6.71 (d, $J = 7.0$ Hz, 4H), 6.71 (d, $J = 7.0$ Hz, 4H), 5.22 (q, $J = 6.7$ Hz, 1H), 5.22 (q, $J = 6.7$ Hz, 1H), 4.11 (t, $J = 3.1$ Hz, 1H), 4.11 (t, $J = 3.1$ Hz, 1H), 3.78-3.67 (m, 2H), 3.78-3.67 (m, 2H), 2.36 (s, 3H), 2.36 (s, 3H), 1.54 (d, $J = 6.7$ Hz, 3H), 1.54 (d, $J = 6.7$ Hz, 3H). ^{13}C NMR (δ , 23 °C, 100 MHz, CDCl_3): 161.7 (d, $^1J_{\text{C-F}} = 240$ Hz), 162.9, 160.5, 143.1, 139.4, 138.8, 137.1, 134.6, 130.3, 130.0, 129.9, 129.4, 127.2, 127.2, 127.2, 126.9, 115.0 (d, $^2J_{\text{C-F}} = 21$ Hz),, 52.5, 45.7, 43.7, 22.5, 21.5. ^{19}F NMR (δ , 23 °C, 376 MHz,

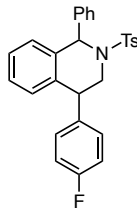
CDCl₃): -116.7. HRMS-ESI: calculated for [M+H] = 396.1428, observed [M+H] = 396.1424.



1-Ethyl-4-(4-fluorophenyl)-2-tosyl-1,2,3,4-tetrahydroisoquinoline (V.5c).

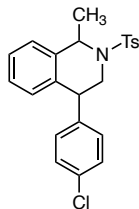
Prepared from 4-fluorostyrene (V.3b) and 1-((4-methyl-*N*-(1-phenylpropyl)phenyl)sulfonamido)pyridin-1-ium triflate (V.2b) and obtained as a colorless oil (19.6 mg, 48% yield, 1:1.1 dr). *Cis isomer*: ¹H NMR (δ, 23 °C, 400 MHz, CDCl₃): 7.65 (d, *J* = 8.3 Hz, 2H), 7.15-7.09 (m, 4H), 7.01-6.97 (m, 5H), 6.58 (d, *J* = 7.8 Hz, 1H), 4.98-4.94 (m, 1H), 4.03 (ddd, *J* = 14.9, 6.8, 1.3 Hz, 1H), 3.76 (dd, *J* = 11.8, 6.8 Hz, 1H), 3.26 (dd, *J* = 14.9, 11.8 Hz, 1H), 2.35 (s, 3H), 1.91-1.86 (m, 2H), 1.06 (t, *J* = 7.4 Hz, 3H). ¹³C NMR (δ, 23 °C, 100 MHz, CDCl₃): 162.0 (d, ¹*J*_{C-F} = 242 Hz), 143.3, 138.3, 138.2, 137.4, 136.1, 130.6, 130.5, 129.6, 129.5, 127.2, 126.9, 126.8, 126.6, 115.8 (d, ²*J*_{C-F} = 21 Hz), 58.2, 46.0, 42.2, 30.7, 21.6, 11.6. ¹⁹F NMR (δ, 23 °C, 376 MHz, CDCl₃): -115.5. *Trans isomer*: ¹H NMR (δ, 23 °C, 400 MHz, CDCl₃): 7.48 (d, *J* = 8.3 Hz, 2H), 7.22-7.08 (m, 5H), 6.80-6.77 (m, 5H), 4.93 (t, *J* = 6.5 Hz, 1H), 4.16 (t, *J* = 5.1 Hz, 1H), 3.88 (dd, *J* = 12.4, 4.9 Hz, 1H), 3.52 (dd, *J* = 12.4, 5.5 Hz, 1H), 2.36 (s, 3H), 2.02-1.90 (m, 2H), 0.96 (t, *J* = 7.5 Hz, 3H). ¹³C NMR (δ, 23 °C, 100 MHz, CDCl₃): 161.8 (d, ¹*J*_{C-F} = 243 Hz), 143.1, 138.5, 137.2, 136.9, 136.1, 130.21, 130.13, 129.5, 129.3, 127.23, 127.20, 126.7, 115.3 (d,

$^2J_{C-F} = 21$ Hz), 58.7, 48.0, 43.3, 31.2, 21.5, 11.0. ^{19}F NMR (δ , 23 °C, CDCl_3): -116.1. HRMS-ESI: calculated for $[\text{M}+\text{H}] = 410.1585$, observed $[\text{M}+\text{H}] = 410.1582$.



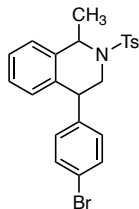
4-(4-Fluorophenyl)-1-phenyl-2-tosyl-1,2,3,4-tetrahydroisoquinoline (**V.5d**).

Prepared from 4-fluorostyrene (**V.3b**) and 1-((*N*-benzhydryl-4-methylphenyl)sulfonamido)pyridin-1-ium triflate (**V.2c**) and obtained as a white solid (9.6 mg, 21% yield, 2.3:1 dr). *Cis isomer*: ^1H NMR (δ , 23 °C, 400 MHz, CDCl_3): 7.60 (d, $J = 8.3$ Hz, 2H), 7.34-7.25 (m, 5H), 7.18-7.10 (m, 4H), 7.06-6.96 (m, 5H), 6.71 (d, $J = 7.7$ Hz, 1H), 6.34 (s, 1H), 3.96-3.84 (m, 2H), 3.13 (dd, $J = 14.2, 11.5$ Hz, 1H), 2.34 (s, 3H). ^{13}C NMR (δ , 23 °C, 100 MHz, CDCl_3): 163.1 (d, $^1J_{C-F} = 244$ Hz), 143.4, 141.5, 137.98, 137.94, 137.88, 137.6, 133.9, 130.57, 130.49, 129.72, 129.53, 129.1, 128.55, 128.47, 128.0, 127.5, 127.2, 126.6, 115.8 (d, $^2J_{C-F} = 21$ Hz), 59.4, 46.2, 42.7, 21.6. ^{19}F NMR (δ , 23 °C, 376 MHz, CDCl_3): -115.4. Isolation of trans isomer was not attempted due to the small quantity generated in this preparation. HRMS-ESI: calculated for $[\text{M}+\text{H}] = 458.1585$, observed $[\text{M}+\text{H}] = 458.1579$.



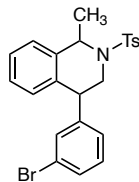
4-(4-Chlorophenyl)-1-methyl-2-tosyl-1,2,3,4-tetrahydroisoquinoline (V.5e).

Prepared from 4-chlorostyrene (V.3c) and 1-((4-methyl-*N*-(1-phenylethyl)phenyl)sulfonamido)pyridin-1-ium triflate (V.2a) and obtained as a white solid (32.1 mg, 78% yield, 1.3:1 dr). *Cis isomer*: ^1H NMR (δ , 23 °C, 400 MHz, CDCl_3): 7.69 (d, $J = 8.4$ Hz, 2H), 7.29 (d, $J = 8.4$ Hz, 2H), 7.22 (d, $J = 8.1$ Hz, 2H), 7.19-7.09 (m, 2H), 7.03 (d, $J = 8.4$ Hz, 3H), 6.67 (d, $J = 7.8$ Hz, 1H), 5.24 (q, $J = 6.9$ Hz, 1H), 4.05-3.96 (m, 2H), 3.28 (dd, $J = 12.6, 10.1$ Hz, 1H), 2.38 (s, 3H), 1.50 (d, $J = 6.8$ Hz, 3H). ^{13}C NMR (δ , 23 °C, 100 MHz, CDCl_3): 143.4, 140.7, 138.36, 138.17, 136.0, 133.2, 130.5, 129.8, 129.6, 129.1, 127.1, 127.0, 126.8, 126.7, 52.3, 45.6, 44.0, 22.9, 21.6. *Trans isomer*: ^1H NMR (δ , 23 °C, 400 MHz, CDCl_3): 7.37 (d, $J = 8.3$ Hz, 2H), 7.28-7.13 (m, 3H), 7.05 (dd, $J = 8.5, 0.6$ Hz, 2H), 6.97 (d, $J = 8.5$ Hz, 2H), 6.92-6.90 (m, 1H), 6.65 (d, $J = 8.3$ Hz, 2H), 5.27-5.22 (m, 1H), 4.10-4.09 (m, 1H), 3.80-3.66 (m, 2H), 2.39 (s, 3H), 1.58 (d, $J = 6.7$ Hz, 3H). ^{13}C NMR (δ , 23 °C, 100 MHz, CDCl_3): 143.2, 142.3, 138.9, 136.9, 134.1, 132.4, 130.3, 129.8, 129.4, 128.3, 127.3, 127.3, 127.2, 127.0, 52.5, 45.4, 43.8, 22.6, 21.6. HRMS-ESI: calculated for $[\text{M}+\text{H}] = 412.1133$, observed $[\text{M}+\text{H}] = 412.1127$.



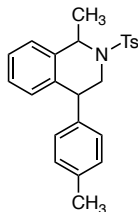
4-(4-Bromophenyl)-1-methyl-2-tosyl-1,2,3,4-tetrahydroisoquinoline (V.5f).

Prepared from 4-bromostyrene (V.3d) and 1-((4-methyl-*N*-(1-phenylethyl)phenyl)sulfonamido)pyridin-1-ium triflate (V.2a) and obtained as a white solid (31.8 mg, 70% yield, 1.6:1 dr). *Cis isomer* ^1H NMR (δ , 23 °C, 400 MHz, CDCl_3): 7.71-7.68 (m, 2H), 7.46-7.43 (m, 2H), 7.22 (dd, $J = 8.5, 0.6$ Hz, 2H), 7.17 (t, $J = 7.4$ Hz, 1H), 7.10 (dd, $J = 7.8, 1.3$ Hz, 1H), 7.03 (td, $J = 7.5, 1.3$ Hz, 1H), 6.99-6.97 (m, 2H), 6.67 (d, $J = 7.8$ Hz, 1H), 5.24 (q, $J = 6.8$ Hz, 1H), 4.06-3.97 (m, 2H), 3.27 (dd, $J = 13.2, 10.7$ Hz, 1H), 2.38 (s, 3H), 1.50 (d, $J = 6.8$ Hz, 3H). ^{13}C NMR (δ , 23 °C, 100 MHz, CDCl_3): 143.4, 141.2, 138.4, 138.1, 135.9, 132.0, 130.9, 129.8, 129.6, 127.1, 127.0, 126.8, 126.7, 121.2, 52.3, 45.5, 44.1, 22.9, 21.6. *Trans isomer* ^1H NMR (δ , 23 °C, 400 MHz, CDCl_3): 7.35 (d, $J = 8.3$ Hz, 2H), 7.27-7.14 (m, 5H), 7.11 (d, $J = 8.5$ Hz, 2H), 7.04 (d, $J = 8.1$ Hz, 2H), 6.89 (d, $J = 7.7$ Hz, 1H), 6.57 (d, $J = 8.4$ Hz, 2H), 5.26-5.21 (m, 1H), 4.06 (dd, $J = 2.3, 0.3$ Hz, 1H), 3.79-3.64 (m, 2H), 2.40 (s, 3H), 1.58 (d, $J = 6.7$ Hz, 3H). ^{13}C NMR (δ , 23 °C, 100 MHz, CDCl_3): 143.3, 142.8, 138.9, 136.8, 134.0, 131.2, 130.3, 130.2, 129.4, 127.3, 127.3, 127.2, 127.0, 120.6, 52.5, 45.3, 43.9, 22.6, 21.7. HRMS-ESI: calculated for $[\text{M}+\text{H}] = 456.0627$, observed $[\text{M}+\text{H}] = 456.0620$.

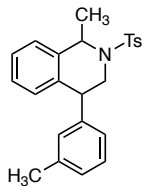


4-(3-Bromophenyl)-1-methyl-2-tosyl-1,2,3,4-tetrahydroisoquinoline (**V.5g**).

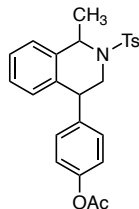
Prepared from 3-bromostyrene (**V.3e**) and 1-((4-methyl-*N*-(1-phenylethyl)phenyl)sulfonamido)pyridin-1-ium triflate (**V.2a**) and obtained as a white solid (30.9 mg, 68% yield, 2.3:1 dr). *Cis isomer*: ^1H NMR (δ , 23 °C, 400 MHz, CDCl_3): 7.72 (d, $J = 8.2$ Hz, 2H), 7.44-7.41 (m, 1H), 7.28-7.05 (m, 8H), 6.71 (d, $J = 7.8$ Hz, 1H), 5.27 (q, $J = 6.7$ Hz, 1H), 4.03 (ddt, $J = 21.0, 13.1, 7.0$ Hz, 2H), 3.32 (dd, $J = 13.5, 11.1$ Hz, 1H), 2.41 (s, 3H), 1.53 (d, $J = 6.8$ Hz, 3H). ^{13}C NMR (δ , 23 °C, 100 MHz, CDCl_3): 144.5, 143.5, 138.3, 138.1, 135.6, 132.1, 130.5, 130.5, 129.8, 129.6, 127.9, 127.1, 127.1, 126.9, 126.7, 122.9, 52.3, 45.5, 44.3, 22.9, 21.6. *Trans isomer*: ^1H NMR (δ , 23 °C, 400 MHz, CDCl_3): 7.39 (d, $J = 8.3$ Hz, 2H), 7.24-7.13 (m, 4H), 7.05 (d, $J = 8.1$ Hz, 2H), 6.95-6.89 (m, 2H), 6.83 (s, 1H), 6.72 (d, $J = 7.9$ Hz, 1H), 5.22 (q, $J = 6.6$ Hz, 1H), 4.08 (dd, $J = 2.9, 2.6$ Hz, 1H), 3.79-3.66 (m, 2H), 2.35 (s, 3H), 1.57 (d, $J = 6.7$ Hz, 3H). ^{13}C NMR (δ , 23 °C, 100 MHz, CDCl_3): 146.1, 143.1, 138.9, 136.5, 133.8, 131.6, 130.3, 129.8, 129.5, 129.5, 127.4, 127.4, 127.3, 127.3, 127.1, 122.5, 52.4, 45.3, 44.1, 22.5, 21.7. HRMS-ESI: calculated for $[\text{M}+\text{H}] = 456.0627$, observed $[\text{M}+\text{H}] = 455.0620$.



1-Methyl-4-(p-tolyl)-2-tosyl-1,2,3,4-tetrahydroisoquinoline (V.5h). Prepared from 4-methylstyrene (**V.3f**) and 1-((4-methyl-*N*-(1-phenylethyl)phenyl)sulfonamido)pyridin-1-ium triflate (**V.2a**) and obtained as a white solid (23.1 mg, 59% yield, 1:2.0 dr). *Cis isomer*: ^1H NMR (δ , 23 °C, 400 MHz, CDCl_3): 7.71 (d, $J = 8.6$ Hz, 2H), 7.21 (d, $J = 8.5$ Hz, 2H), 7.15-7.06 (m, 4H), 6.99 (dd, $J = 18.7, 7.9$ Hz, 3H), 6.68 (dd, $J = 8.5, 0.2$ Hz, 1H), 5.15 (q, $J = 7.1$ Hz, 1H), 3.90-3.76 (m, 2H), 3.11 (dd, $J = 14.3, 11.8$ Hz, 1H), 2.14 (s, 3H), 2.10 (s, 3H), 1.22 (d, $J = 7.2$ Hz, 3H). ^{13}C NMR was not collected due to low quantity. *Trans isomer*: ^1H NMR (δ , 23 °C, 400 MHz, CDCl_3): 7.41 (d, $J = 8.3$ Hz, 2H), 7.24-7.20 (m, 1H), 7.16-7.10 (m, 2H), 7.04 (d, $J = 8.0$ Hz, 2H), 6.90 (t, $J = 7.8$ Hz, 3H), 6.69 (d, $J = 8.1$ Hz, 2H), 5.18 (q, $J = 6.7$ Hz, 1H), 4.11 (t, $J = 3.5$ Hz, 1H), 3.79-3.66 (m, 2H), 2.35 (s, 3H), 2.28 (s, 3H), 1.54 (d, $J = 6.7$ Hz, 3H). ^{13}C NMR (δ , 23 °C, 100 MHz, CDCl_3): 142.8, 140.5, 138.8, 137.0, 136.1, 135.3, 130.2, 129.3, 129.0, 128.5, 127.3, 127.1, 127.0, 126.8, 52.6, 46.0, 44.0, 22.9, 21.6, 21.2. HRMS-ESI: calculated for $[\text{M}+\text{H}] = 392.1679$, observed $[\text{M}+\text{H}] = 392.1672$.

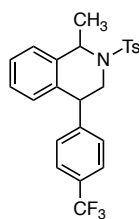


1-Methyl-4-(m-tolyl)-2-tosyl-1,2,3,4-tetrahydroisoquinoline (V.5i). Prepared from 3-methylstyrene (**V.3g**) and 1-((4-methyl-*N*-(1-phenylethyl)phenyl)sulfonamidopyridin-1-ium triflate (**V.2a**) and obtained as a white solid (27.3 mg, 70% yield, 1.2:1 dr). *Cis isomer*: $^1\text{H NMR}$ (δ , 23 °C, 400 MHz, CDCl_3): 77.71-7.69 (m, 2H), 7.23-7.14 (m, 4H), 7.09 (dd, $J = 6.8, 5.4$ Hz, 2H), 7.04-7.00 (m, 1H), 6.91-6.87 (m, 2H), 6.72 (d, $J = 7.8$ Hz, 1H), 5.25 (q, $J = 6.8$ Hz, 1H), 4.07-3.93 (m, 2H), 3.33 (dd, $J = 13.8, 11.3$ Hz, 1H), 2.38 (s, 3H), 2.32 (s, 3H), 1.52 (d, $J = 6.8$ Hz, 3H). $^{13}\text{C NMR}$ (δ , 23 °C, 100 MHz, CDCl_3): 143.2, 142.0, 138.4, 138.2, 138.1, 136.5, 129.7, 129.6, 128.6, 127.9, 127.0, 126.7, 126.4, 126.1, 52.2, 45.5, 44.4, 22.7, 21.5, 21.4. *Trans isomer*: $^1\text{H NMR}$ (δ , 23 °C, 400 MHz, CDCl_3): 7.40 (d, $J = 8.3$ Hz, 2H), 7.22 (dd, $J = 7.1, 0.9$ Hz, 1H), 7.16-7.10 (m, 2H), 7.04-6.97 (m, 3H), 6.94-6.90 (m, 2H), 6.60 (d, $J = 6.3$ Hz, 2H), 5.17 (q, $J = 6.7$ Hz, 1H), 4.11 (t, $J = 3.6$ Hz, 1H), 3.80-3.67 (m, 2H), 2.33 (s, 3H), 2.18 (s, 3H), 1.56 (d, $J = 6.5$ Hz, 3H). HRMS-ESI: 143.4, 142.8, 138.8, 137.7, 136.8, 135.1, 130.2, 129.3, 128.2, 127.3, 127.3, 127.1, 127.0, 126.8, 125.8, 52.6, 46.0, 44.3, 23.0, 21.6, 21.5. HRMS-ESI: calculated for $[\text{M}+\text{H}] = 392.1679$, observed $[\text{M}+\text{H}] = 392.1670$.



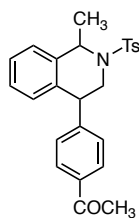
4-(1-Methyl-2-tosyl-1,2,3,4-tetrahydroisoquinolin-4-yl)phenyl acetate (V.5j).

Prepared from 4-acetoxystyrene (**V.3h**) and 1-((4-methyl-*N*-(1-phenylethyl)phenyl)sulfonamido)pyridin-1-ium triflate (**V.2a**) and obtained as a white solid (33.6 mg, 76% yield, 1:2.1 dr). Isolation of *cis* isomer was not successful due to co-elution with H-atom abstraction side products. *Trans* isomer: $^1\text{H NMR}$ (δ , 23 °C, 400 MHz, CDCl_3): 7.40 (d, $J = 7.9$ Hz, 2H), 7.21-7.06 (m, 5H), 6.91 (d, $J = 7.7$ Hz, 1H), 6.78 (s, 4H), 5.19 (q, $J = 6.6$ Hz, 1H), 4.13 (s, 1H), 3.80-3.68 (m, 2H), 2.34 (s, 3H), 2.28 (s, 3H), 1.55 (d, $J = 6.1$ Hz, 3H). $^{13}\text{C NMR}$ (δ , 23 °C, 100 MHz, CDCl_3): 169.4, 149.4, 143.1, 141.1, 138.8, 136.9, 134.6, 130.4, 129.5, 129.5, 127.3, 127.2, 126.9, 121.2, 52.5, 45.7, 43.8, 22.8, 21.5, 21.3. HRMS-ESI: calculated for $[\text{M}+\text{H}] = 436.1577$, observed $[\text{M}+\text{H}] = 436.1574$.



1-Methyl-2-tosyl-4-(4-(trifluoromethyl)phenyl)-1,2,3,4-tetrahydroisoquinoline (V.5k). Prepared from 4-trifluoromethylstyrene (**V.3i**) and 1-((4-methyl-*N*-(1-phenylethyl)phenyl)sulfonamido)-pyridin-1-ium triflate (**V.2a**) and obtained as a pale-

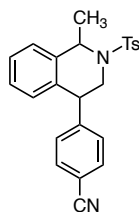
yellow oil (27.1 mg, 61% yield, 2.9:1 dr). *Cis isomer*: ^1H NMR (δ , 23 °C, 400 MHz, CDCl_3): 7.71-7.69 (m, 2H), 7.57 (d, $J = 8.1$ Hz, 2H), 7.23 (d, $J = 8.2$ Hz, 4H), 7.18 (d, $J = 7.3$ Hz, 1H), 7.12 (d, $J = 6.7$ Hz, 1H), 7.05 (t, $J = 7.5$ Hz, 1H), 6.65 (d, $J = 7.8$ Hz, 1H), 5.26 (q, $J = 6.8$ Hz, 1H), 4.12-4.03 (m, 2H), 3.31 (dd, $J = 12.8, 10.2$ Hz, 1H), 2.39 (s, 3H), 1.51 (d, $J = 6.8$ Hz, 3H). ^{19}F NMR (δ , 23 °C, 376 MHz, CDCl_3): -62.5. ^{13}C NMR (δ , 23 °C, 100 MHz, CDCl_3): 146.3, 143.5, 138.4, 138.1, 135.5, 129.8, 129.6, 129.4 ($^2J_{\text{C-F}} = 32.3$ Hz), 127.1, 127.1, 127.0, 126.8, 125.9 ($^3J_{\text{C-F}} = 3.7$ Hz), 124.2 ($^1J_{\text{C-F}} = 270$ Hz), 52.3, 45.5, 44.5, 22.8, 21.6. Isolation of trans isomer was not successful due to co-elution with H-atom abstraction side products. HRMS-ESI: calculated for $[\text{M}+\text{H}] = 446.1396$, observed $[\text{M}+\text{H}] = 446.1391$.



1-(4-(1-Methyl-2-tosyl-1,2,3,4-tetrahydroisoquinolin-4-yl)phenyl)ethan-1-one

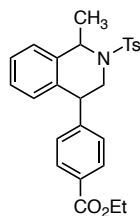
(**V.5l**). Prepared from 1-(4-vinylphenyl)ethan-1-one (**V.3j**) and 1-((4-methyl-*N*-(1-phenylethyl)phenyl)sulfonamido)pyridin-1-ium triflate (**V.2a**) and obtained as a white solid (21.7 mg, 52% yield, 3.2:1 dr). *Cis isomer*: ^1H NMR (δ , 23 °C, 400 MHz, CDCl_3): 7.91 (d, $J = 8.3$ Hz, 2H), 7.70 (d, $J = 8.3$ Hz, 2H), 7.24-7.17 (m, 5H), 7.12-7.10 (m, 1H), 7.03 (dd, $J = 0.6, 0.2$ Hz, 1H), 6.64 (d, $J = 7.8$ Hz, 1H), 5.25 (q, $J = 6.8$ Hz, 1H), 4.11-4.03 (m, 2H), 3.36-3.29 (m, 1H), 2.60 (s, 3H), 2.39 (s, 3H), 1.52 (d, $J = 6.8$ Hz, 3H). ^{13}C NMR (δ , 23 °C, 100 MHz, CDCl_3): 197.7, 147.7, 143.5, 138.3, 138.1, 136.3, 135.6, 129.8, 129.6,

129.4, 129.0, 127.1, 127.0, 126.8, 52.3, 45.4, 44.6, 26.8, 22.9, 21.6. *Trans isomer*: ^1H NMR (δ , 23 °C, 400 MHz, CDCl_3): 7.67 (d, $J = 8.4$ Hz, 2H), 7.41 (d, $J = 8.3$ Hz, 2H), 7.28-7.24 (m, 1H), 7.20-7.14 (m, 2H), 7.01 (d, $J = 8.0$ Hz, 2H), 6.91-6.89 (m, 3H), 5.25 (q, $J = 6.6$ Hz, 1H), 4.19-4.17 (m, 1H), 3.79-3.78 (m, 2H), 2.55 (s, 3H), 2.31 (s, 3H), 1.51 (d, $J = 6.7$ Hz, 3H). ^{13}C NMR (δ , 23 °C, 100 MHz, CDCl_3): 197.7, 149.2, 143.2, 138.8, 137.1, 135.5, 134.0, 130.3, 129.4, 128.8, 128.4, 127.4, 127.3, 127.2, 127.0, 52.5, 45.2, 44.5, 26.7, 22.2, 21.6. HRMS-ESI: calculated for $[\text{M}+\text{H}] = 420.1628$, observed $[\text{M}+\text{H}] = 420.1617$.



4-(1-Methyl-2-tosyl-1,2,3,4-tetrahydroisoquinolin-4-yl)benzonitrile (**V.5m**).

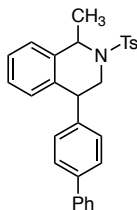
Prepared from 4-cyanostyrene (**V.3k**) and 1-((4-methyl-*N*-(1-phenylethyl)phenyl)sulfonamido)pyridin-1-ium triflate (**V.2a**) and obtained as a white solid (21.3 mg, 53% yield, 8.4:1 dr). *Cis isomer*: ^1H NMR (δ , 23 °C, 400 MHz, CDCl_3): 7.69 (d, $J = 8.3$ Hz, 2H), 7.63-7.60 (m, 2H), 7.25-7.18 (m, 5H), 7.13-7.11 (m, 1H), 7.05 (td, $J = 7.5, 1.2$ Hz, 1H), 6.61 (d, $J = 7.8$ Hz, 1H), 5.24 (q, $J = 6.8$ Hz, 1H), 4.12-4.02 (m, 2H), 3.28 (dd, $J = 13.3, 10.7$ Hz, 1H), 2.39 (s, 3H), 1.50 (d, $J = 6.9$ Hz, 3H). ^{13}C NMR (δ , 23 °C, 100 MHz, CDCl_3): 147.8, 143.6, 138.4, 138.0, 135.0, 132.7, 130.0, 129.8, 129.5, 128.7, 127.2, 127.2, 127.2, 127.1, 126.9, 126.2, 118.7, 111.4, 52.2, 45.4, 44.7, 22.8, 21.7. Isolation of trans isomer was not attempted due to the small quantity generated in this preparation. HRMS-ESI: calculated for $[\text{M}+\text{H}] = 403.1475$, observed $[\text{M}+\text{H}] = 403.1471$.



Ethyl 4-(1-methyl-2-tosyl-1,2,3,4-tetrahydroisoquinolin-4-yl)benzoate (V.5n).

Prepared from ethyl 4-vinylbenzoate (**V.31**) and 1-((4-methyl-*N*-(1-phenylethyl)phenyl)sulfonamido)pyridin-1-ium triflate (**V.2a**) and obtained as a white solid (21.1 mg, 47% yield, 2.4:1 dr). *Cis isomer*: ^1H NMR (δ , 23 °C, 400 MHz, CDCl_3): 8.00-7.98 (m, 2H), 7.71-7.69 (m, 2H), 7.24-7.21 (m, 2H), 7.17 (d, $J = 8.3$ Hz, 3H), 7.11 (dd, $J = 7.7, 1.3$ Hz, 1H), 7.02 (d, $J = 1.2$ Hz, 1H), 6.64 (d, $J = 7.8$ Hz, 1H), 5.25 (q, $J = 6.8$ Hz, 1H), 4.38 (q, $J = 7.1$ Hz, 2H), 4.07-4.04 (m, 2H), 3.32 (dd, $J = 15.7, 13.1$ Hz, 1H), 2.38 (s, 3H), 1.52 (d, $J = 6.8$ Hz, 3H), 1.39 (t, $J = 7.1$ Hz, 3H). ^{13}C NMR (δ , 23 °C, 100 MHz, CDCl_3): 166.4, 147.3, 143.5, 138.3, 138.1, 135.7, 130.2, 129.8, 129.7, 129.6, 129.2, 127.1, 127.0, 126.9, 126.7, 61.1, 52.3, 45.4, 44.6, 22.9, 21.6, 14.5. *Trans isomer*: ^1H NMR (δ , 23 °C, 400 MHz, CDCl_3): 7.70 (d, $J = 8.2$ Hz, 2H), 7.36 (d, $J = 8.2$ Hz, 2H), 7.28-7.24 (m, 1H), 7.21-7.19 (m, 1H), 7.16-7.12 (m, 1H), 6.97 (d, $J = 8.2$ Hz, 2H), 6.89 (d, $J = 7.6$ Hz, 1H), 6.80 (d, $J = 8.3$ Hz, 2H), 5.25 (q, $J = 6.7$ Hz, 1H), 4.36 (q, $J = 7.1$ Hz, 2H), 4.16-4.15 (m, 1H), 3.82-3.71 (m, 2H), 2.30 (s, 3H), 1.56 (d, $J = 7.4$ Hz, 3H), 1.39 (t, $J = 7.1$ Hz, 3H). ^{13}C NMR (δ , 23 °C, 100 MHz, CDCl_3): 166.6, 148.9, 143.1, 138.9, 136.9, 134.0, 130.3, 129.51, 129.38, 128.68, 128.51, 127.36, 127.28, 127.22, 127.04, 61.0, 52.5, 45.2,

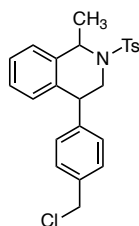
44.4, 22.5, 21.5, 14.5. HRMS-ESI: calculated for [M+H] = 450.1734, observed [M+H] = 450.1728.



4-([1,1'-Biphenyl]-4-yl)-1-methyl-2-tosyl-1,2,3,4-tetrahydroisoquinoline (V.5o).

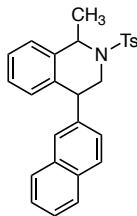
Prepared from 4-vinyl-1,1'-biphenyl (**V.3m**) and 1-((4-methyl-*N*-(1-phenylethyl)phenyl)sulfonamido)pyridin-1-ium triflate (**V.2a**) and obtained as a white solid (21.7 mg, 48% yield, 1:2.2 dr). *Cis isomer*: $^1\text{H NMR}$ (δ , 23 °C, 400 MHz, CDCl_3): 7.56-7.54 (m, 2H), 7.46-7.39 (m, 4H), 7.36-7.32 (m, 1H), 7.30-7.24 (m, 4H), 7.19 (dd, $J = 11.9, 7.2$ Hz, 2H), 6.96 (dd, $J = 7.3, 5.3$ Hz, 3H), 6.83 (d, $J = 8.2$ Hz, 2H), 5.25 (q, $J = 6.6$ Hz, 1H), 4.18 (dd, $J = 3.3, 3.1$ Hz, 1H), 3.85-3.73 (m, 2H), 2.11 (s, 3H), 1.60 (d, $J = 6.7$ Hz, 3H). $^{13}\text{C NMR}$ (δ , 23 °C, 100 MHz, CDCl_3): 143.4, 141.2, 140.8, 140.3, 138.4, 138.3, 136.4, 129.8, 129.7, 129.6, 128.9, 127.6, 127.5, 127.2, 127.1, 126.9, 126.7, 126.6, 52.3, 45.7, 44.2, 22.9, 21.6. *Trans isomer*: $^1\text{H NMR}$ (δ , 23 °C, 400 MHz, CDCl_3): 7.56-7.54 (m, 2H), 7.46-7.39 (m, 4H), 7.36-7.32 (m, 1H), 7.30-7.24 (m, 3H), 7.19 (dd, $J = 11.9, 7.2$ Hz, 2H), 6.96 (dd, $J = 7.3, 5.3$ Hz, 3H), 6.83 (d, $J = 8.2$ Hz, 2H), 5.25 (q, $J = 6.6$ Hz, 1H), 4.18 (dd, $J = 3.3, 3.1$ Hz, 1H), 3.85-3.73 (m, 2H), 2.11 (s, 3H), 1.60 (d, $J = 6.7$ Hz, 3H). $^{13}\text{C NMR}$ (δ , 23 °C, 100 MHz, CDCl_3): 142.9, 142.7, 140.8, 139.2, 138.9, 136.9, 134.7, 130.3, 129.3, 129.0, 128.9, 127.3, 127.3, 127.2, 127.1, 127.1, 127.1, 127.1, 127.1, 127.0, 126.9, 126.8,

126.8, 52.6, 45.8, 44.1, 22.9, 21.3. HRMS-ESI: calculated for [M+H] = 454.1835, observed [M+H] = 454.1827.



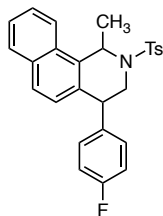
4-(4-(Chloromethyl)phenyl)-1-methyl-2-tosyl-1,2,3,4-tetrahydroisoquinoline

(V.5p). Prepared from 4-(chloromethyl)styrene (**V.3n**) and 1-((4-methyl-*N*-(1-phenylethyl)phenyl)sulfonamido)-pyridin-1-ium triflate (**V.2a**) and obtained as a white solid (32.3 mg, 76% yield, 1.4:1 dr). *Cis isomer*: $^1\text{H NMR}$ (δ , 23 °C, 400 MHz, CDCl_3): 7.73-7.70 (m, 2H), 7.38-7.35 (m, 2H), 7.25 (d, $J = 8.0$ Hz, 2H), 7.19 (t, $J = 7.4$ Hz, 1H), 7.13-7.10 (m, 3H), 7.05 (td, $J = 7.5, 1.3$ Hz, 1H), 6.72 (d, $J = 7.8$ Hz, 1H), 5.27 (q, $J = 6.8$ Hz, 1H), 4.09-4.02 (m, 2H), 3.36-3.29 (m, 1H), 2.39 (dd, $J = 0.7, 0.5$ Hz, 3H), 1.58-1.48 (m, 3H). $^{13}\text{C NMR}$ (δ , 23 °C, 100 MHz, CDCl_3): 143.4, 142.5, 138.4, 138.2, 136.6, 136.1, 129.8, 129.7, 129.6, 129.2, 127.1, 126.9, 126.7, 126.6, 52.3, 46.0, 45.6, 44.3, 22.8, 21.6. *Trans isomer*: $^1\text{H NMR}$ (δ , 23 °C, 400 MHz, CDCl_3): 7.42 (d, $J = 8.3$ Hz, 2H), 7.22-7.06 (m, 7H), 6.90 (d, $J = 7.5$ Hz, 1H), 6.81 (d, $J = 8.1$ Hz, 2H), 5.20 (q, $J = 6.7$ Hz, 1H), 4.52 (s, 2H), 4.14 (t, $J = 3.3$ Hz, 1H), 3.79-3.70 (m, 2H), 2.35 (s, 3H), 1.53 (d, $J = 6.7$ Hz, 3H). $^{13}\text{C NMR}$ (δ , 23 °C, 100 MHz, CDCl_3): 144.0, 143.0, 138.8, 137.0, 135.7, 134.6, 130.3, 129.5, 129.0, 128.5, 127.3, 127.2, 126.9, 52.5, 46.1, 45.6, 44.1, 22.5, 21.6. HRMS-ESI: calculated for [M+H] = 426.1289, observed [M+H] = 426.1285.



1-Methyl-4-(naphthalen-2-yl)-2-tosyl-1,2,3,4-tetrahydroisoquinoline (**V.5q**).

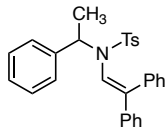
Prepared from 2-vinylnaphthalene (**V.30**) and 1-((4-methyl-*N*-(1-phenylethyl)phenyl)sulfonamido) pyridin-1-ium triflate (**V.2a**) and obtained as a white solid (22.6 mg, 53% yield, 1:1.9 dr). *Cis isomer*: $^1\text{H NMR}$ (δ , 23 °C, 400 MHz, CDCl_3): 7.86-7.81 (m, 3H), 7.75-7.73 (m, 2H), 7.67 (d, $J = 0.9$ Hz, 1H), 7.51 (dt, $J = 6.6, 3.0$ Hz, 2H), 7.26-7.14 (m, 5H), 7.06-7.01 (m, 1H), 6.75 (d, $J = 7.9$ Hz, 1H), 5.32 (q, $J = 6.7$ Hz, 1H), 4.23-4.12 (m, 2H), 3.46 (dd, $J = 13.7, 11.2$ Hz, 1H), 2.41 (s, 3H), 1.58 (d, $J = 6.8$ Hz, 3H). $^{13}\text{C NMR}$ (δ , 23 °C, 100 MHz, CDCl_3): 143.4, 139.4, 138.40, 138.3, 136.3, 133.6, 132.7, 129.8, 129.8, 128.7, 128.4, 127.85, 127.8, 127.1, 126.9, 126.7, 126.6, 126.6, 126.5, 126.1, 52.4, 45.5, 44.7, 22.9, 21.7. *Trans isomer*: $^1\text{H NMR}$ (δ , 23 °C, 400 MHz, CDCl_3): 7.76-7.73 (m, 1H), 7.54 (d, $J = 8.5$ Hz, 1H), 7.52-7.49 (m, 1H), 7.45-7.38 (m, 2H), 7.31-7.23 (m, 2H), 7.19-7.14 (m, 3H), 7.04-7.02 (m, 1H), 6.97-6.96 (m, 1H), 6.92 (s, 1H), 6.52 (d, $J = 8.0$ Hz, 2H), 5.29-5.24 (m, 1H), 4.28 (t, $J = 3.0$ Hz, 1H), 3.83 (qd, $J = 12.9, 3.2$ Hz, 2H), 2.03 (s, 3H), 1.66 (d, $J = 6.7$ Hz, 3H). $^{13}\text{C NMR}$ (δ , 23 °C, 100 MHz, CDCl_3): 142.7, 141.2, 139.1, 136.3, 134.5, 133.3, 132.4, 130.5, 128.9, 128.0, 127.9, 127.6, 127.5, 127.2, 127.2, 127.1, 127.0, 126.7, 125.9, 125.7, 52.5, 45.4, 44.5, 22.9, 21.4. HRMS-ESI: calculated for $[\text{M}+\text{H}] = 428.1712$, observed $[\text{M}+\text{H}] = 428.1677$.



4-(4-Fluorophenyl)-1-methyl-2-tosyl-1,2,3,4-tetrahydrobenzo[h]isoquinoline

(V.5r). Prepared from 4-fluorostyrene (**V.5b**) and 1-((4-methyl-*N*-(1-(naphthalen-1-yl)ethyl)phenyl)sulfonamido) pyridin-1-ium triflate (**V.2d**) and obtained as a white solid (22.7 mg, 51% yield, 1:1.5 dr). *Cis isomer*: $^1\text{H NMR}$ (δ , 23 °C, 400 MHz, CDCl_3): 8.03 (d, $J = 8.5$ Hz, 1H), 7.82 (dd, $J = 8.0, 0.3$ Hz, 1H), 7.64-7.59 (m, 2H), 7.53-7.51 (m, 1H), 7.45 (d, $J = 8.2$ Hz, 2H), 7.05 (d, $J = 8.1$ Hz, 2H), 6.98 (s, 1H), 6.72-6.69 (m, 4H), 5.92 (q, $J = 6.5$ Hz, 1H), 4.23 (d, $J = 3.8$ Hz, 1H), 3.95-3.78 (m, 2H), 2.35 (s, 3H), 1.65 (d, $J = 6.6$ Hz, 3H). $^{13}\text{C NMR}$ (δ , 23 °C, 100 MHz, CDCl_3): 161.7 (d, $^1J_{\text{C-F}} = 240$ Hz), 143.2, 139.59, 139.57, 137.2, 134.0, 133.0, 131.7, 130.07, 130.00, 129.48, 129.45, 129.1, 128.3, 127.9, 127.2, 126.8, 125.9, 123.3, 115.0 (d, $^2J_{\text{C-F}} = 20$ Hz), 49.7, 45.2, 44.2, 21.5, 20.5. $^{19}\text{F NMR}$ (δ , 23 °C, 376 MHz, CDCl_3): -116.7. *Trans isomer*: $^1\text{H NMR}$ (δ , 23 °C, 400 MHz, CDCl_3): 7.99-7.96 (m, 1H), 7.77 (dd, $J = 8.0, 0.3$ Hz, 1H), 7.65 (d, $J = 8.2$ Hz, 2H), 7.61-7.57 (m, 1H), 7.50 (dd, $J = 13.9, 7.8$ Hz, 2H), 7.12-7.06 (m, 4H), 7.01 (t, $J = 8.6$ Hz, 2H), 6.74 (d, $J = 8.6$ Hz, 1H), 5.93-5.88 (m, 1H), 4.22-4.13 (m, 2H), 3.44 (dd, $J = 11.8, 8.9$ Hz, 1H), 2.32 (s, 3H), 1.68 (d, $J = 6.8$ Hz, 3H). $^{13}\text{C NMR}$ (δ , 23 °C, 100 MHz, CDCl_3): 161.6 (d, $^1J_{\text{C-F}} = 240$ Hz), 143.3, 137.7, 133.7, 132.9, 132.4, 130.5, 130.4, 129.5, 129.3, 128.8, 127.4, 127.2, 126.95, 126.76, 125.7, 122.7, 116.0, 115.8 (d, $^2J_{\text{C-F}} = 20$ Hz), 49.4, 45.5, 43.8, 21.4, 21.3.

^{19}F NMR (δ , 23 °C, 376 MHz, CDCl_3): -115.3. HRMS-ESI: calculated for $[\text{M}+\text{H}] = 446.1585$, observed $[\text{M}+\text{H}] = 446.1573$.

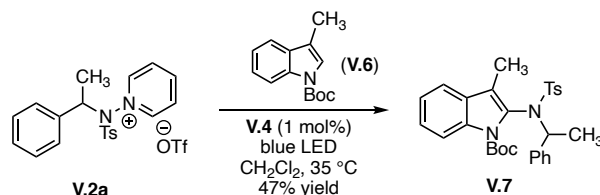


N-(2,2-diphenylvinyl)-4-methyl-*N*-(1-phenylethyl)benzenesulfonamide (**V.5s**).

Prepared from ethene-1,1-diyl-dibenzene (**V.3p**) and 1-((4-methyl-*N*-(1-phenylethyl)phenyl)sulfonamido)pyridin-1-ium triflate (**V.2a**) and obtained as a white solid (44.1 mg, 83% yield). ^1H NMR (δ , 23 °C, 400 MHz, CDCl_3): 7.59 (d, $J = 8.3$ Hz, 2H), 7.26-7.15 (m, 11H), 7.01-6.98 (m, 4H), 6.95-6.93 (m, 2H), 5.89 (s, 1H), 5.04 (q, $J = 7.1$ Hz, 1H), 2.44 (s, 3H), 1.23 (d, $J = 7.1$ Hz, 3H). ^{13}C NMR (δ , 23 °C, 100 MHz, CDCl_3): 147.9, 143.6, 141.1, 139.1, 138.2, 136.4, 130.2, 129.7, 128.5, 128.3, 128.3, 128.2, 128.0, 127.9, 127.8, 127.7, 120.6, 59.8, 21.7, 17.5. HRMS-ESI: calculated for $[\text{M}+\text{H}] = 454.1835$, observed $[\text{M}+\text{H}] = 454.1840$.

Trapping Intermediate Amidyl Radicals with Alternate Nucleophiles

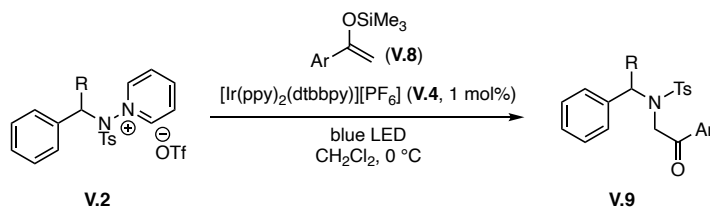
Synthesis of *tert*-butyl 3-methyl-2-((4-methyl-*N*-(1-phenylethyl)phenyl)sulfonamido)-1*H*-indole-1-carboxylate (**V.9**)



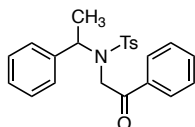
A 25-mL Schlenk tube was charged with 1-((4-methyl-*N*-(1-phenylethyl)phenyl)sulfonamido)pyridin-1-ium triflate (**V.2a**, 50.5 mg, 0.100 mmol, 1.00 equiv), *tert*-butyl 3-methyl-1*H*-indole-1-carboxylate (**V.6**, 69.1 mg, 0.300 mmol, 3.00 equiv), [Ir(ppy)₂(dtbbpy)][PF₆] (**V.4**, 1.0 mg, 1.10 μmol, 1.10 mol%), and CH₂Cl₂ (0.40 mL) under an N₂ atmosphere. The resulting solution was degassed by three freeze-pump-thaw cycles and stirred for 16 h at 35 °C while being irradiated by blue LEDs. The reaction mixture was concentrated under reduced pressure and the obtained residue was purified by SiO₂ gel chromatography (eluent 90:10 hexanes:ethyl acetate) to afford the title compound as a pale-yellow oil (**V.7**, 23.9 mg, 47% yield). Compound **V.7** is obtained as a mixture of two rotamers (characterization details below). Upon heating the mixture of rotamers to 50 °C in CDCl₃, a single compound is obtained (reported here as rotamer 1). For spectra obtained during the thermalization process, see Figure V-86. *Rotamer 1* ¹H NMR (δ, 23 °C, 400 MHz, CDCl₃): 8.15 (d, *J* = 8.4 Hz, 1H), 7.45-7.37 (m, 4H), 7.34-7.29 (m, 3H), 7.27-7.23 (m, 1H), 6.95 (d, *J* = 8.1 Hz, 2H), 6.91-6.89 (m, 2H), 5.57 (q, *J* = 7.1 Hz, 1H),

2.32 (s, 3H), 1.82 (s, 9H), 1.61 (s, 3H), 1.28 (d, $J = 7.1$ Hz, 3H). ^{13}C NMR (δ , 23 °C, 100 MHz, CDCl_3): 149.8, 142.9, 142.4, 138.8, 135.1, 129.0, 128.9, 128.4, 128.3, 128.0, 127.8, 127.5, 125.7, 122.3, 119.3, 119.2, 116.1, 84.6, 61.2, 28.5, 21.6, 21.1, 9.3. *Rotamer 2* ^1H NMR (δ , 23 °C, 400 MHz, CDCl_3): 7.90 (d, $J = 8.4$ Hz, 1H), 7.71 (d, $J = 8.3$ Hz, 2H), 7.43-7.41 (m, 1H), 7.28-7.20 (m, 4H), 7.13-7.08 (m, 5H), 5.43 (q, $J = 7.0$ Hz, 1H), 2.43 (s, 3H), 1.86 (s, 3H), 1.67 (d, $J = 7.0$ Hz, 3H), 1.50 (s, 9H). ^{13}C NMR (δ , 23 °C, 100 MHz, CDCl_3): 148.5, 143.1, 140.3, 139.6, 134.6, 129.4, 129.0, 128.6, 128.1, 128.0, 125.4, 122.2, 119.5, 119.2, 116.2, 83.7, 62.9, 28.5, 28.3, 21.8, 21.7, 10.0. HRMS-ESI: calculated for $[\text{M}+\text{H}] = 505.2156$, observed $[\text{M}+\text{H}] = 505.2158$.

Synthesis of 1-phenyl-2-((1-phenylethyl)amino)ethan-1-one (V.9)

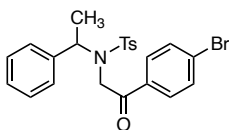


A 25-mL Schlenk tube was charged with *N*-benzylaminopyridinium (**V.2**, 0.100 mmol, 1.00 equiv), vinyl silyl ether (**V.8**, 0.200 mmol, 2.00 equiv), $[\text{Ir}(\text{ppy})_2(\text{dtbbpy})][\text{PF}_6]$ (**V.4**, 1.0 mg, 1.10 μmol , 1.10 mol%), and CH_2Cl_2 (0.40 mL) under an N_2 atmosphere. The resulting solution was degassed by three freeze-pump-thaw cycles and stirred for 16 h at 0 °C while being irradiated by blue LEDs. The reaction mixture was warmed to 23 °C and concentrated under reduced pressure. The obtained residue was purified by SiO_2 gel chromatography (eluent 90:10 hexanes:ethyl acetate) to afford the title compounds **V.9**.



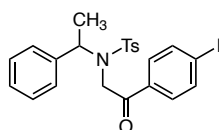
4-Methyl-N-(2-oxo-2-phenylethyl)-N-(1-phenylethyl)benzenesulfonamide (V.9a).

Prepared from 1-((4-methyl-*N*-(1-phenylethyl)phenyl)sulfonamido)pyridin-1-ium triflate (**V.2a**) and trimethyl((1-phenylvinyl)oxy)silane (**V.8a**) and obtained as a white solid (34.2 mg, 87% yield). ¹H NMR (δ , 23 °C, 400 MHz, CDCl₃): 7.93-7.91 (m, 2H), 7.76 (dd, J = 8.4, 1.3 Hz, 2H), 7.53 (t, J = 7.4 Hz, 1H), 7.41-7.34 (m, 4H), 7.24 (m, 1H), 5.18-5.13 (m, 1H), 4.73 (d, J = 18.1 Hz, 1H), 4.70 (d, J = 18.1 Hz, 1H), 4.34 (d, J = 18.1 Hz, 1H), 4.32 (d, J = 18.1 Hz, 1H), 2.47 (s, 3H), 1.43 (d, J = 7.1 Hz, 3H), 1.41 (d, J = 7.1 Hz, 3H). ¹³C NMR (δ , 23 °C, 100 MHz, CDCl₃): 194.9, 143.6, 139.3, 137.9, 135.2, 133.5, 129.6, 128.8, 128.6, 128.2, 128.0, 127.9, 55.8, 49.8, 21.8, 17.2. HRMS-ESI: calculated for [M+H] = 394.1471, observed [M+H] = 394.1467.

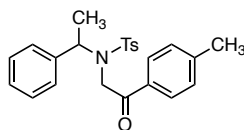


N-(2-(4-Bromophenyl)-2-oxoethyl)-4-methyl-*N*-(1-phenylethyl)benzenesulfonamide (**V.9b**). Prepared from 1-((4-methyl-*N*-(1-phenylethyl)phenyl)sulfonamido)pyridin-1-ium triflate (**V.2a**) and ((1-(4-bromophenyl)vinyl)oxy)trimethylsilane (**V.8b**) and obtained as a white solid (41.8 mg, 89% yield). ¹H NMR (δ , 23 °C, 400 MHz, CDCl₃): 7.89 (d, J = 8.3 Hz, 2H), 7.59 (d, J = 8.6 Hz, 2H), 7.51 (d, J = 8.5 Hz, 2H), 7.36 (d, J = 8.2 Hz, 2H), 7.22 (s, 5H), 5.14 (t, J = 7.1

Hz, 1H), 4.56 (d, $J = 17.8$ Hz, 1H), 4.30 (d, $J = 17.8$ Hz, 1H), 2.47 (s, 3H), 1.37 (d, $J = 7.1$ Hz, 3H). ^{13}C NMR (δ , 23 °C, 100 MHz, CDCl_3): 194.2, 143.8, 139.0, 137.5, 133.9, 132.0, 129.7, 129.6, 128.6, 128.5, 128.1, 128.0, 127.9, 55.8, 49.7, 21.8, 16.7. HRMS-ESI: calculated for $[\text{M}+\text{H}] = 472.0577$, observed $[\text{M}+\text{H}] = 472.0573$.

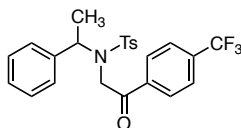


N-(2-(4-Iodophenyl)-2-oxoethyl)-4-methyl-*N*-(1-phenylethyl)benzenesulfonamide (**V.9c**). Prepared from 1-((4-methyl-*N*-(1-phenylethyl)phenyl)sulfonamido)pyridin-1-ium triflate (**V.2a**) and ((1-(4-iodophenyl)vinyl)oxy)trimethylsilane (**V.8c**) and obtained as a pale yellow solid (44.6 mg, 86% yield). ^1H NMR (δ , 23 °C, 400 MHz, CDCl_3): 7.89 (d, $J = 8.3$ Hz, 2H), 7.74 (d, $J = 8.5$ Hz, 2H), 7.43 (d, $J = 8.5$ Hz, 2H), 7.36 (s, 2H), 7.22 (s, 5H), 5.15 (q, $J = 7.1$ Hz, 1H), 4.55 (d, $J = 17.8$ Hz, 1H), 4.28 (d, $J = 17.8$ Hz, 1H), 2.47 (s, 3H), 1.37 (d, $J = 7.1$ Hz, 3H). ^{13}C NMR (δ , 23 °C, 100 MHz, CDCl_3): 194.5, 143.8, 139.0, 138.0, 137.5, 134.4, 129.7, 129.4, 128.6, 128.12, 127.94, 101.4, 55.8, 49.7, 21.8, 16.8. HRMS-ESI: calculated for $[\text{M}+\text{H}] = 520.0438$, observed $[\text{M}+\text{H}] = 520.0435$.

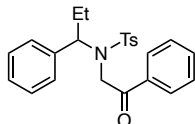


4-Methyl-*N*-(2-oxo-2-(*p*-tolyl)ethyl)-*N*-(1-phenylethyl)benzenesulfonamide (**V.9d**). Prepared from 1-((4-methyl-*N*-(1-phenylethyl)phenyl)sulfonamido)pyridin-1-ium triflate (**V.2a**) and trimethyl((1-(*p*-tolyl)vinyl)oxy)silane (**V.8d**) and obtained as a white solid

(33.1 mg, 81% yield). ^1H NMR (δ , 23 °C, 400 MHz, CDCl_3): 7.92 (d, J = 8.3 Hz, 2H), 7.66 (d, J = 8.3 Hz, 2H), 7.34 (d, J = 8.0 Hz, 2H), 7.26-7.23 (m, 5H), 7.19 (d, J = 8.0 Hz, 2H), 5.15 (q, J = 7.1 Hz, 1H), 4.70 (d, J = 18.2 Hz, 1H), 4.28 (d, J = 18.2 Hz, 1H), 2.46 (s, 3H), 2.38 (s, 3H), 1.40 (d, J = 7.1 Hz, 3H). ^{13}C NMR (δ , 23 °C, 100 MHz, CDCl_3): 194.3, 144.2, 143.4, 139.2, 132.6, 129.4, 129.3, 128.4, 128.1, 128.0, 127.8, 127.7, 56.2, 49.2, 21.7, 21.6, 17.3. HRMS-ESI: calculated for $[\text{M}+\text{H}] = 408.1628$, observed $[\text{M}+\text{H}] = 408.1622$.

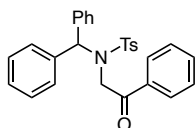


4-Methyl-N-(2-oxo-2-(4-(trifluoromethyl)phenyl)ethyl)-N-(1-phenylethyl)benzenesulfonamide (V.9e). Prepared from 1-((4-methyl-*N*-(1-phenylethyl)phenyl)sulfonamido)pyridin-1-ium triflate (**V.2a**) and trimethyl((1-(4-(trifluoromethyl)phenyl)vinyl)oxy)silane (**V.8e**, 4.00 equiv) and obtained as a yellow oil (36.9 mg, 80% yield). ^1H NMR (δ , 23 °C, 400 MHz, CDCl_3): 7.89 (d, J = 8.4 Hz, 2H), 7.80 (d, J = 8.1 Hz, 2H), 7.62 (d, J = 8.2 Hz, 2H), 7.37 (d, J = 8.0 Hz, 2H), 7.21 (s, 5H), 5.16 (q, J = 7.0 Hz, 1H), 4.55 (d, J = 17.7 Hz, 1H), 4.37 (d, J = 17.7 Hz, 1H), 2.48 (s, 3H), 1.37 (d, J = 7.1 Hz, 3H). ^{13}C NMR (δ , 23 °C, 100 MHz, CDCl_3): 194.4, 143.8, 138.7, 137.8, 137.2, 134.4 ($^2J_{\text{C-F}} = 33.0$ Hz), 129.7, 128.4, 128.3, 128.1, 127.9, 127.8, 125.6 ($^3J_{\text{C-F}} = 3.7$ Hz), 123.5 ($^1J_{\text{C-F}} = 271$ Hz), 55.6, 49.9, 21.6, 16.3. HRMS-ESI: calculated for $[\text{M}+\text{H}] = 462.1345$, observed $[\text{M}+\text{H}] = 462.1339$.



4-Methyl-N-(2-oxo-2-phenylethyl)-N-(1-phenylpropyl)benzenesulfonamide (V.9f).

Prepared from 1-((4-methyl-*N*-(1-phenylpropyl)phenyl)sulfonamido)pyridin-1-ium triflate (**V.2b**) and trimethyl((1-phenylvinyl)oxy)silane (**V.8a**, 4.00 equiv) and obtained as a pale-yellow oil (26.8 mg, 66% yield). ^1H NMR (δ , 23 °C, 400 MHz, CDCl_3): 7.85 (d, $J = 8.3$ Hz, 2H), 7.76 (dd, $J = 8.4, 1.2$ Hz, 2H), 7.54 (tt, $J = 7.4, 1.5$ Hz, 1H), 7.40 (t, $J = 7.7$ Hz, 2H), 7.33 (d, $J = 8.0$ Hz, 2H), 7.25-7.23 (m, 3H), 7.18-7.16 (m, 2H), 4.84 (dd, $J = 9.6, 5.8$ Hz, 1H), 4.71 (d, $J = 18.3$ Hz, 1H), 4.33 (d, $J = 18.3$ Hz, 1H), 2.46 (s, 3H), 1.96-1.78 (m, 2H), 0.78 (t, $J = 7.3$ Hz, 3H). ^{13}C NMR (δ , 23 °C, 100 MHz, CDCl_3): 194.9, 143.5, 138.1, 137.3, 135.3, 133.5, 129.5, 128.8, 128.7, 128.2, 128.1, 128.0, 62.8, 50.0, 24.6, 21.7, 11.6. HRMS-ESI: calculated for $[\text{M}+\text{H}] = 408.1628$, observed $[\text{M}+\text{H}] = 408.1627$.



N-benzhydryl-4-methyl-N-(2-oxo-2-phenylethyl)benzenesulfonamide (V.9g).

Prepared from 1-((*N*-benzhydryl-4-methylphenyl)sulfonamido)pyridin-1-ium triflate (**V.2c**) and trimethyl((1-phenylvinyl)oxy)silane (**V.8a**, 4.00 equiv) and obtained as a white solid (35.1 mg, 77% yield). ^1H NMR (δ , 23 °C, 400 MHz, CDCl_3): 7.79 (d, $J = 8.3$ Hz, 2H), 7.65 (d, $J = 7.1$ Hz, 2H), 7.50 (t, $J = 7.4$ Hz, 1H), 7.36 (t, $J = 7.7$ Hz, 2H), 7.24 (d, $J = 8.1$ Hz, 2H), 7.20-7.18 (m, 6H), 7.13 (dd, $J = 6.7, 2.9$ Hz, 4H), 6.25 (s, 1H), 4.85 (s, 2H),

2.42 (s, 3H). ^{13}C NMR (δ , 23 °C, 100 MHz, CDCl_3): 193.7, 143.4, 138.6, 137.7, 135.3, 133.3, 129.3, 129.2, 128.7, 128.4, 128.4, 127.8, 127.7, 65.4, 51.6, 21.7. HRMS-ESI: calculated for $[\text{M}+\text{H}] = 456.1628$, observed $[\text{M}+\text{H}] = 456.1622$.

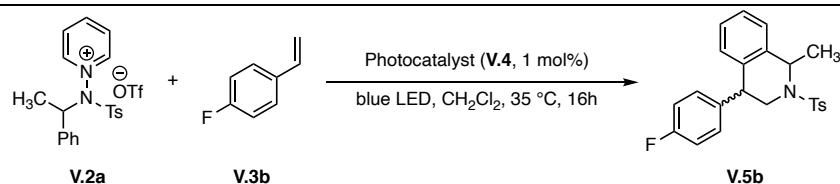
Optimization studies for tetrahydroisoquinoline synthesis

Table V-1. Examination of the impact of solvent on tetrahydroisoquinoline synthesis. A 25-mL Schlenk tube was charged with 1-((4-methyl-*N*-(1-phenylethyl)phenyl)sulfonamido)pyridine-1-ium triflate (**V.2a**, 25.1 mg, 50.0 μmol , 1.00 equiv), 4-fluorostyrene (**V.3b**, 6.1 mg, 50 μmol , 1.0 equiv), $[\text{Ir}(\text{ppy})_2(\text{dtbbpy})][\text{PF}_6]$ (**V.4**, 0.5 mg, 1 mol%), and solvent (2.0 mL) under nitrogen atmosphere. The resulting solution was degassed by three freeze-pump-thaw cycles and stirred at 35 °C under blue LED irradiation for 16 h. The reaction mixture was then concentrated under reduced pressure and analyzed via ^1H and ^{19}F NMR using mesitylene as an internal standard.

Entry	Solvent	Yield (%)
1	CH_2Cl_2	44
2	MeCN	40
3	THF	0
4	HFIP	0
5	Toluene	<5
6	$\text{CH}_2\text{Cl}_2/\text{Toluene}$ (1:1)	<5

Table V-2. Examination of the impact of photocatalyst on tetrahydroisoquinoline synthesis. A 25-mL Schlenk tube was charged with 1-((4-methyl-*N*-(1-

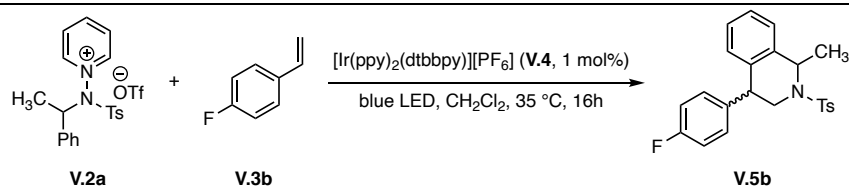
phenylethyl)phenyl)sulfonamido)pyridin-1-ium triflate (**V.2a**, 25.1 mg, 50.0 μmol , 1.00 equiv), 4-fluorostyrene (**V.3b**, 6.1 mg, 50 μmol , 1.0 equiv), photocatalyst (**V.4**, 1 mol%), and CH_2Cl_2 (2.0 mL) under an N_2 atmosphere. The resulting solution was degassed by three freeze-pump-thaw cycles and stirred at 35 $^\circ\text{C}$ under blue LED irradiation for 16 h. The reaction mixture was then concentrated under reduced pressure and analyzed via ^1H and ^{19}F NMR using mesitylene as an internal standard.



Entry	Photocatalyst	Yield (%)
1	$[\text{Ir}(\text{ppy})_2(\text{dtbbpy})][\text{PF}_6]$	44
2	$[\text{Ir}(\text{dF}(\text{CF}_3)\text{ppy})_2(\text{dtbbpy})][\text{PF}_6]$	25
3	$[\text{Ru}(\text{bpy})_3][\text{PF}_6]_2$	<5
4	Eosin Y*	0

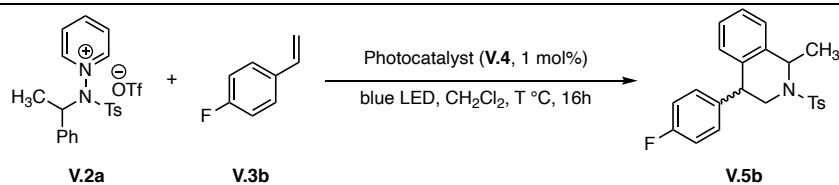
* = green LED instead of blue LED

Table V-3. Examination of the impact of reagent stoichiometry on tetrahydroisoquinoline synthesis. A 25-mL Schlenk tube was charged with 1-((4-methyl-*N*-(1-phenylethyl)phenyl)sulfonamido)pyridin-1-ium triflate (**V.2a**), 4-fluorostyrene (**V.3b**), [Ir(ppy)₂(dtbbpy)][PF₆] (**V.4**, 0.5 mg, 1 mol%), and CH₂Cl₂ under an N₂ atmosphere. The resulting solution was degassed by three freeze-pump-thaw cycles and stirred at 35 °C under blue LED irradiation for 16 h. The reaction mixture was then concentrated under reduced pressure and analyzed via ¹H and ¹⁹F NMR using mesitylene as an internal standard.



Entry	Aminopyridinium (equiv)	4-Fluorostyrene (equiv)	CH ₂ Cl ₂ (mL)	Yield (%)
1	1.5	1.0	2.0	61
2	1.0	4.0	2.0	80
3	1.0	2.5	0.20	81
4	1.0	1.6	0.20	80
5	1.0	1.2	0.20	65

Table V-4. Examination of the impact of temperature on tetrahydroisoquinoline synthesis. A 25-mL Schlenk tube was charged with 1-((4-methyl-*N*-(1-phenylethyl)phenyl)sulfonamido) pyridin-1-ium triflate (**V.2a**, 25.1 mg, 50.0 μmol , 1.00 equiv), 4-fluorostyrene (**V.3b**, 9.8 mg, 80 μmol , 1.6 equiv), [Ir(ppy)₂(dtbbpy)][PF₆] (**V.4**, 0.5 mg, 1 mol%), and CH₂Cl₂ (0.20 mL) under an N₂ atmosphere. The resulting solution was degassed by three freeze-pump-thaw cycles and stirred at the indicated temperature under blue LED irradiation for 16 h. The reaction mixture was then concentrated under reduced pressure and analyzed via ¹H and ¹⁹F NMR using mesitylene as an internal standard.



Entry	Olefin (equiv)	Temp. (°C)	Yield (%)
1	1.6	35	80
2	1.6	0	82
3	2.5	0	67
4	1.6	-35	42 *

* = reaction time 8 h instead of 16 h

X-Ray Diffraction Data

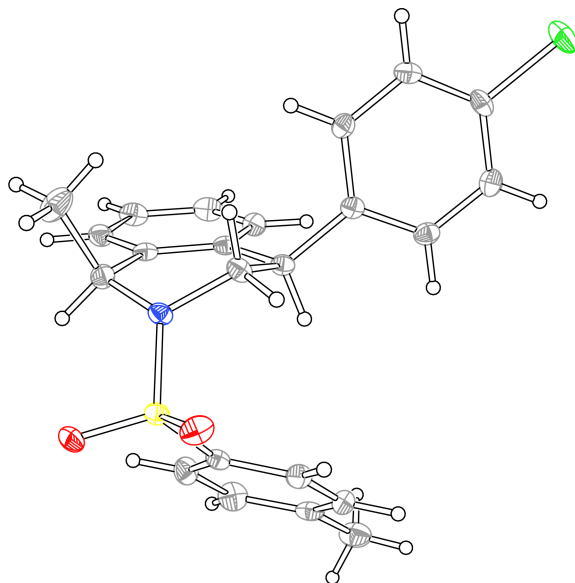


Figure V-6. Displacement ellipsoid plot for *cis*-V.5e plotted at 50% probability. The crystalline sample used in this diffraction experiment was obtained from a concentrated CH_2Cl_2 solution layered with hexanes at 23 °C.

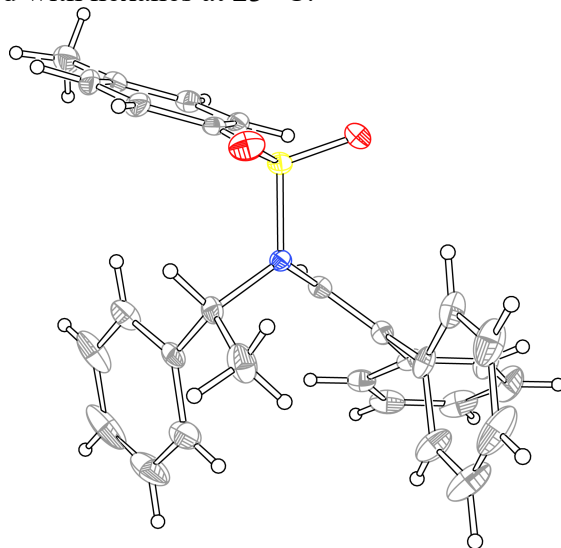


Figure V-7. Displacement ellipsoid plot of V.5s plotted at 50% probability. The crystalline sample used in this diffraction experiment was obtained from a concentrated CH_2Cl_2 solution layered with hexanes at 23 °C.

Table V-5. X-ray experimental details of *cis*-V.5e (CCDC 2084507).

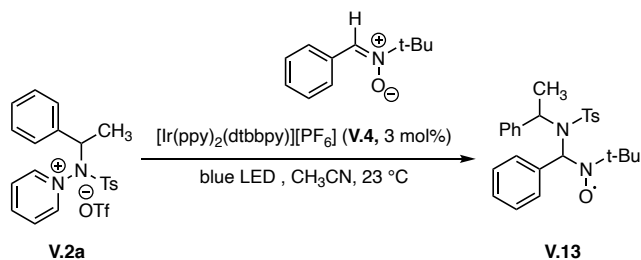
Crystal data	
Chemical formula	2(C ₂₃ H ₂₂ ClNO ₂ S)
<i>M_r</i>	823.85
Crystal system, space group	Orthorhombic, <i>Pbca</i>
Temperature (K)	110
<i>a</i> , <i>b</i> , <i>c</i> (Å)	11.566(1), 18.165(1), 19.229(1)
<i>V</i> (Å ³)	4039.9(5)
<i>Z</i>	4
Radiation type	Mo <i>K</i> α
μ (mm ⁻¹)	0.31
Crystal size (mm)	1.0 × 0.3 × 0.1
Data collection	
Diffractometer	Bruker <i>APEX</i> -II CCD
Absorption correction	Multi-scan <i>SADABS2016/2</i> (Bruker,2016/2) was used for absorption correction. <i>wR2(int)</i> was 0.1155 before and 0.0450 after correction. The ratio of minimum to maximum transmission is 0.8018. The λ/2 correction factor is not present.
<i>T_{min}</i> , <i>T_{max}</i>	0.598, 0.746
No. of measured, independent and observed [<i>I</i> > 2σ(<i>I</i>)] reflections	15721, 4507, 3512
<i>R_{int}</i>	0.051
(sin θ/λ) _{max} (Å ⁻¹)	0.648
Refinement	
<i>R</i> [<i>F</i> ² > 2σ(<i>F</i> ²)], <i>wR</i> (<i>F</i> ²), <i>S</i>	0.045, 0.107, 1.02
No. of reflections	4507
No. of parameters	255
H-atom treatment	H-atom parameters constrained
Δρ _{max} , Δρ _{min} (e Å ⁻³)	0.37, -0.54

Table V-6. X-ray experimental details of V.5s (CCDC 2084508).

Crystal data	
Chemical formula	C ₂₉ H ₂₇ NO ₂ S
<i>M_r</i>	453.57
Crystal system, space group	Monoclinic, <i>P</i> 2 ₁ / <i>c</i>
Temperature (K)	110
<i>a</i> , <i>b</i> , <i>c</i> (Å)	11.070(1), 7.4659(8), 29.942(3)
β (°)	91.619(3)
<i>V</i> (Å ³)	2473.6(5)
<i>Z</i>	4
Radiation type	Mo <i>K</i> α
μ (mm ⁻¹)	0.16
Crystal size (mm)	0.3 × 0.2 × 0.1
Data collection	
Diffractometer	Bruker <i>APEX-II</i> CCD
Absorption correction	Multi-scan <i>SADABS2016/2</i> (Bruker,2016/2) was used for absorption correction. <i>wR2(int)</i> was 0.0815 before and 0.0527 after correction. The ratio of minimum to maximum transmission is 0.9427. The λ/2 correction factor is not present.
<i>T_{min}</i> , <i>T_{max}</i>	0.703, 0.746
No. of measured, independent and observed [<i>I</i> > 2σ(<i>I</i>)] reflections	42772, 5685, 4789
<i>R_{int}</i>	0.046
(sin θ/λ) _{max} (Å ⁻¹)	0.651
Refinement	
<i>R</i> [<i>F</i> ² > 2σ(<i>F</i> ²)], <i>wR</i> (<i>F</i> ²), <i>S</i>	0.045, 0.107, 1.05
No. of reflections	5685
No. of parameters	300
H-atom treatment	H-atom parameters constrained
Δρ _{max} , Δρ _{min} (e Å ⁻³)	0.45, -0.45

Mechanistic Experiments

Spin-Trapping Experiments



A 25-mL Schlenk tube was charged with 1-((4-methyl-*N*-(1-phenylethyl)phenyl)sulfonamido) pyridin-1-ium triflate (**V.2a**, 15.1 mg, 30.0 μ mol, 1.00 equiv), [Ir(ppy)₂(dtbbpy)][PF₆] (**V.4**, 0.8 mg, 2.91 mol%), *N*-*tert*-butyl- α -phenylnitronium (PBN, 6.6 mg, 37 μ mol, 1.2 equiv), and CH₃CN (0.50 mL) under N₂ atmosphere. The resulting solution was degassed by three freeze-pump-thaw cycles and 50 μ L of the resulting solution was transferred to a 2 mm EPR tube inside a glove bag. The EPR tube was inserted into the probe and a background dark spectrum was collected. The tube was irradiated for 45 min at which time an EPR spectrum was collected again (Figure V-8). This spectrum revealed the presence of spin-trapped radical **V.13**.

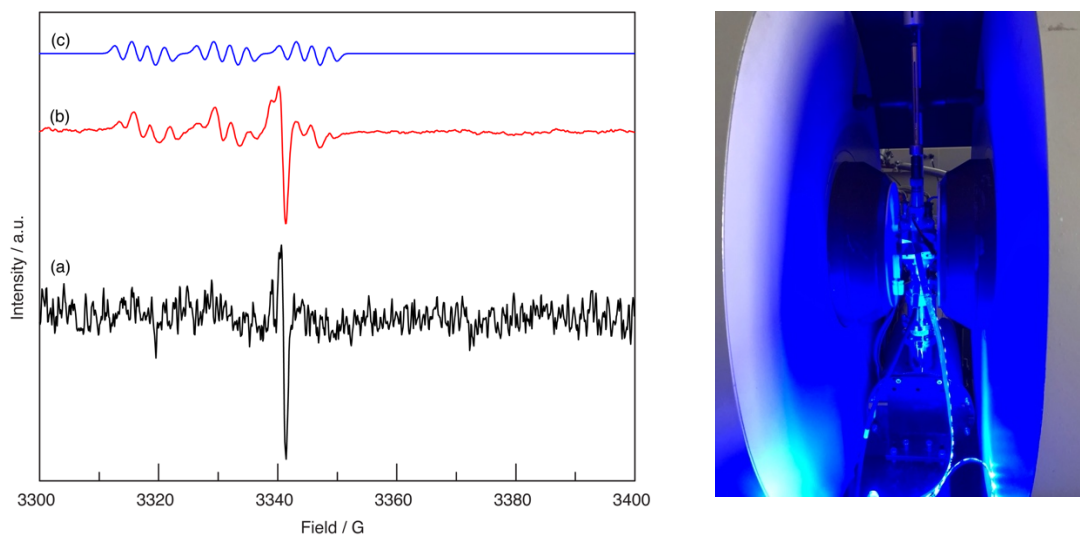


Figure V-8. EPR spectra for photochemical deaminative functionalization of V.2a in presence of PBN was obtained in acetonitrile. Left: EPR spectra of sample (a) without photolysis, (b) with blue light irradiation, and (c) simulated spectrum. The observed triplet of quartet in the photolyzed spectrum is attributed to PBN-trapped amidyl radical (**V.13**) with $a_{N(\text{PBN})} = 13.85$ G, $a_{\text{H}} = 3.20$ G, and $a_{N(\text{amidyl})} = 2.52$ G. The apparent triplet of quartet is due to the unresolved/overlapped hyperfine couplings from a_{H} and $a_{N(\text{amidyl})}$. Formation of PBN-trapped amidyl radical **V.13** was further confirmed by mass analysis of the EPR sample where HRMS-APCI: calculated for $[\text{M}^{\bullet}] = 451.2055$, observed $[\text{M}^{\bullet}] = 451.2037$. Right: Experimental setup used to observe radicals generated by blue light irradiation by EPR spectroscopy.

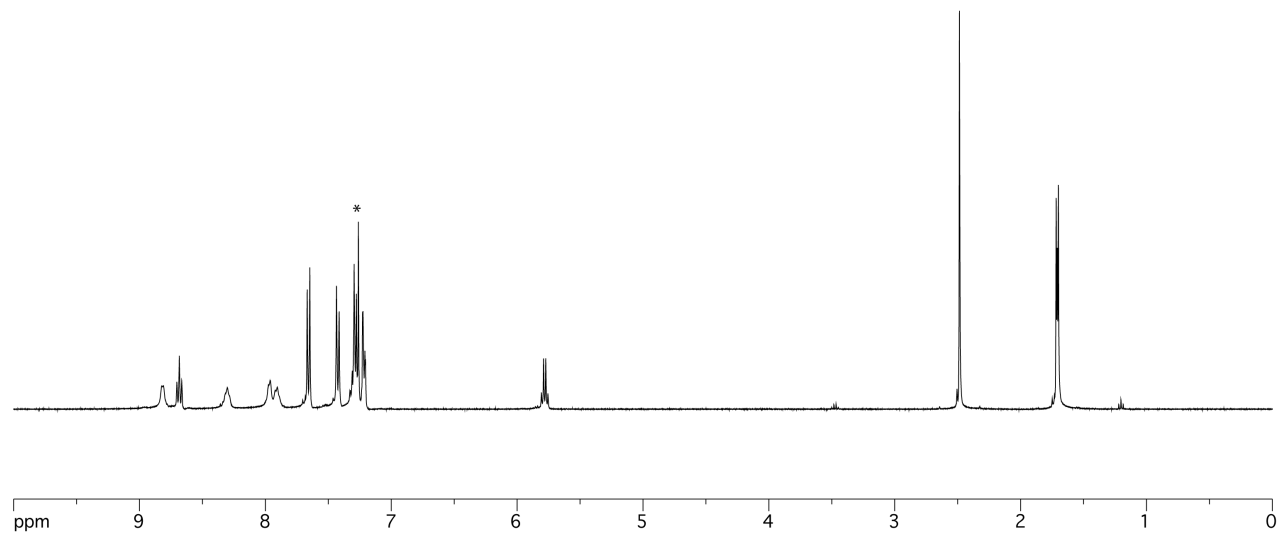
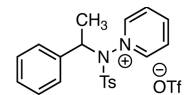


Figure V-9. ¹H NMR spectrum of compound V.2a in CDCl₃ (400 MHz) at 23 °C.*CDCl₃ solvent peak.

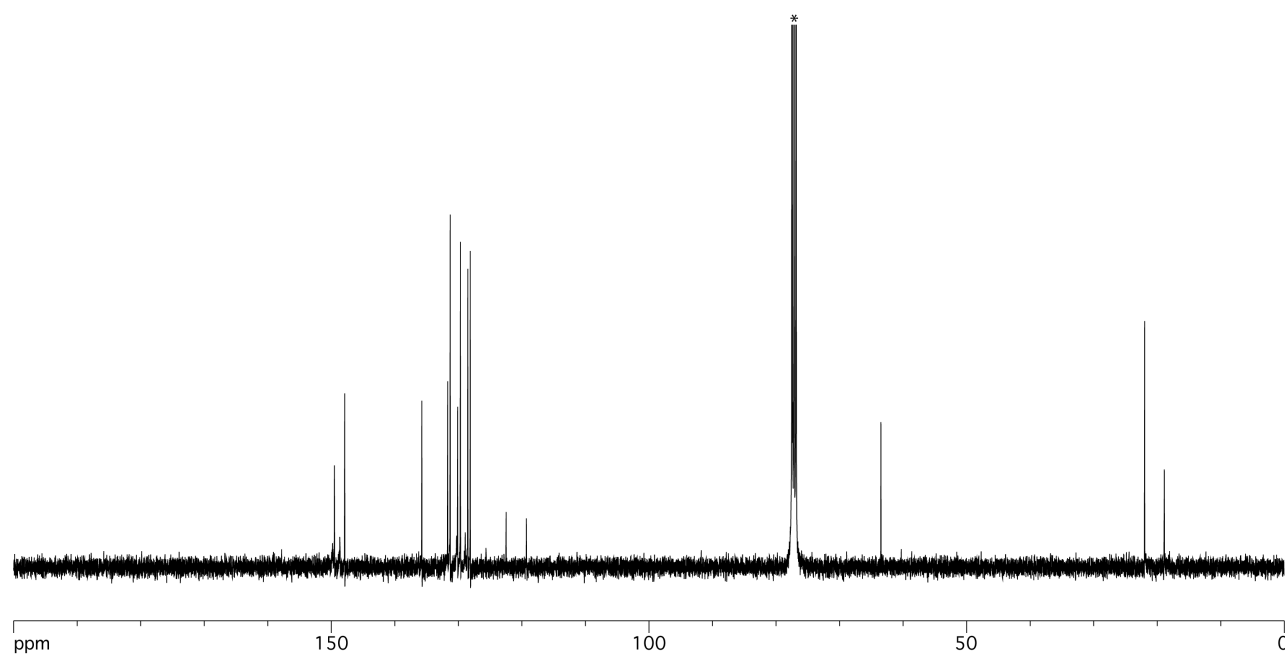
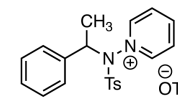


Figure V-10. ^{13}C NMR spectrum of compound V.2a in CDCl_3 (100 MHz) at 23 °C. * CDCl_3 solvent peak.

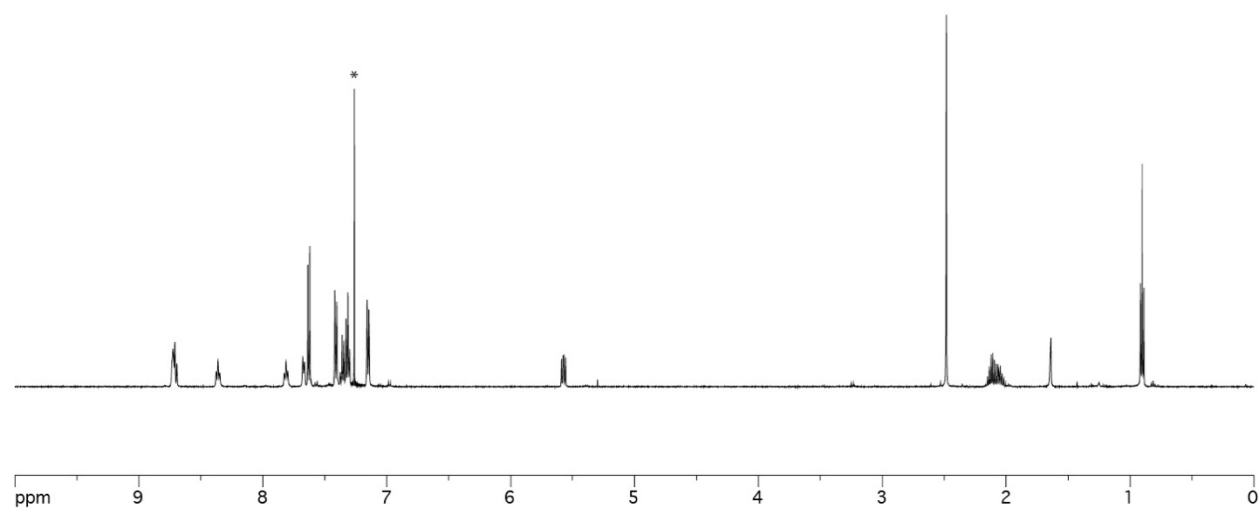
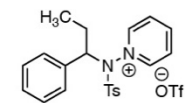


Figure V-11. ¹H NMR spectrum of compound V.2b in CDCl₃ (400 MHz) at 23 °C.*CDCl₃ solvent peak.

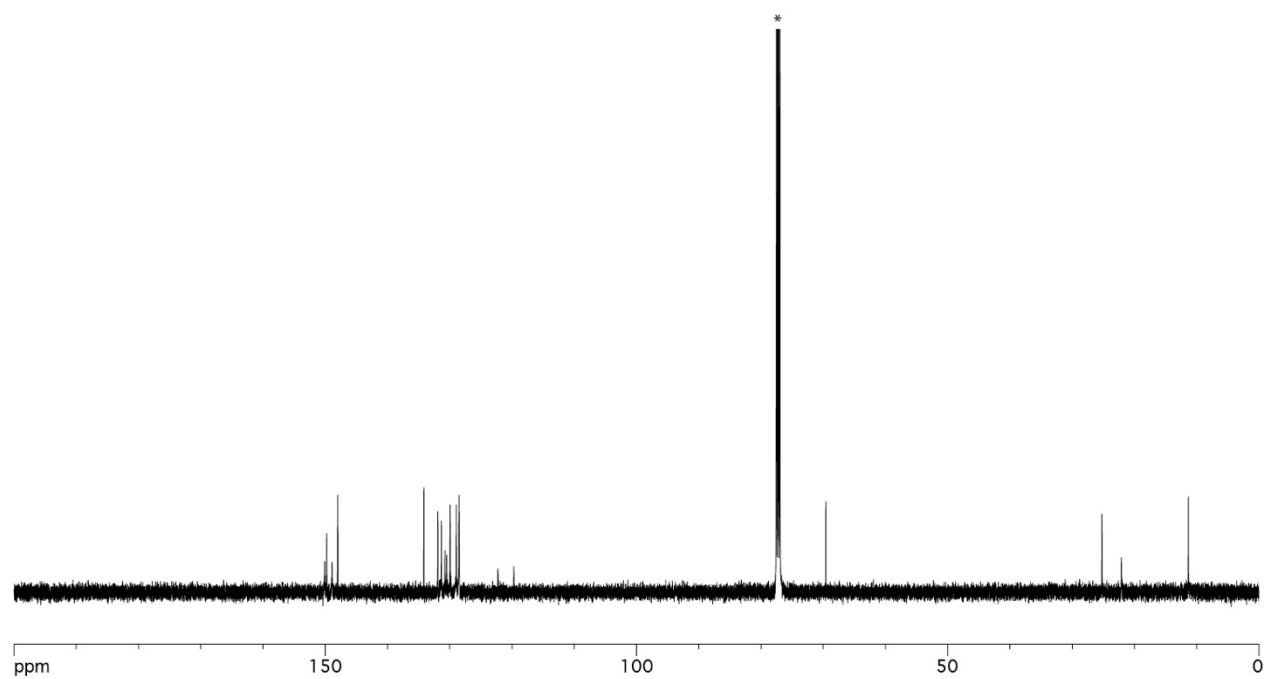
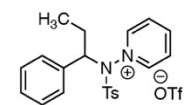


Figure V-12. ¹³C NMR spectrum of compound V.2b in CDCl₃ (100 MHz) at 23 °C.*CDCl₃ solvent peak.

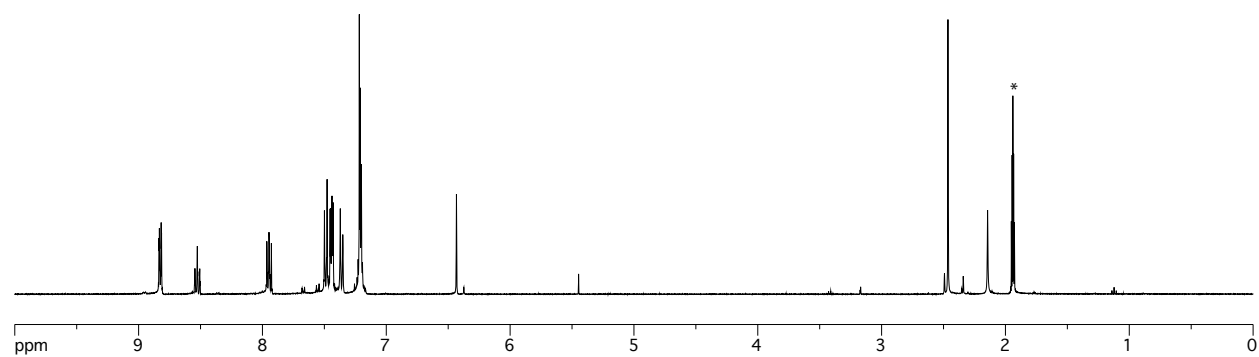
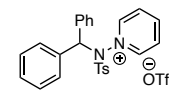


Figure V-13. ^1H NMR spectrum of compound V.2c in CD_3CN (400 MHz) at 23 °C.* CD_3CN solvent peak.

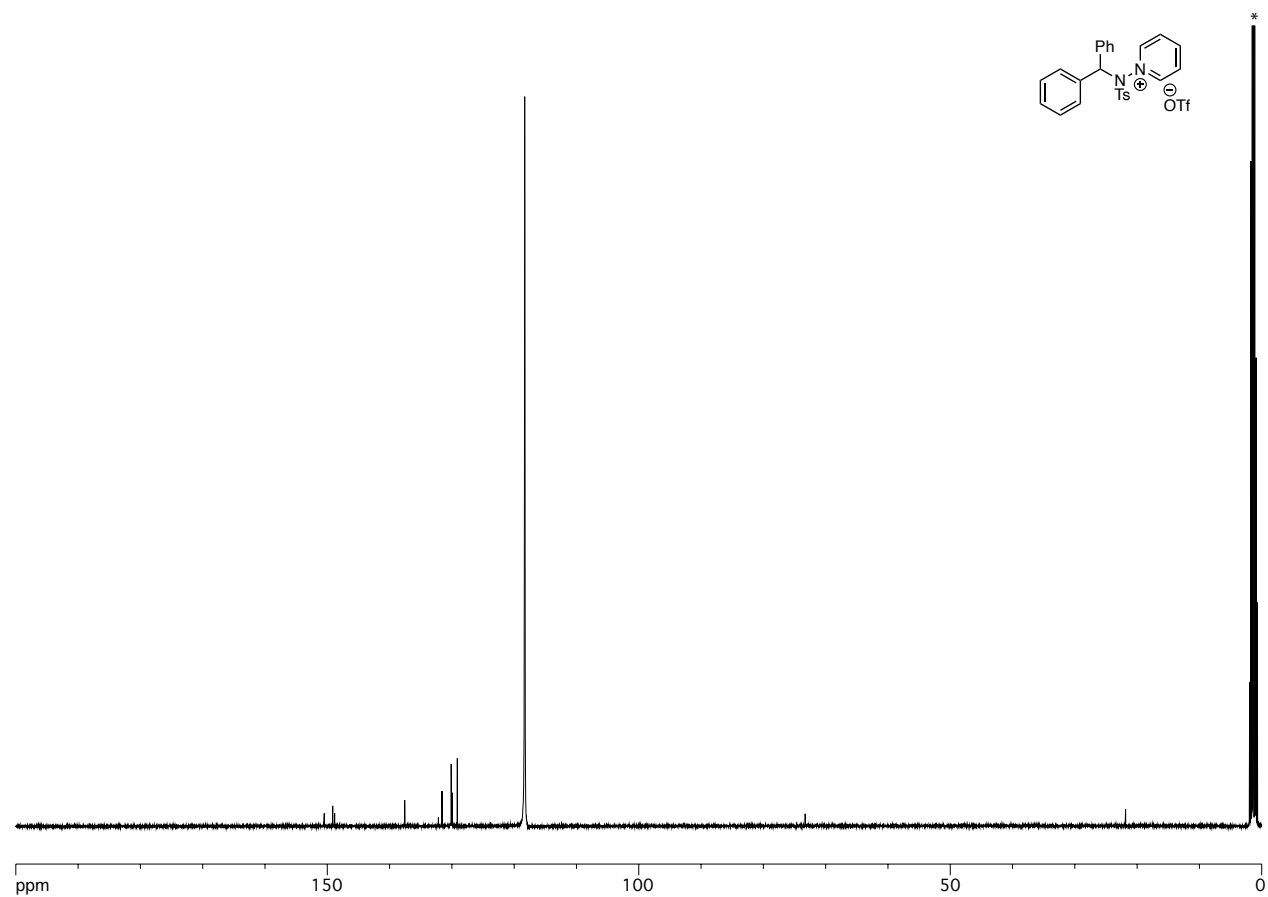


Figure V-14. ^{13}C NMR spectrum of compound V.2c in CD_3CN (100 MHz) at 23 °C. * CD_3CN solvent peak.

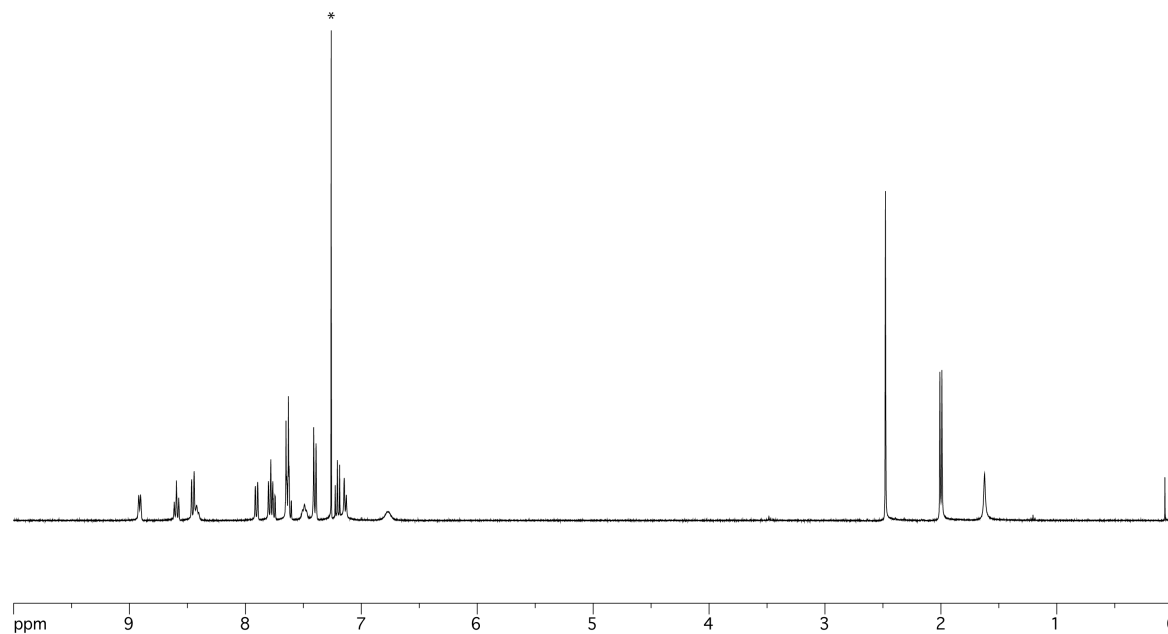
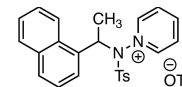


Figure V-15. ^1H NMR spectrum of compound V.2d in CDCl_3 (400 MHz) at 23 °C.* CDCl_3 solvent peak.

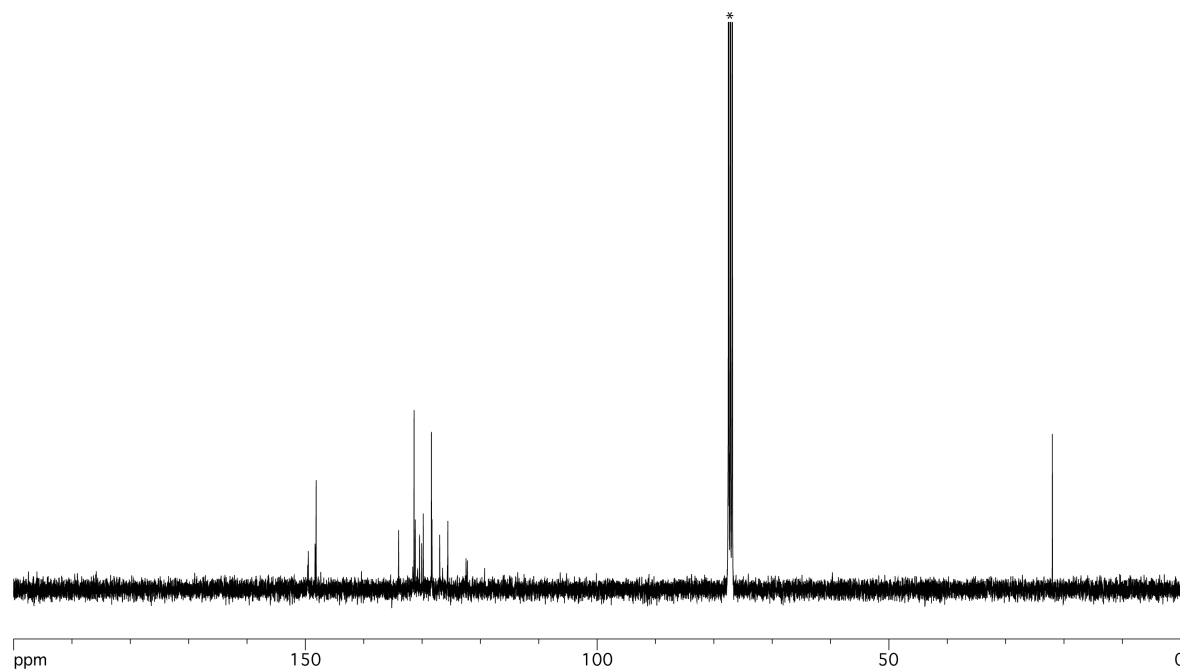
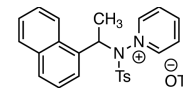


Figure V-16. ^{13}C NMR spectrum of compound V.2d in CDCl_3 (100 MHz) at 23 °C. * CDCl_3 solvent peak.

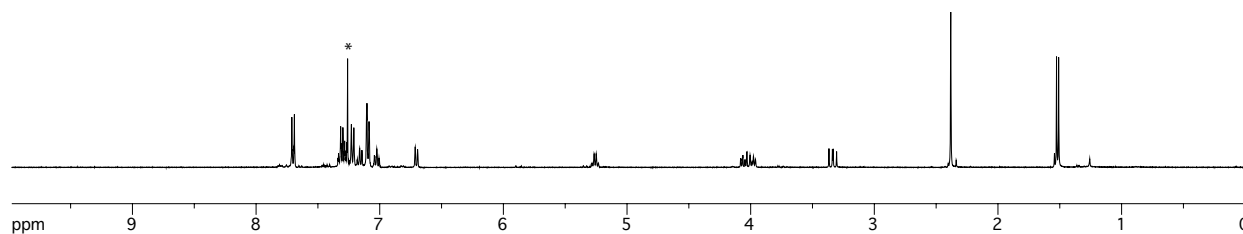
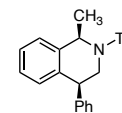


Figure V-17. ^1H NMR spectrum of *cis*-V.5a in CDCl_3 (400 MHz) at 23 °C. * CDCl_3 solvent peak.

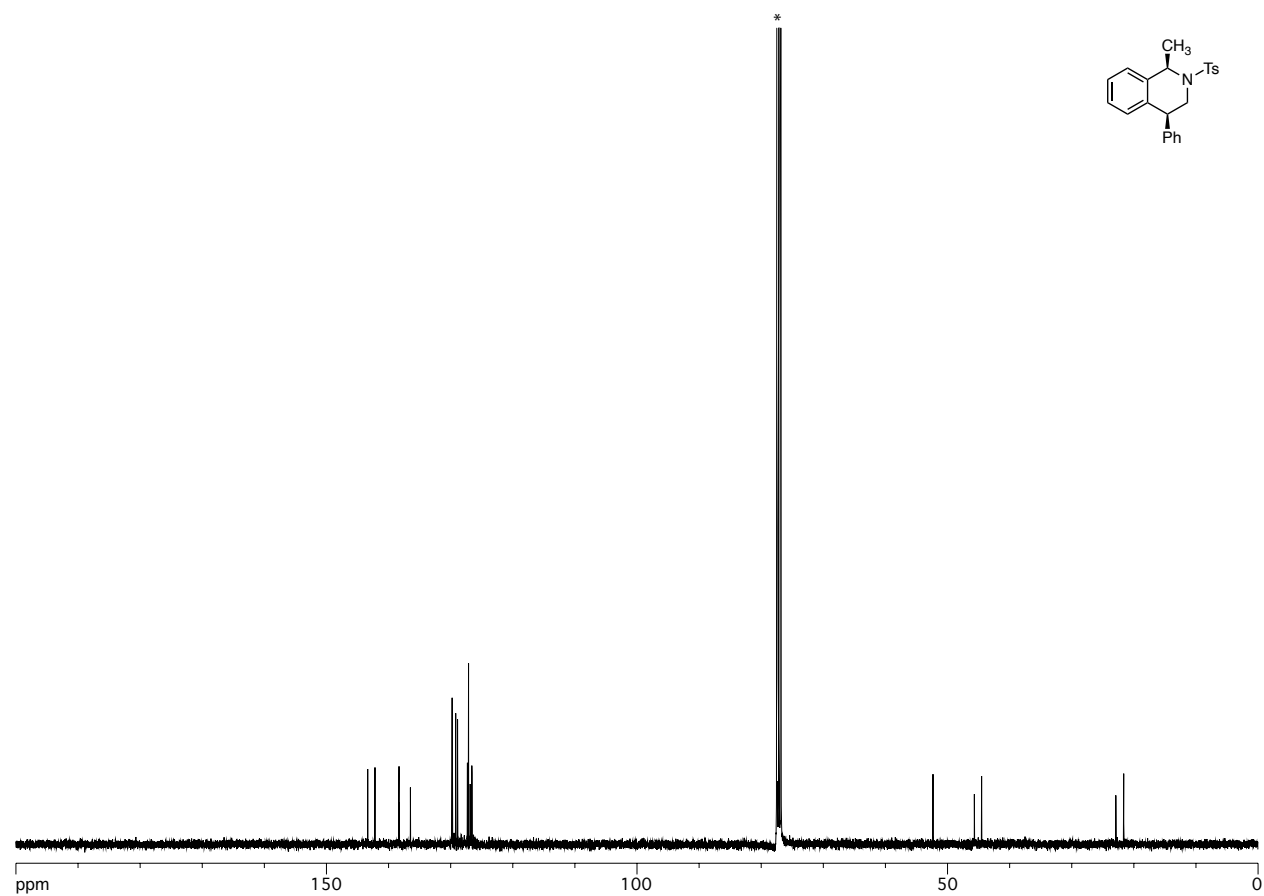


Figure V-18. ¹³C NMR spectrum of *cis*-V.5a in CDCl₃ (100 MHz) at 23 °C.*CDCl₃ solvent peak.

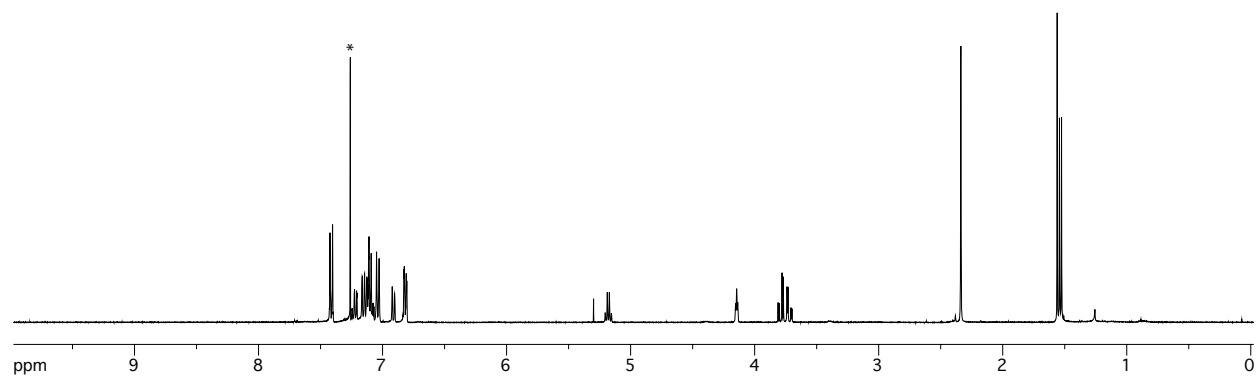
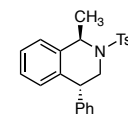


Figure V-19. ¹H NMR spectrum of *trans*-V.5a in CDCl₃ (400 MHz) at 23 °C. *CDCl₃ solvent peak.

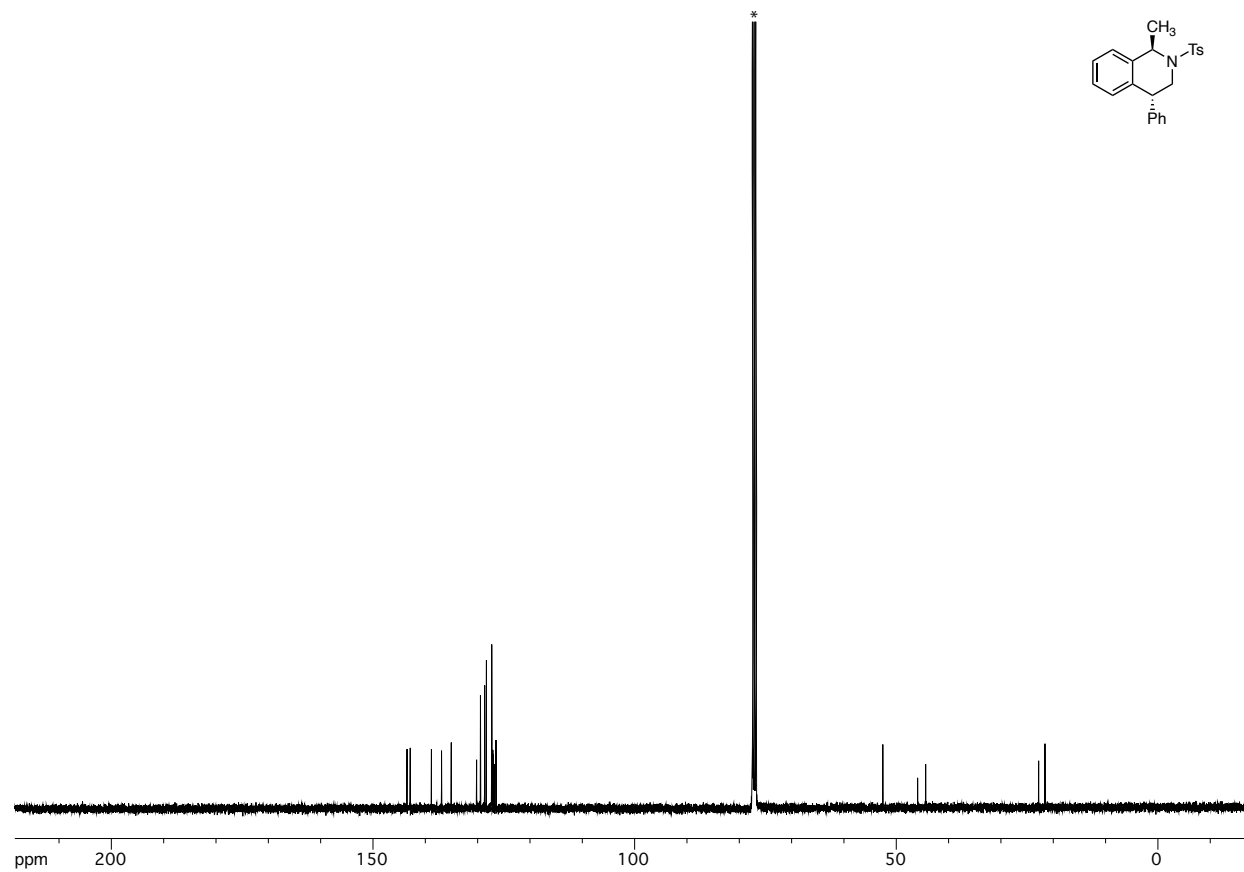


Figure V-20. ¹³C NMR spectrum of *trans*-V.5a in CDCl₃ (100 MHz) at 23 °C.*CDCl₃ solvent peak.

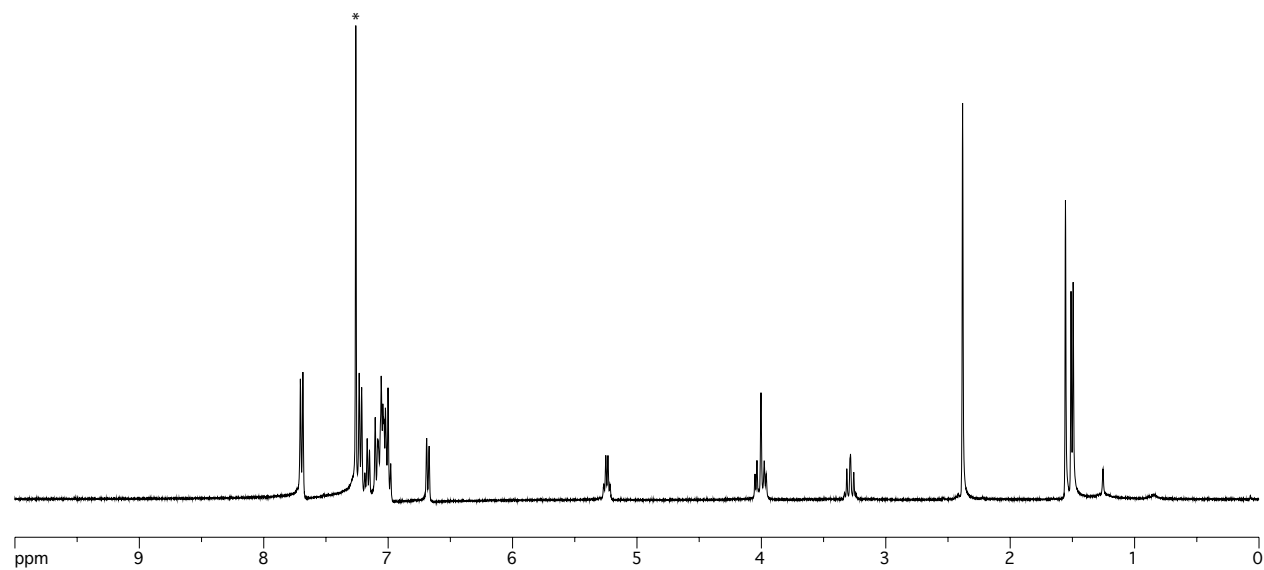
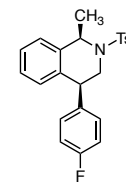


Figure V-21. ¹H NMR spectrum of *cis*-V.5b in CDCl₃ (400 MHz) at 23 °C. *CDCl₃ solvent peak.

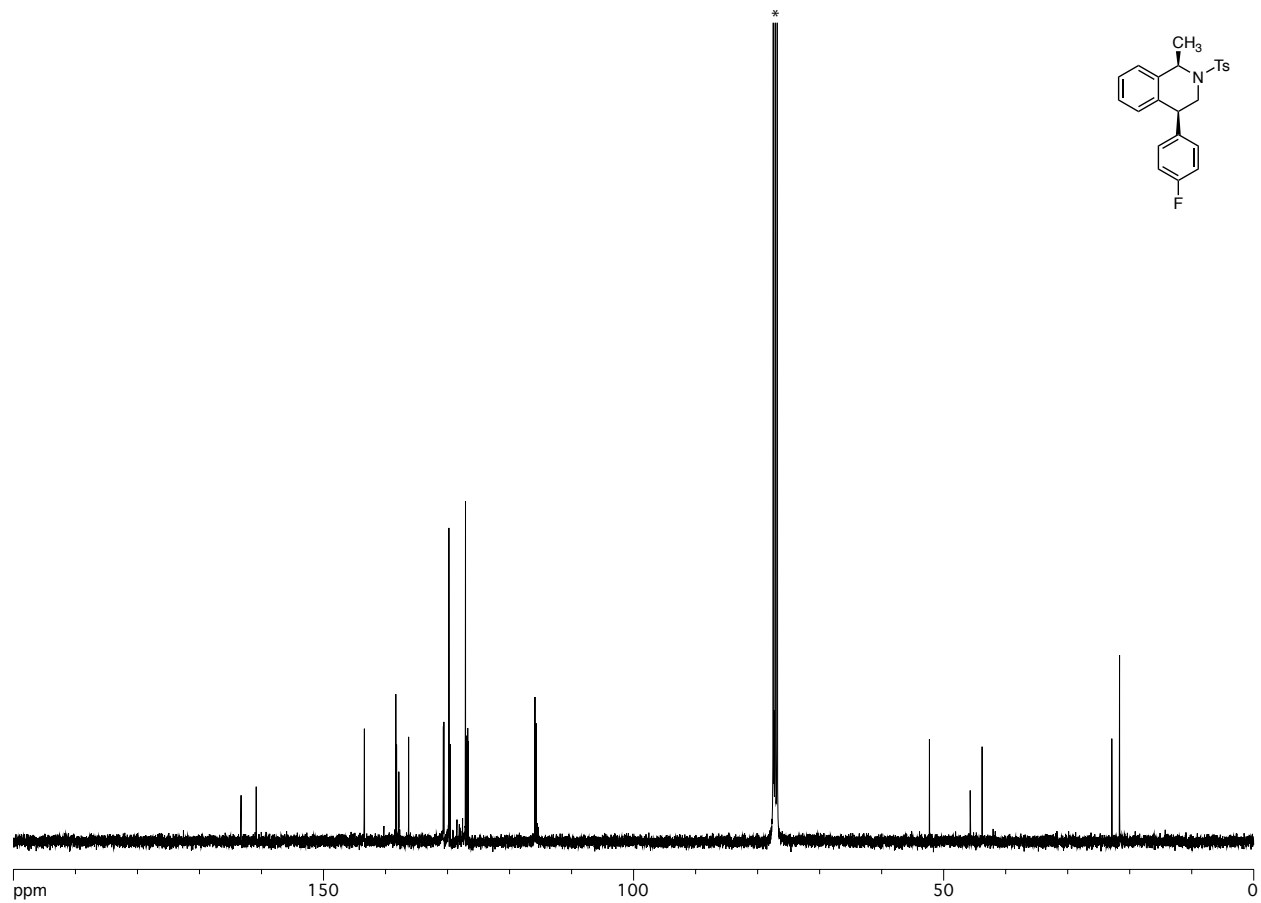


Figure V-22. ^{13}C NMR spectrum of *cis*-V.5b in CDCl_3 (100 MHz) at 23 °C.* CDCl_3 solvent peak.

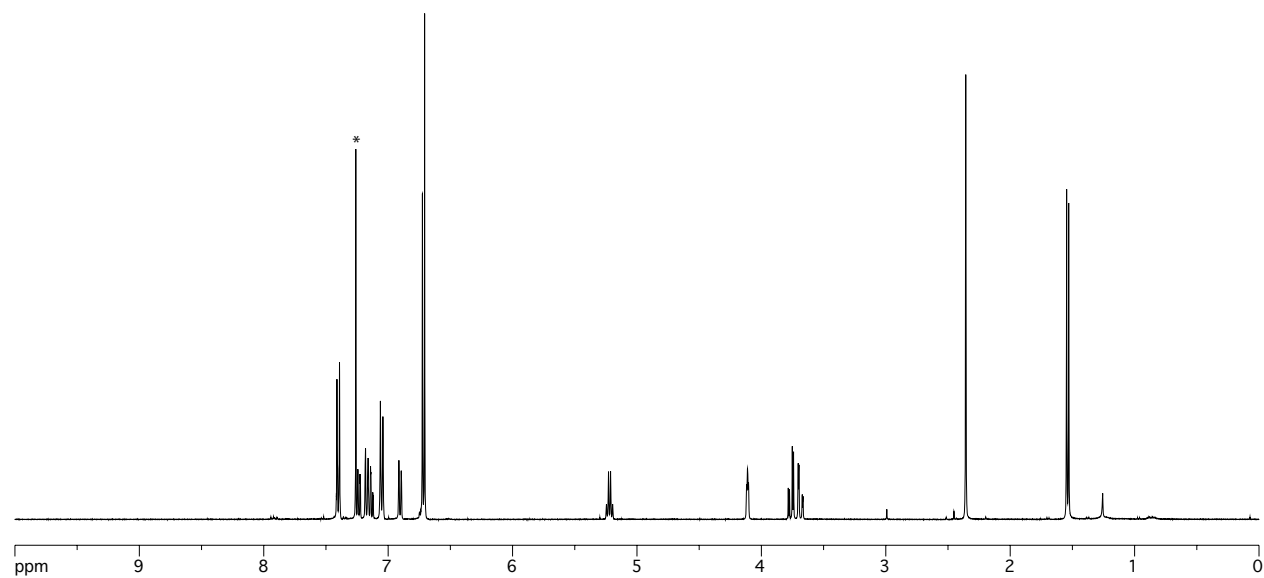
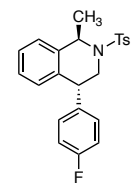


Figure V-23. ^1H NMR spectrum of *trans*-V.5b in CDCl_3 (400 MHz) at 23 °C. * CDCl_3 solvent peak.

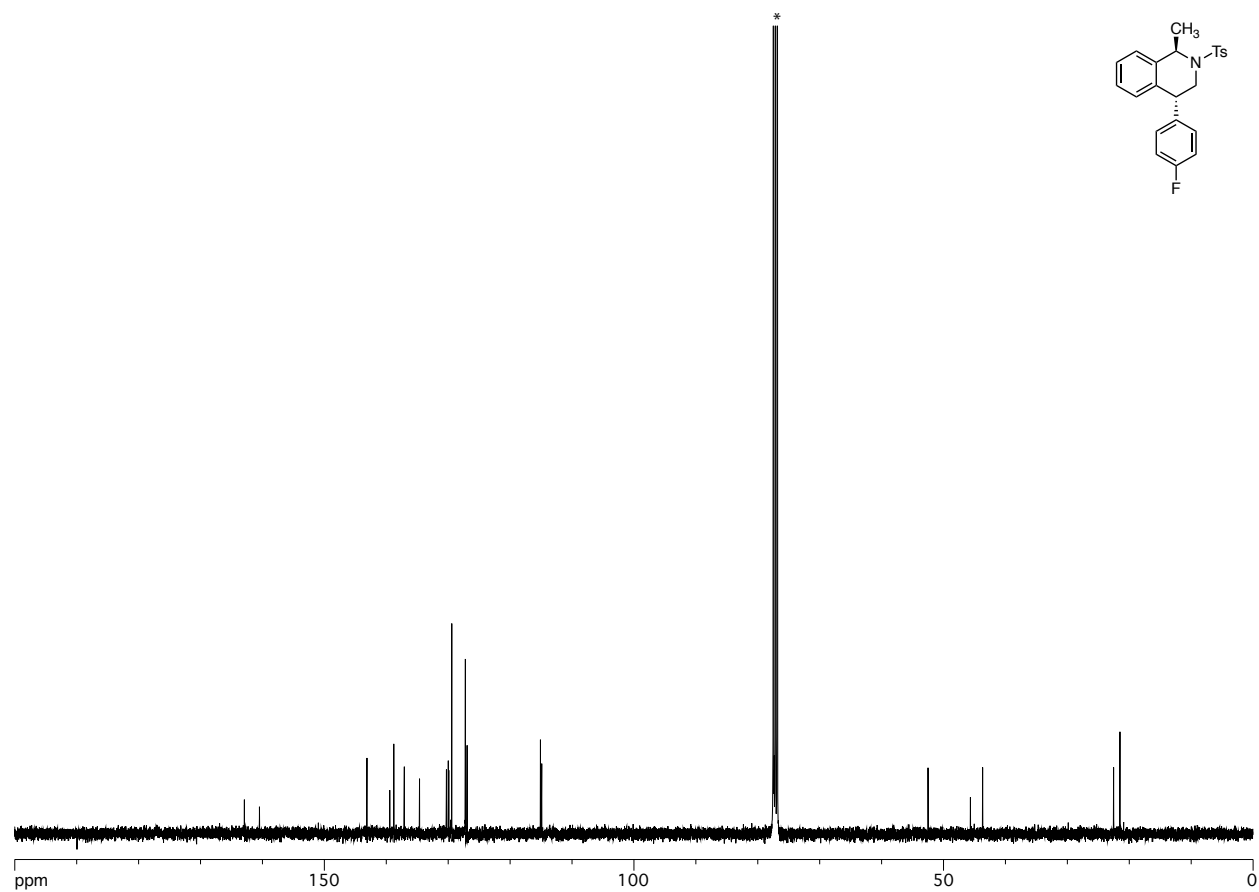


Figure V-24. ^{13}C NMR spectrum of *trans*-V.5b in CDCl_3 (100 MHz) at 23 °C.* CDCl_3 solvent peak.

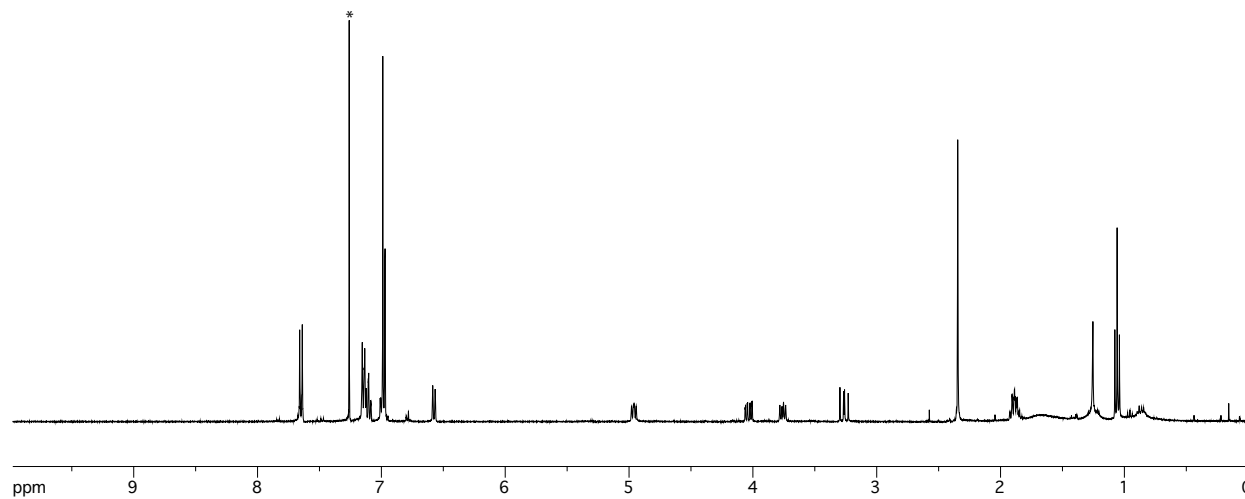
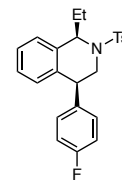


Figure V-25. ^1H NMR spectrum of *cis*-V.5c in CDCl_3 (400 MHz) at 23 °C. * CDCl_3 solvent peak.

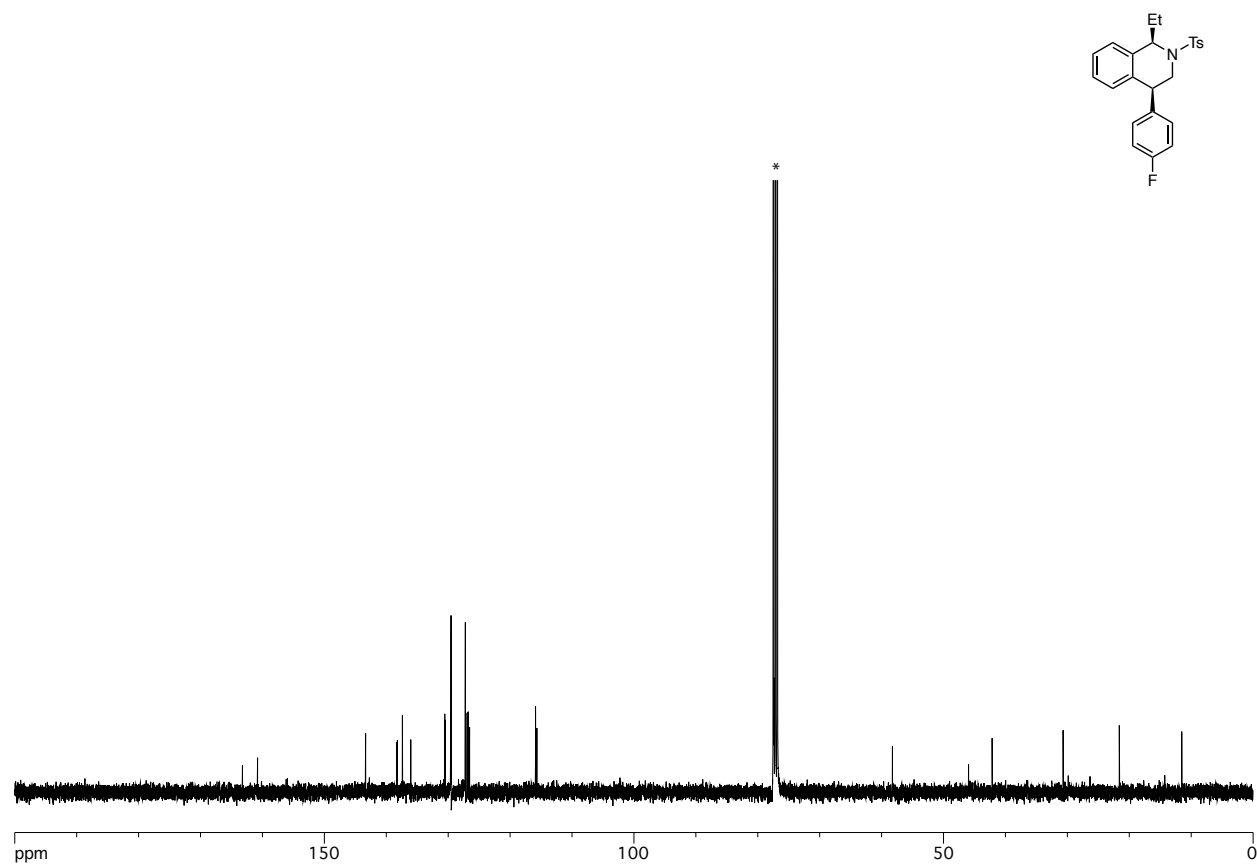


Figure V-26. ¹³C NMR spectrum of *cis*-V.5c in CDCl₃ (100 MHz) at 23 °C.*CDCl₃ solvent peak.

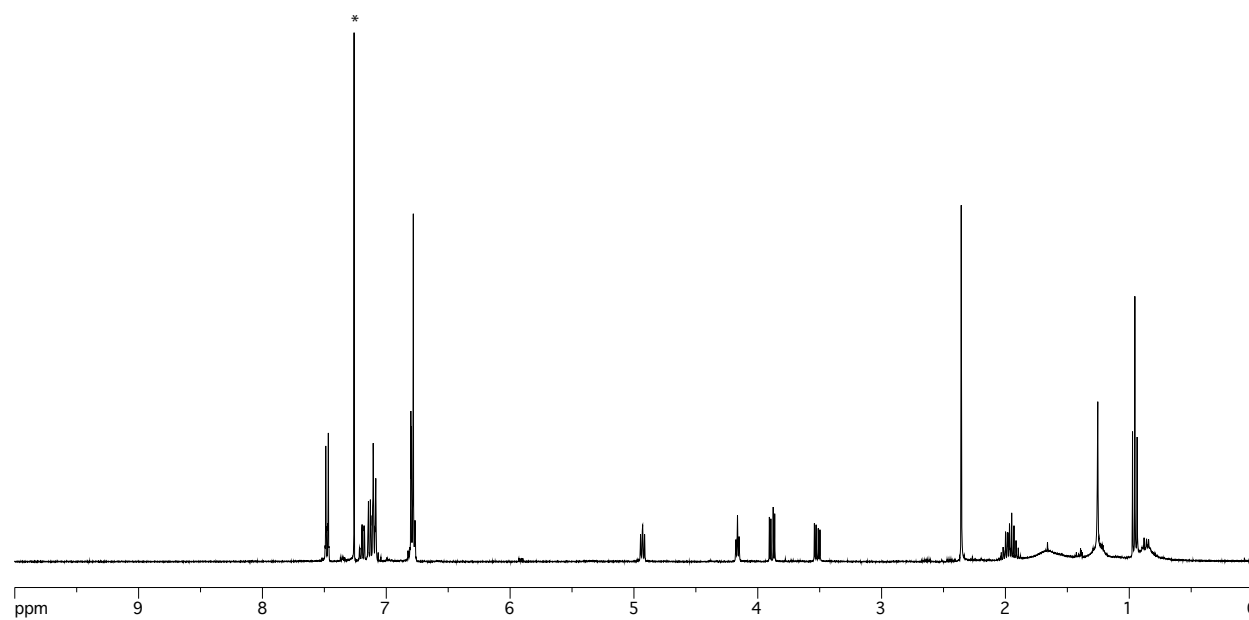
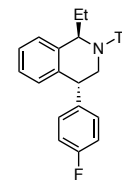


Figure V-27. ¹H NMR spectrum of *trans*-V.5c in CDCl₃ (400 MHz) at 23 °C.*CDCl₃ solvent peak.

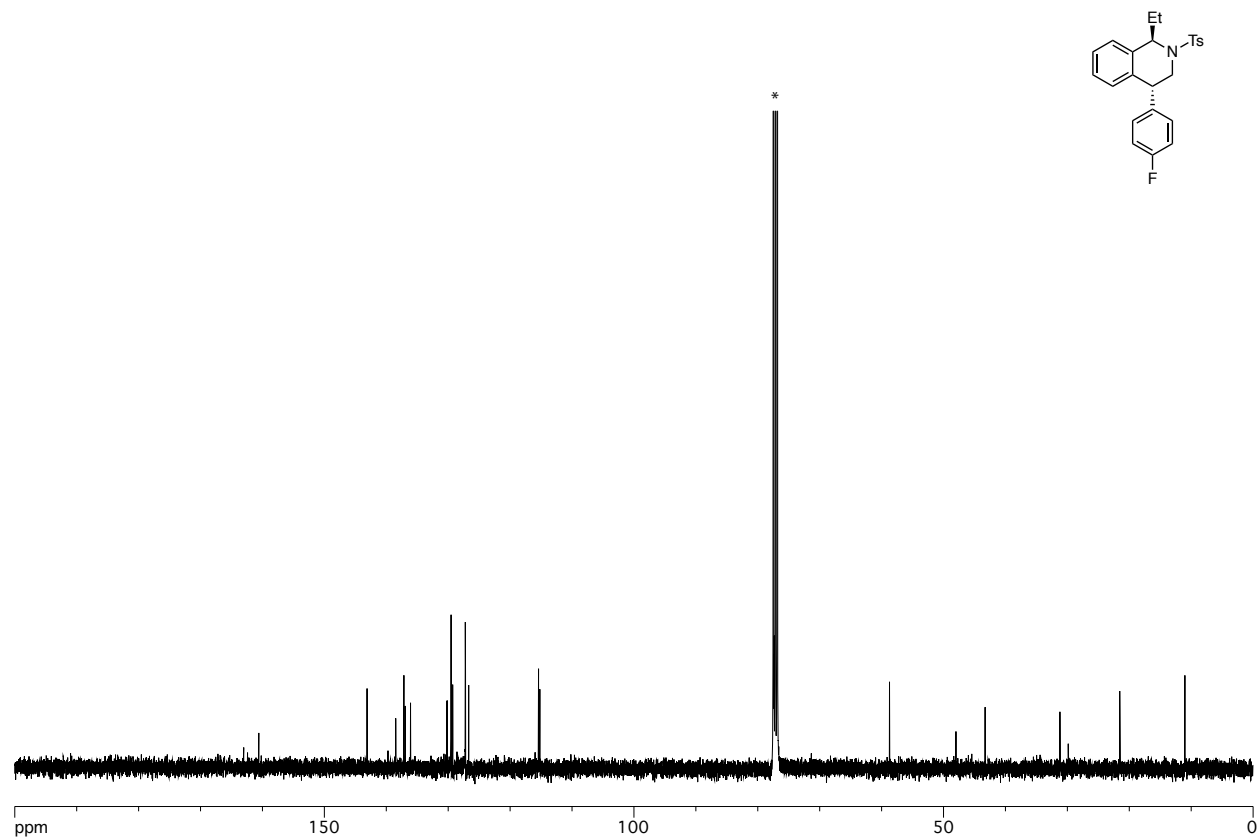


Figure V-28. ^{13}C NMR spectrum of *trans*-V.5c in CDCl_3 (100 MHz) at 23 °C.* CDCl_3 solvent peak.

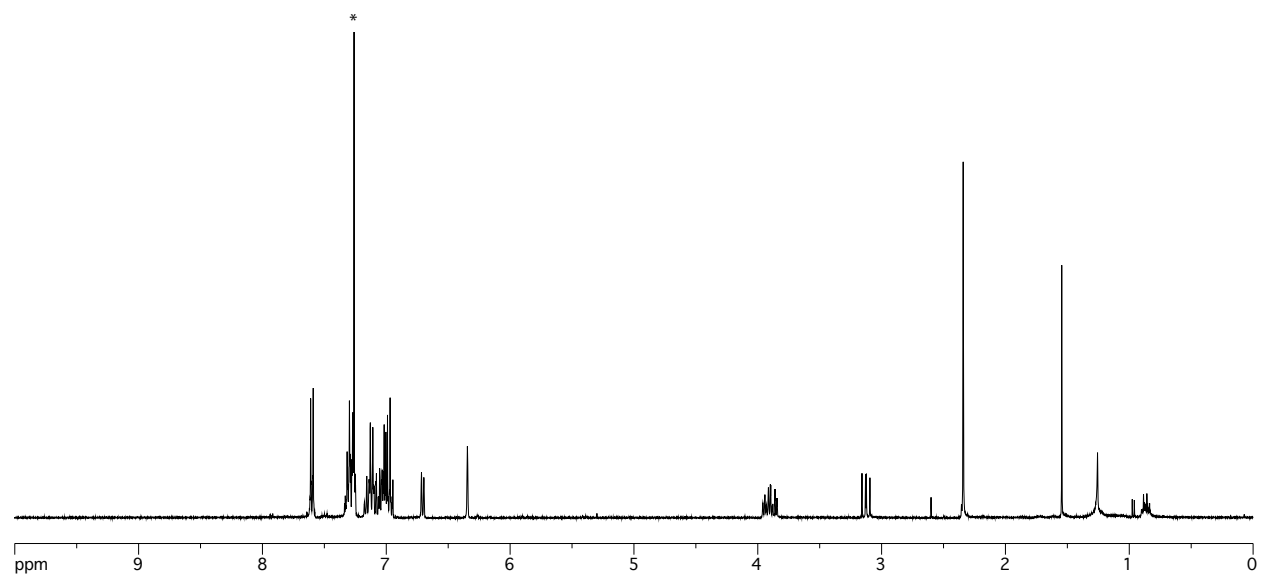
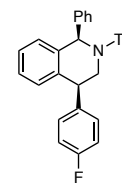


Figure V-29. ^1H NMR spectrum of *cis*-V.5d in CDCl_3 (400 MHz) at 23 °C. * CDCl_3 solvent peak.

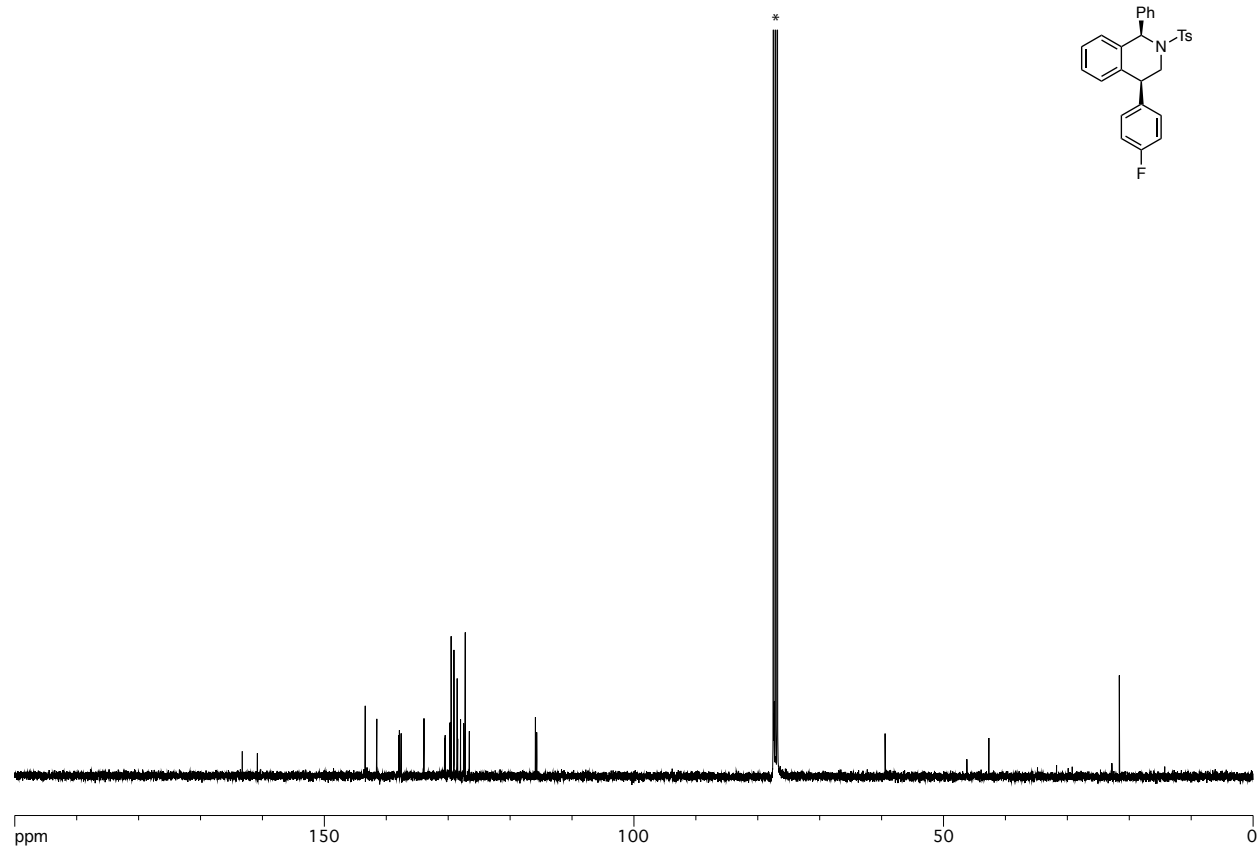


Figure V-30. ¹³C NMR spectrum of *cis*-V.5d in CDCl₃ (100 MHz) at 23 °C.*CDCl₃ solvent peak.

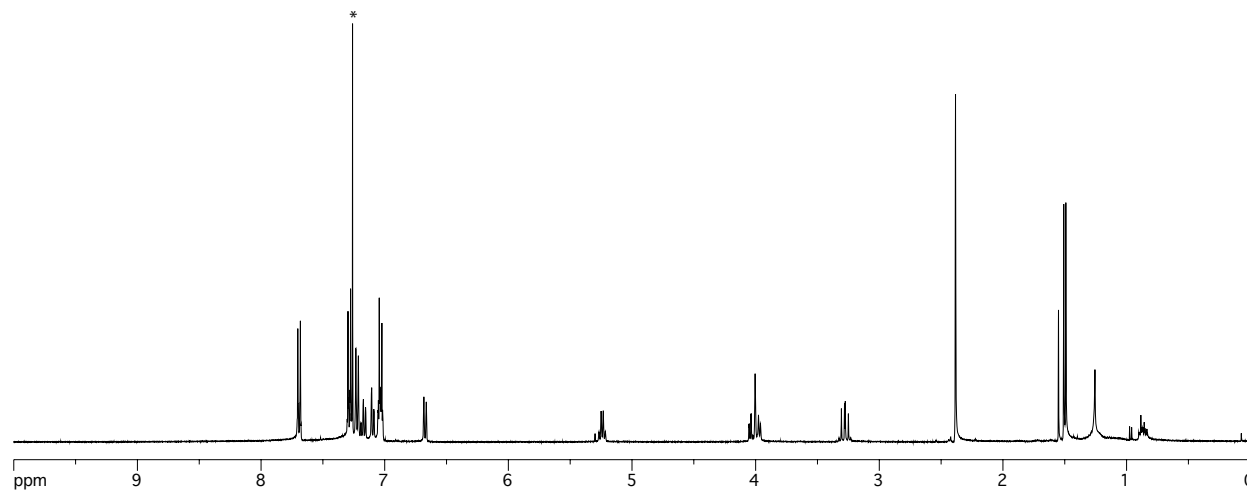
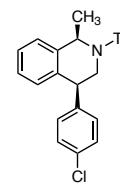


Figure V-31. ^1H NMR spectrum of *cis*-V.5e in CDCl_3 (400 MHz) at 23 °C. * CDCl_3 solvent peak. Peaks with $\delta < 1.4$ ppm are from H grease.

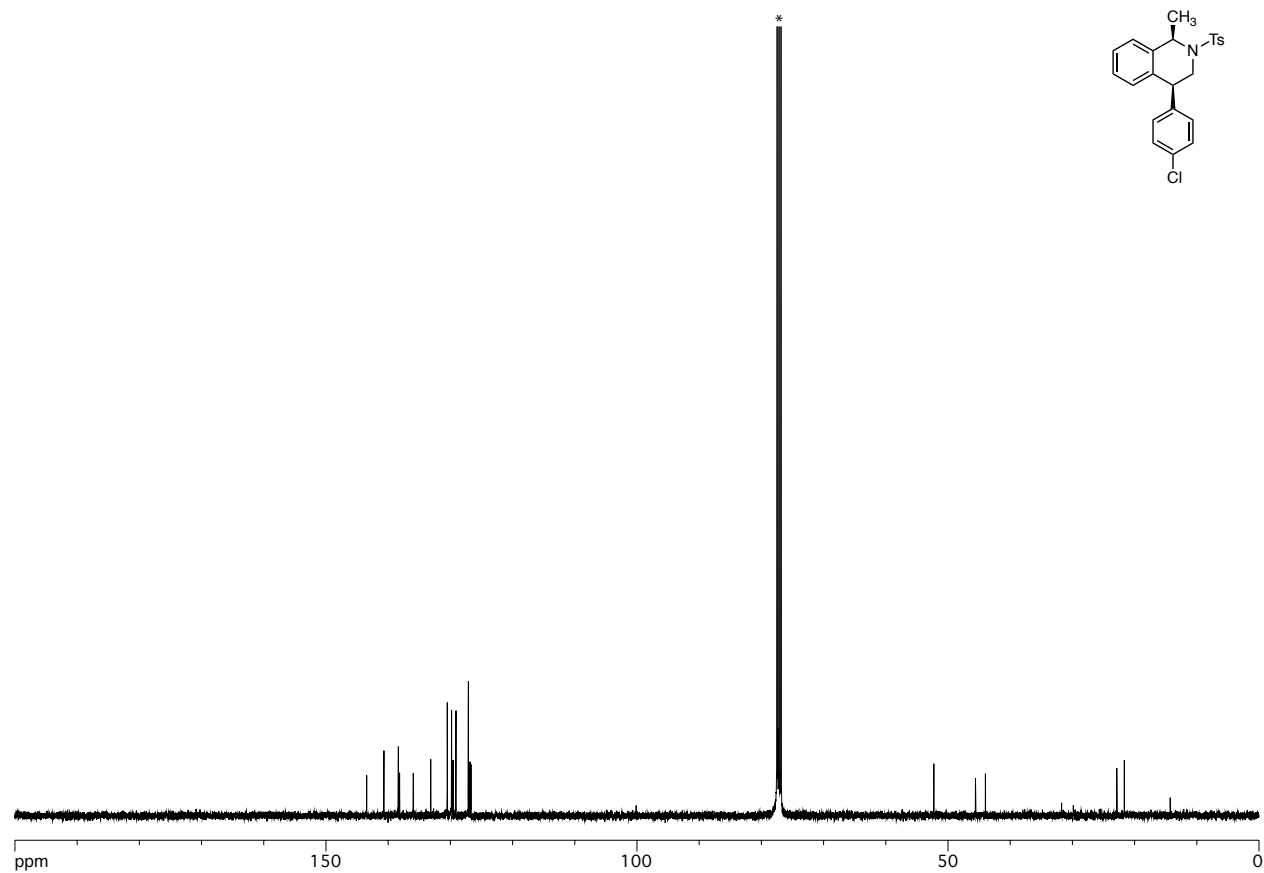


Figure V-32. ^{13}C NMR spectrum of *cis*-V.5e in CDCl_3 (100 MHz) at 23 °C.* CDCl_3 solvent peak.

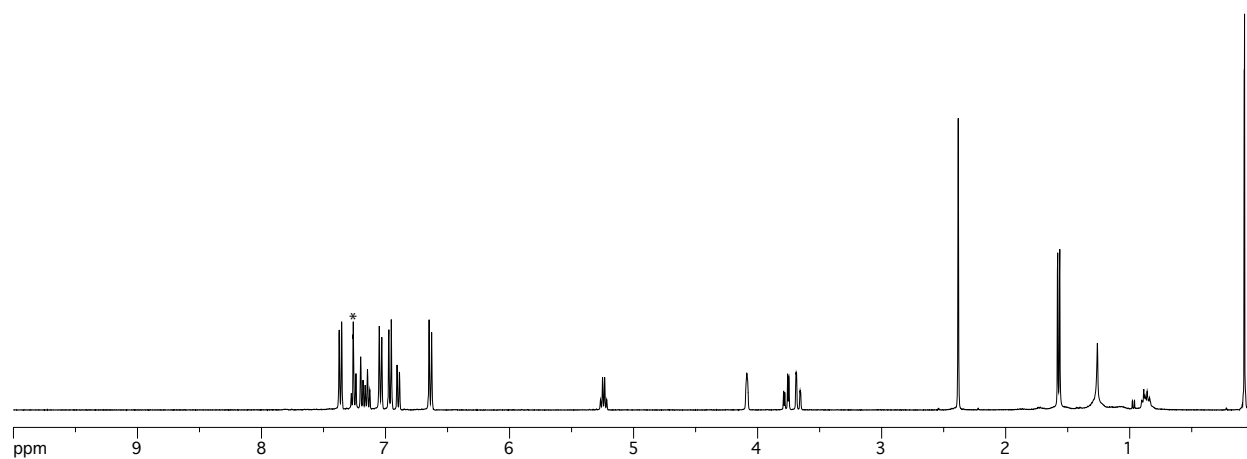
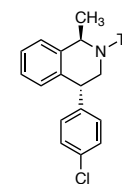


Figure V-33. ¹H NMR spectrum of *trans*-V.5e in CDCl₃ (400 MHz) at 23 °C.*CDCl₃ solvent peak. Peaks with d < 1.4 ppm are from H grease.

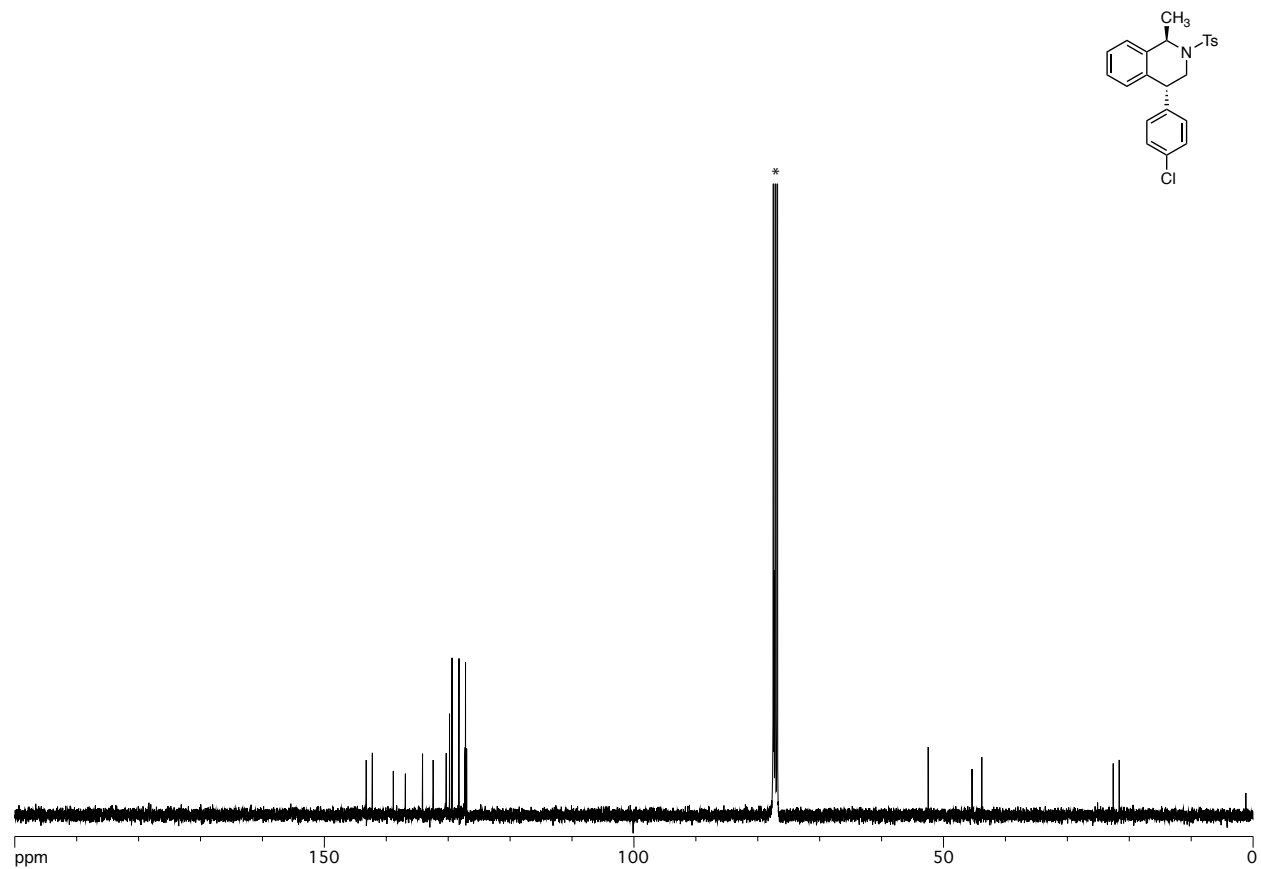


Figure V-34. ¹³C NMR spectrum of *trans*-V.5e in CDCl₃ (100 MHz) at 23 °C.*CDCl₃ solvent peak.

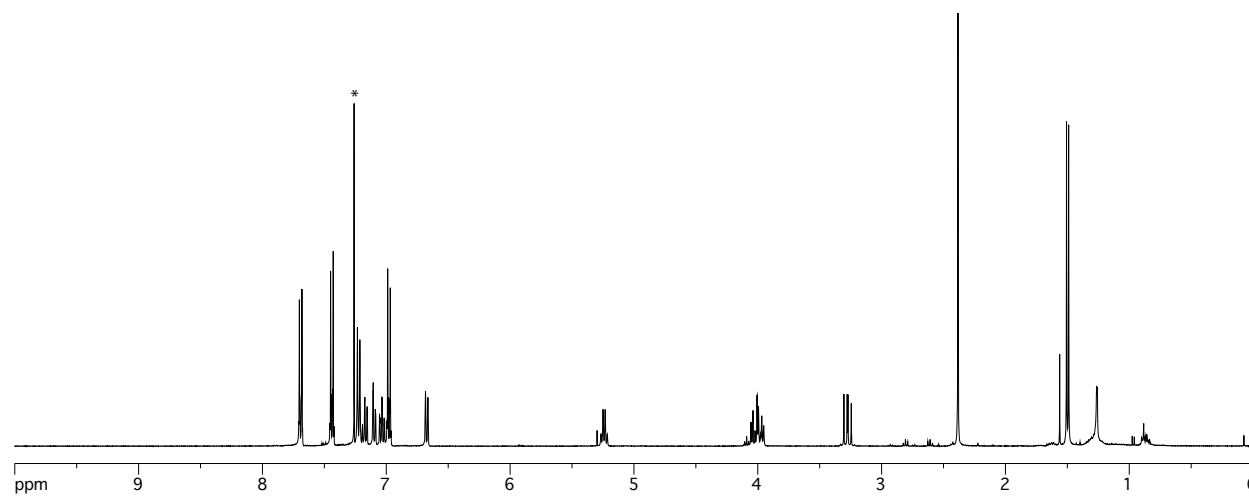
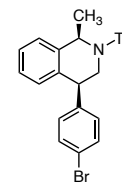


Figure V-35. ¹H NMR spectrum of *cis*-V.5f in CDCl₃ (400 MHz) at 23 °C.*CDCl₃ solvent peak. Peaks with d < 1.4 ppm are from H grease.

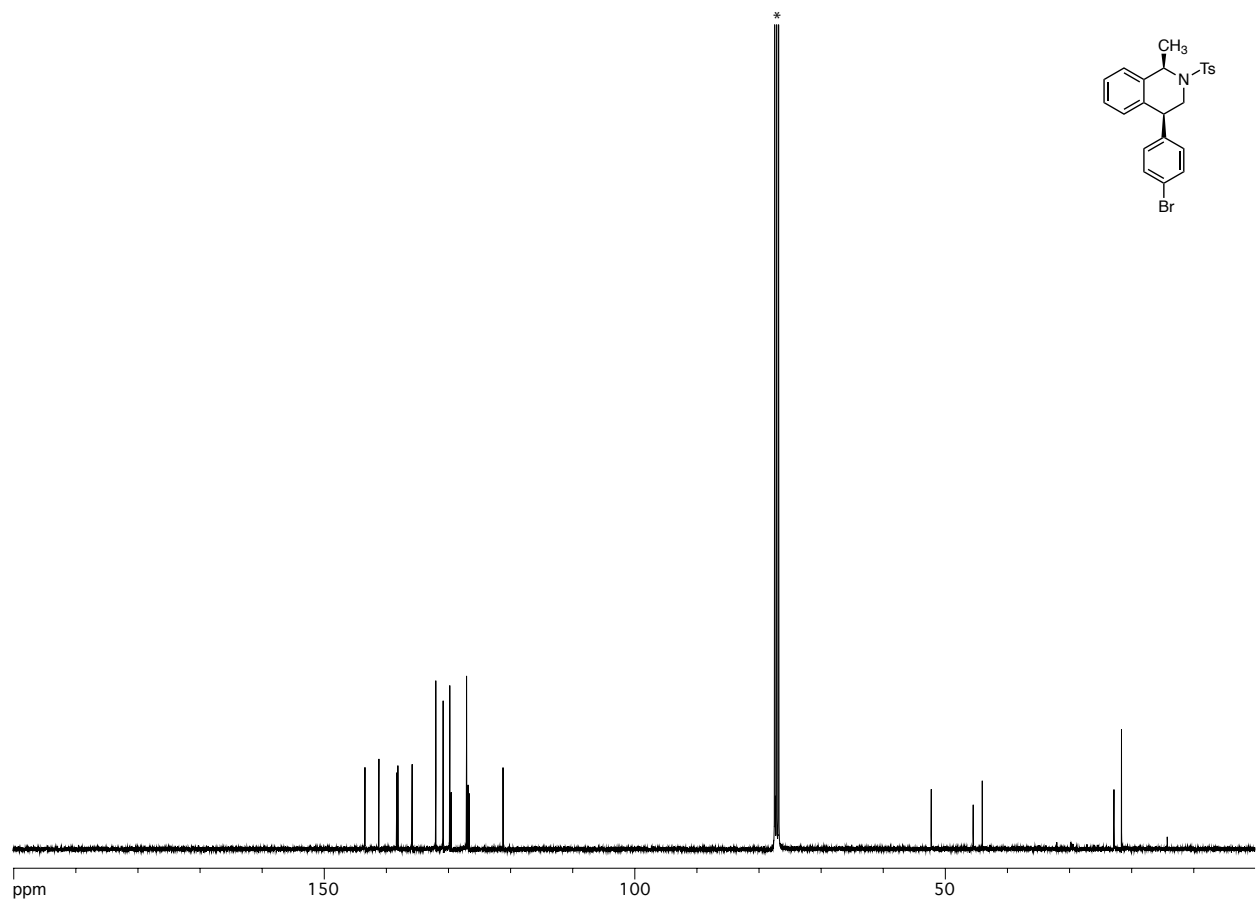


Figure V-36. ^{13}C NMR spectrum of *cis*-V.5f in CDCl_3 (100 MHz) at 23 °C. * CDCl_3 solvent peak. Peaks with $\delta < 1.4$ ppm are from H grease.

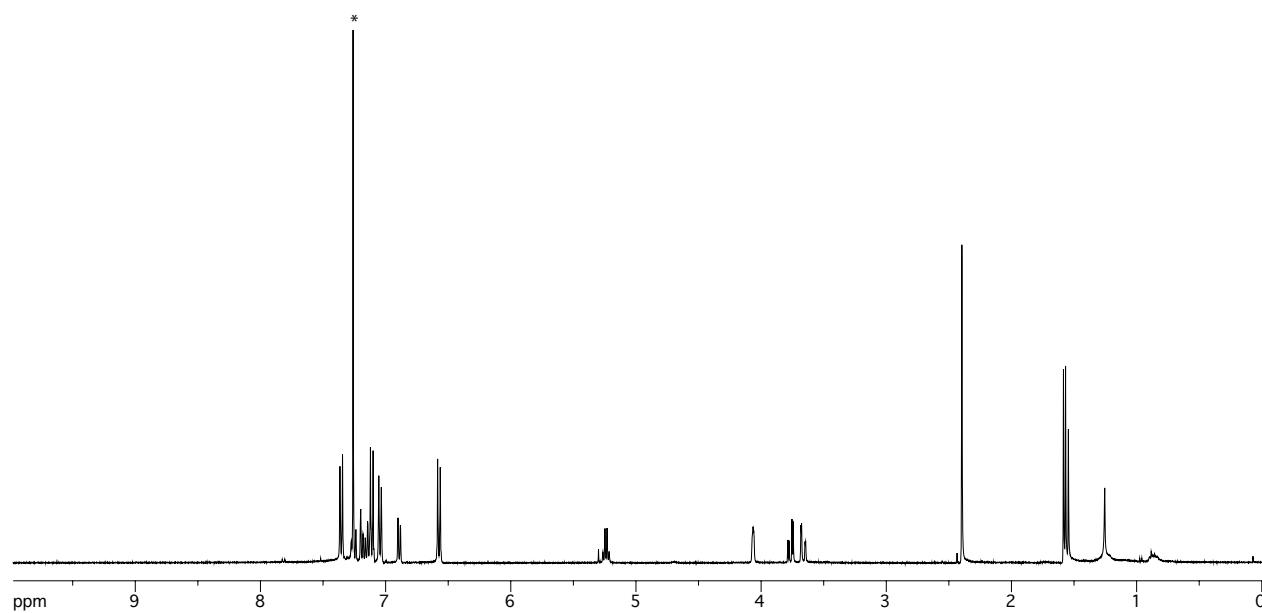
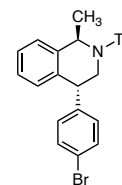


Figure V-37. ^1H NMR spectrum of *trans*-V.5f in CDCl_3 (400 MHz) at 23 °C.* CDCl_3 solvent peak. Peaks with $\delta < 1.4$ ppm are from H grease.

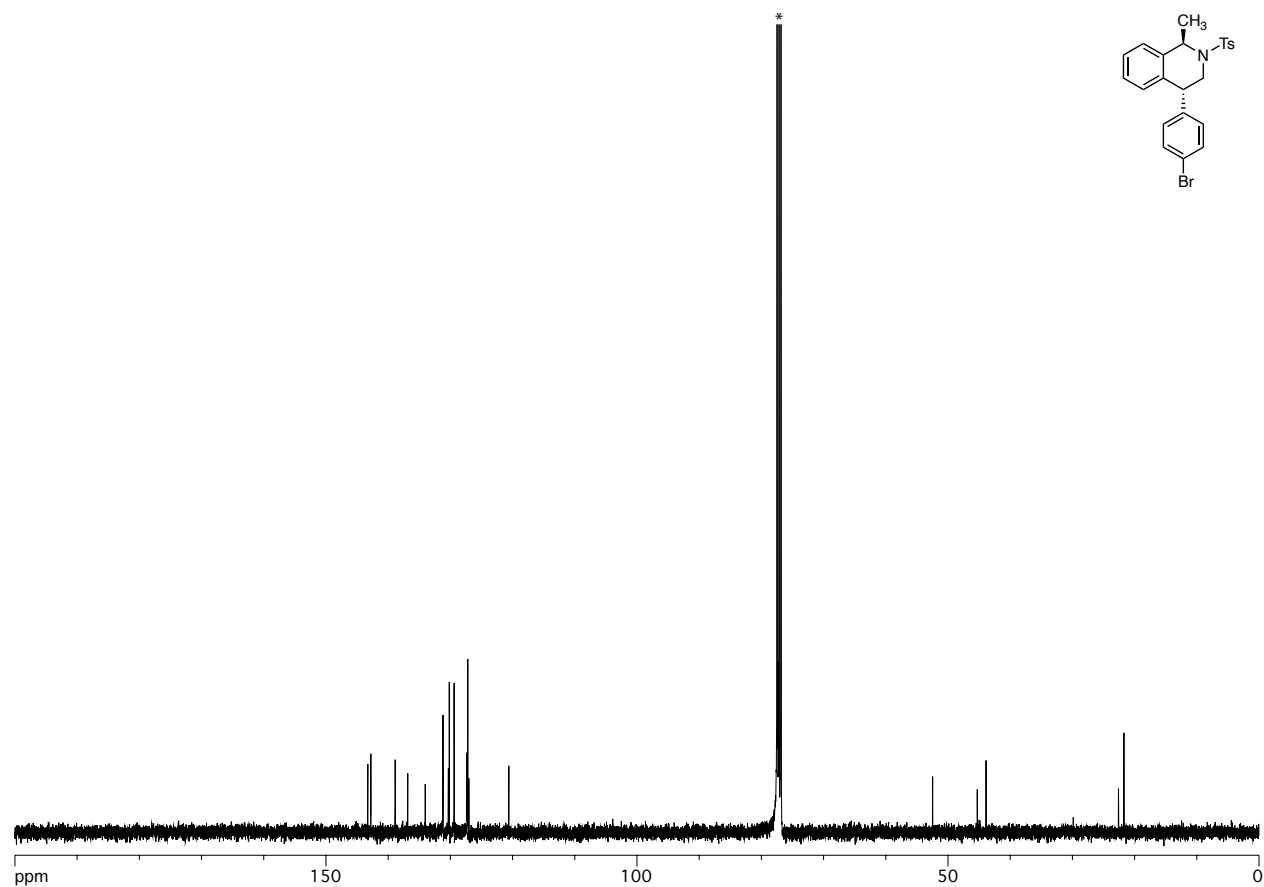


Figure V-38. ¹³C NMR spectrum of *trans*-V.5f in CDCl₃ (100 MHz) at 23 °C.*CDCl₃ solvent peak.

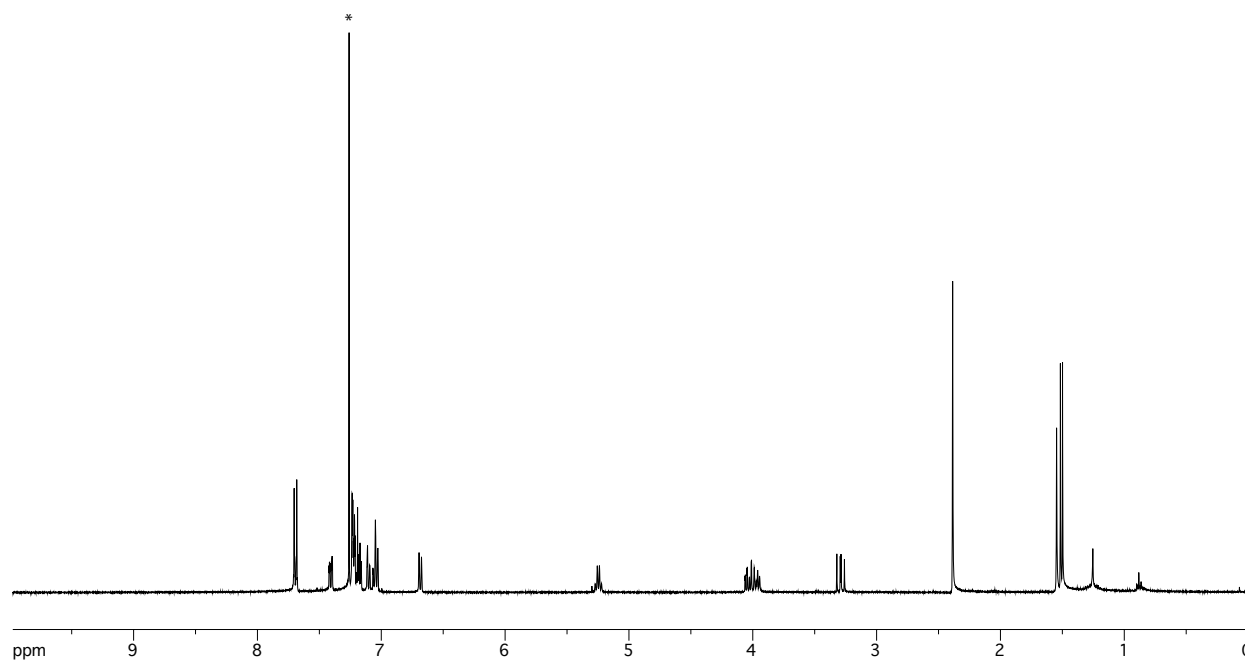
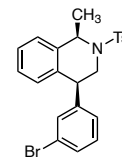


Figure V-39. ¹H NMR spectrum of *cis*-V.5g in CDCl₃ (400 MHz) at 23 °C.*CDCl₃ solvent peak.

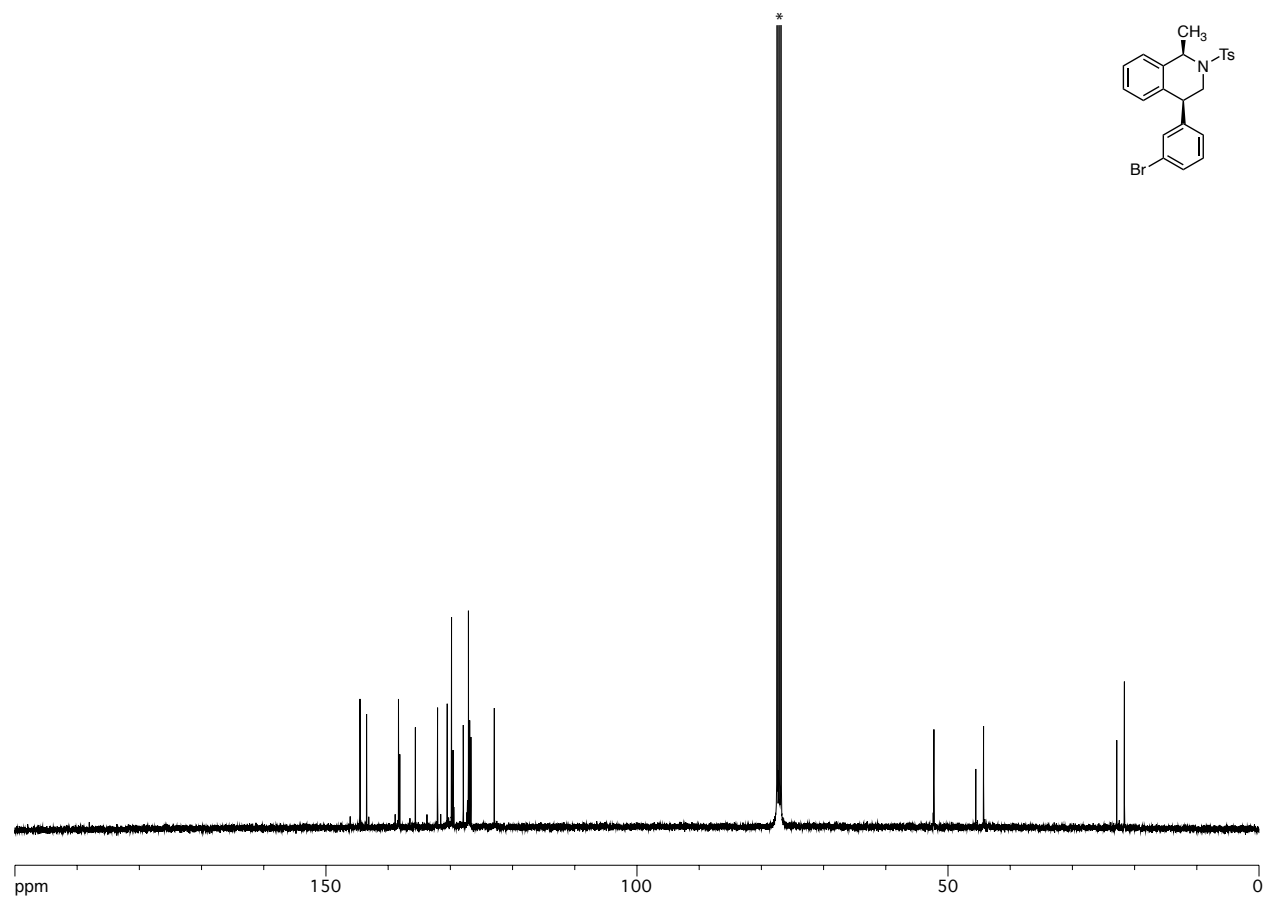


Figure V-40. ¹³C NMR spectrum of *cis*-V.5g in CDCl₃ (100 MHz) at 23 °C.*CDCl₃ solvent peak.

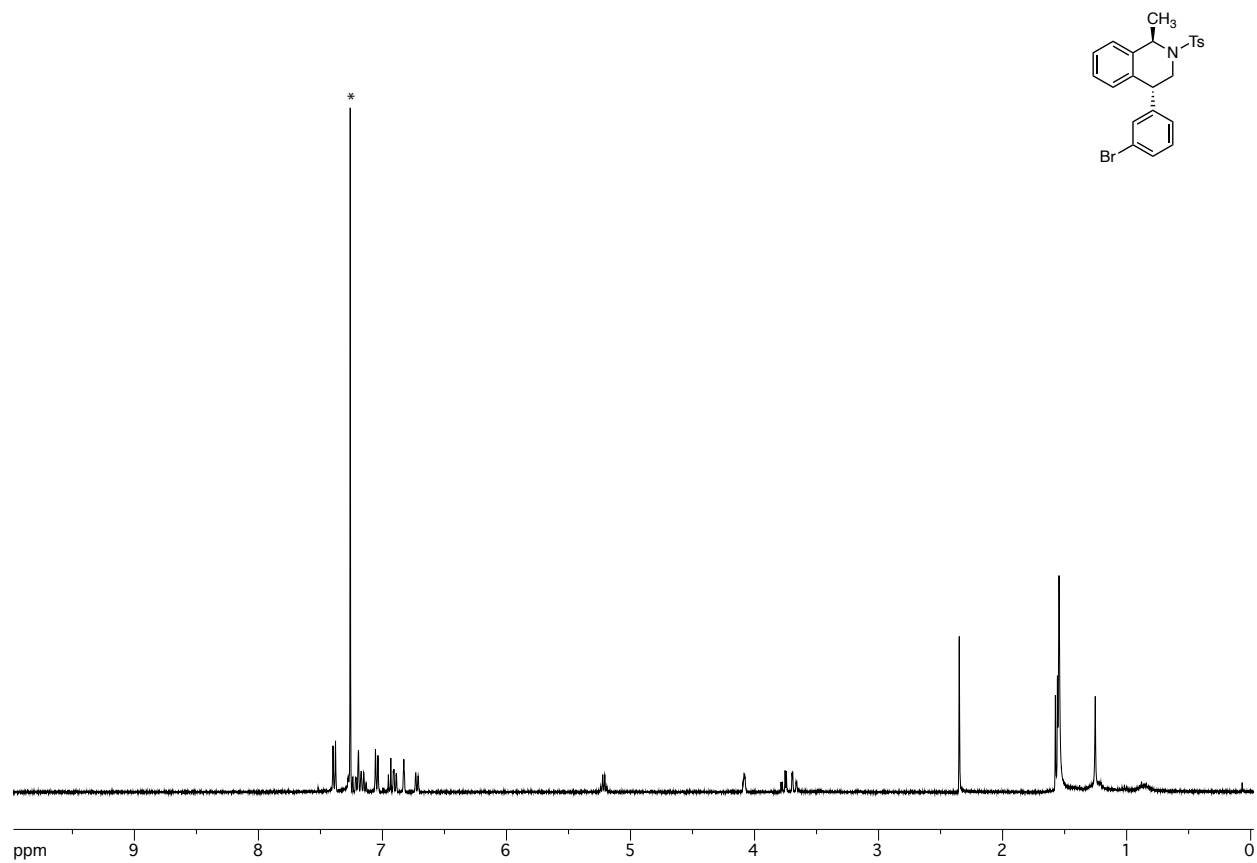


Figure V-41. ¹H NMR spectrum of *trans*-V.5g in CDCl₃ (400 MHz) at 23 °C.*CDCl₃ solvent peak. Peaks with $\delta < 1.4$ ppm are from H grease.

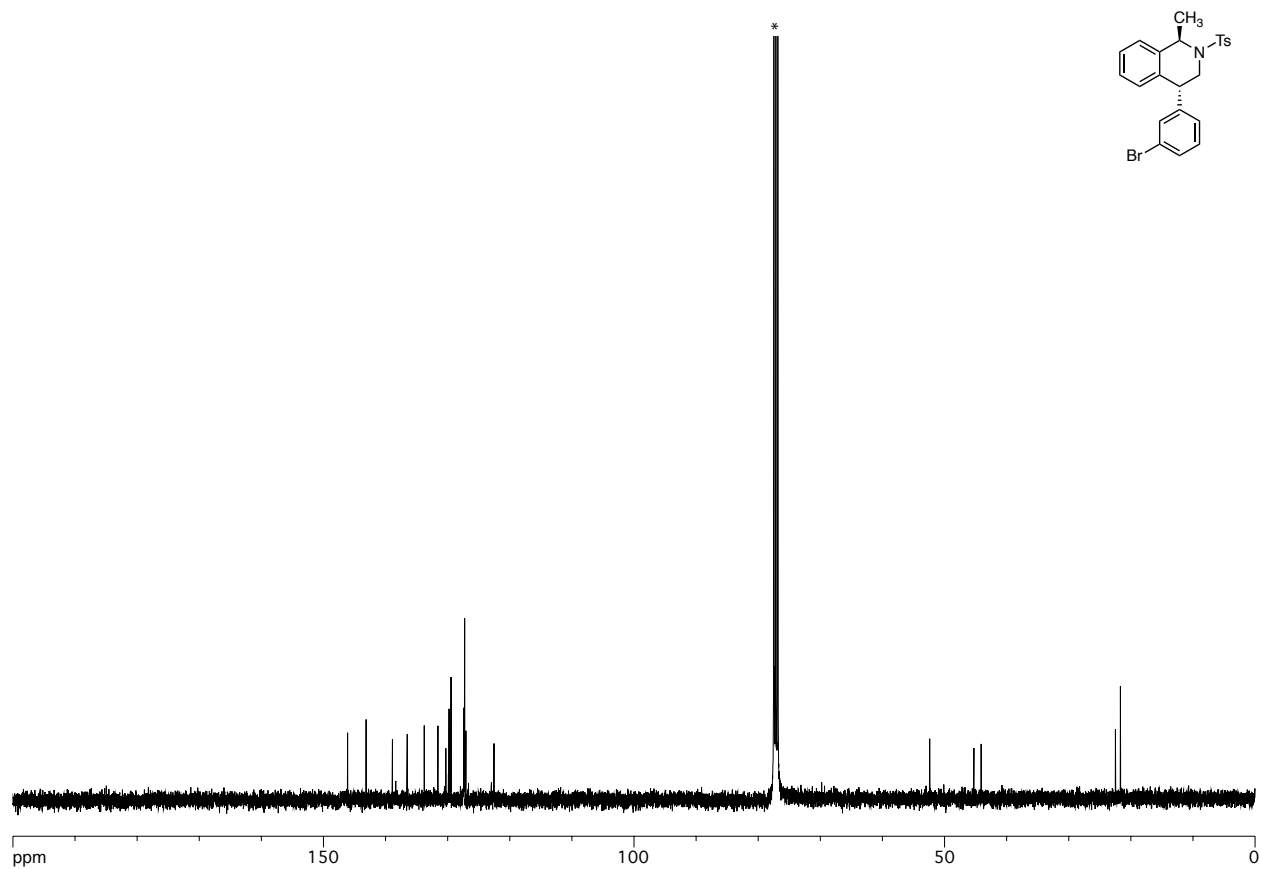


Figure V-42. ¹³C NMR spectrum of *trans*-V.5g in CDCl₃ (100 MHz) at 23 °C.*CDCl₃ solvent peak.

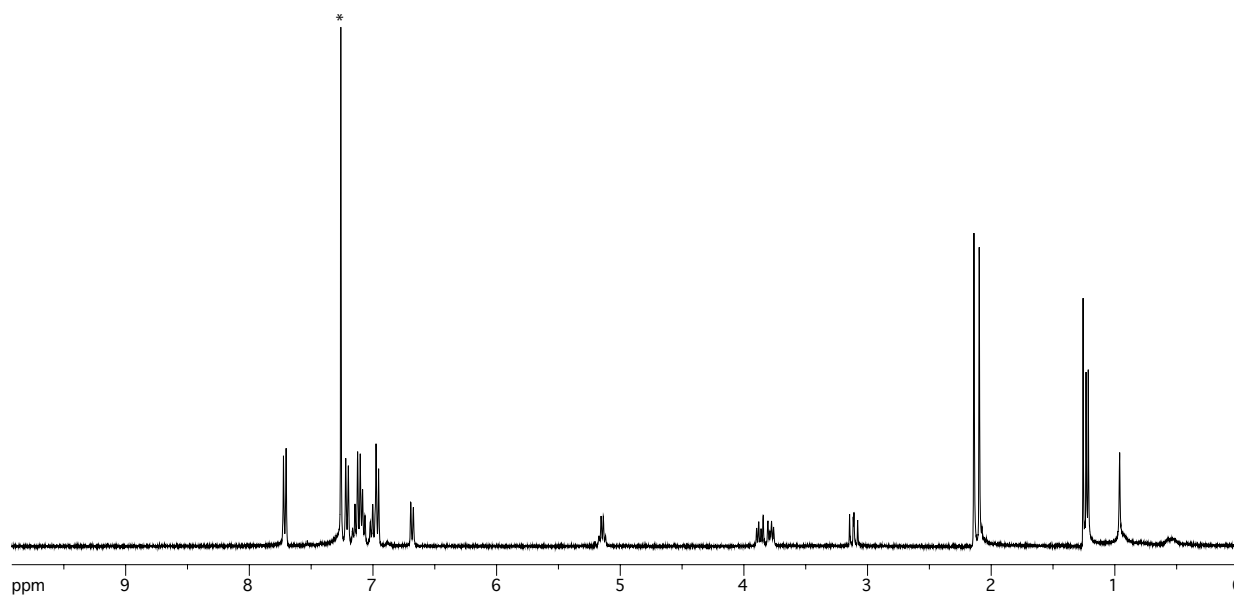
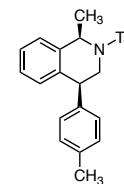


Figure V-43. ^1H NMR spectrum of *cis*-V.5h in CDCl_3 (400 MHz) at 23 °C.* CDCl_3 solvent peak. Peaks with $\delta < 1.4$ ppm are from H grease.

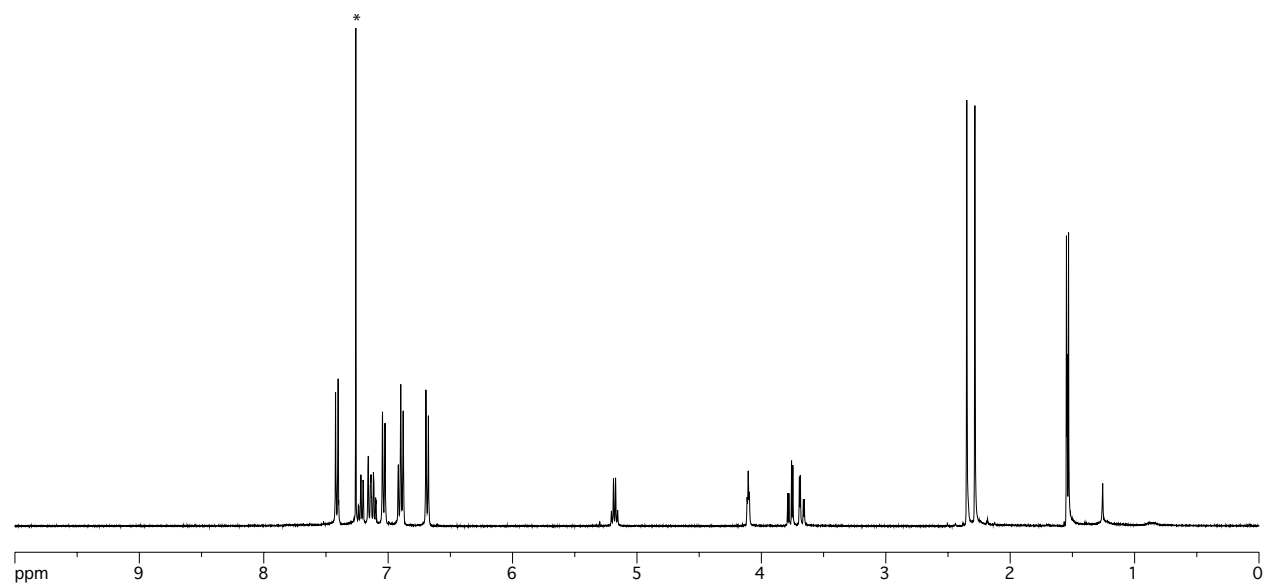
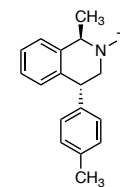


Figure V-44. ¹H NMR spectrum of *trans*-V.5h in CDCl₃ (400 MHz) at 23 °C. *CDCl₃ solvent peak.

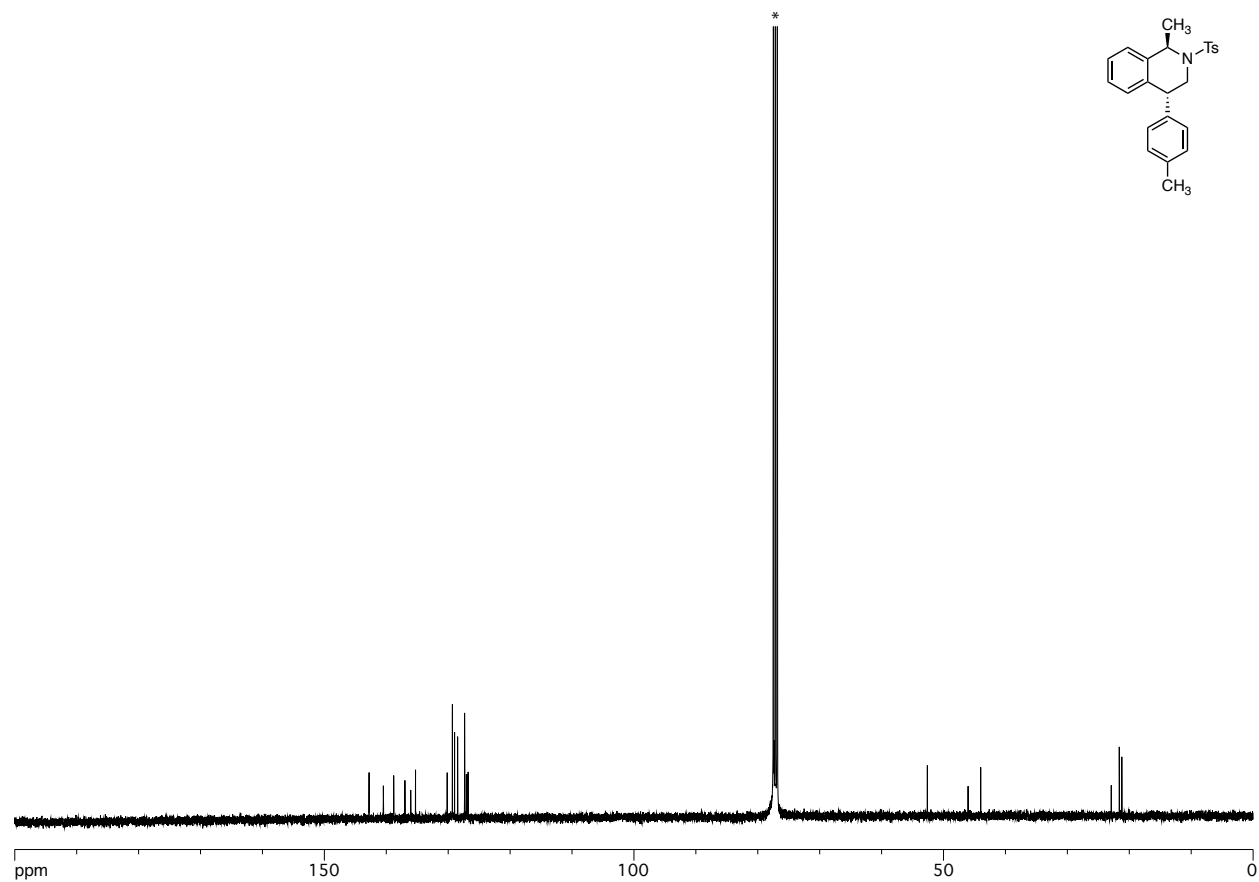


Figure V-45. ^{13}C NMR spectrum of *trans*-V.5h in CDCl_3 (100 MHz) at 23 °C.* CDCl_3 solvent peak.

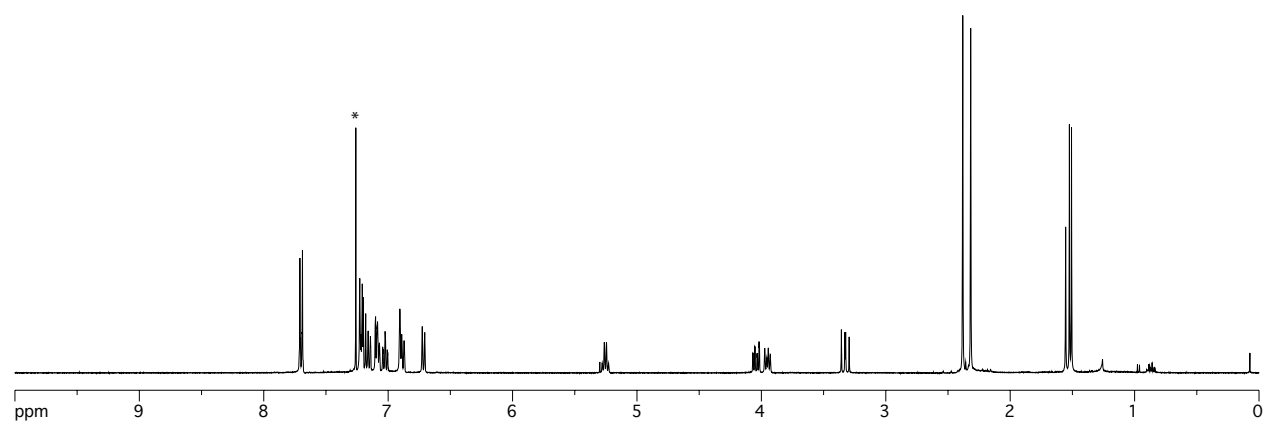
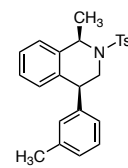


Figure V-46. ^1H NMR spectrum of *cis*-V.5i in CDCl_3 (400 MHz) at 23 °C.* CDCl_3 solvent peak.

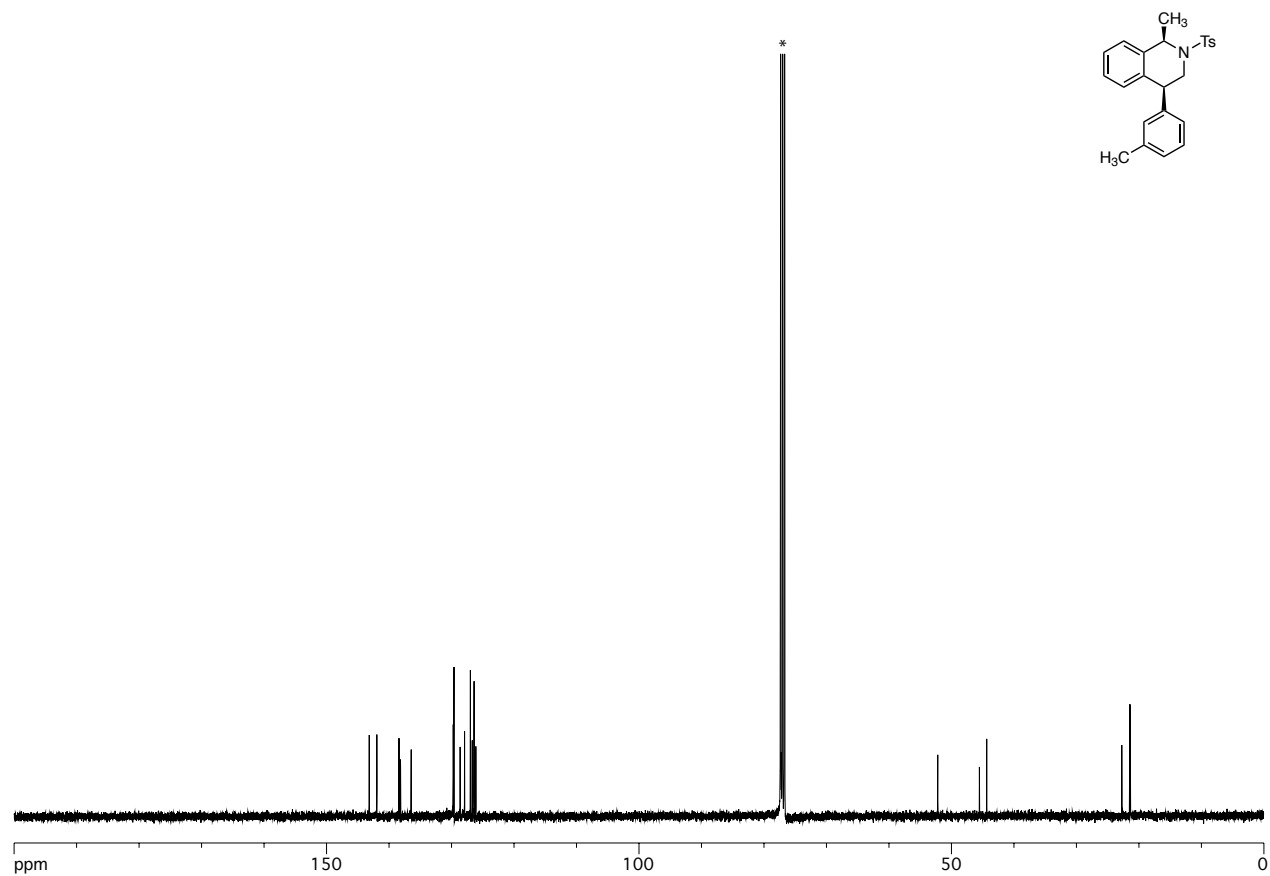


Figure V-47. ^{13}C NMR spectrum of *cis*-V.5i in CDCl_3 (100 MHz) at 23 °C. * CDCl_3 solvent peak.

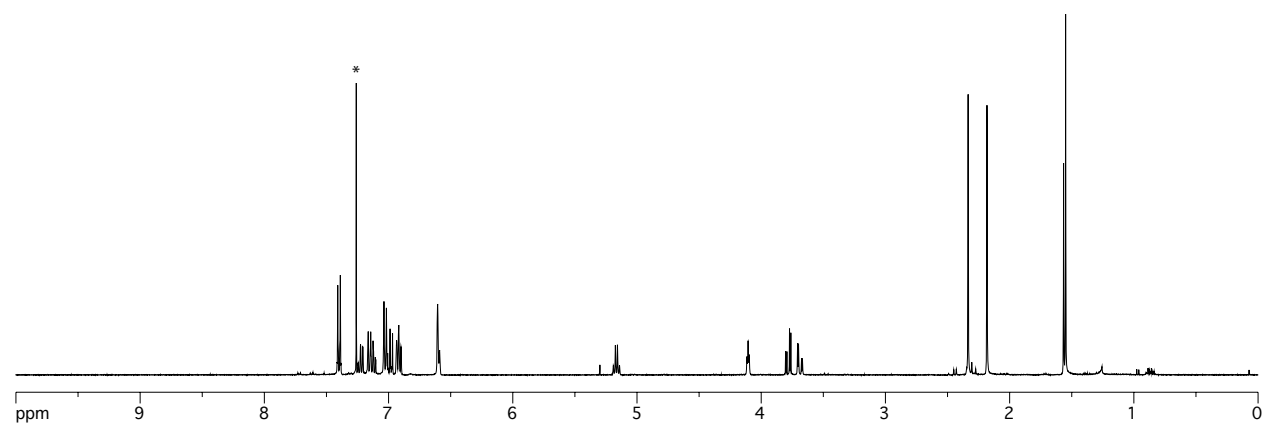
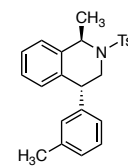


Figure V-48. ¹H NMR spectrum of *trans*-V.5i in CDCl₃ (400 MHz) at 23 °C.*CDCl₃ solvent peak.

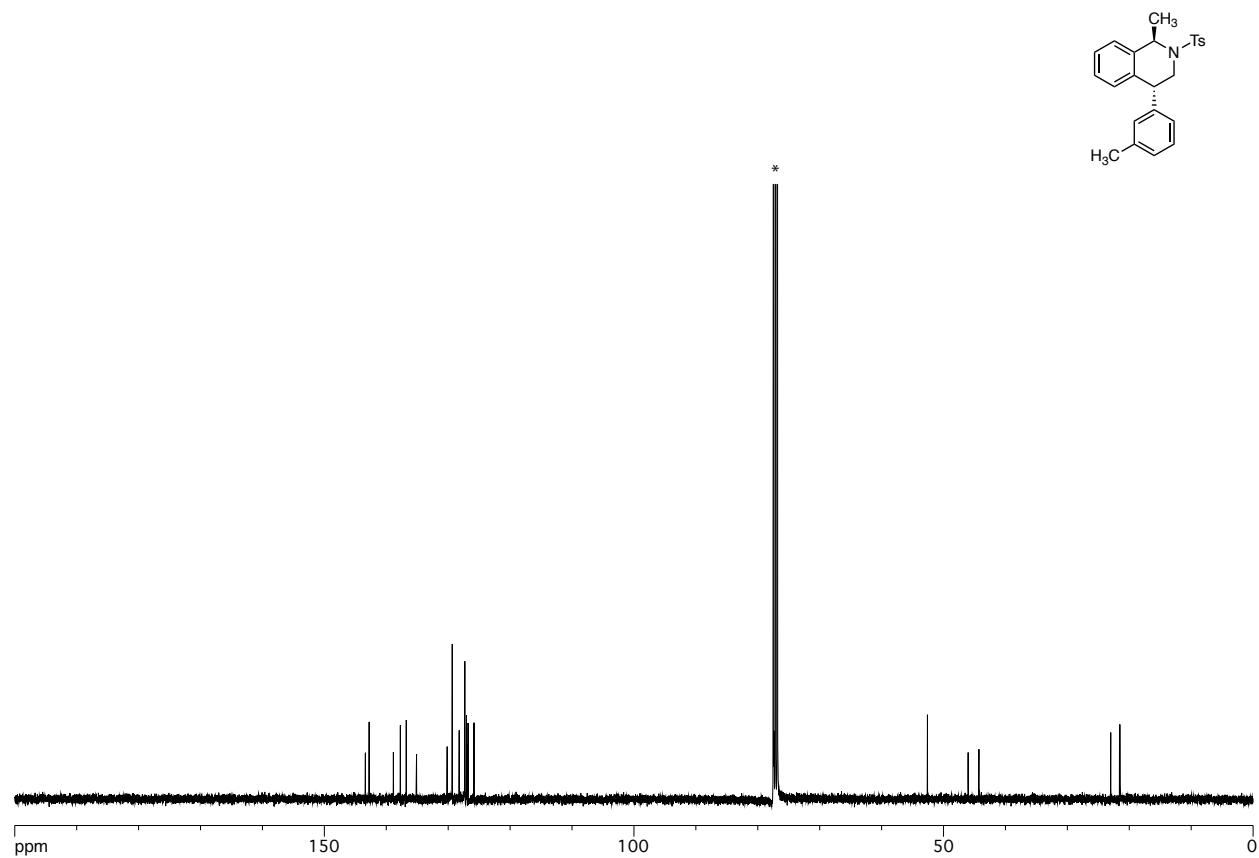


Figure V-49. ^{13}C NMR spectrum of *trans*-V.5i in CDCl_3 (100 MHz) at 23 °C. * CDCl_3 solvent peak.

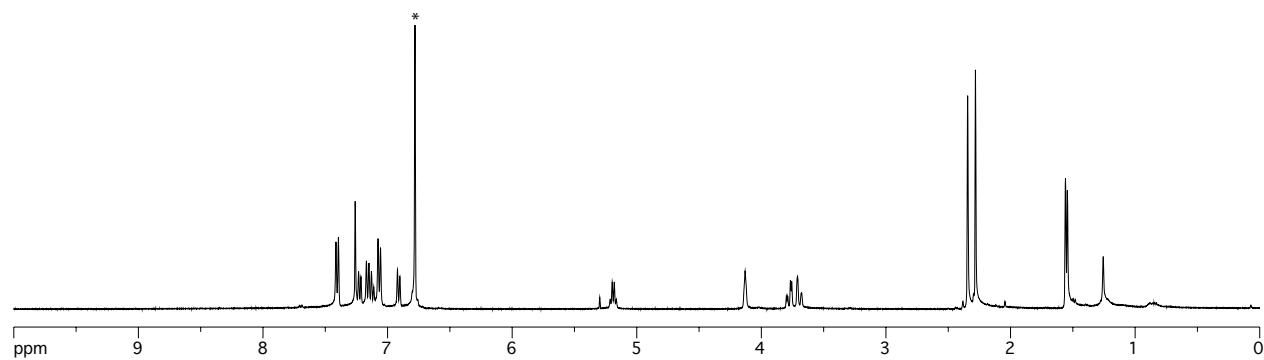
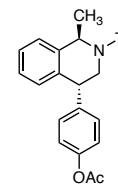


Figure V-50. ¹H NMR spectrum of *trans*-V.5j in CDCl₃ (400 MHz) at 23 °C.*CDCl₃ solvent peak. Peaks with d < 1.4 ppm are from H grease.

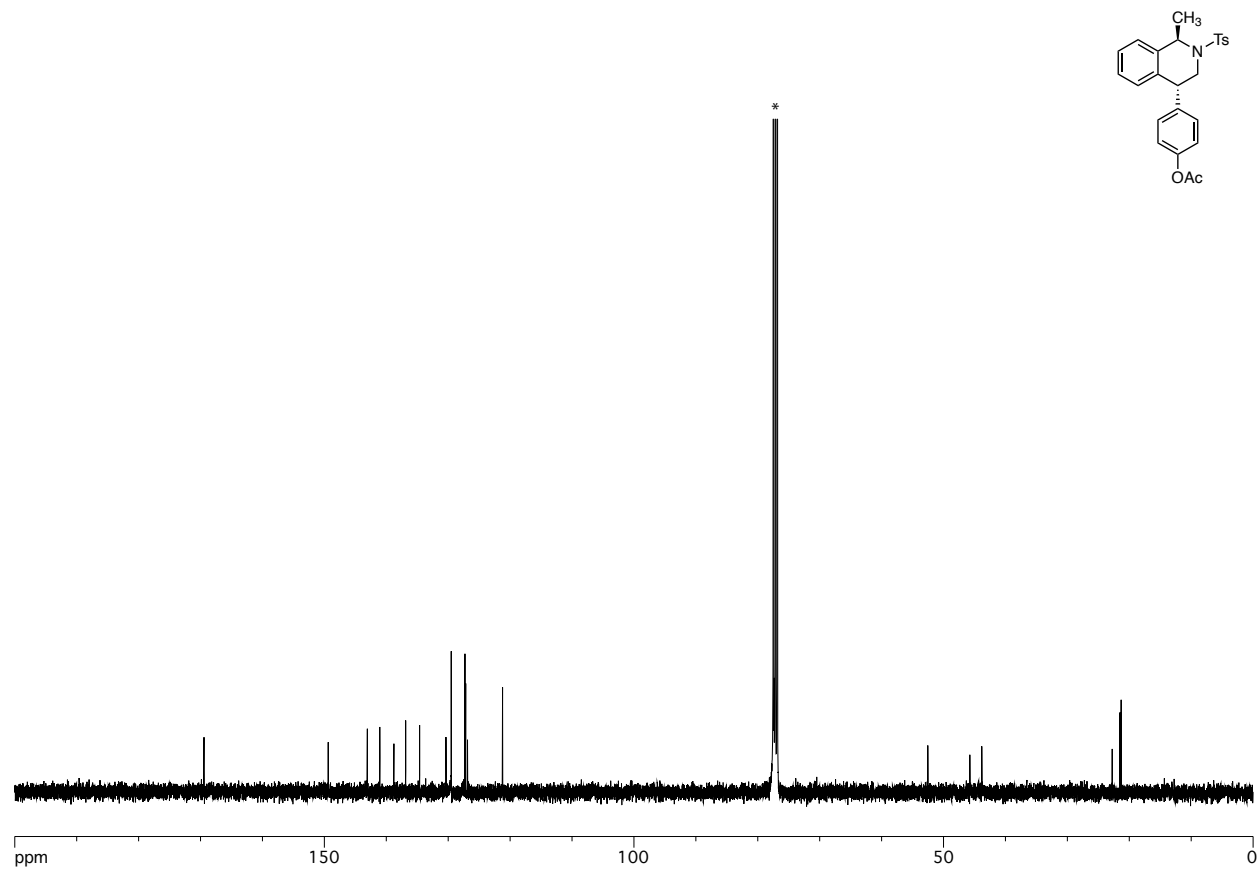


Figure V-51. ¹³C NMR spectrum of *trans*-V.5j in CDCl₃ (100 MHz) at 23 °C.*CDCl₃ solvent peak.

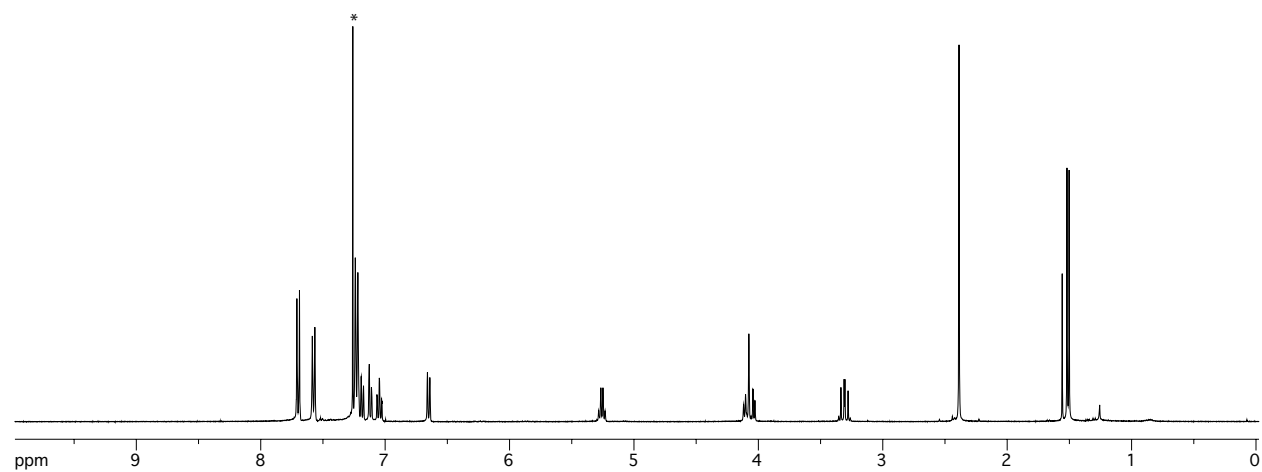
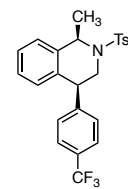


Figure V-52. ¹H NMR spectrum of *cis*-V.5k in CDCl₃ (400 MHz) at 23 °C. *CDCl₃ solvent peak.

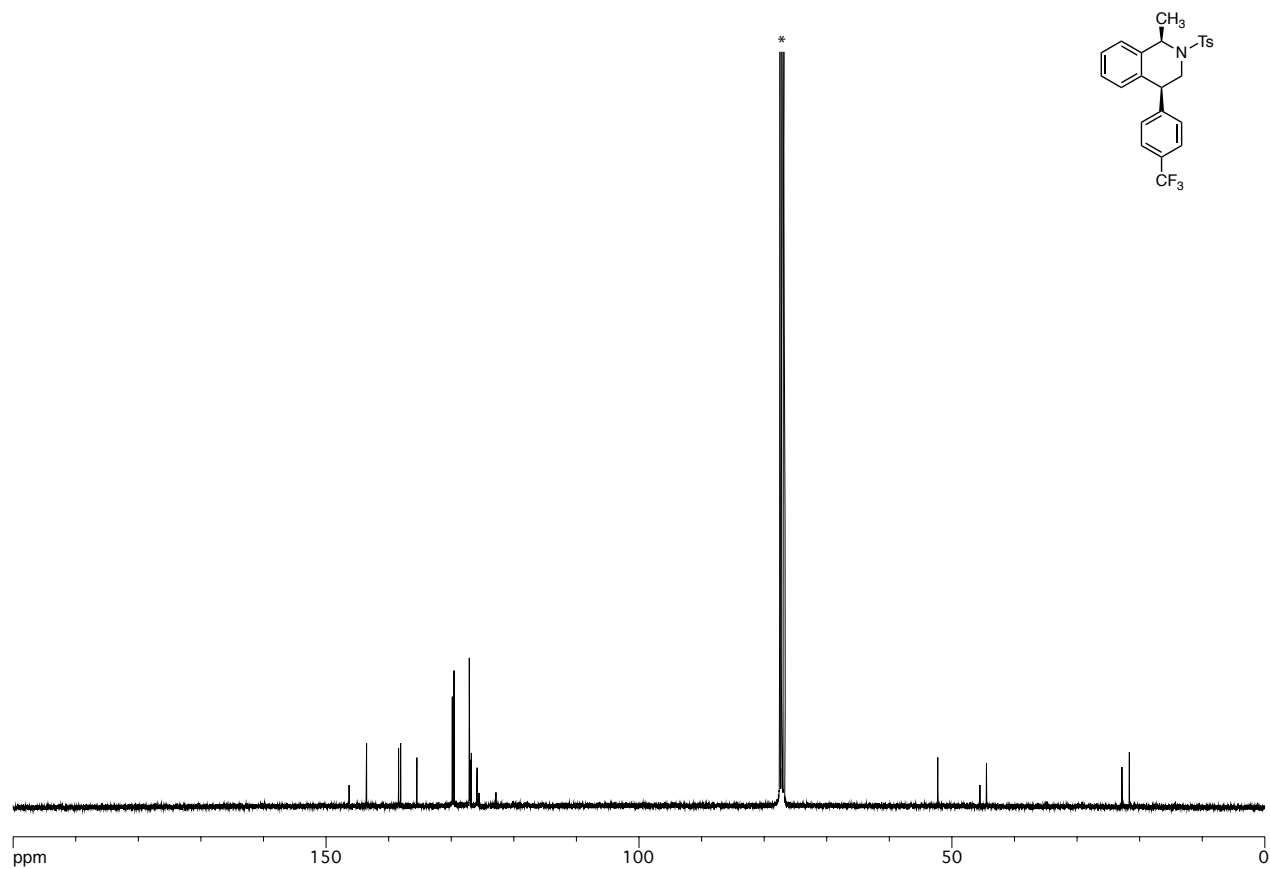


Figure V-53. ¹³C NMR spectrum of *cis*-V.5k in CDCl₃ (100 MHz) at 23 °C.*CDCl₃ solvent peak.

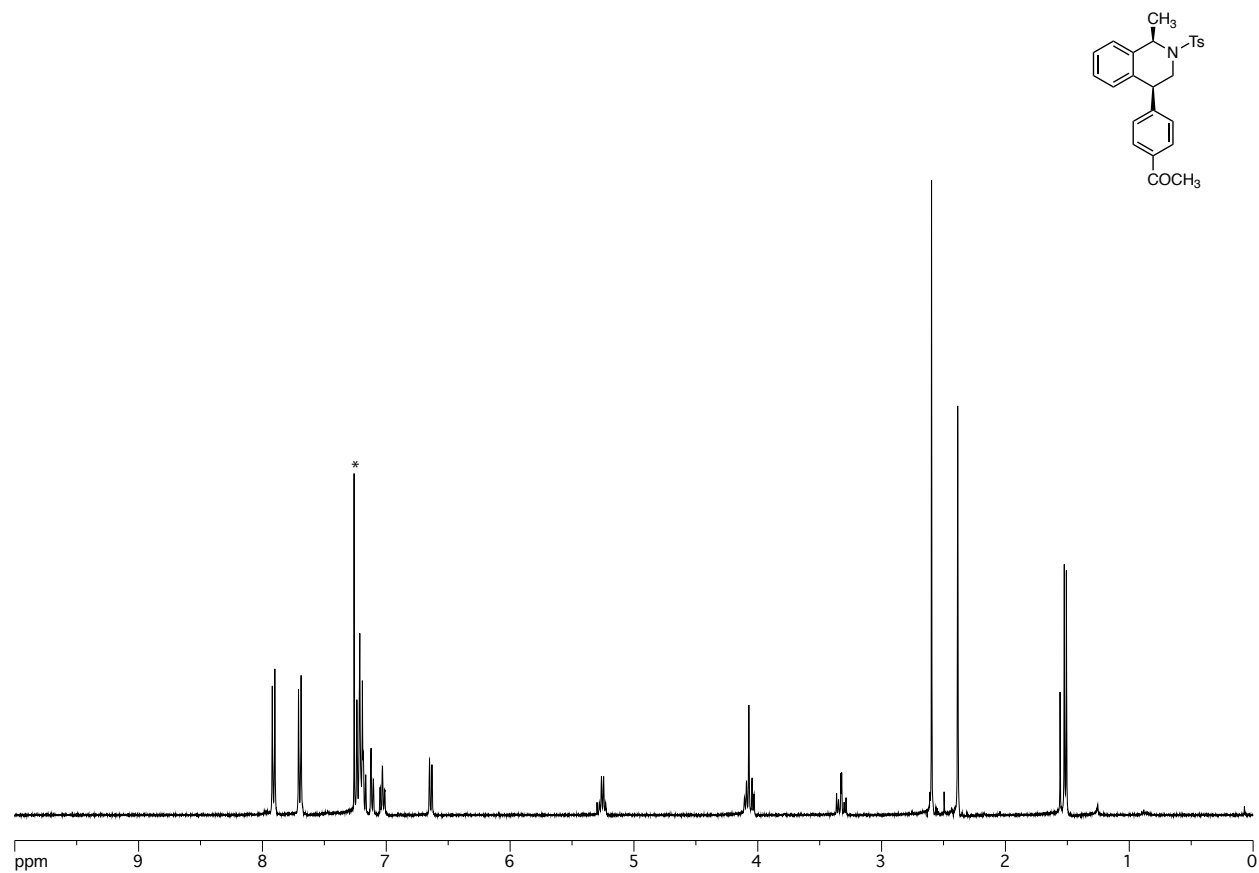


Figure V-54. ¹H NMR spectrum of *cis*-V.51 in CDCl₃ (400 MHz) at 23 °C.*CDCl₃ solvent peak.

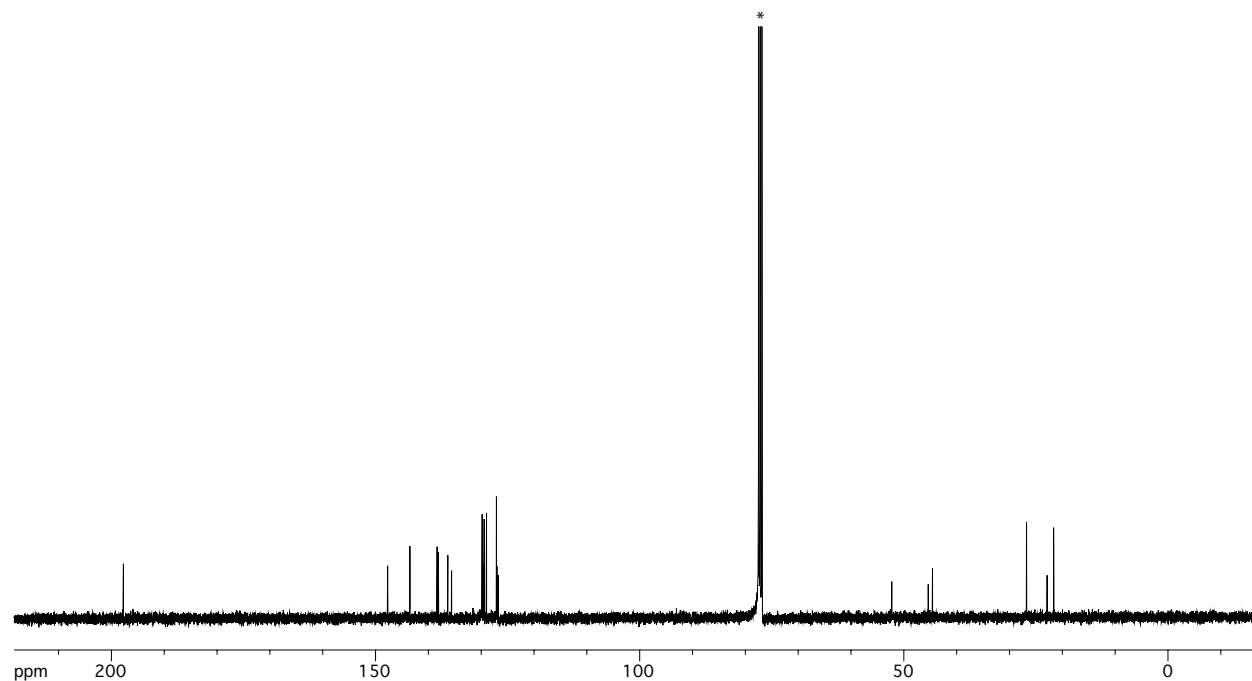
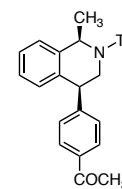


Figure V-55. ¹³C NMR spectrum of *cis*-V.5I in CDCl₃ (100 MHz) at 23 °C. *CDCl₃ solvent peak.

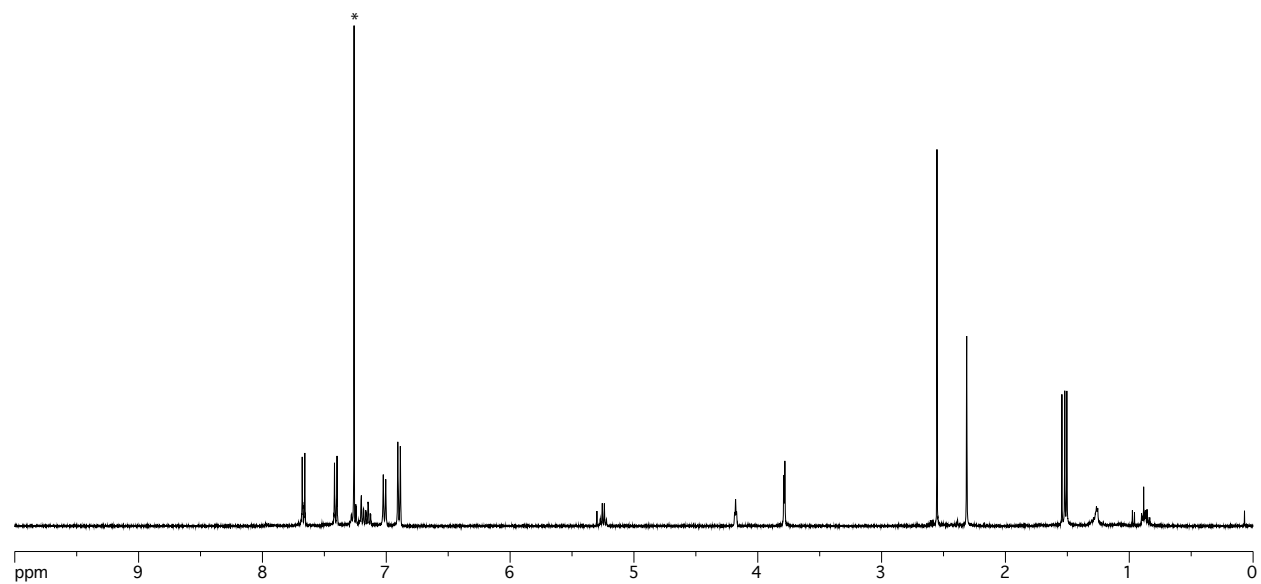
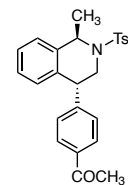


Figure V-56. ^1H NMR spectrum of *trans*-V.51 in CDCl_3 (400 MHz) at 23 °C.* CDCl_3 solvent peak. Peaks with $\delta < 1.4$ ppm are from H grease.

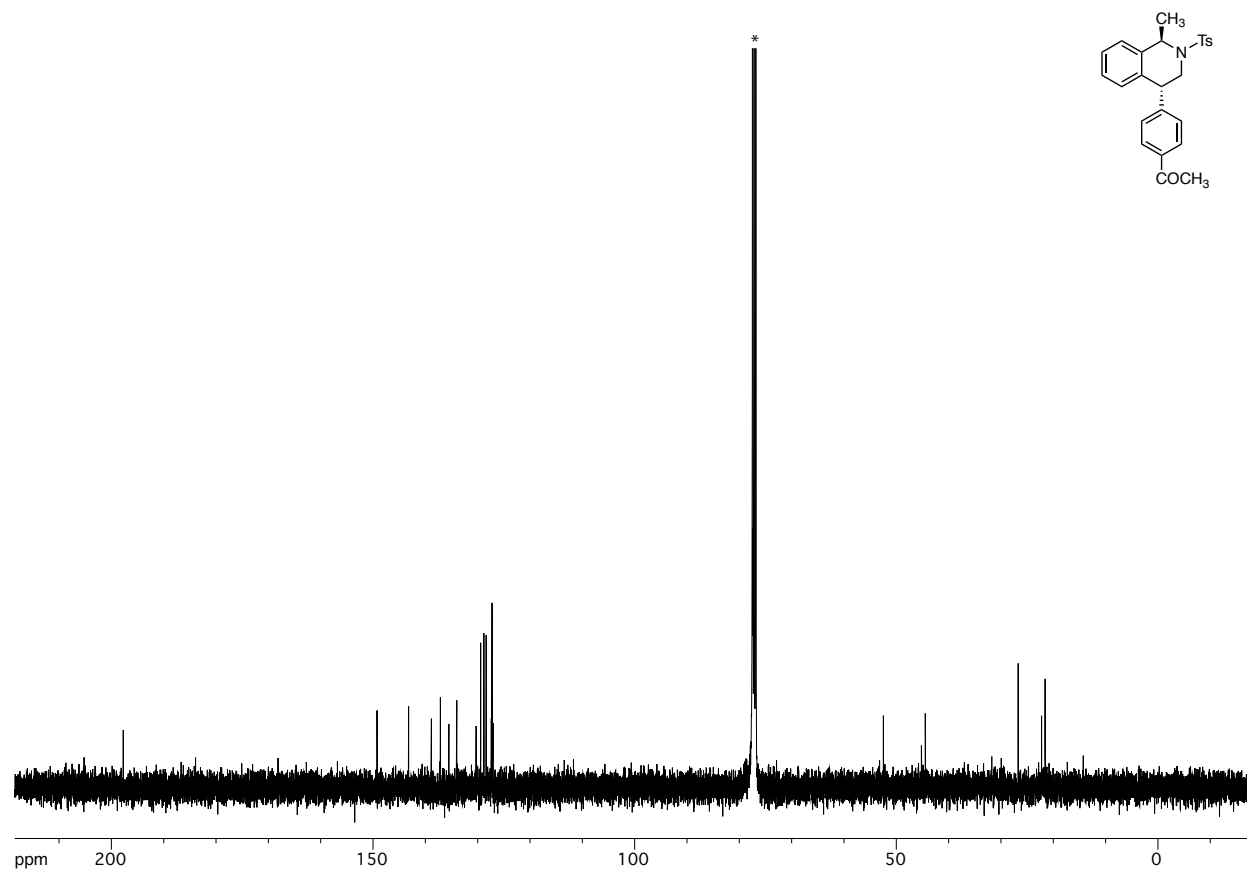


Figure V-57. ¹³C NMR spectrum of *trans*-V.5l in CDCl₃ (100 MHz) at 23 °C.*CDCl₃ solvent peak.

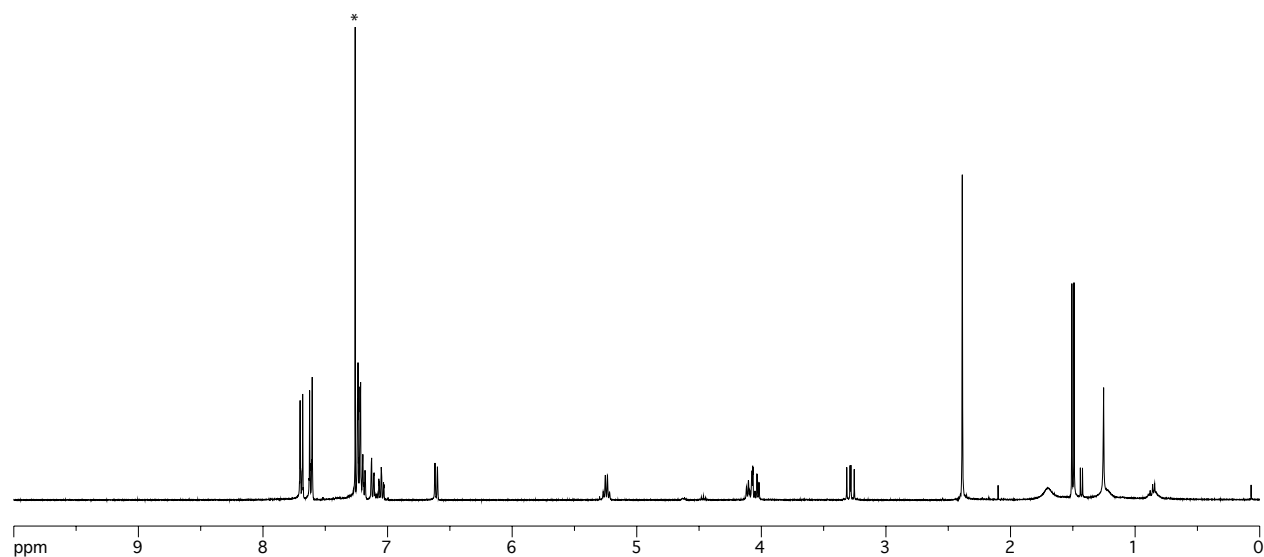
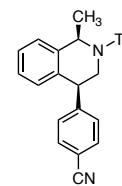


Figure V-58. ^1H NMR spectrum of *cis*-V.5m in CDCl_3 (400 MHz) at 23 °C. * CDCl_3 solvent peak. Peaks with $\delta < 1.4$ ppm are from H grease. The doublet with $\delta = 1.43$ ppm is due to overlapped peak from H-atom abstraction side products.

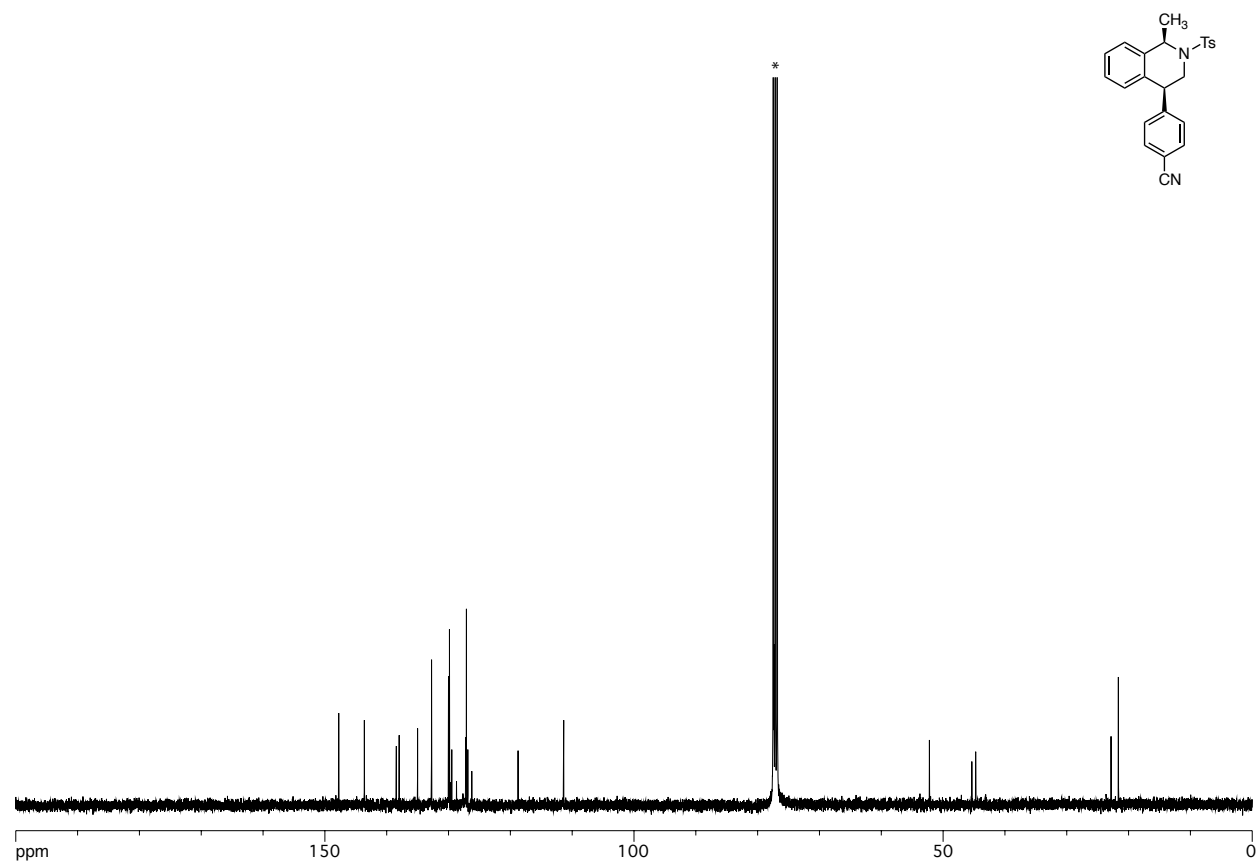


Figure V-59. ¹³C NMR spectrum of *cis*-V.5m in CDCl₃ (100 MHz) at 23 °C.*CDCl₃ solvent peak.

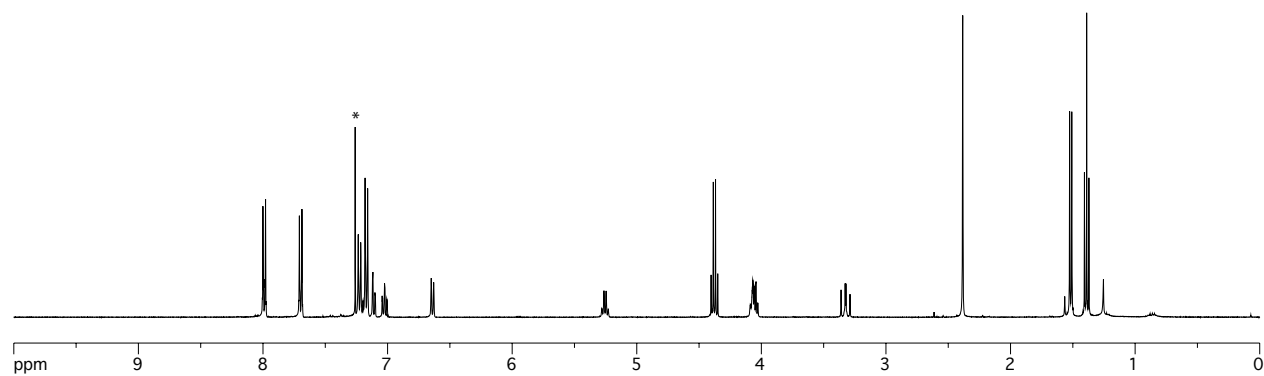
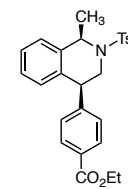


Figure V-60. ¹H NMR spectrum of *cis*-V.5n in CDCl₃ (400 MHz) at 23 °C. *CDCl₃ solvent peak.

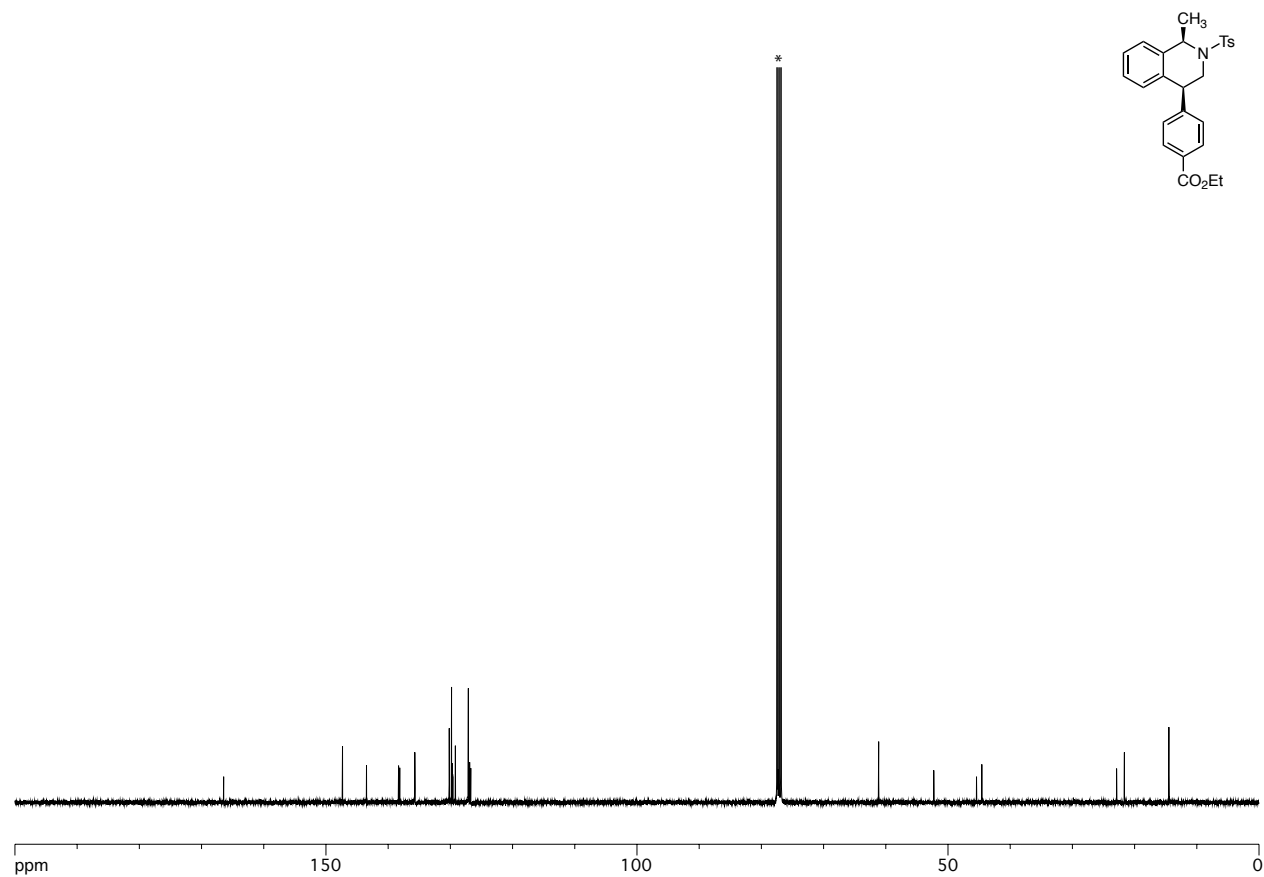


Figure V-61. ¹³C NMR spectrum of *cis*-V.5n in CDCl₃ (100 MHz) at 23 °C.*CDCl₃ solvent peak.

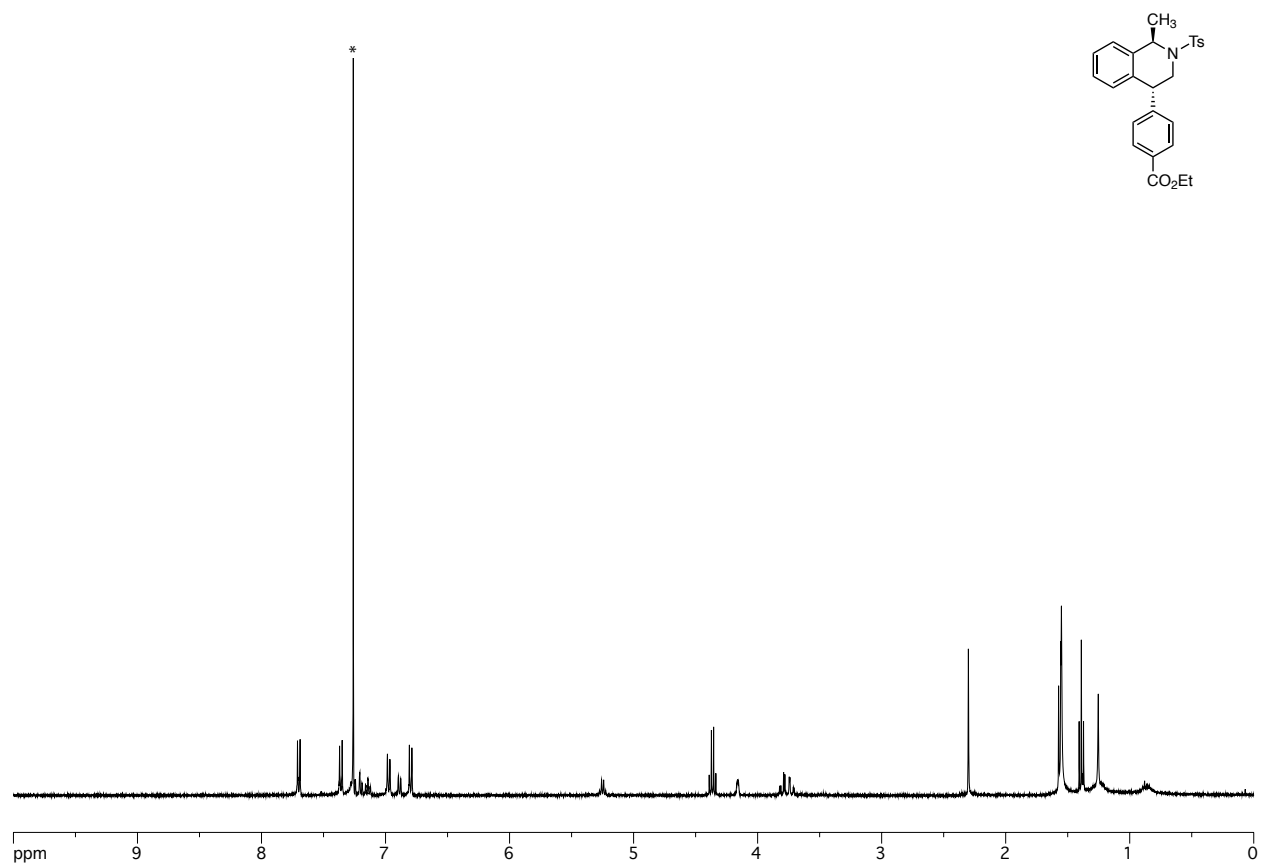


Figure V-62. ¹H NMR spectrum of *trans*-V.5n in CDCl₃ (400 MHz) at 23 °C.*CDCl₃ solvent peak. Peaks with d < 1.4 ppm are from H grease.

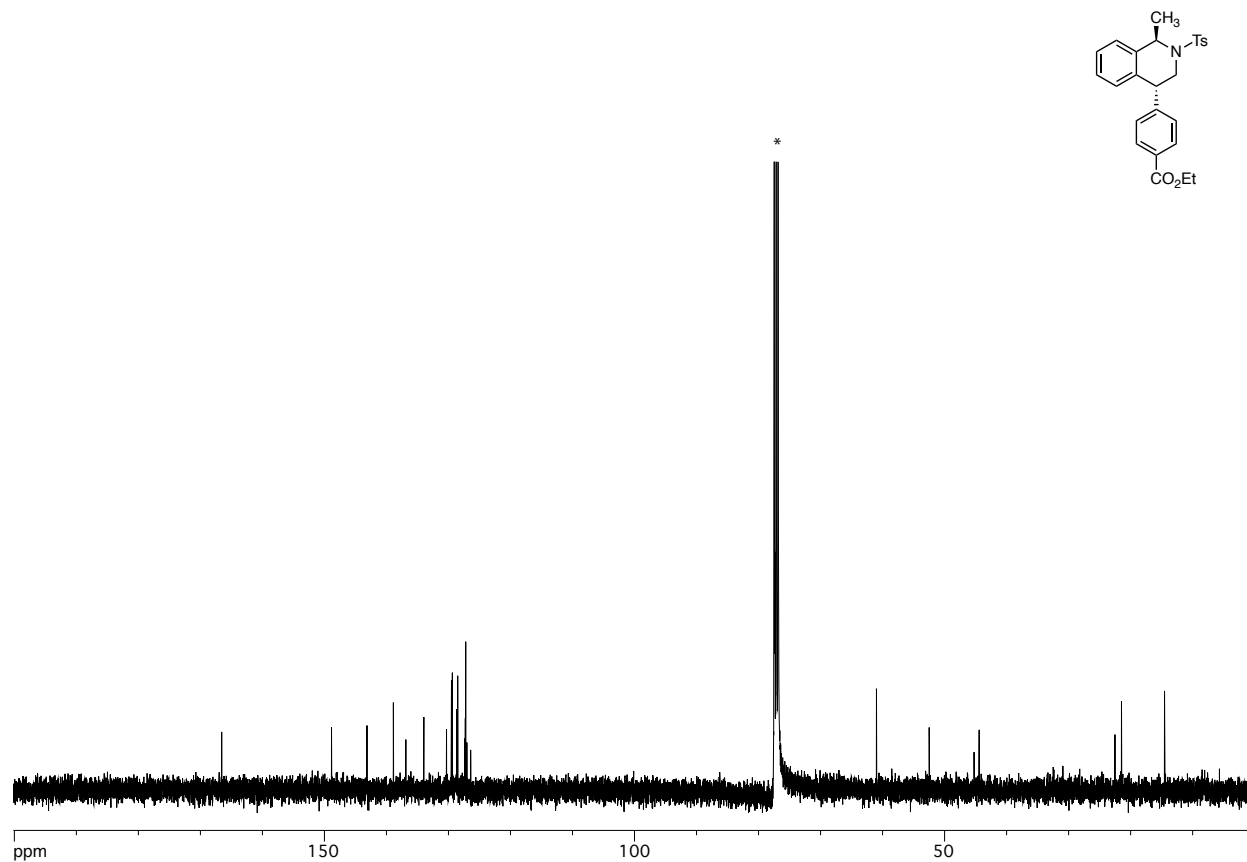


Figure V-63. ¹³C NMR spectrum of *trans*-V.5n in CDCl₃ (100 MHz) at 23 °C.*CDCl₃ solvent peak.

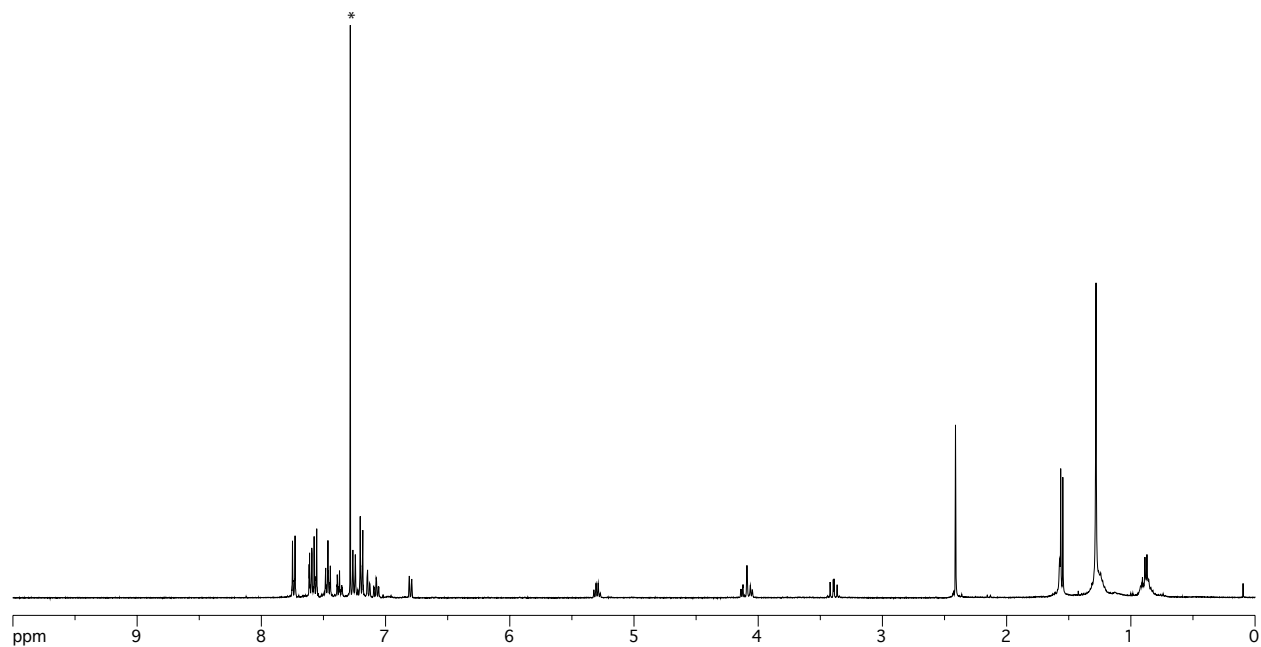
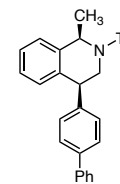


Figure V-64. ¹H NMR spectrum of *cis*-V.50 in CDCl₃ (400 MHz) at 23 °C.*CDCl₃ solvent peak. Peaks with d < 1.4 ppm are from H grease.

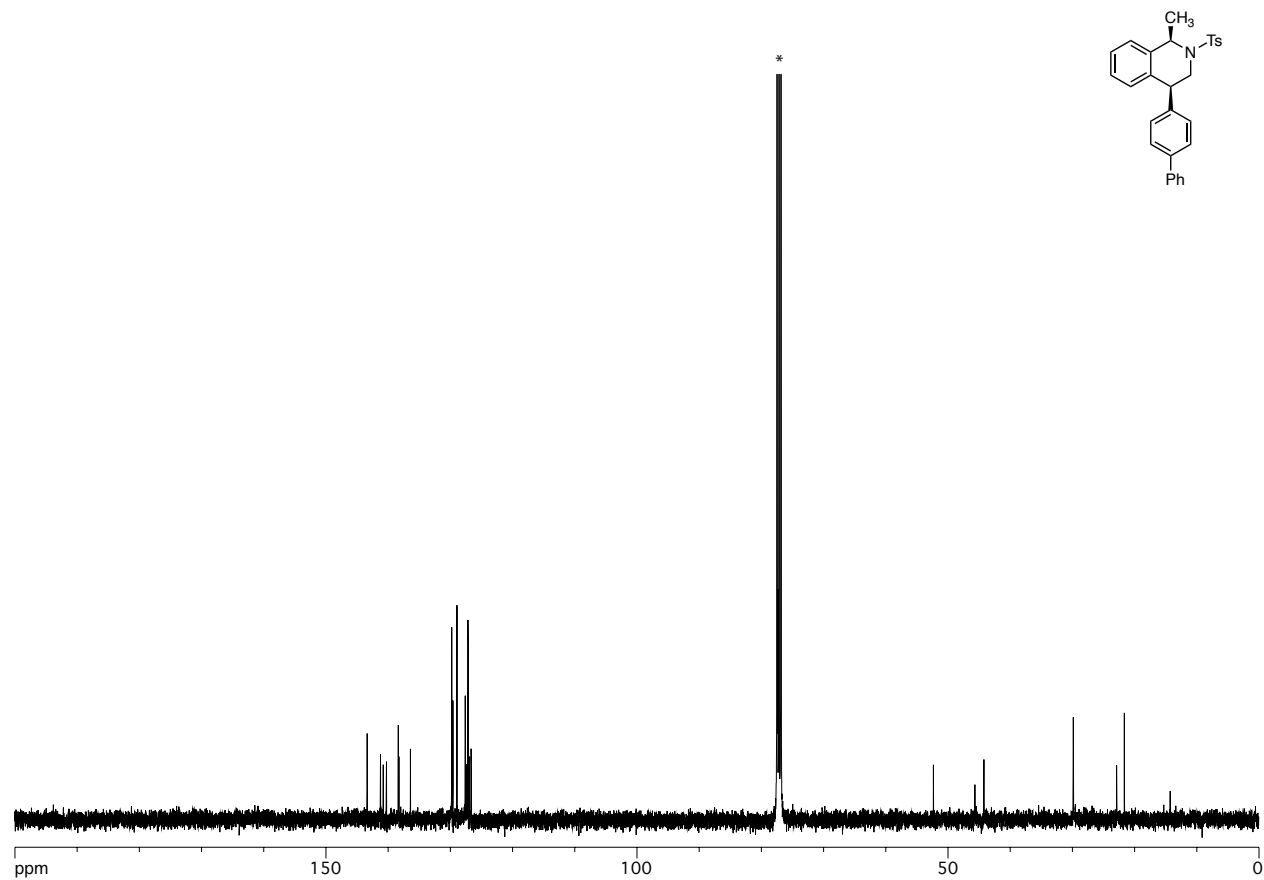


Figure V-65. ¹³C NMR spectrum of *cis*-V.50 in CDCl₃ (100 MHz) at 23 °C.*CDCl₃ solvent peak.

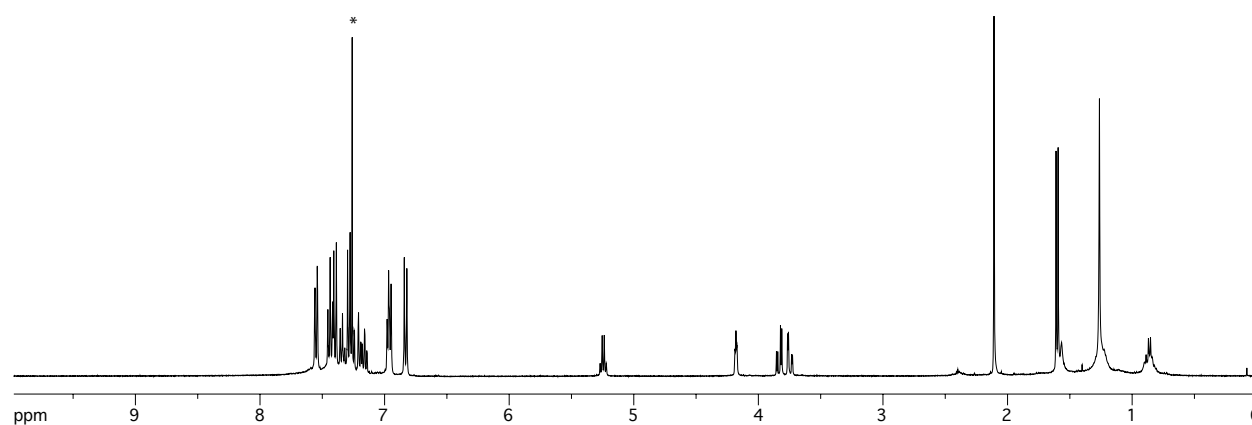
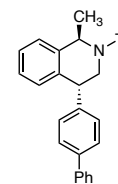


Figure V-66. ¹H NMR spectrum of *trans*-V.5o in CDCl₃ (400 MHz) at 23 °C. *CDCl₃ solvent peak. Peaks with $\delta < 1.4$ ppm are from H grease.

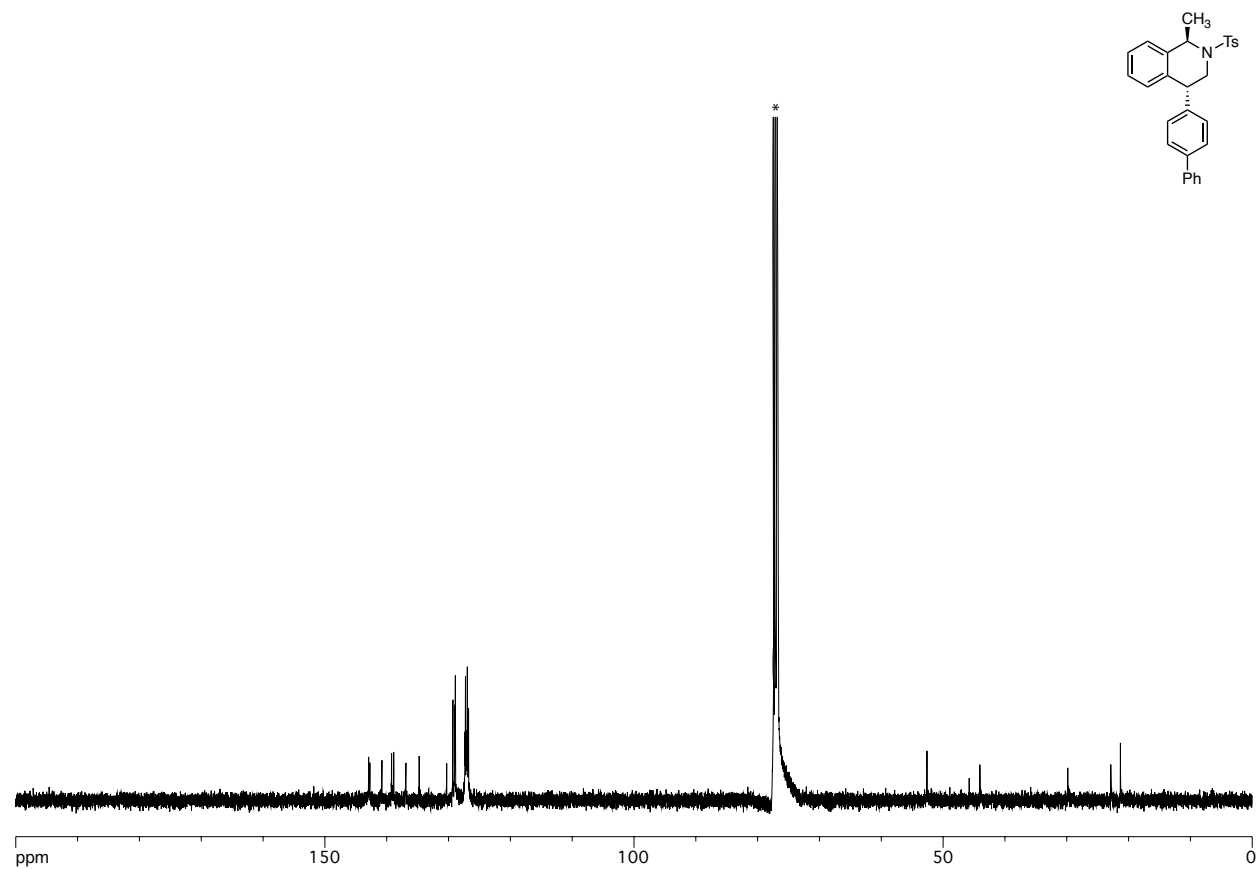


Figure V-67. ¹³C NMR spectrum of *trans*-V.50 in CDCl₃ (100 MHz) at 23 °C.*CDCl₃ solvent peak.

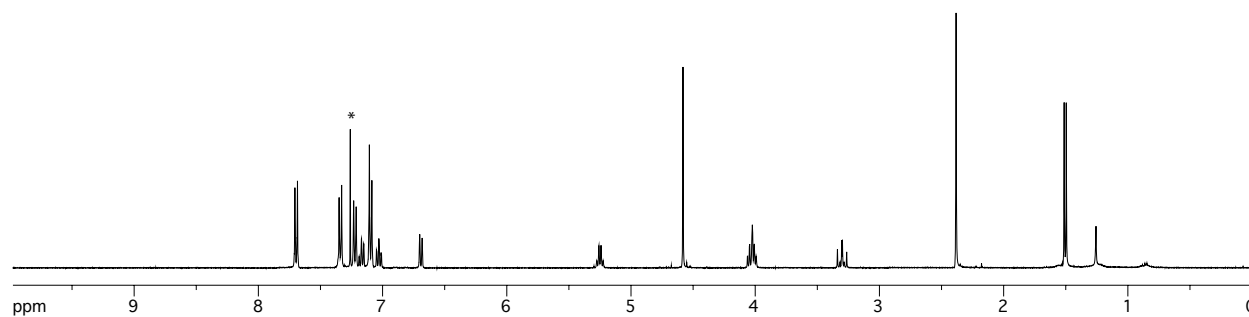
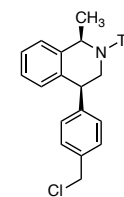


Figure V-68. ^1H NMR spectrum of *cis*-V.5p in CDCl_3 (400 MHz) at 23 °C. * CDCl_3 solvent peak.

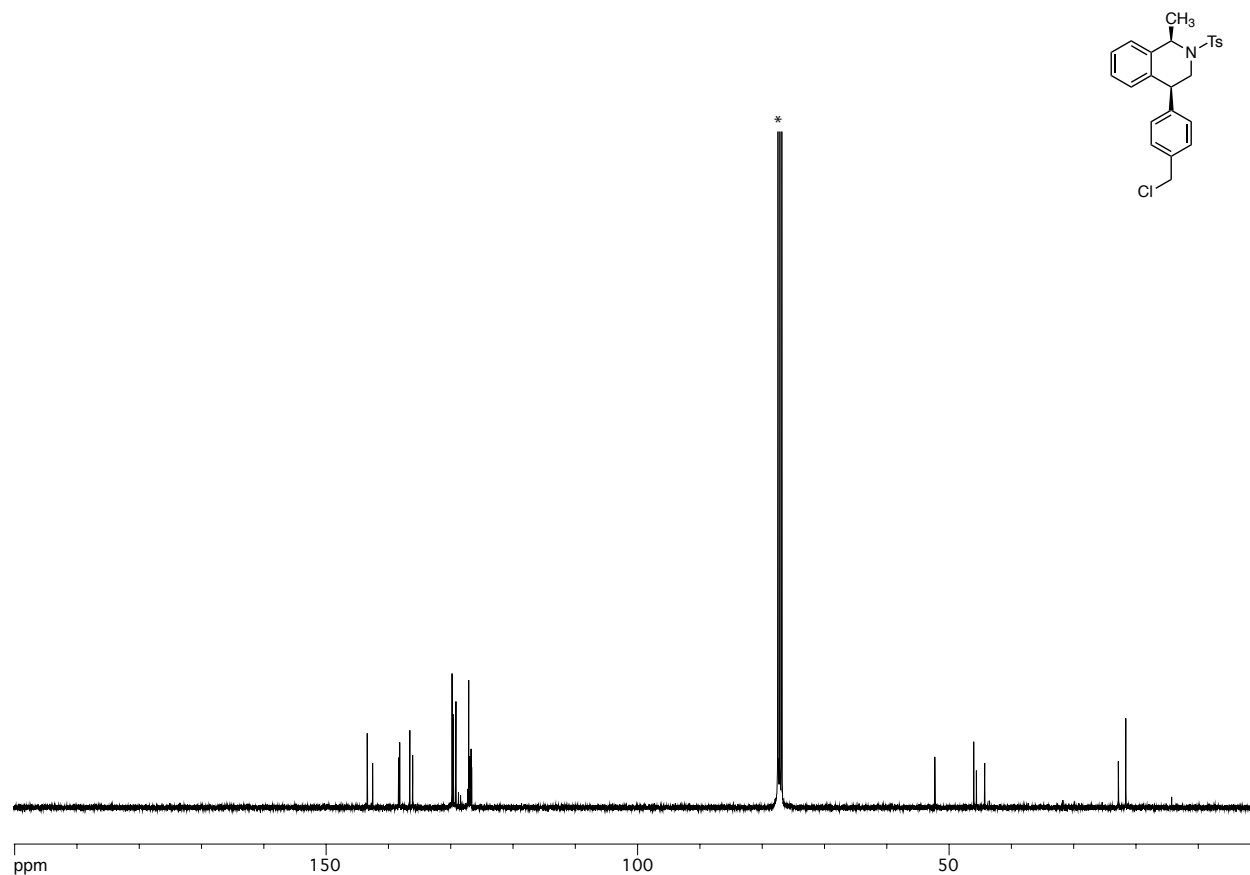


Figure V-69. ^{13}C NMR spectrum of *cis*-V.5p in CDCl_3 (100 MHz) at 23 °C.* CDCl_3 solvent peak.

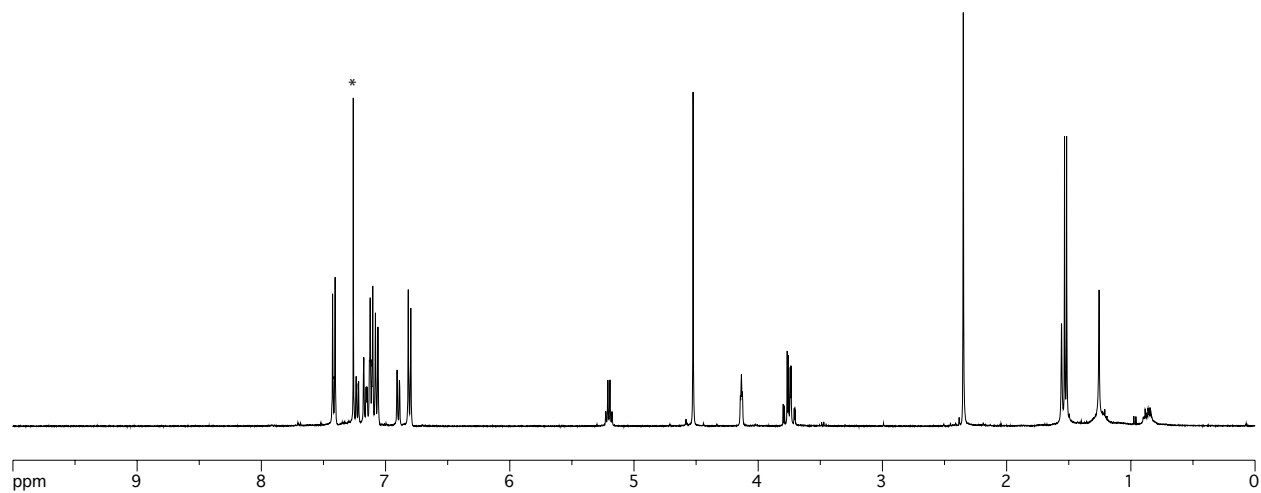
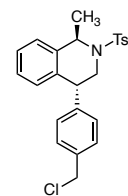


Figure V-70. ^1H NMR spectrum of *trans*-V.5p in CDCl_3 (400 MHz) at 23 °C. * CDCl_3 solvent peak.

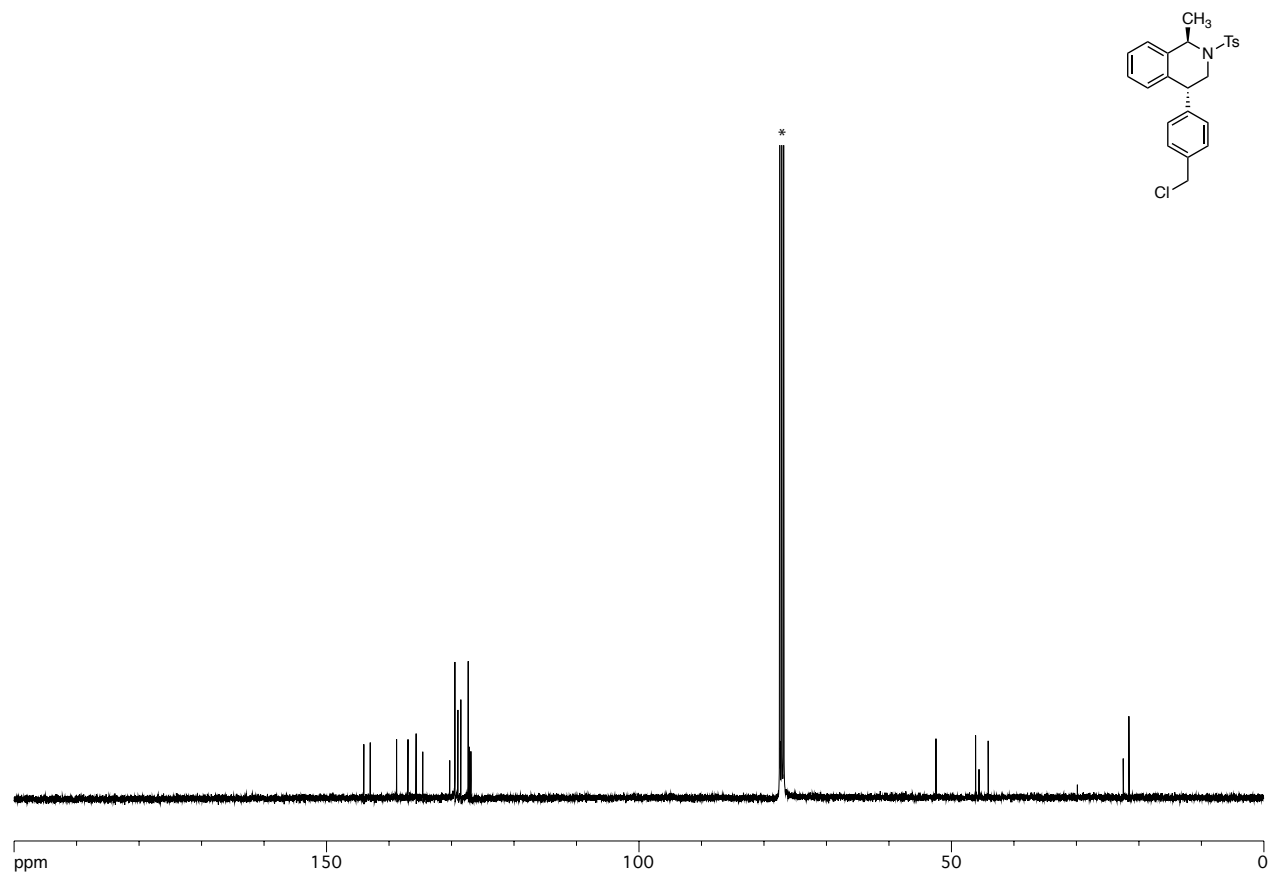


Figure V-71. ^{13}C NMR spectrum of *trans*-V.5p in CDCl_3 (100 MHz) at 23 °C.* CDCl_3 solvent peak.

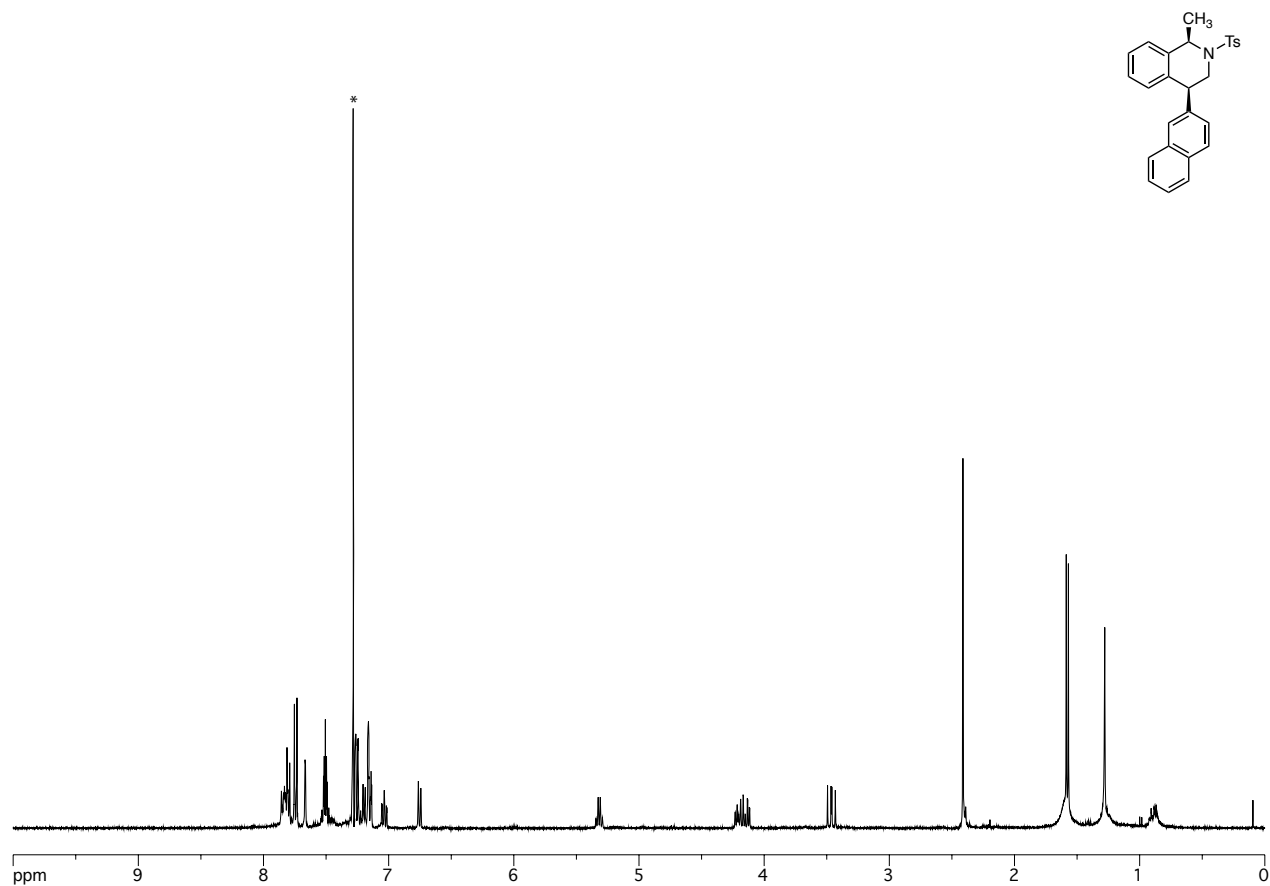


Figure V-72. ¹H NMR spectrum of *cis*-V.5q in CDCl₃ (400 MHz) at 23 °C.*CDCl₃ solvent peak. Peaks with d < 1.4 ppm are from H grease.

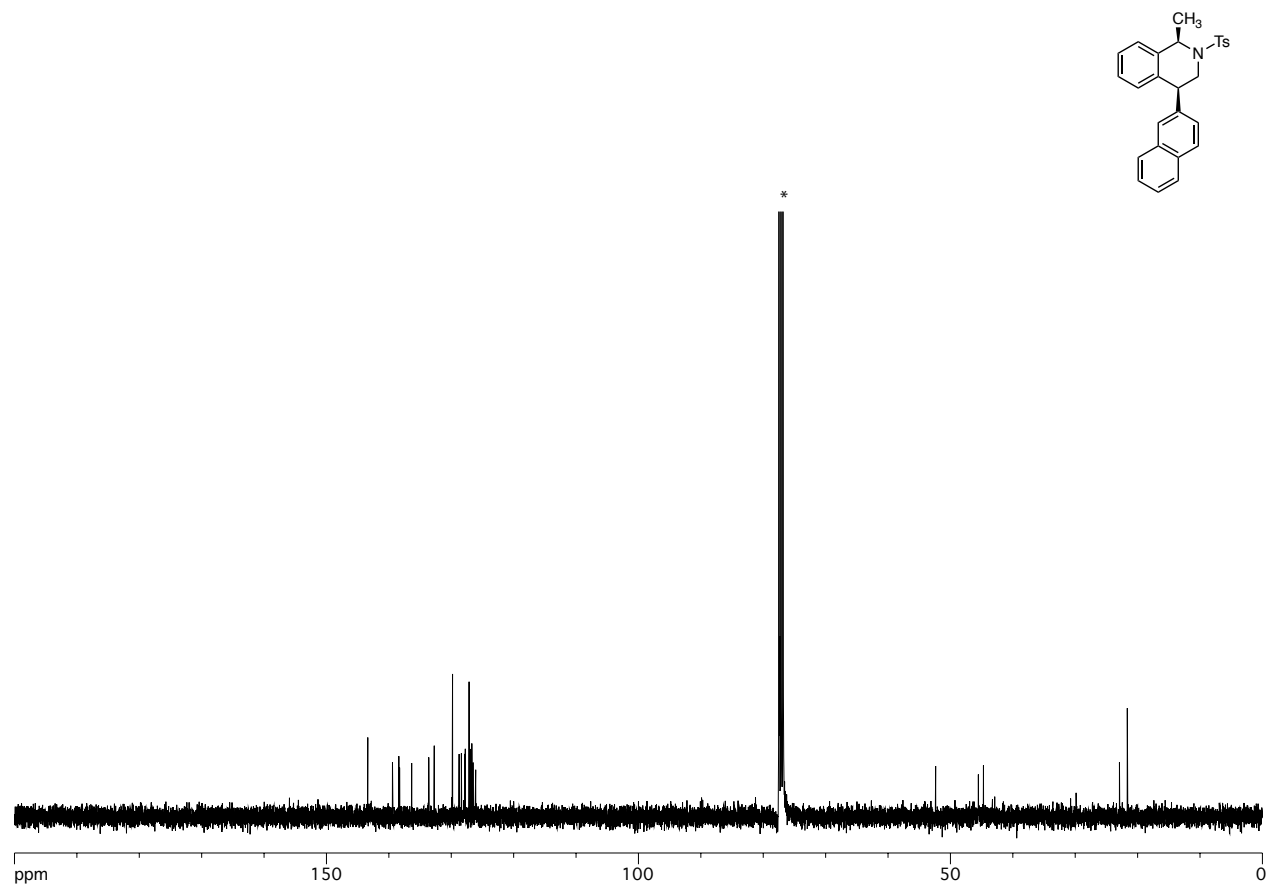


Figure V-73. ¹³C NMR spectrum of *cis*-V.5q in CDCl₃ (100 MHz) at 23 °C.*CDCl₃ solvent peak.

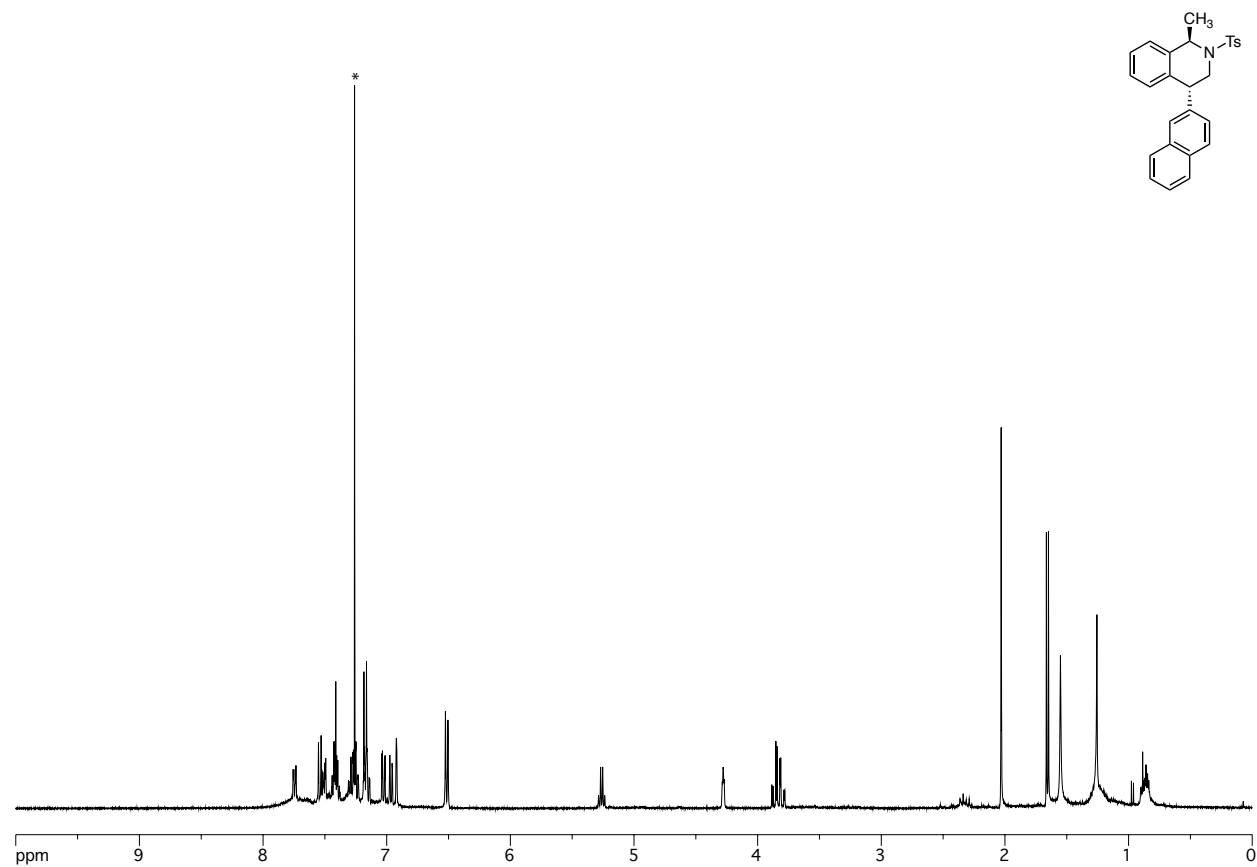


Figure V-74. ¹H NMR spectrum of *trans*-V.5q in CDCl₃ (400 MHz) at 23 °C.*CDCl₃ solvent peak. Peaks with $\delta < 1.4$ ppm are from H grease.

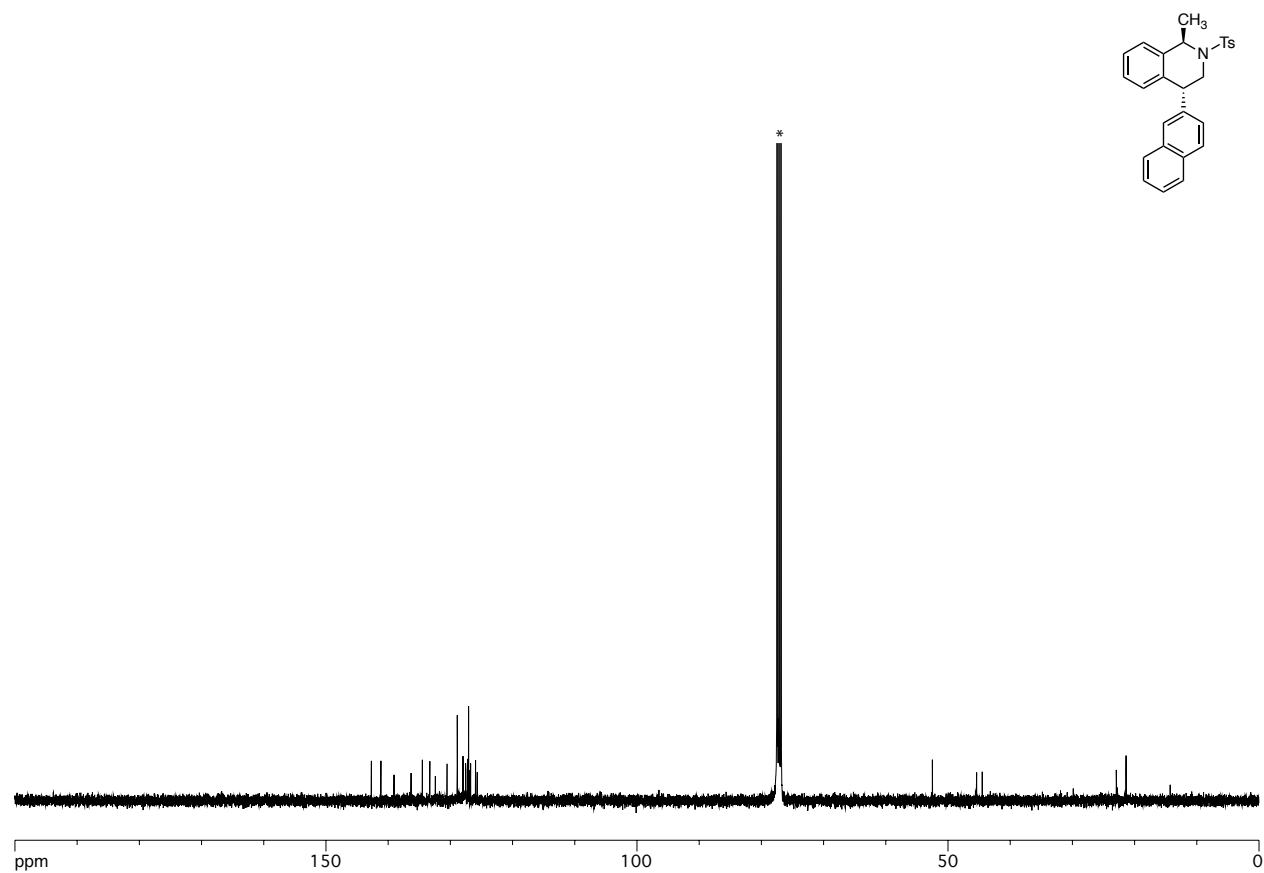


Figure V-75. ¹³C NMR spectrum of *trans*-V.5q in CDCl₃ (100 MHz) at 23 °C.*CDCl₃ solvent peak.

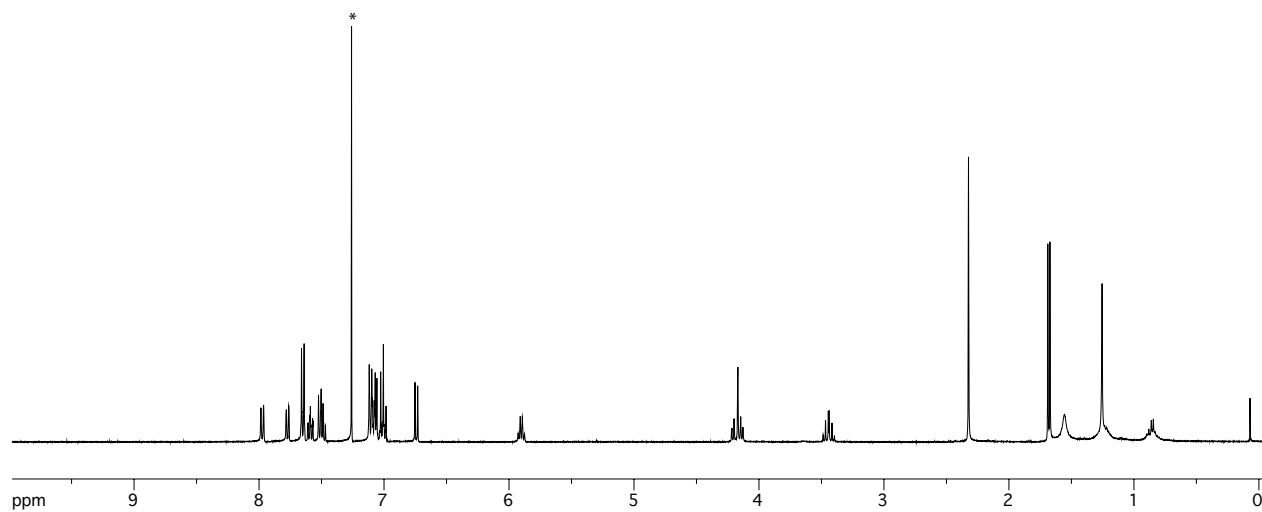
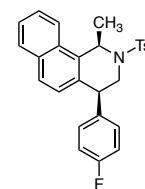


Figure V-76. ¹H NMR spectrum of *cis*-V.5r in CDCl₃ (400 MHz) at 23 °C.*CDCl₃ solvent peak. Peaks with d < 1.4 ppm are from H grease.

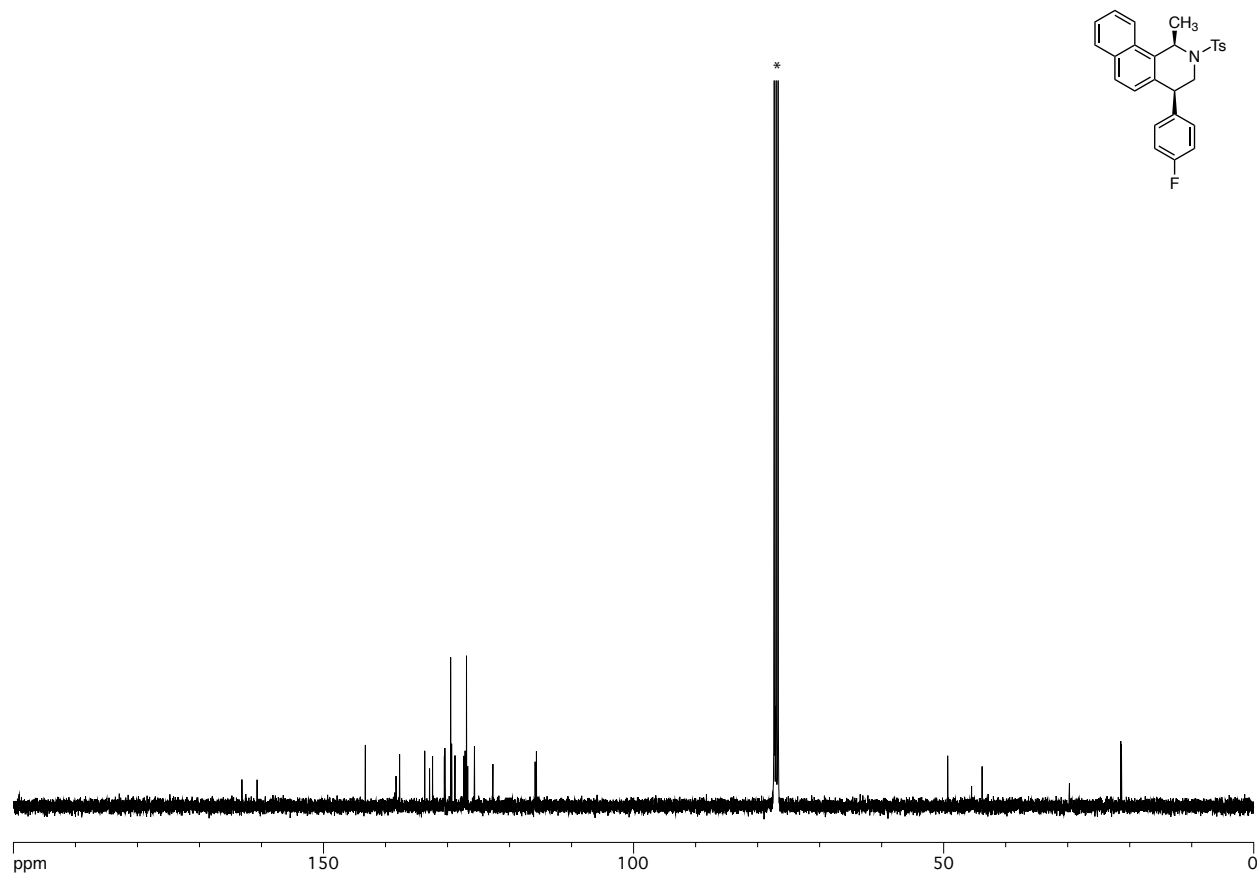


Figure V-77. ¹³C NMR spectrum of *cis*-V.5r in CDCl₃ (100 MHz) at 23 °C.*CDCl₃ solvent peak.

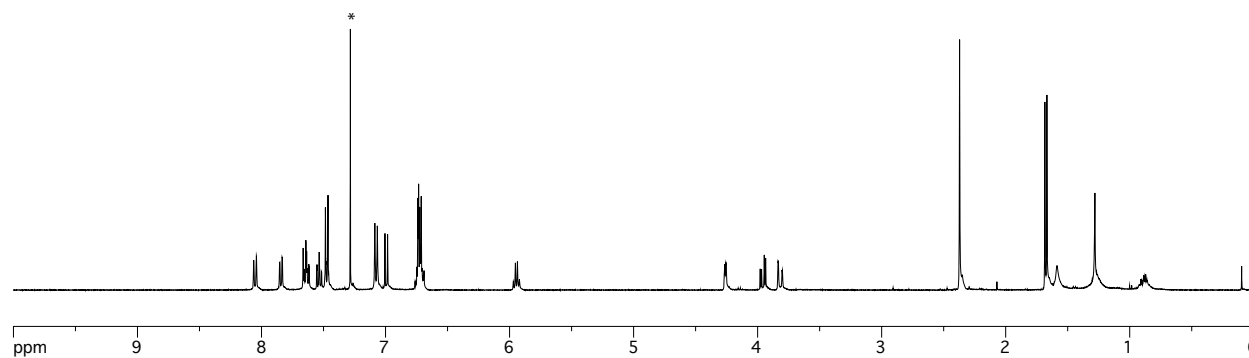
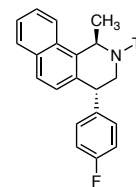


Figure V-78. ¹H NMR spectrum of *trans*-V.5r in CDCl₃ (400 MHz) at 23 °C.*CDCl₃ solvent peak. Peaks with d < 1.4 ppm are from H grease.

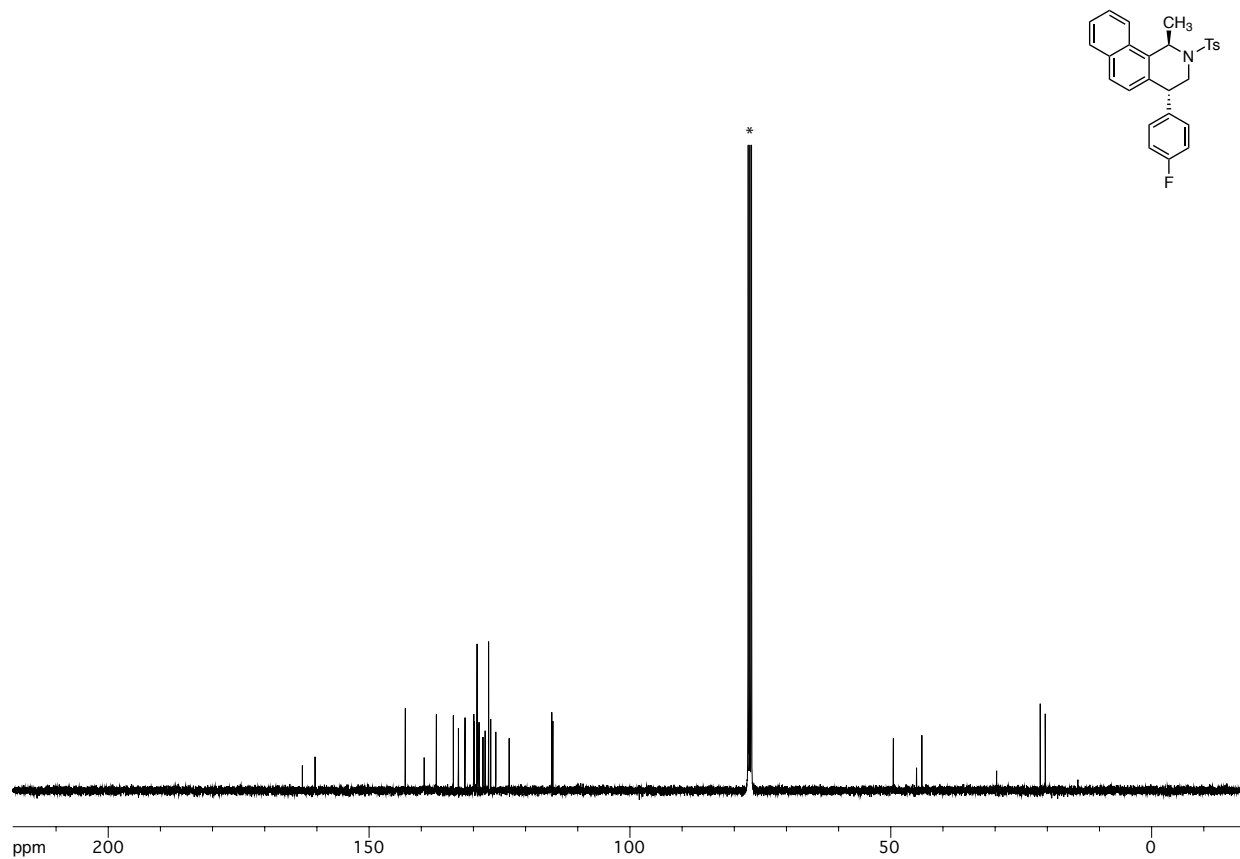


Figure V-79. ¹³C NMR spectrum of *trans*-V.5r in CDCl₃ (100 MHz) at 23 °C.*CDCl₃ solvent peak.

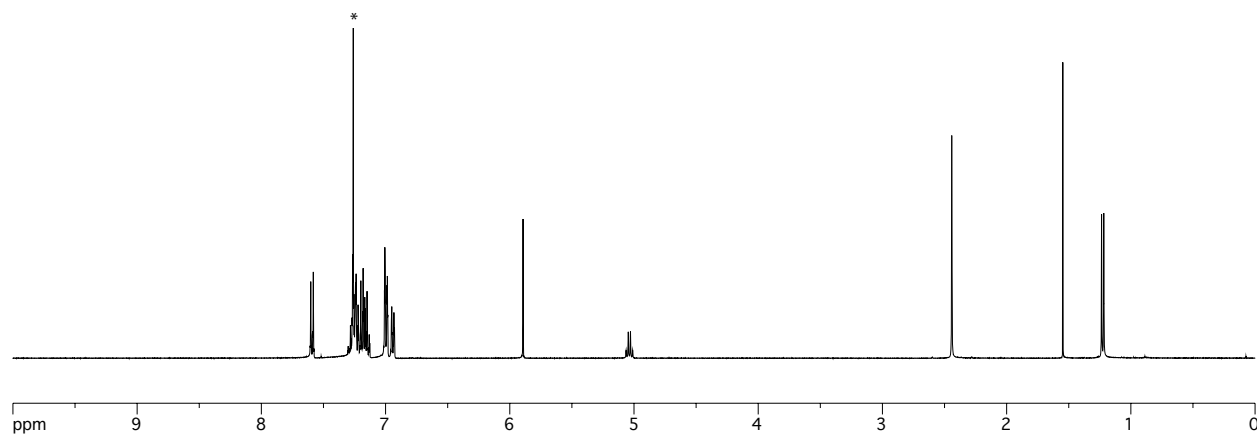
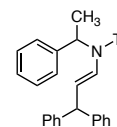


Figure V-80. ^1H NMR spectrum of compound V.5s in CDCl_3 (400 MHz) at 23 °C. * CDCl_3 solvent peak.

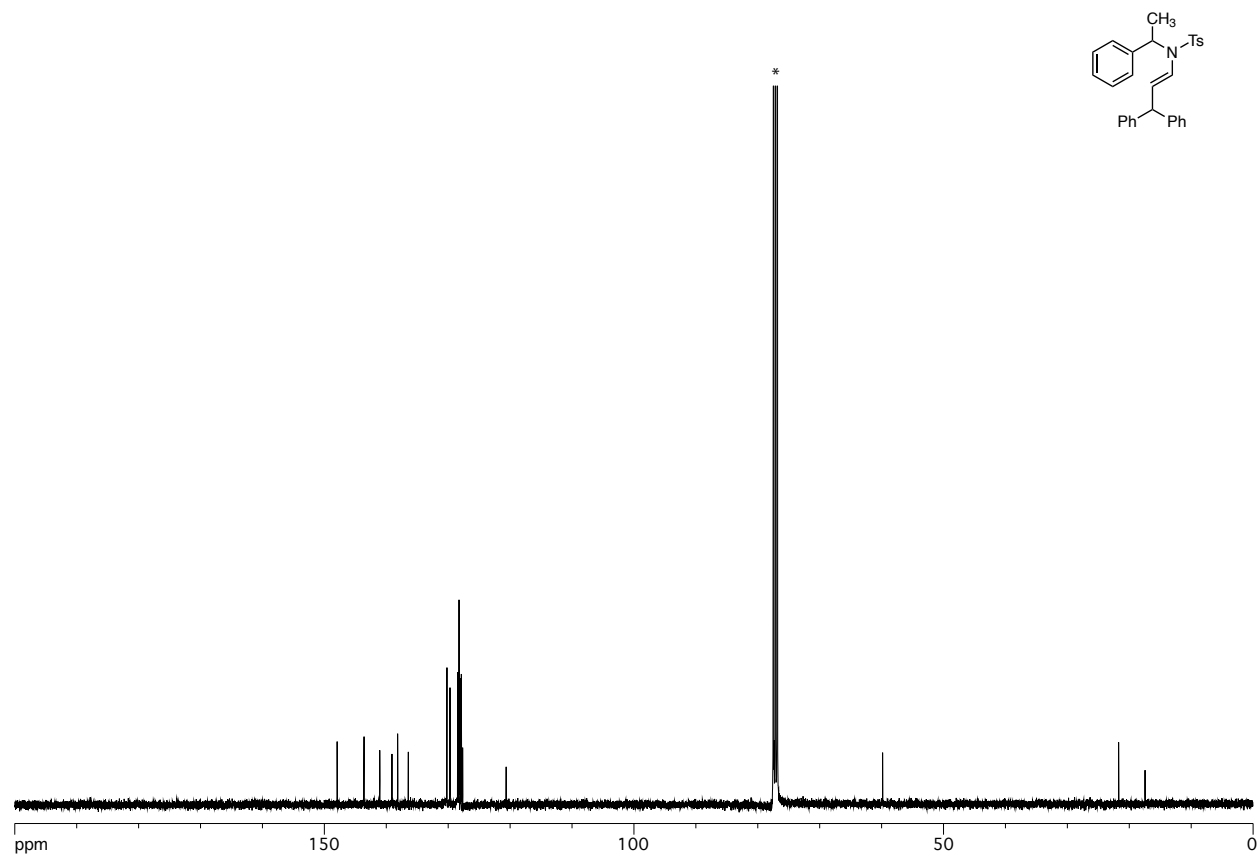


Figure V-81. ¹³C NMR spectrum of compound V.5s in CDCl₃ (100 MHz) at 23 °C.*CDCl₃ solvent peak.

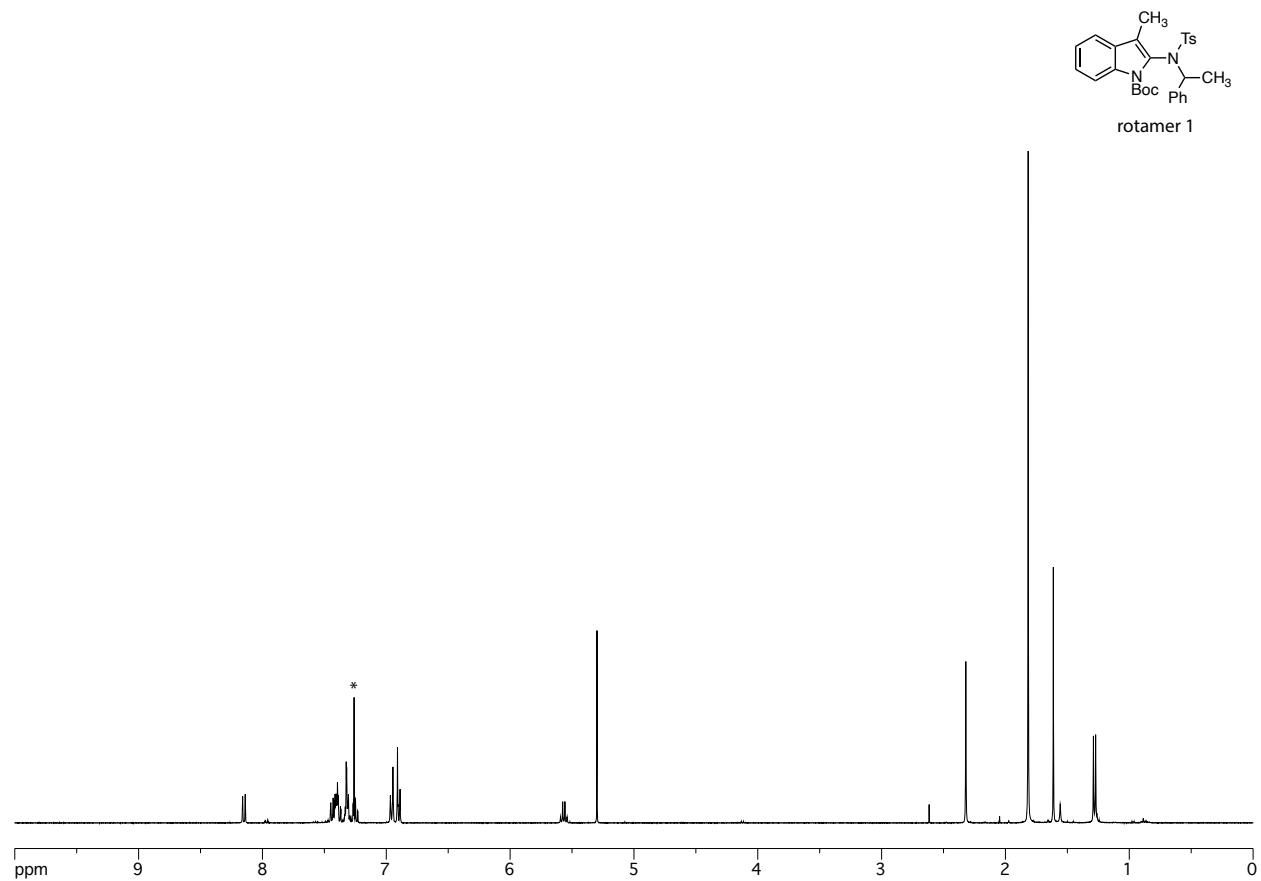


Figure V-82. ^1H NMR spectrum of rotamer 1 of compound V.7 in CDCl_3 (400 MHz) at 23 °C. * CDCl_3 solvent peak. Peaks with $d = 5.30$ ppm is from residual CH_2Cl_2 .

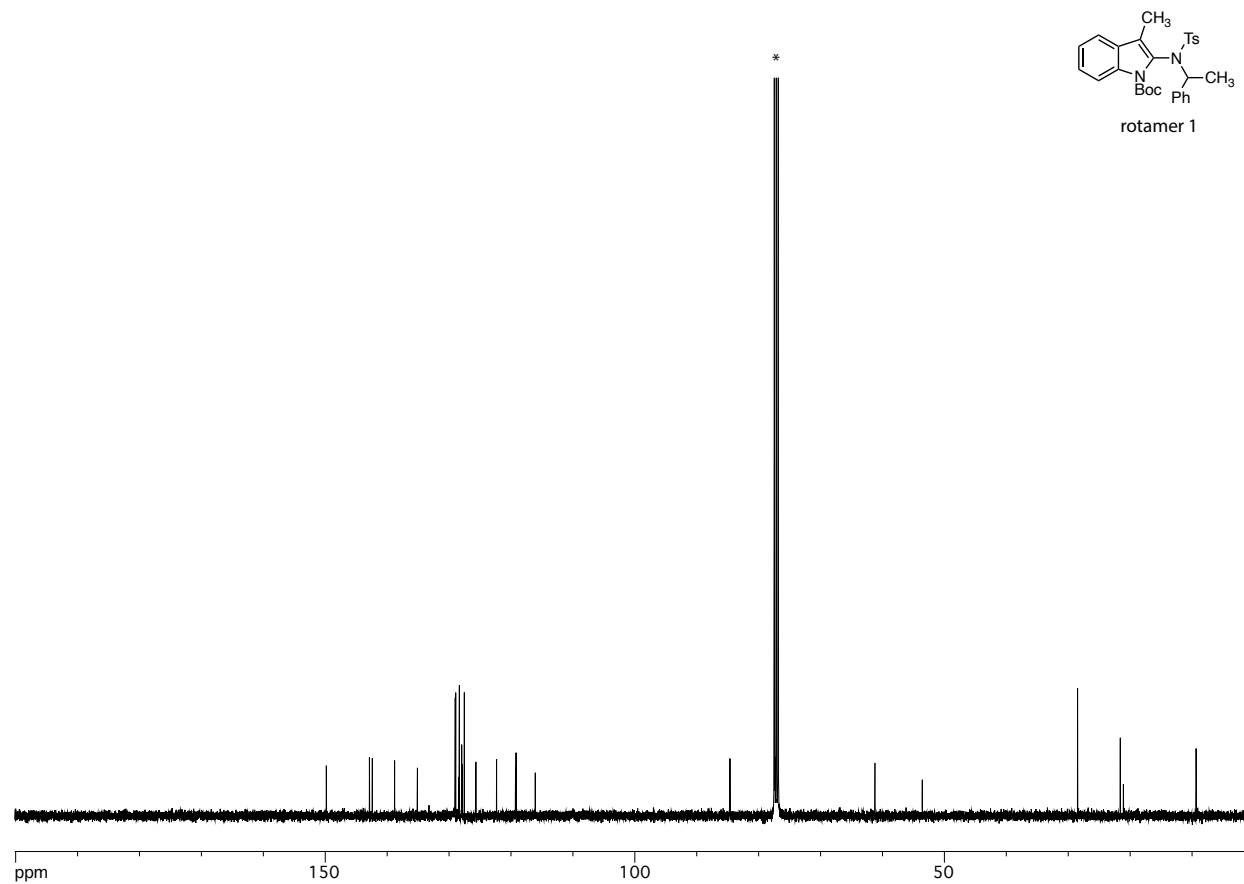


Figure V-83. ¹³C NMR spectrum of rotamer 1 of compound V.7 in CDCl₃ (100 MHz) at 23 °C.*CDCl₃ solvent peak. Peaks with d = 53.2 ppm is from residual CH₂Cl₂.

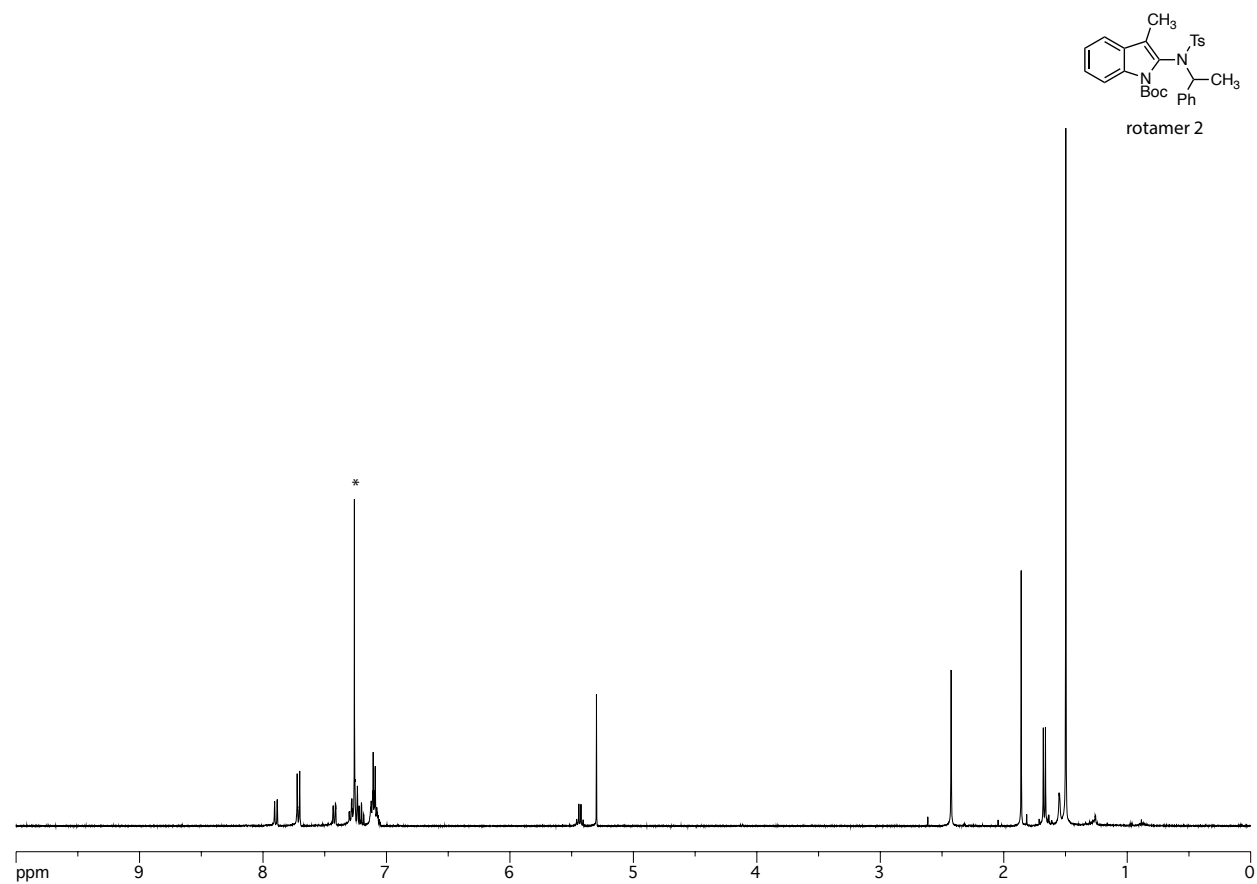


Figure V-84. ^1H NMR spectrum of rotamer 2 of compound V.7 in CDCl_3 (400 MHz) at 23 °C. * CDCl_3 solvent peak. Peaks with $\delta = 5.30$ ppm is from residual CH_2Cl_2 .

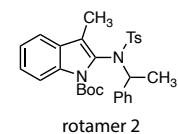
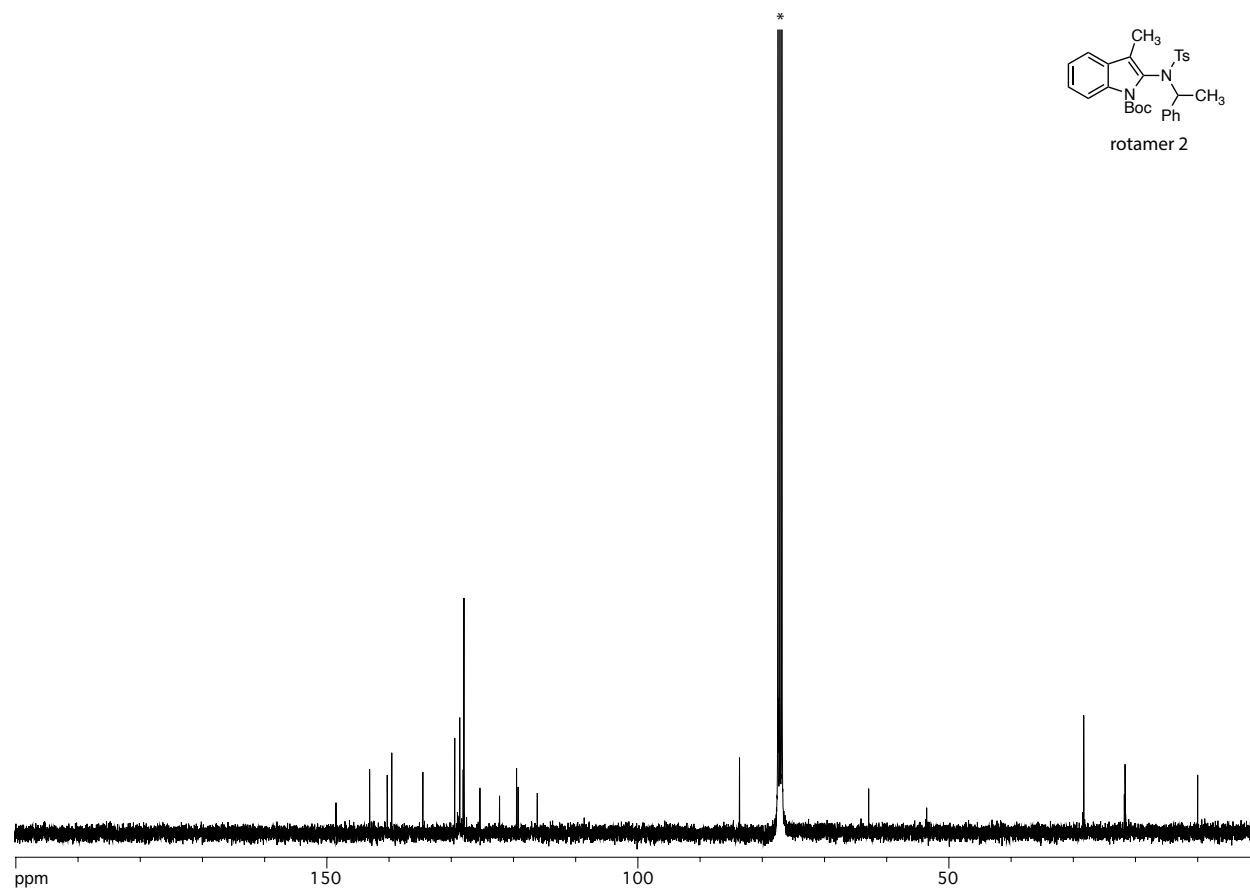


Figure V-85. ¹³C NMR spectrum of rotamer 2 of compound V.7 in CDCl₃ (100 MHz) at 23 °C.*CDCl₃ solvent peak. Peaks with δ = 53.2 ppm is from residual CH₂Cl₂.

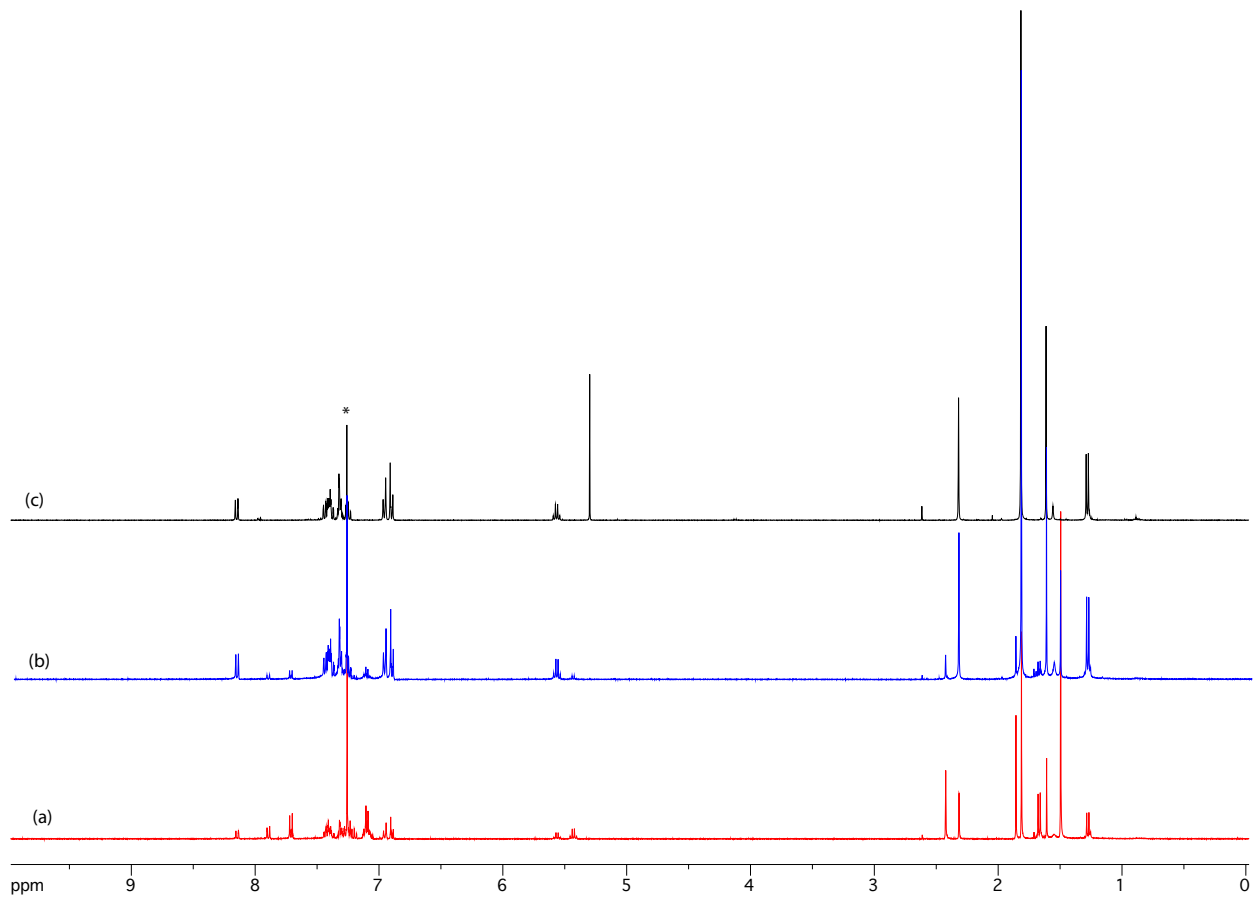


Figure V-86. ¹H NMR spectra for thermal interconversion of rotamers (V.7) at 23 °C in CDCl₃ solvent. *CDCl₃ solvent peak. (a) mixture of rotamers generated from the solution of *rotamer 2* in CDCl₃ upon evacuation and dissolution in CDCl₃, (b) interconversion of *rotamer 2* to *rotamer 1* when heated at 50 °C for 16h, and (c) ¹H NMR spectrum of *rotamer 1*.

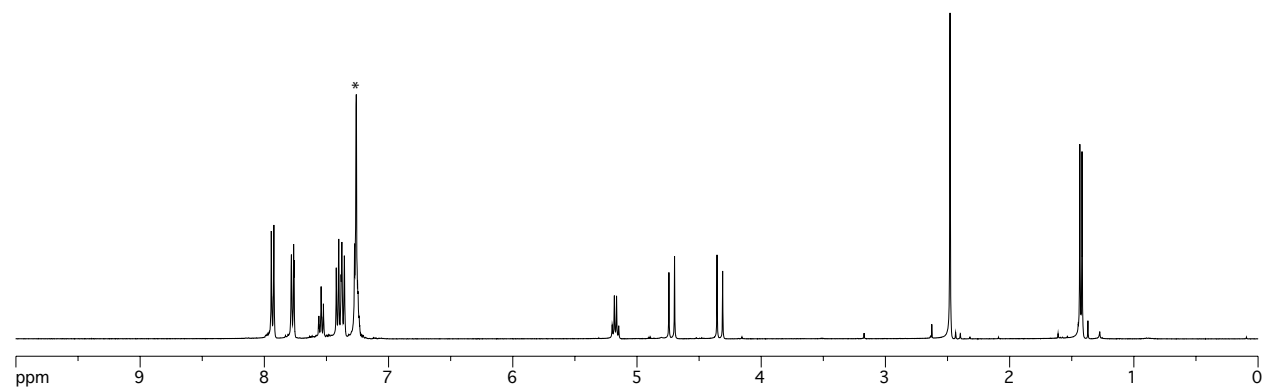
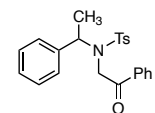


Figure V-87. ¹H NMR spectrum of compound V.9a in CDCl₃ (400 MHz) at 23 °C.*CDCl₃ solvent peak.

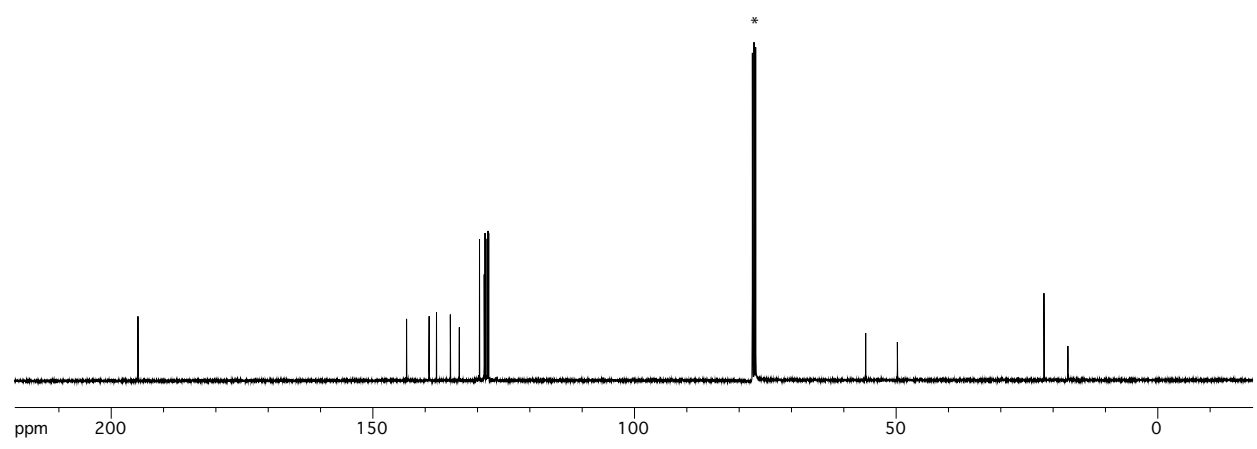
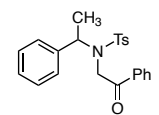


Figure V-88. ¹³C NMR spectrum of compound V.9a in CDCl₃ (100 MHz) at 23 °C.*CDCl₃ solvent peak.

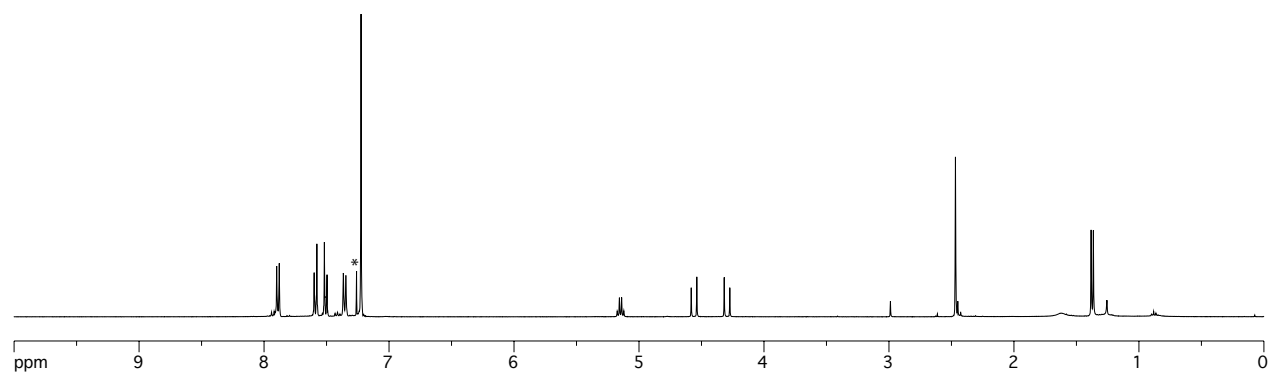
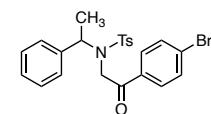


Figure V-89. ¹H NMR spectrum of compound V.9b in CDCl₃ (400 MHz) at 23 °C.*CDCl₃ solvent peak.

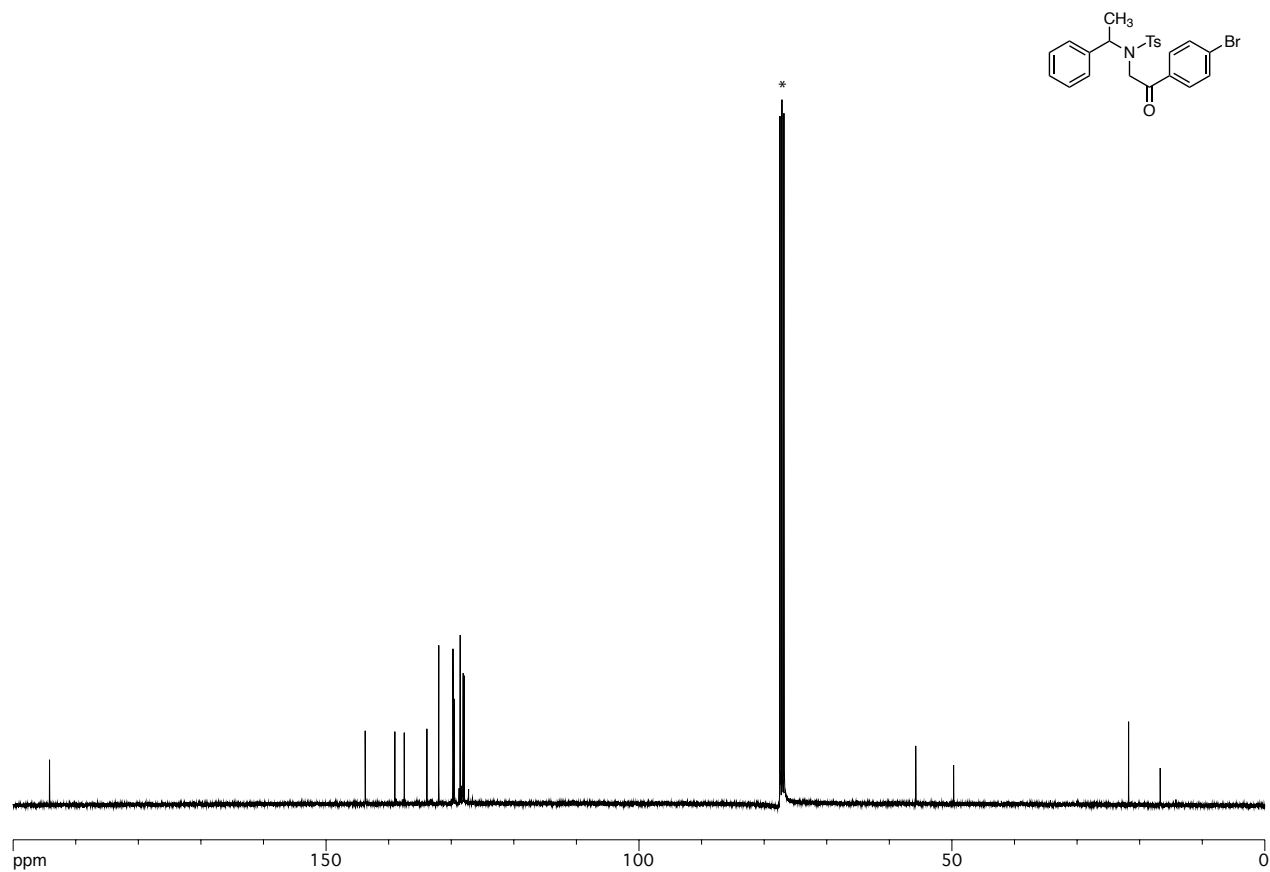


Figure V-90. ^{13}C NMR spectrum of compound V.9b in CDCl_3 (100 MHz) at 23 °C.* CDCl_3 solvent peak.

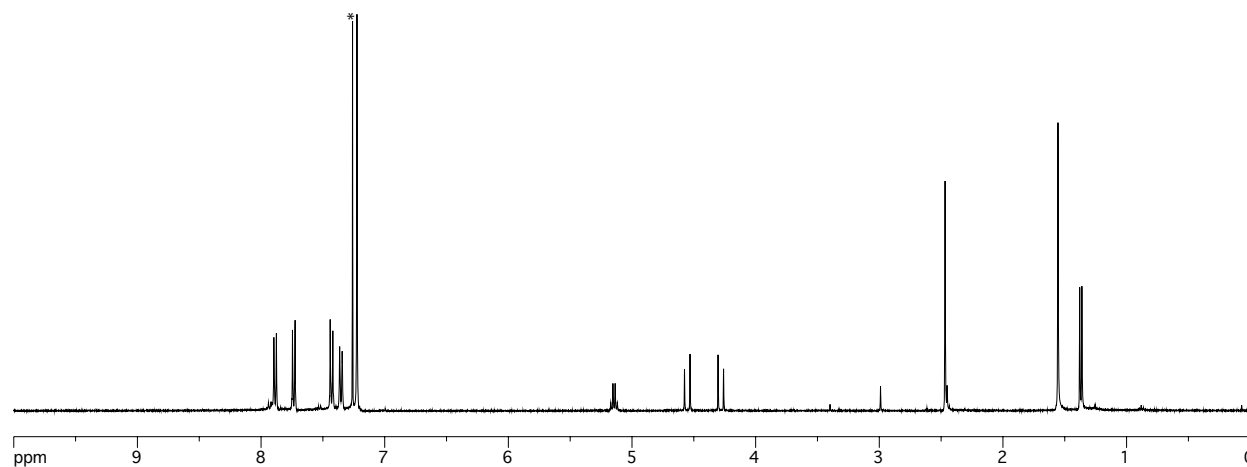
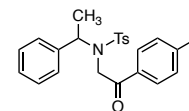


Figure V-91. ¹H NMR spectrum of compound V.9c in CDCl₃ (400 MHz) at 23 °C.*CDCl₃ solvent peak.

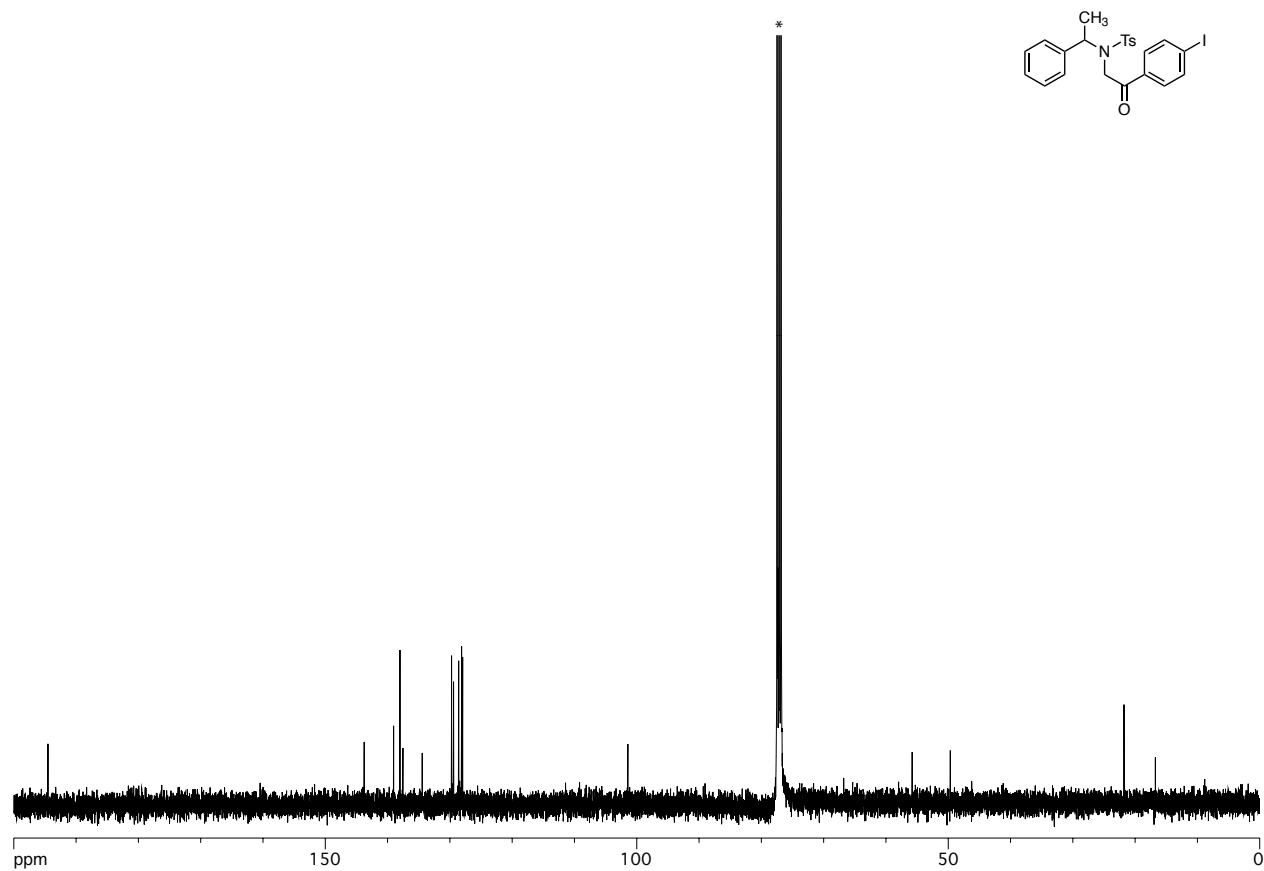


Figure V-92. ¹³C NMR spectrum of compound V.9c in CDCl₃ (100 MHz) at 23 °C. *CDCl₃ solvent peak.

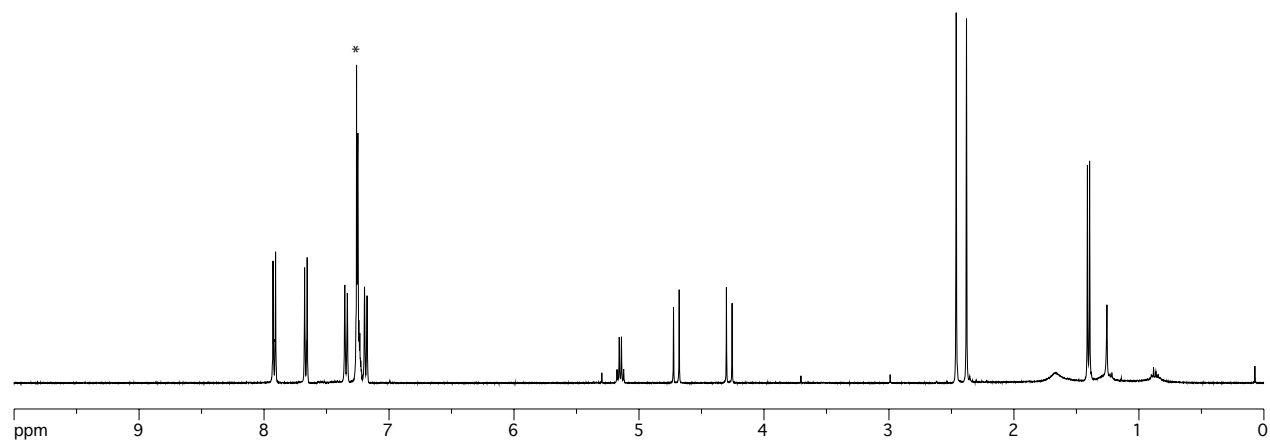
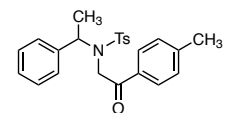


Figure V-93. ^1H NMR spectrum of compound V.9d in CDCl_3 (400 MHz) at 23 °C.* CDCl_3 solvent peak.

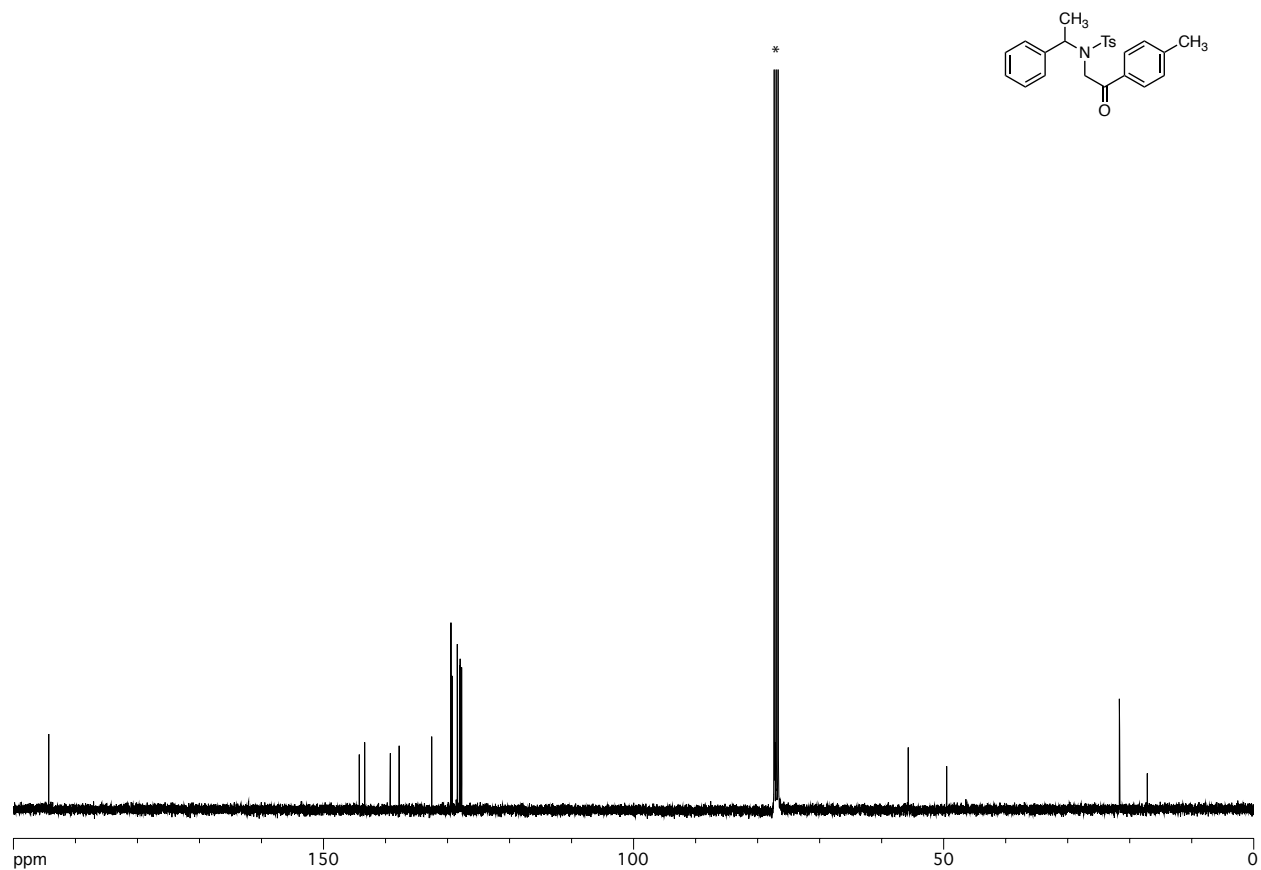


Figure V-94. ¹³C NMR spectrum of compound V.9d in CDCl₃ (100 MHz) at 23 °C. *CDCl₃ solvent peak.

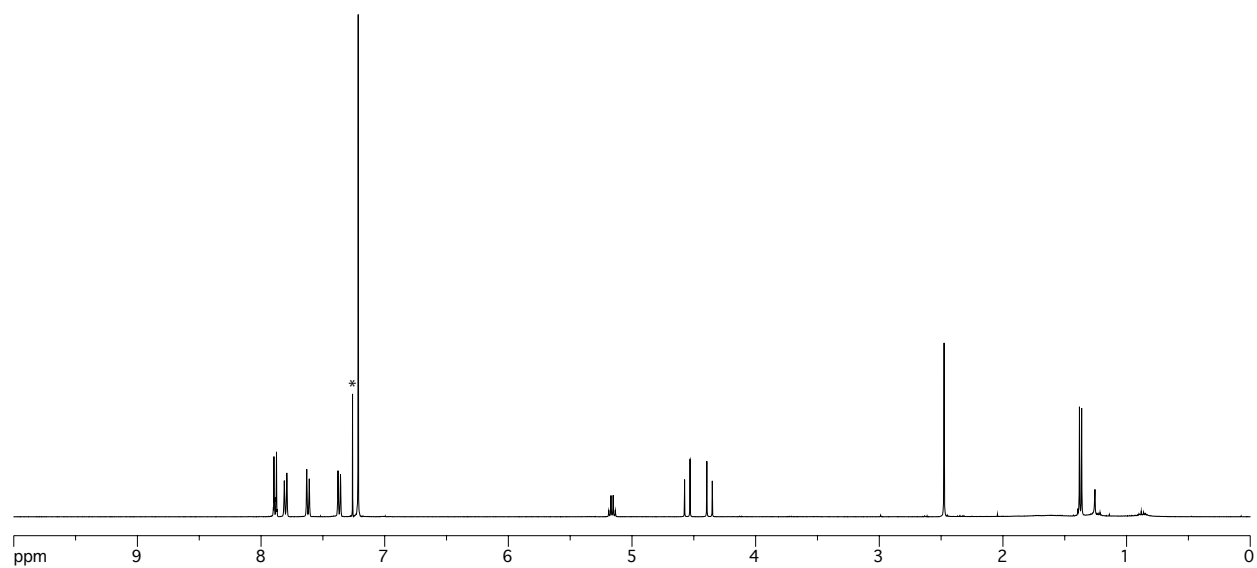
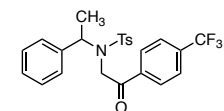


Figure V-95. ^1H NMR spectrum of compound V.9e in CDCl_3 (400 MHz) at 23 °C.* CDCl_3 solvent peak.

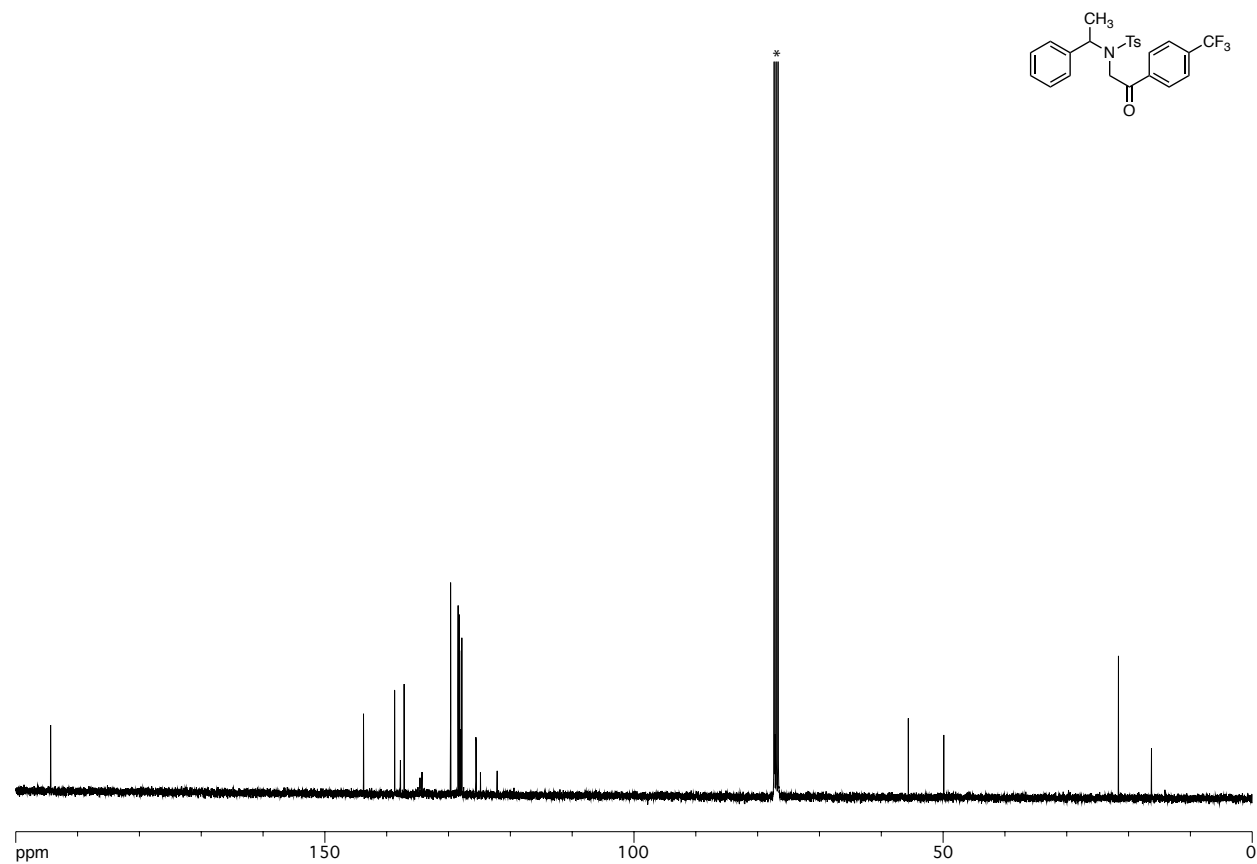


Figure V-96. ¹³C NMR spectrum of compound V.9e in CDCl₃ (100 MHz) at 23 °C.*CDCl₃ solvent peak.

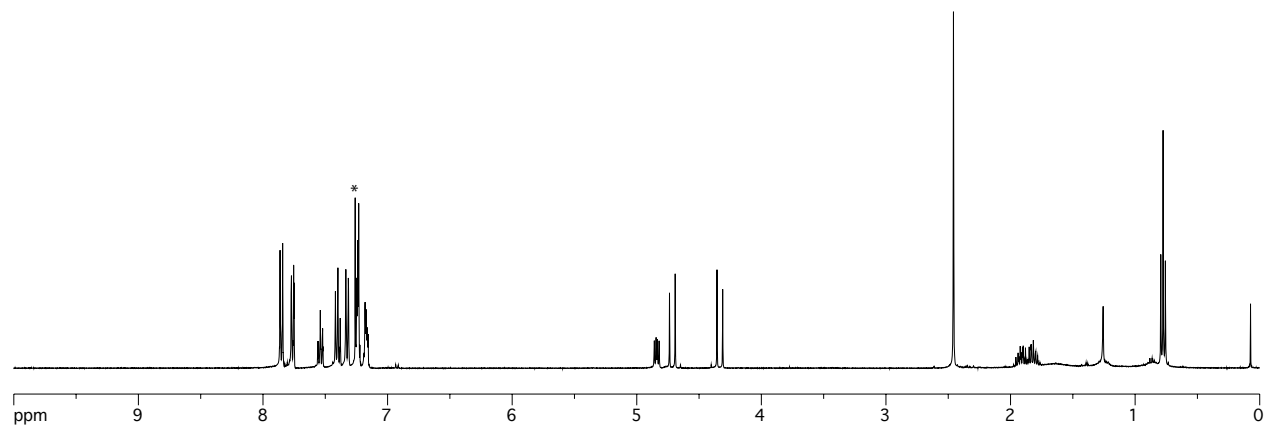
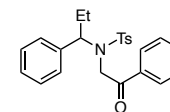


Figure V-97. ^1H NMR spectrum of compound V.9f in CDCl_3 (400 MHz) at 23 °C.* CDCl_3 solvent peak.

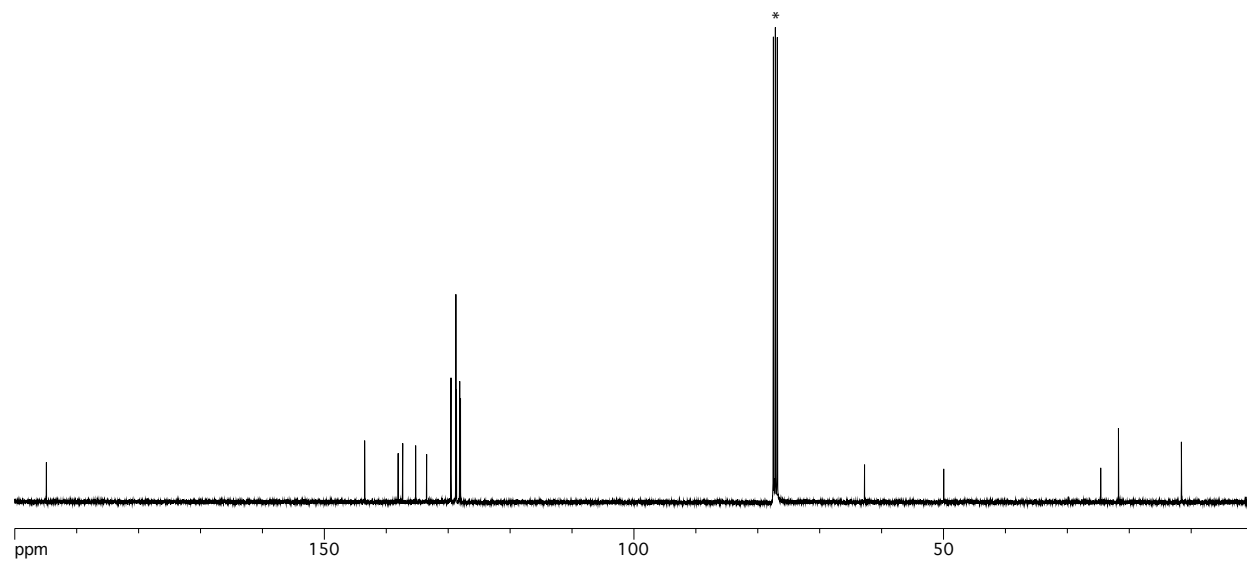
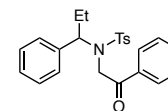


Figure V-98. ¹³C NMR spectrum of compound V.9f in CDCl₃ (100 MHz) at 23 °C.*CDCl₃ solvent peak.

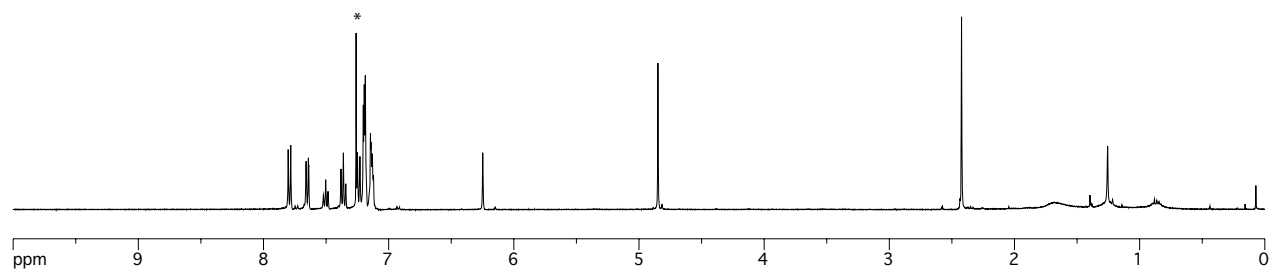
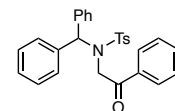


Figure V-99. ¹H NMR spectrum of compound V.9g in CDCl₃ (400 MHz) at 23 °C.*CDCl₃ solvent peak.

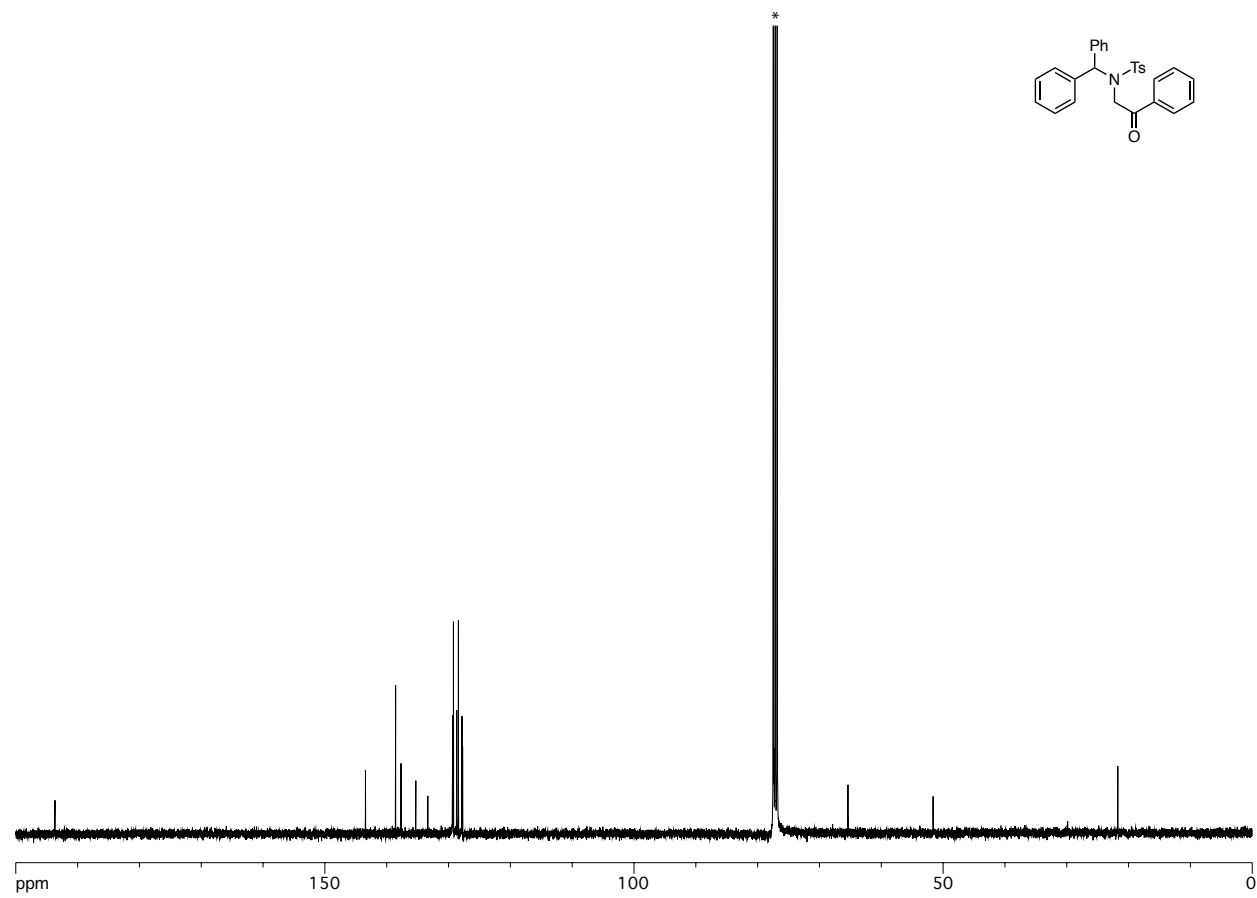


Figure V-100. ¹³C NMR spectrum of compound V.9g in CDCl₃ (100 MHz) at 23 °C.*CDCl₃ solvent peak.

CHAPTER VI

CONCLUDING REMARKS AND OUTLOOK

VI.1 Summary

Hypervalent iodine reagents are a broadly useful class of selective two electron chemical oxidants based on 3-centered, 4-electron (3c-4e) iodine–ligand bonds and are often prepared using hazardous reagents such as peracids or metal-based oxidants. In the preceding chapters of this dissertation, sustainable synthetic methods for hypervalent iodine compounds with O₂ and electrical current as the terminal oxidants were discussed. In Chapter II and III, the development of aerobic hypervalent iodine catalysis as a platform to accomplish an array of organocatalytic aerobic oxidation reactions was illustrated.^{163, 239} This chemistry enabled O₂ to be employed as a terminal oxidant in many of the transformations for which hypervalent iodine intermediates have been developed, including direct C–H/N–H cross coupling, carbonyl α -functionalization, and alcohol oxidation.

Detailed study of the mechanism by which aerobic oxidation is achieved resulted in the recognition that a one-electron mechanism based on addition of aerobically generated acetoxy radicals to aryl iodides was operative.³²² Based on this mechanistic hypothesis, development of aryl-iodide-catalyzed electrochemical C–H amination was described in Chapter IV. Previously reported electrochemical oxidation of aryl iodides significantly suffered from high onset potential required for its oxidation, leading to very limited electrocatalytic application. During our electrocatalytic studies, we have

discovered that anodically generated iodanyl radicals (*i.e.*, I(II)) from some aryl iodides directly engage with the substrate without forming corresponding I(III) compounds.³²³ To accommodate relatively high potential for oxidation of aryl iodides, expansion of library of aminating reagents was discussed in Chapter V.³⁹¹

Hypervalent iodine compounds are often used in stoichiometric amounts to carry out substrate functionalization, and the research described herein using O₂ and electrochemistry would encourage catalytic use of such reagents in diverse chemical settings, rendering more economical and sustainable method for small molecule synthesis.

VI.2 Future Directions

Aerobic Aerobic Asymmetric Hypervalent Iodine Catalysis

While aldehyde autoxidation mediated aerobic hypervalent iodine catalysis serves as an attractive launching platform, generation of reactive radical intermediates from aldehyde autoxidation limits the substrate generality. Thus, development of other mediators for coupling O₂ reduction with aryl iodide oxidation is needed. After our initial report of aerobic hypervalent iodine catalysis, aerobic hypervalent iodine photocatalysis was developed in the context of dearomatization of electron-rich aromatics to afford spirocyclic lactams with very low catalyst loadings (Figure VI-1).⁴²⁹ In this chemistry, sequential oxidation of aryl iodide was proposed by the action of O₂ and photosensitizer (mesityl-2,6-diphenylpyrylium tetrafluoroborate, MDPT) to form the active hypervalent iodine(III) oxidant which undergoes spirocyclization reaction.

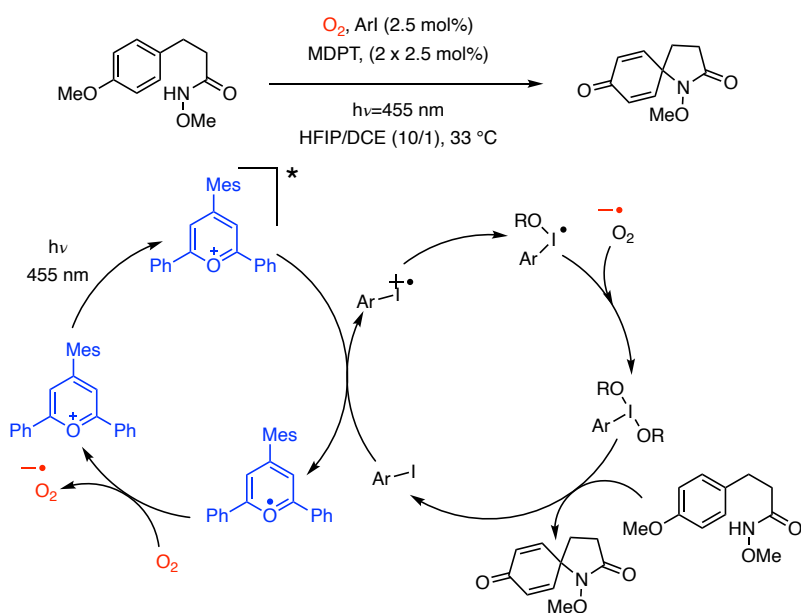


Figure VI-1. Hypervalent iodine catalyzed aerobic spirocyclization reaction under photochemical conditions. MDPT=mesityl-2,6-diphenylpyrylium tetrafluoroborate. Adapted from reference 429.

The potential required for oxidation of aryl iodides significantly varies with the substituents on the aryl ring. With aldehyde autoxidation chemistry, oxidation of aryl iodide is governed by the oxygenated radical species (*i.e.*, acetoxy radical from acetaldehyde autoxidation) with little variability in potential for different aldehyde structure. On the other hand, required potential for oxidation of aryl iodides could be tuned in by varying the structure of photosensitizers. Thus oxidation of more complex aryl iodides (*i.e.*, chiral aryl iodides) could be achieved under mild conditions using O_2 as terminal oxidant whereas reactive radical intermediates from aldehyde autoxidation may not be compatible. Optimization of suitable photosensitizer and aryl iodide structure could lead to asymmetric aerobic hypervalent iodine catalysis.

Green Platform for Metal-Free Cross-Coupling Chemistry

Hypervalent iodine compounds readily engage in the elementary steps necessary for cross-coupling chemistry, namely well-defined two-electron oxidation-reduction chemistry (*i.e.*, oxidative addition and reductive elimination) and facile ligand exchange reactions (*i.e.*, transmetallation reactions) and have thus garnered significant attention as a potential metal-free platform for cross-coupling chemistry. With the sustainable synthesis of hypervalent iodine compounds under aerobic or electrochemical conditions, these intermediates would constitute a green platform for cross-coupling chemistry. For example, both aryl iodide and Pd catalyzed C–N cross-coupling reaction between arene and *N*-methoxy-tosyl amine are compared in light of green chemistry metrics pentagon (Figure VI-2).⁴³⁰ Aryl-iodide-catalyzed reaction is better in terms of yield and atom economy but loses out to Pd catalysis on stoichiometric factor due to higher loading of aryl iodide catalyst. Development of better aryl iodide catalyst structure could address this problem and increase the sustainability.

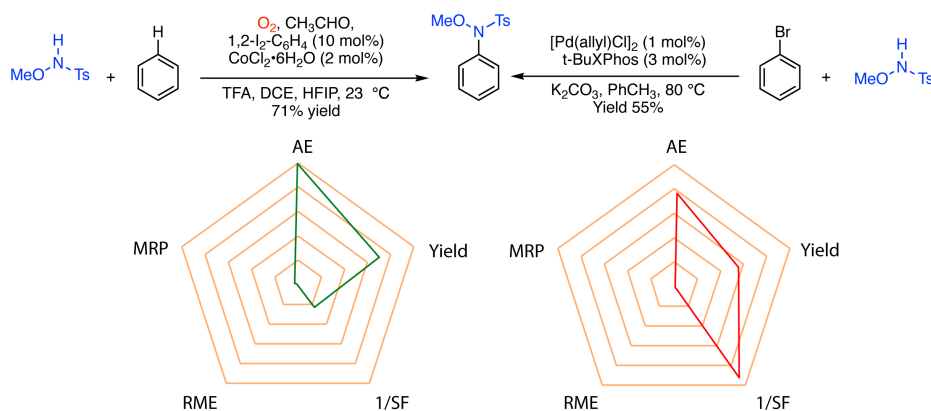


Figure VI-2. Green chemistry comparison between aryl iodide and Pd catalyzed C–N cross coupling reactions. AE = atom economy, SF = stoichiometric factor, MRP = material recovery parameter, RME = reaction mass efficiency. Adapted from reference 430.

The development of electrocatalytic application of hypervalent iodine compounds described in this dissertation could also open up the possibility of performing previously reported *ex cell* reactions under electrocatalytic conditions. For example, an extension of the C–N bond-forming processes to the construction of C–O, and C–X bonds utilizing facile ligand exchange properties of iodine could be envisioned. To develop the electrochemical cross-coupling chemistry of hypervalent iodine compounds, the structure of the aryl iodide catalyst needs to be optimized by examining the effect of substituents both on the oxidation-reduction electrochemistry and also on the efficiency of cross-coupling chemistry.

I(II) Catalysis in Organic Hypervalent Chemistry

While one-electron redox and iodine radical chemistry is well-precedented in the context of inorganic hypervalent iodine chemistry, for example in the iodide-triiodide couple that drives dye-sensitized solar cells,¹⁵ most organic hypervalent iodine chemistry is predicated on the selective two-electron redox couples I(I)/I(III) and I(III)/I(V). Contemporary hypervalent iodine chemistry is predicated on electrophilicity at the iodine center, where substrate functionalization occurs with nucleophilic attack from the substrate at the iodine center followed by formal reductive elimination. But with the generation of I(II) intermediates, other modes of reaction such as hydrogen atom abstraction (HAA) or extrusion of ligand radical to participate in the product formation become available, thus adding to the diversity of hypervalent iodine chemistry. With the new methods described in this dissertation to generate iodanyl radical under aerobic and

electrochemical conditions, we view this research as an opportunity to advance I(II) catalysis as a green alternative to traditional aryl-iodide-catalyzed chemical transformations with peracid or metal-based reagents as terminal oxidants.

REFERENCES

1. Fetzner, S.; Steiner, R. A. Cofactor-Independent Oxidases and Oxygenases. *Appl. Microbiol. Biotechnol.* **2010**, *86*, 791–804.
2. Ho, R. Y.; Liebman, J. F.; Valentine, J. S. Biological Reactions of Dioxygen: An Introduction. In *Active Oxygen in Biochemistry*, Springer: 1995; pp 1–36.
3. Borden, W. T.; Hoffmann, R.; Stuyver, T.; Chen, B. Dioxygen: What Makes This Triplet Diradical Kinetically Persistent? *J. Am. Chem. Soc.* **2017**, *139*, 9010–9018.
4. Filatov, M.; Reckien, W.; Peyerimhoff, S. D.; Shaik, S. What Are the Reasons for the Kinetic Stability of a Mixture of H₂ and O₂? *J. Phys. Chem. A* **2000**, *104*, 12014–12020.
5. Ho, R. Y. N.; Liebman, J. F.; Valentine, J. S. Overview of the Energetics and Reactivity of Oxygen. In *Active Oxygen in Chemistry*, Foote, C. S.; Valentine, J. S.; Greenberg, A.; Liebman, J. F. Eds. Blackie Academic and Professional: New York, 1995; pp 1–23.
6. McCann, S. D.; Stahl, S. S. Copper-Catalyzed Aerobic Oxidations of Organic Molecules: Pathways for Two-Electron Oxidation with a Four-Electron Oxidant and a One-Electron Redox-Active Catalyst. *Acc. Chem. Res.* **2015**, *48*, 1756–1766.
7. Osterberg, P. M.; Niemeier, J. K.; Welch, C. J.; Hawkins, J. M.; Martinelli, J. R.; Johnson, T. E.; Root, T. W.; Stahl, S. S. Experimental Limiting Oxygen Concentrations for Nine Organic Solvents at Temperatures and Pressures Relevant to Aerobic Oxidations in the Pharmaceutical Industry. *Org. Process Res. Dev.* **2015**, *19*, 1537–1543.
8. Anastas, P. Warner J. *Green chemistry: Theory and Practice* **1998**, 30.

9. Anastas, P.; Eghbali, N. Green Chemistry: Principles and Practice. *Chem. Soc. Rev.* **2010**, *39*, 301–312.
10. Goti, A.; Cardona, F. Hydrogen Peroxide in Green Oxidation Reactions: Recent Catalytic Processes. In *Green Chemical Reactions*, Springer: 2008; pp 191–212.
11. Campbell, A. N.; Stahl, S. S. Overcoming the “Oxidant Problem”: Strategies to Use O₂ as the Oxidant in Organometallic C–H Oxidation Reactions Catalyzed by Pd (and Cu). *Acc. Chem. Res.* **2012**, *45*, 851–863.
12. Ibanez, J. G.; Fitch, A.; Frontana–Uribe, B. A.; Vasquez–Medrano, R. Green Electrochemistry. *Encyclopedia of Applied Electrochemistry* **2014**, 964–971.
13. Greenwood, N. N.; Earnshaw, A. *Chemistry of the Elements*. Elsevier: **2012**.
14. Pauling, L. *The Nature of the Chemical Bond*. Cornell University Press Ithaca, NY: **1960**; 260.
15. Boschloo, G.; Hagfeldt, A. Characteristics of the Iodide/Triiodide Redox Mediator in Dye–Sensitized Solar Cells. *Acc. Chem. Res.* **2009**, *42*, 1819–1826.
16. Davies, C. G.; Gillespie, R. J.; Ireland, P. R.; Sowa, J. M. The Preparation and Crystal Structure of [I₂]⁺[Sb₂F₁₁][−]. *Can. J. Chem.* **1974**, *52*, 2048–2052.
17. Kemmitt, R. D. W.; Murray, M.; McRae, V. M.; Peacock, R. D.; Symons, M. C. R.; Odonnell, R. A. Iodine Cation I₂⁺, in Antimony Pentafluoride. *J. Chem. Soc. A* **1968**, 862–866.
18. Faggiani, R.; Gillespie, R. J.; Kapoor, R.; Lock, C. J. L.; Vekris, J. E. Preparation and Solid–State and Solution Studies of Three Compounds of the Tetraiodine Dication I₄²⁺: I₄²⁺(AsF₆[−])₂, I₄²⁺(SbF₆[−])₂, and I₄²⁺(Sb₃F₁₄[−])(SbF₆[−]). *Inorg. Chem.* **1988**, *27*, 4350–4355.

19. Gillespie, R. J.; Kapoor, R.; Faggiani, R.; Lock, C. J. L.; Murchie, M.; Passmore, J. The I_4^{2+} Cation. X-Ray Crystal Structures of $(I_4^{2+})(AsF_6^-)_2$ and $(I_4^{2+})(Sb_3F_{14}^-)(SbF_6^-)$. *J. Chem. Soc. Chem. Commun.* **1983**, 8–9.
20. Willgerodt, C. Ueber Einige Aromatische Jodidchloride. *J. Prakt. Chem.* **1886**, *33*, 154–160.
21. Musher, J. I. The Chemistry of Hypervalent Molecules. *Angew. Chem. Int. Ed.* **1969**, *8*, 54–68.
22. Powell, W. H. Treatment of Variable Valence in Organic Nomenclature (Lambda-Convention). *Pure Appl. Chem.* **1984**, *56*, 769–778.
23. Martin, J. C. “Frozen” Transition States: Pentavalent Carbon *et al.* *Science* **1983**, *221*, 509–514.
24. Perkins, C. W.; Martin, J. C.; Arduengo, A. J.; Lau, W.; Alegria, A.; Kochi, J. K. An Electrically Neutral .Sigma.-Sulfuranyl Radical from the Homolysis of a Perester with Neighboring Sulfenyl Sulfur: 9-S-3 Species. *J. Am. Chem. Soc.* **1980**, *102*, 7753–7759.
25. Zhdankin, V. V.; Stang, P. J. Recent Developments in the Chemistry of Polyvalent Iodine Compounds. *Chem. Rev.* **2002**, *102*, 2523–2584.
26. Stang, P. J.; Zhdankin, V. V. Organic Polyvalent Iodine Compounds. *Chem. Rev.* **1996**, *96*, 1123–1178.
27. Zhdankin, V. V. *Hypervalent Iodine Chemistry: Preparation, Structure and Synthetic Applications of Polyvalent Iodine Compounds*. John Wiley and Sons Ltd.: New York, 2014.

28. Zhdankin, V. V.; Stang, P. J. Chemistry of Polyvalent Iodine. *Chem. Rev.* **2008**, *108*, 5299–5358.
29. Yoshimura, A.; Zhdankin, V. V. Advances in Synthetic Applications of Hypervalent Iodine Compounds. *Chem. Rev.* **2016**, *116*, 3328–3435.
30. Ladziata, U.; Zhdankin, V. V. Hypervalent Iodine (V) Reagents in Organic Synthesis. *ARKIVOC* **2006**, *9*, 26–58.
31. Reed, A. E.; Schleyer, P. v. R. Chemical Bonding in Hypervalent Molecules. The Dominance of Ionic Bonding and Negative Hyperconjugation over d-Orbital Participation. *J. Am. Chem. Soc.* **1990**, *112*, 1434–1445.
32. Hach, R. J.; Rundle, R. E. The Structure of Tetramethylammonium Pentaiodide. *J. Am. Chem. Soc.* **1951**, *73*, 4321–4324.
33. Pimentel, G. C. The Bonding of Trihalide and Bifluoride Ions by the Molecular Orbital Method. *J. Chem. Phys.* **1951**, *19*, 446–448.
34. Wang, W. Halogen Bond Involving Hypervalent Halogen: CSD Search and Theoretical Study. *J. Phys. Chem. A* **2011**, *115*, 9294–9299.
35. Cavallo, G.; Metrangolo, P.; Milani, R.; Pilati, T.; Priimagi, A.; Resnati, G.; Terraneo, G. The Halogen Bond. *Chem. Rev.* **2016**, *116*, 2478–2601.
36. Ochiai, M.; Sueda, T.; Miyamoto, K.; Kiprof, P.; Zhdankin, V. V. Trans Influences on Hypervalent Bonding of Aryl λ^3 -Iodanes: Their Stabilities and Isodesmic Reactions of Benziodoxolones and Benziodazolones. *Angew. Chem. Int. Ed.* **2006**, *45*, 8203–8206.

37. Ivanov, A. S.; Popov, I. A.; Boldyrev, A. I.; Zhdankin, V. V. The I=X (X=O, N, C) Double Bond in Hypervalent Iodine Compounds: Is It Real? *Angew. Chem. Int. Ed.* **2014**, *53*, 9617–9621.
38. Carmalt, C. J.; Crossley, J. G.; Knight, J. G.; Lightfoot, P.; Martín, A.; Muldowney, M. P.; Norman, N. C.; Orpen, A. G. An Examination of the Structures of Iodosylbenzene (PhIO) and the Related Imido Compound, PhINSO₂-4-Me-C₆H₄, by X-Ray Powder Diffraction and EXAFS (Extended X-Ray Absorption Fine Structure) Spectroscopy. *J. Chem. Soc. Chem. Commun.* **1994**, 2367–2368.
39. Nemykin, V. N.; Kuposov, A. Y.; Netzel, B. C.; Yusubov, M. S.; Zhdankin, V. V. Self-Assembly of Hydroxy(Phenyl)Iodonium Ions in Acidic Aqueous Solution: Preparation, and X-Ray Crystal Structures of Oligomeric Phenyliodine(III) Sulfates. *Inorg. Chem.* **2009**, *48*, 4908–4917.
40. Hiller, A.; Patt, J. T.; Steinbach, J. NMR Study on the Structure and Stability of 4-Substituted Aromatic Iodosyl Compounds. *Magn. Reson. Chem.* **2006**, *44*, 955–958.
41. Protasiewicz, J. D. Organoiodine(III) Reagents as Active Participants and Ligands in Transition Metal-Catalyzed Reactions: Iodosylarenes and (Imino)iodoarenes. In *Hypervalent Iodine Chemistry*, Wirth, T. Ed. Springer International Publishing: Cham, 2016; pp 263–288.
42. Kuposov, A. Y.; Karimov, R. R.; Pronin, A. A.; Skrupskaya, T.; Yusubov, M. S.; Zhdankin, V. V. RuCl₃-Catalyzed Oxidation of Iodoarenes with Peracetic Acid: New Facile Preparation of Iodylarenes. *J. Org. Chem.* **2006**, *71*, 9912–9914.
43. Lucas, H. J.; Kennedy, E. R. Iodoxybenzene. *Org. Synth.* **1942**, *22*, 72–73.

44. Vasconcelos, R. S.; Silva, L. F.; Lopes, N. P. Study by Mass Spectrometry of Solutions of Hydroxy(Tosyloxy)Iodo Benzene: Proposed Disproportionation Mechanisms. *Quim. Nova* **2012**, *35*, 1593–1599.
45. Ochiai, M. *Reactivities, Properties and Structure*. Springer-Verlag: Berlin Heidelberg, 2003; Vol. 224.
46. Koser, G. F.; Wettach, R. H. Synthesis and Characterization of [Methoxy(Tosyloxy)Iodo]Benzene, an Acyclic Monoalkoxyiodinane. *J. Org. Chem.* **1980**, *45*, 4988–4989.
47. Moriarty, R. M.; Prakash, O. Hypervalent Iodine in Organic Synthesis. *Acc. Chem. Res.* **1986**, *19*, 244–250.
48. McDonald, A. R.; Que Jr, L. High-Valent Nonheme Iron-Oxo Complexes: Synthesis, Structure, and Spectroscopy. *Coord. Chem. Rev.* **2013**, *257*, 414–428.
49. Yamada, Y.; Kashima, K.; Okawara, M. Substituent Effect in the Nucleophilic Attack by the Bromide Ion on the *p*-Tolyl-Substituted Phenyliodonium Ions. *Bull. Chem. Soc. Japan* **1974**, *47*, 3179–3180.
50. England, J.; Guo, Y.; Farquhar, E. R.; Young Jr, V. G.; Münck, E.; Que Jr, L. The Crystal Structure of a High-Spin Oxoiron(IV) Complex and Characterization of Its Self-Decay Pathway. *J. Am. Chem. Soc.* **2010**, *132*, 8635–8644.
51. England, J.; Martinho, M.; Farquhar, E. R.; Frisch, J. R.; Bominaar, E. L.; Münck, E.; Que Jr, L. A Synthetic High-Spin Oxoiron(IV) Complex: Generation, Spectroscopic Characterization, and Reactivity. *Angew. Chem. Int. Ed.* **2009**, *48*, 3622–3626.

52. White, M. C.; Zhao, J. Aliphatic C–H Oxidations for Late-Stage Functionalization. *J. Am. Chem. Soc.* **2018**, *140*, 13988–14009.
53. Kang, Y.; Li, X.-X.; Cho, K.-B.; Sun, W.; Xia, C.; Nam, W.; Wang, Y. Mutable Properties of Nonheme Iron(III)–Iodosylarene Complexes Result in the Elusive Multiple-Oxidant Mechanism. *J. Am. Chem. Soc.* **2017**, *139*, 7444–7447.
54. Singh, F. V.; Wirth, T. Hypervalent Iodine-Catalyzed Oxidative Functionalizations Including Stereoselective Reactions. *Chem. Asian. J.* **2014**, *9*, 950–971.
55. Yusubov, M. S. Y. A. Zhdankin, V. V Iodonium Ylides in Organic Synthesis. *ARKIVOC* **2016**, *2016*, 342–364.
56. Dunn, N. L.; Ha, M.; Radosevich, A. T. Main Group Redox Catalysis: Reversible P^{III}/P^V Redox Cycling at a Phosphorus Platform. *J. Am. Chem. Soc.* **2012**, *134*, 11330–11333.
57. Hilton, M. C.; Zhang, X.; Boyle, B. T.; Alegre-Requena, J. V.; Paton, R. S.; McNally, A. Heterobiaryl Synthesis by Contractive C–C Coupling via P(V) Intermediates. *Science* **2018**, *362*, 799–804.
58. Nykaza, T. V.; Cooper, J. C.; Li, G.; Mahieu, N.; Ramirez, A.; Luzung, M. R.; Radosevich, A. T. Intermolecular Reductive C–N Cross Coupling of Nitroarenes and Boronic Acids by P^{III}/P^V=O Catalysis. *J. Am. Chem. Soc.* **2018**, *140*, 15200–15205.
59. Nykaza, T. V.; Harrison, T. S.; Ghosh, A.; Putnik, R. A.; Radosevich, A. T. A Biphilic Phosphetane Catalyzes N–N Bond-Forming Cadogan Heterocyclization via P^{III}/P^V=O Redox Cycling. *J. Am. Chem. Soc.* **2017**, *139*, 6839–6842.
60. Hans-Joachim, R.; Georg, P. Production of Hydrogen Peroxide. Google Patents: 1939.

61. Marzzacco, C. J. The Enthalpy of Decomposition of Hydrogen Peroxide: A General Chemistry Calorimetry Experiment. *J. Chem. Educ.* **1999**, *76*, 1517–1518.
62. Lu, C.-S.; Hughes, E.; Giguère, P. A. The Crystal Structure of the Urea—Hydrogen Peroxide Addition Compound $\text{Co}(\text{NH}_2)_2 \cdot \text{H}_2\text{O}_2$. *J. Am. Chem. Soc.* **1941**, *63*, 1507–1513.
63. Catir, M.; Kilic, H.; Nardello-Rataj, V.; Aubry, J.-M.; Kazaz, C. Singlet Oxygen Generation from [Bis(trifluoroacetoxy)iodo]benzene and Hydrogen Peroxide. *J. Org. Chem.* **2009**, *74*, 4560–4564.
64. Boeseken, J.; Schneider, G. C. C. *J. Prakt. Chem.* **1935**, *131*, 285.
65. Pausacker, K. 18. The Oxidation of Glycols by Aryl Iodosoacetates. a Kinetic Study. *J. Chem. Soc.* **1953**, 107–109.
66. Colomer, I.; Batchelor-McAuley, C.; Odell, B.; Donohoe, T. J.; Compton, R. G. Hydrogen Bonding to Hexafluoroisopropanol Controls the Oxidative Strength of Hypervalent Iodine Reagents. *J. Am. Chem. Soc.* **2016**, *138*, 8855–8861.
67. Zhdankin, V. V.; Scheuller, M. C.; Stang, P. J. A General Approach to Aryl(cyano) Iodonium Triflates-Versatile Iodonium Transfer Reagents. *Tetrahedron Lett.* **1993**, *34*, 6853–6856.
68. Spyroudis, S. Dehydrogenations with Phenyliodine Ditrifluoroacetate. **1975**.
69. White, J. D.; Caravatti, G.; Kline, T. B.; Edstrom, E.; Rice, K. C.; Brossi, A. Biomimetic Total Synthesis of (–)-Codeine. *Tetrahedron* **1983**, *39*, 2393–2397.
70. Alcock, N. W.; Waddington, T. C. 780. Chemistry of Positive Iodine. Part II. Reactions of Iodobenzene Dichloride with Silver Salts. *J. Chem. Soc.* **1963**, 4103–4109.

71. Zefirov, N.; Safronov, S.; Kaznacheev, A.; Zhdankin, V. General Method for the Synthesis of Aryliodoso Derivatives under Aprotic Conditions by the Reaction of Iodosobenzene with Substituted Trimethylsilanes. *ChemInform* **1989**, *20*.
72. Page, T. K.; Wirth, T. Simple Direct Synthesis of [Bis(trifluoroacetoxy)iodo]arenes. *Synthesis* **2006**, *2006*, 3153–3155.
73. Knight, D. W.; Russell, G. A. Phenyliodine(III) Dichloride. *Encyclopedia of Reagents for Organic Synthesis* **2001**.
74. Krassowska-wiebocka, B.; Prokopienko, G.; Skulski, L. Biphasic Chlorination of Iodoarenes to (Dichloroiodo)arenes. *Synlett* **1999**, *1999*, 1409–1410.
75. Obeid, N.; Skulski, L. Novel Oxidative, Liquid-Phase Chlorination Procedures for the Preparation of (Dichloroiodo)arenes from Iodoarenes. *Pol. J. Chem.* **2000**, *74*, 1609–1615.
76. Baranowski, A.; Płachta, D.; Skulski, L.; Klimaszewska, M. Liquid-Phase and Biphasic Chlorination of Some Iodoarenes to Form (Dichloroiodo)arenes with Sodium Peroxodisulfate as the Oxidant. *J. Chem. Res.* **2000**, *2000*, 435–437.
77. Kaźmierczak, P.; Skulski, L.; Obeid, N. Oxidative Chlorination of Various Iodoarenes to (Dichloroiodo)arenes with Chromium(VI) Oxide as the Oxidant. *J. Chem. Res.* **1999**, 64–65.
78. Zhao, X.-F.; Zhang, C. Iodobenzene Dichloride as a Stoichiometric Oxidant for the Conversion of Alcohols into Carbonyl Compounds; Two Facile Methods for Its Preparation. *Synthesis* **2007**, *2007*, 551–557.

79. Podgoršek, A.; Iskra, J. Conversion of Aryl Iodides into Aryliodine(III) Dichlorides by an Oxidative Halogenation Strategy Using 30% Aqueous Hydrogen Peroxide in Fluorinated Alcohol. *Molecules* **2010**, *15*, 2857–2871.
80. Schmidt, H.; Meinert, H. Zum Mechanismus Der Elektrochemischen Fluorierung Und Über Die Bildung Von Jod-Monofluorid. *Angew. Chem.* **1960**, *72*, 109–110.
81. Rozhkov, I. N. Radical-Cation Mechanism of the Anodic Fluorination of Organic Compounds. *Russ. Chem. Rev.* **1976**, *45*, 615–619.
82. Fuchigami, T.; Fujita, T. Electrolytic Partial Fluorination of Organic Compounds. 14. The First Electrosynthesis of Hypervalent Iodobenzene Difluoride Derivatives and Its Application to Indirect Anodic Gem-Difluorination. *J. Org. Chem.* **1994**, *59*, 7190–7192.
83. Hara, S.; Hatakeyama, T.; Chen, S.-Q.; Ishii, K.; Yoshida, M.; Sawaguchi, M.; Fukuhara, T.; Yoneda, N. Electrochemical Fluorination of β -Dicarbonyl Compounds Using *p*-Iodotoluene Difluoride as a Mediator. *J. Fluorine Chem.* **1998**, *87*, 189–192.
84. Lund, H.; Hammerich, O. *Organic Electrochemistry*. Marcel Dekker New York: 2001; Vol. 4.
85. Simonet, J.; Pilard, J. *Organic Electrochemistry* Ed Lund, H., Hammerich, O. Marcel Dekker Inc. New York, 2001; pp 1163–1225.
86. Kajiyama, D.; Saitoh, T.; Nishiyama, S. Application of Electrochemically Generated Hypervalent Iodine Oxidant to Natural Products Synthesis. *Electrochemistry* **2013**, *81*, 319–324.

87. Inoue, K.; Ishikawa, Y.; Nishiyama, S. Synthesis of Tetrahydropyrroloiminoquinone Alkaloids Based on Electrochemically Generated Hypervalent Iodine Oxidative Cyclization. *Org. Lett.* **2010**, *12*, 436–439.
88. Kajiyama, D.; Inoue, K.; Ishikawa, Y.; Nishiyama, S. A Synthetic Approach to Carbazoles Using Electrochemically Generated Hypervalent Iodine Oxidant. *Tetrahedron* **2010**, *66*, 9779–9784.
89. Dohi, T.; Ito, M.; Yamaoka, N.; Morimoto, K.; Fujioka, H.; Kita, Y. Hypervalent Iodine(III): Selective and Efficient Single-Electron-Transfer (SET) Oxidizing Agent. *Tetrahedron* **2009**, *65*, 10797–10815.
90. Dohi, T.; Yamaoka, N.; Kita, Y. Fluoroalcohols: Versatile Solvents in Hypervalent Iodine Chemistry and Syntheses of Diaryliodonium(III) Salts. *Tetrahedron* **2010**, *66*, 5775–5785.
91. Ebersson, L.; Hartshorn, M. P.; Persson, O.; Radner, F. Making Radical Cations Live Longer. *Chem. Commun.* **1996**, 2105–2112.
92. Broese, T.; Francke, R. Electrosynthesis Using a Recyclable Mediator-Electrolyte System Based on Ionically Tagged Phenyl Iodide and 1,1,1,3,3,3-Hexafluoroisopropanol. *Org. Lett.* **2016**, *18*, 5896–5899.
93. Koleda, O.; Broese, T.; Noetzel, J.; Roemelt, M.; Suna, E.; Francke, R. Synthesis of Benzoxazoles Using Electrochemically Generated Hypervalent Iodine. *J. Org. Chem.* **2017**, *82*, 11669–11681.

94. Roesel, A. F.; Broese, T.; Májek, M.; Francke, R. Iodophenylsulfonates and Iodobenzoates as Redox-Active Supporting Electrolytes for Electrosynthesis. *ChemElectroChem* **2019**, *6*, 4229–4237.
95. Watts, K.; Gattrell, W.; Wirth, T. A Practical Microreactor for Electrochemistry in Flow. *Beilstein J. Org. Chem.* **2011**, *7*, 1108–1114.
96. Gemoets, H. P.; Laudadio, G.; Verstraete, K.; Hessel, V.; Noël, T. A Modular Flow Design for the Meta-Selective C–H Arylation of Anilines. *Angew. Chem. Int. Ed.* **2017**, *56*, 7161–7165.
97. Gao, W.-C.; Xiong, Z.-Y.; Pirhaghani, S.; Wirth, T. Enantioselective Electrochemical Lactonization Using Chiral Iodoarenes as Mediators. *Synthesis* **2019**, *51*, 276–284.
98. Elsherbini, M.; Winterson, B.; Alharbi, H.; Folgueiras-Amador, A. A.; Génot, C.; Wirth, T. Continuous-Flow Electrochemical Generator of Hypervalent Iodine Reagents: Synthetic Applications. *Angew. Chem. Int. Ed.* **2019**, *58*, 9811–9815.
99. Plutschack, M. B.; Pieber, B. u.; Gilmore, K.; Seeberger, P. H. The Hitchhiker’s Guide to Flow Chemistry^{ll}. *Chem. Rev.* **2017**, *117*, 11796–11893.
100. Asprion, N.; Mollner, S.; Poth, N.; Rumpf, B. Energy Management in Chemical Industry. *Ullmann's Encyclopedia of Industrial Chemistry* **2000**.
101. Britton, J.; Raston, C. L. Multi-Step Continuous-Flow Synthesis. *Chem. Soc. Rev.* **2017**, *46*, 1250–1271.
102. Adamo, A.; Beingessner, R. L.; Behnam, M.; Chen, J.; Jamison, T. F.; Jensen, K. F.; Monbaliu, J.-C. M.; Myerson, A. S.; Revalor, E. M.; Snead, D. R. On-Demand

- Continuous-Flow Production of Pharmaceuticals in a Compact, Reconfigurable System. *Science* **2016**, *352*, 61–67.
103. Kennedy, R. J.; Stock, A. M. The Oxidation of Organic Substances by Potassium Peroxymonosulfate. *J. Org. Chem.* **1960**, *25*, 1901–1906.
104. Kazmierczak, P.; Skulski, L.; Kraszkiewicz, L. Syntheses of (Diacetoxyiodo)arenes or Iodylarenes from Iodoarenes, with Sodium Periodate as the Oxidant. *Molecules* **2001**, *6*, 881–891.
105. Kraszkiewicz, L.; Skulski, L. Optimized Syntheses of Iodylarenes from Iodoarenes, with Sodium Periodate as the Oxidant. Part II. *ARKIVOC* **2003**, *6*, 120–125.
106. Soldatova, N.; Postnikov, P.; Troyan, A. A.; Yoshimura, A.; Yusubov, M. S.; Zhdankin, V. V. Mild and Efficient Synthesis of Iodylarenes Using Oxone as Oxidant. *Tetrahedron Lett.* **2016**, *57*, 4254–4256.
107. Sharefkin, J.; Saltzman, H. Iodoxybenzene. *Org. Synth. Coll* **1973**, *43*, 65–66.
108. Lucas, H. J.; Kennedy, E. R. Iodoxybenzene. *Org. Synth.* **1942**, *22*, 72–75.
109. Yusubov, M. S.; Chi, K.-W.; Park, J. Y.; Karimov, R.; Zhdankin, V. V. Highly Efficient RuCl₃-Catalyzed Disproportionation of (Diacetoxyiodo)benzene to Iodylbenzene and Iodobenzene; Leading to the Efficient Oxidation of Alcohols to Carbonyl Compounds. *Tetrahedron Lett.* **2006**, *47*, 6305–6308.
110. Bystron, T.; Horbenko, A.; Syslova, K.; Hii, K. K.; Hellgardt, K.; Kelsall, G. 2-Iodoxybenzoic Acid Synthesis by Oxidation of 2-Iodobenzoic Acid at a Boron-Doped Diamond Anode. *ChemElectroChem* **2018**, *5*, 1002–1005.

111. Devadas, B.; Svoboda, J.; Krupička, M.; Bystron, T. Electrochemical and Spectroscopic Study of 2-Iodobenzoic Acid and 2-Iodosobenzoic Acid Anodic Oxidation in Aqueous Environment. *Electrochim. Acta* **2020**, 136080.
112. Moriarty, R. M.; Prakash, O. Oxidation of Carbonyl Compounds with Organohypervalent Iodine Reagents. In *Organic Reactions*, Paquette, L. A. Ed. John Wiley & Sons, Inc.: 2004; Vol. 54, pp 273–415.
113. Nicolaou, K. C.; Simmons, N. L.; Ying, Y.; Heretsch, P. M.; Chen, J. S. Enantioselective Dichlorination of Allylic Alcohols. *J. Am. Chem. Soc.* **2011**, *133*, 8134–8137.
114. Turner, C. D. C. M. A. Oxidation of Oximes with Hypervalent Iodine Reagents: Opportunities, Development, and Applications. *ARKIVOC* **2011**, 410–428.
115. Ciufolini, M. A.; Norbert, A. B.; Canesi, S.; Ousmer, M.; Chang, J.; Chai, D. Oxidative Amidation of Phenols through the Use of Hypervalent Iodine Reagents: Development and Applications. *Synthesis* **2007**, *2007*, 3759–3772.
116. Moriarty, R. M.; Prakash, O. Oxidation of Phenolic Compounds with Organohypervalent Iodine Reagents. In *Organic Reactions*, Overman, L. E. Ed. John Wiley & Sons, Inc.: **2001**; *57*, 327–415.
117. Pouységu, L.; Deffieux, D.; Quideau, S. Hypervalent Iodine–Mediated Phenol Dearomatization in Natural Product Synthesis. *Tetrahedron* **2010**, *66*, 2235–2261.
118. Samanta, R.; Matcha, K.; Antonchick, A. P. Metal-Free Oxidative Carbon-Heteroatom Bond Formation through C–H Bond Functionalization. *Eur. J. Org. Chem.* **2013**, *2013*, 5769–5804.

119. Moreno, I.; Tellitu, I.; Herrero, M. T.; SanMartin, R.; Dominguez, E. New Perspectives for Iodine(III) Reagents in (Hetero)biaryl Coupling Reactions. *Curr. Org. Chem.* **2002**, *6*, 1433–1452.
120. Charpentier, J.; Früh, N.; Togni, A. Electrophilic Trifluoromethylation by Use of Hypervalent Iodine Reagents. *Chem. Rev.* **2015**, *115*, 650–682.
121. Cavani, F.; Teles, J. H. Sustainability in Catalytic Oxidation: An Alternative Approach or a Structural Evolution? *Chemsuschem* **2009**, *2*, 508–534.
122. Wertz, S.; Studer, A. Nitroxide–Catalyzed Transition-Metal-Free Aerobic Oxidation Processes. *Green Chem.* **2013**, *15*, 3116–3134.
123. Stahl, S. S. Palladium Oxidase Catalysis: Selective Oxidation of Organic Chemicals by Direct Dioxygen–Coupled Turnover. *Angew. Chem. Int. Ed.* **2004**, *43*, 3400–3420.
124. Bäckvall, J.-E.; Hopkins, R. B.; Grennberg, H.; Mader, M. M.; Awasthi, A. K. Multistep Electron-Transfer in Palladium-Catalyzed Aerobic Oxidations via a Metal Macrocycle–Quinone System. *J. Am. Chem. Soc.* **1990**, *112*, 5160–5166.
125. Bäckvall, J.-E.; Awasthi, A. K.; Renko, Z. D. Biomimetic Aerobic 1,4-Oxidation of 1,3-Dienes Catalyzed by Cobalt Tetraphenylporphyrin-Hydroquinone-Palladium(II) - An Example of Triple Catalysis. *J. Am. Chem. Soc.* **1987**, *109*, 4750–4752.
126. Wendlandt, A. E.; Stahl, S. S. Quinone–Catalyzed Selective Oxidation of Organic Molecules. *Angew. Chem. Int. Ed.* **2015**, *54*, 14638–14658.
127. Gligorich, K. M.; Sigman, M. S. Recent Advancements and Challenges of Palladium(II)-Catalyzed Oxidation Reactions with Molecular Oxygen as the Sole Oxidant. *Chem. Commun.* **2009**, 3854–3867.

128. Kotov, V.; Scarborough, C. C.; Stahl, S. S. Palladium-Catalyzed Aerobic Oxidative Amination of Alkenes: Development of Intra- and Intermolecular Aza-Wacker Reactions. *Inorg. Chem.* **2007**, *46*, 1910–1923.
129. Hoover, J. M.; Stahl, S. S. Highly Practical Copper(I)/TEMPO Catalyst System for Chemoselective Aerobic Oxidation of Primary Alcohols. *J. Am. Chem. Soc.* **2011**, *133*, 16901–16910.
130. Ryland, B. L.; Stahl, S. S. Practical Aerobic Oxidations of Alcohols and Amines with Homogeneous Copper/TEMPO and Related Catalyst Systems. *Angew. Chem. Int. Ed.* **2014**, *53*, 8824–8838.
131. Melone, L.; Punta, C. Metal-Free Aerobic Oxidations Mediated by N-Hydroxyphthalimide. A Concise Review. *Beilstein J. Org. Chem.* **2013**, *9*, 1296–1310.
132. Yokota, T.; Sakaguchi, S.; Ishii, Y. Aerobic Oxidation of Benzene to Biphenyl Using a Pd(II)/Molybdovanadophosphoric Acid Catalytic System. *Adv. Synth. Catal.* **2002**, *344*, 849–854.
133. Burton, H. A.; Kozhevnikov, I. V. Biphasic Oxidation of Arenes with Oxygen Catalysed by Pd(II)–Heteropoly Acid System: Oxidative Coupling Versus Hydroxylation. *J. Mol. Catal. A: Chem.* **2002**, *185*, 285–290.
134. Stowers, K. J.; Fortner, K. C.; Sanford, M. S. Aerobic Pd-Catalyzed sp^3 C–H Olefination: A Route to Both *N*-Heterocyclic Scaffolds and Alkenes. *J. Am. Chem. Soc.* **2011**, *133*, 6541–6544.
135. Obora, Y.; Ishii, Y. Pd(II)/HPMoV-Catalyzed Direct Oxidative Coupling Reaction of Benzenes with Olefins. *Molecules* **2010**, *15*, 1487–1500.

136. Yokota, T.; Fujibayashi, S.; Nishiyama, Y.; Sakaguchi, S.; Ishii, Y. Molybdovanadophosphate (NPMoV)/Hydroquinone/O₂ System as an Efficient Reoxidation System in Palladium–Catalyzed Oxidation of Alkenes. *J. Mol. Catal. A Chem.* **1996**, *114*, 113–122.
137. Bergstad, K.; Backvall, J. E. Mild and Efficient Flavin–Catalyzed H₂O₂ Oxidation of Tertiary Amines to Amine N–Oxides. *J. Org. Chem.* **1998**, *63*, 6650–6655.
138. Chan, D. M. T.; Monaco, K. L.; Wang, R. P.; Winters, M. P. New N– and O–Arylations with Phenylboronic Acids and Cupric Acetate. *Tetrahedron Lett.* **1998**, *39*, 2933–2936.
139. Evans, D. A.; Katz, J. L.; West, T. R. Synthesis of Diaryl Ethers through the Copper–Promoted Arylation of Phenols with Arylboronic Acids. An Expedient Synthesis of Thyroxine. *Tetrahedron Lett.* **1998**, *39*, 2937–2940.
140. Lam, P. Y. S.; Clark, C. G.; Saubern, S.; Adams, J.; Winters, M. P.; Chan, D. M. T.; Combs, A. New Aryl/Heteroaryl C–N Bond Cross–Coupling Reactions via Arylboronic Acid Cupric Acetate Arylation. *Tetrahedron Lett.* **1998**, *39*, 2941–2944.
141. Antilla, J. C.; Buchwald, S. L. Copper–Catalyzed Coupling of Arylboronic Acids and Amines. *Org. Lett.* **2001**, *3*, 2077–2079.
142. King, A. E.; Brunold, T. C.; Stahl, S. S. Mechanistic Study of Copper–Catalyzed Aerobic Oxidative Coupling of Arylboronic Esters and Methanol: Insights into An Organometallic Oxidase Reaction. *J. Am. Chem. Soc.* **2009**, *131*, 5044–5045.

143. Semmelhack, M. F.; Schmid, C. R.; Cortés, D. A.; Chou, C. S. Oxidation of Alcohols to Aldehydes with Oxygen and Cupric Ion, Mediated by Nitrosonium Ion. *J. Am. Chem. Soc.* **1984**, *106*, 3374–3376.
144. Markó, I. E.; Giles, P. R.; Tsukazaki, M.; Brown, S. M.; Urch, C. J. Copper–Catalyzed Oxidation of Alcohols to Aldehydes and Ketones: An Efficient, Aerobic Alternative. *Science* **1996**, *274*, 2044–2046.
145. McCann, S. D.; Stahl, S. S. Mechanism of Copper/Azodicarboxylate–Catalyzed Aerobic Alcohol Oxidation: Evidence for Uncooperative Catalysis. *J. Am. Chem. Soc.* **2016**, *138*, 199–206.
146. Ryland, B. L.; McCann, S. D.; Brunold, T. C.; Stahl, S. S. Mechanism of Alcohol Oxidation Mediated by Copper(II) and Nitroxyl Radicals. *J. Am. Chem. Soc.* **2014**, *136*, 12166–12173.
147. Wang, W. X.; Liang, A. D.; Lippard, S. J. Coupling Oxygen Consumption with Hydrocarbon Oxidation in Bacterial Multicomponent Monooxygenases. *Acc. Chem. Res.* **2015**, *48*, 2632–2639.
148. Bilgrien, C.; Davis, S.; Drago, R. S. The Selective Oxidation of Primary Alcohols to Aldehydes by O₂ Employing a Trinuclear Ruthenium Carboxylate Catalyst. *J. Am. Chem. Soc.* **1987**, *109*, 3786–3787.
149. Bäckvall, J.–E.; Chowdhury, R. L.; Karlsson, U. Ruthenium–Catalyzed Aerobic Oxidation of Alcohols Via Multistep Electron–Transfer. *J. Chem. Soc. Chem. Commun.* **1991**, 473–475.

150. Markó, I. E.; Giles, P. R.; Tsukazaki, M.; Chellé–Regnaut, I.; Urch, C. J.; Brown, S. M. Efficient, Aerobic, Ruthenium–Catalyzed Oxidation of Alcohols into Aldehydes and Ketones. *J. Am. Chem. Soc.* **1997**, *119*, 12661–12662.
151. Csjernyk, G.; Éll, A. H.; Fadini, L.; Pugin, B.; Bäckvall, J. E. Efficient Ruthenium–Catalyzed Aerobic Oxidation of Alcohols Using a Biomimetic Coupled Catalytic System. *J. Org. Chem.* **2002**, *67*, 1657–1662.
152. Samec, J. S. M.; Éll, A. H.; Bäckvall, J.–E. Efficient Ruthenium–Catalyzed Aerobic Oxidation of Amines by Using a Biomimetic Coupled Catalytic System. *Chem. Eur. J.* **2005**, *11*, 2327–2334.
153. Meunier, B.; de Visser, S. P.; Shaik, S. Mechanism of Oxidation Reactions Catalyzed by Cytochrome P450 Enzymes. *Chem. Rev.* **2004**, *104*, 3947–3980.
154. Poulos, T. L.; Finzel, B. C.; Howard, A. J. High–Resolution Crystal–Structure of Cytochrome–P450cam. *J. Mol. Biol.* **1987**, *195*, 687–700.
155. Rittle, J.; Green, M. T. Cytochrome P450 Compound I: Capture, Characterization, and C–H Bond Activation Kinetics. *Science* **2010**, *330*, 933–937.
156. Basch, H.; Mogi, K.; Musaev, D. G.; Morokuma, K. Mechanism of the Methane→Methanol Conversion Reaction Catalyzed by Methane Monooxygenase: a Density Functional Study. *J. Am. Chem. Soc.* **1999**, *121*, 7249–7256.
157. Liu, K. E.; Valentine, A. M.; Qiu, D.; Edmondson, D. E.; Appelman, E. H.; Spiro, T. G.; Lippard, S. J. Characterization of a Diiron(III) Peroxo Intermediate in the Reaction Cycle of Methane Monooxygenase Hydroxylase from *Methylococcus–Capsulatus* (Bath). *J. Am. Chem. Soc.* **1995**, *117*, 4997–4998.

158. Varvoglis, A. Hypervalent Iodine in Organic Synthesis. *Academic Press, Inc. San Diego, CA*, 1997; pp 201–210.
159. Brand, J. P.; González, D. F.; Nicolai, S.; Waser, J. Benziodoxole–Based Hypervalent Iodine Reagents for Atom–Transfer Reactions. *Chem. Commun.* **2011**, *47*, 102–115.
160. Banik, S. M.; Mennie, K. M.; Jacobsen, E. N. Catalytic 1, 3–Difunctionalization via Oxidative C–C Bond Activation. *J. Am. Chem. Soc.* **2017**, *139*, 9152–9155.
161. Mu, R. H.; Liu, Z. Q.; Yang, Z. J.; Liu, Z. G.; Wu, L. M.; Liu, Z. L. An Efficient Catalytic Aerobic Oxidation of Alcohols in Water Using Hypervalent Iodine(V). *Adv. Synth. Catal.* **2005**, *347*, 1333–1336.
162. Uyanik, M.; Fukatsu, R.; Ishihara, K. Bromine–Catalyzed Aerobic Oxidation of Alcohols. *Chem. Asian J.* **2010**, *5*, 456–460.
163. Maity, A.; Hyun, S. M.; Powers, D. C. Oxidase Catalysis Via Aerobically Generated Hypervalent Iodine Intermediates. *Nat. Chem.* **2018**, *10*, 200–204.
164. Reich, L.; Stivala, S. S. *Autoxidation of Hydrocarbons and Polyolefins*. Marcell Dekker, Inc.: New York, 1969.
165. Wöhler, F.; von Liebig, J. F. Untersuchungen Über Das Radikal Der Benzoesäure. *Liebigs Ann.* **1832**, *3*, 249–282.
166. Bäckström, H. L. J. The Chain–Reaction Theory of Negative Catalysis. *J. Am. Chem. Soc.* **1927**, *49*, 1460–1472.
167. Baeyer, A.; Villiger, V. Benzoylwasserstoffsperoxyd Und Die Oxydation Des Benzaldehyds an Der Luft. *Ber. Dtsch. Chem. Ges.* **1900**, *33*, 1569–1585.

168. Chudasama, V.; Ahern, J. M.; Fitzmaurice, R. J.; Caddick, S. Synthesis of γ -Ketophosphonates via Aerobic Hydroacylation of Vinyl Phosphonates. *Tetrahedron Lett.* **2011**, *52*, 1067–1069.
169. Chudasama, V.; Akhbar, A. R.; Bahou, K. A.; Fitzmaurice, R. J.; Caddick, S. Metal-Free, Hydroacylation of C=C and N=N Bonds Via Aerobic C–H Activation of Aldehydes, and Reaction of the Products Thereof. *Org. Biomol. Chem.* **2013**, *11*, 7301–7317.
170. Chudasama, V.; Fitzmaurice, R. J.; Ahern, J. M.; Caddick, S. Dioxygen Mediated Hydroacylation of Vinyl Sulfonates and Sulfones on Water. *Chem. Commun.* **2010**, *46*, 133–135.
171. Chudasama, V.; Fitzmaurice, R. J.; Caddick, S. Hydroacylation of α,β -Unsaturated esters via Aerobic C–H Activation. *Nat. Chem.* **2010**, *2*, 592–596.
172. Paul, S.; Guin, J. Dioxygen-Mediated Decarbonylative C–H Alkylation of Heteroaromatic Bases with Aldehydes. *Chem. Eur. J.* **2015**, *21*, 17618–17622.
173. Yamada, T.; Takai, T.; Rhode, O.; Mukaiyama, T. Direct Epoxidation of Olefins Catalyzed by Nickel(II) Complexes with Molecular-Oxygen and Aldehydes. *Bull. Chem. Soc. Jpn.* **1991**, *64*, 2109–2117.
174. Kaneda, K.; Haruna, S.; Imanaka, T.; Hamamoto, M.; Nishiyama, Y.; Ishii, Y. a Convenient Synthesis of Epoxides from Olefins Using Molecular-Oxygen in the Absence of Metal-Catalysts. *Tetrahedron Lett.* **1992**, *33*, 6827–6830.
175. Mizuno, N.; Weiner, H.; Finke, R. G. Co-Oxidative Epoxidation of Cyclohexene with Molecular Oxygen, Isobutyraldehyde Reductant, and the Polyoxoanion-Supported Catalyst Precursor $[(n\text{-C}_4\text{H}_9)_4\text{N}]_5\text{Na}_3[(1,5\text{-COD})\text{Ir}\cdot\text{P}_2\text{W}_{15}\text{Nb}_3\text{O}_{62}]$. The Importance of

Key Control Experiments Including Omitting the Catalyst and Adding Radical–Chain Initiators *J. Mol. Catal. A Chem.* **1996**, *114*, 15–28.

176. Nam, W. W.; Kim, H. J.; Kim, S. H.; Ho, R. Y. N.; Valentine, J. S. Metal Complex-Catalyzed Epoxidation of Olefins by Dioxygen with Co-Oxidation of Aldehydes. A Mechanistic Study. *Inorg. Chem.* **1996**, *35*, 1045–1049.

177. Das, P.; Saha, D.; Saha, D.; Guin, J. Aerobic Direct C(sp²)-H Hydroxylation of 2-Arylpyridines by Palladium Catalysis Induced with Aldehyde Auto-Oxidation. *ACS Catal.* **2016**, *6*, 6050–6054.

178. Larkin, D. R. The Role of Catalysts in the Air Oxidation of Aliphatic-Aldehydes. *J. Org. Chem.* **1990**, *55*, 1563–1568.

179. Lehtinen, C.; Brunow, G. Factors Affecting the Selectivity of Air oxidation of 2-Ethylhexanal, an A-Branched Aliphatic Aldehyde. *Org. Process Res. Dev.* **2000**, *4*, 544–549.

180. Muller, P.; Godoy, J. Ru-Catalyzed Oxidations with Iodosylbenzene Derivatives - Substituent Effects on Selectivity in Oxidation of Sulfides and Alcohols. *Helv. Chim. Acta* **1983**, *66*, 1790–1795.

181. Katritzky, A. R.; Gallos, J. K.; Durst, H. D. Structure of and Electronic Interactions in Aromatic Polyvalent Iodine Compounds - A ¹³C NMR-Study. *Magn. Reson. Chem.* **1989**, *27*, 815–822.

182. Koser, G. F.; Wettach, R. H.; Troup, J. M.; Frenz, B. A. Hypervalent Organoiodine - Crystal-Structure of Phenylhydroxytosyloxyiodine. *J. Org. Chem.* **1976**, *41*, 3609–3611.

183. Macikenas, D.; Skrzypczak-Jankun, E.; Protasiewicz, J. D. A New Class of Iodonium Ylides Engineered as Soluble Primary Oxo and Nitrene Sources. *J. Am. Chem. Soc.* **1999**, *121*, 7164–7165.
184. Zhong, W. H.; Yang, J.; Meng, X. B.; Li, Z. J. $\text{BF}_3 \cdot \text{OEt}_2$ -Promoted diastereoselective Diacetoxylation of Alkenes by $\text{PhI}(\text{OAc})_2$. *J. Org. Chem.* **2011**, *76*, 9997–10004.
185. Yamamoto, Y.; Togo, H. PhI -Catalyzed *A*-Tosyloxylation of Ketones with *m*-Chloroperbenzoic acid and *p*-Toluenesulfonic Acid. *Synlett* **2006**, 798–800.
186. Dohi, T.; Takenaga, N.; Fukushima, K.; Uchiyama, T.; Kato, D.; Shiro, M.; Fujioka, H.; Kita, Y. Designer μ -Oxo-Bridged Hypervalent Iodine(III) Organocatalysts for Greener Oxidations. *Chem. Commun.* **2010**, *46*, 7697–7699.
187. Lucchetti, N.; Scalone, M.; Fantasia, S.; Muniz, K. An Improved Catalyst for Iodine (I/III)-Catalysed Intermolecular C–H Amination. *Adv. Synth. Catal.* **2016**, *358*, 2093–2099.
188. Yablonskii, O. P.; Vinogradov, M. G.; Kereselidze, R. V.; Nikishin, G. I. Mechanism of Oxidation of Aldehydes by Oxygen. *Bull. Acad. Sci. USSR* **1969**, *18*, 272–275.
189. Iwasaki, M.; Araki, Y.; Iino, S.; Nishihara, Y. Synthesis of Multisubstituted Triphenylenes and Phenanthrenes by Cascade Reaction of *o*-Iodobiphenyls or (*Z*)- β -Halostyrenes with *o*-Bromobenzyl Alcohols through Two Sequential C–C Bond Formations Catalyzed by a Palladium Complex. *J. Org. Chem.* **2015**, *80*, 9247–9263.
190. Macikenas, D.; Skrzypczak-Jankun, E.; Protasiewicz, J. D. A New Class of Iodonium Ylides Engineered as Soluble Primary Oxo and Nitrene Sources. *J. Am. Chem. Soc.* **2011**, *133*, 4151–4151.

191. Fulmer, G. R.; Miller, A. J. M.; Sherden, N. H.; Gottlieb, H. E.; Nudelman, A.; Stoltz, B. M.; Bercaw, J. E.; Goldberg, K. I. NMR Chemical Shifts of Trace Impurities: Common Laboratory Solvents, Organics, and Gases in Deuterated Solvents Relevant to the Organometallic Chemist. *Organometallics* **2010**, *29*, 2176–2179.
192. Iinuma, M.; Moriyama, K.; Togo, H. Simple and Practical Method for Preparation of (Diacetoxy)iiodoarenes with Iodoarenes and *m*-Chloroperoxybenzoic Acid. *Synlett* **2012**, 2663–2666.
193. Zheng, X.; Oviedo, I. R.; Twyman, L. J. Pseudo-Generational Effects Observed for a Series of Hyperbranched Polymers When Applied as Epoxidation Catalysts. *Macromolecules* **2008**, *41*, 7776–7779.
194. Haskali, M. B.; Telu, S.; Lee, Y. S.; Morse, C. L.; Lu, S. Y.; Pike, V. W. An Investigation of (Diacetoxyiodo)arenes as Precursors for Preparing No-Carrier-Added [¹⁸F] Fluoroarenes from Cyclotron-Produced [¹⁸F] Fluoride Ion. *J. Org. Chem.* **2016**, *81*, 2201–2201.
195. Moriarty, R. M.; Bailey, B. R.; Prakash, O.; Prakash, I. Capture of Electron-Deficient Species with Aryl Halides - New Syntheses of Hypervalent Iodonium Ylides. *J. Am. Chem. Soc.* **1985**, *107*, 1375–1378.
196. Sawaguchi, M.; Ayuba, S.; Hara, S. A Practical Synthetic Method of Iodoarene Difluorides without Fluorine Gas and Mercury Salts. *Synthesis-Stuttgart* **2002**, 1802–1803.

197. Hossain, D.; Kitamura, T. Unexpected, Drastic Effect of Triflic Acid on Oxidative Diacetoxylation of Iodoarenes by Sodium Perborate. A Facile and Efficient One-Pot Synthesis of (Diacetoxyiodo)arenes. *J. Org. Chem.* **2005**, *70*, 6984–6986.
198. Wu, Y. C.; Izquierdo, S.; Vidossich, P.; Lledos, A.; Shafir, A. NH-Heterocyclic Aryliodonium Salts and Their Selective Conversion into N1-Aryl-5-Iodoimidazoles. *Angew. Chem. Int. Ed.* **2016**, *55*, 7152–7156.
199. Miyamoto, K.; Yokota, Y.; Suefuji, T.; Yamaguchi, K.; Ozawa, T.; Ochiai, M. Reactivity of Hydroxy- and Aquo(Hydroxy)- λ^3 -Iodane Crown Ether Complexes. *Chem. Eur. J.* **2014**, *20*, 5447–5453.
200. Hamnett, D. J.; Moran, W. J. Improving Alkynyl(aryl)iodonium Salts: 2-Anisyl as a Superior Aryl Group. *Org. Biomol. Chem.* **2014**, *12*, 4156–4162.
201. Yamamoto, Y.; Togo, H. Facile One-Pot Preparation of Hydroxy(sulfonyloxy)iodoarenes from Iodoarenes with *m*CPBA in the Presence of Sulfonic Acids. *Synlett* **2005**, 2486–2488.
202. Wang, Y.; Zhang, L.; Yang, Y. H.; Zhang, P.; Du, Z. T.; Wang, C. Y. Alkene Oxyalkylation Enabled by Merging Rhenium Catalysis with Hypervalent Iodine(III) Reagents via Decarboxylation. *J. Am. Chem. Soc.* **2013**, *135*, 18048–18051.
203. Frei, R.; Waser, J. A Highly Chemoselective and Practical Alkynylation of Thiols. *J. Am. Chem. Soc.* **2013**, *135*, 9620–9623.
204. Vita, M. V.; Waser, J. Azidation of β -Keto Esters and Silyl Enol Ethers with a Benziodoxole Reagent. *Org. Lett.* **2013**, *15*, 3246–3249.

205. Eisenberger, P.; Gischig, S.; Togni, A. Novel 10-I-3 Hypervalent Iodine-Based Compounds for Electrophilic Trifluoromethylation. *Chem. Eur. J.* **2006**, *12*, 2579–2586.
206. Feng, Y. Y.; Huang, R. F.; Hu, L. Z.; Xiong, Y.; Coeffard, V. Chiral C(2)–Symmetric Iodoarene–Catalyzed Asymmetric α -Oxidation of β -Keto Esters. *Synthesis–Stuttgart* **2016**, *48*, 2637–2644.
207. Yamamoto, Y.; Togo, H. PhI-Catalyzed α -Tosyloxylation of Ketones with *m*-Chloroperbenzoic Acid and *p*-Toluenesulfonic Acid. *Synlett* **2006**, 798–800.
208. Ohkata, K.; Tamura, Y.; Shetuni, B. B.; Takagi, R.; Miyanaga, W.; Kojima, S.; Paquette, L. A. Stereoselectivity Control by Oxaspiro Rings During Diels-Alder Cycloadditions to Cross-Conjugated Cyclohexadienones: The Syn Oxygen Phenomenon. *J. Am. Chem. Soc.* **2004**, *126*, 16783–16792.
209. Frings, M.; Bolm, C. Enantioselective Halogenation of β -Oxo Esters Catalyzed by a Chiral Sulfoximine-Copper Complex. *Eur. J. Org. Chem.* **2009**, 4085–4090.
210. Piera, J.; Bäckvall, J. E. Catalytic Oxidation of Organic Substrates by Molecular Oxygen and Hydrogen Peroxide by Multistep Electron Transfer - a Biomimetic Approach. *Angew. Chem. Int. Ed.* **2008**, *47*, 3506–3523.
211. Miyamoto, K.; Yamashita, J.; Narita, S.; Sakai, Y.; Hirano, K.; Saito, T.; Wang, C.; Ochiai, M.; Uchiyama, M. Iodoarene-Catalyzed Oxidative Transformations Using Molecular Oxygen. *Chem. Commun.* **2017**, *53*, 9781–9784.
212. Duschek, A.; Kirsch, S. F. 2-Iodoxybenzoic Acid-a Simple Oxidant with a Dazzling Array of Potential Applications. *Angew. Chem. Int. Ed.* **2011**, *50*, 1524–1552.

213. Yoshimura, A.; Yusubov, M. S.; Zhdankin, V. V. Synthetic Applications of Pseudocyclic Hypervalent Iodine Compounds. *Org. Biomol. Chem.* **2016**, *14*, 4771–4781.
214. Zhdankin, V. V. Organoiodine(V) Reagents in Organic Synthesis. *J. Org. Chem.* **2011**, *76*, 1185–1197.
215. Satam, V.; Harad, A.; Rajule, R.; Pati, H. 2-Iodoxybenzoic Acid (IBX): An Efficient Hypervalent Iodine Reagent. *Tetrahedron* **2010**, *66*, 7659–7706.
216. Wirth, T. Oxidations and Rearrangements. In *Hypervalent Iodine Chemistry: Modern Developments in Organic Synthesis*, Wirth, T. Ed. Springer-Verlag Berlin: Berlin, 2003; Vol. 224, pp 185–208.
217. Yusubov, M. S.; Postnikov, P. S.; Yusubova, R. Y.; Yoshimura, A.; Jürjens, G.; Kirschning, A.; Zhdankin, V. V. 2-Iodoxybenzoic Acid Tosylates: The Alternative to Dess–Martin Periodinane Oxidizing Reagents. *Adv. Synth. Catal.* **2017**, *359*, 3207–3216.
218. Dess, D. B.; Martin, J. C. Readily Accessible 12-I-5 Oxidant for the Conversion of Primary and Secondary Alcohols to Aldehydes and Ketones. *J. Org. Chem.* **1983**, *48*, 4155–4156.
219. Dess, D. B.; Martin, J. C. A Useful 12-I-5 Triacetoxyperiodinane (the Dess-Martin Periodinane) for the Selective Oxidation of Primary or Secondary Alcohols and a Variety of Related 12-I-5 Species. *J. Am. Chem. Soc.* **1991**, *113*, 7277–7287.
220. Hartmann, C.; Meyer, V. Ueber Jodbenzoësäure. *Chem. Ber.* **1893**, *26*, 1727–1732.
221. Frigerio, M.; Santagostino, M. A Mild Oxidizing Reagent for Alcohols and 1,2-Diols : *o*-Iodoxybenzoic Acid (IBX) in DMSO. *Tetrahedron Lett.* **1994**, *35*, 8019–8022.

222. Frigerio, M.; Santagostino, M.; Sputore, S.; Palmisano, G. Oxidation of Alcohols with O-Iodoxybenzoic Acid (IBX) in DMSO: A New Insight into an Old Hypervalent Iodine Reagent. *J. Org. Chem.* **1995**, *60*, 7272–7276.
223. DeMunari, S.; Frigerio, M.; Santagostino, M. Hypervalent Iodine Oxidants: Structure and Kinetics of the Reactive Intermediates in the Oxidation of Alcohols and 1,2-Diols by *o*-Iodoxybenzoic Acid (IBX) and Dess-Martin Periodinane. A Comparative ¹H-NMR Study. *J. Org. Chem.* **1996**, *61*, 9272–9279.
224. Corey, E. J.; Palani, A. A Mechanistic Model for the Selective Oxidation of 1,4-Diols to α -Lactols by *o*-Iodoxybenzoic Acid. *Tetrahedron Lett.* **1995**, *36*, 7945–7948.
225. Corey, E. J.; Palani, A. A Method for the Selective Oxidation of 1,4-Diols to Lactols. *Tetrahedron Lett.* **1995**, *36*, 3485–3488.
226. Nicolaou, K. C.; Mathison, C. J. N.; Montagnon, T. O-Iodoxybenzoic Acid (IBX) as a Viable Reagent in the Manipulation of Nitrogen- and Sulfur-Containing Substrates: Scope, Generality, and Mechanism of IBX-Mediated Amine Oxidations and Dithiane Deprotections. *J. Am. Chem. Soc.* **2004**, *126*, 5192–5201.
227. de Graaff, C.; Bensch, L.; van Lint, M. J.; Ruijter, E.; Orru, R. V. A. IBX-Mediated Oxidation of Unactivated Cyclic Amines: Application in Highly Diastereoselective Oxidative Ugi-Type and Aza-Friedel–Crafts Reactions. *Org. Biomol. Chem.* **2015**, *13*, 10108–10112.
228. Nicolaou, K. C.; Montagnon, T.; Baran, P. S. Modulation of the Reactivity Profile of IBX by Ligand Complexation: Ambient Temperature Dehydrogenation of Aldehydes and

Ketones to α , β -Unsaturated Carbonyl Compounds. *Angew. Chem. Int. Ed.* **2002**, *41*, 993–996.

229. Nicolaou, K. C.; Montagnon, T.; Baran, P. S.; Zhong, Y. L. Iodine(V) Reagents in Organic Synthesis. Part 4. *o*-Iodoxybenzoic Acid as a Chemospecific Tool for Single Electron Transfer-Based Oxidation Processes. *J. Am. Chem. Soc.* **2002**, *124*, 2245–2258.

230. Nicolaou, K. C.; Zhong, Y. L.; Baran, P. S. A New Method for the One-Step Synthesis of α , β -Unsaturated Carbonyl Systems from Saturated Alcohols and Carbonyl compounds. *J. Am. Chem. Soc.* **2000**, *122*, 7596–7597.

231. Nicolaou, K. C.; Baran, P. S.; Zhong, Y.-L. Selective Oxidation at Carbon Adjacent to Aromatic Systems with IBX. *J. Am. Chem. Soc.* **2001**, *123*, 3183–3185.

232. Chandra, A.; Parida, K. N.; Moorthy, J. N. One-Pot Synthesis of α -Bromo- and α -Azidoketones from Olefins by Catalytic Oxidation with in situ-Generated Modified IBX as the Key Reaction. *Tetrahedron* **2017**, *73*, 5827–5832.

233. Mishra, A. K.; Moorthy, J. N. Mechanochemical Catalytic Oxidations in the Solid State with in situ-Generated Modified IBX from 3,5-Di-Tert-Butyl-2-Iodobenzoic Acid (DTB-IA)/Oxone. *Org. Chem. Front.* **2017**, *4*, 343–349.

234. Moorthy, J. N.; Parida, K. N. Oxidative Cleavage of Olefins by in situ-Generated Catalytic 3,4,5,6-Tetramethyl-2-Iodoxybenzoic Acid/Oxone. *J. Org. Chem.* **2014**, *79*, 11431–11439.

235. Seth, S.; Jhulki, S.; Moorthy, J. N. Catalytic and Chemoselective Oxidation of Activated Alcohols and Direct Conversion of Diols to Lactones with in situ-Generated Bis-IBX Catalyst. *Eur. J. Org. Chem.* **2013**, *2013*, 2445–2452.

236. Bikshapathi, R.; Prathima, P. S.; Rao, V. J. Hypervalent Iodine Catalysis for Selective Oxidation of Baylis–Hillman Adducts via in situ Generation of *o*-Iodoxybenzoic Acid (IBX) from 2-Iodosobenzoic Acid (IBA) in the Presence of Oxone. *New J. Chem.* **2016**, *40*, 10300–10304.
237. Yakura, T.; Horiuchi, Y.; Nishimura, Y.; Yamada, A.; Nambu, H.; Fujiwara, T. Efficient Oxidative Cleavage of Tetrahydrofuran-2-Methanols to γ -Lactones by a 2-Iodobenzamide Catalyst in Combination with Oxone. *Adv. Synth. Catal.* **2016**, *358*, 869–873.
238. Thottumkara, A. P.; Bowsher, M. S.; Vinod, T. K. In situ Generation of *o*-Iodoxybenzoic Acid (IBX) and the Catalytic Use of It in Oxidation Reactions in the Presence of Oxone as a Co-Oxidant. *Org. Lett.* **2005**, *7*, 2933–2936.
239. Maity, A.; Hyun, S.-M.; Wortman, A. K.; Powers, D. C. Oxidation Catalysis by an Aerobically Generated Dess–Martin Periodinane Analogue. *Angew. Chem. Int. Ed.* **2018**, *57*, 7205–7209.
240. Macikenas, D.; Skrzypczak-Jankun, E.; Protasiewicz, J. D. Redirecting Secondary Bonds to Control Molecular and Crystal Properties of an Iodosyl- and an Iodylbenzene. *Angew. Chem. Int. Ed.* **2000**, *39*, 2007–2010.
241. Bawn, C. E. H.; Jolley, J. E. The Cobalt-Salt-Catalyzed Autoxidation of Benzaldehyde. *Proc. R. Soc. Lond. Ser. A* **1956**, *237*, 297–312.
242. Moorthy, J. N.; Singhal, N.; Senapati, K. Oxidative Cleavage of Vicinal Diols: IBX Can Do What Dess–Martin Periodinane (DMP) Can. *Org. Biomol. Chem.* **2007**, *5*, 767–771.

243. Morimoto, T.; Hirano, M.; Hamaguchi, T.; Shimoyama, M.; Zhuang, X. Oxidation of Alcohols with Peracetic Acid in Ethyl Acetate in the Presence of Sodium Bromide. *Bull. Chem. Soc. Jpn.* **1992**, *65*, 703–706.
244. Morimoto, T.; Hirano, M.; Wachi, M.; Murakami, T. Oxidation of Alcohols to Carbonyl Compounds with Peracetic Acid Catalysed by Cobalt(III) Acetate. *J. Chem. Soc. Perkin Trans. 2* **1984**, 1949–1951.
245. Richter, H. W.; Cherry, B. R.; Zook, T. D.; Koser, G. F. Characterization of Species Present in Aqueous Solutions of [Hydroxy(Mesyloxy)Iodo]Benzene and [Hydroxy(Tosyloxy)Iodo]Benzene. *J. Am. Chem. Soc.* **1997**, *119*, 9614–623.
246. Silva, L. F.; Vasconcelos, R. S.; Lopes, N. P. Application of High-Resolution Electrospray Mass Spectrometry for the Elucidation of the Disproportionation Reaction of Iodobenzene Diacetate. *Int. J. Mass spectrom.* **2008**, *276*, 24–30.
247. Cardenal, A. D.; Maity, A.; Gao, W.-Y.; Ashirov, R.; Hyun, S.-M.; Powers, D. C. Iodosylbenzene Coordination Chemistry Relevant to Metal–Organic Framework Catalysis. *Inorg. Chem.* **2019**, *58*, 10543–10553.
248. Sankar, M.; Nowicka, E.; Carter, E.; Murphy, D. M.; Knight, D. W.; Bethell, D.; Hutchings, G. J. The Benzaldehyde Oxidation Paradox Explained by the Interception of Peroxy Radical by Benzyl Alcohol. *Nat. Commun.* **2014**, *5*, 3332.
249. Domae, M.; Katsumara, Y.; Jiang, P. Y.; Nagaishi, R.; Hasegawa, C.; Ishigure, K.; Yoshida, Y. Observation of Chlorine Oxide (ClO₃) Radical in Aqueous Chlorate Solution by Pulse Radiolysis. *J. Phys. Chem.* **1994**, *98*, 190–192.

250. Zhao, Y.; Truhlar, D. G. The M06 Suite of Density Functionals for Main Group Thermochemistry, Thermochemical Kinetics, Noncovalent Interactions, Excited States, and Transition Elements: Two New Functionals and Systematic Testing of Four M06-Class Functionals and 12 Other Functionals. *Theor. Chem. Acc.* **2008**, *120*, 215–241.
251. Hay, P. J.; Wadt, W. R. Ab Initio Effective Core Potentials for Molecular Calculations. Potentials for the Transition Metal Atoms Sc to Hg. *J. Chem. Phys.* **1985**, *82*, 270–283.
252. Hay, P. J.; Wadt, W. R. Ab Initio Effective Core Potentials for Molecular Calculations. Potentials for K to Au Including the Outermost Core Orbitals. *J. Chem. Phys.* **1985**, *82*, 299–310.
253. Wadt, W. R.; Hay, P. J. Ab Initio Effective Core Potentials for Molecular Calculations. Potentials for Main Group Elements Na to Bi. *J. Chem. Phys.* **1985**, *82*, 284–298.
254. Ditchfield, R.; Hehre, W. J.; Pople, J. A. Self-Consistent Molecular-Orbital Methods. IX. An Extended Gaussian-Type Basis for Molecular-Orbital Studies of Organic Molecules. *J. Chem. Phys.* **1971**, *54*, 724–728.
255. Frisch, M. J.; Pople, J. A.; Binkley, J. S. Self-Consistent Molecular Orbital Methods 25. Supplementary Functions for Gaussian Basis Sets. *J. Chem. Phys.* **1984**, *80*, 3265–3269.
256. Marenich, A. V.; Cramer, C. J.; Truhlar, D. G. Universal Solvation Model Based on Solute Electron Density and on a Continuum Model of the Solvent Defined by the Bulk

Dielectric Constant and Atomic Surface Tensions. *J. Phys. Chem. B* **2009**, *113*, 6378–6396.

257. Schnapperelle, I.; Hummel, W.; Groger, H. Formal Asymmetric Hydration of Non-Activated Alkenes in Aqueous Medium through a "Chemoenzymatic Catalytic System". *Chem. Eur. J.* **2012**, *18*, 1073–1076.

258. Tsuchiya, D.; Moriyama, K.; Togo, H. Swern Oxidation of Alcohols with Ion-Supported Methyl Sulfoxide and Oxalyl Chloride. *Synlett* **2011**, 2701–2704.

259. Kumar, R.; Gleissner, E. H.; Tiu, E. G. V.; Yamakoshi, Y. C-70 as a Photocatalyst for Oxidation of Secondary Benzylamines to Imines. *Org. Lett.* **2016**, *18*, 184–187.

260. Hughey, J. L.; Knapp, S.; Schugar, H. Dehydrogenation of 2-Imidazolines to Imidazoles with Barium Manganate. *Synthesis-Stuttgart* **1980**, 489–490.

261. Pascanu, V.; Gomez, A. B.; Ayats, C.; Platero-Prats, A. E.; Carson, F.; Su, J.; Yao, Q. X.; Pericas, M. A.; Zou, X. D.; Martin-Matute, B. Double-Supported Silica-Metal-Organic Framework Palladium Nanocatalyst for the Aerobic Oxidation of Alcohols under Batch and Continuous Flow Regimes. *ACS Catal.* **2015**, *5*, 472–479.

262. Komagawa, H.; Maejima, Y.; Nagano, T. Sodium Bromide-Catalyzed Oxidation of Secondary Benzylic Alcohols Using Aqueous Hydrogen Peroxide as Terminal Oxidant. *Synlett* **2016**, *27*, 789–793.

263. Guo, S.; Zeng, R. Y.; Li, C. Y. Nitrite-Containing Resin as an Efficient and Recyclable Catalyst for Aerobic Oxidation of Oximes to Carbonyl Compounds. *Synth. Commun.* **2016**, *46*, 1446–1453.

264. Rueping, M.; Vila, C.; Szadkowska, A.; Koenigs, R. M.; Fronert, J. Photoredox Catalysis as an Efficient Tool for the Aerobic Oxidation of Amines and Alcohols: Bioinspired Demethylations and Condensations. *ACS Catal.* **2012**, *2*, 2810–2815.
265. Moriyama, K.; Takemura, M.; Togo, H. Selective Oxidation of Alcohols with Alkali Metal Bromides as Bromide Catalysts: Experimental Study of the Reaction Mechanism. *J. Org. Chem.* **2014**, *79*, 6094–6104.
266. Lauber, M. B.; Stahl, S. S. Efficient Aerobic Oxidation of Secondary Alcohols at Ambient Temperature with an ABNO/NO_x Catalyst System. *ACS Catal.* **2013**, *3*, 2612–2616.
267. Zhu, Y. G.; Zhao, B. G.; Shi, Y. Highly Efficient Cu(I)-Catalyzed Oxidation of Alcohols to Ketones and Aldehydes with Diaziridinone. *Org. Lett.* **2013**, *15*, 992–995.
268. Feng, Q.; Song, Q. L. Aldehydes and Ketones Formation: Copper-Catalyzed Aerobic Oxidative Decarboxylation of Phenylacetic Acids and α -Hydroxyphenylacetic Acids. *J. Org. Chem.* **2014**, *79*, 1867–1871.
269. Clennan, E. L.; Pan, G. L. Zeolite-Promoted Oxidations of 1,1-Diarylethylenes. *Org. Lett.* **2003**, *5*, 4979–4982.
270. Steves, J. E.; Stahl, S. S. Copper(I)/ABNO-Catalyzed Aerobic Alcohol Oxidation: Alleviating Steric and Electronic Constraints of Cu/TEMPO Catalyst Systems. *J. Am. Chem. Soc.* **2013**, *135*, 15742–15745.
271. Chen, F. N.; Liu, A. C.; Yan, Q. J.; Liu, M. X.; Zhang, D. M.; Shao, L. Y. Tetrabutylammonium Peroxydisulfate in Organic Synthesis; IV. An Efficient, Highly

- Selective and Oxidative Deoxygenation by Tetrabutylammonium Peroxydisulfate. *Synth. Commun.* **1999**, *29*, 1049–1056.
272. Iosub, A. V.; Stahl, S. S. Palladium-Catalyzed Aerobic Oxidative Dehydrogenation of Cyclohexenes to Substituted Arene Derivatives. *J. Am. Chem. Soc.* **2015**, *137*, 3454–3457.
273. Dodd, R. H.; Lehyaric, M. The Oxidation of Aromatic-Aldehydes to Carboxylic-Acids Using Hydrogen-Peroxide in Formic-Acid. *Synthesis-Stuttgart* **1993**, 295–297.
274. Dohi, T.; Takenaga, N.; Goto, A.; Fujioka, H.; Kita, Y. Clean and Efficient Benzylic C-H Oxidation in Water Using a Hypervalent Iodine Reagent: Activation of Polymeric Iodosobenzene with KBr in the Presence of Montmorillonite-K10. *J. Org. Chem.* **2008**, *73*, 7365–7368.
275. Jain, S. L.; Sain, B. An Unconventional Cobalt-Catalyzed Aerobic Oxidation of Tertiary Nitrogen Compounds to N-Oxides. *Angew. Chem. Int. Ed.* **2003**, *42*, 1265–1267.
276. Das, A.; Reibenspies, J. H.; Chen, Y. S.; Powers, D. C. Direct Characterization of a Reactive Lattice-Confined Ru₂-Nitride by Photocrystallography. *J. Am. Chem. Soc.* **2017**, *139*, 2912–2915.
277. Lee, C. T.; Yang, W. T.; Parr, R. G. Development of the Colle-Salvetti Correlation-Energy Formula into a Functional of the Electron-Density. *Phys. Rev. B* **1988**, *37*, 785–789.
278. Rassolov, V. A.; Ratner, M. A.; Pople, J. A.; Redfern, P. C.; Curtiss, L. A. 6-31g* Basis Set for Third-Row Atoms. *J. Comput. Chem.* **2001**, *22*, 976–984.

279. Zhao, Y.; Truhlar, D. G. Density Functionals with Broad Applicability in Chemistry. *Acc. Chem. Res.* **2008**, *41*, 157–167.
280. Zhao, Y.; Truhlar, D. G. A New Local Density Functional for Main-Group Thermochemistry, Transition Metal Bonding, Thermochemical Kinetics, and Noncovalent Interactions. *J. Chem. Phys.* **2006**, *125*, 194101–194117.
281. Frontana-Uribe, B. A.; Little, R. D.; Ibanez, J. G.; Palma, A.; Vasquez-Medrano, R. Organic Electrosynthesis: A Promising Green Methodology in Organic Chemistry. *Green Chem.* **2010**, *12*, 2099–2119.
282. Lund, H. A Century of Organic Electrochemistry. *J. Electrochem. Soc.* **2002**, *149*, S21–S33.
283. Horn, E. J.; Rosen, B. R.; Baran, P. S. Synthetic Organic Electrochemistry: An Enabling and Innately Sustainable Method. *ACS Cent. Sci.* **2016**, *2*, 302–308.
284. Chiba, K.; Okada, Y. Electron–Transfer–Induced Molecular Reactions: Electrode Processes in Organic Synthesis. *Curr. Opin. Electrochem.* **2017**, *2*, 53–59.
285. Yan, M.; Kawamata, Y.; Baran, P. S. Synthetic Organic Electrochemical Methods since 2000: On the Verge of a Renaissance. *Chem. Rev.* **2017**, *117*, 13230–13319.
286. Kärkäs, M. D. Electrochemical Strategies for C–H Functionalization and C–N Bond Formation. *Chem. Soc. Rev.* **2018**, *47*, 5786–5865.
287. Möhle, S.; Zirbes, M.; Rodrigo, E.; Gieshoff, T.; Wiebe, A.; Waldvogel, S. R. Modern Electrochemical Aspects for the Synthesis of Value-Added Organic Products. *Angew. Chem. Int. Ed.* **2018**, *57*, 6018–6041.
288. Morrow, G. Organic Electrochemistry. Marcel Dekker New York: 2001.

289. Amatore, C.; Saveant, J.; Tessier, D. Kinetics of Electron Transfer to Organic Molecules at Solid Electrodes in Organic Media. *J. Electroanal. Chem. Interfacial Electrochem.* **1983**, *146*, 37–45.
290. Evans, D. H. One-Electron and Two-Electron Transfers in Electrochemistry and Homogeneous Solution Reactions. *Chem. Rev.* **2008**, *108*, 2113–2144.
291. Steckhan, E. Indirect Electroorganic Syntheses—a Modern Chapter of Organic Electrochemistry [New Synthetic Methods (59)]. *Angew. Chem. Int. Ed.* **1986**, *25*, 683–701.
292. Steckhan, E. Organic Syntheses with Electrochemically Regenerable Redox Systems. *Electrochemistry I* **1987**, 1–69.
293. Ogibin, Y. N.; Elinson, M. N.; Nikishin, G. I. Mediator Oxidation Systems in Organic Electrosynthesis. *Russ. Chem. Rev.* **2009**, *78*, 89–140.
294. Francke, R.; Little, R. D. Redox Catalysis in Organic Electrosynthesis: Basic Principles and Recent Developments. *Chem. Soc. Rev.* **2014**, *43*, 2492–2521.
295. Utley, J.; Rozenberg, G. Electroorganic Reactions. Part 57.† Ddq Mediated Anodic Oxidation of 2-Methyl- and 2-Benzyl-naphthalenes. *J. Appl. Electrochem.* **2003**, *33*, 525–532.
296. Amatore, C.; Cammoun, C.; Jutand, A. Electrochemical Recycling of Benzoquinone in the Pd/Benzoquinone-Catalyzed Heck-Type Reactions from Arenes. *Adv. Synth. Catal.* **2007**, *349*, 292–296.

297. Shen, Y.; Suzuki, K.; Atobe, M.; Fuchigami, T. Indirect Anodic Fluorodesulfurization of S-Aryl Thiobenzoates Using a Triarylamine Mediator. *J. Electroanal. Chem.* **2003**, *540*, 189–194.
298. Wu, X.; Davis, A. P.; Fry, A. J. Electrocatalytic Oxidative Cleavage of Electron-Deficient Substituted Stilbenes in Acetonitrile– Water Employing a New High Oxidation Potential Electrocatalyst. An Electrochemical Equivalent of Ozonolysis. *Org. Lett.* **2007**, *9*, 5633–5636.
299. Park, Y. S.; Little, R. D. Redox Electron-Transfer Reactions: Electrochemically Mediated Rearrangement, Mechanism, and a Total Synthesis of Daucene. *J. Org. Chem.* **2008**, *73*, 6807–6815.
300. Semmelhack, M. F.; Chou, C. S.; Cortes, D. A. Nitroxyl-Mediated Electrooxidation of Alcohols to Aldehydes and Ketones. *J. Am. Chem. Soc.* **1983**, *105*, 4492–4494.
301. Inokuchi, T.; Matsumoto, S.; Torii, S. Indirect Electrooxidation of Alcohols by a Double Mediatory System with Two Redox Couples of $[R_2N^+=O]/R_2NO^\bullet$ And $[Br^\bullet \text{ Or } Br^+]/Br^-$ in an Organic-Aqueous Two-Phase Solution. *J. Org. Chem.* **1991**, *56*, 2416–2421.
302. Hickey, D. P.; McCammant, M. S.; Giroud, F.; Sigman, M. S.; Minter, S. D. Hybrid Enzymatic and Organic Electrocatalytic Cascade for the Complete Oxidation of Glycerol. *J. Am. Chem. Soc.* **2014**, *136*, 15917–5920.
303. Rafiee, M.; Miles, K. C.; Stahl, S. S. Electrocatalytic Alcohol Oxidation with TEMPO and Bicyclic Nitroxyl Derivatives: Driving Force Trumps Steric Effects. *J. Am. Chem. Soc.* **2015**, *137*, 14751–14757.

304. Cha, H. G.; Choi, K.-S. Combined Biomass Valorization and Hydrogen Production in a Photoelectrochemical Cell. *Nat. Chem.* **2015**, *7*, 328–333.
305. Badalyan, A.; Stahl, S. S. Cooperative Electrocatalytic Alcohol Oxidation with Electron-Proton-Transfer Mediators. *Nature* **2016**, *535*, 406–410.
306. Folgueiras-Amador, A. A.; Philipps, K.; Guilbaud, S.; Poelakker, J.; Wirth, T. An Easy-to-Machine Electrochemical Flow Microreactor: Efficient Synthesis of Isoindolinone and Flow Functionalization. *Angew. Chem. Int. Ed.* **2017**, *56*, 15446–15450.
307. Zhu, L.; Xiong, P.; Mao, Z. Y.; Wang, Y. H.; Yan, X.; Lu, X.; Xu, H. C. Electrocatalytic Generation of Amidyl Radicals for Olefin Hydroamidation: Use of Solvent Effects to Enable Anilide Oxidation. *Angew. Chem. Int. Ed.* **2016**, *55*, 2226–2229.
308. Fu, N.; Sauer, G. S.; Saha, A.; Loo, A.; Lin, S. Metal-Catalyzed Electrochemical Diazidation of Alkenes. *Science* **2017**, *357*, 575–579.
309. Sauermann, N.; Meyer, T. H.; Tian, C.; Ackermann, L. Electrochemical Cobalt-Catalyzed C–H Oxygenation at Room Temperature. *J. Am. Chem. Soc.* **2017**, *139*, 18452–18455.
310. Tang, S.; Wang, D.; Liu, Y.; Zeng, L.; Lei, A. Cobalt-Catalyzed Electrooxidative C–H/N–H [4+ 2] Annulation with Ethylene or Ethyne. *Nat. commun.* **2018**, *9*, 1–7.
311. Tian, C.; Massignan, L.; Meyer, T. H.; Ackermann, L. Electrochemical C–H/N–H Activation by Water-Tolerant Cobalt Catalysis at Room Temperature. *Angew. Chem.* **2018**, *130*, 2407–2411.
312. Sauermann, N.; Mei, R.; Ackermann, L. Electrochemical C–H Amination by Cobalt Catalysis in a Renewable Solvent. *Angew. Chem. Int. Ed.* **2018**, *57*, 5090–5094.

313. Yang, Q.-L.; Wang, X.-Y.; Lu, J.-Y.; Zhang, L.-P.; Fang, P.; Mei, T.-S. Copper-Catalyzed Electrochemical C–H Amination of Arenes with Secondary Amines. *J. Am. Chem. Soc.* **2018**, *140*, 11487–11494.
314. Jiao, K.-J.; Xing, Y.-K.; Yang, Q.-L.; Qiu, H.; Mei, T.-S. Site-Selective C–H Functionalization via Synergistic Use of Electrochemistry and Transition Metal Catalysis. *Acc. Chem. Res.* **2020**, *53*, 300–310.
315. Sousa e Silva, F. C.; Tierno, A. F.; Wengryniuk, S. E. Hypervalent Iodine Reagents in High Valent Transition Metal Chemistry. *Molecules* **2017**, *22*, 780.
316. Elsherbini, M.; Wirth, T. Hypervalent Iodine Reagents by Anodic Oxidation: A Powerful Green Synthesis. *Chem. Eur. J.* **2018**, *24*, 13399–13407.
317. Amano, Y.; Nishiyama, S. Oxidative Synthesis of Azacyclic Derivatives through the Nitrenium Ion: Application of a Hypervalent Iodine Species Electrochemically Generated from Iodobenzene. *Tetrahedron Lett.* **2006**, *47*, 6505–6507.
318. Yoshiyama, T.; Fuchigami, T. Anodic Gem-Difluorination of Dithioacetals. *Chem. Lett.* **1992**, *21*, 1995–998.
319. Sawamura, T.; Kuribayashi, S.; Inagi, S.; Fuchigami, T. Use of Task-Specific Ionic Liquid for Selective Electrocatalytic Fluorination. *Org. Lett.* **2010**, *12*, 644–646.
320. Sawamura, T.; Kuribayashi, S.; Inagi, S.; Fuchigami, T. Recyclable Polymer-Supported Iodobenzene-Mediated Electrocatalytic Fluorination in Ionic Liquid. *Adv. Synth. Catal.* **2010**, *352*, 2757–2760.

321. Doobary, S.; Sedikides, A. T.; Caldora, H. P.; Poole, D. L.; Lennox, A. J. Electrochemical Vicinal Difluorination of Alkenes: Scalable and Amenable to Electron-Rich Substrates. *Angew. Chem.* **2020**, *132*, 1171–1176.
322. Hyun, S.-M.; Yuan, M.; Maity, A.; Gutierrez, O.; Powers, D. C. The Role of Iodanyl Radicals as Critical Chain Carriers in Aerobic Hypervalent Iodine Chemistry. *Chem* **2019**, *5*, 2388–2404.
323. Maity, A.; Frey, B. L.; Hoskinson, N. D.; Powers, D. C. Electrocatalytic C–N Coupling via Anodically Generated Hypervalent Iodine Intermediates. *J. Am. Chem. Soc.* **2020**, *142*, 499–4995.
324. Cho, S. H.; Yoon, J.; Chang, S. Intramolecular Oxidative C–N Bond Formation for the Synthesis of Carbazoles: Comparison of Reactivity between the Copper-Catalyzed and Metal-Free Conditions. *J. Am. Chem. Soc.* **2011**, *133*, 5996–6005.
325. Antonchick, A. P.; Samanta, R.; Kulikov, K.; Lategahn, J. Organocatalytic, Oxidative, Intramolecular C–H Bond Amination and Metal-Free Cross-Amination of Unactivated Arenes at Ambient Temperature. *Angew. Chem. Int. Ed.* **2011**, *50*, 8605–8608.
326. Samanta, R.; Kulikov, K.; Strohmam, C.; Antonchick, A. P. Metal-Free Electrocyclization at Ambient Temperature: Synthesis of 1-Arylcarbazoles. *Synthesis* **2012**, *44*, 2325–2332.
327. Elgrishi, N.; Rountree, K. J.; McCarthy, B. D.; Rountree, E. S.; Eisenhart, T. T.; Dempsey, J. L. A Practical Beginner's Guide to Cyclic Voltammetry. *J. Chem. Educ.* **2018**, *95*, 197–206.

328. Dohi, T.; Sasa, H.; Dochi, M.; Yasui, C.; Kita, Y. Oxidative Coupling of N-Methoxyamides and Related Compounds toward Aromatic Hydrocarbons by Designer μ -Oxo Hypervalent Iodine Catalyst. *Synthesis* **2019**, *51*, 1185–1195.
329. Ito, C.; Katsuno, S.; Ohta, H.; Omura, M.; Kajiura, I.; Furukawa, H. Constituents of *Clausena Excavata*. Isolation and Structural Elucidation of New Carbazole Alkaloids. *Chem. Pharm. Bull.* **1997**, *45*, 48–52.
330. Meragelman, K. M.; McKee, T. C.; Boyd, M. R. Siamenol, a New Carbazole Alkaloid from *Murraya Siamensis*. *J. Nat. Prod.* **2000**, *63*, 427–428.
331. Samanta, R.; Bauer, J. O.; Strohmman, C.; Antonchick, A. P. Organocatalytic, Oxidative, Intermolecular Amination and Hydrazination of Simple Arenes at Ambient Temperature. *Org. Lett.* **2012**, *14*, 5518–5521.
332. Ragnarsson, U. Synthetic Methodology for Alkyl Substituted Hydrazines. *Chem. Soc. Rev.* **2001**, *30*, 205–213.
333. van der Vlugt, J. I. Advances in Selective Activation and Application of Ammonia in Homogeneous Catalysis. *Chem. Soc. Rev.* **2010**, *39*, 2302–2322.
334. Galicia, M.; González, F. Electrochemical Oxidation of Tetrabutylammonium Salts of Aliphatic Carboxylic Acids in Acetonitrile. *J. Electrochem. Soc.* **2002**, *149*, D46–D50.
335. Bard, A. J.; Faulkner, L. R. Fundamentals and Applications. *Electrochemical methods* **2001**, *2*, 580–632.
336. Savéant, J.-M. *Elements of Molecular and Biomolecular Electrochemistry: An Electrochemical Approach to Electron Transfer Chemistry*. John Wiley & Sons: 2006; Vol. 13.

337. Filler, R.; Schure, R. M. Highly Acidic Perhalogenated Alcohols. A New Synthesis of Perfluoro-tert-Butyl Alcohol. *J. Org. Chem.* **1967**, *32*, 1217–1219.
338. Collins, K. D.; Glorius, F. A Robustness Screen for the Rapid Assessment of Chemical Reactions. *Nat. Chem.* **2013**, *5*, 597–601.
339. Powers, D. C.; Lee, E.; Ariaferd, A.; Sanford, M. S.; Yates, B. F.; Canty, A. J.; Ritter, T. Connecting Binuclear Pd(III) and Mononuclear Pd(IV) Chemistry by Pd–Pd Bond Cleavage. *J. Am. Chem. Soc.* **2012**, *134*, 12002–12009.
340. Mörsdorf, J.-M.; Wadepohl, H.; Ballmann, J. A Tautomeric Λ^3/Λ^5 -Phosphane Pair and Its Ambiphilic Reactivity. *Inorg. Chem.* **2019**, *58*, 3502–3508.
341. Brosse, N.; Pinto, M. F.; Jamart-Gregoire, B. Preparation of Multiply Protected Alkylhydrazine Derivatives by Mitsunobu and Ptc Approaches. *Eur. J. Org. Chem.* **2003**, *2003*, 4757–4764.
342. Liang, Z.; Ju, L.; Xie, Y.; Huang, L.; Zhang, Y. Free-Amine-Directed Alkenylation of C(sp²)-H and Cycloamination by Palladium Catalysis. *Chem. Eur. J.* **2012**, *18*, 15816–15821.
343. Singh, D. K.; Kim, I. Convergent Synthesis of Diptoindonesin G. *Tetrahedron Lett.* **2019**, *60*, 300–301.
344. Huq, M. M.; Rahman, M. R.; Naher, M.; Khan, M. M. R.; Masud, M. K.; Hossain, G. M. G.; Zhu, N.; Lo, Y. H.; Younus, M.; Wong, W.-Y. Synthesis, Characterization and Catalytic Activities of Palladium(II) Nitroaryl Complexes. *J. Inorg. Organomet. Polym. Mater.* **2016**, *26*, 1243–1252.

345. Wang, W.; Guo, Y.; Sun, K.; Wang, S.; Zhang, S.; Liu, C.; Chen, Q.-Y. Visible Light-Induced Radical Cyclization of Tertiary Bromides with Isonitriles to Construct Trifluoromethylated Quaternary Carbon Center. *J. Org. Chem.* **2018**, *83*, 14588–14599.
346. Chatterjee, T.; Lee, D. S.; Cho, E. J. Extended Study of Visible-Light-Induced Photocatalytic [4+ 2] Benzannulation: Synthesis of Polycyclic (Hetero)aromatics. *J. Org. Chem.* **2017**, *82*, 4369–4378.
347. Zuo, Z.; Liu, J.; Nan, J.; Fan, L.; Sun, W.; Wang, Y.; Luan, X. Highly Stereoselective Synthesis of Imine-Containing Dibenzo [*b*, *d*] Azepines by a Palladium(II)-Catalyzed [5+ 2] Oxidative Annulation of *o*-Arylanilines with Alkynes. *Angew. Chem. Int. Ed.* **2015**, *54*, 15385–15389.
348. Kayser-Bricker, K. J.; Glenn, M. P.; Lee, S. H.; Sebti, S. M.; Cheng, J. Q.; Hamilton, A. D. Non-Peptidic Substrate-Mimetic Inhibitors of Akt as Potential Anti-Cancer Agents. *Bioorg. Med. Chem.* **2009**, *17*, 1764–1771.
349. Jiang, J.; Zhang, W.-M.; Dai, J.-J.; Xu, J.; Xu, H.-J. Visible-Light-Promoted C–H Arylation by Merging Palladium Catalysis with Organic Photoredox Catalysis. *J. Org. Chem.* **2017**, *82*, 3622–3630.
350. Guerra, W. D.; Rossi, R. A.; Pierini, A. B.; Barolo, S. M. “Transition-Metal-Free” Synthesis of Carbazoles by Photostimulated Reactions of 2'-Halo[1, 1'-biphenyl]-2-amines. *J. Org. Chem.* **2015**, *80*, 928–941.
351. Simó Padial, J.; Poater, J.; Nguyen, D. T.; Tinnemans, P.; Bickelhaupt, F. M.; Mecinović, J. Stabilization of 2, 6-Diarylanilinum Cation by through-Space Cation– π Interactions. *J. Org. Chem.* **2017**, *82*, 9418–9424.

352. Jasch, H.; Scheumann, J.; Heinrich, M. R. Regioselective Radical Arylation of Anilines with Arylhydrazines. *J. Org. Chem.* **2012**, *77*, 10699–10706.
353. Yang, L.; Zhang, Y.; Zou, X.; Lu, H.; Li, G. Visible-Light-Promoted Intramolecular C–H Amination in Aqueous Solution: Synthesis of Carbazoles. *Green Chem.* **2018**, *20*, 1362–1366.
354. Smith, G.; Martin, N.; Menear, K.; Hummersone, M.; Cockcroft, X.-L.; Frigerio, M.; Griffin, R.; Golding, B.; Hardcastle, I.; Newell, D. R.; Calvert, H. A.; Curtin, N. J.; Desage-El Murr, M. Preparation of Chromen-4-Ones and Their Analogs as DNA-PK Inhibitors. US Patents, 2006109084, October 19, 2006.: 2006.
355. Albaugh, P. A.; Dominguez-Manzanares, E.; Hong, J. E.; Hornback, W. J.; Jiang, D.; Ornstein, P. L.; Thompson, M. L.; Tromiczak, E. G.; Wu, Z.; Zarrinmayeh, H. Pyrrole and Pyrazole Derivatives as Potentiators of Glutamate Receptors. US Patent, 7,625,932, December 1, 2009: 2009.
356. Trost, B. M.; Pissot-Soldermann, C.; Chen, I. A Short and Concise Asymmetric Synthesis of Hamigeran B. *Chem. Eur. J.* **2005**, *11*, 951–959.
357. Xi, J.; Dong, Q.-L.; Liu, G.-S.; Wang, S.; Chen, L.; Yao, Z.-J. Efficient Synthesis of Phenanthridines Using Hendrickson Reagent Initiated Cascade Reaction under Mild Conditions. *Synlett* **2010**, *2010*, 1674–1678.
358. Kim, J.; Moon, Y.; Lee, S.; Hong, S. A Pd-Catalyzed One-Pot Dehydrogenative Aromatization and Ortho-Functionalization Sequence of N-Acetyl Enamides. *Chem. Commun.* **2014**, *50*, 3227–3230.

359. Annamalai, P.; Hsu, K.-C.; Raju, S.; Hsiao, H.-C.; Chou, C.-W.; Lin, G.-Y.; Hsieh, C.-M.; Chen, P.-L.; Liu, Y.-H.; Chuang, S.-C. Palladium(II)-Catalyzed Mono-and Bis-alkenylation of N-Acetyl-2-aminobiaryls through Regioselective C–H Bond Activation. *J. Org. Chem.* **2018**, *83*, 3840–3856.
360. Chinnagolla, R. K.; Jeganmohan, M. Ruthenium-Catalyzed Ortho-Arylation of Acetanilides with Aromatic Boronic Acids: An Easy Route to Prepare Phenanthridines and Carbazoles. *Chem. Commun.* **2014**, *50*, 2442–2444.
361. Hyodo, K.; Hasegawa, G.; Oishi, N.; Kuroda, K.; Uchida, K. Direct and Catalytic Amide Synthesis from Ketones via Transoximation and Beckmann Rearrangement under Mild Conditions. *J. Org. Chem.* **2018**, *83*, 13080–13087.
362. Arumugam, V.; Kaminsky, W.; Nallasamy, D. Pd(II) Pincer Type Complex Catalyzed Tandem C–H and N–H Activation of Acetanilide in Aqueous Media: A Concise Access to Functionalized Carbazoles in a Single Step. *Green Chem.* **2016**, *18*, 3295–3301.
363. Natarajan, P.; Chuskit, D. Transition-Metal-Free and Organic Solvent-Free Conversion of N-Substituted 2-Aminobiaryls into Corresponding Carbazoles via Intramolecular Oxidative Radical Cyclization Induced by Peroxodisulfate. *Green Chem.* **2017**, *19*, 5854–5861.
364. Wang, S.; Mao, H.; Ni, Z.; Pan, Y. Pd(II)-Catalyzed Intramolecular C–H Activation/C–C Cross Coupling for the Synthesis of Carbazoles from Diaryl Acetamides. *Tetrahedron Lett.* **2012**, *53*, 505–508.
365. Tsang, W. C. P.; Zheng, N.; Buchwald, S. L. Combined C–H Functionalization/C–N Bond Formation Route to Carbazoles. *J. Am. Chem. Soc.* **2005**, *127*, 14560–14561.

366. Zhou, S.; Wang, J.; Zhang, F.; Song, C.; Zhu, J. A Versatile, Traceless C–H Activation-Based Approach for the Synthesis of Heterocycles. *Org. Lett.* **2016**, *18*, 2427–2430.
367. Drago, R. S. *Physical Methods for Chemists*. 2 ed.; Surfside Scientific Publishers: Gainesville, FL, 1992.
368. Hili, R.; Yudin, A. K. Making Carbon-Nitrogen Bonds in Biological and Chemical Synthesis. *Nat. Chem. Biol.* **2006**, *2*, 284–287.
369. Vitaku, E.; Smith, D. T.; Njardarson, J. T. Analysis of the Structural Diversity, Substitution Patterns, and Frequency of Nitrogen Heterocycles among US FDA Approved Pharmaceuticals: Miniperspective. *J. Med. Chem.* **2014**, *57*, 10257–10274.
370. Richter, M. F.; Drown, B. S.; Riley, A. P.; Garcia, A.; Shirai, T.; Svec, R. L.; Hergenrother, P. J. Predictive Compound Accumulation Rules Yield a Broad-Spectrum Antibiotic. *Nature* **2017**, *545*, 299–304.
371. Clark, J. R.; Feng, K.; Sookezian, A.; White, M. C. Manganese-Catalysed Benzylic C (sp³)–H Amination for Late-Stage Functionalization. *Nat. Chem.* **2018**, *10*, 583–591.
372. Park, Y.; Kim, Y.; Chang, S. Transition Metal-Catalyzed C–H Amination: Scope, Mechanism, and Applications. *Chem. Rev.* **2017**, *117*, 9247–9301.
373. Dequierez, G.; Pons, V.; Dauban, P. Nitrene Chemistry in Organic Synthesis: Still in Its Infancy? *Angew. Chem. Int. Ed.* **2012**, *51*, 7384–7395.
374. Wentrup, C. Carbenes and Nitrenes: Recent Developments in Fundamental Chemistry. *Angew. Chem. Int. Ed.* **2018**, *57*, 11508–11521.

375. Davies, H. M.; Manning, J. R. Catalytic C–H Functionalization by Metal Carbenoid and Nitrenoid Insertion. *Nature* **2008**, *451*, 417–424.
376. Breslow, R.; Gellman, S. H. Tosylamidation of Cyclohexane by a Cytochrome P-450 Model. *J. Chem. Soc. Chem. Commun.* **1982**, 1400–1401.
377. Espino, C. G.; Du Bois, J. A Rh-Catalyzed C–H Insertion Reaction for the Oxidative Conversion of Carbamates to Oxazolidinones. *Angew. Chem. Int. Ed.* **2001**, *40*, 598–600.
378. Zalatan, D. N.; Du Bois, J. A Chiral Rhodium Carboxamidate Catalyst for Enantioselective C–H Amination. *J. Am. Chem. Soc.* **2008**, *130*, 9220–9221.
379. Hinman, A.; Du Bois, J. A Stereoselective Synthesis of (–)-Tetrodotoxin. *J. Am. Chem. Soc.* **2003**, *125*, 11510–11511.
380. Paradine, S. M.; Griffin, J. R.; Zhao, J.; Petronico, A. L.; Miller, S. M.; White, M. C. A Manganese Catalyst for Highly Reactive yet Chemoselective Intramolecular C(sp³)–H Amination. *Nat. Chem.* **2015**, *7*, 987–994.
381. Chiappini, N. D.; Mack, J. B.; Du Bois, J. Intermolecular C(sp³)–H Amination of Complex Molecules. *Angew. Chem. Int. Ed.* **2018**, *57*, 4956–4959.
382. Noda, H.; Asada, Y.; Shibasaki, M. O-Benzoylhydroxylamines as Alkyl Nitrene Precursors: Synthesis of Saturated N-Heterocycles from Primary Amines. *Org. Lett.* **2020**, *22*, 8769–8773.
383. Romero, N. A.; Margrey, K. A.; Tay, N. E.; Nicewicz, D. A. Site-Selective Arene C–H Amination via Photoredox Catalysis. *Science* **2015**, *349*, 1326–1330.
384. See, Y. Y.; Sanford, M. S. C–H Amination of Arenes with Hydroxylamine. *Org. Lett.* **2020**, *22*, 2931–2934.

385. Anugu, R. R.; Munnuri, S.; Falck, J. R. Picolinate-Directed Arene Meta-C–H Amination via FeCl₃ Catalysis. *J. Am. Chem. Soc.* **2020**, *142*, 5266–5271.
386. D'Amato, E. Börgel J. Ritter T. *Chem. Sci.* **2019**, *10*, 2424–2428.
387. Kim, H.; Heo, J.; Kim, J.; Baik, M.-H.; Chang, S. Copper-Mediated Amination of Aryl C–H Bonds with the Direct Use of Aqueous Ammonia via a Disproportionation Pathway. *J. Am. Chem. Soc.* **2018**, *140*, 14350–14356.
388. Legnani, L.; Prina Cerai, G.; Morandi, B. Direct and Practical Synthesis of Primary Anilines through Iron-Catalyzed C–H Bond Amination. *ACS Catal.* **2016**, *6*, 8162–8165.
389. Paudyal, M. P.; Adebessin, A. M.; Burt, S. R.; Ess, D. H.; Ma, Z.; Kürti, L.; Falck, J. R. Dirhodium-Catalyzed C–H Arene Amination Using Hydroxylamines. *Science* **2016**, *353*, 1144–1147.
390. Huang, H.-M.; Bellotti, P.; Ma, J.; Dalton, T.; Glorius, F. Bifunctional Reagents in Organic Synthesis. *Nat. Rev. Chem.* **2021**, *5*, 301–321.
391. Roychowdhury, P.; Maity, A.; Powers, D. Bifunctional *N*-Aminopyridinium Reagents Enable C–H Amination, Olefin Carboamination Cascades. **2021**, 10.26434/chemrxiv.14677533.v1.
392. Chen, J.-Q.; Yu, W.-L.; Wei, Y.-L.; Li, T.-H.; Xu, P.-F. Photoredox-Induced Functionalization of Alkenes for the Synthesis of Substituted Imidazolines and Oxazolidines. *J. Org. Chem.* **2017**, *82*, 243–249.
393. Zhao, Y.; Shi, C.; Su, X.; Xia, W. Synthesis of Isoquinolones by Visible-Light-Induced Deaminative [4+ 2] Annulation Reactions. *Chem. Commun.* **2020**, *56*, 5259–5262.

394. Mo, J.-N.; Yu, W.-L.; Chen, J.-Q.; Hu, X.-Q.; Xu, P.-F. Regiospecific Three-Component Aminofluorination of Olefins via Photoredox Catalysis. *Org. Lett.* **2018**, *20*, 4471–4474.
395. Miyazawa, K.; Koike, T.; Akita, M. Regiospecific Intermolecular Aminohydroxylation of Olefins by Photoredox Catalysis. *Chem. Eur. J.* **2015**, *21*, 11677–11680.
396. Miyazawa, K.; Koike, T.; Akita, M. Aminohydroxylation of Olefins with Iminopyridinium Ylides by Dual Ir Photocatalysis and Sc(OTf)₃ Catalysis. *Tetrahedron* **2016**, *72*, 7813–7820.
397. Guo, W.; Wang, Q.; Zhu, J. Selective 1,2-Aminoisothiocyanation of 1,3-Dienes under Visible-Light Photoredox Catalysis. *Angew. Chem. Int. Ed.* **2021**, *60*, 4085–4089.
398. Yu, W.-L.; Chen, J.-Q.; Wei, Y.-L.; Wang, Z.-Y.; Xu, P.-F. Alkene Functionalization for the Stereospecific Synthesis of Substituted Aziridines by Visible-Light Photoredox Catalysis. *Chem. Commun.* **2018**, *54*, 1948–1951.
399. Moon, Y.; Park, B.; Kim, I.; Kang, G.; Shin, S.; Kang, D.; Baik, M.-H.; Hong, S. Visible Light Induced Alkene Aminopyridylation Using *N*-Aminopyridinium Salts as Bifunctional Reagents. *Nat. Commun.* **2019**, *10*, 1–9.
400. Rössler, S. L.; Jelier, B. J.; Tripet, P. F.; Shemet, A.; Jeschke, G.; Togni, A.; Carreira, E. M. Pyridyl Radical Cation for C–H Amination of Arenes. *Angew. Chem. Int. Ed.* **2019**, *58*, 526–531.

401. Ham, W. S.; Hillenbrand, J.; Jacq, J.; Genicot, C.; Ritter, T. Divergent Late-Stage (Hetero)aryl C–H Amination by the Pyridinium Radical Cation. *Angew. Chem.* **2019**, *131*, 542–546.
402. Hillenbrand, J.; Ham, W. S.; Ritter, T. C–H Pyridonation of (Hetero-)arenes by Pyridinium Radical Cations. *Org. Lett.* **2019**, *21*, 5363–5367.
403. Pictet, A.; Spengler, T. Über Die Bildung Von Isochinolin-Derivaten Durch Einwirkung Von Methylal Auf Phenyl-Äthylamin, Phenyl-Alanin Und Tyrosin. *Ber. Dtsch. Chem. Ges.* **1911**, *44*, 2030–2036.
404. Yokoyama, A.; Ohwada, T.; Shudo, K. Prototype Pictet–Spengler Reactions Catalyzed by Superacids. Involvement of Dicationic Superelectrophiles. *J. Org. Chem.* **1999**, *64*, 611–617.
405. Maryanoff, B. E.; Zhang, H.-C.; Cohen, J. H.; Turchi, I. J.; Maryanoff, C. A. Cyclizations of N-Acyliminium Ions. *Chem. Rev.* **2004**, *104*, 1431–1628.
406. Uematsu, N.; Fujii, A.; Hashiguchi, S.; Ikariya, T.; Noyori, R. Asymmetric Transfer Hydrogenation of Imines. *J. Am. Chem. Soc.* **1996**, *118*, 4916–4917.
407. Berhal, F.; Wu, Z.; Zhang, Z.; Ayad, T.; Ratovelomanana-Vidal, V. Enantioselective Synthesis of 1-Aryl-Tetrahydroisoquinolines through Iridium Catalyzed Asymmetric Hydrogenation. *Org. Lett.* **2012**, *14*, 3308–3311.
408. Berkowitz, W. F.; John, T. V. An Internal Imino-Diels-Alder Route to a Tetrahydroisoquinoline. *J. Org. Chem.* **1984**, *49*, 5269–5271.

409. Sirvent, A.; García-Muñoz, M. J.; Yus, M.; Foubelo, F. Stereoselective Synthesis of Tetrahydroisoquinolines from Chiral 4-Azaocta-1, 7-Diynes and 4-Azaocta-1, 7-Enynes. *Eur. J. Org. Chem.* **2020**, *2020*, 113–126.
410. Kotha, S.; Sreenivasachary, N. A New Synthetic Approach to 1,2,3,4-Tetrahydroisoquinoline-3-carboxylic Acid (Tic) Derivatives via Enyne Metathesis and the Diels–Alder Reaction. *Chem. Commun.* **2000**, 503–504.
411. Qian, G.; Bai, M.; Gao, S.; Chen, H.; Zhou, S.; Cheng, H. G.; Yan, W.; Zhou, Q. Modular One-Step Three-Component Synthesis of Tetrahydroisoquinolines Using a Catellani Strategy. *Angew. Chem. Int. Ed.* **2018**, *57*, 10980–10984.
412. Li, J. J.; Mei, T. S.; Yu, J. Q. Synthesis of Indolines and Tetrahydroisoquinolines from Arylethylamines by Pdii-Catalyzed C–H Activation Reactions. *Angew. Chem.* **2008**, *120*, 6552–6555.
413. Zhou, Z.; Cheng, Q.-Q.; Kürti, L. Aza-Rubottom Oxidation: Synthetic Access to Primary α -Aminoketones. *J. Am. Chem. Soc.* **2019**, *141*, 2242–2246.
414. Golszewska, K.; Rybicka-Jasińska, K.; Szurmak, J.; Gryko, D. Visible-Light-Mediated Amination of π -Nucleophiles with N-Aminopyridinium Salts. *J. Org. Chem.* **2019**, *84*, 15834–15844.
415. Jiang, H.; Studer, A. Intermolecular Radical Carboamination of Alkenes. *Chem. Soc. Rev.* **2020**, *49*, 1790–1811.
416. Jelier, B. J.; Tripet, P. F.; Pietrasiak, E.; Franzoni, I.; Jeschke, G.; Togni, A. Radical Trifluoromethoxylation of Arenes Triggered by a Visible-Light-Mediated N–O Bond Redox Fragmentation. *Angew. Chem. Int. Ed.* **2018**, *57*, 13784–13789.

417. Pangborn, A. B.; Giardello, M. A.; Grubbs, R. H.; Rosen, R. K.; Timmers, F. J. Safe and Convenient Procedure for Solvent Purification. *Organometallics* **1996**, *15*, 1518–1520.
418. Gordillo, A.; Ortuño, M. A.; López-Mardomingo, C.; Lledós, A.; Ujaque, G.; De Jesús, E. Mechanistic Studies on the Pd-Catalyzed Vinylation of Aryl Halides with Vinylalkoxysilanes in Water: The Effect of the Solvent and NaOH Promoter. *J. Am. Chem. Soc.* **2013**, *135*, 13749–13763.
419. Gao, S.; Zhao, L.; Zhao, P.; Huang, Y.; Zhao, H. Synthesis, Structure and Characterization of a New Highly Porous Zirconium-Based Metal-Organic Frameworks. *Inorg. Chim. Acta* **2018**, *480*, 173–176.
420. Zhang, J. z.; Tang, Y. Iron-Catalyzed Regioselective Oxo- and Hydroxy-Phthalimidation of Styrenes: Access to α -Hydroxyphthalimide Ketones. *Adv. Synth. Catal.* **2016**, *358*, 752–764.
421. Song, C.-x.; Chen, P.; Tang, Y. Carboxylation of Styrenes with CBr_4 and DMSO via Cooperative Photoredox and Cobalt Catalysis. *RSC Adv.* **2017**, *7*, 11233–11243.
422. Kuwano, R.; Kashiwabara, M. Ruthenium-Catalyzed Asymmetric Hydrogenation of N-Boc-Indoles. *Org. Lett.* **2006**, *8*, 2653–2655.
423. Khan, I.; Reed-Berendt, B. G.; Melen, R. L.; Morrill, L. C. FLP-Catalyzed Transfer Hydrogenation of Silyl Enol Ethers. *Angew. Chem.* **2018**, *130*, 12536–12539.
424. Stoll, S.; Schweiger, A. Easyspin, a Comprehensive Software Package for Spectral Simulation and Analysis in EPR. *J. Magn. Res.* **2006**, *178*, 42–55.
425. Sheldrick, G. M. A Short History of Shelx. *Acta Cryst.* **2008**, *64*, 112–122.

426. Dolomanov, O. V.; Bourhis, L. J.; Gildea, R. J.; Howard, J. A.; Puschmann, H. Olex2: A Complete Structure Solution, Refinement and Analysis Program. *J. Appl. Cryst.* **2009**, *42*, 339–341.
427. Sheldrick, G. M. Crystal Structure Refinement with Shelxl. *Acta Cryst.* **2015**, *71*, 3–8.
428. Gosl, R.; Meuwsen, A. 1-Aminopyridinium Iodide. *Org. Synth.* **1973**, *5*, 43–45.
429. Habert, L.; Cariou, K. Photoinduced Aerobic Iodoarene-Catalyzed Spirocyclization of N-Oxy-Amides to N-Fused Spirolactams. *Angew. Chem. Int. Ed.* **2021**, *60*, 171–175.
430. Cosio, M. N.; Cardenal, A. D.; Maity, A.; Hyun, S.-M.; Akwaowo, V. E.; Hoffman, C. W.; Powers, T. M.; Powers, D. C. Exploring Green Chemistry with Aerobic Hypervalent Iodine Catalysis. *J. Chem. Educ.* **2020**, *97*, 3816–3821.